ANALYSIS OF MASONRY ARCH BRIDGES

Kwooi-Hock NG BEng (Hons)

A thesis submitted to Napier University,

in partial fulfilment of the requirements for the

Degree of Doctor of Philosophy

School of the Built Environment

Napier University

Edinburgh, UK

1999

This copy of the thesis has been supplied on condition that anyone who consults it is understood to recognise that the copyright rests with its author and that no quotation from the thesis and no information derived from it may be published without the prior written consent of the author or the University (as may be appropriate).

PAGE NUMBERING AS ORIGINAL

Abstract

In January 1999, the maximum axle weight increased from 10t to 11.5t for the assessment of highway bridges and structures. At the same time, the maximum vehicle weight also increased from 38t to 44t. Highway authorities are urgently searching for a more refined assessment method to predict the behaviour of masonry arch bridges. LUSAS finite element analysis was used to study the behaviour of masonry arch bridges. Load *versus* deflection curves and collapse loads are given for some of the full and large scale arches previously tested to collapse. A parametric study was also performed to determine the influence of the arch material properties and the load dispersal angle: the arch tensile strength and the load dispersal angle were found to have the most significant influence on the collapse load predictions.

Repeatability tests were carried out by building three nominally identical large scale arch bridges in the laboratory and testing them to collapse. The first, second and third arches collapsed at 21kNm^{-1}, 16kNm^{-1}, and 25kNm^{-1} respectively. Finite element analysis predicted a range of 18kNm^{-1} to 39kNm^{-1} for the same arches. This led to an examination of a statistical, risk based, approach to bridge assessment.

Two novel risk assessment programs were developed by integrating Monte Carlo simulation with the MEXE and the mechanism methods. Statistical information about the predicted collapse load and allowable axle load is given. These risk assessment tools are offered for incorporation within routine assessment methods. Their principal benefit lies in providing engineers with a feel for the reliability of their analyses.

A modification has been made to the mechanism method by considering arch deflection. A mechanism prediction is accurate only when all the forces and their positions are accurately located. The modified mechanism method was used to analyse some of the full scale arch bridges, previously tested to collapse, which revealed that arch deflections had a significant influence on the collapse load prediction.

Declaration

This thesis is submitted to Napier University for the Degree of Doctor of Philosophy. The work described in this thesis was carried out under the supervision of Dr Charles Fairfield and Professor Alan Sibbald. The work was undertaken in The School of the Built Environment, Napier University, Edinburgh.

In accordance with the Regulations of Napier University governing the requirements for the Degree of Doctor of Philosophy, the candidate submits that the work presented in this thesis is original unless otherwise referenced within the text. The finite element analysis, large scale arch bridge tests, Monte Carlo simulation, and the modified mechanism method are claimed as original.

The following papers published in journals or conference proceedings were derived from the work in this thesis. Those papers published by the time this thesis is prepared are included in the Appendix. Full permission from the relevant publisher or copyright holder has been obtained.

1 NG, K. H., FAIRFIELD, C. A. & SIBBALD, A. (1998). Track bed geotechnology: its effect on the collapse load of railway arch bridges. Proc. 1st Int. Conf. Railway Engng., Uxbridge, pp. 163-168.

2 NG, K. H., FAIRFIELD, C. A. & SIBBALD, A. (1999). Finite-element analysis of masonry arch bridges. Proc. Instn Civ. Engnrs J. Structs & Bldgs, 134, pp. 119-127.

3 NG, K. H., FAIRFIELD, C. A. & SIBBALD, A. (1999). Arch bridge mechanism method assessment incorporating deflection dependent soil pressure updating algorithms. Proc. 2nd Int. Conf. Railway Engng., London, ISBN 0-947644-39-3. (Highly recommended for conference award)

4 NG, K. H. & FAIRFIELD, C. A. (1999). Reliability of arch bridges by Monte Carlo simulation. Proc. 8th Int. Conf. Struct. Faults & Repair, London, ISBN 0-947644-41-5. (Highly recommended for conference award)

5 NG, K. H. & FAIRFIELD, C. A. (1999). Collapse load repeatability tests on brickwork arches. Proc. 8th Int. Conf. Struct. Faults & Repair, London, ISBN 0-947644-41-5.

6 NG, K. H., FAIRFIELD, C. A. & SIBBALD, A. Arch bridge assessment based on risk analysis. Computers & Structures, *under review*, 1999.

7 NG, K. H., FAIRFIELD, C. A. & SIBBALD, A. Repeatability tests and risk analyses of masonry arch bridges. Proc. Instn Civ. Engrs Structs & Bldgs., *under review*, 1999.

8 FAIRFIELD, C. A., REID, A. J., HOUNSOME, I. W. S. & NG, K. H. Transport infrastructure: engineering issues. Conf. Scottish Roads & Traffic Management, Edinburgh, oral presentation, 1998.

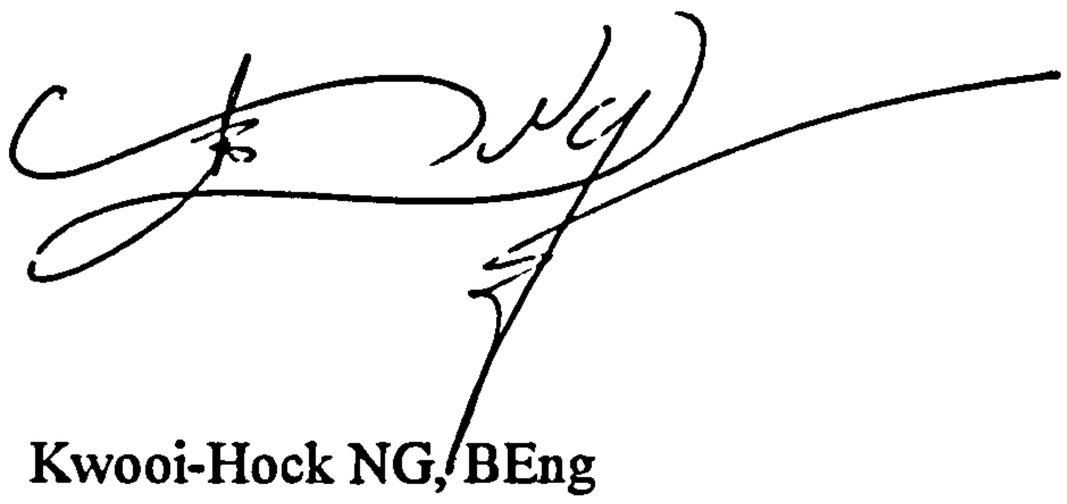

Kwooi-Hock NG, BEng

Acknowledgement

The author is indebted to Dr Charles Fairfield and Professor Alan Sibbald for their active supervision and encouragement throughout the course of this research at Napier University.

The author is grateful to Napier University for providing a Postgraduate Research Scholarship to support this research throughout the three years of the project.

The facilities provided by The School of the Built Environment, Napier University, are hereby gratefully acknowledged. The author also thanks the entire Department Technical Staff, in particular: William Laing, Colin Gardner, and John Callaghan for their help in carrying out laboratory tests.

The author thanks Dr Abdelmadjid Bensalem, previously a research fellow based at the then Department of Civil and Transportation Engineering, Napier University, for giving valuable technical advice during this research.

The author thanks Dr Fraser Smith (University of Dundee) for the use of program ARCHIE, Dr Tim Hughes (University of Wales College, Cardiff) for the use of Program CTAP and Dr Selwyn Davies (formerly The University of Edinburgh) for the use of program MARCH.

Finally but by no means least, the author would like to thank his parents, brothers, sister, and Miss Siew-Fei Tan for their continued support and encouragement throughout the course of this research.

CONTENTS

List of Figures

CHAPTER 3

CHAPTER 4

CHAPTER 5

CHAPTER 6

CHAPTER 7

CHAPTER 8

CHAPTER 9

There are no Figures in Chapter 9

CHAPTER 10

There are no Figures in Chapter 10

List of Tables

CHAPTER 8

CHAPTER 9

There are no Tables in Chapter 9

CHAPTER 10

There are no Tables in Chapter 10

Notation

Unless otherwise stated in the text, the symbols used in this document are listed below. Roman characters are given first followed by Greek characters.

Roman characters

c	apparent cohesion of the backfill
d	ring thickness at the crown
d_a	vertical ring thickness at the abutment
d_b	brick thickness
d_q	vertical ring thickness at the quarter span point
D_{ACT}	ultimate active horizontal deflection
D_{PAS}	ultimate passive horizontal deflection
E_b	elastic modulus of the brick
E_m	elastic modulus of the mortar
F	collapse load
F_c	the condition factor in the MEXE method
F_j	the joint factor in the MEXE method
F_m	the material factor in the MEXE method
F_p	the profile factor in the MEXE method
F_{sr}	the span to rise ratio factor in the MEXE method
f_{tb}	brick-mortar flexural bond strength
F_{tb}	total bonding force
h	depth of backfill over the crown
H_q	rise to the intrados at the quarter span point
I_n	live load influence factor at point n
I_p	the sum of live load influence factors in the region enclosed within a specified load dispersal angle or Boussinesq's limiting live load influence factor
K_o	coefficient of earth pressure at rest

K_p	passive coefficient of earth pressure
L	intrados span of the arch
L_b	length of a brick
L_m	length of a mortar joint
P	ultimate applied load to overcome the brick-mortar bond strength
P_F	probability of failure
q	applied stress
R	rise to the intrados at the crown
R_a	vertical reaction at point A
R_b	vertical reaction at point B
R_{LH}	left hand horizontal support reaction
R_{LV}	left hand vertical support reaction
R_{RH}	right hand horizontal support reaction
R_{RV}	right hand vertical support reaction
t_m	mortar thickness
W	brick self-weight
W^n_{ACT}	backfill equivalent active force acting at point n
W^n_{FILL}	weight of backfill acting at point n
W_p	width of the load platen
W^n_{PAS}	backfill equivalent passive force acting at point n
W^n_{PL}	equivalent point load acting at point n
W^n_V	weight of arch acting at point n
X^n	horizontal distance at point n measured from the origin
X/R	dimensionless horizontal co-ordinate
Y^n	vertical distance at point n measured from the origin
Y^n_{EX}	vertical distance at point n on the arch extrados measured from the origin
Y^n_{IN}	vertical distance at point n on the arch intrados measured from the origin

Greek characters

γ_b	backfill bulk unit weight
ε_b	strain in the brick
ε_m	strain in the mortar
ε_{ult}	ultimate tensile strain
θ	allowable live load dispersal angle
θ^n	live load dispersal angle at point n measured from the edge of the load platen
μ	mean
ν_b	Poisson's ratio of the brick
ν_m	Poisson's ratio of the mortar
σ	standard deviation
σ_b	stress in the brick
σ_c	compressive strength
σ_m	stress in the mortar
σ_n	normal stress
σ_t	tensile strength
σ_x	horizontal stress
σ_y	vertical stress
σ_1	major principal stress
σ_3	minor principal stress
τ	shear stress
τ_{xy}	complementary shear stress
ϕ	backfill angle of shearing resistance
χ^2	chi-squared statistic

CHAPTER 1

Introduction

1.1 General introduction to masonry arch bridges in the UK

Masonry arch bridges have been built in the United Kingdom from the time of the Romans onwards. There are approximately 75,000 masonry arch bridges in service on road, railway and waterway networks in the United Kingdom with the majority of these bridges built between the 17th and 19th centuries. The assessment of old masonry arch bridges is not a simple matter as such bridges have been serving the traffic over centuries and the material may be deteriorated and weathered to a certain extent. These bridges are now carrying weights far beyond those envisaged by their builders. Since January 1999, under new European Commission Directives, the maximum allowable gross vehicle weight has been increased from 38t to 44t and simultaneously the maximum axle load increased from 10t to 11.5t. Figure 1.1 shows the increase in the maximum allowable single axle load from 1967 to 1999. The increases in traffic load have compelled both local and national highway authorities to undertake assessment and strengthening of their stocks of masonry arch bridges. Abnormally large heavy loads also require special one-off assessments typical of which was the 240t oil rig leg seen in Figure 1.2 crossing Balmoor bridge, Inverugie in 1991.

In the past few decades, only a few new masonry arch bridges were built in the United Kingdom. This is because the construction of masonry arch bridges requires a high standard of design and craftsmanship if they are to achieve a satisfactory appearance. The high initial construction cost coupled with a limited demand in incorporating this type of ancient-look structure into the modern world, renders the chances of new

masonry arch bridges being constructed as somewhat pessimistic. In China, however, arch bridges are still being constructed. The world's longest single span masonry arch bridge, Jiuxigou bridge, was built in Sichuan, China, in 1972 with span, rise, and transverse width of 116m, 14.5m, and 7.5m respectively (see Figure 1.3). The ring thickness varies from 1.6m to 2.15m. The arch was built in random stonework took only a year to complete.

However, apart from environmental reasons, low maintenance cost and durability favour the commissioning of new masonry arch bridges. With a large stock of masonry arch bridges in the United Kingdom and the potential for construction of new bridges of this kind, more research is still needed to unveil the secrets of this complex soil-arch system. Hopefully this research will add to the body of knowledge and spur what may be a short-term arch construction revival.

1.2 Current assessment methods and their deficiencies

There are mainly four methods for the assessment of masonry arch bridges in the United Kingdom: the Military Engineering Experimental Establishment (MEXE) method (empirical), mechanism (limit state analysis), elastic cracking (Castigliano's strain energy approach), and finite element analysis. This section presents a review of these methods; problems associated with each method are outlined.

1.2.1 The MEXE method

This method was derived by the Military Engineering Experimental Establishment based on the work done by PIPPARD *et al.*, (1936, 1938, 1941, 1948, 1951, 1952 & 1968). The method is empirical and based on some classic elastic theories and a series of experimental studies. Various assumptions are made in the MEXE method: the arch is parabolic, it has a span to rise ratio of four, both abutments are pinned, it is of a

specified unit weight ($21.97kNm^{-3}$), and the arch is loaded at the crown with a transverse line load. The permitted maximum arch compressive and tensile stresses are 1.4MPa and 0.7MPa respectively. The MEXE method involves the evaluation of the provisional axle load (PAL) which is then adjusted by a series of modification factors to account for the geometry, material, and condition of the arch bridge. The expression for the modified axle load is given in Eqn 1.1. The modified axle load is multiplied by axle factors to convert it to single and multiple axle loads which are then translated into maximum vehicle weights.

$$\text{Modified axle load} = \frac{740(d+h)^2}{L^{1.3}} \times F_{sr} \times F_p \times F_m \times F_j \times F_c \qquad 1.1$$

Details of the values of these modification factors may be found in the current departmental standard (BD21/97, 1997a) for the assessment of highway bridges and structures.

The PAL depends equally on the arch and backfill thickness although the ring thickness has a significantly greater influence on the arch behaviour than the backfill. The modification factors are introduced without taking account of the arch geometry; the backfill depth, ring thickness, and even the mortar thickness could have differing influences on arches with different geometries. The application of condition factor is subjective and a wide range of arch capacity could be legitimately assessed. Excellent photographs are provided in the advice note (BA16/97, 1997b) which gives examples of arches and suggested condition factors. These however are unable to do away with much of the subjectivity inherent in choosing F_c.

1.2.2 The mechanism method

This method assumes the arch is on the verge of collapse and there are four or five hinges in the arch ring. Figures 1.4a and 1.4b show a typical four- and a five-hinge

collapse modes respectively. These hinges are necessary, in this method, to turn the arch into a statically determinate structure. The arch is assumed to be incapable of bearing tensile stress and has an infinite elastic modulus; no arch deflections are considered even at the moment of collapse. The arch is divided into small segments which are acted upon by an assumed configuration of live and dead loads, and the backfill lateral forces. Static equilibrium equations are then derived to solve for the collapse load and abutment reactions.

The application of backfill passive pressure coefficient is subjective. Furthermore, a constant backfill lateral pressure coefficient is used in this method regardless of the arch deflection. It is understood that the mechanism method is only reliable if all forces and their positions are accurately considered. The author has developed a modified mechanism based assessment method which takes the arch deflection into consideration. Results revealed that the mechanism prediction for the arch collapse load was significantly affected by arch deflections.

1.2.3 Elastic cracking method

This method was developed at the University Of Wales, Cardiff (BRIDLE & HUGHES, 1989; 1990) and is based on Castigliano's strain energy method (CASTIGLIANO, 1876; 1879). The method is available in a computer program known as CTAP in which a mechanism based analysis option is also available. Incremental loads, after being distributed by a specified load distribution, are applied to the arch and stresses in the arch ring are evaluated. Tensile zones in the arch ring are eliminated which results in the progressive development of hinges. Loads are applied until the ultimate limit state is reached. The actual collapse load can not be defined exactly as it lies between the last two load increments. The problem is easily overcome by using a small load increment. Figure 1.5 shows an illustration of the thinning of the arch in CTAP. Unlike the MEXE and mechanism methods, the elastic cracking method predicts the collapse load, the arch deflections, and is able to model snap through

buckling failure. A typical snap through buckling failure of an arch is presented in Figure 1.6.

A much lower elastic modulus, compared with that of the voussoirs, is assigned to the arch to account for the presence of much weaker mortar joints. A lower elastic modulus is also required to simulate large deflections due to rotation of arch segments. A similar problem occurs with the finite element method as will be noted in Section 1.2.4. Apart from the difficulty in deciding the arch and backfill material properties, the method also involves complex computations.

1.2.4 Finite element analyses

Finite element analysis became famous in the last few decades mainly due to the development of powerful computers. The advantage of this method over other conventional structural analyses is that it can be used for statically indeterminate structures with irregular shapes and different boundary conditions. Non-linear material properties can also be defined giving non-linear structural behaviour up to ultimate limit state.

Various researchers (CRISFIELD *et al.*, 1984; 1985a & b; 1988; TOWLER, 1981; 1985; SAWKO *et al.*, 1982; 1985; ROUF, 1984; CHOO *et al.*, 1990a & b ; 1991; GONG, 1992; LOO *et al.*, 1991a & b; 1995) have assisted in the development of finite element analyses for arch bridges. One and two dimensional finite element analyses are undertaken ignoring the spandrel walls, parapet, wing walls and skew effects. While three dimensional finite element modelling is more realistic, it is rather more complicated and time consuming. Figure 1.7 shows a typical 3-D finite element output.

Most finite element programs written specifically for arches assume that the arch has no tensile strength. This is undoubtedly a safe assumption but it may be too safe and therefore conservative. It is unlikely that in an arch's loading history any applied force

was large enough to cause full separation between voussoirs. The author's FE results will show that the arch's tensile strength had a significant influence on the collapse load prediction. There remains, of course, the risk of attaching too much importance to the tensile capacity in any assessment and the obvious point about all analyses; rubbish in = rubbish out applies equally to the finite element method.

Field elements are used to model the backfill lateral resistance. To the author's knowledge, previous non-linear finite element analyses on arch bridges were performed by imposing the live load directly onto the arch extrados. This is done by assuming a stress dispersal angle; the resultant distribution could be either based on Boussinesq's or the codified (BD21/97, 1997a) method. This is to avoid premature foundation failure directly under the load platen as encountered by CRISFIELD (1988).

A series of parametric studies was performed by the author which revealed that the collapse load prediction was very sensitive to variations in arch tensile strength. Unfortunately, the tensile strength of an existing arch is almost impossible to determine. As in the case of CTAP's elastic cracking method, a much lower elastic modulus, compared with that of the voussoirs, should usually be assigned to the arch to account for the presence of mortar joints. Finite element analysis remains a powerful tool provided interpretation is carried out expertly and the cost is fully justified. In many cases a highway authority would, like a doctor's patient, be advised to seek collaborative evidence in the form of a second opinion from MEXE, ARCHIE or CTAP.

1.3 Research domain

Extensive experimental and theoretical work has been carried out on arch bridges for about 300 years to date. Detailed literature reviews are presented in Chapter 2 of this thesis. The deficiencies in each current assessment method have manifested themselves so that further research is required to reveal the true potential of arch bridges.

This research concentrates mainly on both the theoretical and experimental studies of arch bridges. The following items were the objectives of this research:

i To review the current assessment methods and examine their deficiencies.

ii To develop a 2-D FE model which considers all modes of soil-structure interactions including stress distribution and backfill lateral resistance. A series of parametric studies is to be performed to examine the influence of the arch material properties and the load dispersal angle on the collapse load prediction.

iii To construct three nominally identical large scale arch bridges to examine the repeatability of such large scale tests. Both backfill and arch samples are to be tested for their properties and, if required, used as input variables in the subsequent collapse load predictions by various arch bridge assessment methods.

iv To integrate Monte Carlo simulation into two arch bridge assessment routines, the MEXE and mechanism methods, to perform risk analyses on arch bridges.

v To modify the mechanism method by including arch deflections and a deflection dependent backfill lateral pressure distribution model.

1.4 Outline of the thesis

This section outlines what is included in the thesis. A brief summary of each chapter is presented. A total of ten chapters with references and an Appendix are bound in this thesis.

Chapter 2 A Review Of Literature On Arch Bridges

Both theoretical and experimental work carried out before the 20th century is briefly reviewed. Following this, a more comprehensive review is given on more recent theoretical studies (the MEXE, mechanism, Castigliano's strain energy, and finite element assessments). Detailed critical appraisal of both full and large scale arch bridge tests is included.

Chapter 3 Two Dimensional Linear Elastic Analysis Of Stresses In Arch Bridges

A 2-D linear elastic finite element model has been developed, using LUSAS (1997), to investigate the way in which live load is distributed from the road surface to the arch extrados. A large scale semicircular arch is modelled in this Chapter. Comparisons are made with the load distributions predicted by Boussinesq's and the codified methods of dispersal, and the stresses recorded during the test.

Chapter 4 Non-Linear Two Dimensional Analysis Of Arch Bridges

A non-linear finite element model is used to analyse three full scale single span and one large scale multi-span arch bridges recently tested to collapse by other researchers. A parametric study has been performed by varying the arch material properties and load dispersal angle. The arch tensile strength has been identified to be the most influential arch material property in the collapse load prediction by this method. Collapse modes predicted by the finite element method on each arch bridge are presented which showed a close agreement with those observed in the tests.

Chapter 5 Material Testing

This chapter describes the experimental evaluation of the material properties for the arch and mortar which are used for constructing three nominally identical arch bridges. Compression tests have been carried out on bricks, mortar cubes, and masonry prisms. The elastic moduli for both the arch and mortar are evaluated using strain gauges. The brick-mortar bond strength is also investigated and results showed that the flexural tensile strength between the brick-mortar interface varied significantly.

Chapter 6 Repeatability Tests On Large Scale Arch Bridges

Three nominally identical arch bridges with span, rise, and ring thickness of 2000mm, 500mm, and 102.5mm respectively have been built and tested to collapse to examine the repeatability of large scale arch bridge tests. The collapse loads were 21kNm^{-1}, 16kNm^{-1}, and 25kNm^{-1} width perpendicular to the arch span. The main conclusion was, nominally identical arches do not always collapse at the same load. It was suspected that the variation of arch tensile strength was responsible for the discrepancy in the experimental collapse loads.

Chapter 7 Risk Analysis Using Monte Carlo Simulation

A Monte Carlo simulation has been incorporated into the MEXE and mechanism methods to perform risk analysis on arch bridges. Risk analyses have been carried out by these two arch bridge assessment methods on seven full scale bridges and one large scale model. All random variables were drawn using a random number generator on a computer. Each input parameter was assumed to be distributed in accordance with a Gaussian distribution with a set mean and standard deviation. The risk involved in each analysis was indicated by the extent to which the predicted results, the allowable axle

load or the collapse load, deviated from its mean. The probability of failure could also be evaluated if the actual arch collapse load was available.

Chapter 8 A Modified Mechanism Method Incorporating Arch Deflections

A modification has been made to the mechanism method by considering arch deflections and incorporating a deflection dependent backfill lateral pressure distribution model. Three full scale arch bridges are analysed by this modified mechanism method. Results revealed that arch deflections significantly affected the collapse load prediction by the mechanism method.

Chapter 9 Conclusions

A global summary of this research project is given. Following this, conclusions from each chapter are also presented to provide a succinct summary of the key findings arising from each strand of the project. In this way the individual threads represented by each chapter are woven into the rope represented by the whole thesis.

Chapter 10 Recommendations For Future Research

Future work is suggested so that some of the current research could be further developed. It is suggested that large scale repeatability arch bridge tests should be continued by building more nominally identical arches similar to those by the author. The two arch bridge risk assessment programs are ready to be used. However, to ensure a large number of users, these programs are to be further developed so that both the pre- and post-processing could be performed in a more user friendly way. Development of graphical input and output is recommended. More research is needed on the modified mechanism method before it could be used as a reliable arch bridge

assessment tool: the deflection at which the arch is on the verge of collapse is yet to be established.

The thesis is completed by the list of cited works and an Appendix containing the author's publications.

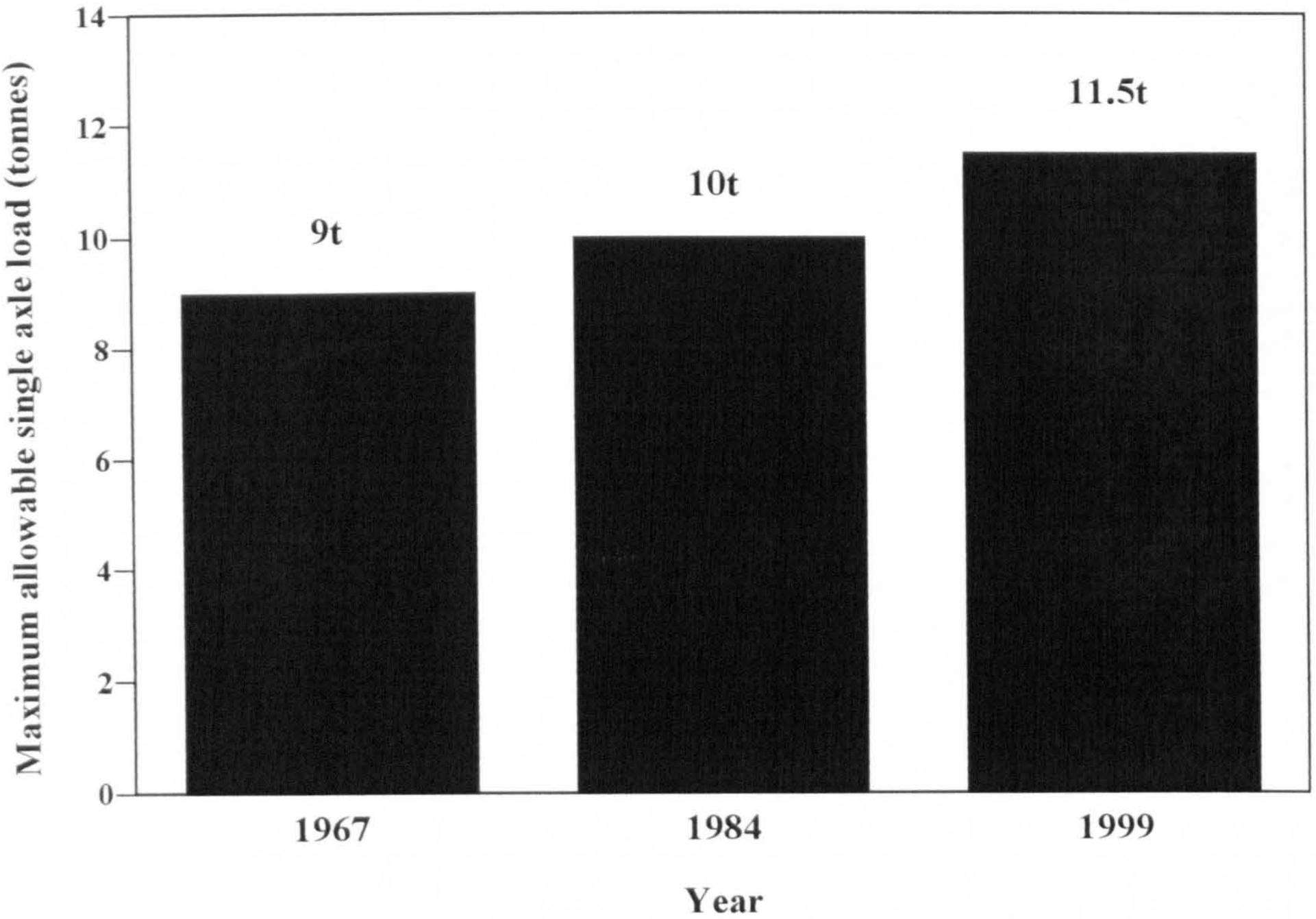

Figure 1.1 Increase in the maximum allowable single axle load

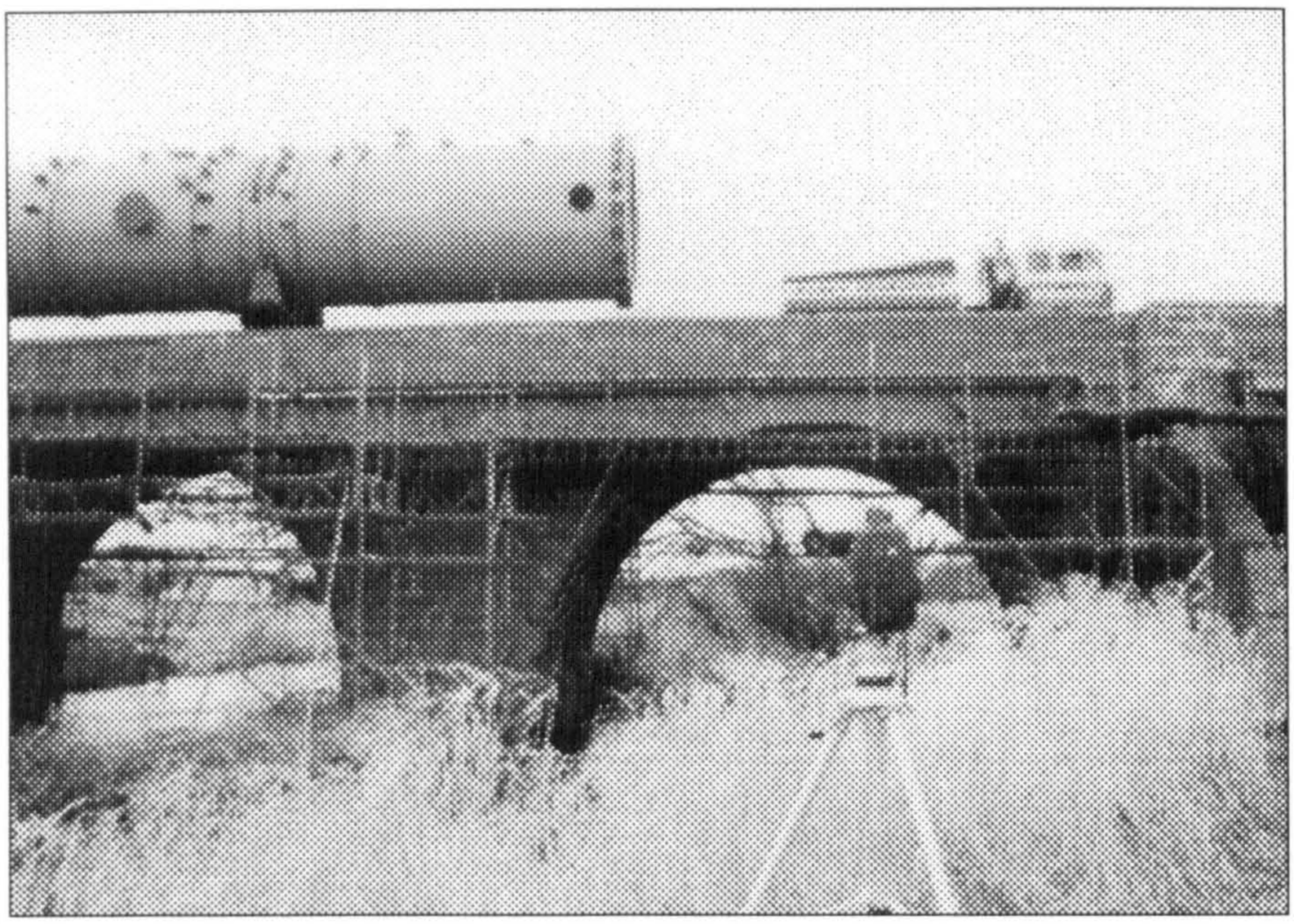

Figure 1.2 A 240t oil rig on Balmoor bridge, Inverugie in 1991

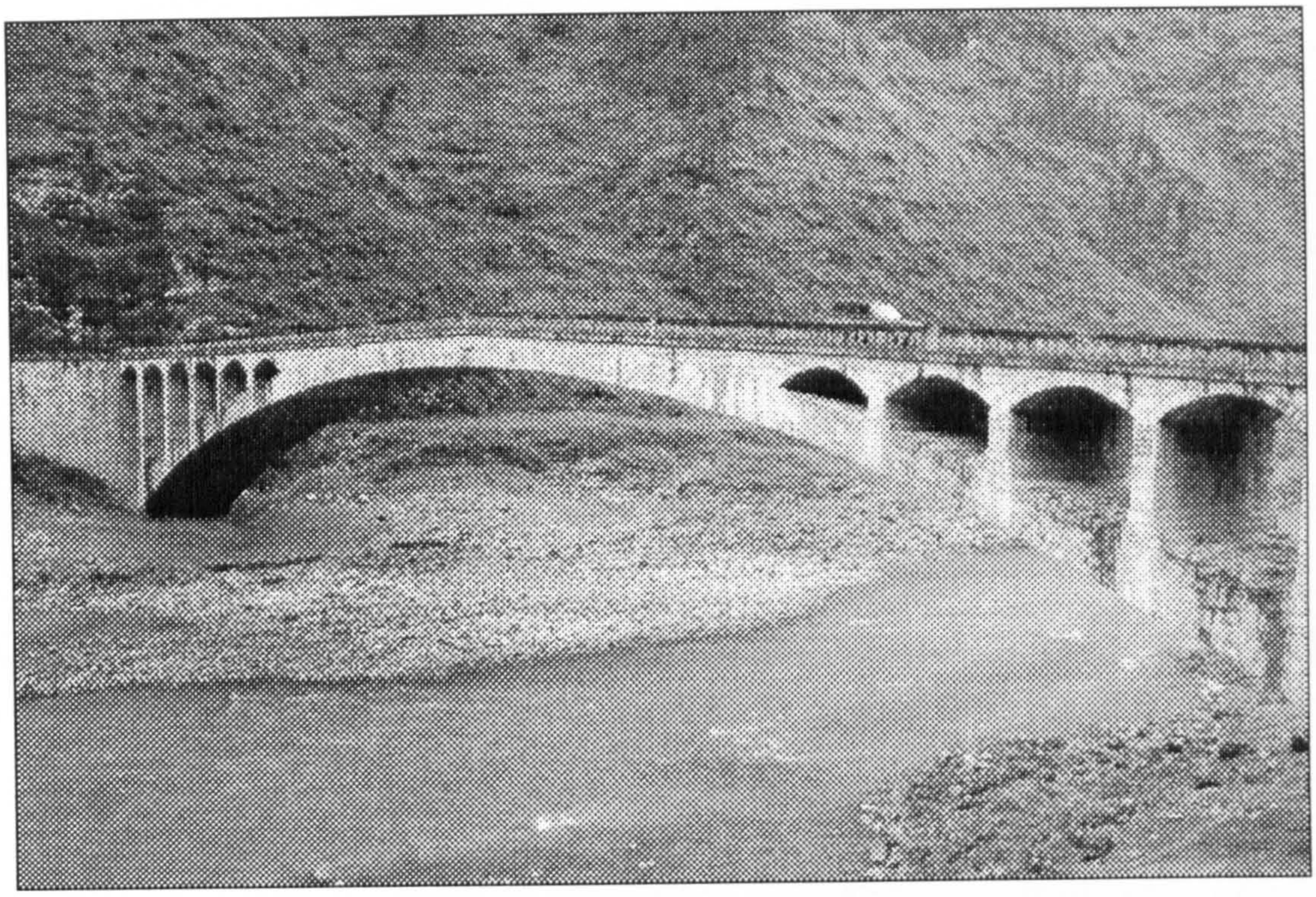

Figure 1.3 The world's longest masonry arch bridge, Jiuxigou bridge, China (After LU, 1992)

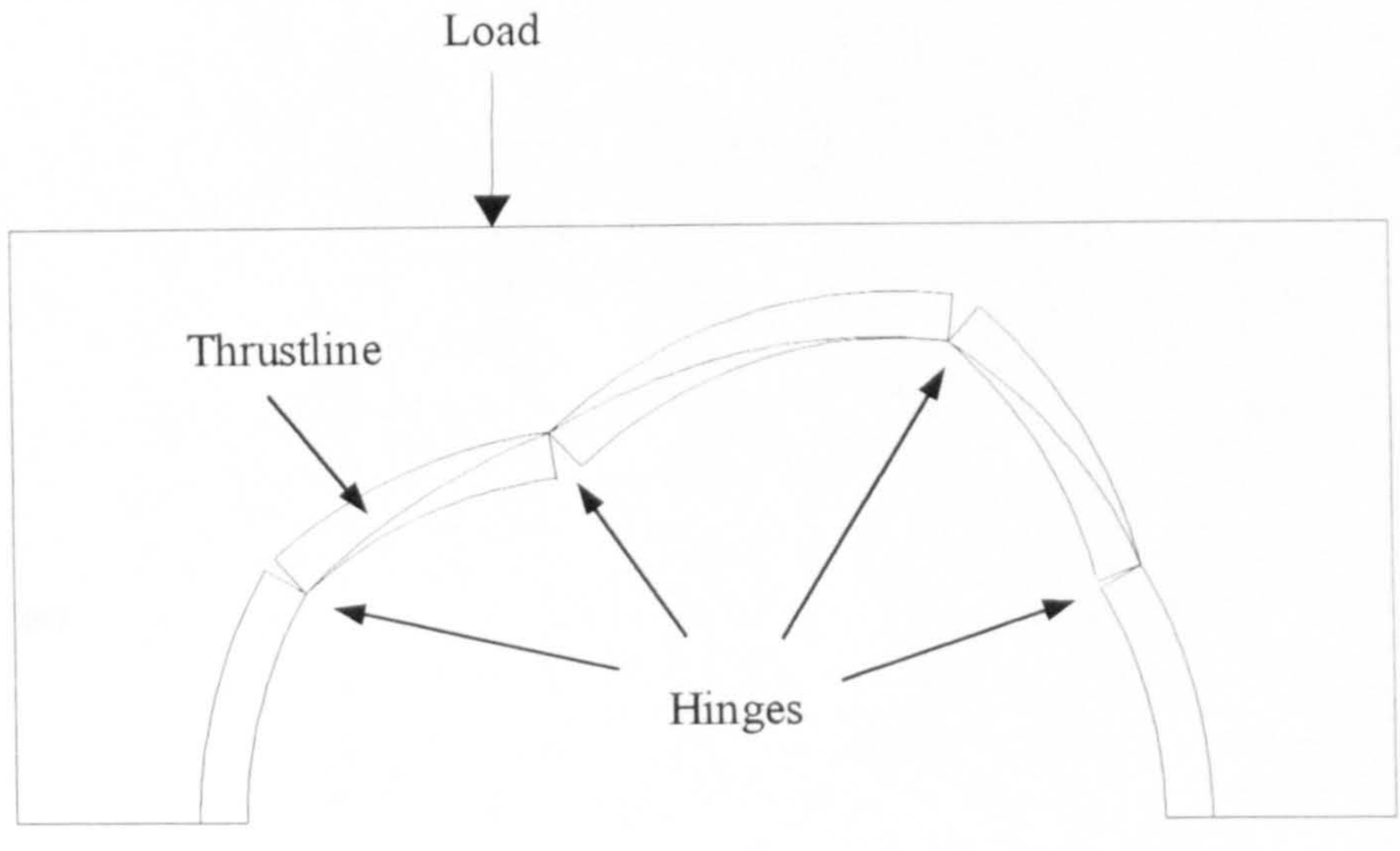

Figure 1.4a A typical four-hinged collapse mechanism

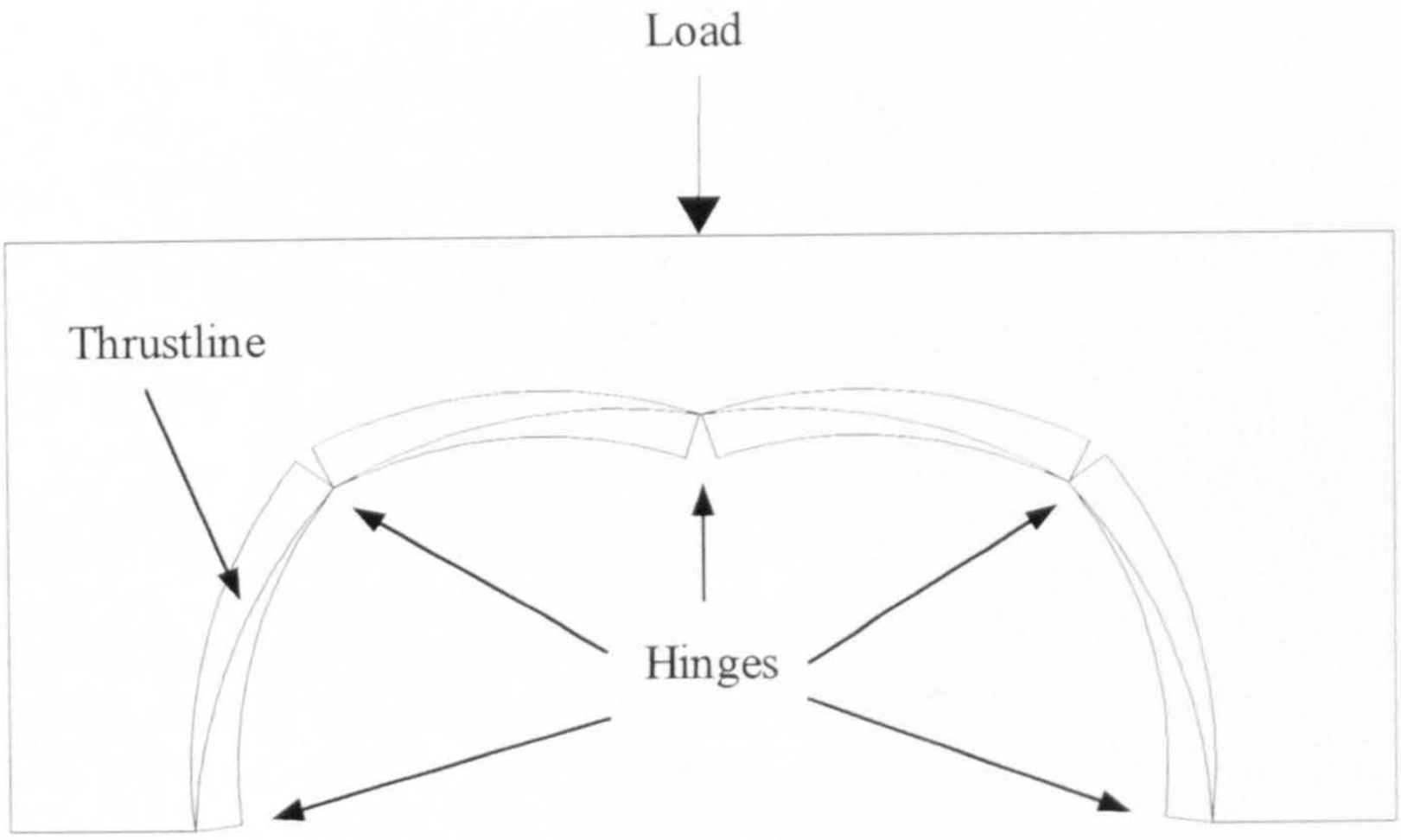

Figure 1.4b A typical five-hinged collapse mechanism

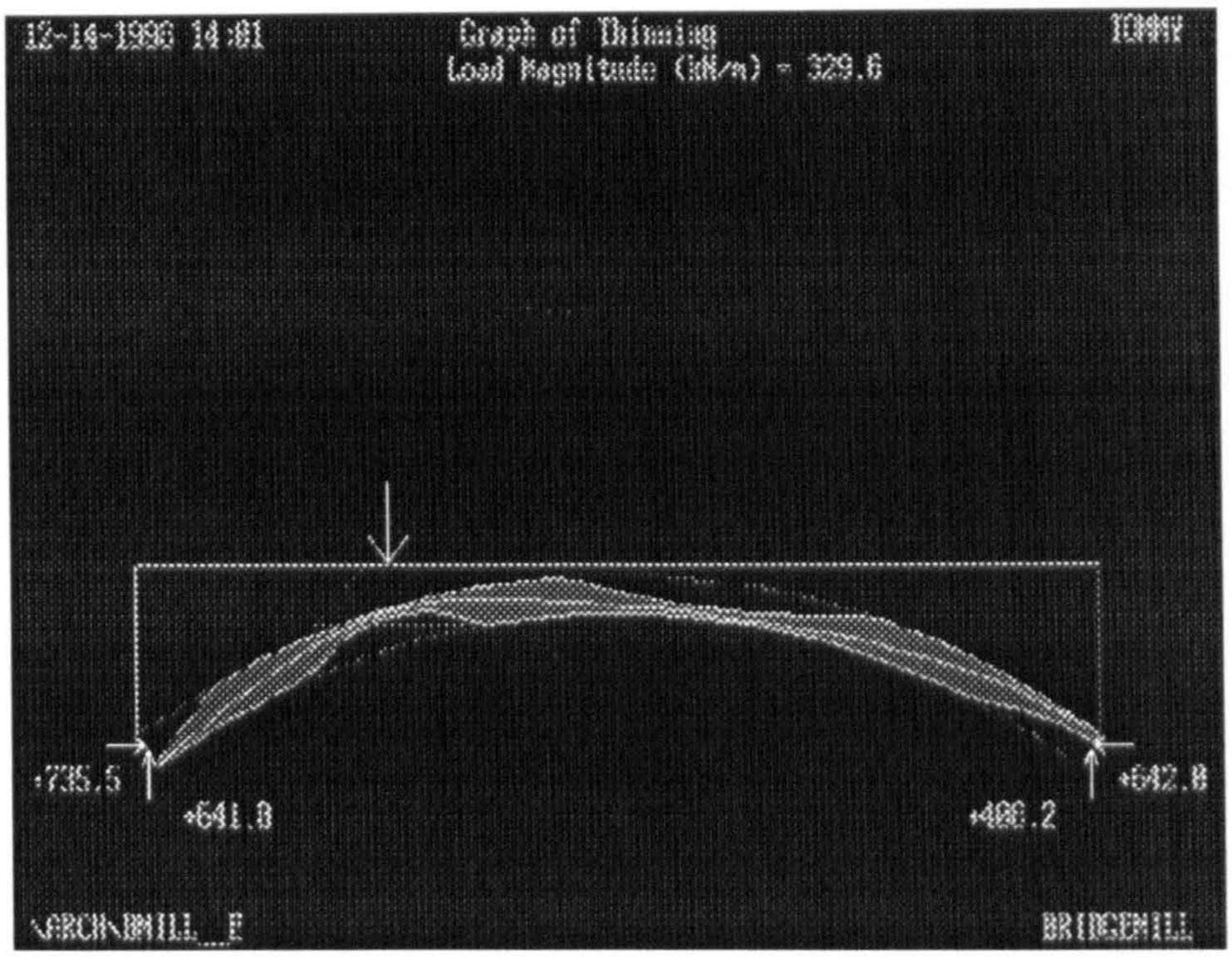

Figure 1.5 An illustration of the thinning of the arch in CTAP on Bridgemill bridge

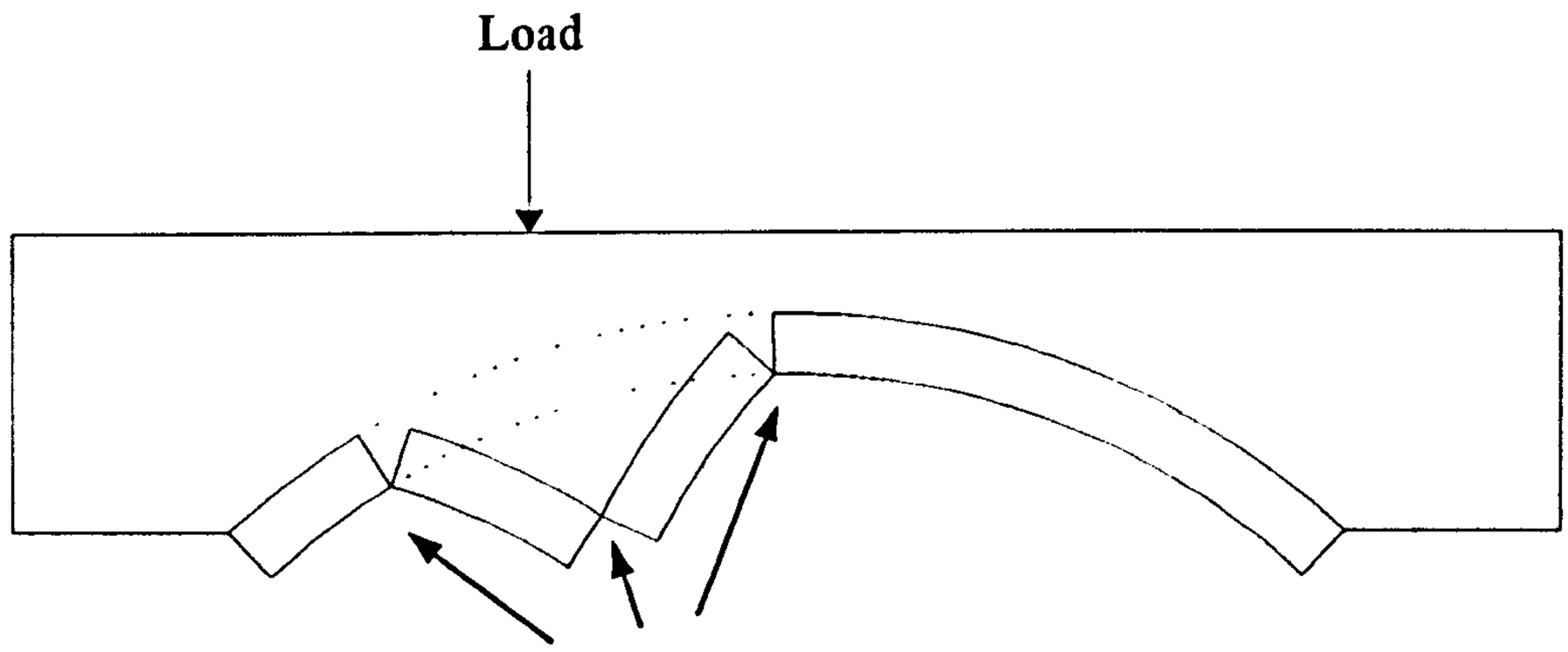

Figure 1.6 A typical snap through buckling failure of the arch

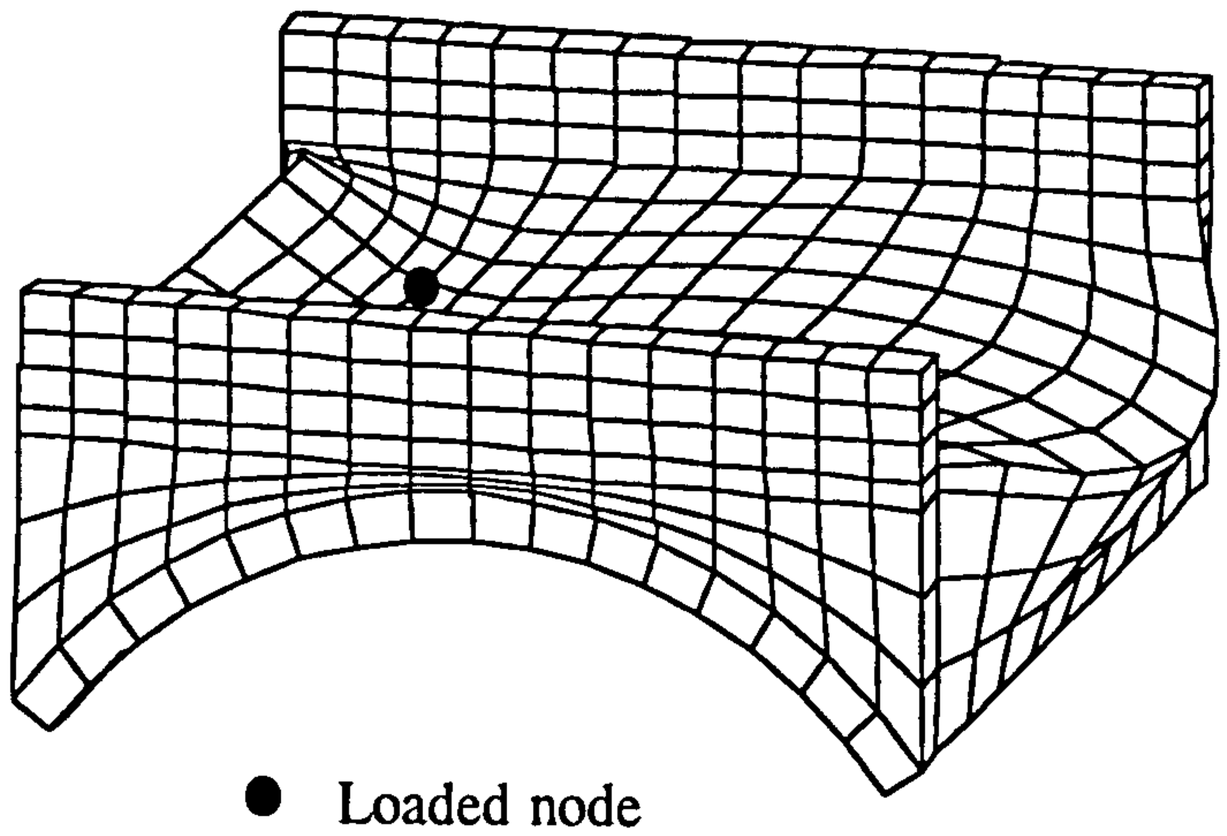

Figure 1.7 A typical 3-D finite element output (After BENSALEM *et al.*, 1998)

CHAPTER 2

A Review Of Literature On Arch Bridges

2.1 General history of ancient arch bridges

Masonry arches have been used for bridges and in buildings for several thousand years. Early builders relied on rules of thumb to design their arches. Surprisingly, some of these ancient arches still stand although scientific structural knowledge was not available at that time. This is because this form of structure is more honest to its material and function. It is also an unforgiving form because its profile must be accurate to be suitable for the imposed loads. Many older arches are preceded by unsuccessful attempts at crossings which collapsed because they were the wrong shape.

Arches have been a popular structural profile in China up to 5000 years ago. Even today, the Chinese still treat arches as the most desirable form of structure from aesthetical and engineering standpoints. The most precise masonry arch bridge still in use today is the Zhau Zhou Bridge (see Figure 2.1) in China with the span of 37.02 m built in the Sui Dynasty nearly 1400 years ago. This bridge has a span to rise ratio of 5.25 and 1.03m ring thickness. QIAN (1987) investigated this bridge using the mechanism method. He revealed that this ancient bridge was very similar to a modern bridge in its appearance and he proved by calculation that the design was in good accord with modern bridge building thinking. Qian's mechanism analysis showed that for an imposed line load of $80kNm^{-1}$ located at the ¼-span point, the bridge is safe with a geometrical factor of safety of 3.7.

The Romans were also great arch builders and many of these arches are still in use despite their age. The largest well preserved Roman arch is the Pont du Gard (see Figure 2.2) located in southern France which was built between 63 - 13 BC. Figure 2.3 shows another ancient arch bridge, the Ponte San Martino, located in Italy.

2.2 Theoretical work on arch bridges

Robert Hooke was the first to carry out scientific research on arches. His main finding was about the shape of an arch which could stand on its own. He published his finding in an anagram (HOOKE, 1675) which in English reads;

' As hangs the flexible line, so but inverted will stand the rigid arch '

About two decades later, GREGORY(1697) suggested the theoretical correct shape for an arch centreline where the arch took the form of Hooke's catenary. He concluded that an arch will stand only if a catenary can be wholly contained within the thickness of the arch ring. At about half a century later, both concepts by Hooke and Gregory were adopted by POLENI (1748) to investigate the safety of St. Peter's dome. COUPLET (1729) produced a 'Memoire' which demonstrated the idea of thrustline and the mechanism of failure of a voussoir arch.

The concepts of the thrustline and the mechanism have been developed even until today. In the past few decades, with the advent of modern computers, many arch bridge assessment programs, based on the concepts of thrustline and failure mechanism, have been developed and are still widely used for routine assessments.

2.2.1 Pippard *et al.*: Elastic theory for arch bridges

Pippard worked in conjunction with Baker, Chitty, Ashby and Tranter on arch bridge problems from 1936 to 1968 (PIPPARD *et al.*, 1936; 1938; 1941; 1948; 1951; 1952; 1968). He conducted a series of experiments on model arches and concluded that the voussoir arch behaved elastically within certain limiting loads. He also demonstrated that the collapse of arch bridges was due to formation of hinges as the result of cracking. He then derived several equations using strain energy methods to calculate collapse loads based on the assumption that the arch ring was made of a homogeneous linear elastic material. His first attempt ignored tensile stress in the arch ring by limiting the analysis to the middle third rule (see Figure 2.4). He then found that it was safe to reduce this limitation to the middle half rule, as illustrated in Figure 2.5, by allowing some tensile stress to develop in the arch ring.

From his analysis based on these two limiting rules, he derived an expression relating the span, rise, thickness and fill depth over the crown to vehicle type. This was a simple approach to assess arch bridges and was used during the wartime by untrained personnel who oversaw heavy vehicles and goods crossing previously unassessed arch bridges. The expression was then modified by the Military Engineering Experimental Establishment (MEXE) in the form of a nomograph (see Figure 2.6) and is currently recommended by the Department of Transport in its Departmental standard (BD21/97, 1997a). However, he didn't consider the effect of lateral resistance from the backfill surrounding the arch ring. This influence is particularly significant for steep haunched arches.

2.2.2 Heyman: The plastic method and mechanism approach

Heyman's work was mainly based on the concept of mechanism failure with the incorporation of plastic theorems. Over many years, he produced a large amount of publications on this subject (HEYMAN, 1966; 1969; 1972a & b; 1980; 1982; 1996).

He developed a simplified approach based on the plastic theorem for the collapse of an arch rib. A plastic moment was assumed to be reached when the thrustline at a section in the arch ring reached either the intrados or the extrados. A major problem of this method, as pointed out by SAWKO *et al.*, (1982), was that the plastic moment was derived based on a constant vertical thickness of arch. For an arch with a constant radial thickness, which is the most common type of arch, the vertical arch thickness varies along the arch ring. This is illustrated for a typical arch geometry in Figure 2.7.

Heyman also carried out work on the mechanism method related to the mechanism procedures of COUPLET(1729) and COULOMB(1773). Heyman made a strong statement about the stability of voussoir arches which reads;

' If a thrustline can be found, for the complete arch, which is in equilibrium with the external loading including self-weight, and which lies everywhere within the masonry of the arch ring, then the arch is safe '

The terminology of the plastic method was also used by Heyman to describe the mechanism method. In an attempt to simplify the mechanism method, Heyman ignored the live load distribution and the contribution of backfill lateral resistance. Moreover, the arch ring was divided equally along the horizontal span into four arch segments and a hinge was assumed to form at the end of each arch segment. By assuming further the arch and backfill unit weights were similar, he derived a 'quick assessment method' as shown in Eqn 2.1 and Figure 2.8.

$$F = \frac{(1+3\beta-\alpha)\left\{\alpha+\left(1-\frac{1}{4}k\right)\tau\right\}-(6+9\beta-5\alpha)\left\{(1-\alpha)-\left(1+\frac{1}{4}k\right)\tau\right\}}{(3-2\alpha)-(2+k)\tau}\times\left\{\frac{1}{6}\gamma LR\right\} \qquad 2.1$$

Where,

$$\alpha=\frac{H_q}{R} \qquad \beta=\frac{d+h}{R} \qquad \tau=\frac{d_q}{R} \qquad k=\frac{d_s}{d_q} \qquad 2.2$$

The method given by Eqns 2.1 and 2.2 is subsequently referred to as Heyman's plastic method in this thesis. Most recently, this method was adopted by PENG (1997a & b) in an optimisation design using genetic algorithms.

2.2.3 Sawko, Towler & Rouf: Finite element analysis

Sawko, Towler and Rouf based at the University of Liverpool were working on arch bridges using finite element analysis. Large scale model arches were built and tested to collapse to confirm the validity of their finite element programs. Relevant papers can be found (SAWKO *et al.*, 1982; 1985; TOWLER, 1981; 1985; ROUF, 1984). Curved beam elements were used for the arch ring with non-linear stress strain material properties. No backfill element was introduced in the FE analysis and the backfill surrounding the arch was treated as a series of vertical dead loads.

The large scale bridges built were all bare arches. However, equivalent weights were placed on the extrados of the arch ring to simulate the dead load of the backfill but giving no contribution to the lateral stiffness from the 'backfill'. These artificial arches are perfectly suitable to validate their FE model which does not consider the influence of lateral stresses from the backfill surrounding the arch ring.

In spite of the omission of lateral backfill forces, the program was used to predict collapse loads of arches tested to collapse by various workers. Good agreements in terms of the load *versus* deflection curve and collapse load were obtained. No further comment has to be made on the accuracy of this program as the omission of lateral soil forces does not actually model the real behaviour of arch bridges. The load *versus* deflection curve and the final collapse load can be 'adjusted' by varying the material properties of the arch.

2.2.4 Harvey & Smith: Mechanism method with program ARCHIE

Harvey and Smith analysed arch bridges using the mechanism method and developed a computer program ARCHIE (HARVEY *et al.*, 1987; 1988a & b; 1991a & b; SMITH *et al.*, 1990; 1991a & b). The thrustline for a given applied load acting on an arch is calculated. By specifying the compressive yield strength of the arch, the zone of thrust is obtained by dividing the thrust by the yield strength. Minimum arch thickness can then be defined based on this zone of thrust. The most important contribution of this program is the inclusion of soil-structure interaction effects. Load dispersal angle, passive pressure distribution, and the position of any backing can be defined in this program. The height of backing is simply a level at which the thrustline is allowed to leave the ring before reaching the springers. This program can also be used to analyse multi-span viaducts and arches. Figure 2.9 shows a typical output from program ARCHIE on Dundee large scale arch.

The ARCHIE program has been widely used for arch bridge assessments because of its ease of use. However, this mechanism based method can work only when all variable loads and reactions are proportional and their proportionality is known or determinate. A fixed soil pressure configuration has to be defined before the analysis is run. This means the load capacity obtained from this method is only pertinent to that pressure configuration which may or may not be the correct distribution at failure. It is therefore not appropriate for arch bridges where soil resistance is important. The ARCHIE program was used by the Department of Transport to analyse ten full scale bridges (BA16/97, 1997b). It was concluded that the program may produce arbitrary results due to the unrealistic soil model incorporated in this program.

A modified mechanism has been developed by the author by incorporating a deflection dependent backfill lateral pressure distribution model and arch deflections. Results are presented in Chapter 8 of this thesis which revealed that the mechanism prediction for the arch collapse load is highly influenced by arch deflections.

2.2.5 Davies: MARCH program with funicular polygon

DAVIES (1989a & b) developed a computer program known as MARCH based on the funicular polygon method. A mechanism program also developed based on Heyman's method with the addition of an iterative procedure to obtain a thrustline occupying the whole arch ring. Four different distribution patterns of lateral soil forces are incorporated in the program; it is up to the user to select one of them. Figure 2.10a shows an illustration of the notation for the lateral pressure distribution model used in program MARCH; its soil pressure distribution options are presented in Figure 2.10b. Load dispersal angles can also be defined in this program. As in the case of the mechanism method, a fixed backfill pressure configuration is to be defined in a speculative manner. Furthermore, this program is not suitable for solving steep haunched arches due to its inherent difficulty in allowing the thrustline to reach the springers without heading outwards into the backfill.

2.2.6 Crisfield: Mechanism and finite element analyses

Crisfield developed a mechanism (CRISFIELD *et al.*, 1987) and two finite element (CRISFIELD *et al.*, 1984; 1985a & b; 1988) programs while he was at the then Transport and Road Research Laboratory. His mechanism program incorporated yield blocks at the hinge locations and calculations were performed by virtual work equations rather than the more common static equilibrium equations. Lateral backfill forces were used in his mechanism program which could overestimate the ultimate collapse load by as much as 25% in some cases particularly for arches where the soil resistance is important (CRISFIELD, 1984).

The finite element idealisation involved a smeared continuum so that no direct allowance was made for the joints. The material property with a lower modulus should be assigned to arch ring to indirectly consider the joints. His two dimensional finite element program adopted isoparametric elements with conditions of plane stress

assumed for ring and plane strain assumed for backfill. The backfill was modelled with the aid of a Mohr-Coulomb (MOHR, 1871) yield criterion. Both material and geometrical non-linearities were considered. Numerical analyses were performed on some of the arches previously tested to collapse using his two finite element programs. From his analyses, he showed that the contribution of the backfill elements varied with arch span to rise ratio. For reasons unknown to the author Crisfield's work is little used today.

2.2.7 Hughes *et al.*: Castigliano's and mechanism methods

BRIDLE & HUGHES (1989 & 1990) developed a computer program known as CTAP based on Castigliano's strain energy analysis. The arch ring is treated as a linear elastic material fixed at both ends. A load is applied incrementally and stresses at every section are calculated. Areas subjected to tensile stress are discounted which reduces the effective depth of the ring at those sections. The same procedure is repeated until the thrustline is just contained within the reduced cross-sectional area. The load *versus* deflection curve is non-linear due to the elimination of tensile zones at every load increment. Soil-structure interaction is considered in this analysis by incorporating active and passive forces around the arch extrados.

A mechanism method was also used to analyse single and twin span arches (HUGHES, 1995a & b). A seven-pin mechanism analysis was applied to twin span masonry arches. A parametric study was carried out over a wide range of geometrical parameters for both single and twin span arches and empirical expressions were derived relating the arch geometry to its collapse load. An expression relating the collapse loads of a single and twin span arches was also derived. Predictions of the collapse loads on some of the recent full scale tests yielded a close agreement.

HUGHES & BLACKLER (1997a) reviewed some of the current assessment tools used in the UK namely the MEXE, pinned-elastic, mechanism and elastic cracking

methods. They expressed concerns over the modification factors used in the MEXE method as those factors are considered independently of each other. Furthermore, the basis of those modification factors is still unknown. For the pinned-elastic method, the arch tensile strength is a major concern as it could significantly influence the collapse load prediction. The 2-D non-linear finite element analysis performed by the author in Chapter 4 of this thesis reached a similar conclusion. The mechanism method is said to be too sensitive to the magnitude of backfill lateral forces. For the crack-elastic method, the soil and arch stiffness are difficult to determine. The method is also claimed to involve complex computation for efficient implementation of the technique.

A series of centrifuge model tests on small scale arch bridges was also conducted (HUGHES *et al.*, 1998). A large scale arch bridge of a span, ring thickness, and span to rise ratio of 3m, 0.215m, and 4 respectively was scaled at a ratio of 1/6 to the prototype arch. The model arch was placed into a centrifuge and rotated to give an acceleration of six times gravity. That produced a vertical self-weight stress that was equivalent to the full scale stress. Results revealed that the scaled model arches under increased gravity produced consistent results and replicated all the features of full scale behaviour. Of note are Hughes' observations about active pressures on the loaded area of the extrados. Most other methods ignore these and merely concentrate on the more obvious passive pressure mobilisation on the side of the arch remote from the load. The author hopes to show how the FE analysis incorporates realistic earth pressure distributions yet acknowledges that the modified mechanism method (see Chapter 8) needs further development in this respect.

2.2.8 Choo and Gong: The MAFEA suite

CHOO *et al.* (1990a, 1990b & 1991) and GONG (1992) worked in conjunction with British Rail Research at Nottingham University to develop a finite element program for arch bridge assessment. One, two and three dimensional finite element programs have been developed and are known as the MAFEA suite. The most notable change in the

program is the use of tapered beam elements (see Figure 2.11). The effective depth of a particular section is defined as the depth of the section after eliminating tensile and compressive yielded zones. Yielded compressive zones are assumed to be capable of transmitting compressive forces and continue their contribution to the overall stiffness.

Backfill elements with a Mohr-Coulomb failure criterion are used to account for the effects of soil-structure interaction. The applied load is distributed by Boussinesq's method with a fixed dispersal angle. A limitation is imposed such that no further distribution is possible on the arch extrados where the gradient of the arch is greater than the friction angle of the backfill. Slipping is assumed to occur beyond this point. Extensive numerical analyses were carried out on arch bridges which were tested to collapse and obtained good correlation with some of the experimental results. It is noticed that some of the results obtained from the 3-D analysis with spandrel walls were some 50% higher than the results from 1-D and 2-D analyses without the spandrel walls. It is a matter of common sense that the 3-D model with spandrel walls is the most realistic model. However, most of the excellent results were obtained from 1-D and 2-D models which in the case of 3-D model with spandrel walls should not be so accurate. The neglect of the arch tensile strength has also made the model unrealistic. What may account for these seemingly strange discrepancies between 1-, 2-, and 3-D FE data could be the fact that in an old arch the spandrels may have yielded laterally. They would then merely serve to retain the fill and not act as truly structured walls. This could paradoxically make a 2-D analysis more representative.

2.2.9 Melbourne *et al.*: Rigid-block analysis

Melbourne and Gilbert introduced a new technique known as the rigid-block method for analysing arch bridges (GILBERT *et al.*, 1994; 1998; MELBOURNE *et al.*, 1995a; 1997). This method has been computer coded and used to determine the collapse load of structures comprising a number of masonry blocks. The method uses the upper-bound theory of plasticity in conjunction with geometrical compatibility criteria to

obtain solutions to problems of single and multi-span arches. Specific parameters such as ring separation and attached or detached spandrel walls can be modelled using this method. The removal of the 'no-sliding' restriction increases the generality of the method, permitting adjacent blocks greater freedom of movement. However, there are limitations associated with the rigid-block method such as the assumption of normality at frictional interfaces and from the utilisation of small-deflection theory.

An analysis on open spandrel masonry arch bridges was also carried out by MELBOURNE & TAO (1995b). The findings showed that the proportions of the main span are critical to the overall stability of the bridge whilst the spandrel arches and piers are of secondary importance. Unlike the case of filled spandrel arches, once the horizontal restraint capacity of an open spandrel arch has been reached then no spare capacity is available, and brittle failure is possible.

2.2.10 Loo & Yang: Cracking and failure analysis

A 2-D finite element program was developed at Griffith University in Australia to analyse the behaviour of arch bridges (LOO *et al.*, 1991a & b; 1995). Smeared cracks were assumed to occur if the tensile stress exceeded the tensile strength in the arch elements. A simplified von Mises (MISES, 1913) criterion was used to define the yielding of the material under bi-axial stress states. Difficulties were encountered in convergence when a cracked element released its tension suddenly. This problem was minimised by introducing a parameter to control stress release.

Numerical analyses were carried out on five full-scale arch bridges and good agreement in terms of the ultimate loads was obtained. However, as for other finite element analyses, the results depend highly on input material properties. Loo found that only the arch tensile strength and strain softening parameter have a significant influence on arch collapse loads. The strain softening parameter governs the stress-strain behaviour of the material once its yield strength is reached (see Figure 6.28). The

arch elastic modulus and compressive strength were rather insensitive to the predicted ultimate loads. The recommended values for tensile strength and strain softening parameter were 1.6MPa and 12 (dimensionless) respectively for stone arch bridges; 0.3MPa and 4 respectively for brickwork arches.

2.2.11 Hogg: Scale effects and dimensional analysis

A dimensionless analysis was carried out to study the scale effects in masonry arch bridges (CHOO *et al.*, 1994). The results from scale model test (ROYLES *et al.*, 1991) were used to compare with prototype results. A 3-D FE method was also used to model the specific weight of the arch material which can not be modelled in small scale arches. The influence of the ratio of arch-fill was investigated and it was concluded that the predicted collapse load was directly proportional to the arch-backfill weight ratio.

However, the arch material properties can not be modelled accurately with small scale arches. The arch tensile strength which is the most influential material property was not considered in the 3-D FE analysis. The arch elastic modulus and the arch compressive strength are interchangeable in her model due to the similarity of dimension of unit of both material properties. It must be noted that the arch elastic modulus and the arch compressive strength have significantly different contributions to the collapse load and must not be ' interchangeable '.

2.2.12 Peng: Optimisation of Heyman's plastic method

An optimal design of arch bridges integrating genetic algorithms and Heyman's plastic method was developed (PENG *et al.*, 1997a; 1999). Three different optimisations were presented: 1) optimise the design with respect to minimising the ratio of the ¼-span ring thickness to the rise to the intrados at the crown, 2) optimise with respect to

minimising the arch cross-sectional area, and 3) optimise with respect to maximising the ultimate load.

This genetic algorithm based optimisation method has been widely used over the last thirty years until today and is accepted by many as an efficient optimisation tool. However, integrating genetic algorithms and Heyman's plastic method to obtain an optimal design is unreliable. Heyman's plastic method is a simplified mechanism method which ignores the live load distribution and no backfill lateral forces are considered. Furthermore, the arch ring was divided into only four segments and a hinge is assumed to form at the end of each arch segment. The unit weights of both the backfill and the arch are considered to be similar. Such a simplified method, albeit integrated with sophisticated genetic algorithms, is hardly believed to be able to reach a reliable optimal design. The author acknowledges that Peng's solution is optimal within the constraints of Heyman's method. It is the aforementioned constraints that the author queries.

2.3 Experimental research on arch bridges

Possibly, the earliest recorded test was carried out by GAUTIER (1717) in France. Half arches of nine wooden voussoirs were constructed between the ground and a vertical surface to determine horizontal thrust due to the self-weight. DANYZY (1778) constructed small plaster voussoirs and tested them to determine the manner in which those arches failed. His works were mainly concentrated on failure modes and minimum pier sizes for arch stability. LESAGE (1810) recorded the work done by Boistard in which he constructed 22 model arches and tested to find the abutment thrust exerted by the self-weight of the arch ring. BARLOW (1846) demonstrated different possible positions of the thrustline within the arch. Timber voussoirs were used and joints were made up of wooden strips which could be inserted and withdrawn between the voussoirs. By removing the three of the four strips at each joint in different configurations, different positions of thrustlines were demonstrated. A

detailed review of the experimental work done in the modern era is presented in the following sections.

2.3.1 Pippard *et al.*: Elastic voussoirs

Extensive experiments on model arches were carried out by PIPPARD *et al.* (1936, 1938, 1941 & 1951). The first test involved 23 steel voussoirs with span and rise of 3048mm and 762mm respectively giving a span to rise ratio of four. The ring thickness was 254mm and the width was 152mm. The dead load of the fill was represented by hanging equivalent weights at the centre of each voussoir. Series of tests were carried out on this model and results were then compared with those obtained from a similarly proportioned solid steel rib. He concluded that the voussoir arch behaved elastically within a limiting load and failed by 4-hinged mechanism. His second test was carried out using mass concrete voussoirs with similar geometries. Non-hydraulic lime mortar and rapid hardening Portland cement mortar were used as jointing material. The conclusions drawn from these tests were the arch behaved elastically until formation of the first hinge or crack and it failed in a similar manner by 4-hinged mechanism. Pippard noticed that after the first hinge occurred, there was a significant amount of reserve strength in the arch before collapse. Dynamic tests were also carried out but no significant decrease in strength was noted. From these tests, Pippard concluded that it was reasonable to analyse an arch as a linear elastic material and it was also safe to adopt a middle half rule rather than the more conventional middle third rule. It must be noted that Pippard did not consider the structural contribution of the backfill in these tests.

2.3.2 Davey: Twenty one full scale tests

DAVEY (1953) at the Building Research Station in Britain conducted a series of tests to destruction on 21 real arch bridges. He observed that the load required to cause

cracks was relatively low compared with the collapse load. This is consistent with the results of Pippard. The contribution of each element of the structure to its overall capacity was also investigated on three arch bridges. Davey found that the collapse load was two and a half times higher in the presence of fill than in its absence.

2.3.3 Chettoe & Henderson: Elastic tests

CHETTOE & HENDERSON (1957) carried out elastic tests on 13 real bridges in Britain. All bridges tested were in good condition. The maximum applied load was limited to 90 tonnes so as to prevent any significant damage to those bridges. The load *versus* deflection measurements obtained were elastic and agreed with the findings of Pippard's work. They concluded that the 45° load dispersal angle was appropriate for assessment purpose. However, FAIRFIELD (1994a) commented that such a conclusion was purely speculative because the dispersal angle was an unknown without any pressure measurements in the fill and extrados.

2.3.4 Sawko, Towler & Rouf: Validation of FE analyses

Sawko, Towler and Rouf, at Liverpool University, constructed large scale arches and tested them to collapse to check the validity of their finite element program (TOWLER, 1981; 1985; SAWKO *et al.*, 1982; ROUF, 1984). Two brick arches were constructed by Towler with span and rise of 4m and 1m respectively. The ring thickness was 0.215m for a 2-course ring and 0.335m for a 3-course ring. The width was 1.1m. Self-weight of fill was represented by equivalent weights located on steps cast on the extrados. In such a manner, the effect of lateral soil restraint was not taken into consideration. A line load was applied at about third span to the 3-course arch and at the crown to the 2-course arch. Rouf later constructed a similar 3-course arch and tested to collapse by applying a line load at the crown. Numerical analyses were carried out on these arches and good correlation was achieved. Rouf noticed that some shear

failure of the tangential mortar joints within the middle span of the arch occurred during the tests. It was concluded that a multi-ring arch has a lower collapse load than a similar single ring arch of identical geometry.

2.3.5 Harvey & Smith: Large semicircular arch test

A large scale semicircular arch bridge was constructed and tested to collapse (HARVEY *et al.*, 1989; SMITH *et al.*, 1989; 1991a). The span and ring thickness of the arch were 2m and 0.25m respectively. The width was 6m and consisted of 40 bricks. The depth of backfill over the crown including the surfacing was 0.2m. Two 100-tonne screw jacks were used to apply the imposed load. The imposed load was located onto a spreader beam to represent a line load covering the whole width of the arch. They noticed that the assumption of load dispersal angle of 45° was appropriate at low loads. However, this angle reduced significantly with a sudden cut off of pressure recorded at higher loads. They believed that, under low loads, the soil was undisturbed and the load was distributed downwards by dint of particles resting on top of other particles. With the larger load and displacement at the ultimate limit state, failure within the soil would have concentrated the load over a narrower width. The arch behaviour was analysed by ARCHIE and they concluded that refinements built into ARCHIE were correct and appropriate. These tests were amongst the first to focus on soil pressures and the array of instrumentation included to that end was impressive. From a soil mechanics viewpoint, earlier work by The University of Edinburgh and the then TRRL on Bridgemill and Bargower was limited by lack of budget for soil pressure measurement. This work represented a turning point which possibly inspired later researchers at Edinburgh University (PONNIAH *et al.*, 1989; MALLINSON, 1989; FAIRFIELD, 1994a; PRENTICE, 1996) to focus with greater clarity upon soil-structure interaction effects.

2.3.6 Hendry *et al.*: Full scale and model arch tests

Hendry, based at The University of Edinburgh tested two full scale arch bridges for the Transport and Road Research Laboratory: Bridgemill (HENDRY *et al.*, 1985) and Bargower (HENDRY *et al.*, 1986). The experimental collapse loads for Bridgemill and Bargower were 361kNm^{-1} and 645kNm^{-1} respectively. Experiments were also carried out on 24 model arch bridges with spans of 1.0, 2.08 and 2.48m (ROYLES *et al.*, 1991). The objective of these tests was to examine the general behaviour of these structures, which had span to rise ratios between 2.0 and 6.4 and to establish the effect of spandrel and wing walls on the arch capacity. It was found that the effect of the spandrel and wing walls depended on the span to rise ratio with maximum contribution on semicircular arches.

These bridge models were built based on those three actual bridges: Bridgemill, Bargower and Carron. The object of basing the models on actual bridges was to ensure that the geometrical proportions would be representative and to permit comparison of model and full scale results. The scale factor between model and prototype relating maximum loads was investigated using Heyman's approximate formula as given by Eqn 2.1. It was found that the full scale test results indicated fair agreement in terms of general behaviour and scaled maximum loads. However, it must be noted that the effect of lateral restraint from surrounding backfill was not taken into consideration. The validity of the scale factor was also limited by the fact that material properties of the structure can not be modelled or scaled.

2.3.7 Page: Full scale arch bridge tests

Page, based at the Department of Transport carried out a series of full scale tests as part of the national arch bridge research programme to re-examine the validity of the MEXE method for evaluating arch carrying capacity. Tests were mainly concerned with the load *versus* deflection relationships, collapse mechanisms and collapse loads.

A total of six arch bridge tests were supervised by Page; Preston on the Wealds Moor (PAGE, 1987), Prestwood, (PAGE, 1987), Torksey (PAGE, 1988), Shinafoot (PAGE, 1988), Strathmashie (PAGE, 1989) and Barlae (PAGE, 1989). All arch bridge tests undertaken by Page were tested to collapse using a line load located at quarter span with the exception of Preston on the Wealds Moor Bridge where the load was applied at the third span. These tests formed the basis for much of Das's work at the Highway Agency (DAS, 1990) where he compared the efficiency of the commonest arch assessment methods. The results from Das's comparisons are shown in Figures 2.12a to 2.12e inclusive. Page has since retired and the focus of arch research at TRL has shifted towards repair strategies; SUMON (1998), rather than assessment or design.

2.3.8 Melbourne: Tests on large scale arches

His experimental research interests on arch bridges are arch construction techniques (MELBOURNE, 1987; 1989c), large scale single span arch bridges (MELBOURNE *et al.*, 1988; 1989a; 1990a; 1994b; 1995d), large scale multi-span bridges (MELBOURNE *et al.*, 1992a & c; 1993; 1995a; 1997), effect of defects on arch bridges (MELBOURNE *et al.*, 1990b; 1992b), multi-ring arch bridges (MELBOURNE *et al.*, 1989b; 1992d; 1995e) and skewed arch bridges (MELBOURNE *et al.*, 1994a; 1995c). Most notable were the three large scale multi-span arch bridges each consisting of three spans of 3m. Parameters investigated in these tests were load positions, contribution from spandrel walls, soil pressures and collapse mechanism. It was found that one or more of the spans adjacent to the loaded span were involved in the failure mechanism. Melbourne's former Ph.D. researcher Gilbert has since moved to Sheffield where his research has broadened into the area of impact loads caused by vehicles on parapet walls; GILBERT *et al.* (1995).

2.3.9 Fairfield: Soil-structure interaction in arch bridges

Fairfield has conducted extensive experimental tests examining soil-structure interaction effects in arch bridges. Tests mainly concentrated on the effect of load distribution, lateral soil pressure and zones of fill displacement. Three small scale models were constructed from timber voussoirs, each spanning 700mm with span to rise ratios of 2, 4 and 10. A total number of 220 results from parametric tests were generated by varying backfill depths, load positions and backfill bulk unit weights (FAIRFIELD *et al.*, 1994b). Hughes submitted a detailed discussion of this work; HUGHES (1997b) where he had used program CTAP to assess the small scale timber arches. In nearly every aspect, except for the formation of a fifth crown hinge in centrally loaded cases, CTAP modelled even these dry jointed timber and sand models extremely well. Smith during a private discussion with Fairfield made numerous suggestions to improve the models and these led to the development of most of his own small scale models at Dundee University and also the multi-span version used by PRENTICE (1996) and ROBINSON *et al.* (1997a).

A large scale semicircular arch bridge was also constructed with span and ring thickness of 2m and 102.5mm respectively. Pressure measurements were undertaken during the test. From the results of large and small scale model tests, the contributions of soil-structure interaction in arch bridges were clearly demonstrated. Primary modes of interaction were the load dispersal and mobilisation of lateral pressures. Fairfield also showed that the addition of backfill depth over the crown of an arch bridge could be implemented to increase the load carrying capacity economically. Other relevant works are well documented elsewhere (FAIRFIELD *et al.*, 1992a - c; 1993a - d; 1994a; 1994b; 1996).

Fairfield also worked in conjunction with the Transport Research Laboratory to install and monitor pressure measurement devices in a newly constructed bridge at Kimbolton Butts, Cambridgeshire (FAIRFIELD, 1993b; 1994a; PONNIAH *et al.*, 1997). A series of elastic tests was carried out and pressure changes were recorded. Fairfield noticed

that the peak influence value was some 16% lower than the BD21/97's peak allowable influence value and the loaded influence zone was considerably larger than that allowed by BD21/97. Passive pressure mobilisation was observed at about 18% of the classical Rankine value. Monitoring, especially of the temperature effects at Kimbolton Butts continues under the care of ROBINSON *et al.* (1997b & 1998).

2.3.10 Sibbald *et al.*: Non-destructive tests

Sibbald, Fairfield and Bensalem based at Napier University, analysed the dynamic response of arch bridges using non-destructive testing (BENSALEM *et al.*, 1997a). A large scale semicircular arch ring was constructed and tested in the laboratory. Experimental results were compared with dynamic finite element analyses and close agreements were achieved both in time and frequency domains. A void defect was introduced in the backfill over the crown and was detected in the change in behaviour of the frequency response function. A 3-D finite element model was also generated to study the effect of material stiffness on the dynamic characteristics of arch bridges (BENSALEM *et al.*, 1997b). The results indicated that the introduction of the backfill increased the damping ratios and decreased the resonant frequencies. The work also forms part of the ongoing monitoring of Kimbolton Butts bridge; ALI-AHMED (1999).

2.3.11 Peng *et al.*: Tests on flat arch bridges

Peng, based at Napier University, constructed three flat arch bridges and tested them to collapse in the laboratory (PENG *et al.*, 1997a & b). The span, width and ring thickness of each arch bridge were 2.0m, 1.0m and 102.5mm respectively. The first bridge was constructed with attached spandrel and wing walls. The second test involved only an arch ring. The third bridge was built with non-structural spandrel walls so that the wall only served to retain the backfill above the arch ring. The backfill

depth over the crown for the first and third bridges was 230mm. All arches were loaded to collapse using a line load located at quarter span. The collapse loads for the first, second and third bridge were 37kNm^{-1}, 14kNm^{-1} and 45.5kNm^{-1} respectively. The results of the first and third tests seem to be contrary to engineering principles and common sense. The arch bridge with attached spandrel walls should have failed at a higher collapse load compared with the one without attached spandrel walls. This discrepancy has, in part, led the author to research risk analysis (Chapter 7) procedures as applied to arch bridge collapse load assessment.

2.4 Concluding remarks

Both theoretical and experimental works are still being carried out on arch bridges although this type of structure has been studied for more than 300 years. Many classical theories on arch bridges are still in use today such as the theory of thrustline and mechanism of collapse. Classical structural theory such as Castigliano's method is also used to analyse arch bridges. This doesn't mean that the current analytical methods are merely imitations of the old. Many classical theories have been refined or improved due to advances in scientific structural knowledge. The advent of high-speed electronic digital computers has given tremendous impetus to all numerical analyses. Many classical analyses on arch bridges have been computer coded thus enabling such complex structures to be analysed more easily, more rapidly and more accurate.

Experimental works form a major part in arch bridge research. It may be because the complexity of arch behaviour such as the influence of soil-structure interaction can not be explained or quantified theoretically and realistically. It is believed that proper understanding of soil-structure interaction is vital in order to solve the mystery of arch bridges.

It is quite unfortunate that most of the full scale arch bridge tests carried out by Davey and Page did not consider soil pressure measurements. Full scale tests provide valuable

information if properly monitored. The chance to have full scale tests these days is slender due to financial and environmental reasons as well as the lack of availability of abandoned arch bridges.

Most of the currently available arch bridge assessment methods are idealised representations of reality. Many unrealistic or subjective assumptions have to be made in order to make the analysis more easy or indeed even possible. In the mechanism and Castigliano's strain energy methods, assumptions such as the load dispersal angle and the mobilisation of backfill lateral resistance are always made in a speculative manner. This is because their magnitudes have yet to be discovered for the complex arch-soil system. Most of the FE codes, written specifically for the analysis of arch bridges, are sensitive to variations of arch material properties.

Although arch bridges have been subjected to scientific research for 300 hundred years, the scope for further research is wide. This study involves a wide spectrum of research on arch bridges: finite element analyses, repeatability analysis of large scale arch bridge tests, Monte Carlo risk analyses, and a new modification to the mechanism method.

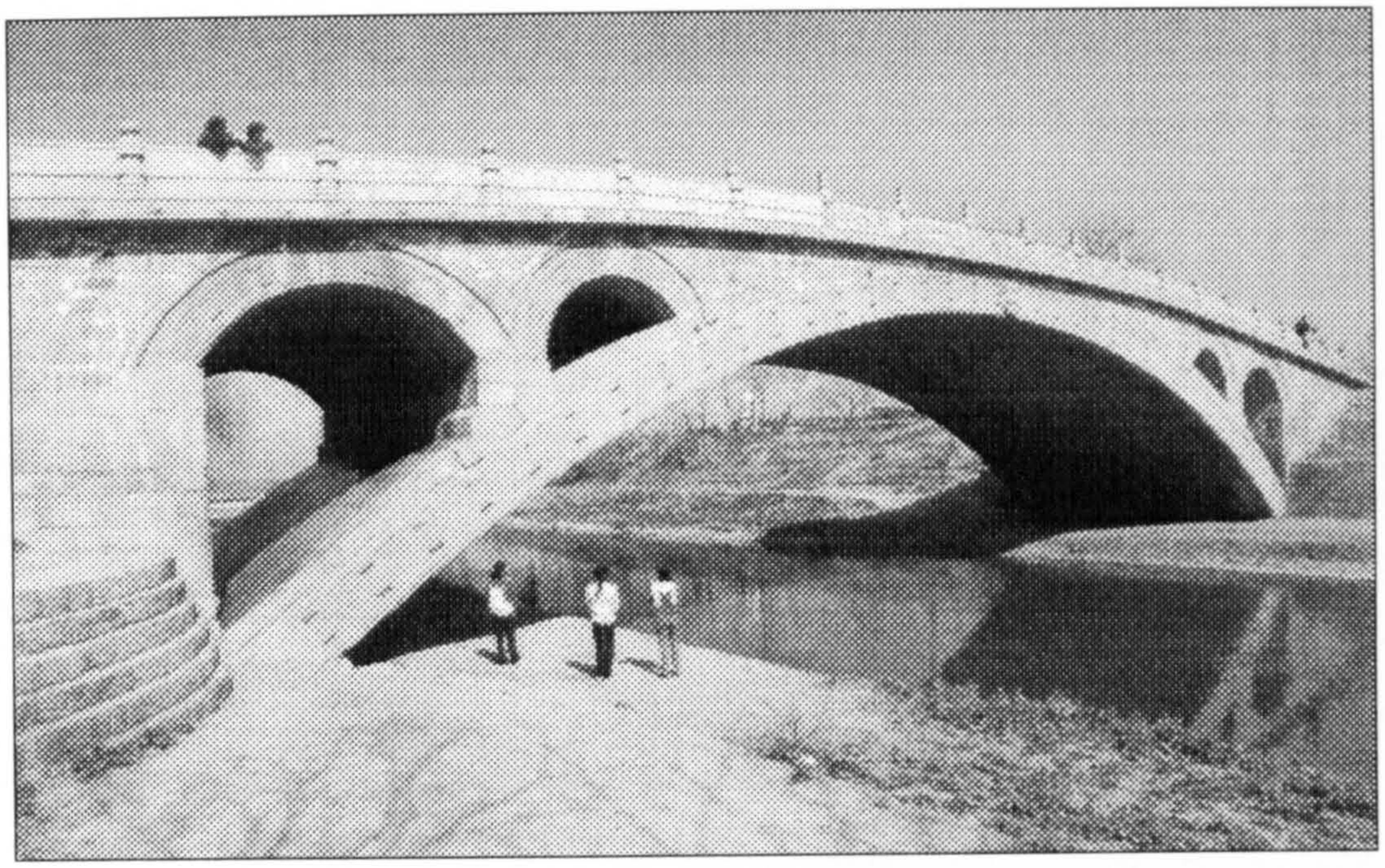

Figure 2.1　Zhau Zhou bridge in China: 1400 years old (After LU, 1992)

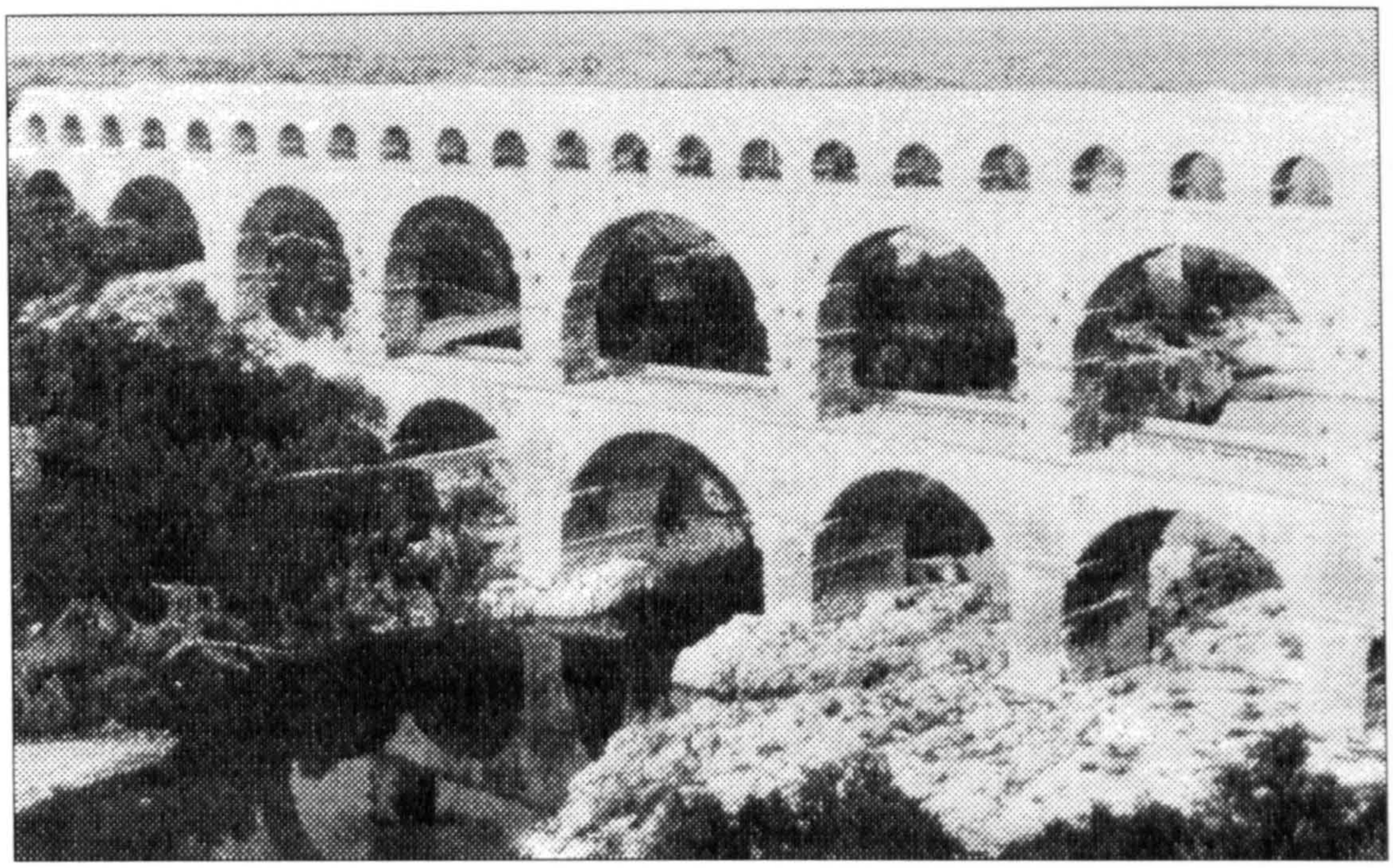

Figure 2.2　Pont du Gard in France: 2000 years old (After HOPKINS, 1970)

Figure 2.3 Ponte San Martino in Italy: 2000 years old (After HOPKINS, 1970)

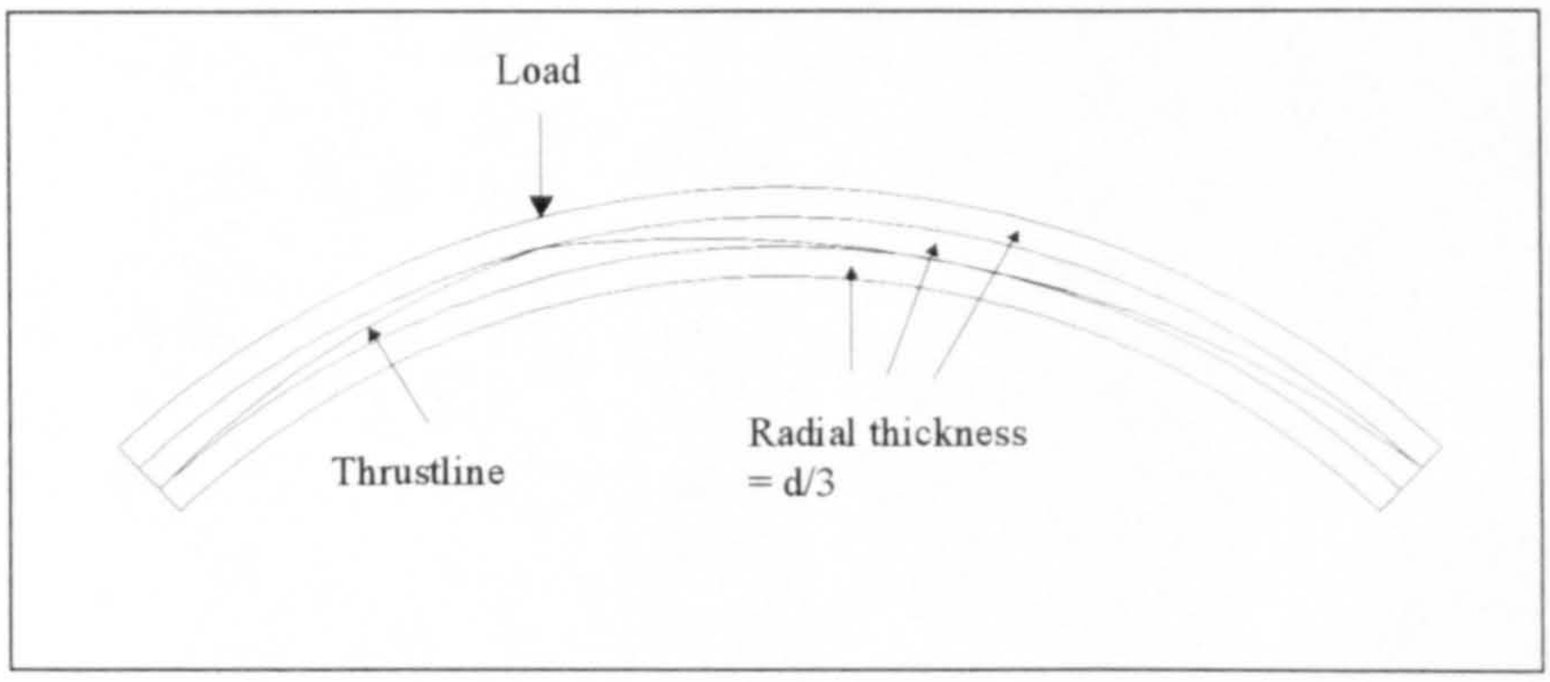

Figure 2.4 An illustration of the middle third rule

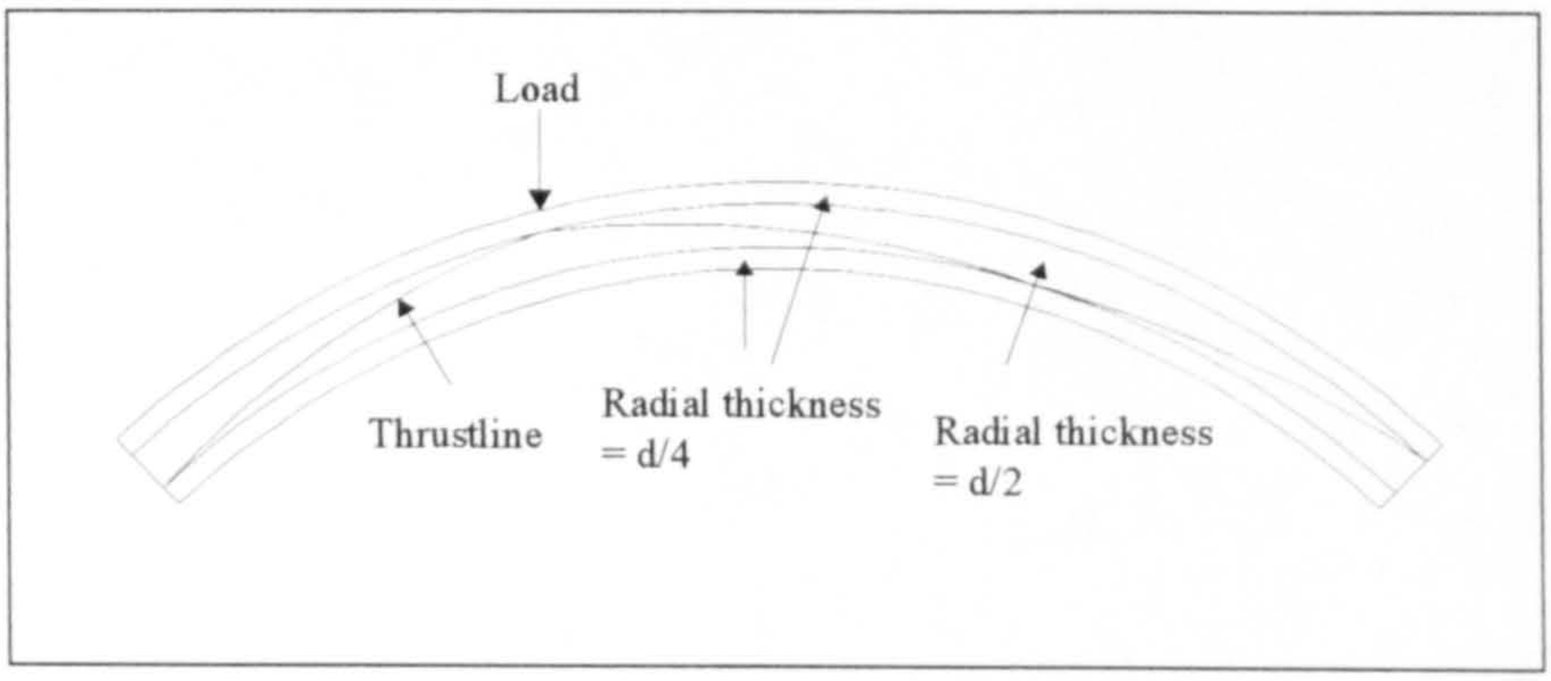

Figure 2.5 An illustration of the middle half rule

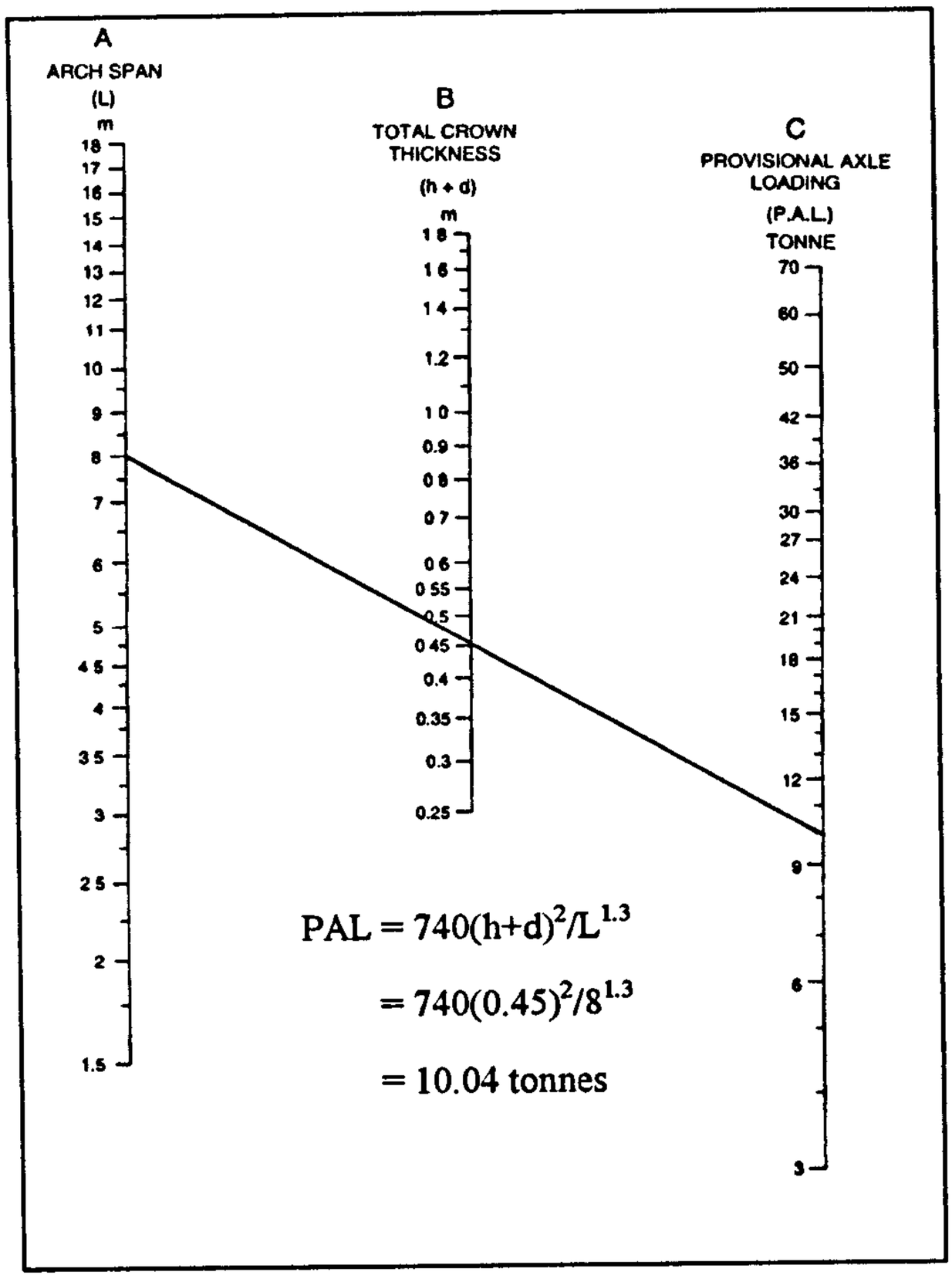

$$PAL = 740(h+d)^2/L^{1.3}$$

$$= 740(0.45)^2/8^{1.3}$$

$$= 10.04 \text{ tonnes}$$

Figure 2.6 The MEXE nomograph (BA16/97, 1997b)

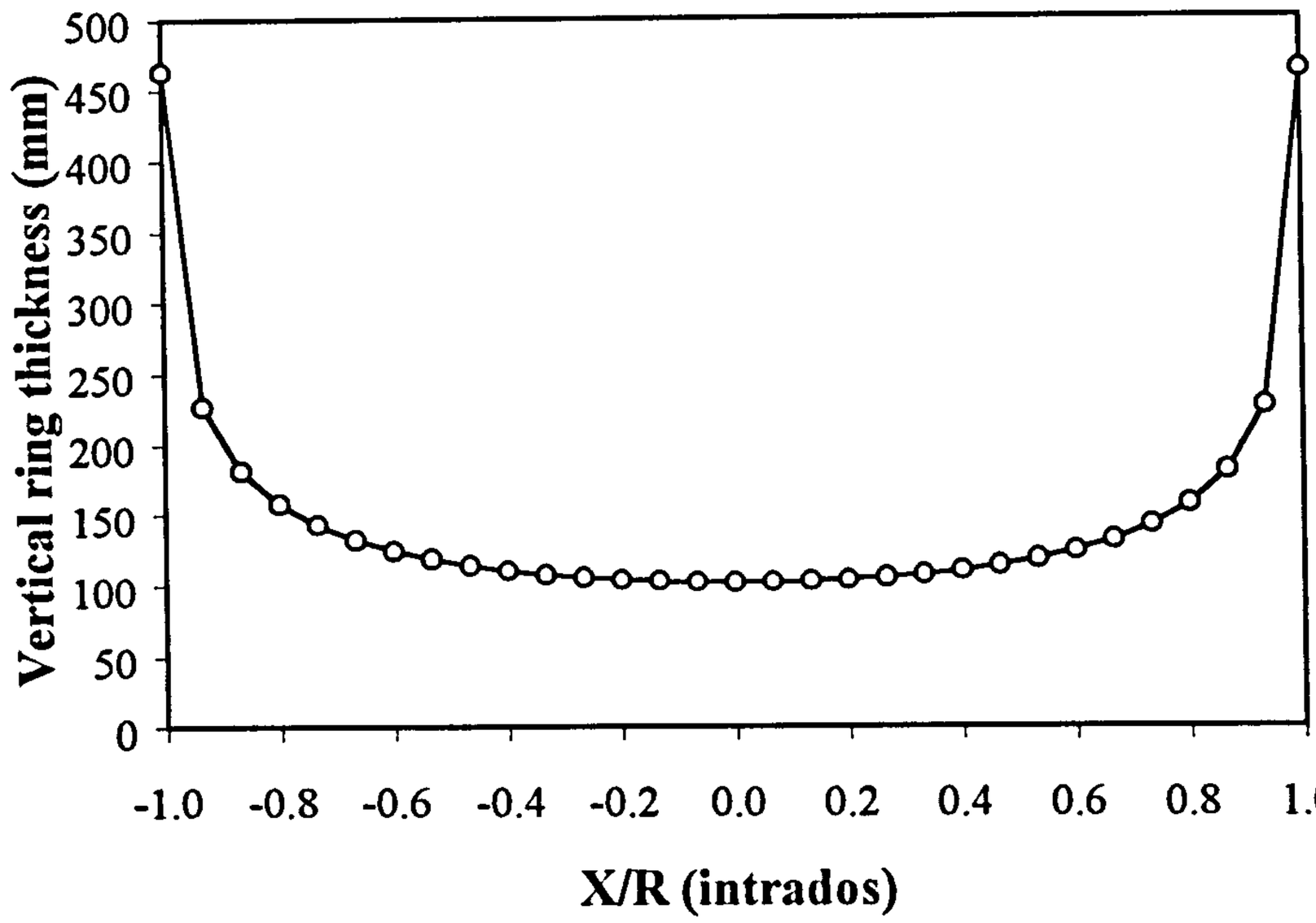

Figure 2.7 The variation of arch vertical thickness

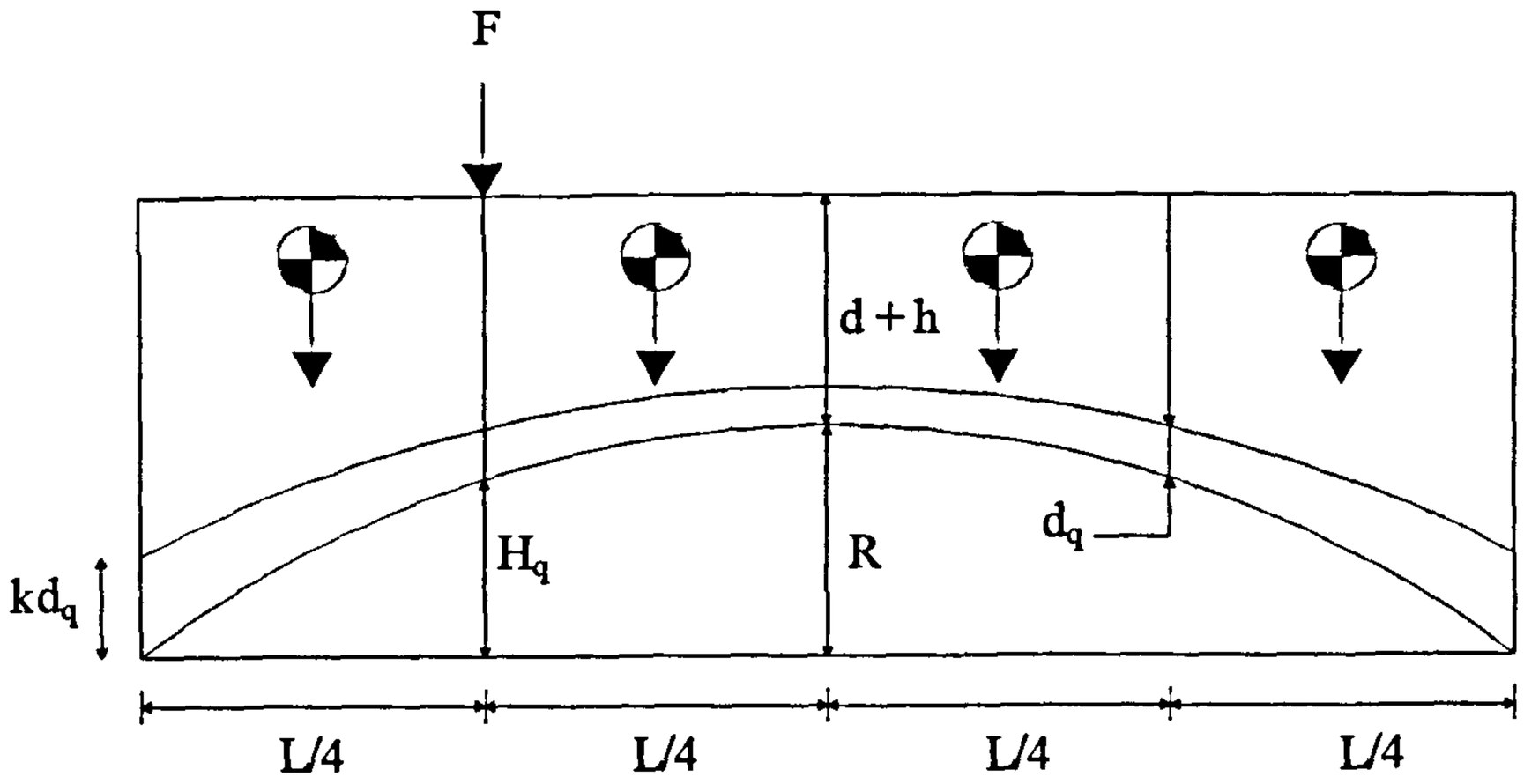

Figure 2.8 Assumed behaviour for Heyman's plastic method

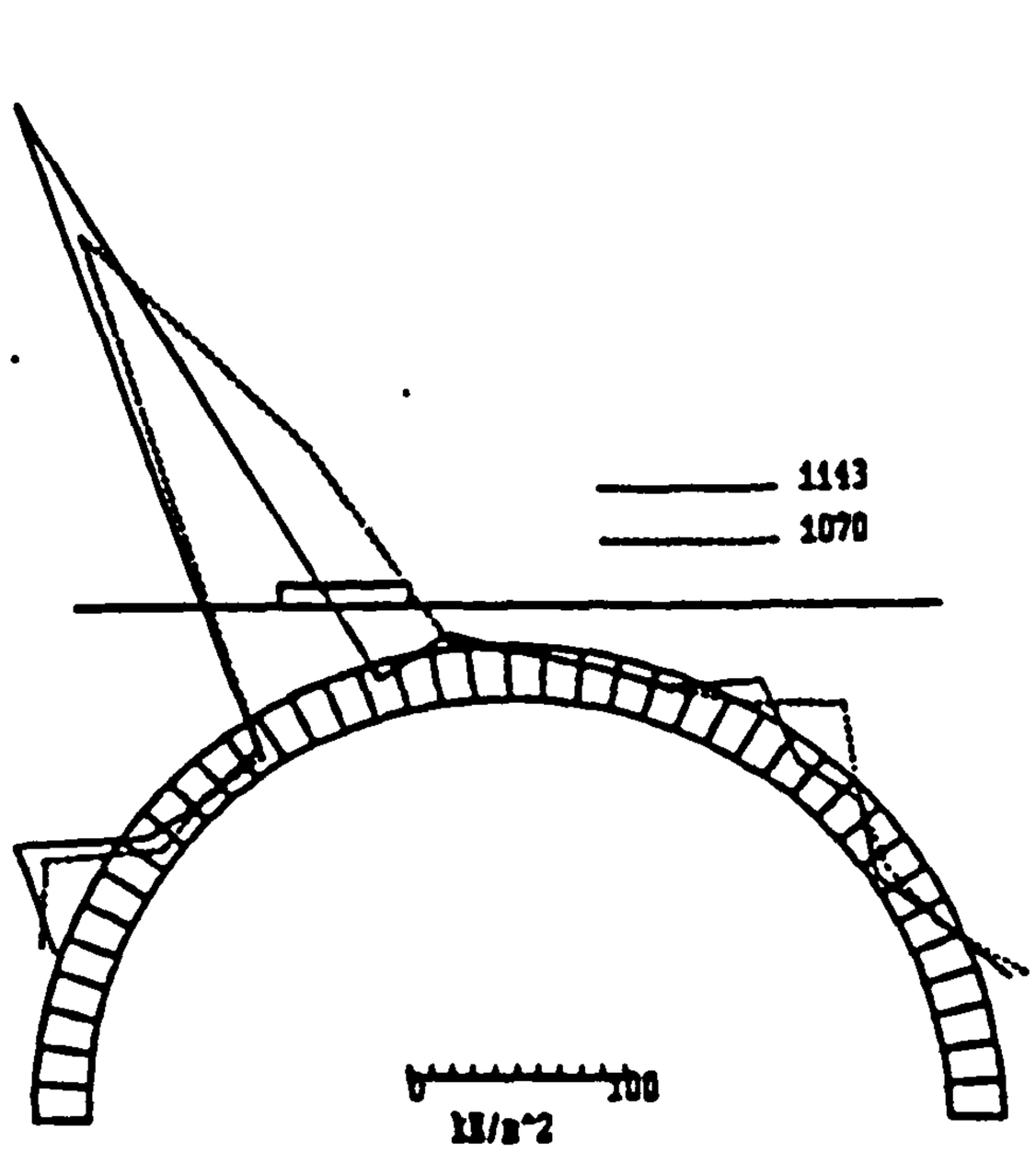

Figure 2.9 A typical output from program ARCHIE (SMITH, 1991a)

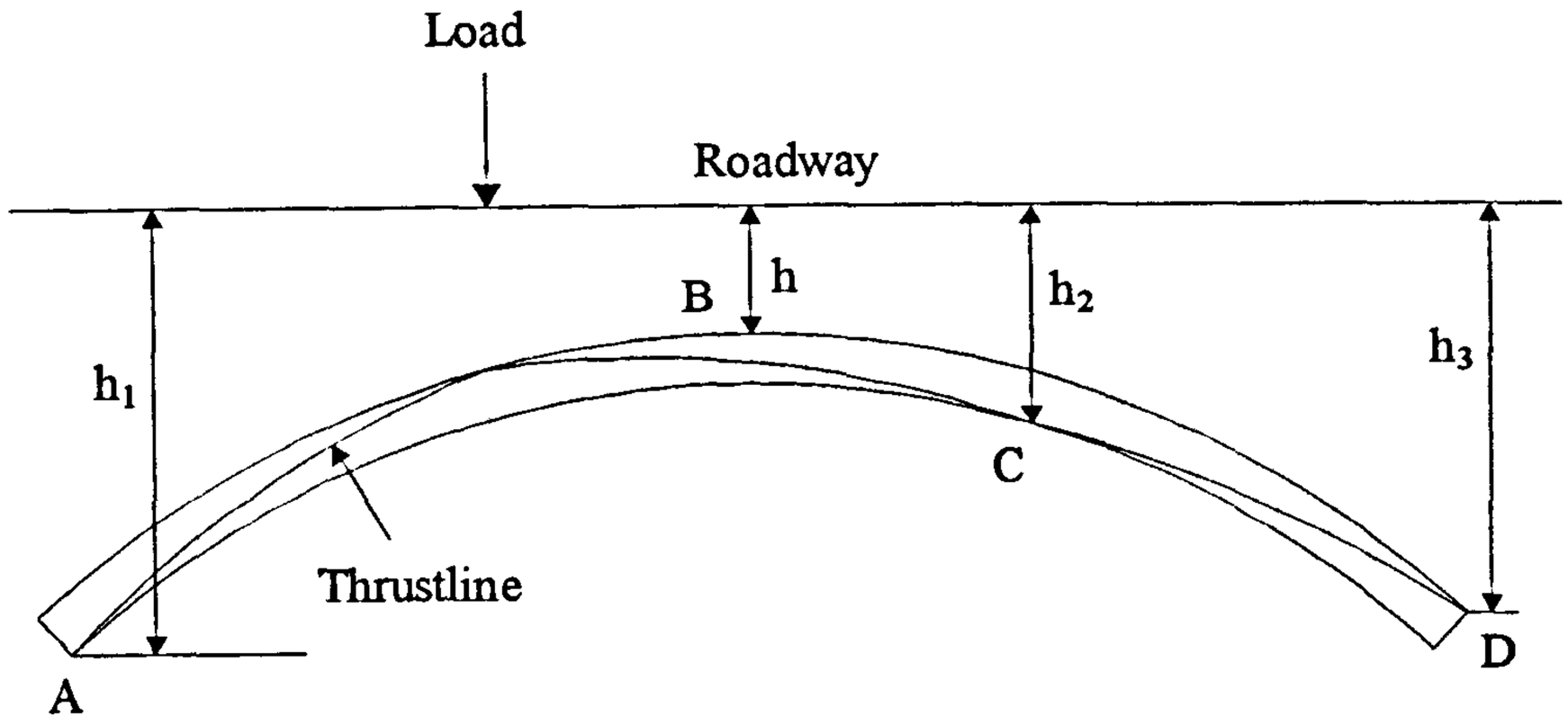

Figure 2.10a Illustration of the notation for the lateral pressure distribution model used in program MARCH

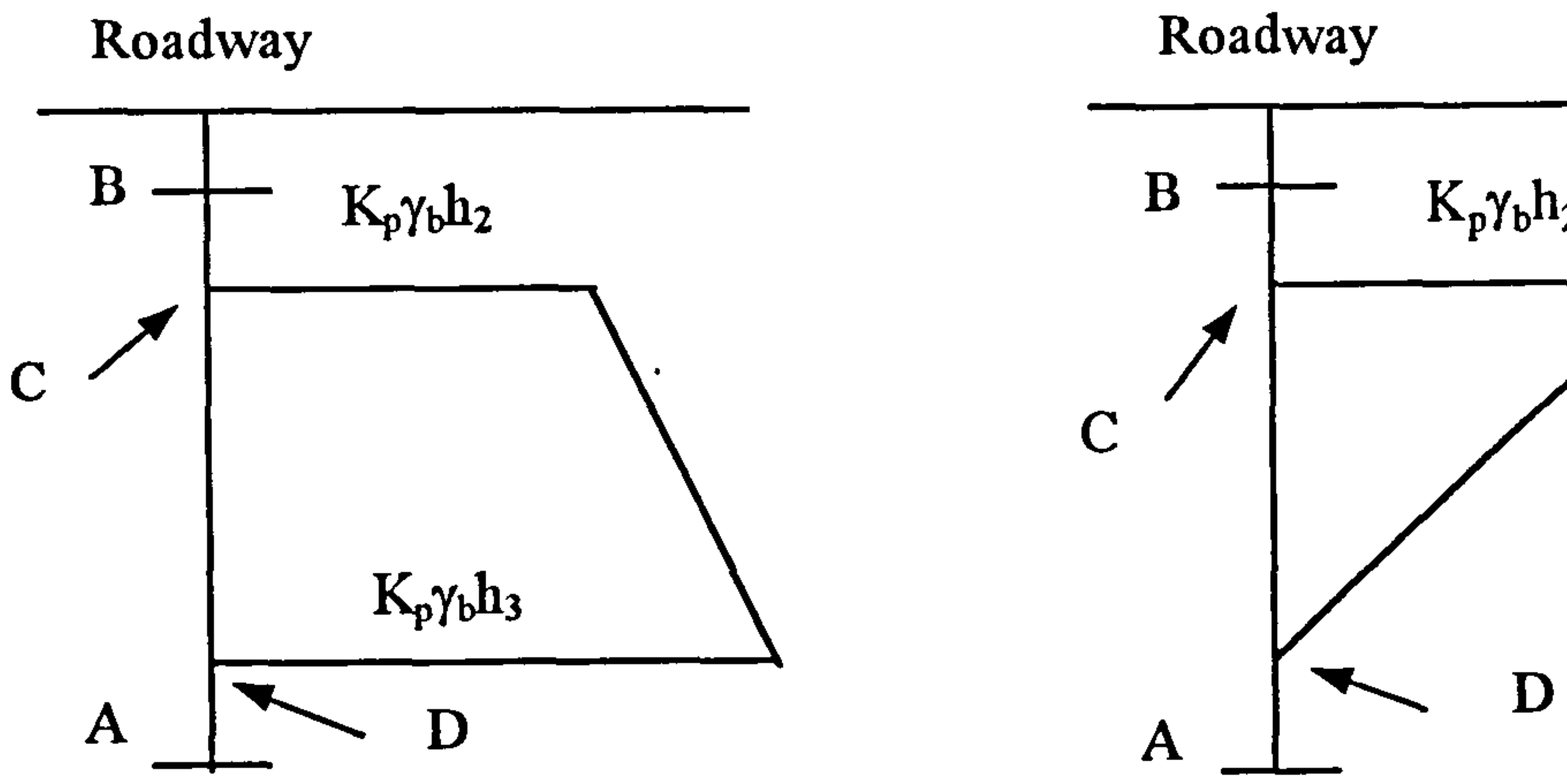

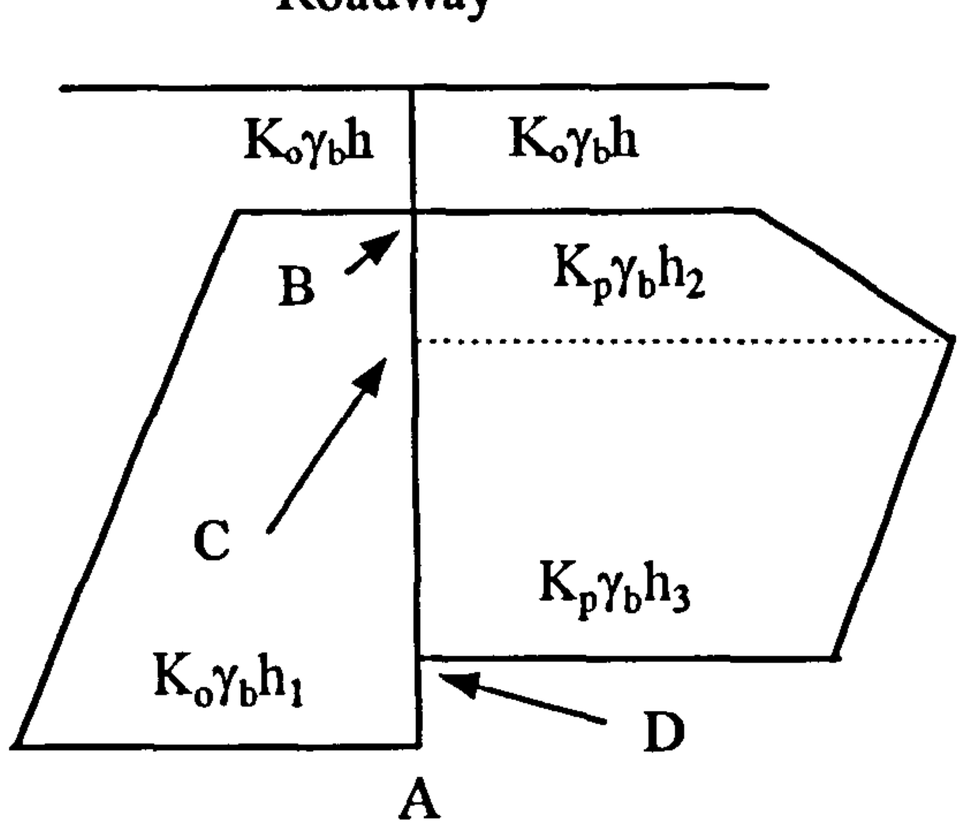

Figure 2.10b Soil pressure distribution options in program MARCH

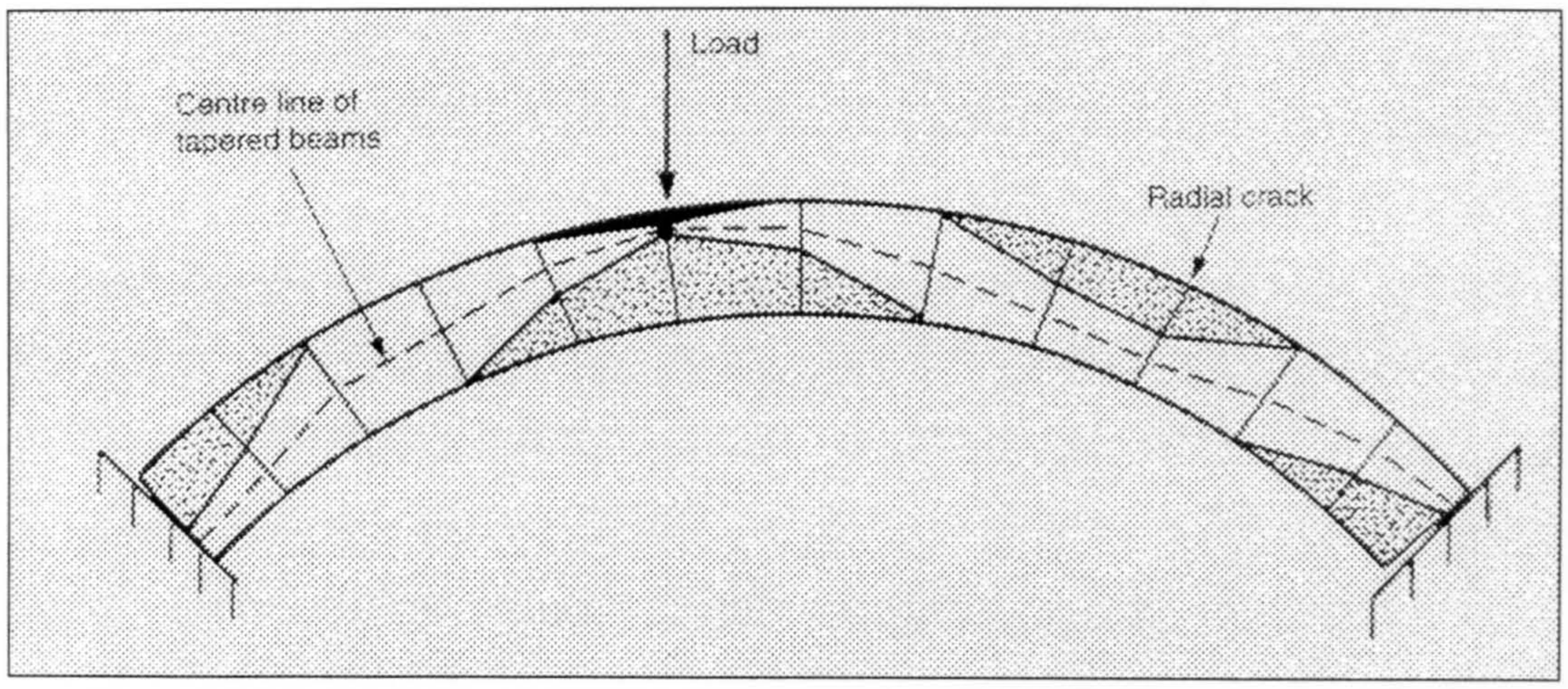

Figure 2.11 Typical use of tapered beam elements in MAFEA (After CHOO *et al.*, 1991)

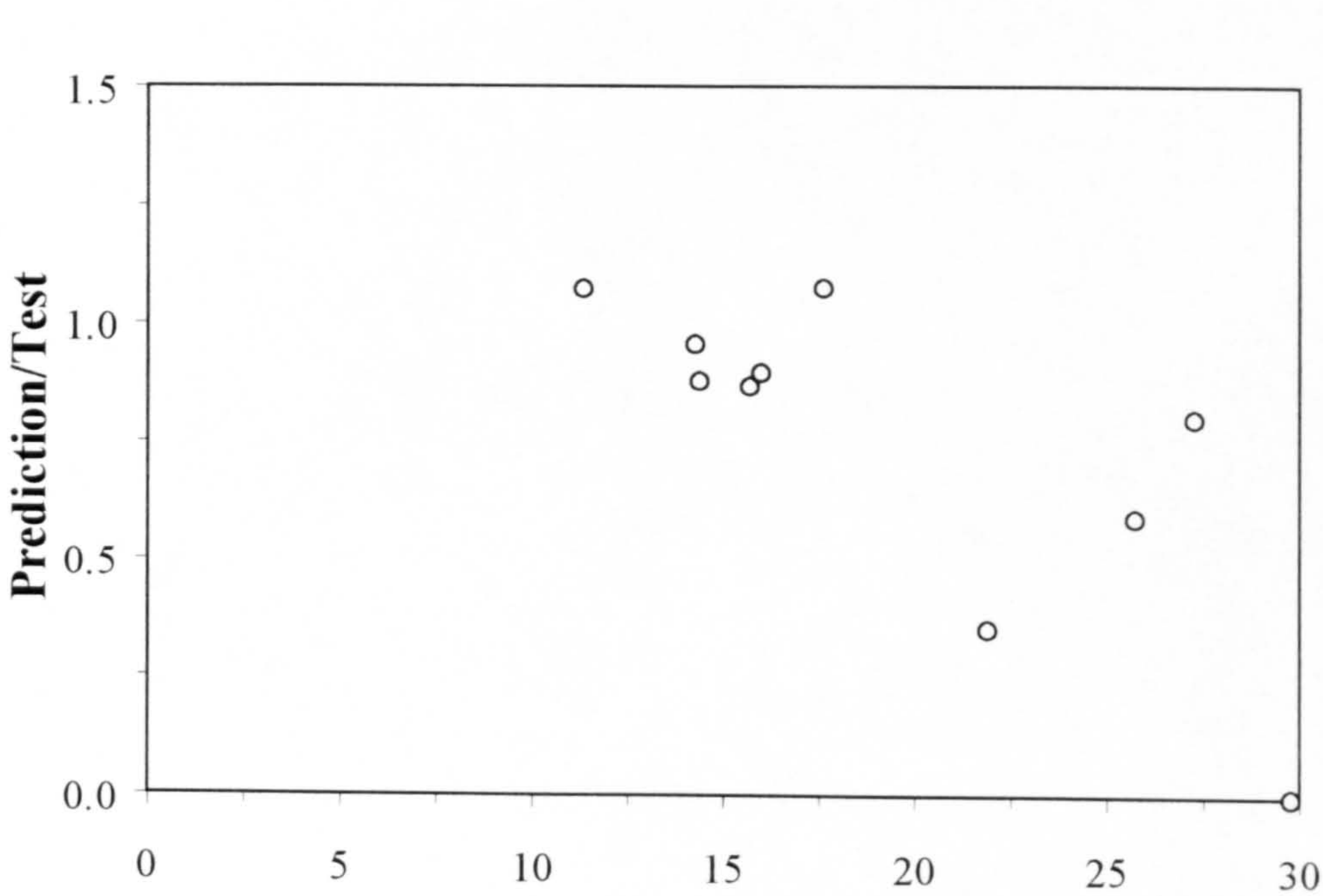

Figure 2.12a Comparison of results using CTAP (After DAS, 1990)

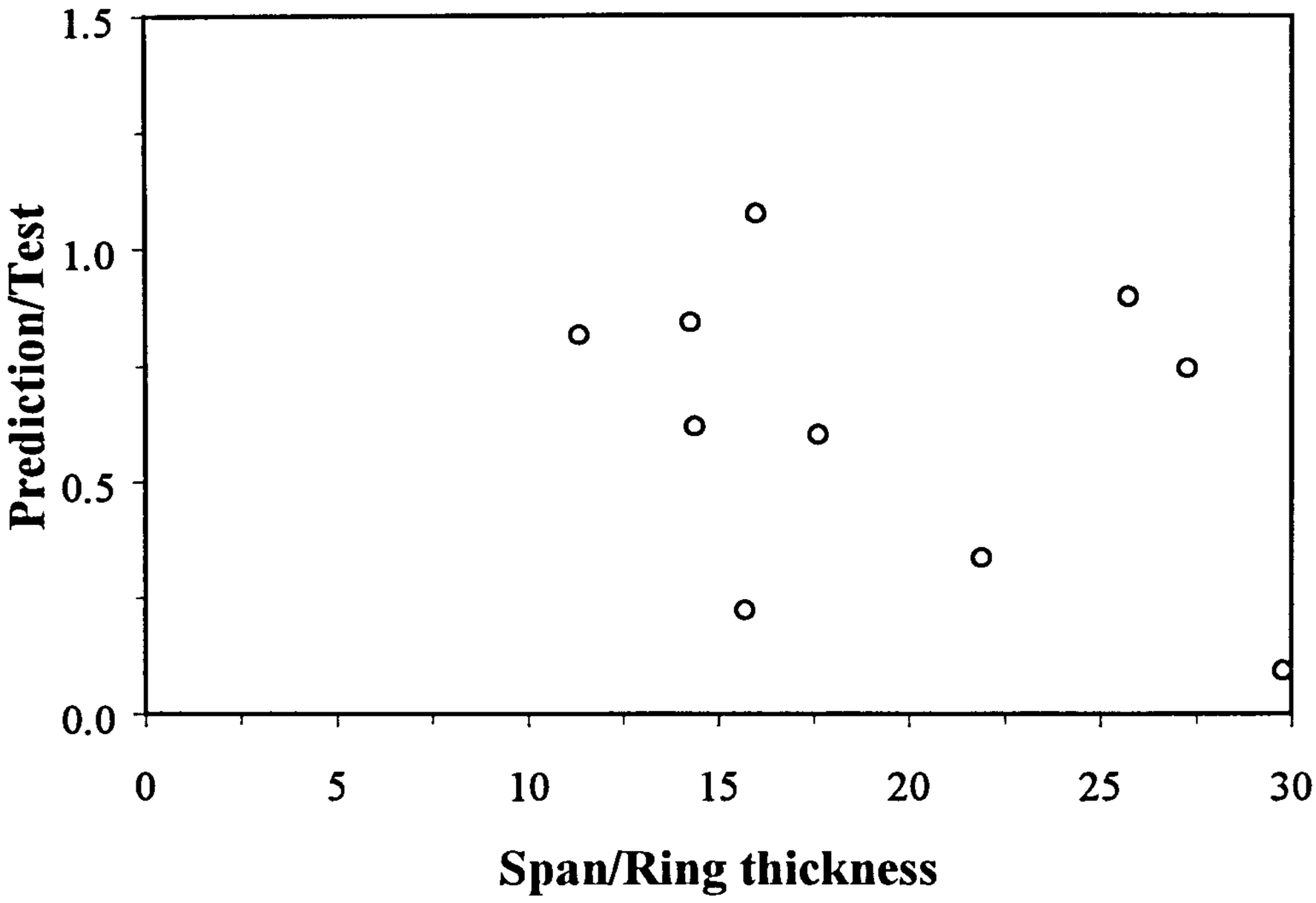

Figure 2.12b Comparison of results using ARCHIE (After DAS, 1990)

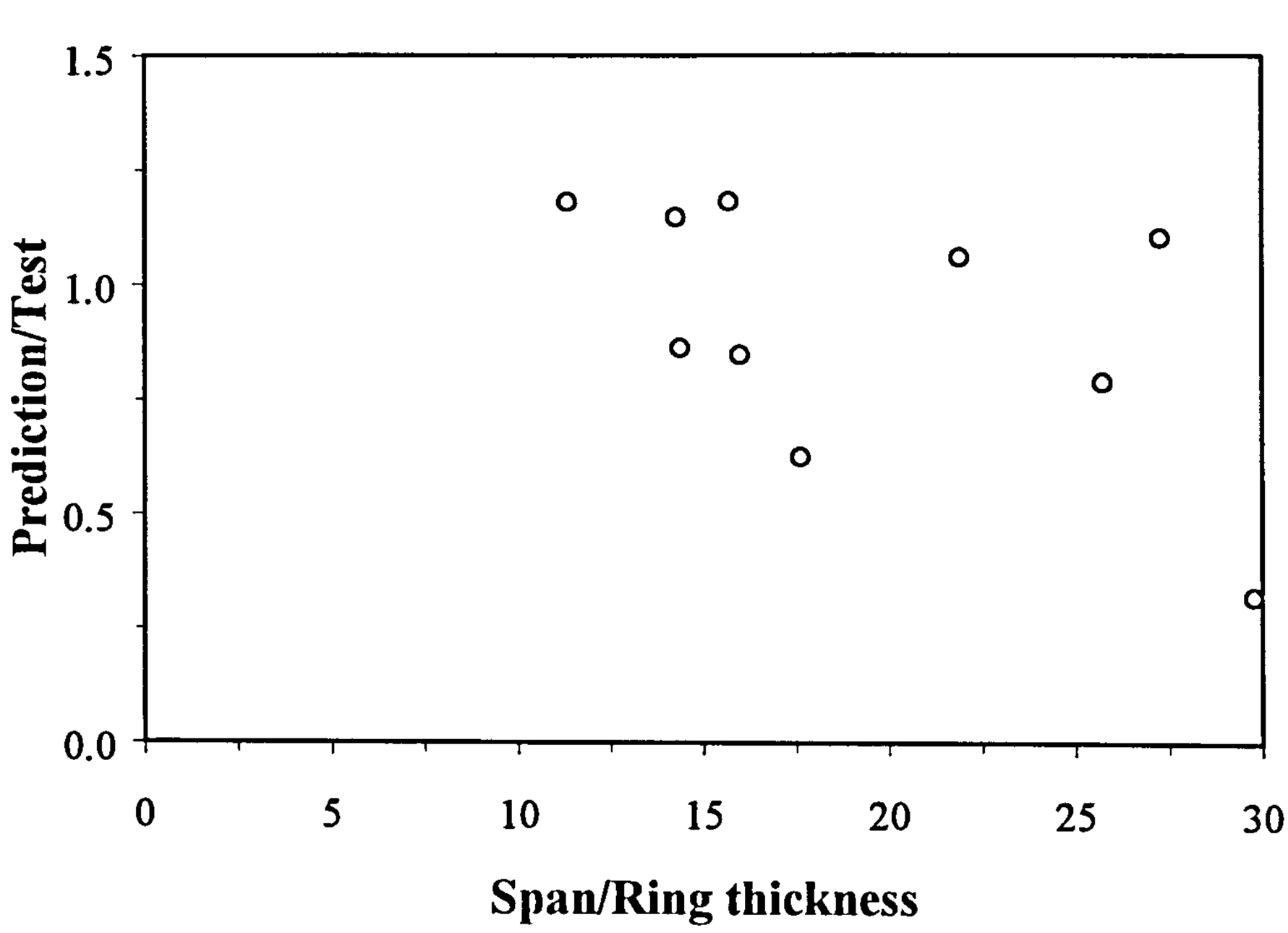

Figure 2.12c Comparison of results using MINIPONT (After DAS, 1990)

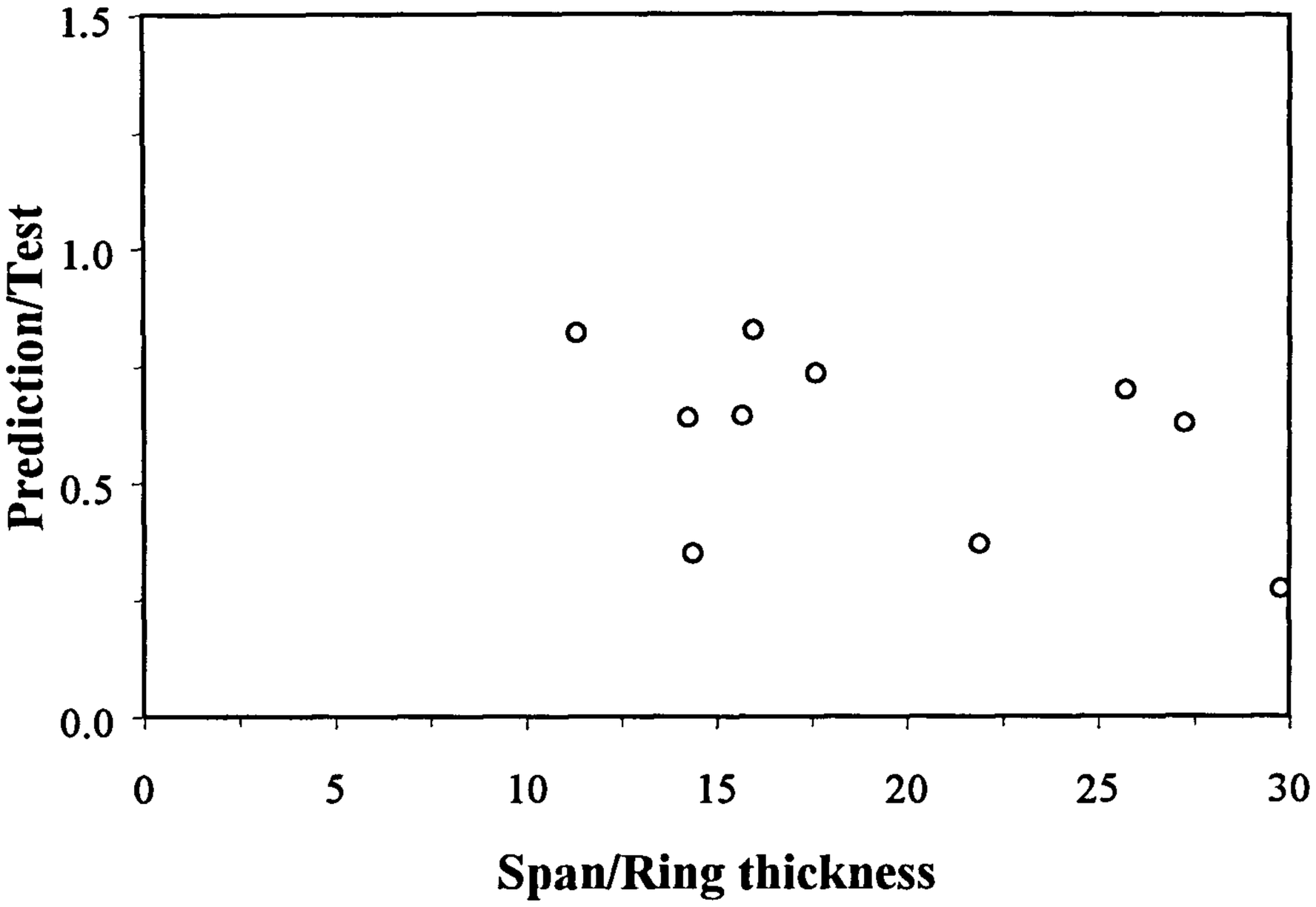

Figure 2.12d Comparison of results using ARCH (After DAS, 1990)

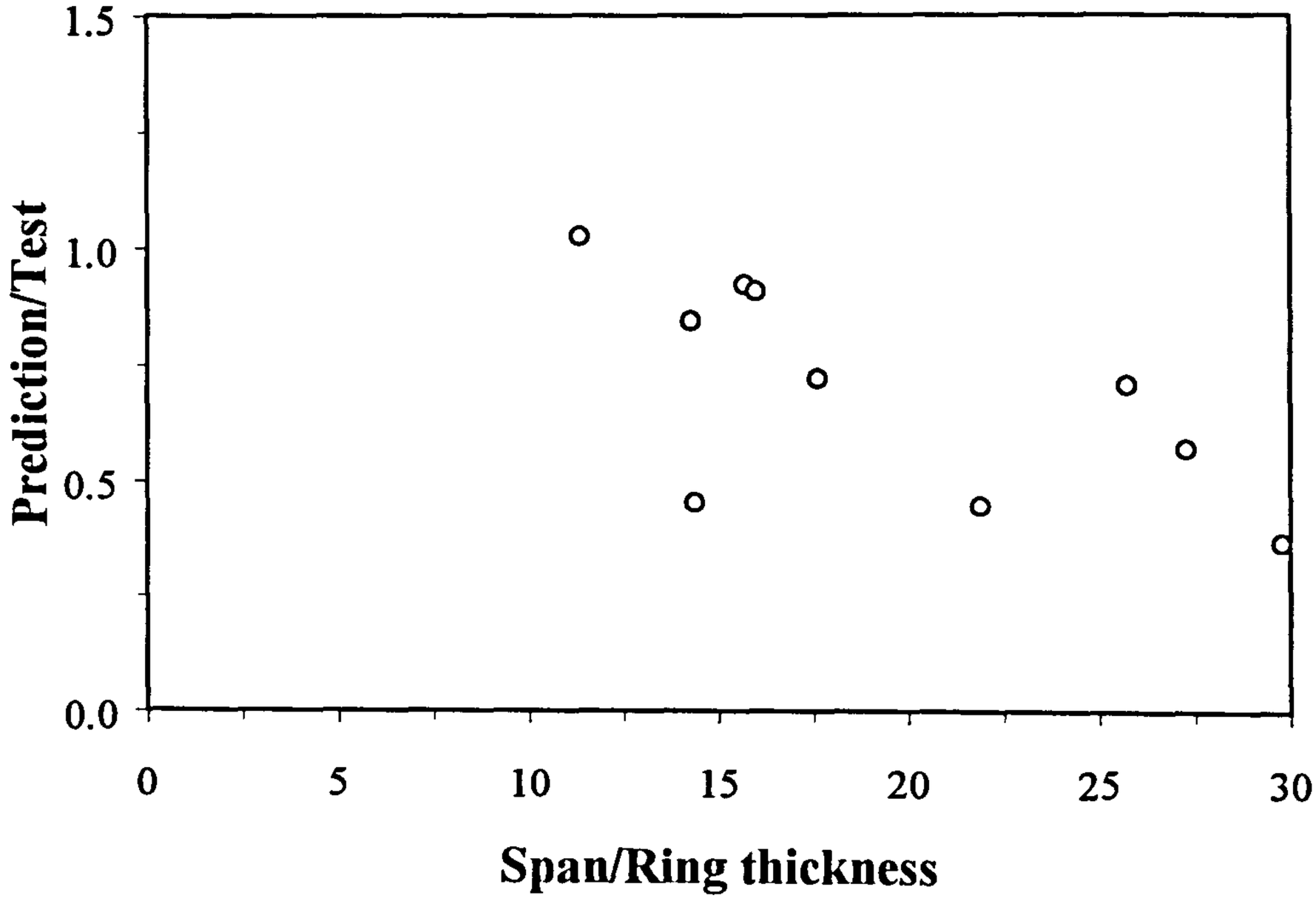

Figure 2.12e Comparison of results using MAFEA (After DAS, 1990)

CHAPTER 3

Two Dimensional Linear Elastic Analysis Of Stresses In Arch Bridges

3.1 Introduction

It is always believed that the difficulty in assessing arch bridges is due to lack of knowledge about quantifying soil-arch interactions. A concentrated load applied on the pavement's surface above an arch bridge will be distributed downwards onto the extrados. The extent to which the load can be distributed depends on the soil's stiffness and to a lesser degree on the stiffness of the arch. The current standard, BD21/97 (1997a), allows a load distribution of 1 horizontal to 2 vertical. FAIRFIELD *et al.* (1993b) recorded load dispersal angles in full and large scale tests far beyond that recommended by BD21/97.

As an arch deforms due to the action of applied load, active and passive pressures are mobilised. This effect is most significant in the case of steep haunched arches. The extent to which these pressures are mobilised is still unknown. Many arch assessment programs account for the influence of lateral forces but this is often only done in a speculative manner. The contribution of lateral forces in arch bridge assessments must be recognised and yet the current recommended assessment method (MEXE) was derived in such a way that no lateral forces were considered.

This chapter attempts to quantify the soil-arch interaction theoretically. The analysed bridge is similar to the large scale semicircular arch built and tested to collapse by FAIRFIELD (1994a). The bridge was fully instrumented and all pressure

measurements were recorded at each load increment. The details of the experiment are given in Section 3.2 of this thesis.

Three analytical methods were used to derive the stresses induced in the backfill and arch ring. They are the 2-D linear elastic FE (ZIENKIEWICZ *et al.*, 1989), Boussinesq's (BOUSSINESQ, 1885) and the codified or BD21/97 (BD21/97, 1997a) methods. Among the three analytical methods adopted, the 2-D linear elastic FE method is the most realistic method since it accounts for non-homogeneous materials and also the deflections of the arch ring under applied load. The stresses obtained from each individual method at different load levels are presented. Comparisons were also made between results obtained from different analytical methods and experiments.

3.2 The arch bridge analysed and test procedures used

The bridge analysed in this chapter was a semicircular arch bridge with span, ring thickness and crown backfill depth of 2.0m, 0.1025m and 0.15m respectively. The width of the bridge was 1.79m. A line load was applied to the bridge through a 0.18m wide spreader beam located on the surface of backfill. Figure 3.1 shows a schematic of the arch bridge with its salient dimensions.

Table 3.1 Test procedures at various stages, 2m semicircular arch bridge

Test	Load point, (X/R)	Load stage	Applied stress (kPa)
1	-1.0	1, 2, 3, 4	21, 39, 58, 78
2	-0.75	1, 2, 3, 4	18, 38, 56, 76
3	-0.50	1, 2, 3, 4	18, 37, 54, 75
4	0.0	1, 2, 3, 4	18, 37, 56, 75
5	-0.33	1, 2, 3, 4, 5	17, 52, 82, 96, 115

Tests were carried out at five different positions as *per* in Table 3.1. Different loads were applied to the bridge at each position and corresponding pressure changes recorded. A series of elastic tests was carried out on the bridge in tests 1 to 4 before it was collapsed in test 5.

3.3 Analytical methods

As mentioned in Section 3.1, there were three analytical methods used in the analysis: the 2-D linear elastic FE, Boussinesq's and the codified methods. The analysis of stresses due to the action of self-weight was carried out using the classical geostatic relationship given in Eqns 3.1 and 3.2 for vertical and horizontal stresses respectively. The coefficient of earth pressure at rest, K_o, was assumed to be 0.67. This value was used for compatibility of Poisson's ratio as also used in the FE analysis. Poisson's ratio is the ratio of horizontal strain to vertical strain assuming a vertical applied load. Horizontal stresses increase with increasing Poisson's ratio. The backfill bulk unit weight and its depth were denoted as γ_b and y respectively.

$$\sigma_y = \gamma_b y \qquad 3.1$$

$$\sigma_x = K_o \gamma_b y \qquad 3.2$$

$$\sigma_n = \frac{1}{2}[\sigma_y + \sigma_x] + \frac{1}{2}[\sigma_y - \sigma_x]\cos 2\theta - \tau_{xy}\sin 2\theta \qquad 3.3$$

$$\tau = \frac{1}{2}[\sigma_y - \sigma_x]\sin 2\theta + \tau_{xy}\cos 2\theta \qquad 3.4$$

Figure 3.2 shows the sign convention used in this analysis. All directions shown are positive. The normal and shear stresses are calculated using Eqns 3.3 and 3.4 respectively. It is clearly shown in Figure 3.2 that the direction of stresses on the arch extrados is opposite to that in the arch ring.

3.3.1 The finite element method

The finite element analysis was performed using a commercial finite element package LUSAS (1997). Its companion pre- and post-processing software MYSTRO (1997)

was used for data generation and graphical presentation of the computed results. Two meshes were generated to account for five different load points. Figure 3.3 shows the mesh used for tests 1, 3 and 4 while Figure 3.4 applies to tests 2 and 5. Four-noded quadrilateral elements were used for both the backfill and arch ring whilst 8-noded quadrilateral elements were assigned to the pavement since a more refined mesh was required to distribute applied loads more evenly. All elements were used in conjunction with 4 Gauss integration points. Similar analyses were also carried out with 8-noded elements in conjunction with 9 Gauss points and no significant changes to the stress state were found. In the case in which the applied load was acting right above the crown, the sign of shear stress changed rapidly over a narrow distance and therefore 8-noded elements were used to discretise the whole arch bridge. The arch ring was rigidly fixed in both vertical and horizontal directions. This was appropriate since no support movement was noticed during later tests. Backfill elements were restrained horizontally in both sides of the wing walls and rigidly fixed at the base. The above support conditions and mesh density were altered to examine their corresponding influences on the predictions.

Figure 3.5 shows the location of Gauss points at which the stresses in the arch ring were considered. All materials of the arch bridge were assumed to be linear elastic, homogeneous and isotropic. A plane strain condition was assigned to all elements. It was assumed that the backfill above the arch ring was more likely to be close to a plane strain condition due to transverse confinement by the spandrel walls. A series of parametric studies was carried out by varying the conditions in both the backfill and arch. A layer of thin interface elements was generated between the arch ring and backfill to account for soil-arch interaction. An analysis was also carried out without the interface element.

Table 3.2 presents the material properties of the arch, backfill, interface and pavement. A parametric study on these material properties was carried out to determine the influence of material variations on the stress state on the arch extrados. The range of

parametric study is clearly indicated in the relevant section of the text or corresponding graphs.

Table 3.2 Material properties, 2m semicircular arch bridge

Property	Arch	Backfill	Interface	Pavement
Elastic modulus (MPa)	5000	10	5	50
Poisson's ratio	0.2	0.4	0.4	0.35
Bulk unit weight (kNm^{-3})	21.5	14.5	14.5	14.5

3.3.2 Boussinesq's method

This method was published by Boussinesq in 1885 (BOUSSINESQ, 1885) for determining stresses induced in a soil mass under the action of an applied stress on the soil surface. The model was derived by treating the soil mass as semi-infinite, elastic, homogeneous, and isotropic the boundaries of which were sufficiently remote from the point of applied stress. Apparently, soils do not comply with such ideal conditions, but providing the stresses stay well below the yield point, the magnitude of error will be small.

It is clear that none of the above assumptions made in this model matches the situation in arch bridges. The assumptions treating the soil as a semi-infinite half-space and as a homogeneous material are clearly violated in the presence of an arch ring with a much higher stiffness. The application of a high stress causes considerable settlement which also reduces the distance between the applied load and the arch ring. This method was used only for the purpose of comparisons.

3.3.3 The codified method (BD21/97)

This method is currently recommended in the Department of Transport Standard, most recently, BD21/97 (1997a) and its associated Advice Note, BA16/97 (1997b). The

load applied on the road surface is to be dispersed through the backfill at a slope of 2 vertical to 1 horizontal. This gives a dispersal angle of 26.6° from each side of the loading edge.

3.4 Analysis of stresses due to self-weight

This section presents the stresses induced on the arch extrados and through the arch ring due to the action of self-weight only. The stress ratio and friction angle mobilised were also investigated. The stresses on the arch extrados were obtained from both the FE and geostatic methods. The geostatic vertical and horizontal stresses are evaluated using Eqn 3.1 and Eqn 3.2 respectively which assumed a linear variation of vertical and horizontal stresses with depth of backfill.

The self-weight in the FE analysis was applied by allowing the elemental body forces to be applied at the relevant nodes of all elements. The results obtained from the FE analysis should be identical to those obtained from the geostatic method if the soil mass is homogeneous and the boundary far enough from the point under consideration. However, these assumptions were clearly violated with the inclusion of an arch ring with a much higher elastic modulus.

Neither the FE nor the geostatic method accounts for arching action in the backfill. In reality, the self-weight vertical stresses induced in the backfill do not increase linearly with the depth of backfill due to the presence of vertical shear stresses between the soil particles. This phenomenon is particularly important if the backfill is horizontally confined within a small boundary and the depth of backfill considered is large compared with the horizontal confinement. However, the maximum depth of backfill in an arch bridge is likely to be much less than the distance between the spandrel walls; this reduces its influence on the self-weight vertical stress distribution. The results obtained from FE analysis are more realistic as they consider the arch, backfill and

pavement material properties. The FE method also considers the change in stress state as the arch deforms.

3.4.1 Stresses on the arch extrados

The normal and shear stresses obtained by the FE and geostatic methods are presented in Figure 3.6a. The normal stresses obtained by both methods were quite close to each other at the region over the crown. This was expected since the depth of backfill over the crown is not much influenced by the presence of the arch ring which was oriented in a horizontal direction. At X/R = ±0.4 and outwards to the springer, stress differences became more significant. This was because the normal stresses in the backfill were affected by the inclusion of the arch ring, with its significantly higher modulus, which was oriented in a much steeper direction. The normal stresses evaluated by the FE method were higher than those by the geostatic method over the region between X/R = ±0.4 to ±0.8. The maximum discrepancy of the normal stress obtained by these two methods was found to be 22% at X/R = ±0.65. This was because the high stiffness of the arch material was able to attract considerable stresses. The stresses at the region near the springers were severely affected by the presence of the rigid boundary in the FE analysis. Stresses predicted by the FE method at region near X/R = ±1.0 are significantly affected by the support: normal and shear stresses at X/R = -8.0 to -1.0 are presented in Figure 3.6b. At X/R = ±1.0, the FE and geostatic methods predicted a normal stress of 3.95kPa and 12.11kPa respectively; 1.29kPa and 0kPa respectively for the shear stress. The fluctuation of the FE and geostatic results was because the geostatic method did not take into account the presence of different materials. It is derived in such a way that the boundary is far enough from the point of consideration to have any significant influence on the stress state.

For the analysis of shear stresses, a similar behaviour as in the case of normal stresses was noticed. The dissimilarity of results obtained from both methods was due to the presence of the arch ring. The geostatic shear stresses were zero at the crown and

springers where the slope of the arch was either horizontal or vertical. These were the principal planes and no shear stress acts thereon. A small shear stress was recorded by the FE method at the springers due to the presence of complementary shear stresses. The maximum shear stress obtained by the geostatic method occurred at X/R = ± 0.88 which compared well with X/R = ± 0.82 predicted by the FE method. However, the maximum shear stress predicted by the FE method was 4.3kPa or 70% higher than that predicted by the geostatic method. This was because the FE method was able to model complementary shear stresses around the arch extrados which become more significant at the region near both springers where the arch ring was steeper.

Further analyses were carried out on the stress ratio and mobilisation of angle of shearing resistance: results are presented in Figure 3.7. The stress ratio in this case was taken as the ratio of vertical to horizontal stresses. The stress ratios predicted by the geostatic method were constant since a constant coefficient of lateral soil pressure was assumed in this method. The stress ratios predicted by both methods were in agreement at the region over the crown. This was because the orientation of the arch profile was flatter in this region and therefore it was more likely to be under geostatic conditions. From X/R = ± 0.4 outwards, the stress ratios predicted by the FE method were larger than those mobilised by the geostatic method. This was because the effect of inclusion of the arch ring was more significant in this region. The FE method predicted a maximum stress ratio of 2.57 at X/R = ± 0.8 which was about 70% higher than that by the geostatic method.

The normal and shear stresses on the arch extrados were used to define the mobilisation of friction angle. No significant difference of results was noticed at the region over the crown. The maximum friction angles mobilised by the FE and geostatic methods were 26.5° and 11.5° respectively at X/R = ± 0.85. These results also suggest that no shear failure in the backfill on the arch extrados should be expected under the action of self-weight unless the angle of shearing resistance on the soil-masonry interface is less than 26.5°. The soil-masonry friction angle is about 0.67 times the soil friction angle (CRAIG, 1997): a soil-masonry friction angle of 26.5° is therefore

equates to a soil friction angle of about 41°. The backfill angle of shearing resistance is 40°. Yielding of the soil-arch interface is therefore predicted at X/R = ±0.85 under self-weight.

3.4.2 Stresses in the arch ring

The normal and shear stresses in the arch ring due to the action of self-weight are presented in Figure 3.8. Stresses were taken from four Gauss points along a section in the radial direction as indicated in Figure 3.5. The sign convention for these stresses is shown in Figure 3.2.

From Figure 3.8, it could be seen that the whole arch ring was under compression as all normal stresses were positive. It would be expected from a classical structural analysis that the arch is in compression under its self-weight. The maximum normal stress (200kPa) was recorded at both springers near the intrados. At the crown, the highest normal stress (132kPa) was found at the intrados. At the region about X/R = ±0.8, the highest normal stress (136kPa) was recorded near the extrados. Based on the variation of normal stresses along the whole arch ring, it was clear that the crown moved upwards under the action of self-weight. This was because considerable lateral stresses were induced on both sides of the arch. Analysis of arch deflections showed that the crown moved upwards by 0.0115mm under the action of self-weight. It is therefore not always true to say that newly built arches will settle upon decentering. This depends mainly on the arch profile and stresses induced during the process of backfilling. It may be true for flat arches on which the lateral stresses have no significant influence in restricting horizontal arch deformations. It is not worthy to discuss material failure at this stage given the maximum normal compressive stress of about 200kPa which is too low to cause material crushing.

As in the case of the normal stresses, shear stresses were symmetrical about the mid-span. The shear stress at the crown was zero as the arch profile was horizontal. The

maximum shear stress was found to be about ± 9kPa at X/R = ± 0.45. Ratios of shear to normal stresses would give an idea of the friction angle mobilised but this was deemed to be unnecessary at this stage. This was because the self-weight stresses are low relative to the live load stresses.

3.5 Analysis of stresses due to live loads

This section presents all results obtained from the live-load analyses by three analytical methods mentioned in Section 3.3: the 2-D FE, Boussinesq's and the codified methods. The results from analytical methods are presented separately and the comparisons of each analytical method are carried out in Section 3.6. The normal and shear stresses on the arch extrados were analysed using all analytical methods while the stress state in the arch ring was predicted by only the FE method. Among all the analytical methods used in this analysis, the FE method was the only method able to predict stresses in the arch ring. Both normal and shear stresses were calculated using Eqn 3.3 and Eqn 3.4 respectively. It must be noted that the codified method gave only the vertical stresses but not horizontal and complementary shear stresses. Therefore, the normal and shear stresses obtained from the codified method were not compared with those obtained by the FE and Boussinesq's methods. As the result, only the influence factors for vertical stresses by all analytical methods were used in these comparisons. As mentioned in Section 3.2, five load points were considered; the loading regimes were indicated in Table 3.1. The FE results are presented first, followed by the results from Boussinesq's method and finally the codified method's results.

3.5.1 Finite element results

All results from the live load analyses by the FE method are presented here. Both the normal and shear stresses on the arch extrados and in the arch ring were analysed. The

influence of material properties, support conditions, boundary proximity and mesh refinement were carried out. Analyses were also carried out by varying the conditions (plane strain and plane stress) in the arch and backfill. An analysis was also performed without the interface elements. For the sake of clarity, the results of each study above are presented separately in the following sections.

3.5.1.1 Stresses on the arch extrados with constant material properties

This section examines the normal and shear stresses on the extrados using the material properties given in Table 3.2. Table 3.3 shows the test number for each test and its associated peak normal and shear influence factors. The normal and shear stresses in tests 1 to 5 are presented in Figures 3.9 to 3.13 respectively.

The distributions of normal and shear stresses were very similar to those predicted by classical stress distribution methods in the form of a bell shape curve. All peak stresses were found right beneath the loaded points with the exception of tests with the loads applied at X/R = -1.0 and -0.75 where the peak stresses were found away from the load point towards the crown. The influence factors were affected by both the vertical and horizontal distances from the load point and the location of peak stress was not fixed and varied with different arch geometries.

The highest normal influence factor was found in test 4 when the load was applied just above the crown. It would be expected since the vertical distance from the load to the arch was minimised at this point. For all the tests carried out in this section, no significant amount of normal stress was found on the side remote from the load. Mobilisation of passive pressure on the side remote from the load was mainly due to arch deformations in such a way that the arch was being pushed into the backfill. Figure 3.14 shows the horizontal and vertical arch deformations with the load applied at X/R = -0.33. The maximum horizontal deflection was 0.33 mm towards the backfill

at X/R = +0.65 with an applied load of 115kPa. Given such a small amount of horizontal deflection, the mobilisation of passive pressure could never reach its ultimate limit. The maximum ratio of the horizontal to vertical stresses on the side remote from the load was found to be 0.802 recorded at X/R = +0.706. If the angle of shearing resistance of the backfill was taken as 35°, only 22% of the classical Rankine passive pressure was mobilised.

Table 3.3 Peak influence factors for normal and shear stresses on the arch extrados, FEM

Test No.	Load point X/R	Peak influence factor	
		Normal stress	Shear stress
1	-1.0	0.196	0.106
2	-0.75	0.311	0.154
3	-0.5	0.44	0.185
4	0.0	0.763	0.139
5	-0.33	0.568	0.191

It was impossible, in this case, to quantify the mobilisation of active pressure on the arch extrados under the load point as the pressure actually increased from the at-rest state due to the action of the live load. It was true that the arch ring moved downwards after the application of live load but an intimate contact was still maintained between the backfill and the arch extrados. The backfill was actually being pushed towards the arch ring which subsequently caused the arch ring to move downwards. This situation is different from the classical Rankine active state in which 'the wall moves away from the soil'. It may be true at the moment the arch collapses that no intimate support is provided by the arch ring to the backfill.

The maximum influence factor for the shear stress on the arch extrados was found to be 0.191 with the load applied at X/R = -0.33. No doubt, the circumferential shear stresses have a strengthening effect on arch bridges as such stresses prevent the arch moving in circumferential directions. However, the contribution of circumferential shear stresses is difficult to be quantified as it also depends on both vertical and horizontal stresses which are still not fully elucidated.

3.5.1.2 Stresses in the arch ring

This section analyses the stresses induced in the arch ring with an imposed stress of 115kPa located at X/R = -0.33. Figure 3.5 shows the location of Gauss points at which the normal and shear stresses were considered. The sign convention for these stresses is shown in Figure 3.2. The normal and shear stresses induced in the arch ring are presented in Figure 3.15.

Referring to Figure 3.15, it was clear that there were four sections in which the stresses changed from positive to negative or *vice versa*. These sections indicated the possible hinge locations. Most notably was the section right under the applied load at X/R = -0.33 with a maximum compressive and tensile stresses of 939kPa and 790kPa respectively. This predicted hinge location coincided exactly with that observed later in the relevant experiment. Three other hinge locations were predicted at X/R = -0.89, 0.52 and 1.0. It is unlikely that a hinge will form at the springer of a semicircular arch bridge due to the considerable lateral restraint offered by the backfill. This linear elastic analysis is only valid until the first Gauss point reaches its ultimate limit. It is not sensible to use a linear elastic analysis to predict ultimate limit results. However, this elastic analysis forms a basis for comparisons with more realistic non-linear analyses and also to show the limitations of elastic analyses.

The maximum shear stress was found to be about 100kPa at X/R = -0.16. The maximum ratio of the shear to normal stresses was found to be 2.28 at X/R = -0.97 on the arch extrados. This gave a friction angle of 66.3°. This friction angle might be too large to be sustained on the soil-masonry interface and yielding would have occurred in reality. Such a high friction angle was predicted by the FE method which did not consider material yielding.

3.5.1.3 Stresses on the arch extrados with different material properties

This section examines the influence of material properties on the stress distribution on the arch extrados. The study was carried out by varying the arch, backfill and pavement elastic moduli. Table 3.4 shows the peak normal and shear stresses with different material moduli. The relevant factor was the ratio of the current peak stress to that obtained with standard material properties given in Table 3.1. The normal and shear stresses on the arch extrados with different arch, backfill and pavement moduli are presented in Figures 3.16, 3.17 and 3.18 respectively.

Table 3.4. Peak stresses with different material properties

Material	Elastic modulus MPa	Peak stress (kPa)		Relative factor	
		Normal	Shear	Normal	Shear
Arch	3000	63.97	23.15	0.98	1.05
	5000	65.27	22.01	1.00	1.00
	10000	66.36	21.01	1.02	0.95
	15000	66.76	20.56	1.02	0.93
Backfill	5	66.51	22.97	1.02	1.04
	10	65.27	22.01	1.00	1.00
	50	58.34	18.70	0.89	0.85
	100	53.02	17.92	0.81	0.81
Pavement	50	65.27	22.01	1.00	1.00
	500	61.87	20.63	0.95	0.94
	1000	58.57	19.64	0.90	0.89
	2000	54.31	18.35	0.83	0.83

The modulus of the arch had little influence on the normal stresses on the arch extrados. The influence factor for normal stress increased by 2.3% for a 300% increase in the arch modulus. Unlike the case of the normal stresses, the shear stress decreased with the increase in arch modulus. This was because the arch with a lower modulus behaved more flexibly and thus mobilised more circumferential shear stresses. An increase of 5.2% in the shear stress was recorded with a decrease in the arch modulus from 5000MPa to 3000MPa.

Higher modulus backfills dispersed the applied stress over a wider area. By increasing the modulus of backfill from 10MPa to 100MPa, the normal and shear stresses were decreased by 18.8% and 18.6% respectively. Similarly, both the normal and shear stresses decreased by increasing the pavement modulus. The normal and shear stresses decreased by 16.8% and 16.7% with a pavement modulus of 50MPa and 2000MPa respectively.

3.5.1.4 The effects of mesh refinement

No doubt, the finer the mesh the better the result will be in any FE analysis. Cost and time may be the main issues deciding the mesh density. As mentioned in Section 3.3.1, 4-noded quadrilateral elements were used to model the backfill and the arch except for the test in which the applied load was acting right above the crown. This section examines the influence of 4-noded and 8-noded quadrilateral elements on the prediction of normal and shear stresses on the arch extrados. The 8-noded quadrilateral element was used in conjunction with a 3x3, 9 point Gaussian integration routine. This analysis was carried out with an imposed stress of 115kPa located at X/R = -0.33. The normal and shear stresses on the arch extrados were evaluated and compared with those obtained from the analysis with 4-noded elements.

The normal and shear stresses on the arch extrados obtained from the analyses with both meshes are presented in Figure 3.19. It can be seen from Figure 3.19 that the magnitude and the trend of stress distributions obtained with both meshes seemed to be almost identical. A slight variation in the shear stresses was noticed on the side remote from the load but its magnitude was insignificant.

3.5.1.5 The effects of support conditions

The effect of varying the support condition of the backfill elements on the prediction of both the normal and shear stresses on arch extrados is described in this section. The arch ring was deemed to be rigidly fixed at both abutments. The analysis was carried out for the test with an imposed load of 115kPa located at X/R = -0.33. The normal and shear stresses with different support conditions are presented in Figure 3.20a. Three different support conditions were examined which were referred to as Case 1, Case 2 and Case 3. Case 1 being the standard support condition used in all analyses as mentioned in Section 3.3.1. In Case 2, the backfill elements were rigidly fixed on both lateral sides and the base of both wing walls. In Case 3, the boundary of each wing wall was restrained horizontally on both lateral sides and supported vertically at the base. Cases 1, 2, and 3 are shown schematically in Figures 3.20b, 3.20c, and 3.20d respectively.

It can be seen from Figure 3.20 that the normal and shear stresses on the arch extrados obtained with different backfill support conditions were almost identical. This was because the boundary was far enough away for it to have any significant influence on the stress state on the arch extrados. The maximum difference in the normal stress obtained from Case 1 and Case 2 was found to be only 1kPa at X/R = 0.92. At no point did the shear-stress difference exceed 0.3kPa.

3.5.1.6 The effects of boundary proximity

The boundary proximity used in all FE analyses in this study was similar to that in the test. Therefore, this section does not serve to examine the accuracy of this FE analysis associated with the variations of boundary proximity. However, the sensitivity of support conditions is directly related to the boundary proximity. If the boundary is at a considerable distance, results may not be significantly affected no matter what type of support conditions are used provided the mesh density is kept constant.

Three different boundary proximities were examined under an imposed stress of 115kPa located at X/R = -0.33. The normal and shear stresses on the arch extrados with these boundary proximities are presented in Figure 3.21a. Case 1 being the standard case used in all analyses with the length of the wing wall being 572mm. The length of wing wall was 286mm in Case 2 and 1145mm in Case 3. The bridge geometry of Cases 1, 2, and 3 are depicted in Figures 3.21b, 3.21c, and 3.21d respectively.

The stress states obtained in Case 1 and Case 3 were almost identical. Stresses from Case 2 were predicted to be higher than those from Case 1 and Case 3. This was because, in Case 2, the length of the wing wall was only half the original size which increased the degree of confinement to the arch. The peak normal stress in Case 2 was predicted at 1.4kPa higher than that in Case 1. A more significant change of stress state was found at the region close to both springers. The normal stress in Case 2 was predicted at 2.95kPa higher than that in Case 1 on the side remote from the load. This was because the arch deformations on the side remote from the load were restricted due to a higher degree of backfill confinement. The shear stresses in Case 2 were also predicted to be higher than those in Case 1 and Case 3 on the side remote from the load. The maximum shear stress difference, in Case 1 and Case 2, was 1.2kPa recorded on the side remote from the load.

The results of these analyses showed that the boundary proximity used in the FE mesh was appropriate. No significant changes were found in terms of peak stresses and the trend of stress distributions. The boundary proximity was also examined experimentally (FAIRFIELD, 1994a) by installing vibrating wire gauges on the end walls which found that the boundary was too far away to have any significant influence on the stress state.

3.5.1.7 The effect of using plane strain or plane stress states for the arch and backfill

Four different conditions were assigned to the backfill and arch as given in Table 3.5. The corresponding vertical and horizontal arch deflections are presented in Figure 3.22. The conditions of the interface element and the pavement were similar to that of the backfill. All analyses were carried out with an imposed stress of 115kPa located at X/R = -0.33.

Table 3.5 Different conditions for the backfill and the arch

Condition	Backfill	Arch
Case 1	Plane strain	Plane strain
Case 2	Plane stress	Plane stress
Case 3	Plane strain	Plane stress
Case 4	Plane stress	Plane strain

Referring to Figure 3.22, it is obvious that the conditions of both the backfill and arch had no significant effect on predicted deflection. The maximum arch vertical deflections with conditions assigned in Case 1, Case 2, Case 3, and Case 4 were 0.446mm, 0.454mm, 0.461mm, and 0.444mm: all recorded at X/R = -0.233. The maximum arch horizontal deflections were found to be 0.355mm, 0.365mm, 0.364mm, and 0.357mm with conditions assigned in Case 1 to Case 4 inclusive respectively: all recorded at X/R = +0.648. This indicates that using either plane strain or plane stress will only result in a slight variation in the deflection or stress and the point subjected to the maximum deflection is unaffected in this study. In most cases, the behaviour of an arch bridge is dominated by the arch ring since it is much stronger and stiffer than any other components of the system. Any variation in the backfill properties is therefore unable to induce a significant change in the behaviour of the bridge. Either plane strain or plane stress conditions can be assigned to the backfill in a FE analysis and the resulting variation should not be perceptible. It has been shown in Chapter 6 of this thesis that varying the condition of the backfill yielded a similar predicted collapse load in a non-linear 2-D FE analysis.

The condition of the arch was also shown to have no effect on the prediction of arch deflection. This was because the Poisson's ratio of the arch was only 0.2 in this study. The arch material is unlikely to have a high Poisson's ratio. This indicates that the arch ring, in any 2-D FE analysis, could be idealised in either a plane strain or plane stress condition without having much variation in the prediction provided a reasonably small Poisson's ratio is assigned to the arch.

3.5.1.8 The effects of extrados interface elements

The effect of the interface elements was analysed in this section. Two analyses were carried out with an imposed stress of 115kPa located at X/R = -0.33, with and without interface elements. The corresponding vertical and horizontal arch deflections are presented in Figure 3.23.

No significant changes to both the arch vertical and horizontal deflections were noticed. The maximum arch vertical deflections recorded with and without interface elements were 0.446mm and 0.438mm respectively, recorded at X/R = -0.233, and 0.355mm and 0.345mm respectively for the arch horizontal deflections recorded at X/R = +0.648.

3.5.2 Boussinesq's results

This section presents the normal and shear stresses on the arch extrados obtained by the classical Boussinesq method (BOUSSINESQ, 1885). The properties of this method are described in Section 3.3.2. The test procedures are given in Table 3.1. Only live loads were considered in this section. The vertical, horizontal and complementary shear stresses were obtained using Eqns 3.5, 3.6 and 3.7 respectively. The identities of the parameters in these equations are clearly shown in Figure 3.2. Table 3.6 shows the test reference number for each test and its associated peak

influence factors for normal and shear stresses. The normal and shear stresses for tests 1 to 5 are presented in Figures 3.24 to 3.28 respectively.

$$\sigma_y = \frac{q}{\pi}\{\alpha + \sin\alpha\cos(\alpha + 2\beta)\} \qquad 3.5$$

$$\sigma_x = \frac{q}{\pi}\{\alpha - \sin\alpha\cos(\alpha + 2\beta)\} \qquad 3.6$$

$$\tau_{xy} = \frac{q}{\pi}\{\sin\alpha\sin(\alpha + 2\beta)\} \qquad 3.7$$

The distributions of the normal and shear stresses were all in the form of a bell shape. All maximum influence factors for the normal and shear stresses were found to be closer to the crown. Most notably was the case where the load was acting at X/R = -1.0, the peak influence factor for the normal stress was found at X/R = -0.648. Needless to say, the normal stress close to the springers, for a semicircular arch, was mainly contributed to by horizontal stresses. The maximum ratio of horizontal to vertical stresses for the load acting at X/R = -1.0 was only 0.01 between the region X/R = -1.0 to -0.76. These low ratios of horizontal to vertical stresses were probably responsible for the migration of peak normal stress closer to the crown.

Table 3.6 Peak influence factors for normal and shear stresses on the arch extrados, Boussinesq's method

Test No.	Load point X/R	Peak influence factor	
		Normal stress	Shear stress
1	-1.0	0.185	0.090
2	-0.75	0.273	0.125
3	-0.5	0.409	0.162
4	0.0	0.625	0.205
5	-0.33	0.495	0.192

None of the assumptions made in Boussinesq's method remained intact with this complex soil-arch system. The assumption of a homogeneous material was violated

due to the presence of an arch ring. The arch ring itself was also a boundary to the surrounding backfill which violated the assumption of a semi-infinite half-space material. The stresses on the side remote from the load were obtained in a speculative manner due to the absence of soil medium under the arch ring. Despite the violation of the assumptions made in this method, the results obtained were nevertheless quite satisfactory in terms of the trend of stress distribution (a bell shape curve). This is because Boussinesq method is geometrical and its distribution is inversely proportional to both vertical and horizontal distance away from the loaded area.

3.5.3 The codified (BD21/97) method's results

The details of this method were described in Section 3.3.3. The test procedures were similar to those in the FE and Boussinesq's methods given in Table 3.1. It must be noticed that this method does not give horizontal and complementary shear stresses. The normal and shear stresses are therefore obtained by considering vertical stresses only. Table 3.7 shows the test reference number for each test and its associated peak influence factors for normal and shear stresses. The normal and shear stresses for tests 1 to 5 are presented in Figures 3.29 to 3.33 respectively.

Table 3.7 Peak influence factors for normal and shear stresses on the arch extrados, codified (BD21/97) method

Test No.	Load point X/R	Peak influence factor	
		Normal stress	Shear stress
1	-1.0	0.176	0.150
2	-0.75	0.267	0.163
3	-0.5	0.425	0.138
4	0.0	0.545	0.042
5	-0.33	0.511	0.163

The distributions of normal and shear stresses were somewhat absurd. The maximum normal stress was found at the point, within the region covered by the distribution, lying nearest to the crown. This was because the vertical stress is calculated in such a

way that it is only proportional to the vertical distance. A sudden curtailment of normal stress was found in every test, indicating a point from which no stress distribution was allowed. This was because a fixed dispersal angle, 26.5° in this case, was assumed in this method. It is highly unlikely that such a distribution of stresses would occur in reality.

The maximum influence factor for normal stress was found to be 0.545 with the load acting right above the crown. This was because the vertical distance from the load to the arch extrados was the lowest among all the tests. The maximum influence factor for shear stress was found to be 0.163 with the load acting at X/R = -0.75. As mentioned previously, these normal and shear stresses were evaluated by considering vertical stresses alone and therefore should not be used for comparison with results by the FE and Boussinesq's methods. However, the behaviour of vertical stresses is worth further analysis. Comparison of influence factors of vertical stresses was made with the results obtained by the FE and Boussinesq's methods in Section 3.6.1. Despite the stress distribution being so unrealistic, this method is currently recommended by the Department of Transport, most recently, BD21/97 (1997a) and its associated advice note, BA16/97 (1997b).

3.6 Comparisons of analytical and experimental results

This section presents the comparisons of the results obtained by three analytical methods; the FE, Boussinesq's and the codified methods. The analytical results were also compared with those observed experimentally (FAIRFIELD, 1994a). All comparisons were carried out on each test associated with peak applied stresses.

3.6.1 Comparison of analytical results

This section examines the behaviour of all theoretical results generated in this chapter. They are the results obtained by the FE, Boussinesq's and the codified methods. Only the influence factors for vertical stresses were compared. The comparisons were made with loads applied at X/R = -1.0, -0.75, -0.5, 0.0 and -0.33 and results are presented in Figures 3.34 to 3.38 respectively. Only these results associated with maximum applied load at each load point were considered. Figure 3.39 shows a summary of peak influence factors obtained by each analytical method in each test.

It can be seen from Figures 3.34 to 3.38 that the stress distributions were basically in agreement in terms of the load spread but with different stress distributions. All peak influence factors were found to be closer to the crown rather than just below the loaded points. Different arch profiles and backfill depths may have different influences on the migration of peak stresses. However, it is often believed that a slight variation of load position in any analysis does not lead to any notable change in the arch behaviour.

If a limiting influence factor of 0.1 is chosen to confine the extent of stress distribution, then it became clear that all analytical methods in this study predicted almost a similar extent of stress distribution at every load point. This seems to indicate that the assumption made in the current standard, BD21/97 (1997a); that the stress distribution of 2 vertical to 1 horizontal is appropriate. However, it is understood that the behaviour of the stress distributions from all analytical methods used in this study are greatly sensitive to the arch geometry. Therefore, the acceptability of the stress distribution recommended by BD21/97 (1997a) should not be confirmed unless similar analyses are carried out on arches with different span to rise ratios. Figure 3.39 presents the summary of all peak influence factors for vertical stresses predicted by all analytical methods used in this study. The ratios of these influence factors are presented in Table 3.8.

All peak influence factors predicted by Boussinesq's method were lower than those obtained by the FE method with a maximum discrepancy of 20% in the test with the load applied at X/R = -0.75. This was because Boussinesq's method assumes the backfill mass to be a semi-infinite half-space and homogeneous; facts clearly violated with the presence of an arch with a much higher modulus.

Table 3.8 Ratios of influence factors for vertical stresses

X/R	FEM	Boussinesq	Codified
-1.00	1	0.81	0.80
-0.75	1	0.80	1.10
-0.50	1	0.86	1.01
-0.33	1	0.84	0.88
0.00	1	0.82	0.71

The peak influence factors predicted by the codified method were lower than those obtained by the FE method in the test with the loads applied at X/R = -1.0, -0.33 and 0.0. The maximum discrepancy of 28.6% was in the test with the load applied at X/R = 0.0 where the distance between the surface of the backfill to the arch extrados was at a minimum.

The FE method the most realistic method among those used in this study as it takes into account the soil-structure interactions. Boussinesq's method, albeit based on various assumptions that do not pertain to this soil-arch system, did give satisfactory trends of stress distributions similar to those given by the FE method. The codified method did not seem to give a sensible shape of stress distribution as a fixed dispersal angle had to be assumed in this method.

3.6.2 Comparison of theoretical and experimental results

This section presents the comparison of the results obtained by three analytical methods used in this study with those observed experimentally. Details of the experimental results are well documented elsewhere (FAIRFIELD, 1994a). In the

experiment on the 2m semicircular arch, five stress transducers were mounted on the arch extrados at X/R = -0.62, -0.35, 0.0, +0.35 and +0.62 to measure both the normal and shear stresses. The normal and shear stresses from tests 1 to 5, associated with peak applied stresses, were used for comparisons with the experimental stress states. The experimental and analytical stress states in tests 1 to 5 are presented in Figures 3.40 to 3.44 respectively. The summary of the analytical peak normal and shear stresses is presented in Table 3.9.

Table 3.9 Peak normal and shear stresses

X/R	Applied stress (kPa)	FE method (kPa)		Boussinesq's method (kPa)		Codified method (kPa)	
		Normal	Shear	Normal	Shear	Normal	Shear
-1.00	78	15.3	8.3	14.3	7.0	13.7	11.7
-0.75	76	23.6	11.7	20.8	9.5	20.3	12.4
-0.50	75	33.0	13.9	30.7	12.2	31.8	12.2
0.00	75	57.2	10.4	46.8	15.3	40.9	3.16
-0.33	115	65.3	22.0	56.9	22.1	58.8	18.7

Good agreements in terms of the trend of stress distribution were achieved. The experimental normal stresses were higher than those obtained analytically in the tests with loads applied at X/R = -1.0, -0.75, -0.5 and 0.0. The best prediction of the analytical normal stresses was in test 3. The experimental peak normal stress was 38kPa which compared well with the peak normal stresses predicted by the FE (33kPa), Boussinesq's (30.7kPa) and the codified (31.8kPa) methods. All analytical peak normal stresses (FE = 65.3kPa, Boussinesq = 56.9kPa, and codified = 58.8kPa) were predicted as being higher than the experimental peak normal stress of 34kPa in the test to destruction (load applied at X/R = -0.33; maximum applied stress of 115kPa). Stress decreases were recorded at higher load levels before the collapse of the arch. The decrease in stress was due to deformation of the arch ring which subsequently redistributed stresses around the arch ring and surrounding backfill. The FE and Boussinesq's methods were found to give excellent predictions in terms of the trend of stress distribution and the peak normal stresses especially at low load levels.

It is understood that any experimental results are subjected, to some extent, to experimental errors. In test 4 with the load applied at X/R = 0.0, the peak experimental influence factor for normal stress was 2.07. An influence factor of more than one is not possible from a theoretical point of view. The application of a uniform pressure on the surface of backfill was only a hypothesis. Due to the different degree of confinement in the soil mass beneath the load platen, the stress would be concentrated at the middle point of the soil-platen interface where the degree of confinement was the greatest and the peak applied stress would be larger than the average applied stress. This was why an influence factor of more than one was obtained during the experiment. Figures 3.45a and 3.45b show the stress distributions under a rigid and a flexible foundations on cohesionless soil mass.

The analytical shear stresses compared well with the experimental results in terms of the trend of the stress distribution in tests 1 to 3. In test 5, the test to destruction, an experimental peak shear stress of 70kPa was recorded at the crown. This was because a considerable amount of circumferential shearing resistance was mobilised at the crown during the test as the arch deformed. The shear stress at the crown predicted by the FE, Boussinesq's, and the codified methods were only -0.96kPa, -6.4kPa, and 0kPa respectively. Although the FE method does consider arch deformations, it was only valid at low loads when the arch was still within its elastic limit.

This study has demonstrated the efficacy of elastic analyses to model stress distributions in a soil-arch system. It is obvious that both the FE and Boussinesq's methods were able to predict a realistic trend of stress distribution and peak stresses on the arch extrados at low loads. The increase in normal stress on the side remote from the load was only predicted by the FE method but was lower than that observed experimentally. All peak normal stresses predicted by the codified method were lower than those obtained by the FE method with discrepancies of 10.5%, 14.0%, 3.6%, 28.5%, and 10% in tests 1 to 5 respectively.

The above observations may only be true for the geometry of the arch analysed in this study. Arches with different span to rise ratios might have a different stress distribution from those observed in this study.

3.7 Conclusions

1 The linear elastic FE method was the most realistic analytical method in this study which successfully responded to the variation of material homogeneity for this soil-arch system.

2 Results by the FE and geostatic methods for the dead-load analysis were found to be in agreement over the region around the crown where the effect of the foreign inclusion of the arch ring was not significant.

3 Results by the FE analysis showed that the whole arch ring was in compression under the action of self-weight.

4 The FE method was the only analytical method in this study that detected the mobilisation of passive stresses on the side remote from the applied load as the result of arch deformations.

5 Stresses in the arch ring derived by the FE method in test 5 predicted four possible hinge locations with the one right beneath the applied load coincident with the hinge location in the experiment.

6 The arch's elastic modulus was found to have no significant effect on the prediction of stresses on the arch extrados.

7 Stresses were found to be reduced significantly with the increase of backfill and pavement moduli.

8 Analysis of boundary conditions revealed that the current FE mesh was appropriate with respect to the mesh refinement, support conditions and boundary proximity.

9 Varying the conditions of the backfill and the arch (plane strain and plane stress) had no effect on the prediction of arch deflection.

10 No significant changes to the arch deflection were noticed in an analysis without interface elements.

11 Normal and vertical stresses from the FE analysis were higher than those from Boussinesq's method.

12 The stress distribution by the codified method was found to be unrealistic with a sudden curtailment of peak stresses.

13 The extent of distribution of vertical stresses obtained from the FE, Boussinesq's and codified methods was found to be quite similar for this particular arch geometry.

14 Stresses on the arch extrados calculated from all analytical methods used in this study were in agreement with experimental results in terms of the trend of stress variation.

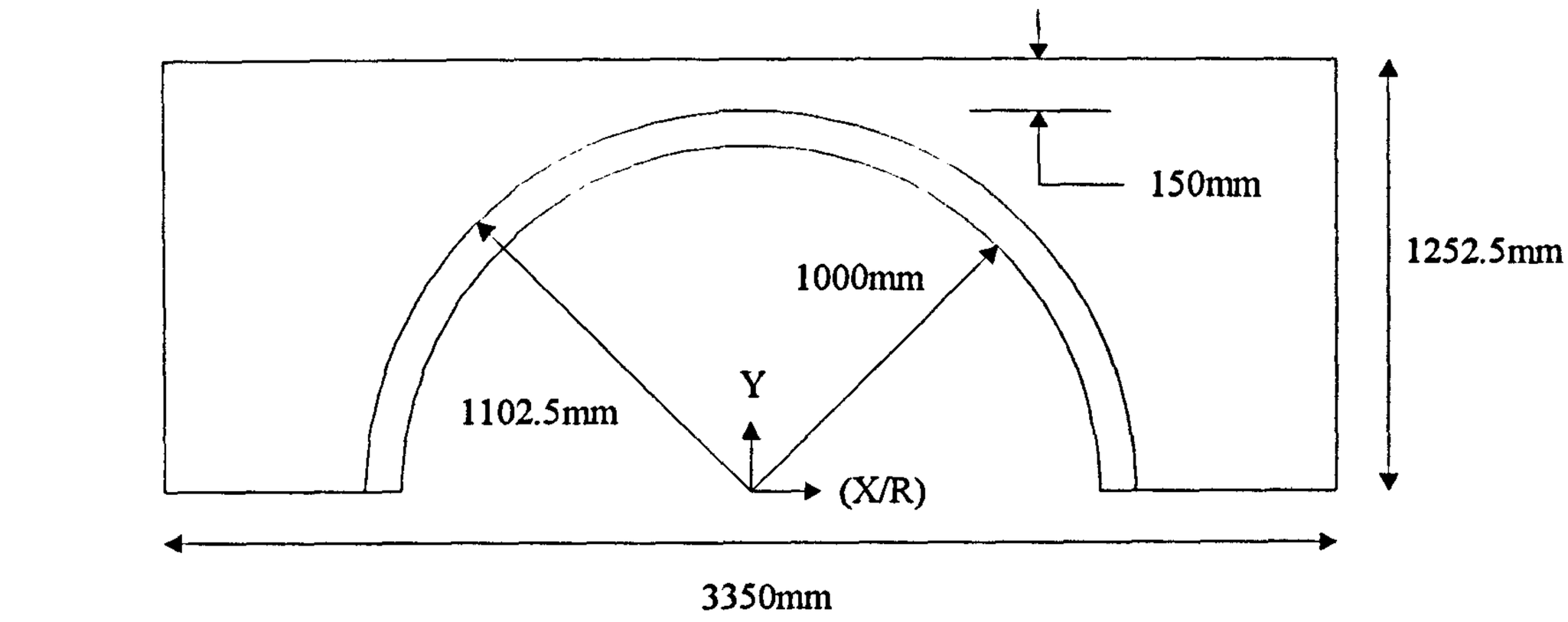

Figure 3.1 Salient dimensions of the semicircular arch bridge

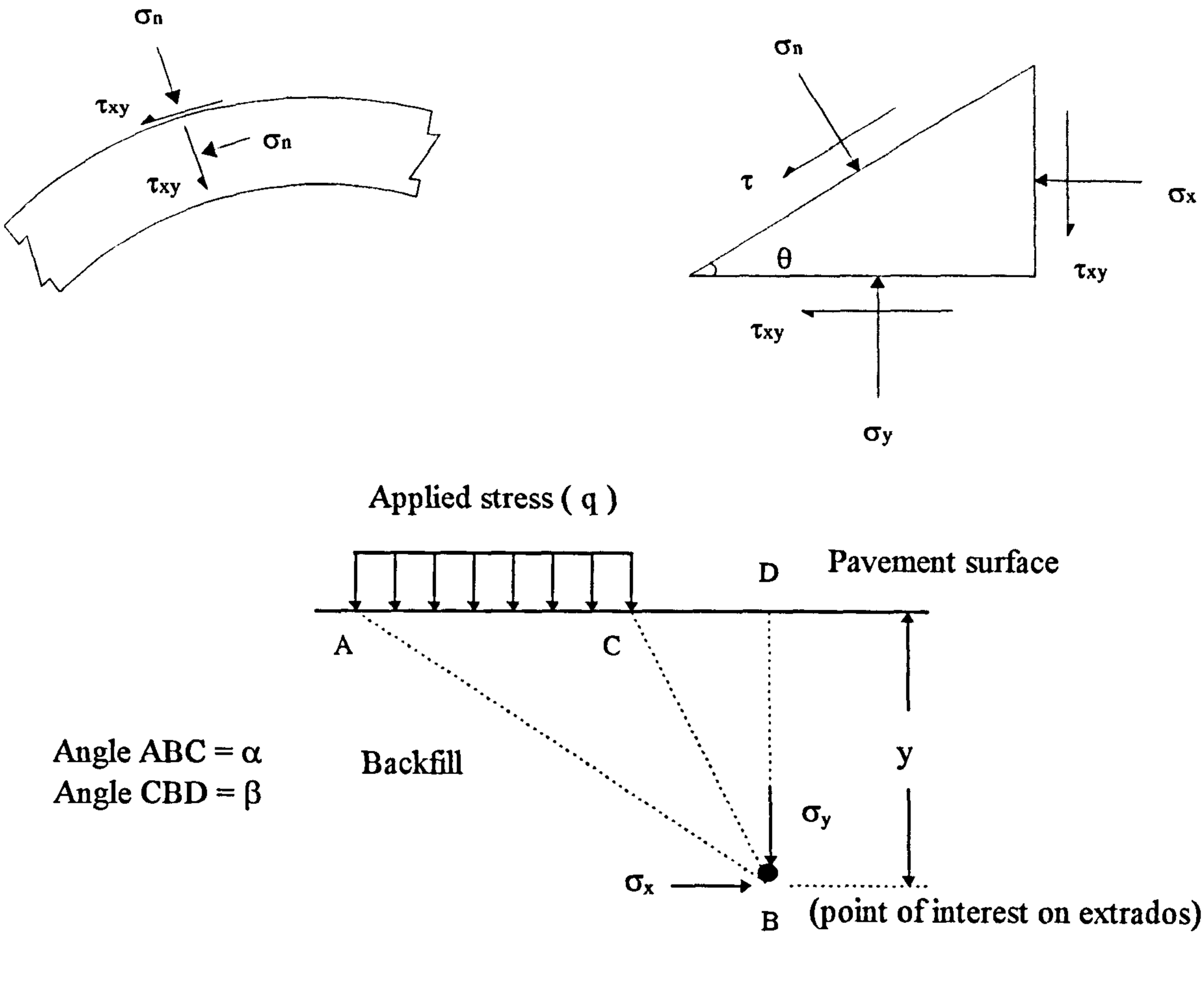

Figure 3.2 Direction of stresses

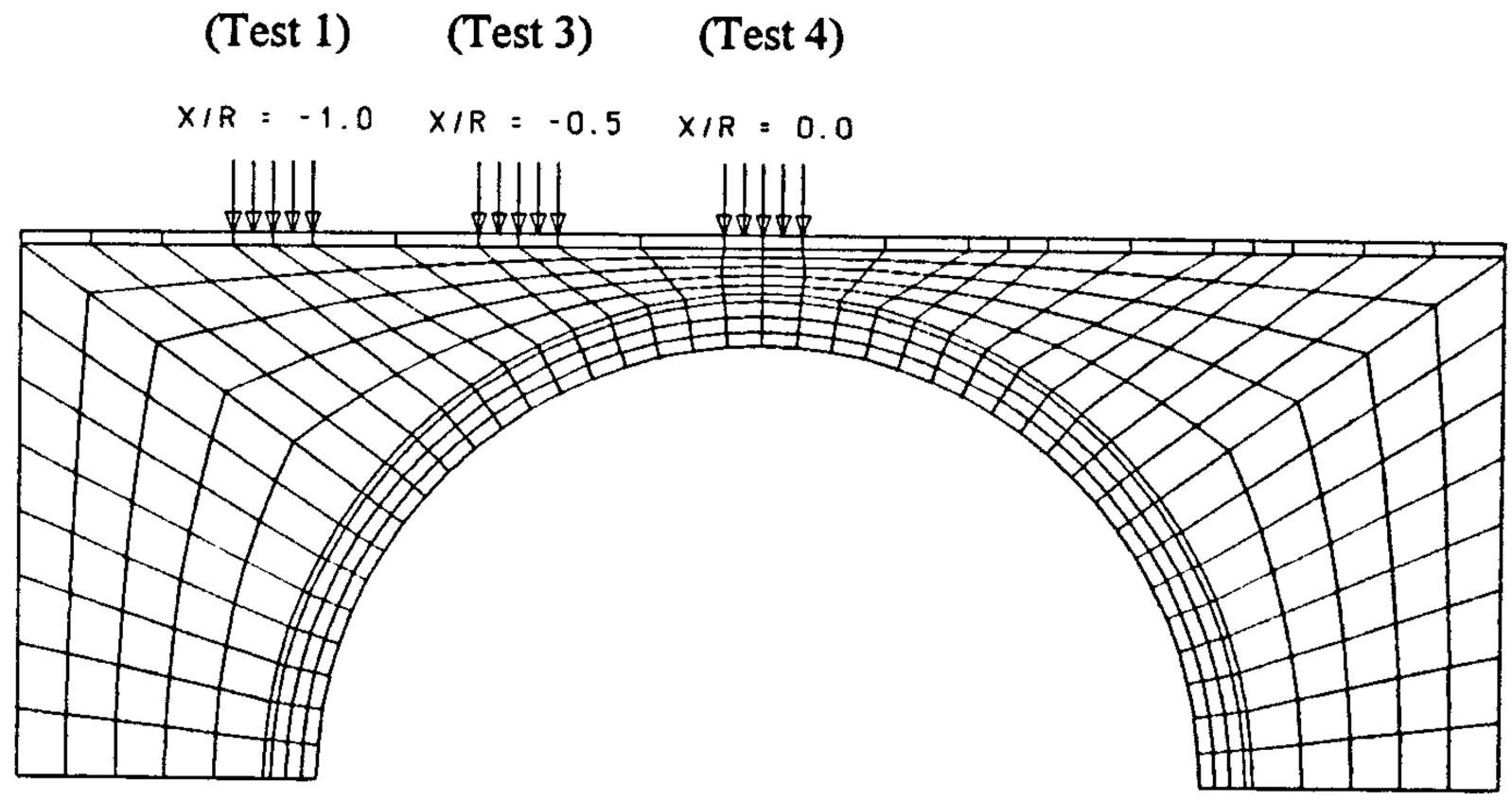

Figure 3.3 Finite element mesh for tests 1, 3 and 4

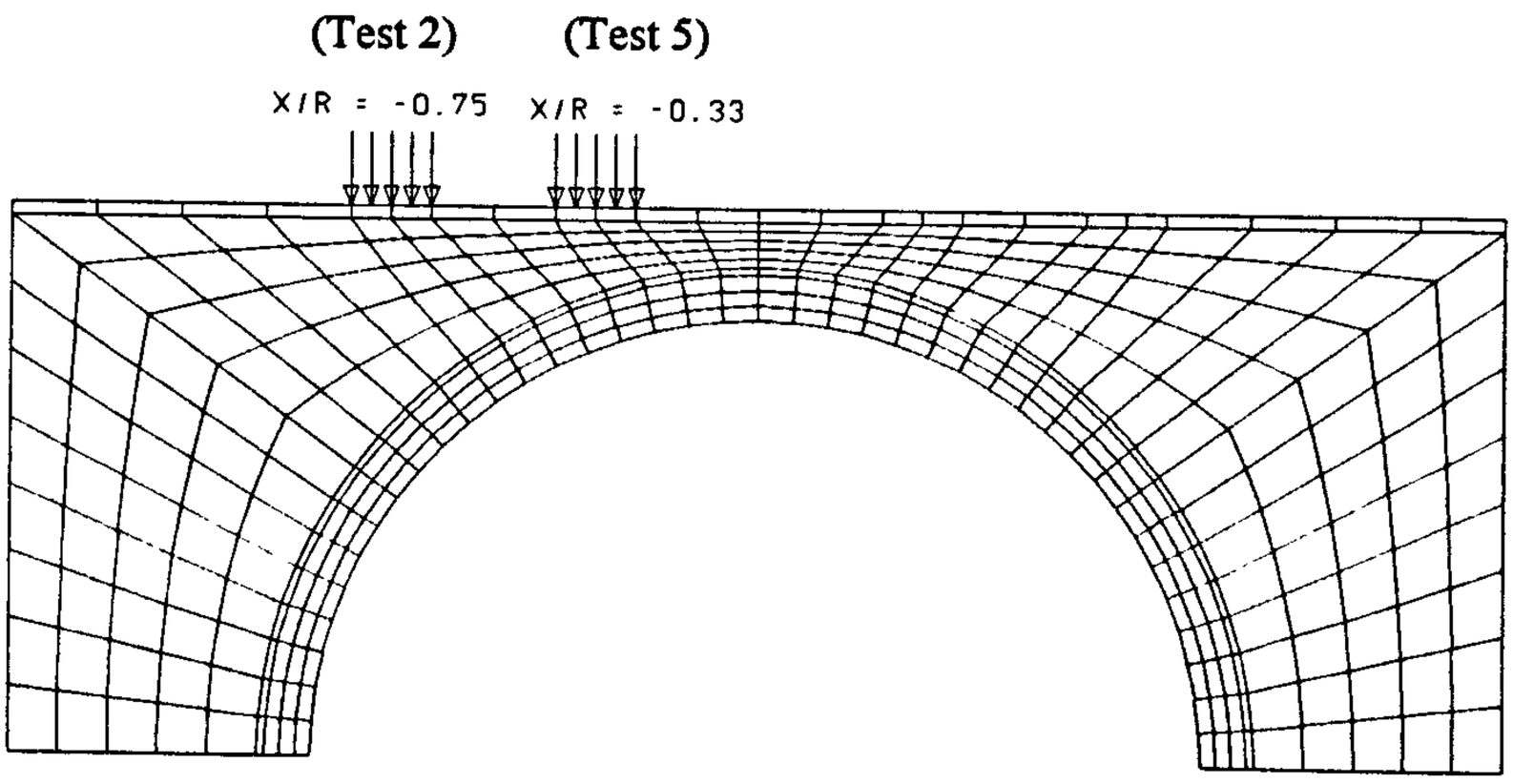

Figure 3.4 Finite element mesh for tests 2 and 5

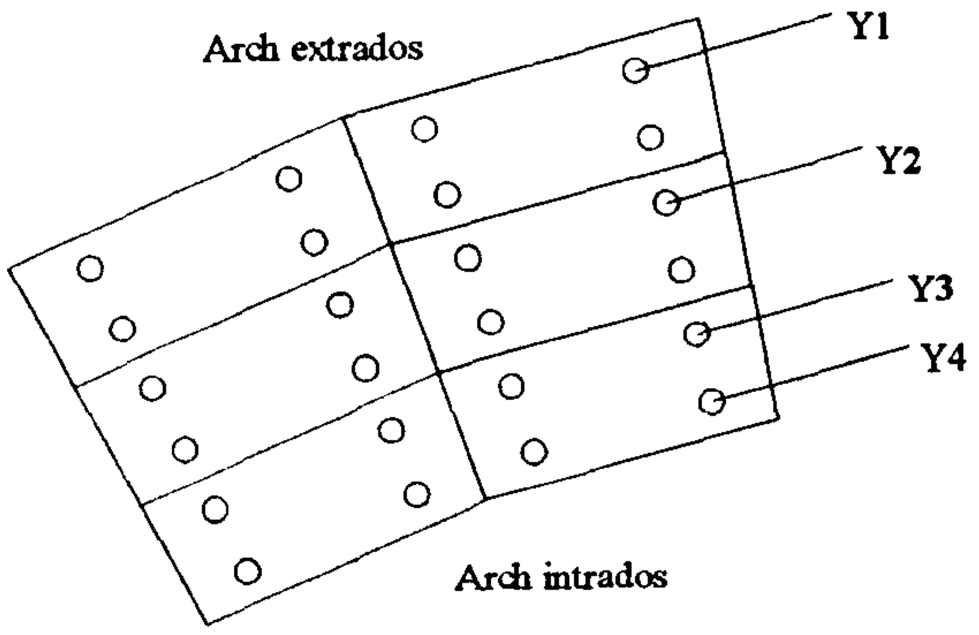

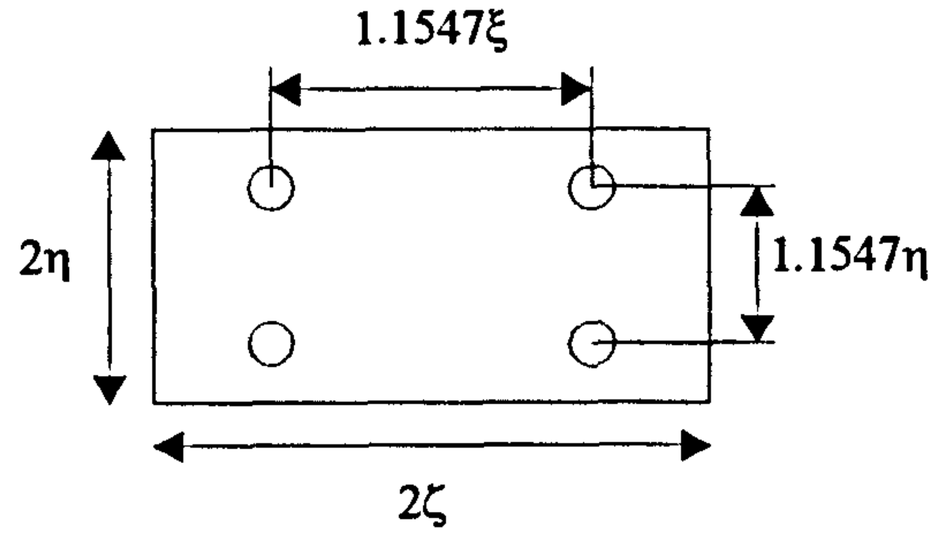

Figure 3.5 Location of Gauss points

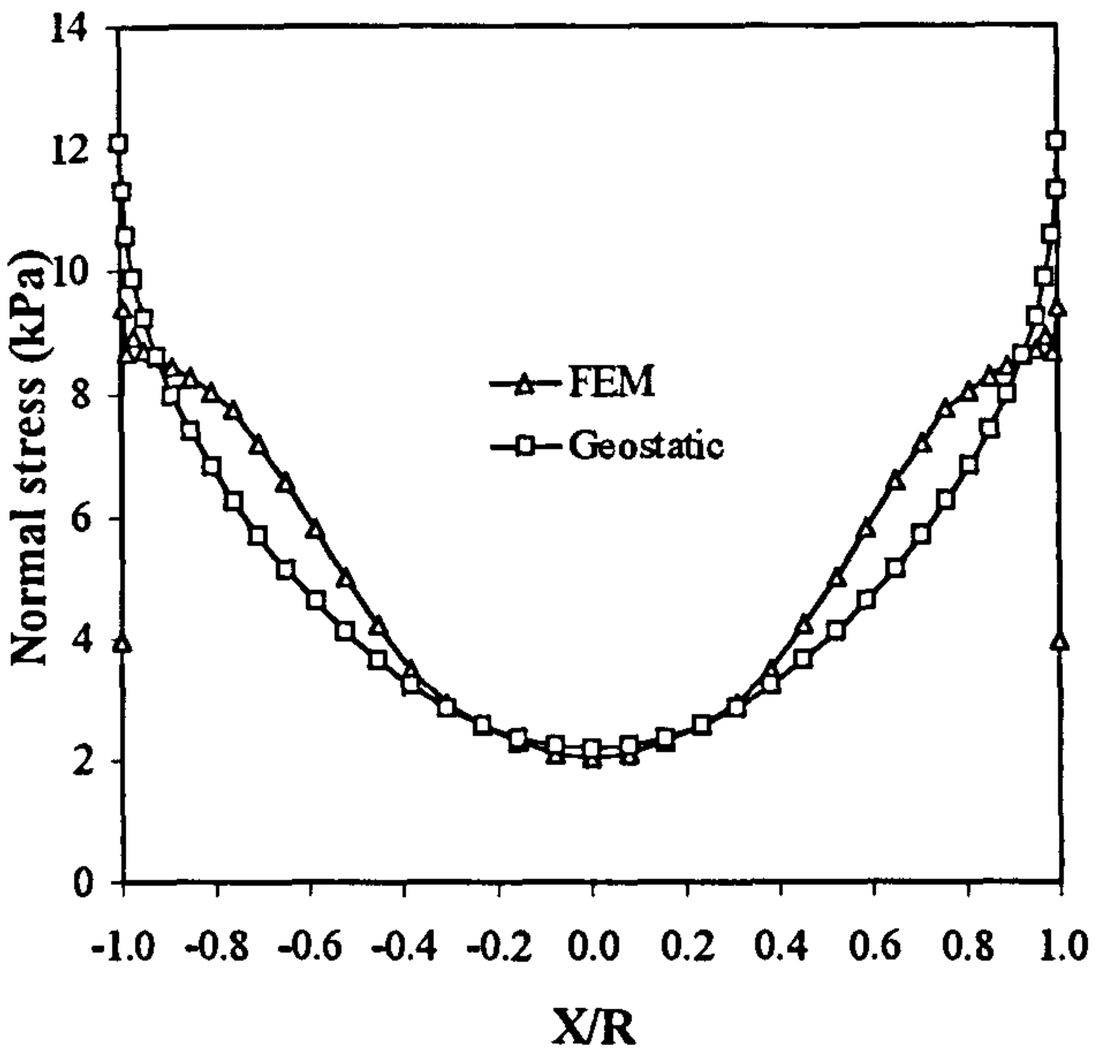

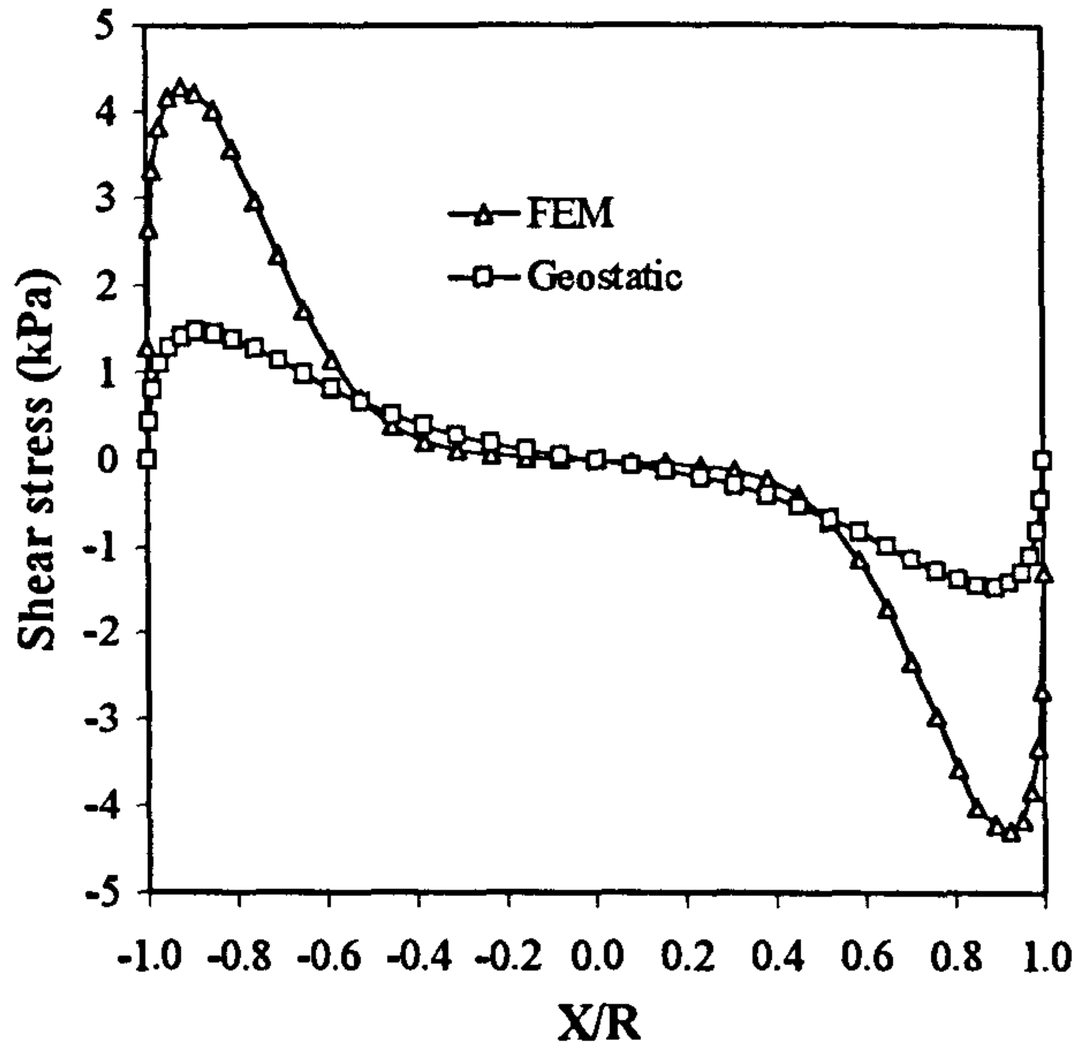

Figure 3.6a Stresses on the arch extrados, self-weight only

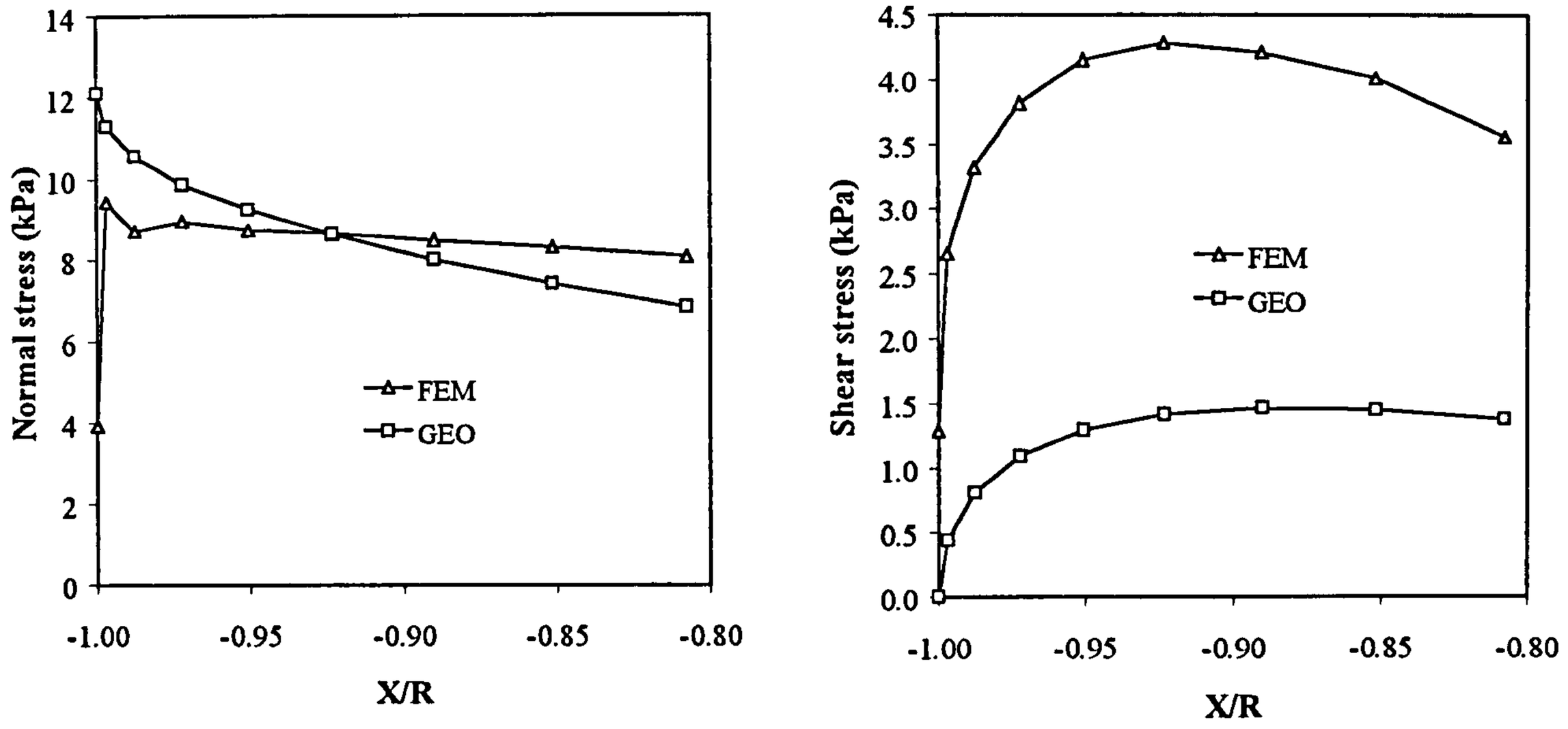

Figure 3.6b Call-outs from Figure 3.6a for X/R = -0.8 to -1.0

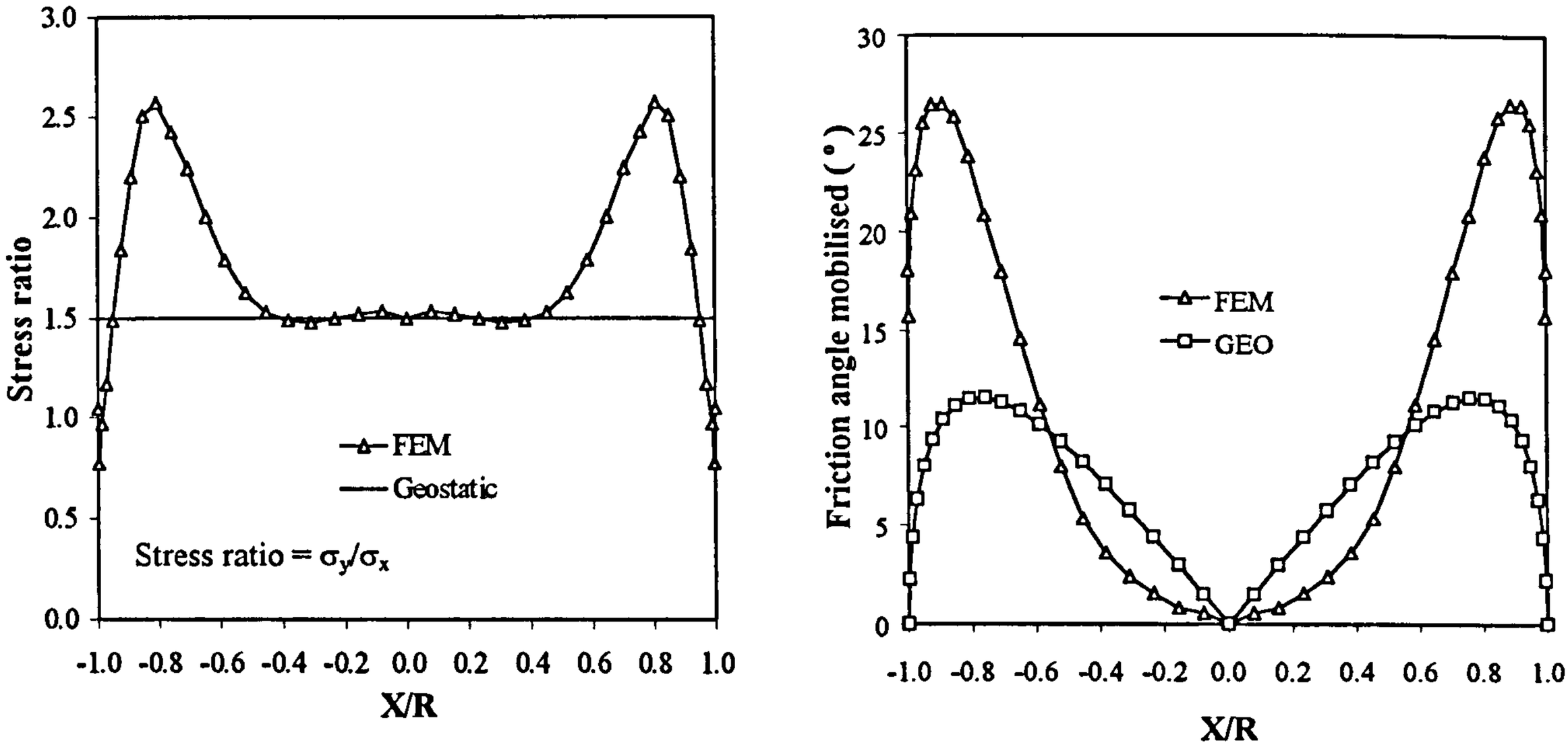

Figure 3.7 Stress ratio and friction angle mobilised, self-weight only

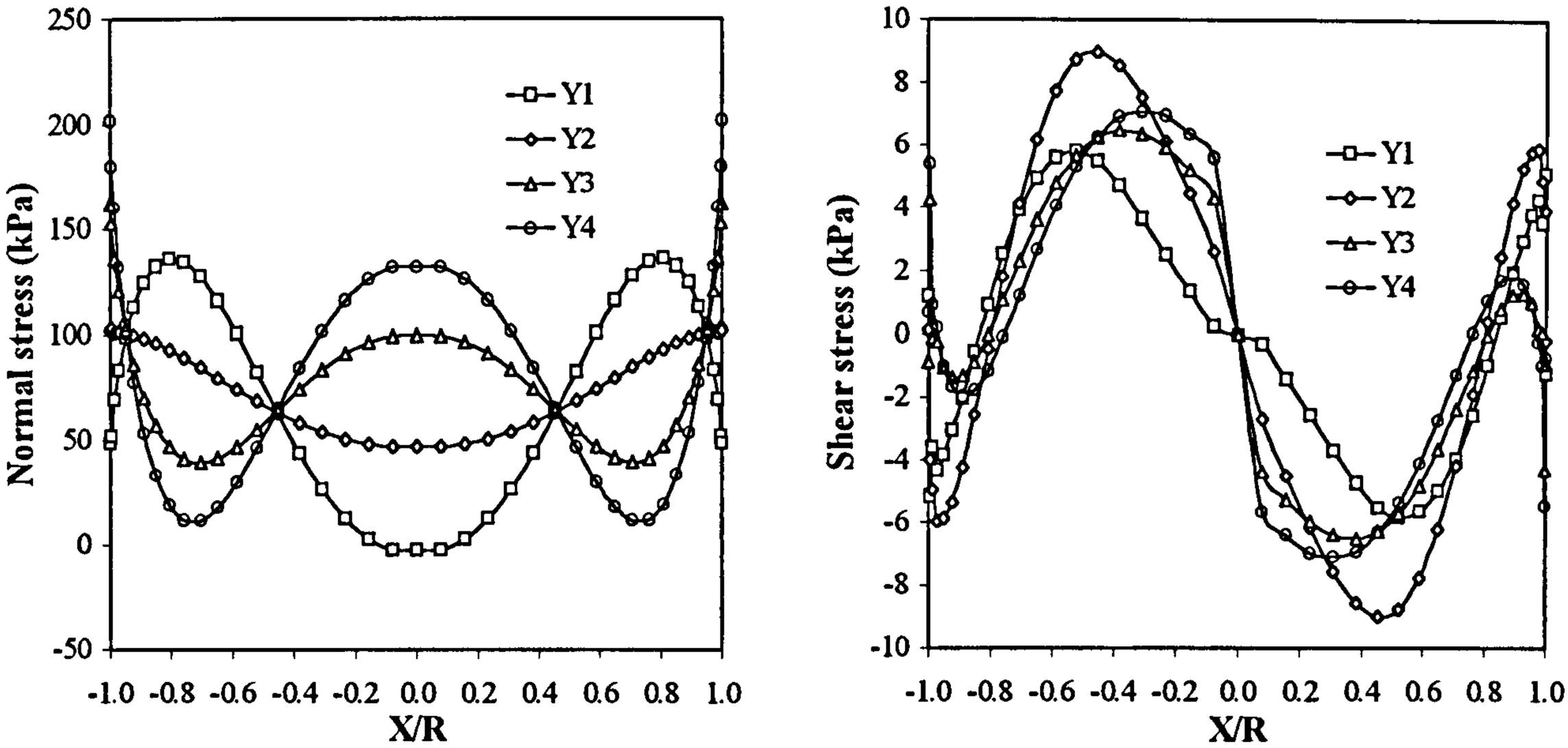

Figure 3.8 Stresses through the arch ring, self-weight only, FEM

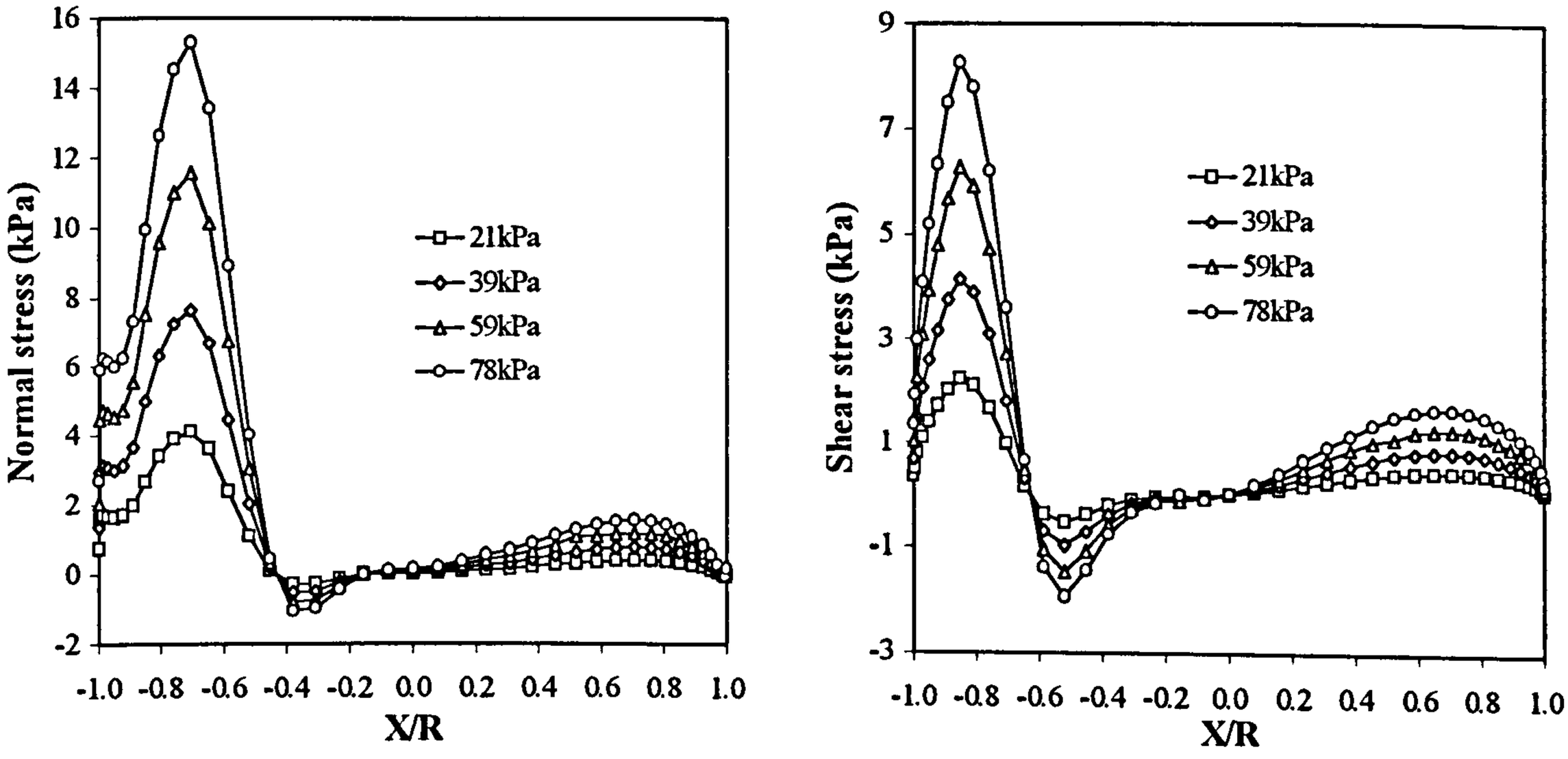

Figure 3.9 Stresses on the arch extrados, load at (X/R) = -1.0, FEM

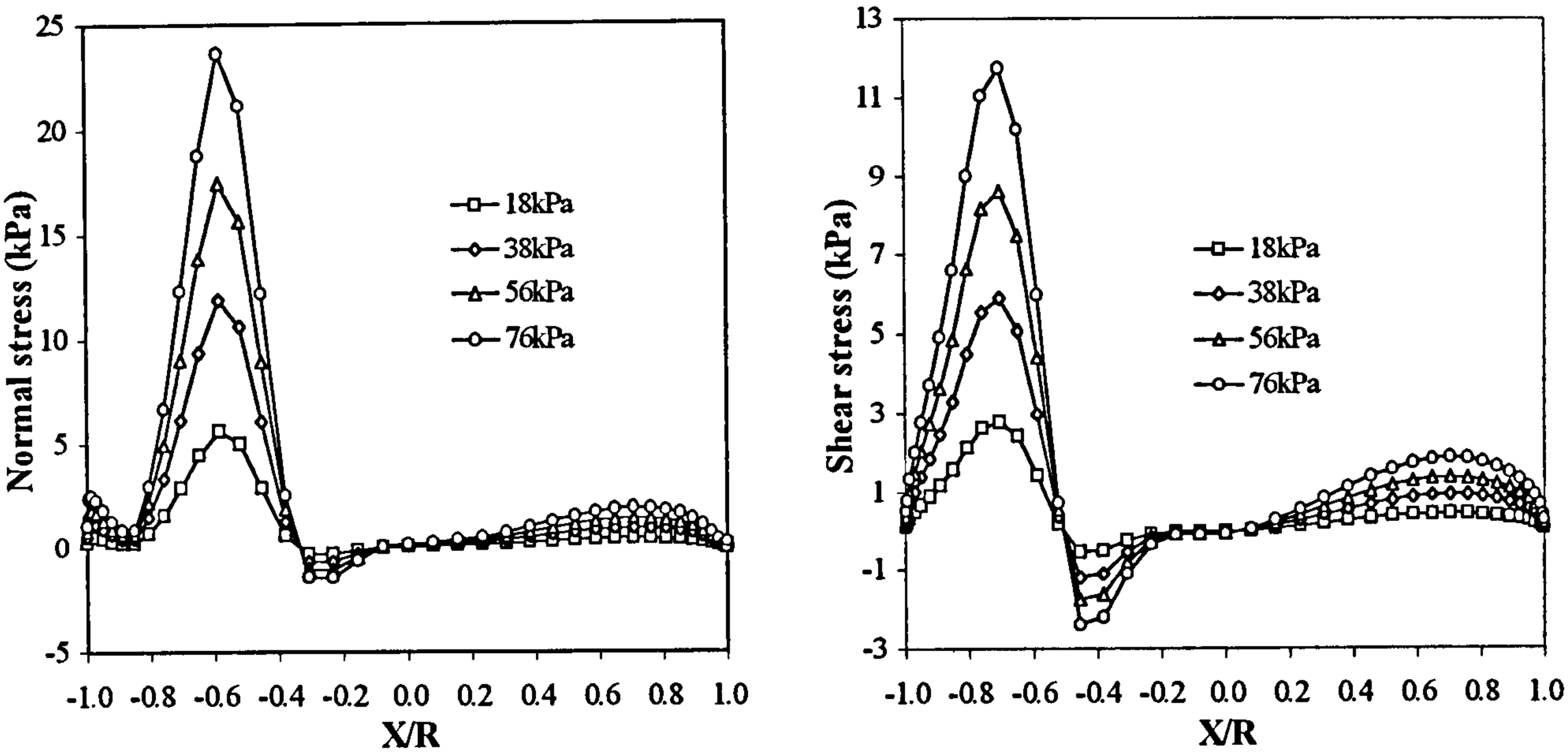

Figure 3.10 Stresses on the arch extrados, load at (X/R) = -0.75, FEM

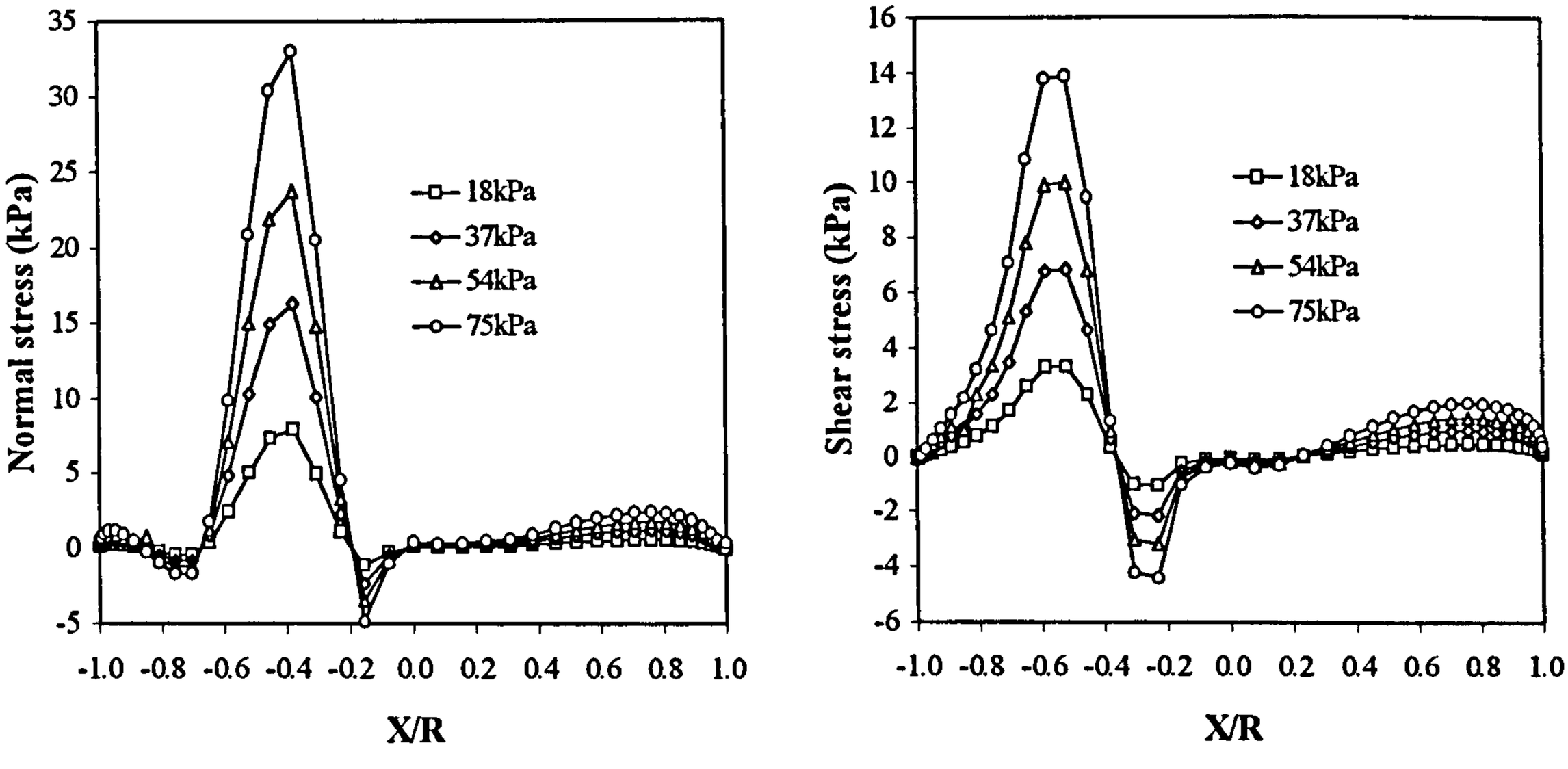

Figure 3.11 Stresses on the arch extrados, load at (X/R) = -0.5, FEM

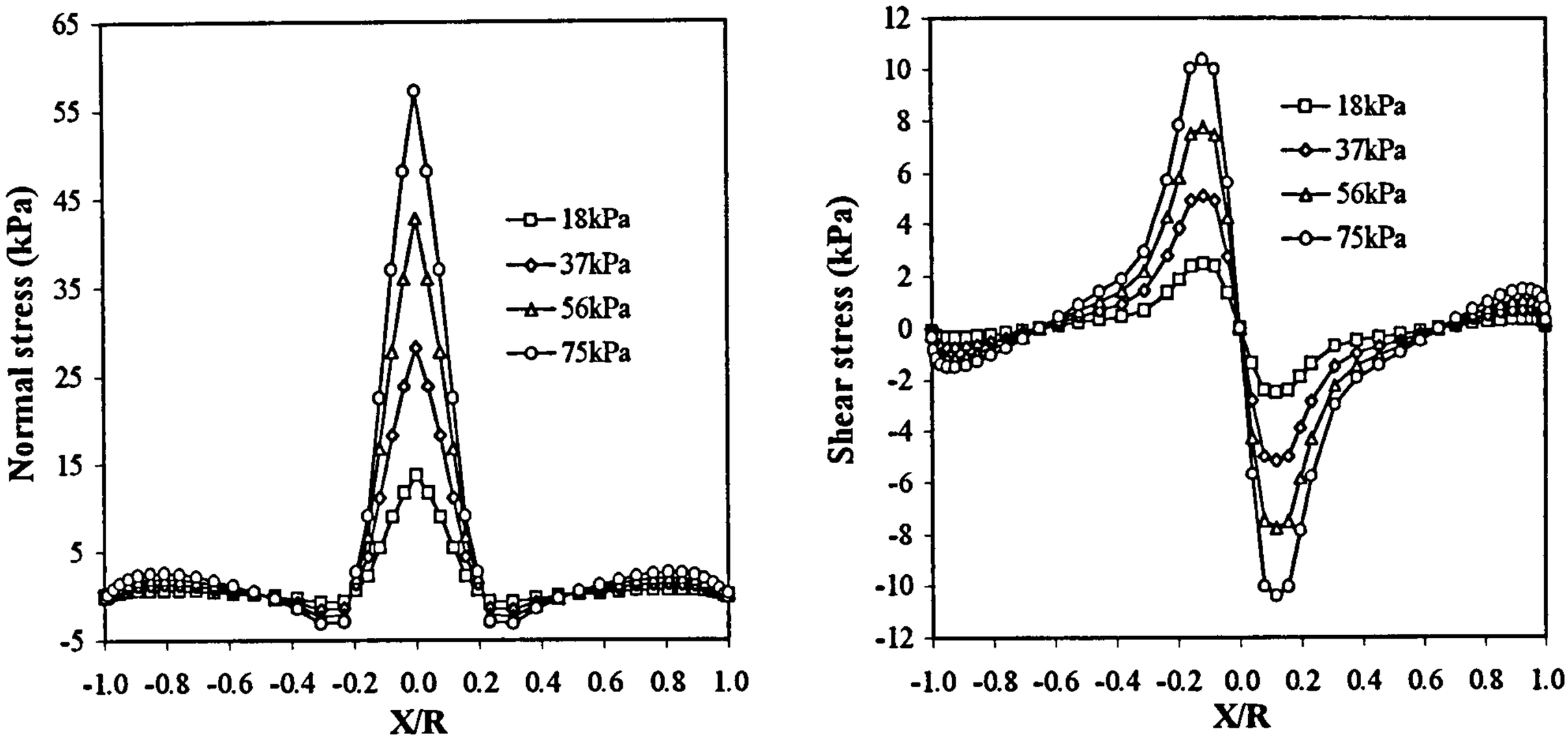

Figure 3.12 Stresses on the arch extrados, load at (X/R) = 0.0, FEM

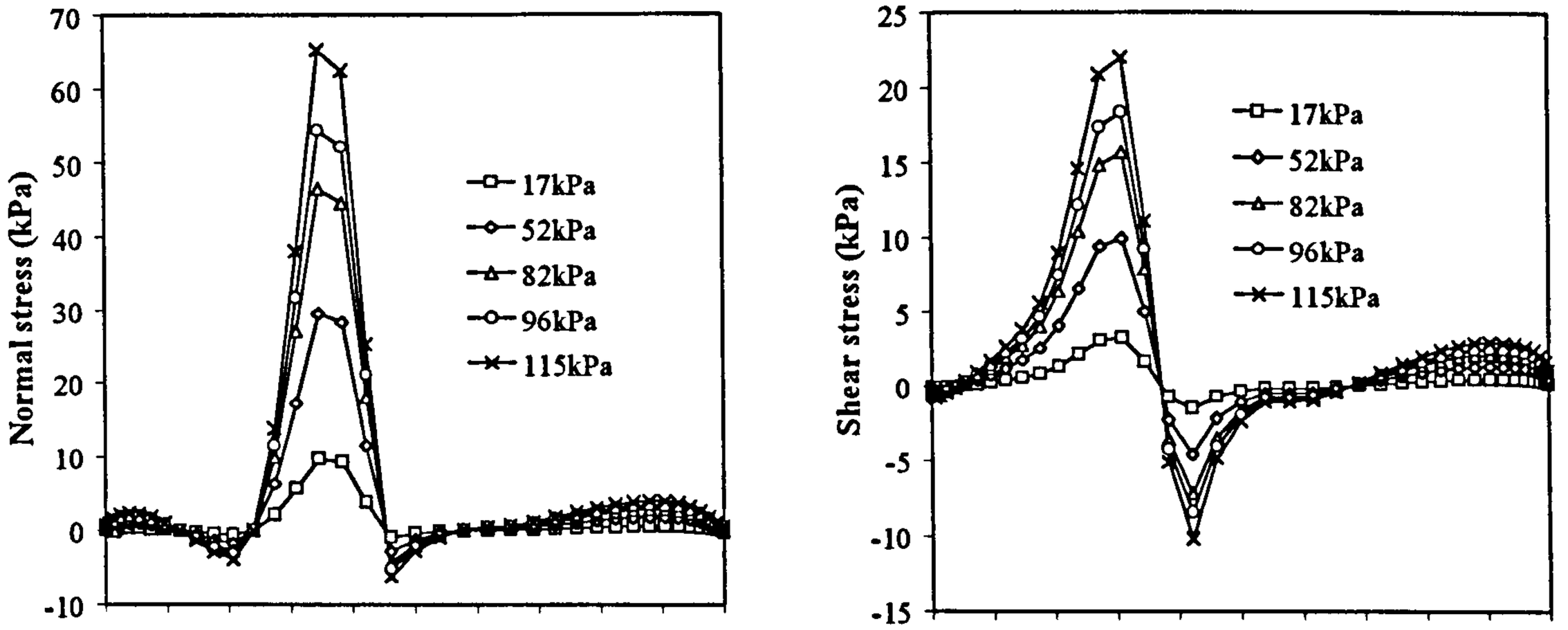

Figure 3.13 Stresses on the arch extrados, load at (X/R) = -0.33, FEM

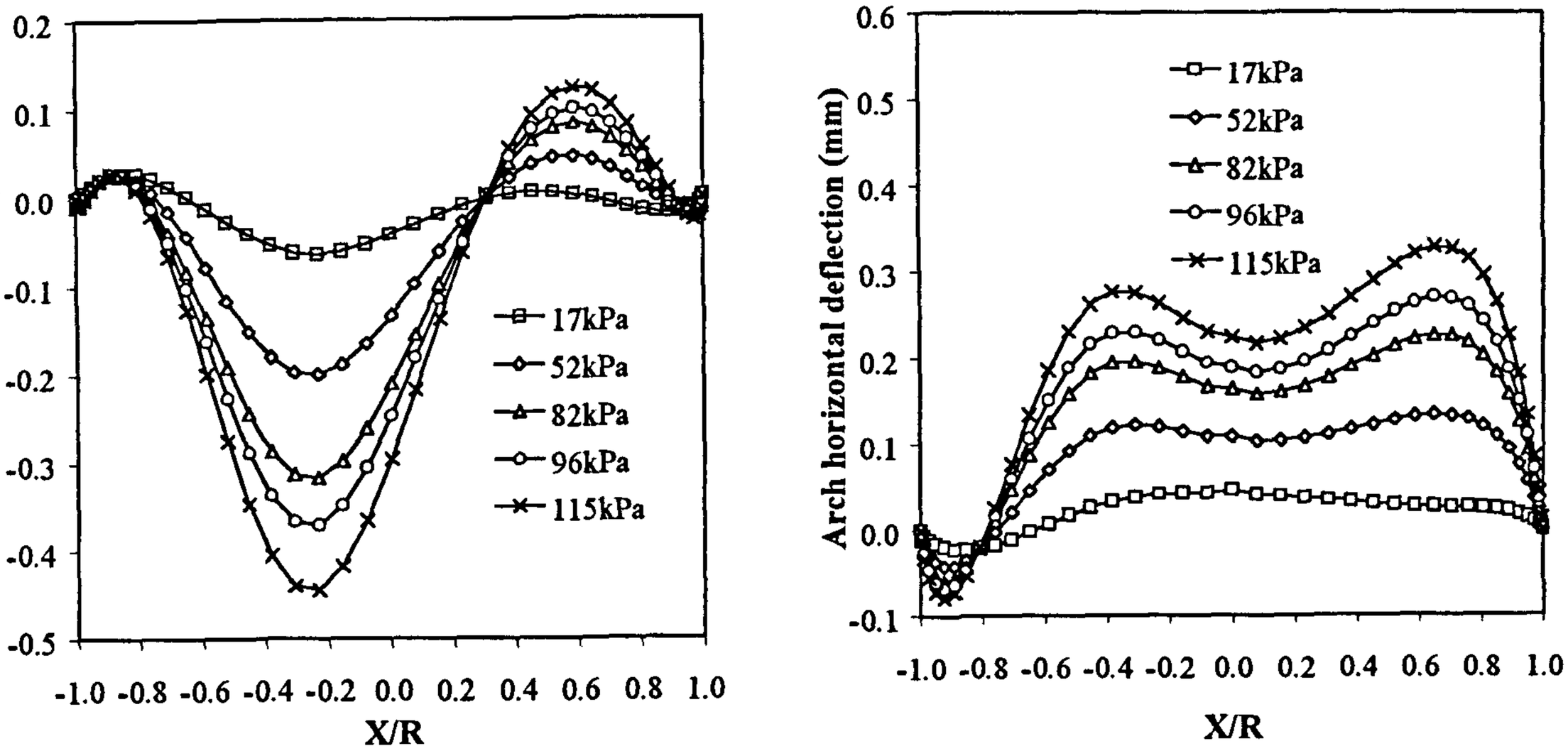

Figure 3.14 Arch deflections, load at (X/R) = -0.33, FEM

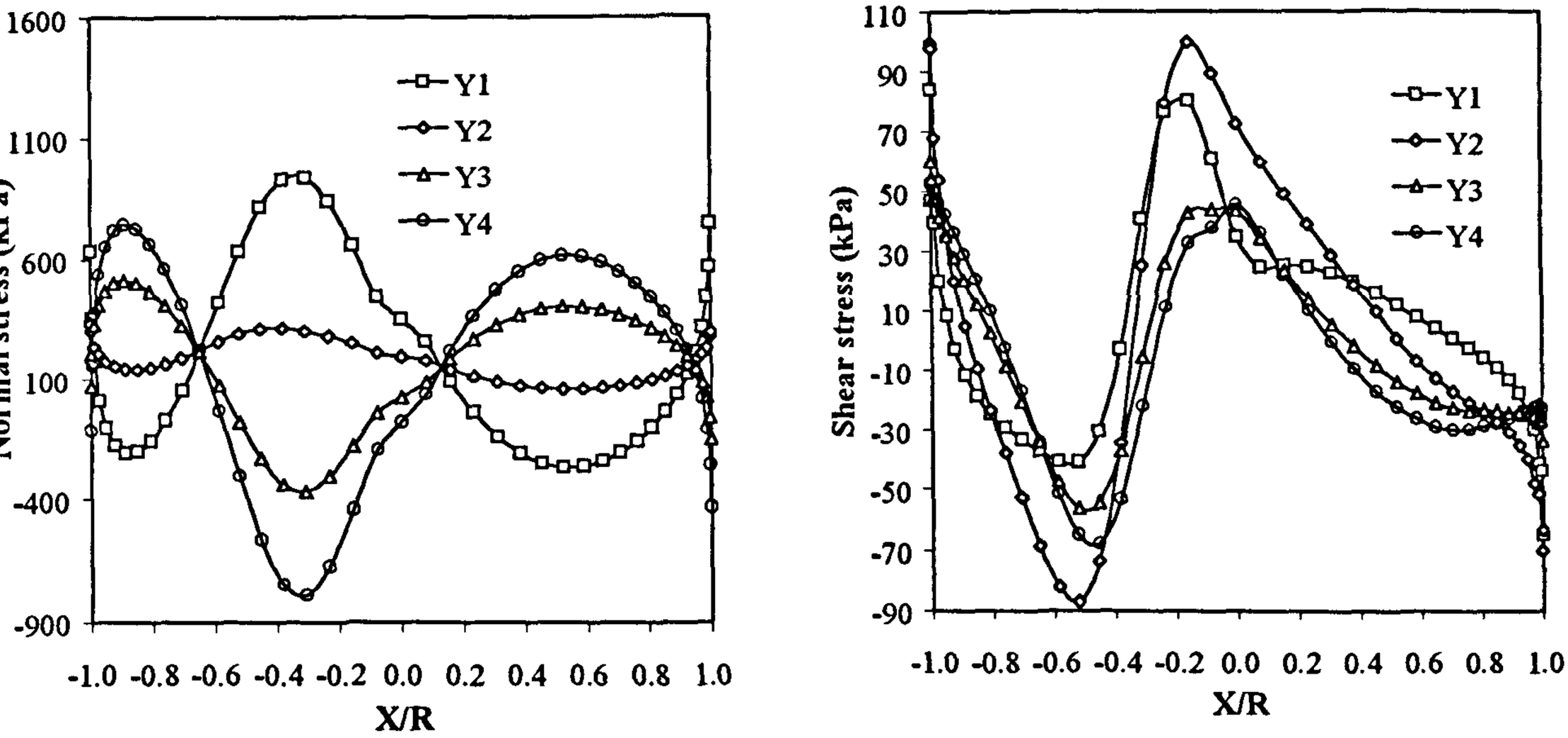

Figure 3.15 Stresses through the arch ring, load at (X/R) = -0.33, FEM

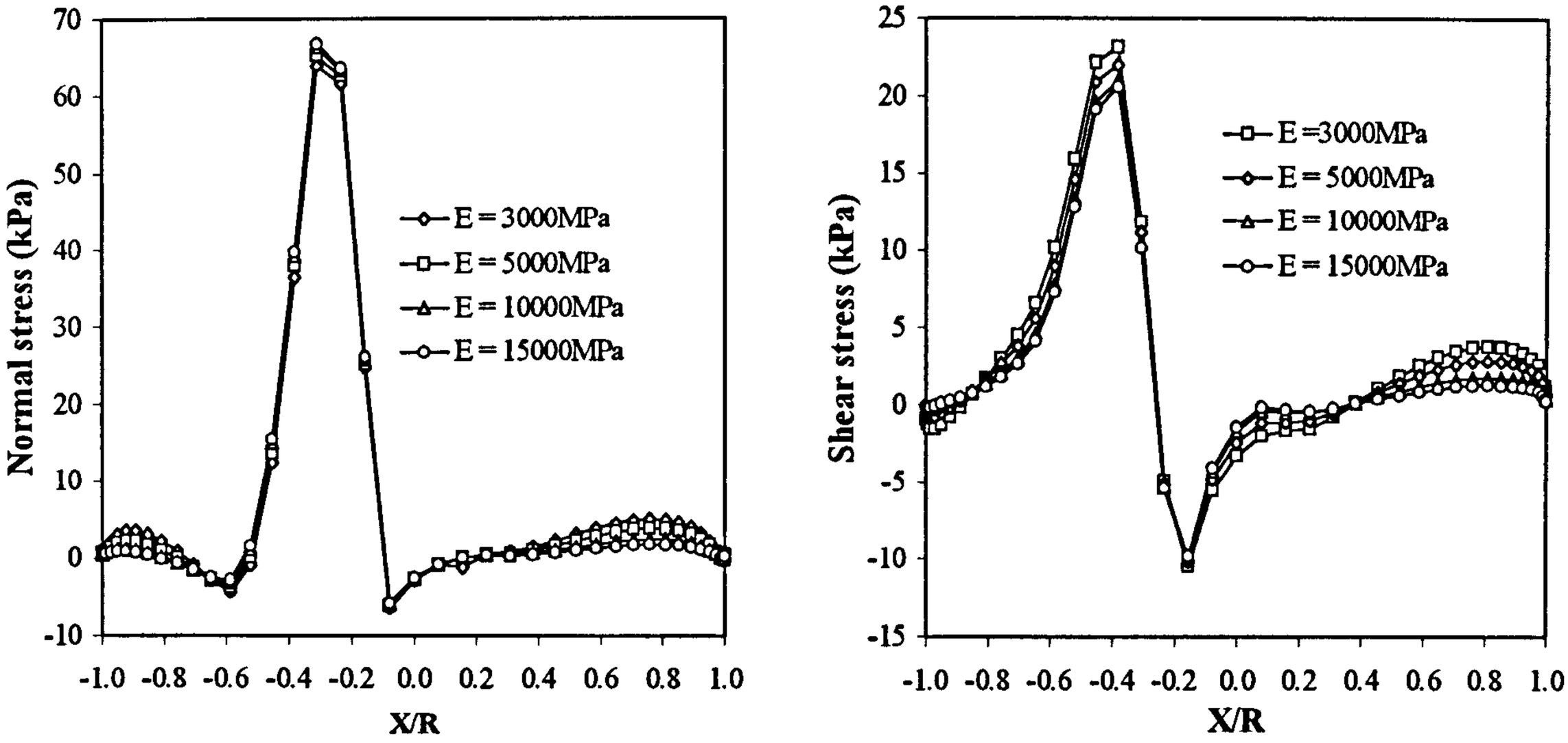

Figure 3.16 Stresses on the arch extrados for different arch moduli

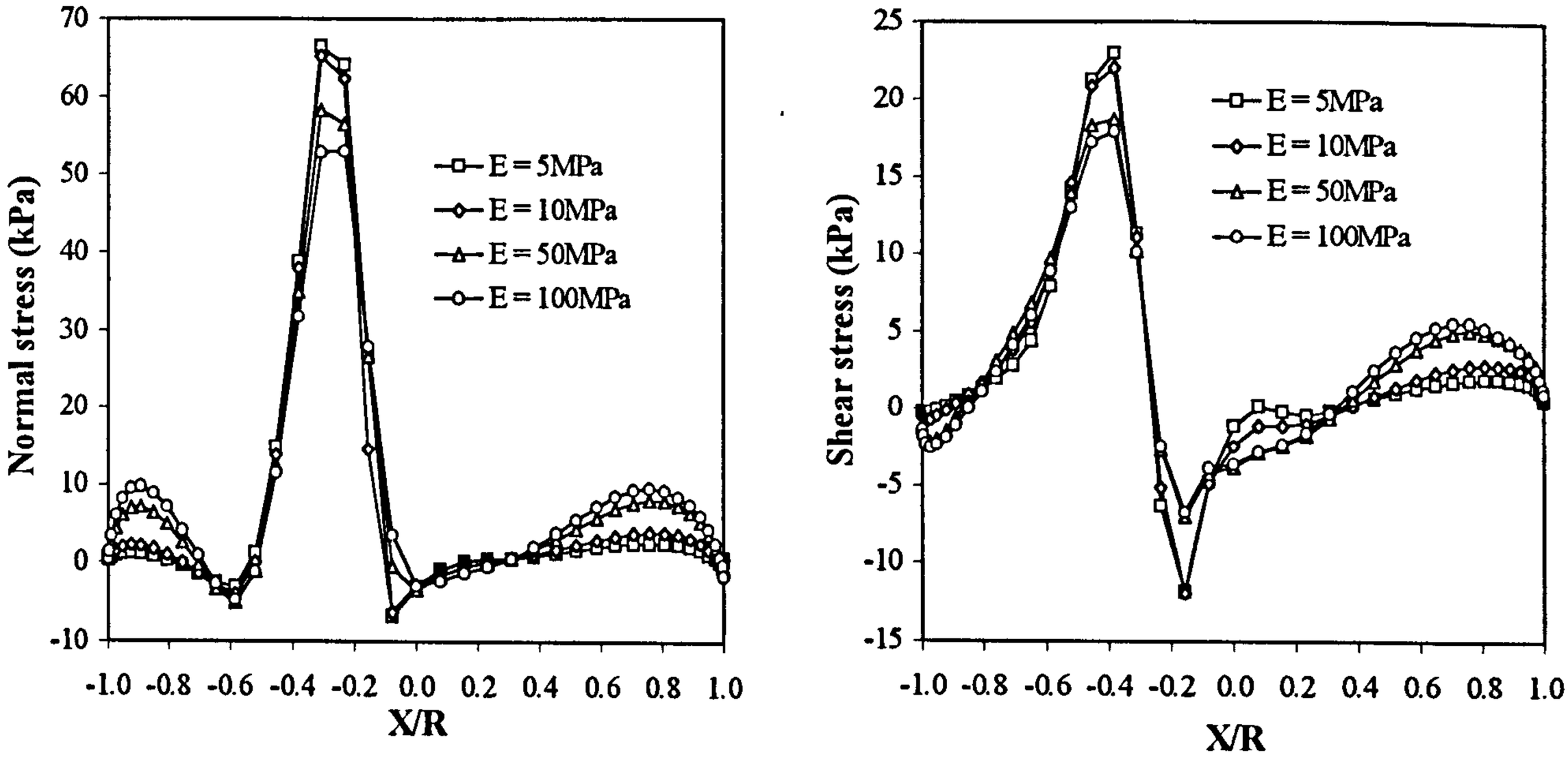

Figure 3.17 Stresses on the arch extrados for different backfill moduli

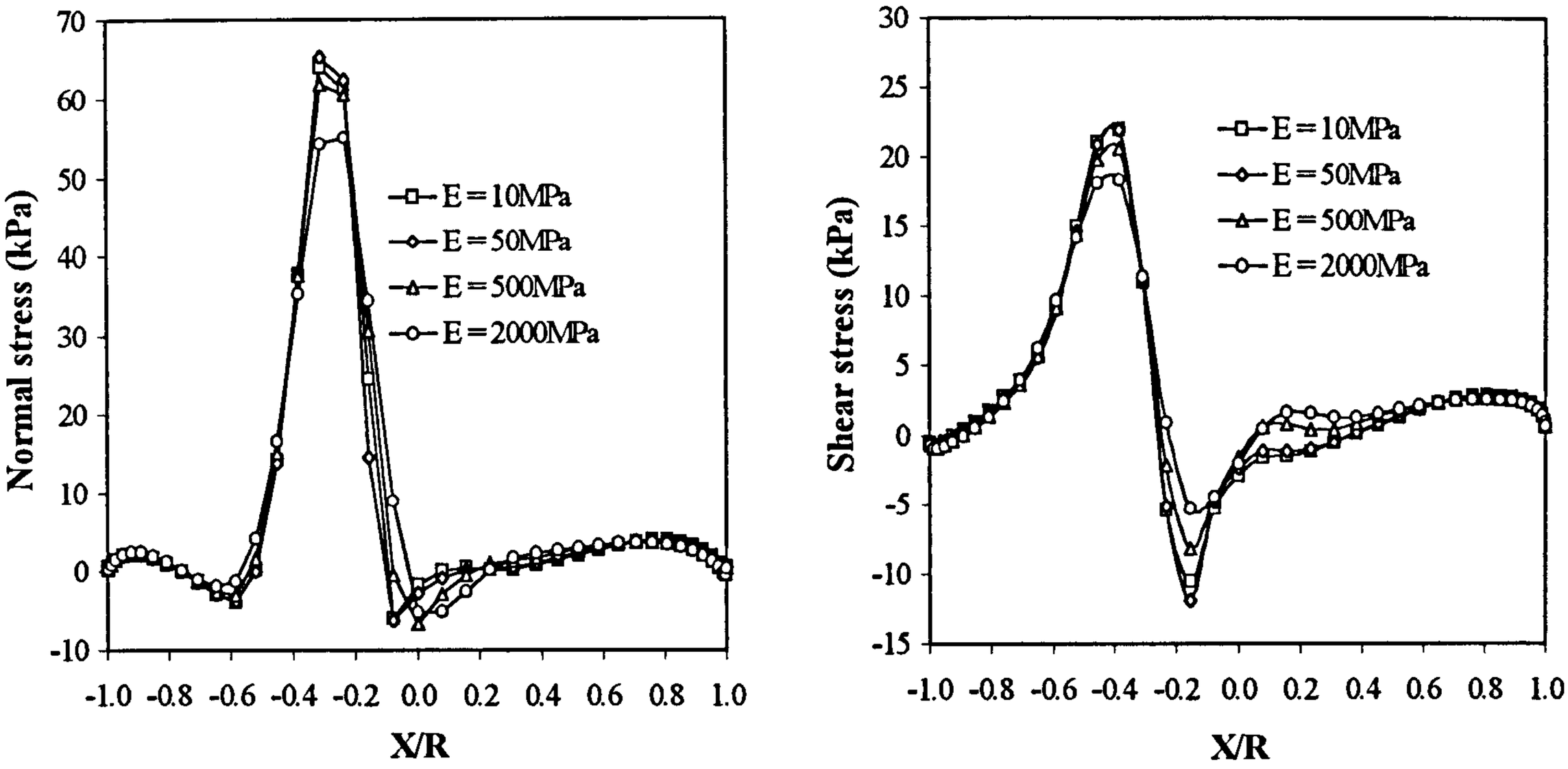

Figure 3.18 Stresses on the arch extrados for different pavement moduli

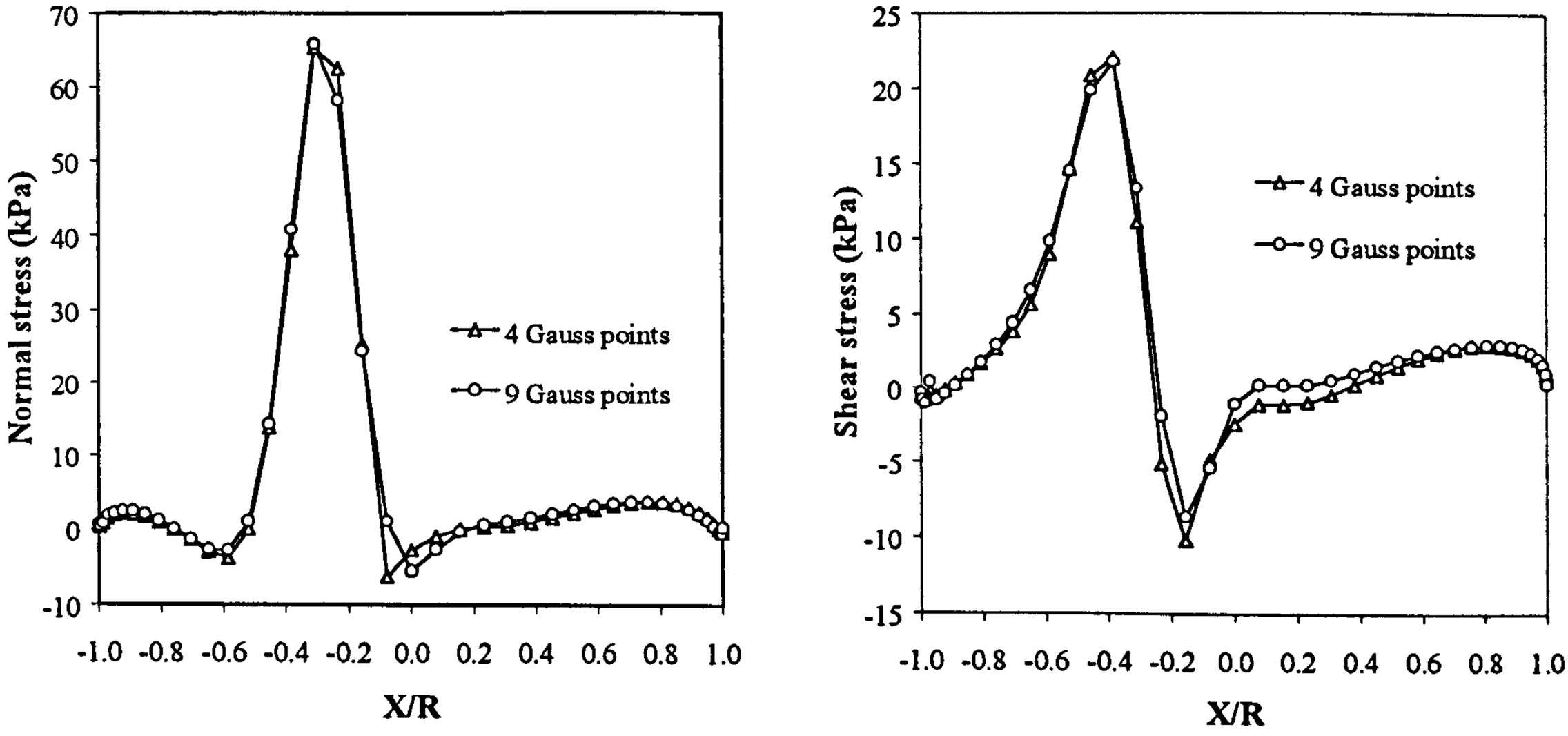

Figure 3.19 Stresses on the arch extrados for different integration methods

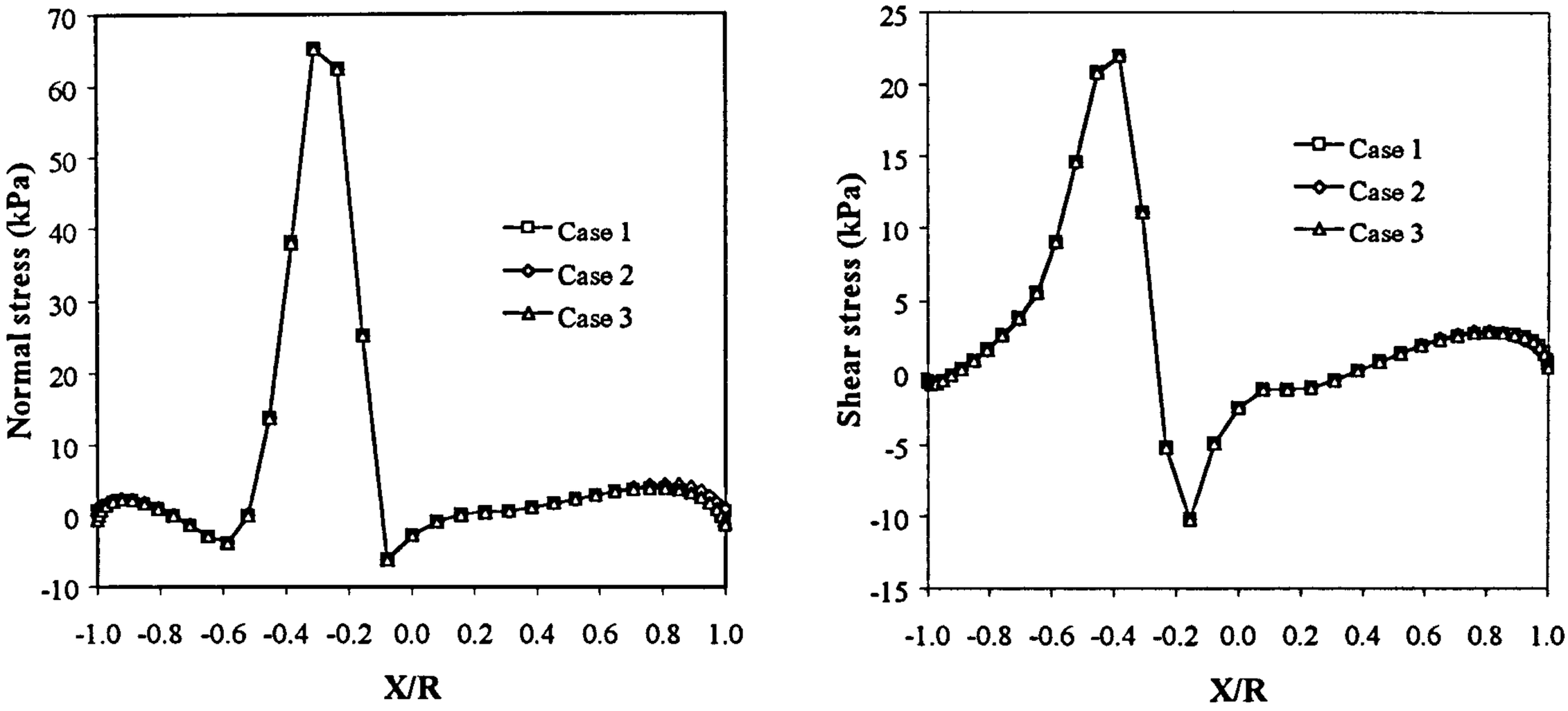

Figure 3.20a Stresses on the arch extrados for different support conditions

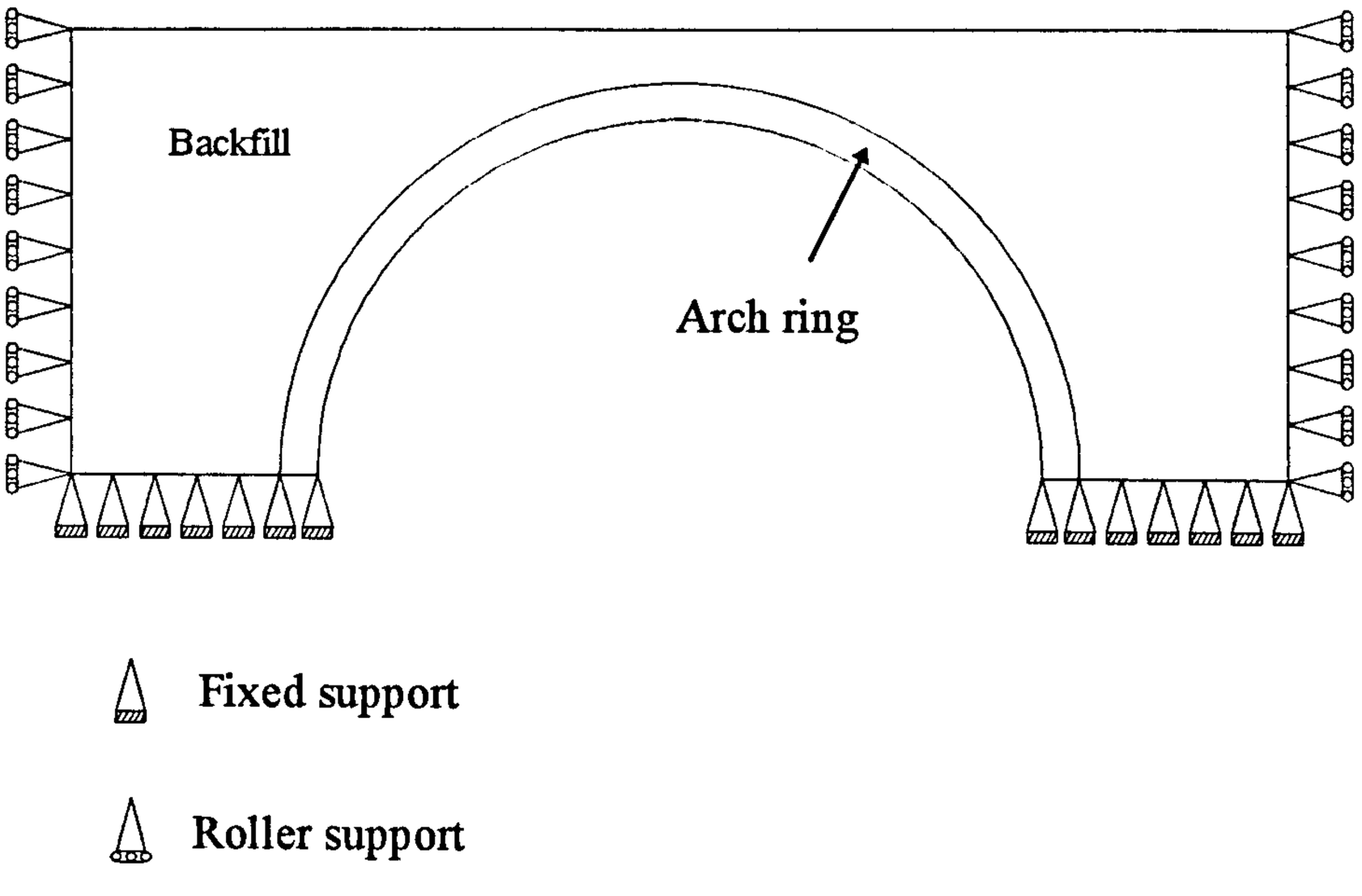

Figure 3.20b Support condition of Case 1

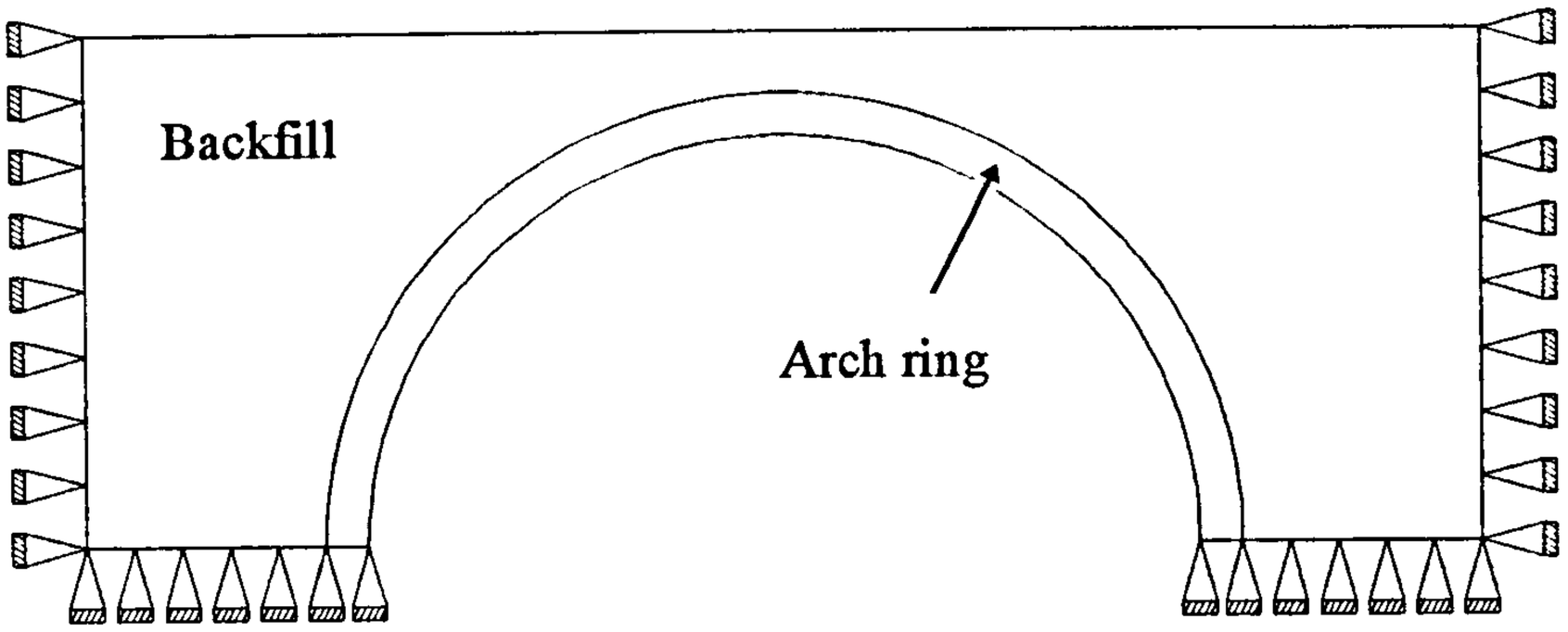

Fixed support

Figure 3.20c Support condition of Case 2

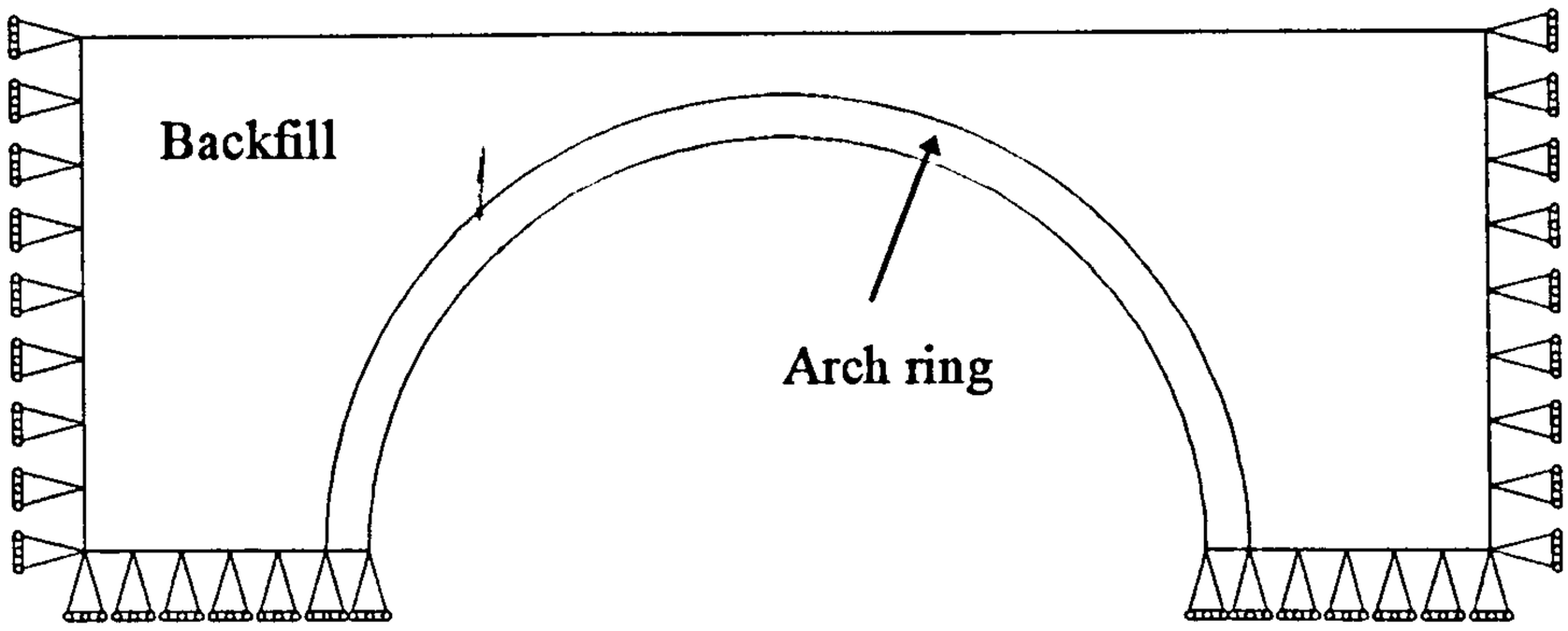

Roller support

Figure 3.20d Support condition of Case 3

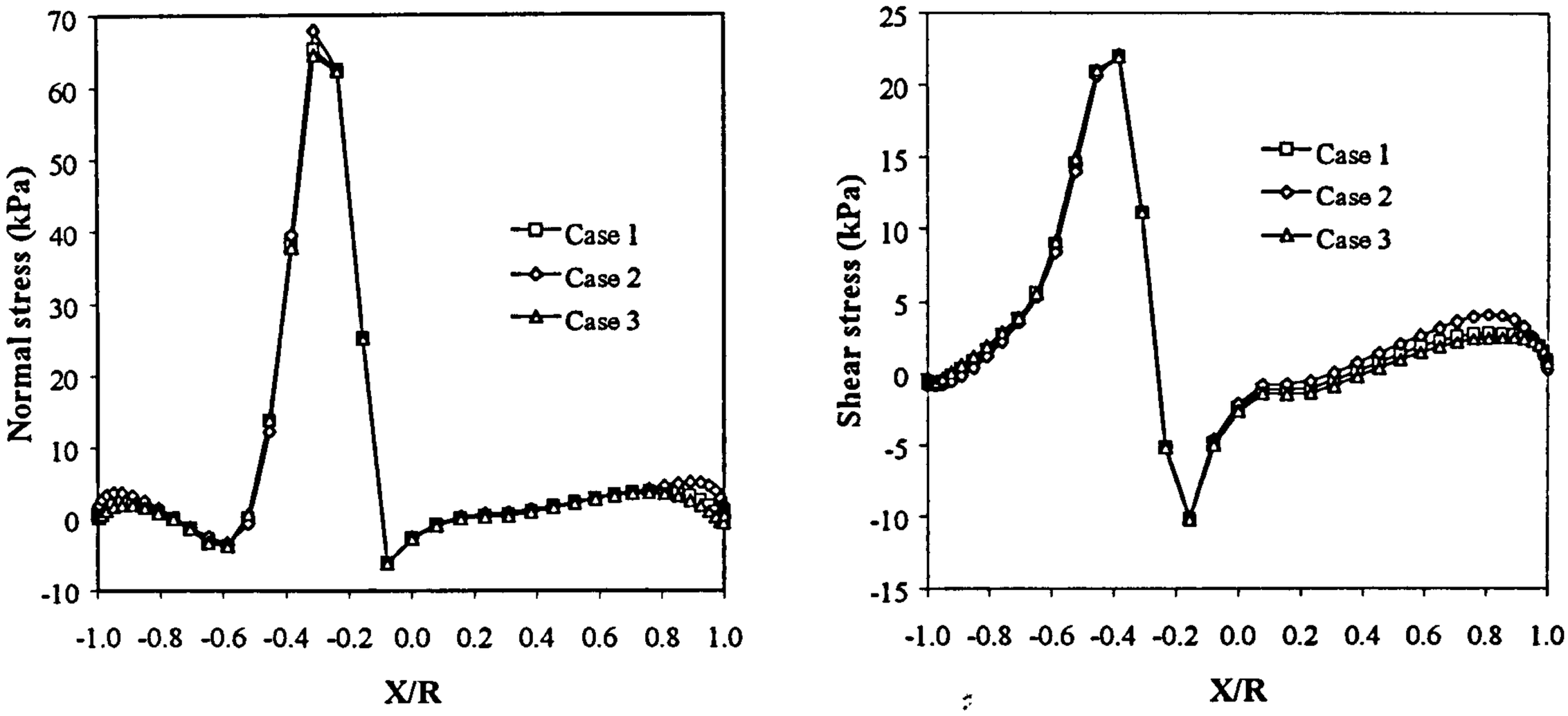

Figure 3.21a Stresses on the arch extrados for different boundary proximities

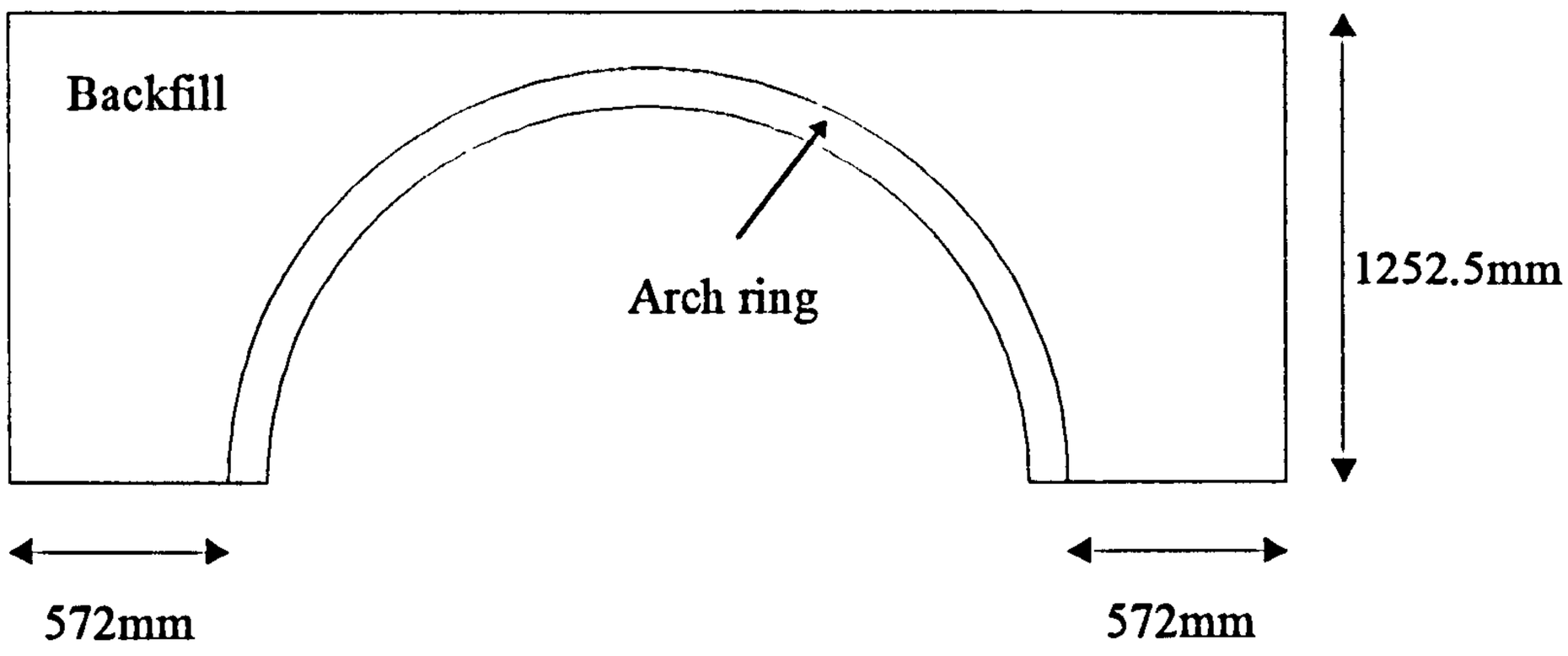

Figure 3.21b Wing walls of Case 1

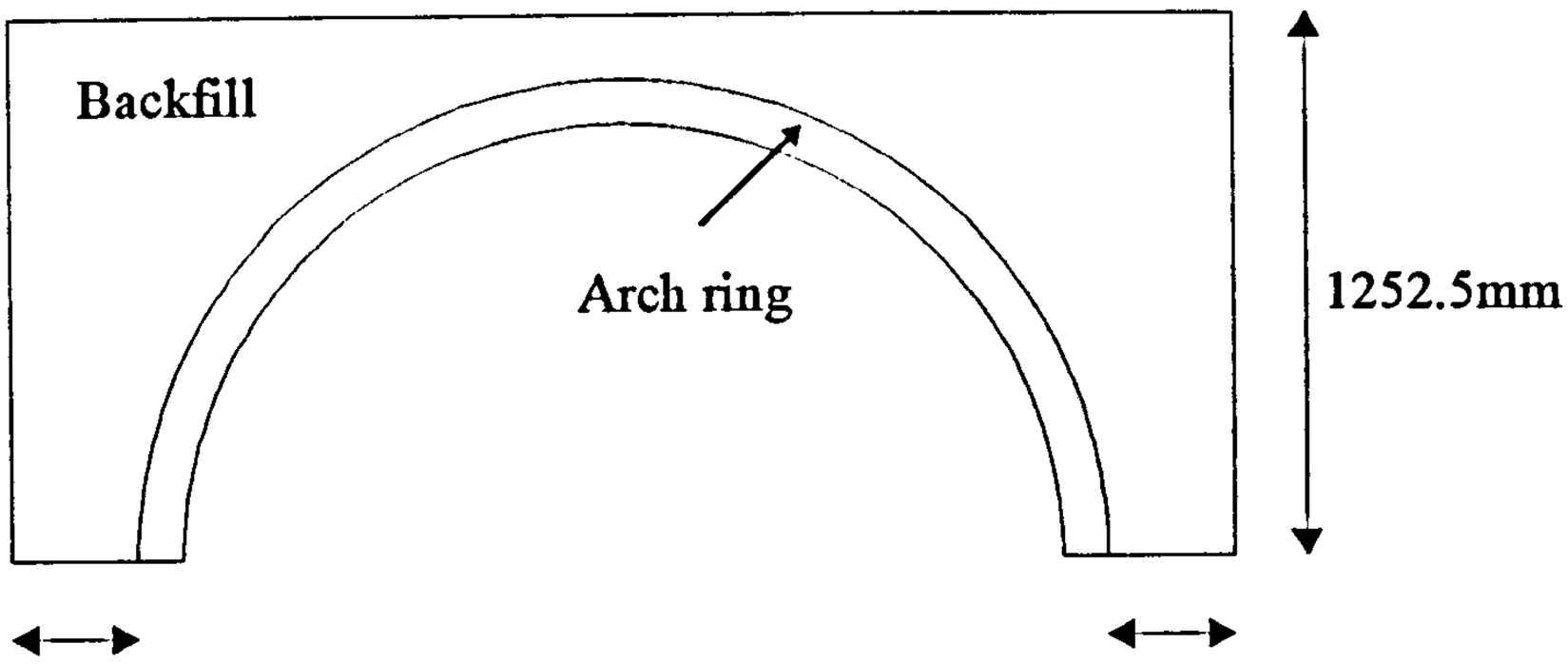

Figure 3.21c Wing walls of Case 2

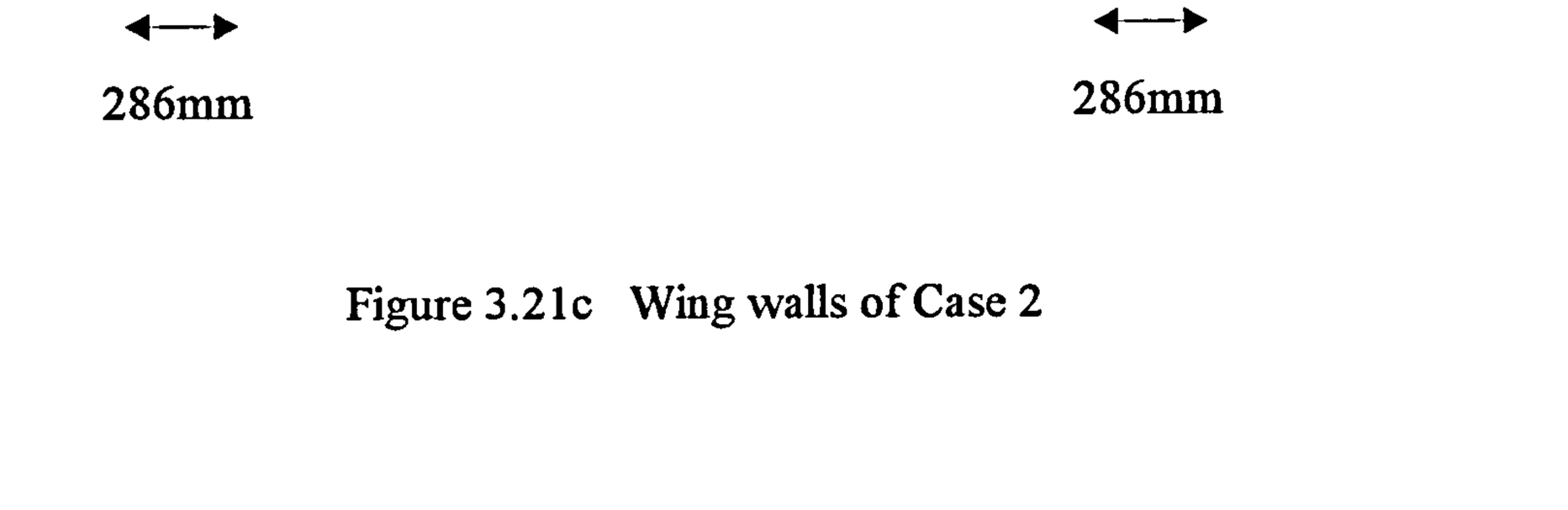

Figure 3.21d Wing walls of Case 3

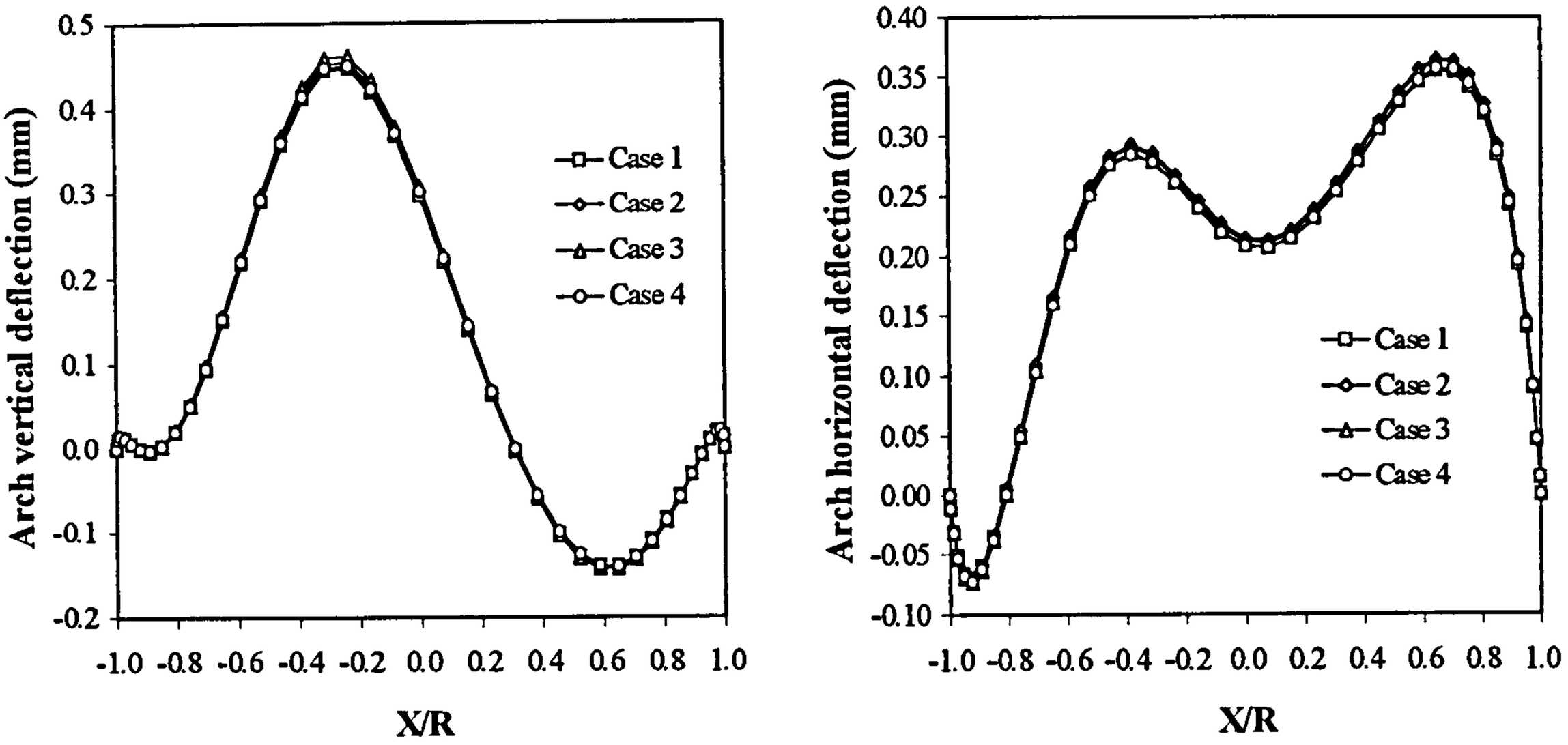

Figure 3.22 The difference between plane strain and plane stress

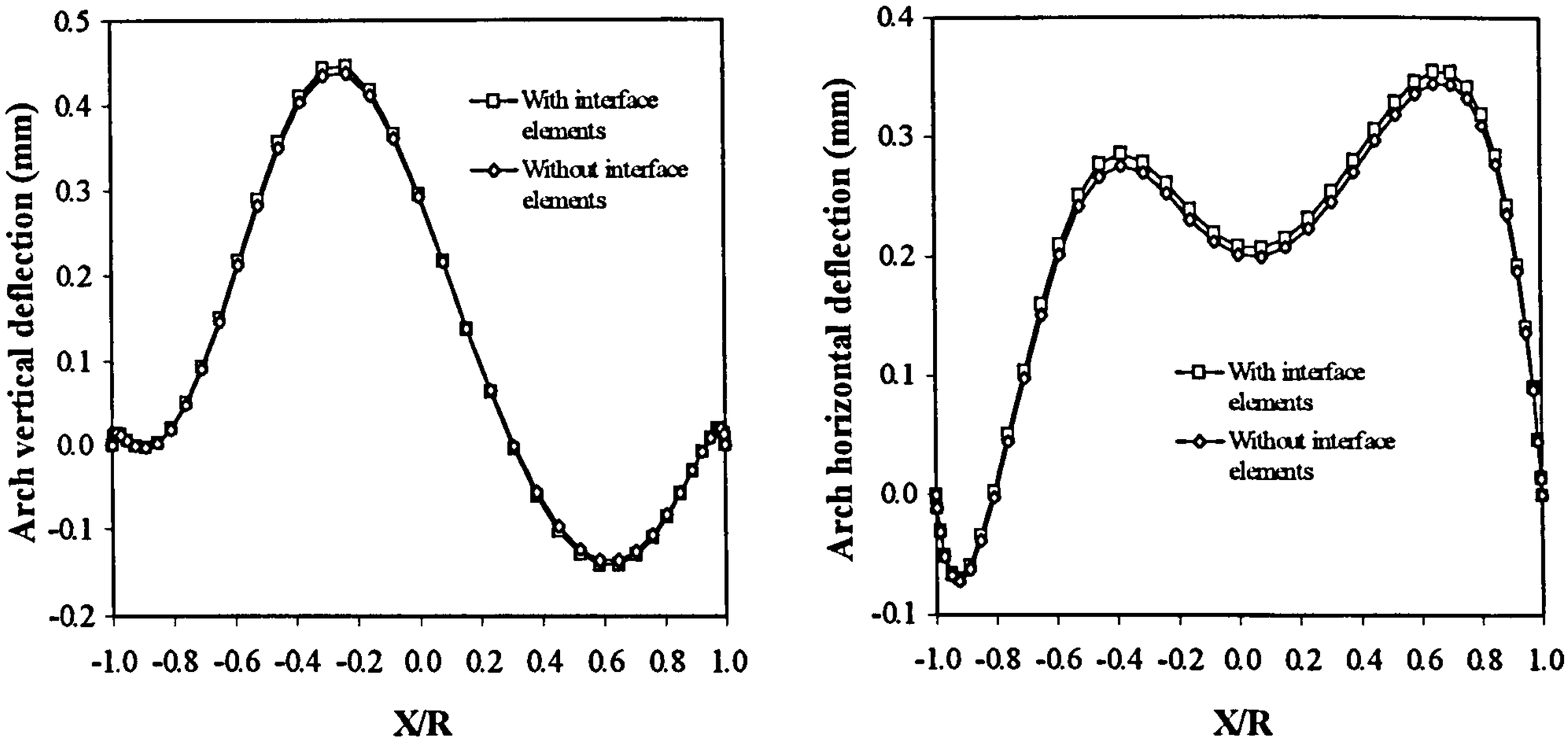

Figure 3.23 The effects of the interface element

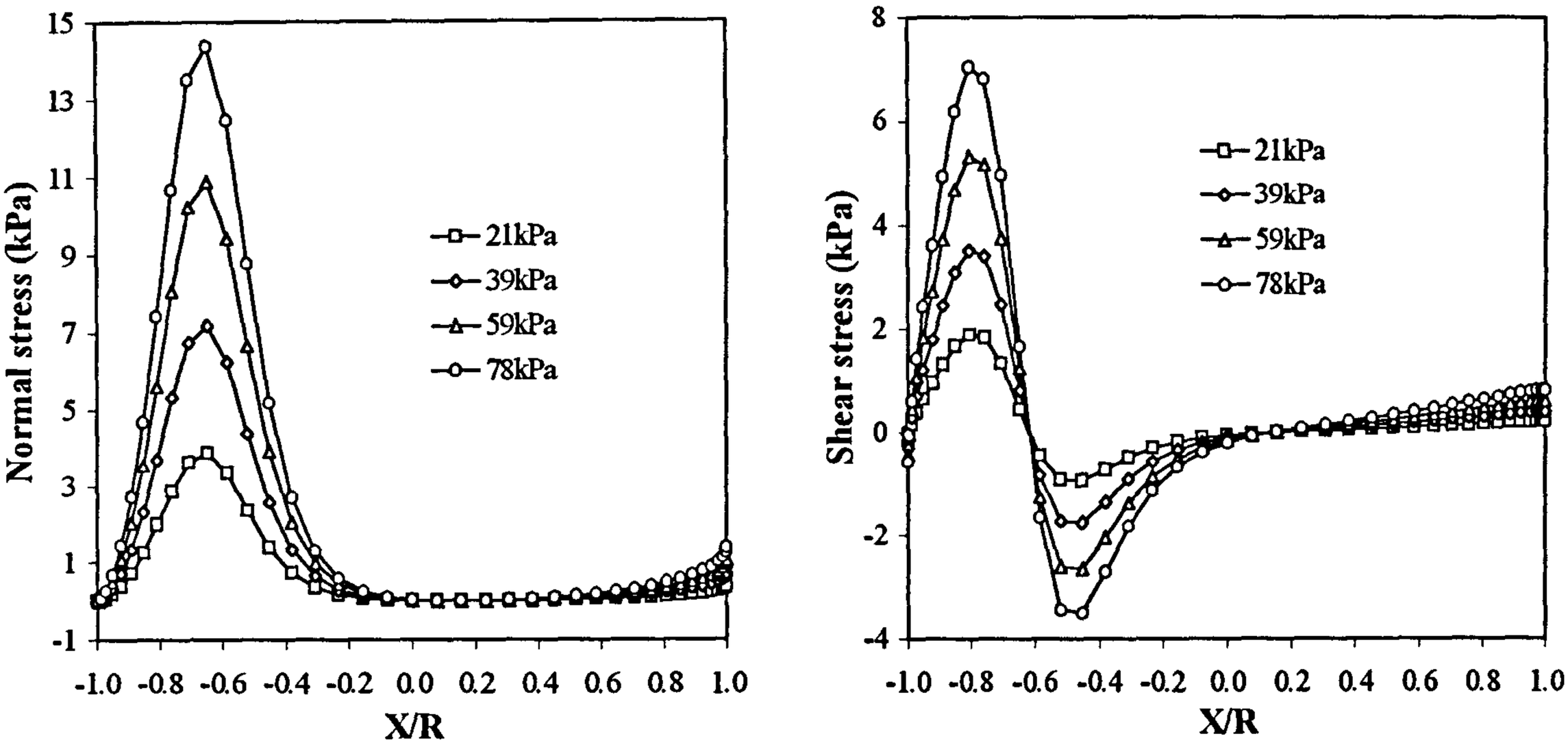

Figure 3.24 Stresses on the arch extrados, load at (X/R) = -1.0, Boussinesq's method

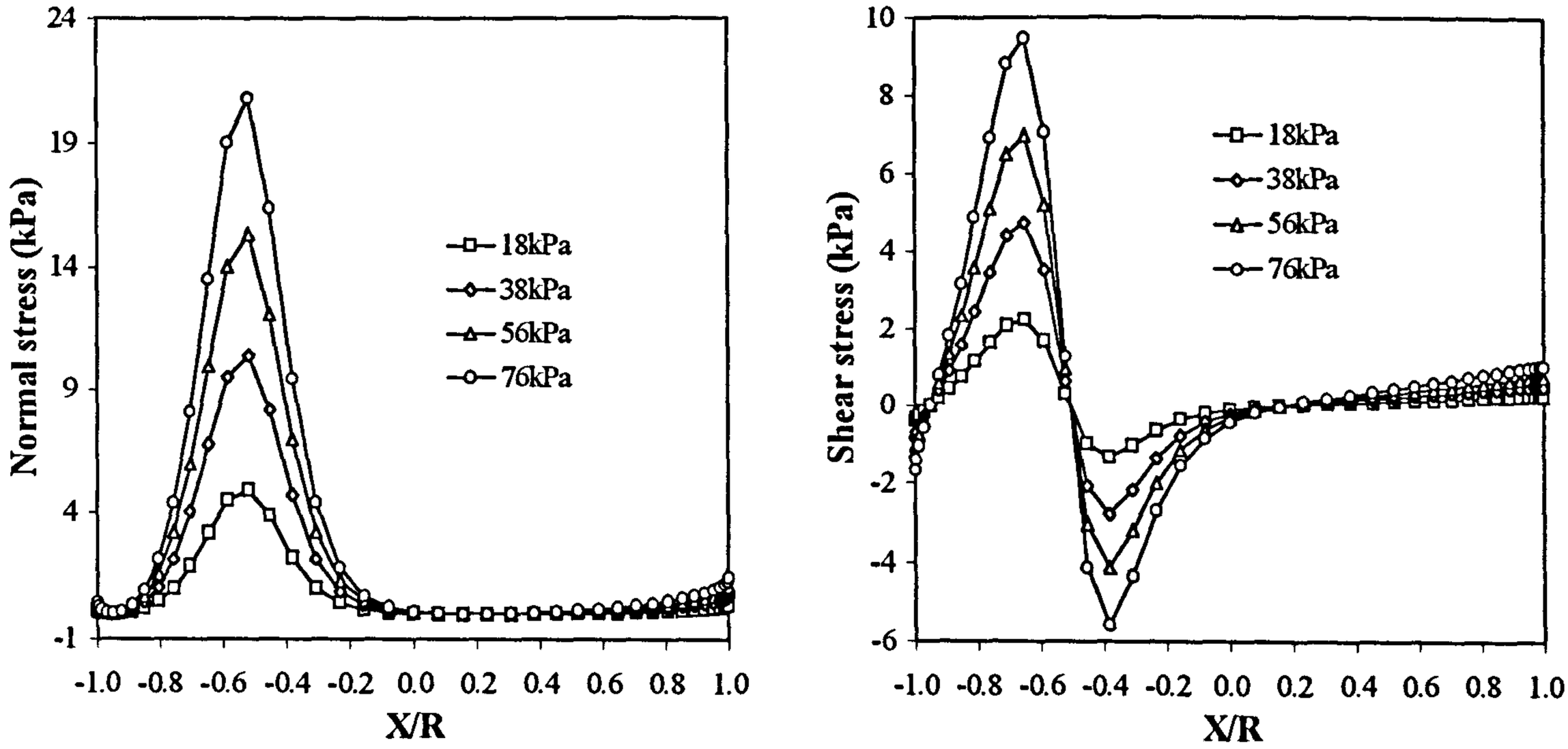

Figure 3.25 Stresses on the arch extrados, load at (X/R) = -0.75, Boussinesq's method

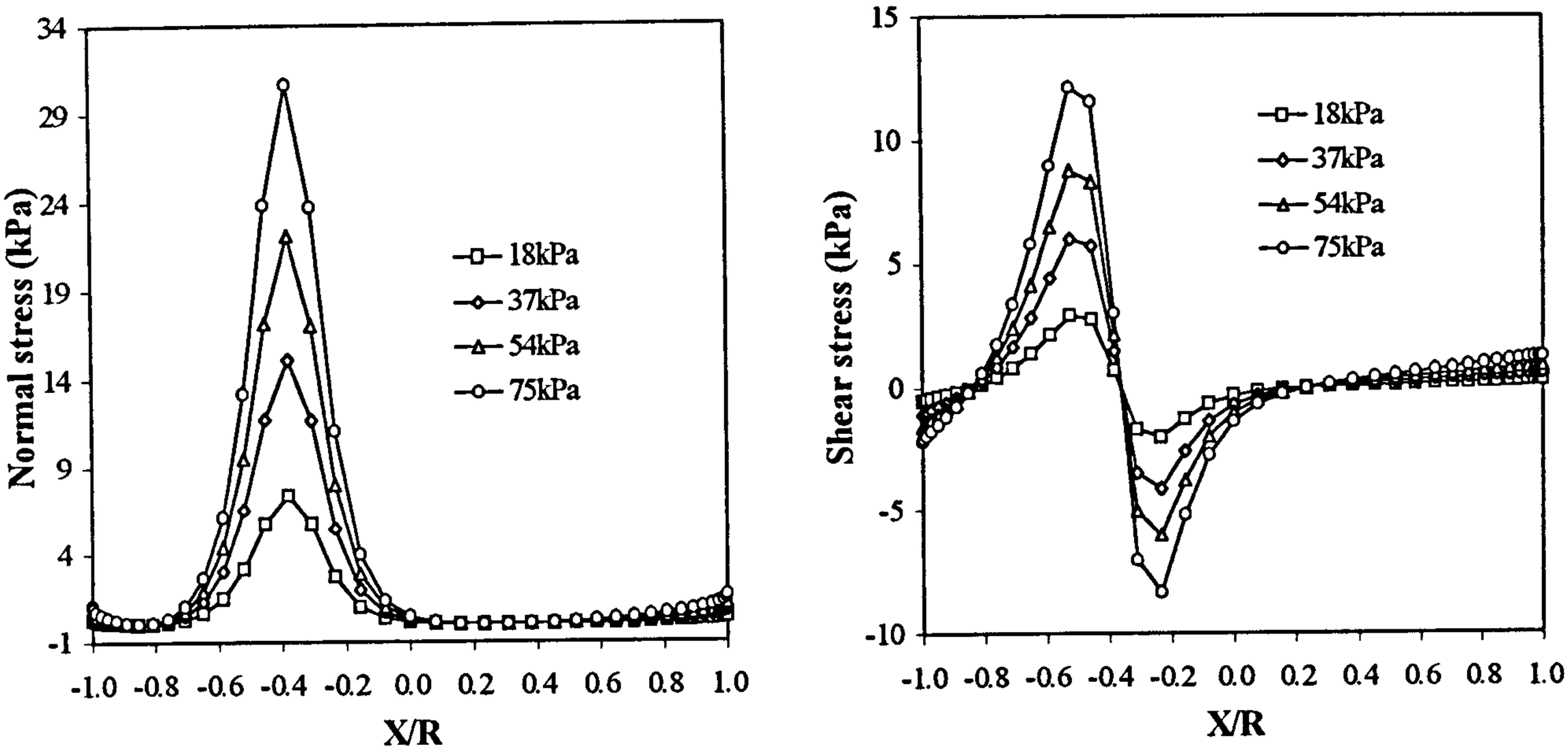

Figure 3.26 Stresses on the arch extrados, load at (X/R) = -0.50, Boussinesq's method

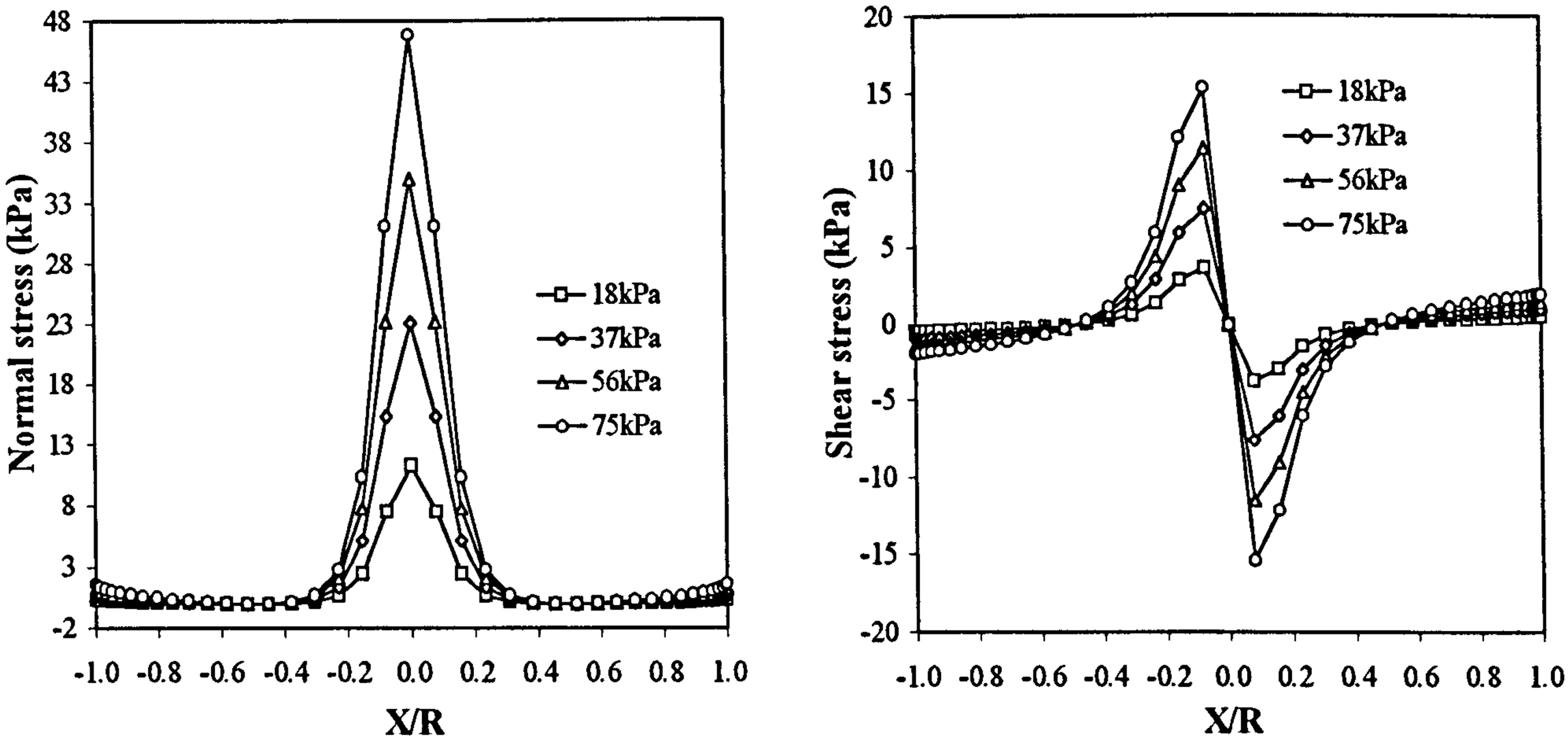

Figure 3.27 Stresses on the arch extrados, load at (X/R) = 0.0, Boussinesq's method

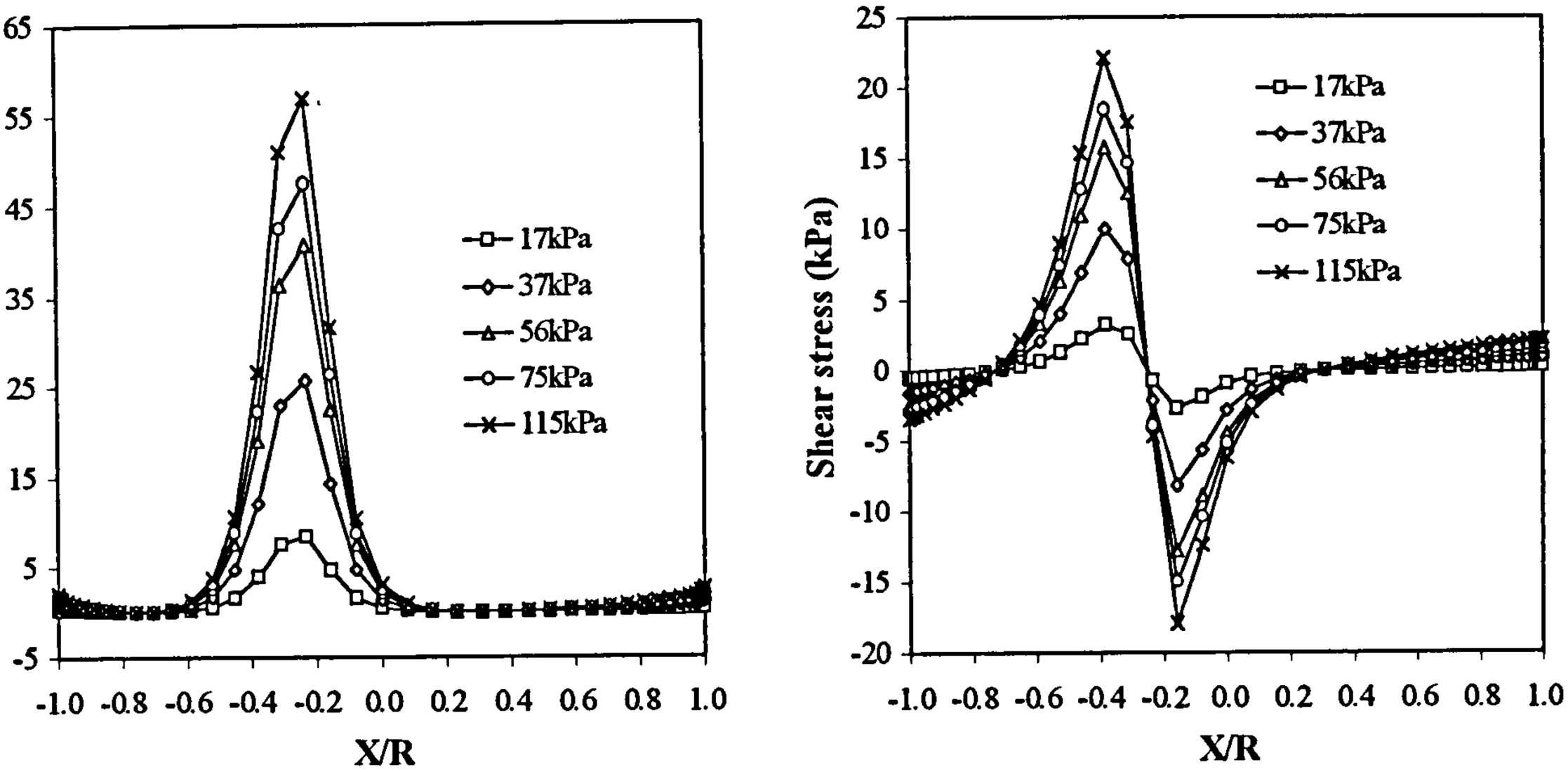

Figure 3.28 Stresses on the arch extrados, load at (X/R) = -0.33, Boussinesq's method

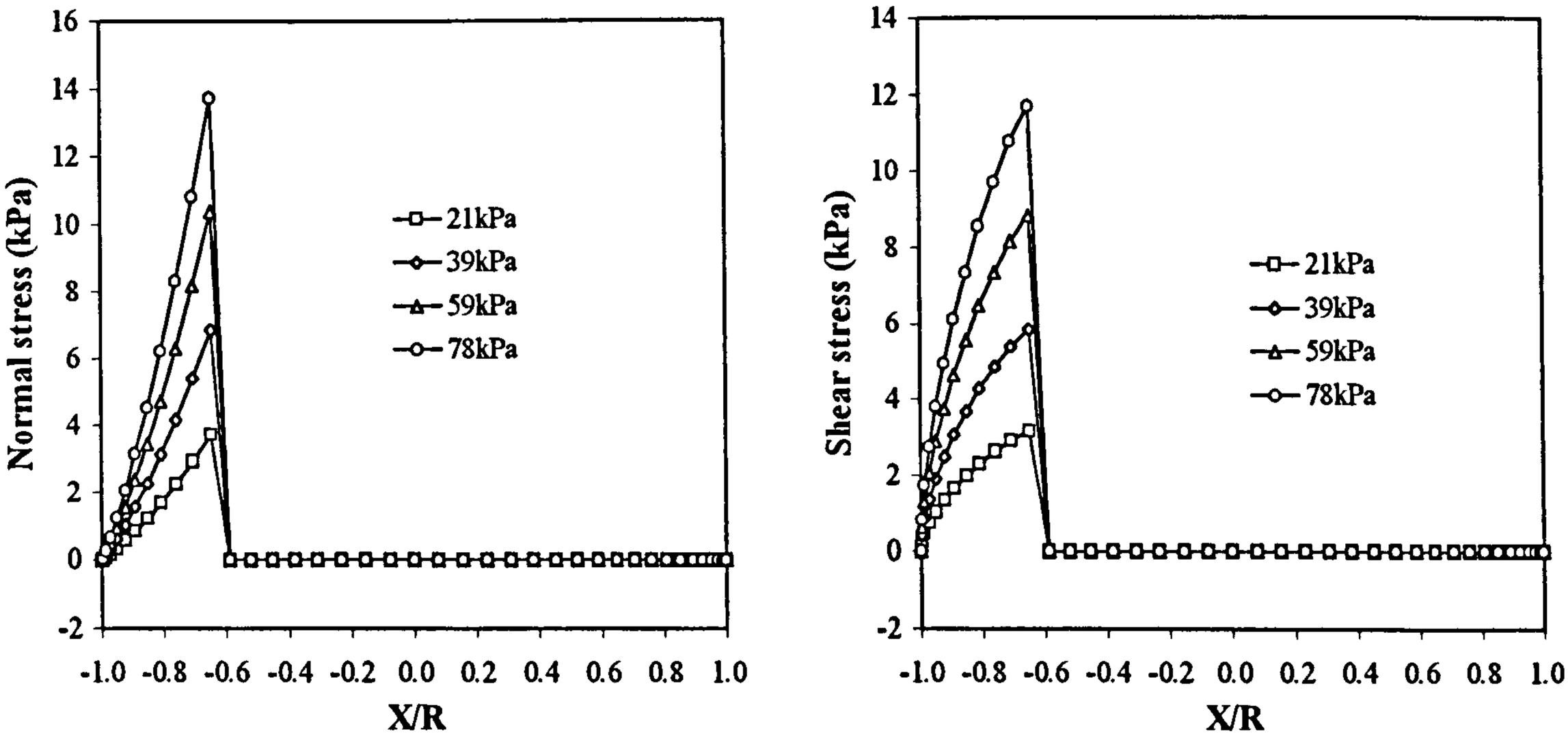

Figure 3.29 Stresses on the arch extrados, load at (X/R) = -1.0, codified method

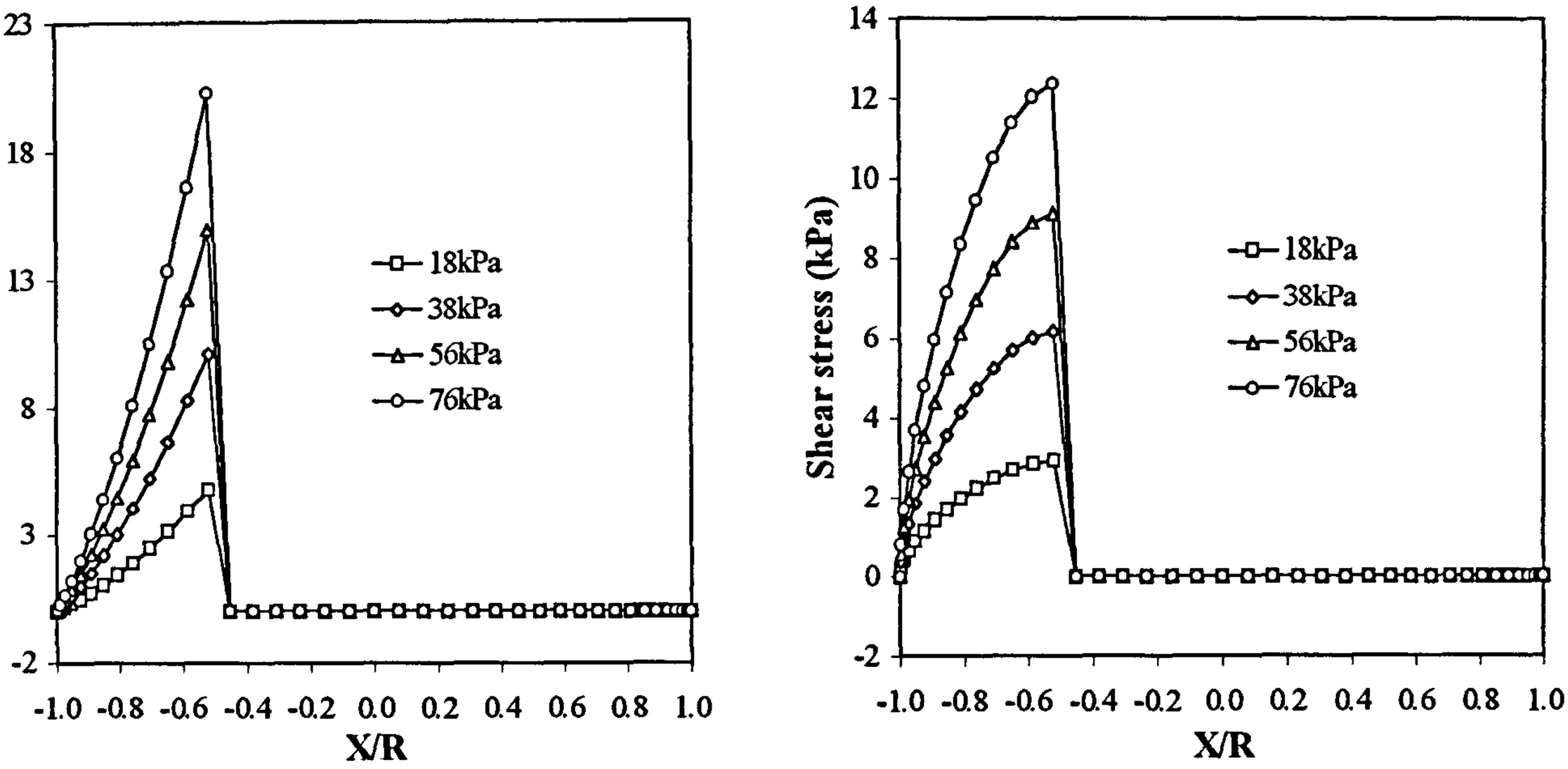

Figure 3.30 Stresses on the arch extrados, load at (X/R) = -0.75, codified method

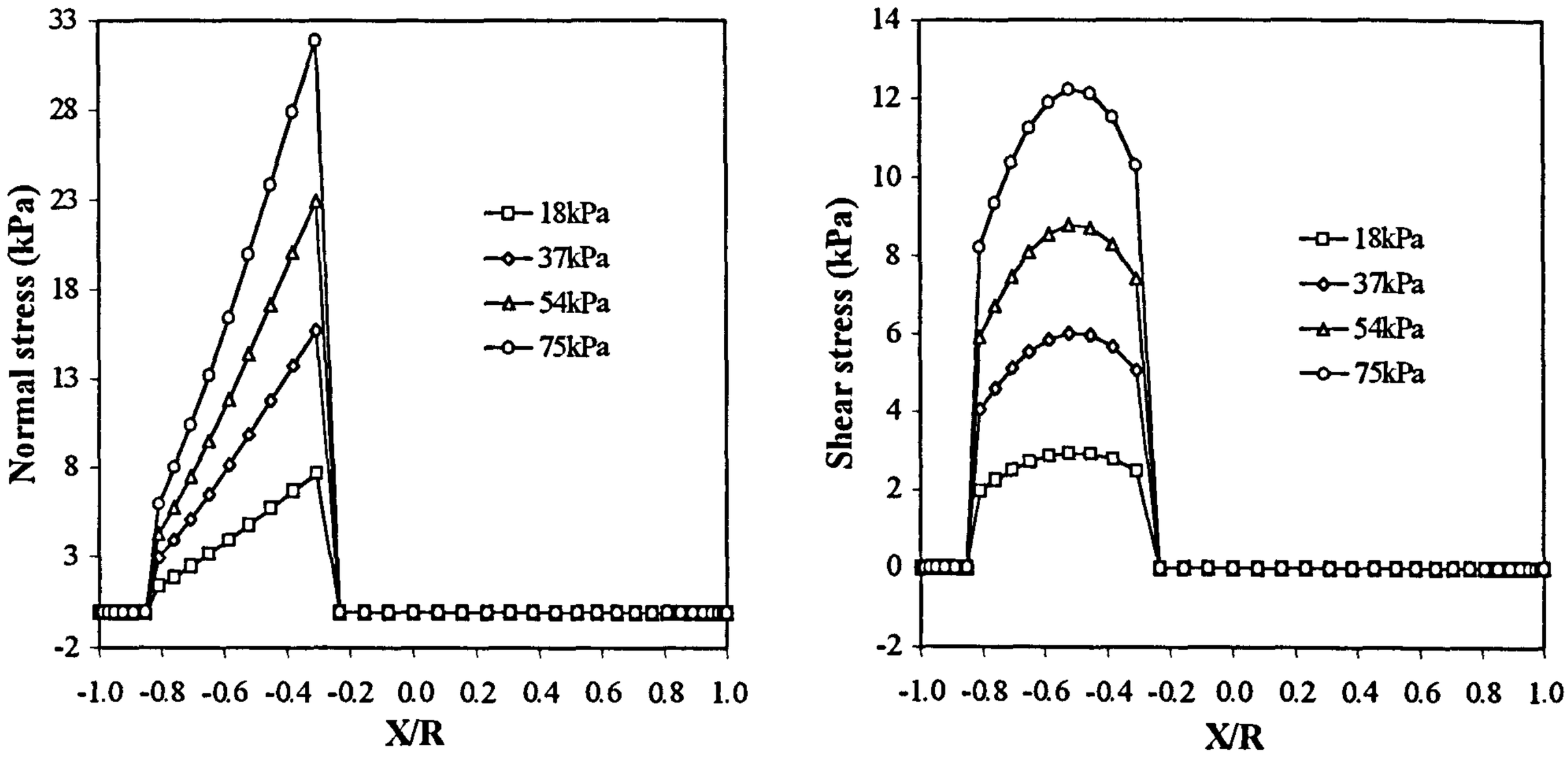

Figure 3.31 Stresses on the arch extrados, load at (X/R) = -0.50, codified method

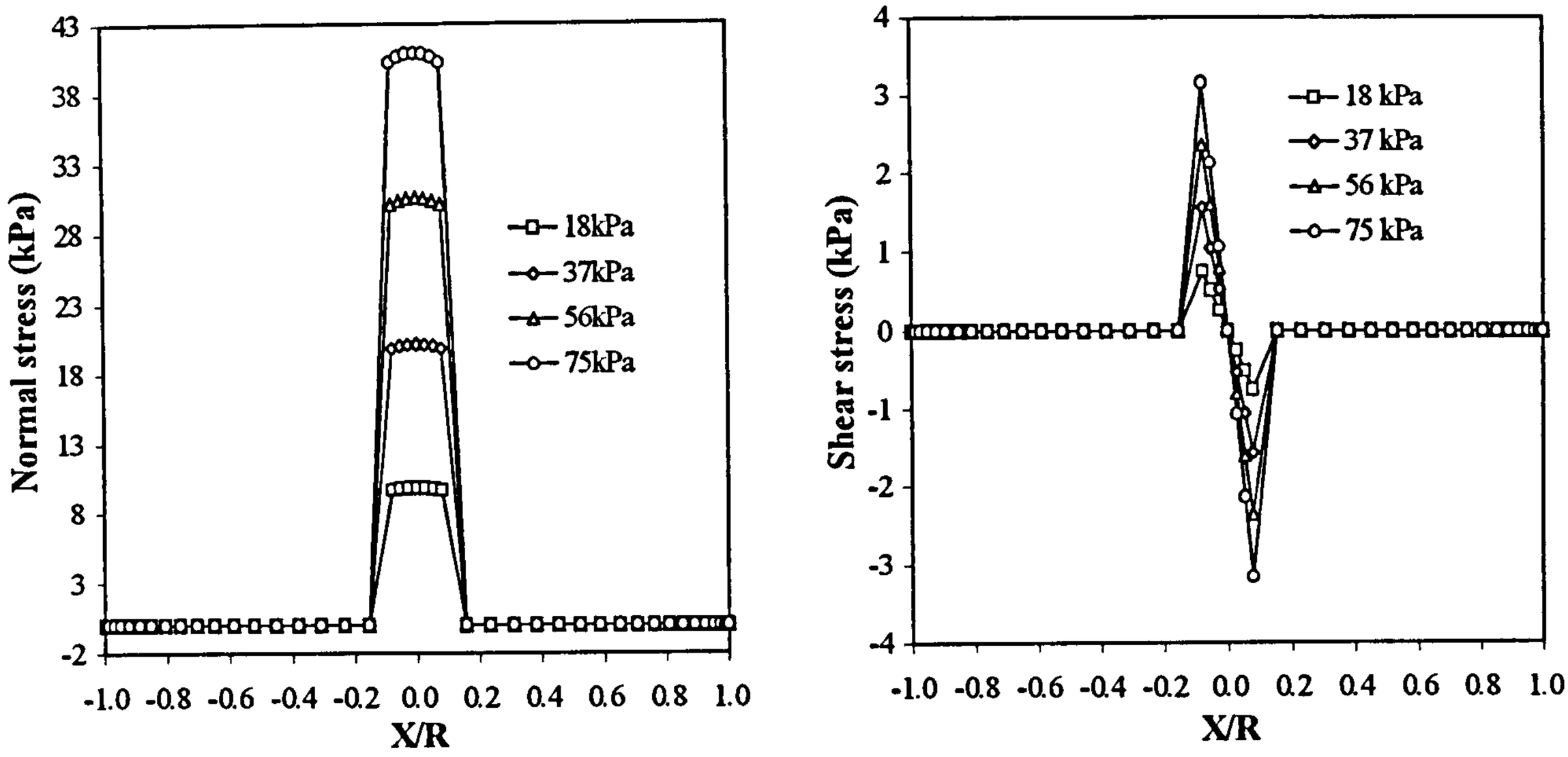

Figure 3.32 Stresses on the arch extrados, load at (X/R) = 0.0, codified method

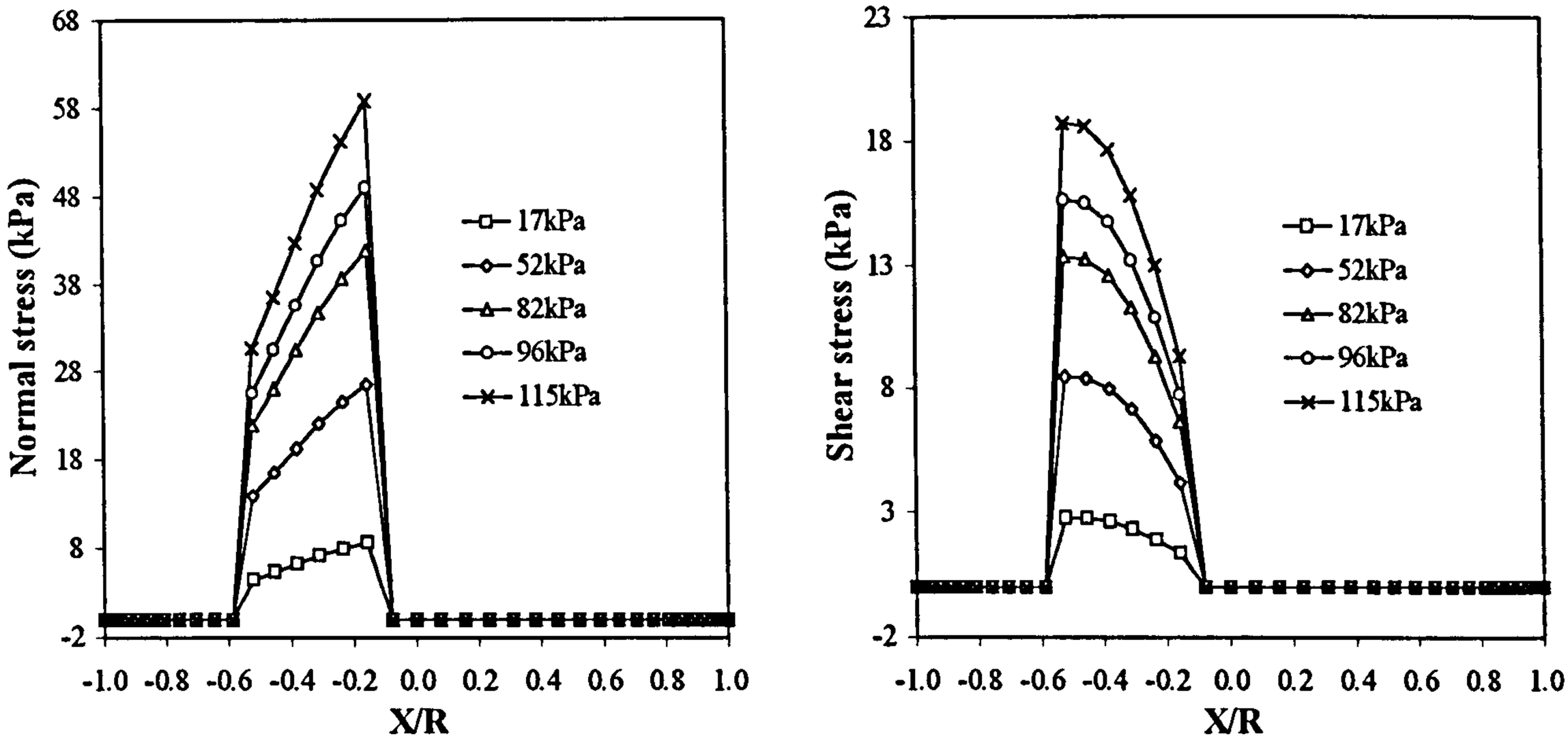

Figure 3.33 Stresses on the arch extrados, load at (X/R) = -0.33, codified method

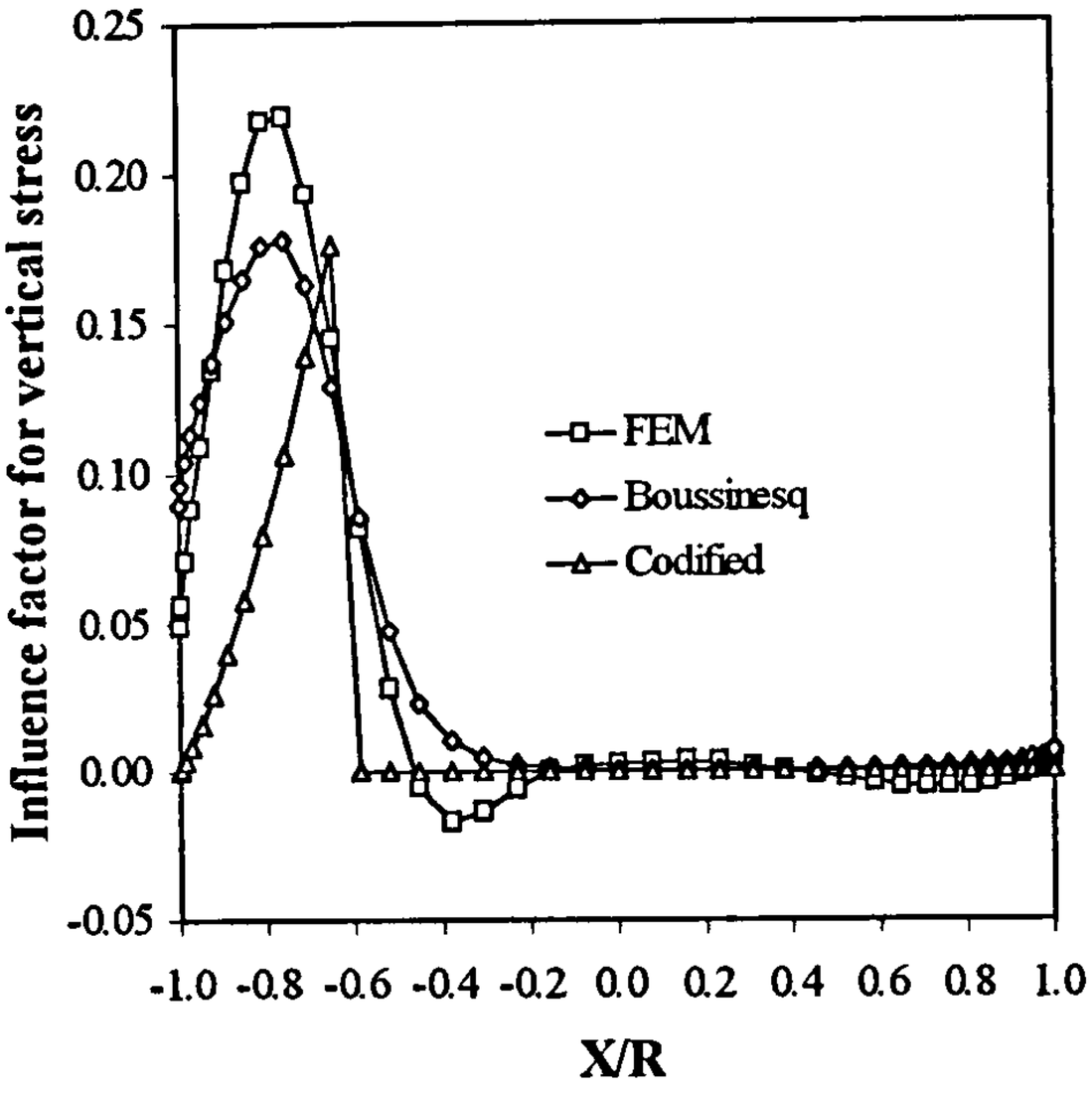

Figure 3.34 Comparison of theoretical results, load at (X/R) = -1.0

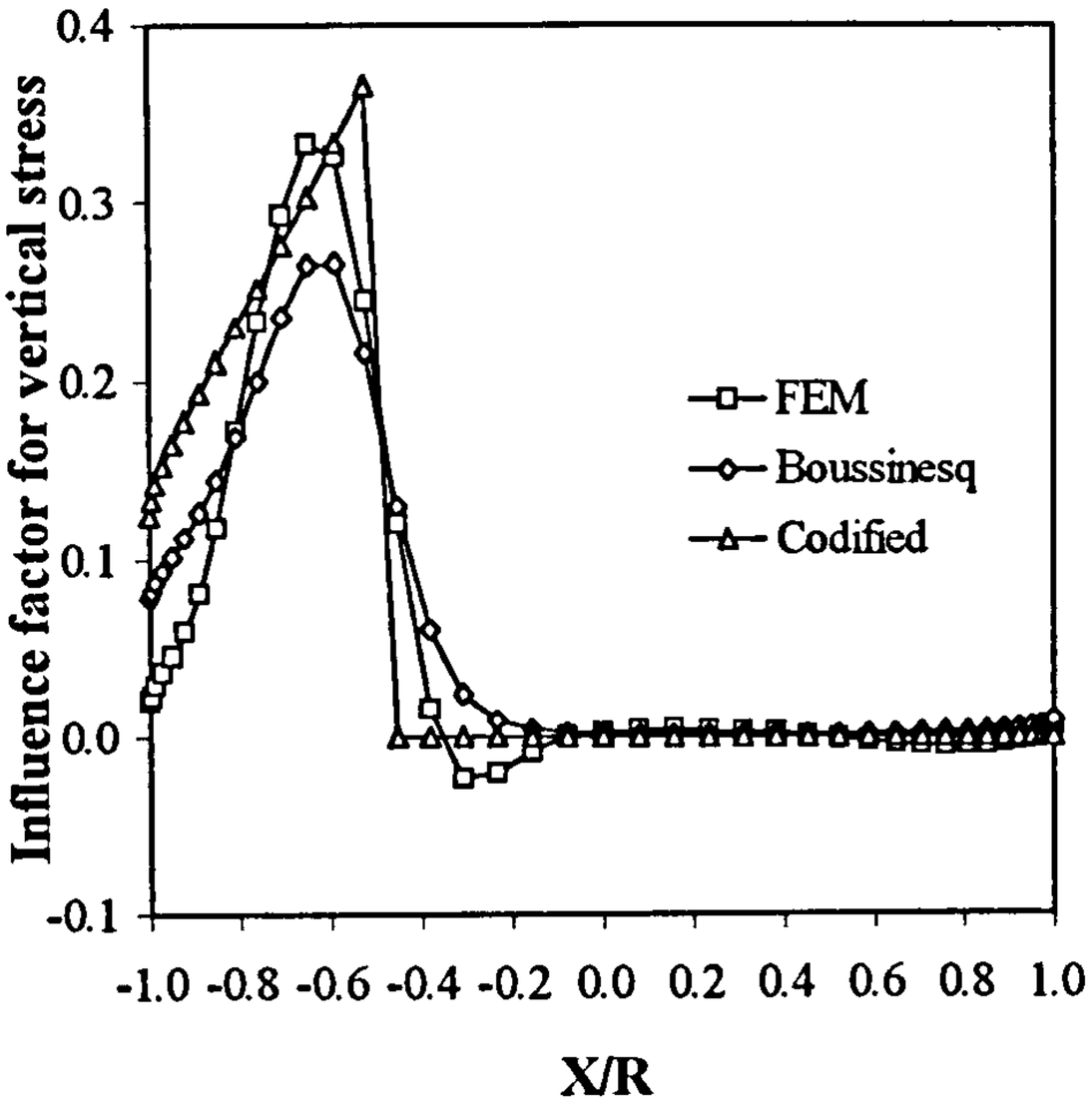

Figure 3.35 Comparison of theoretical results, load at (X/R) = -0.75

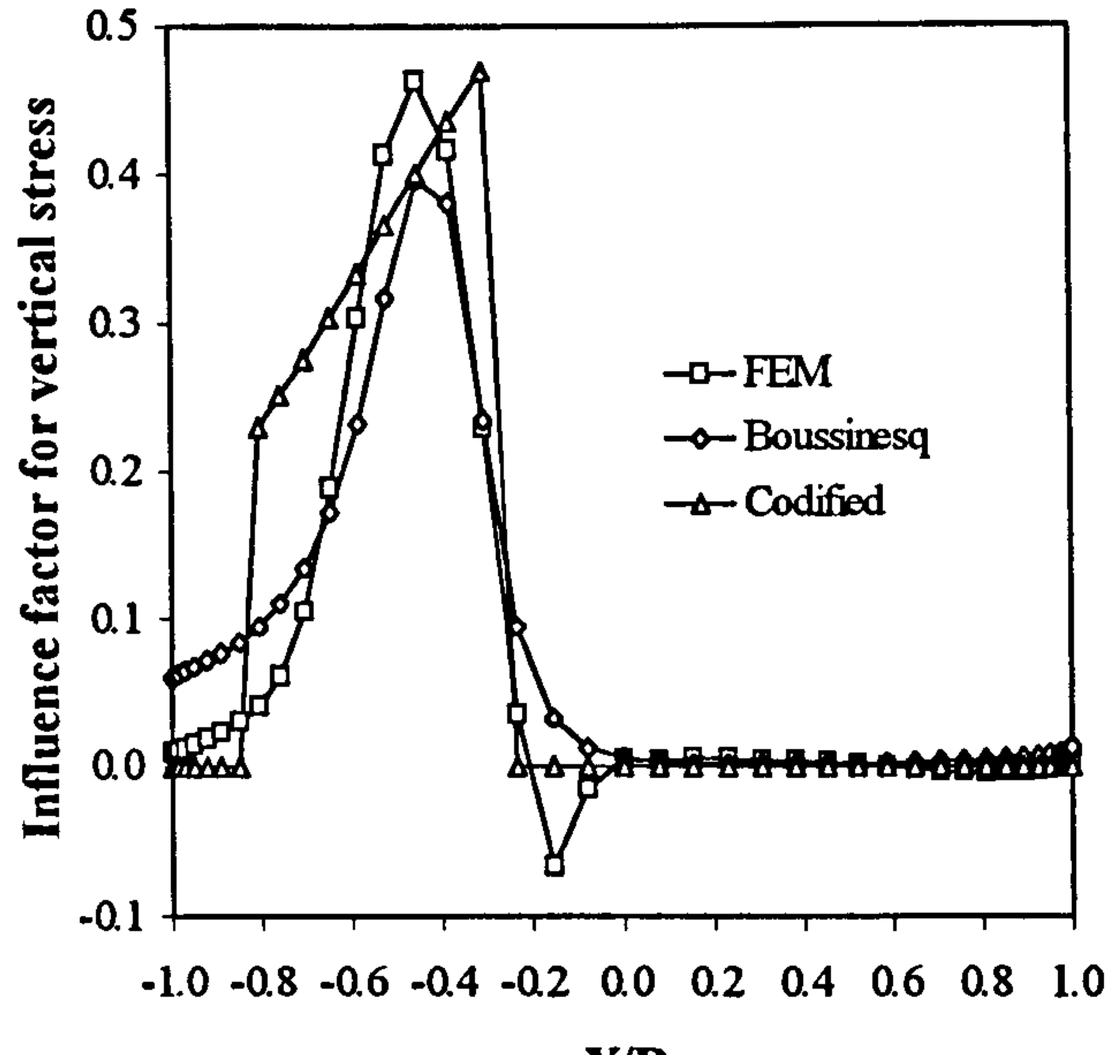

Figure 3.36 Comparison of theoretical results, load at (X/R) = -0.5

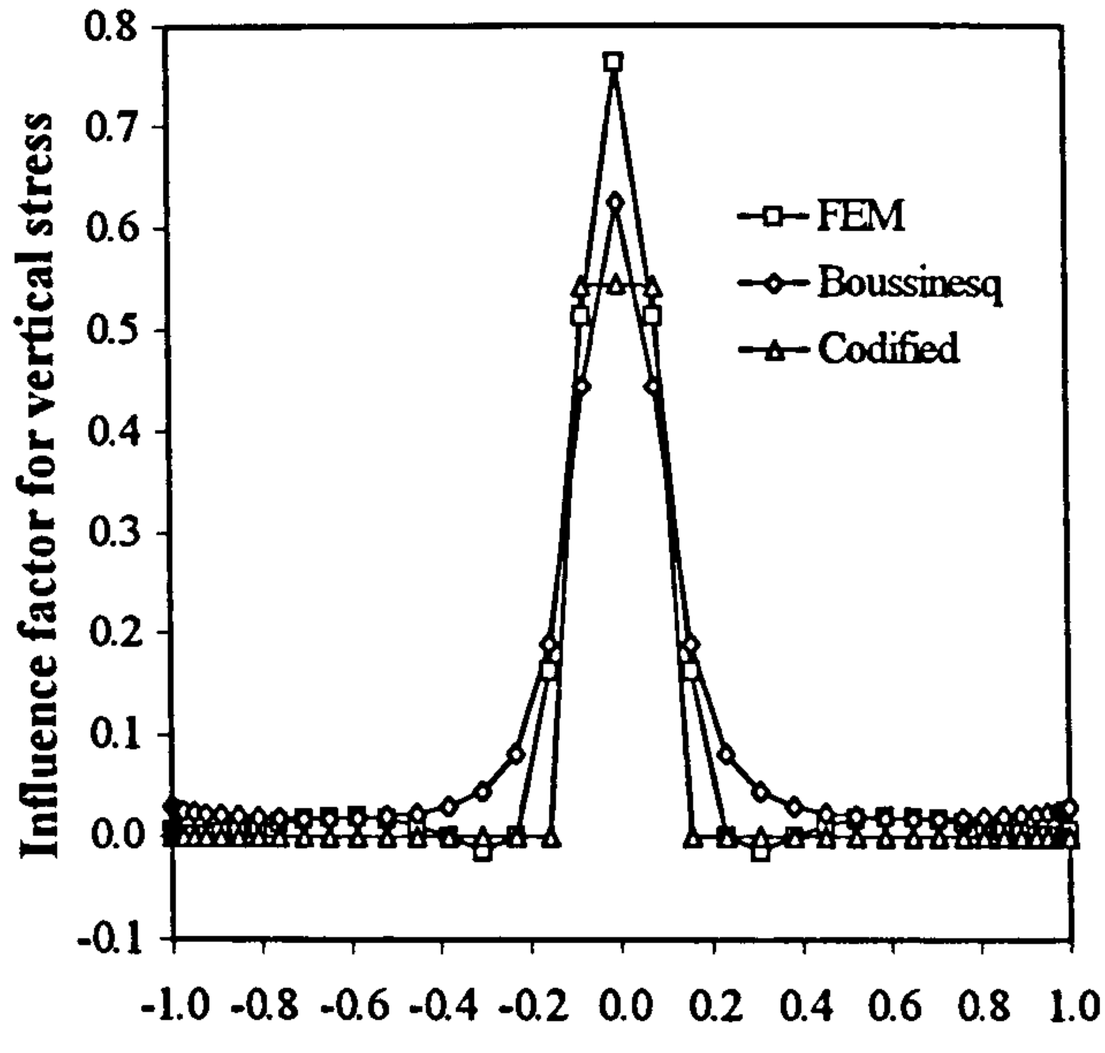

Figure 3.37 Comparison of theoretical results, load at (X/R) = 0.0

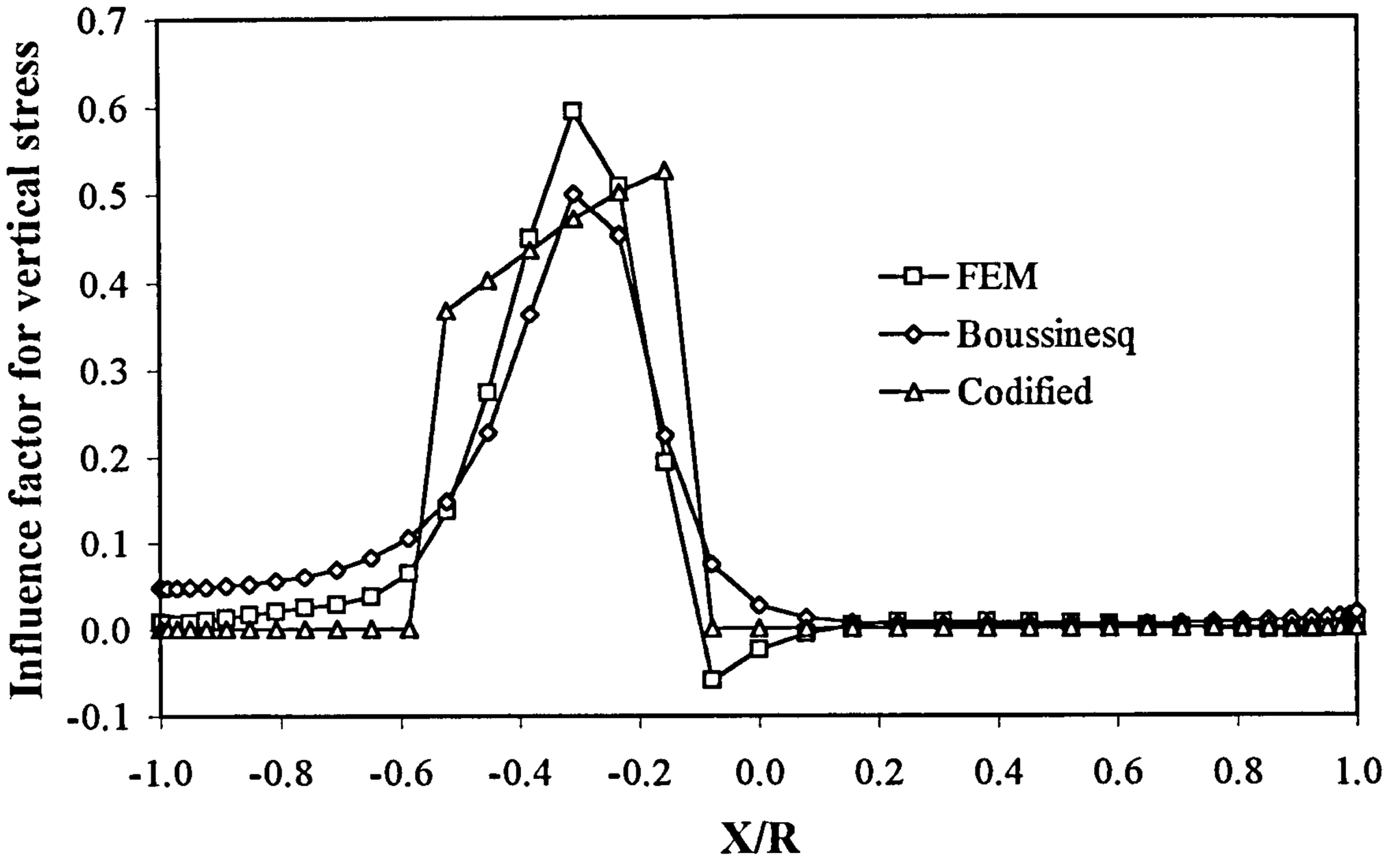

Figure 3.38 Comparison of theoretical results, load at (X/R) = -0.33

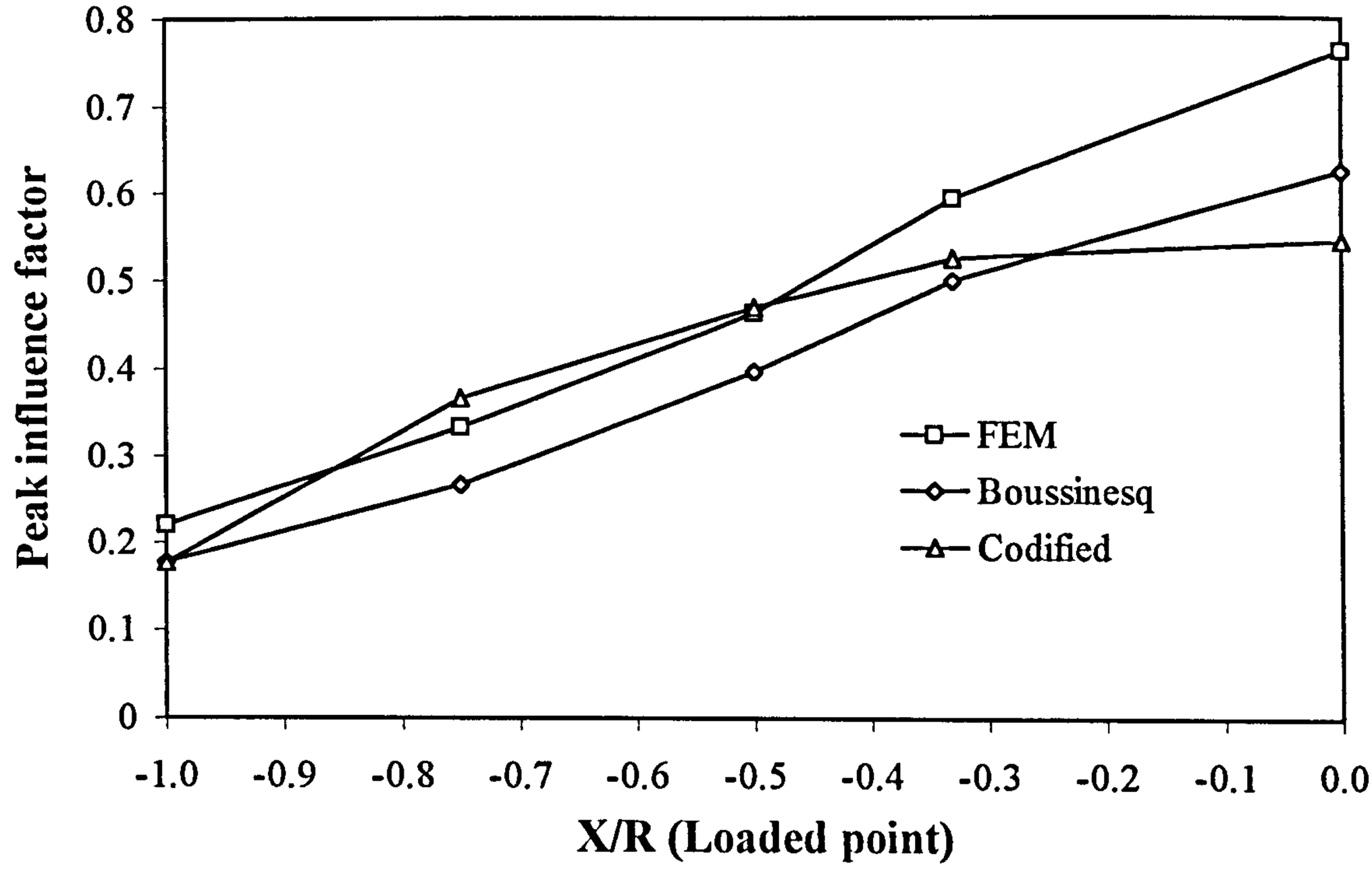

Figure 3.39 Comparison of peak influence factors for vertical stresses

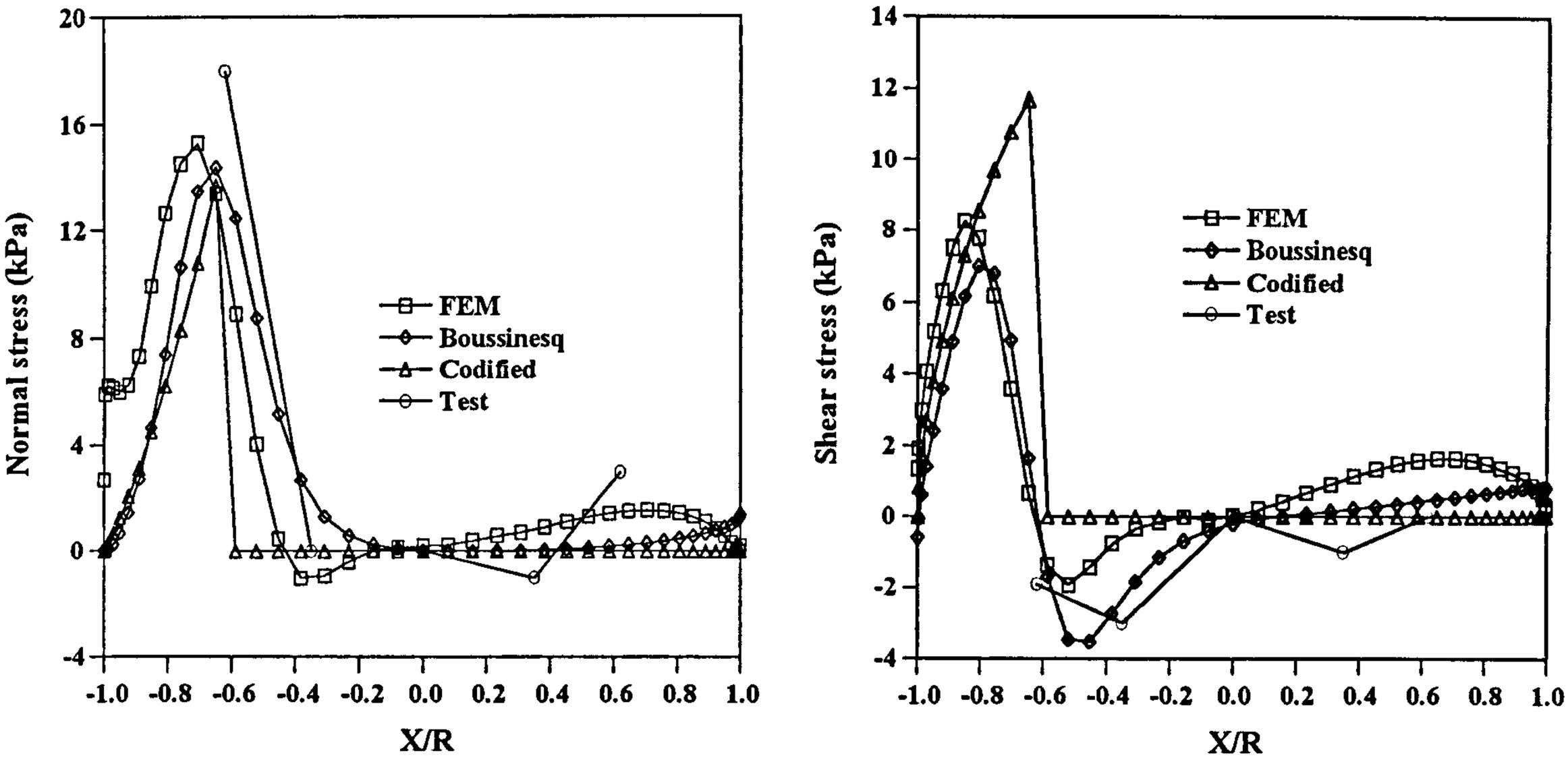

Figure 3.40 Comparison with experimental results, load at (X/R) = -1.0

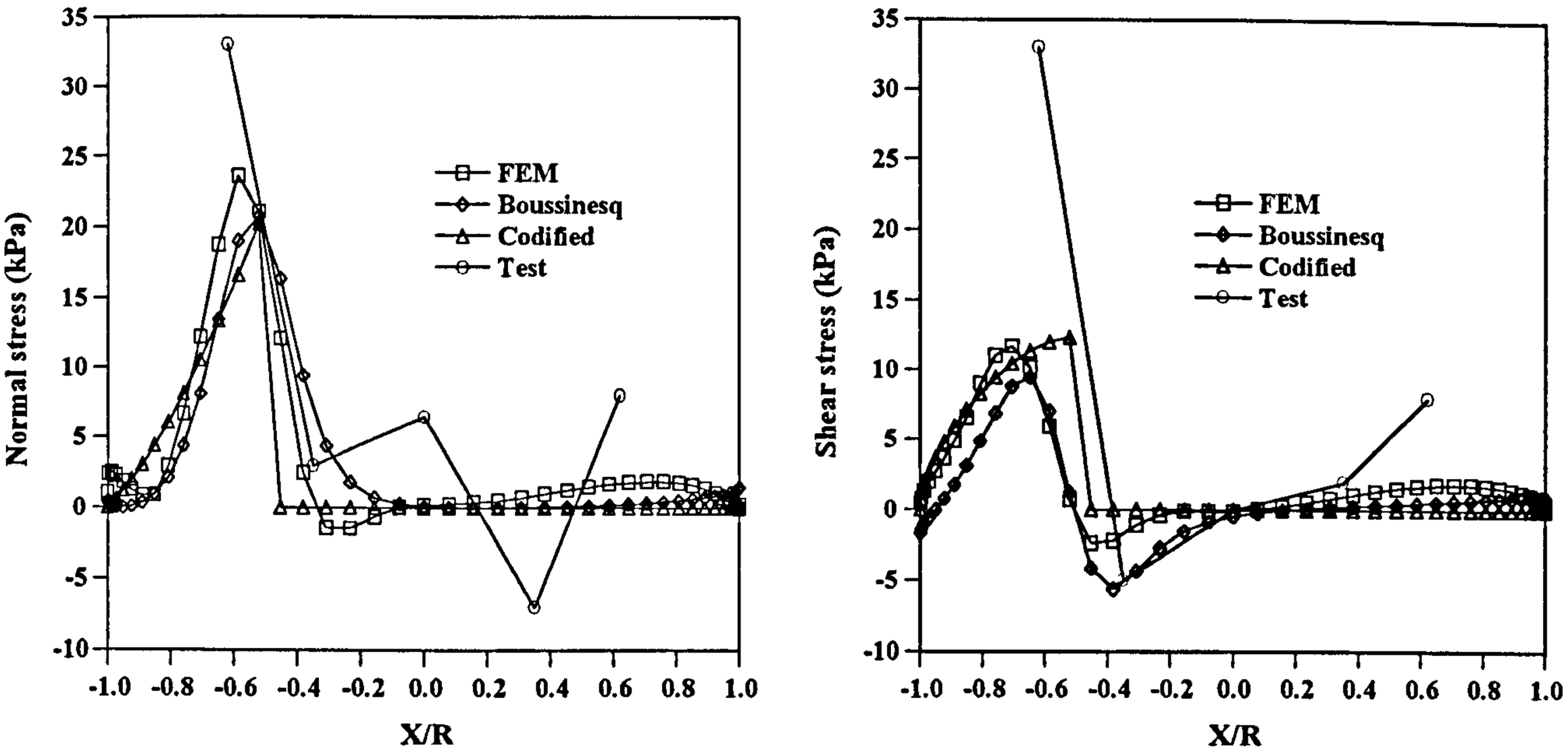

Figure 3.41 Comparison with experimental results, load at (X/R) = -0.75

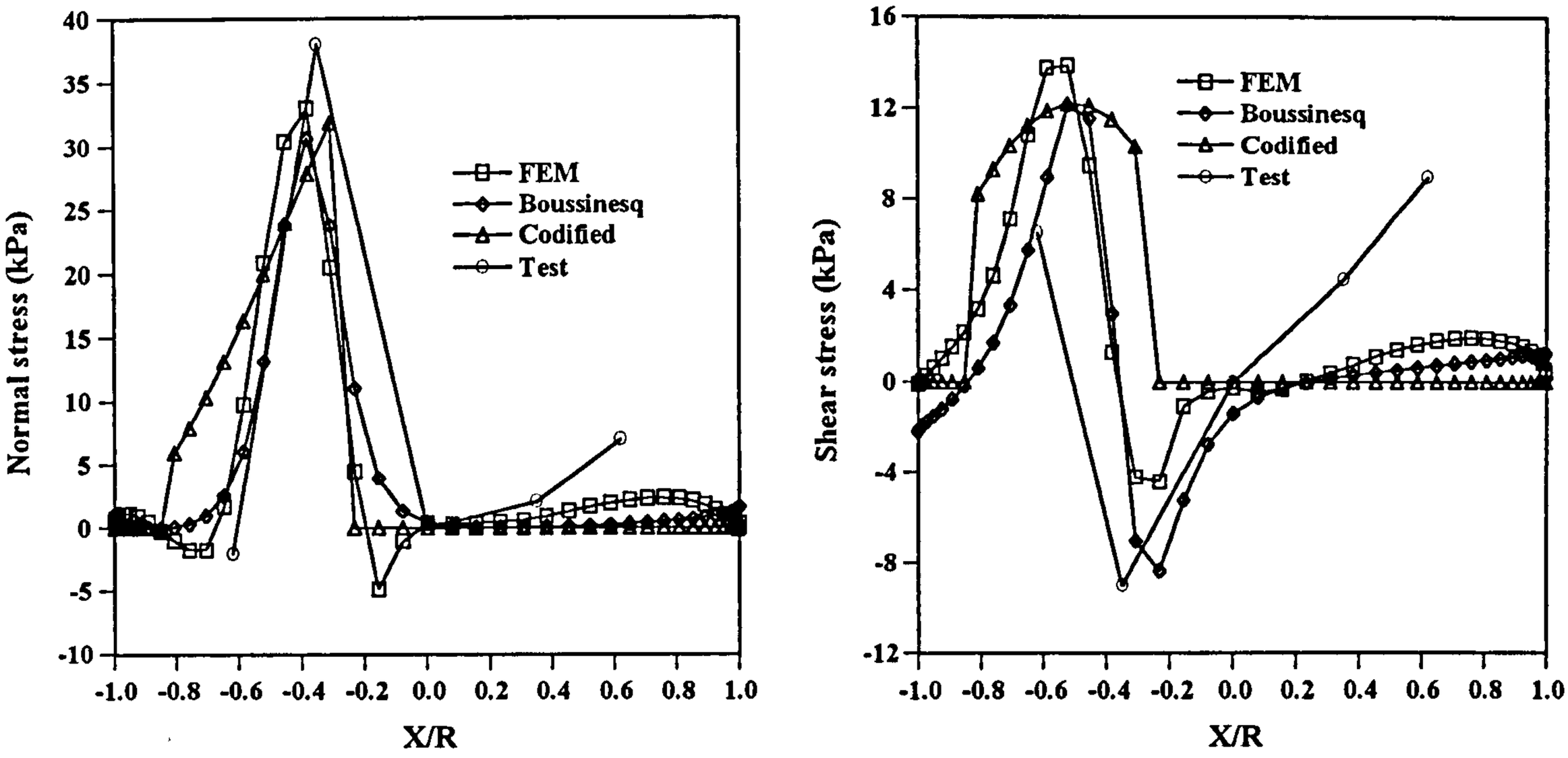

Figure 3.42 Comparison with experimental results, load at (X/R) = -0.50

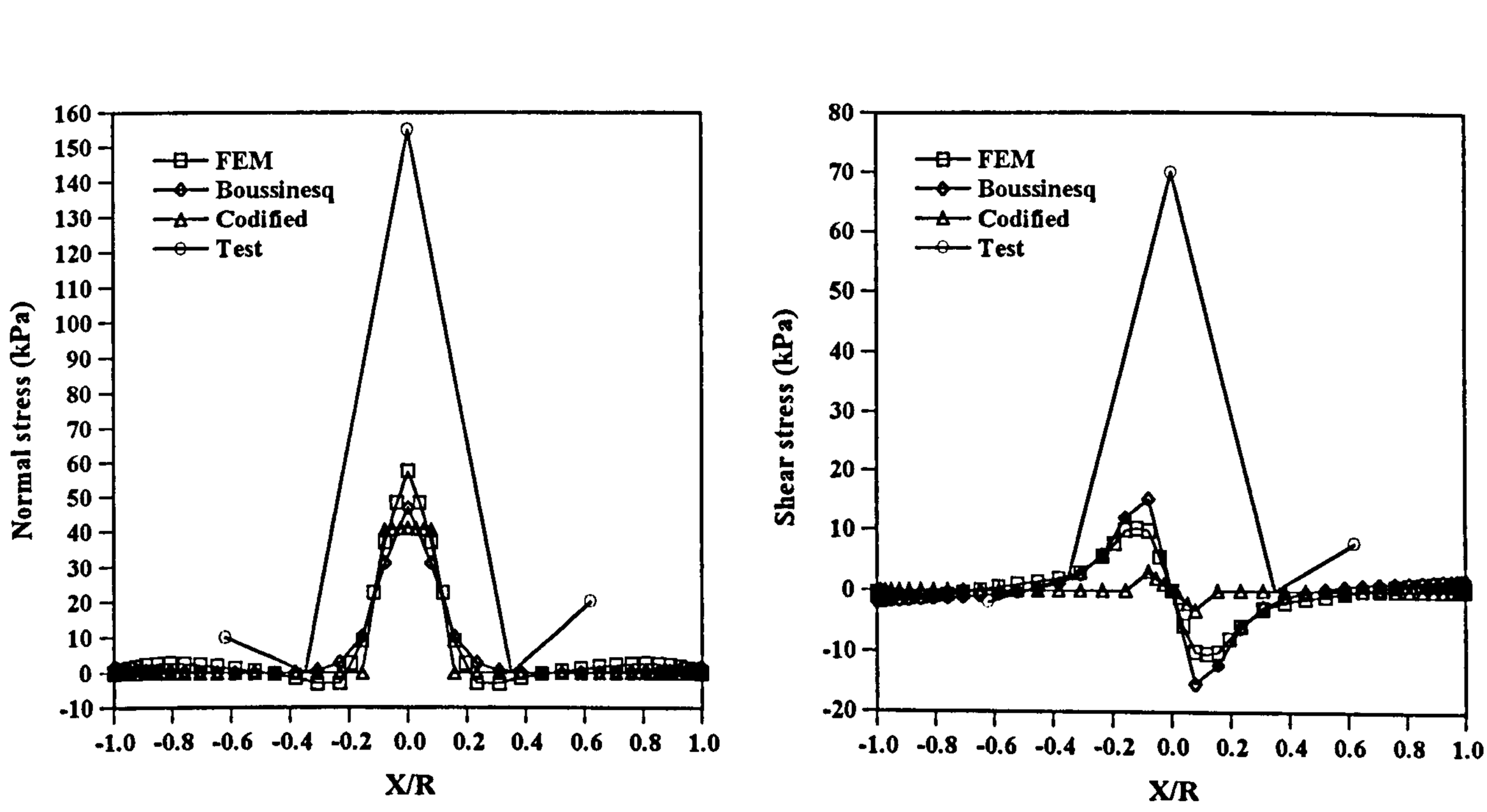

Figure 3.43 Comparison with experimental results, load at (X/R) = 0.0

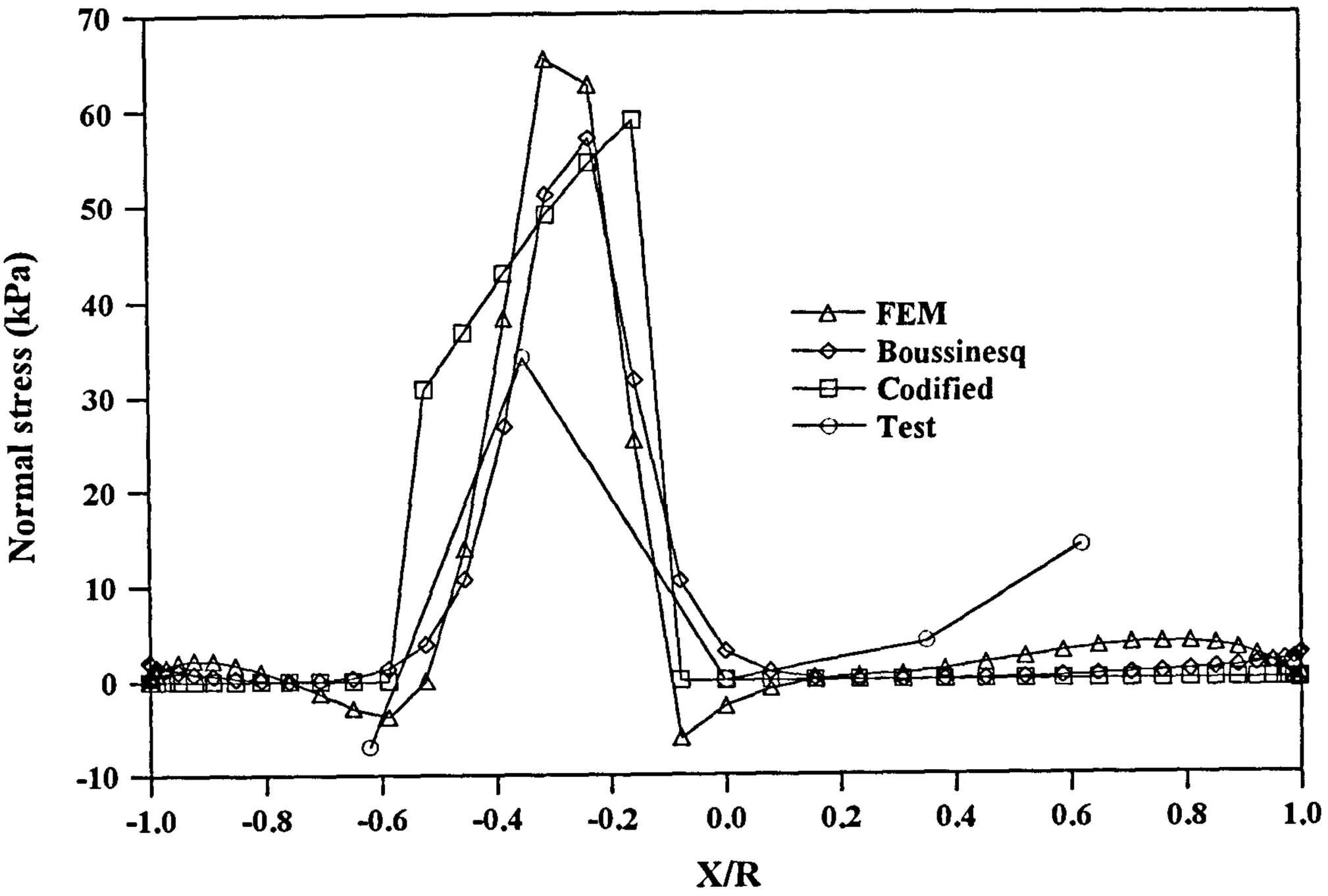

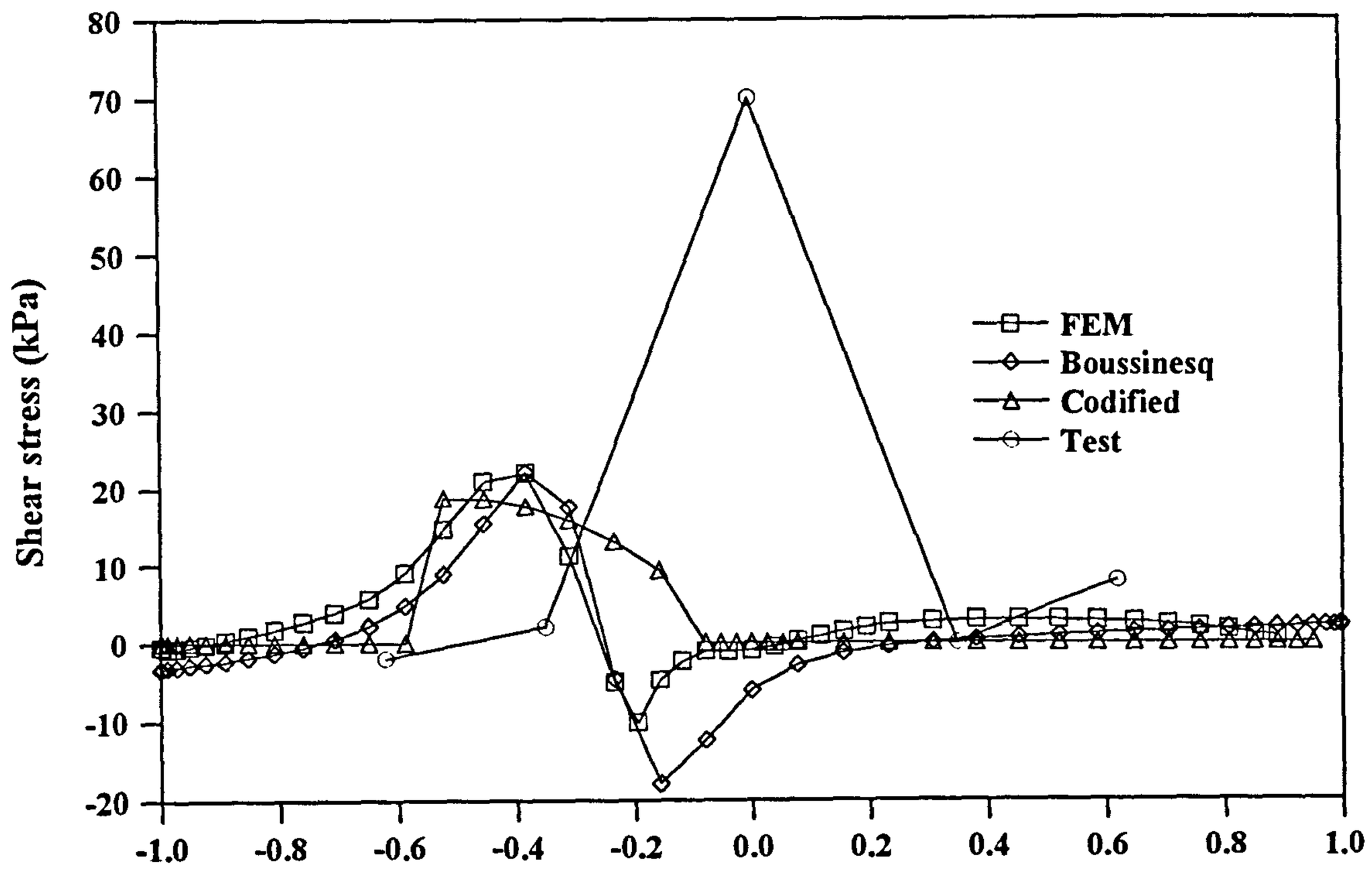

Figure 3.44 Comparison with experimental results, load at (X/R) = -0.33

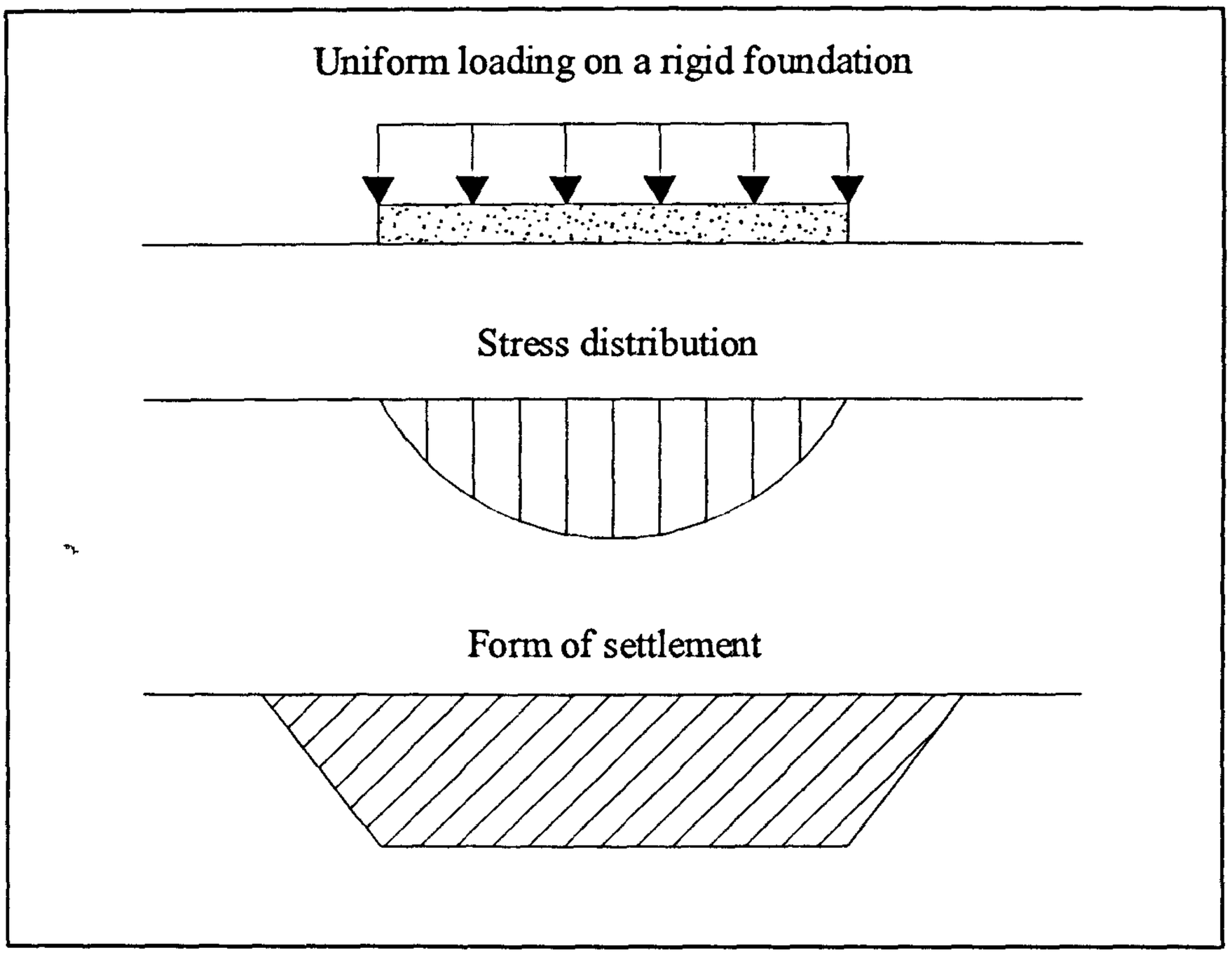

Figure 3.45a Uniform loading on a rigid foundation

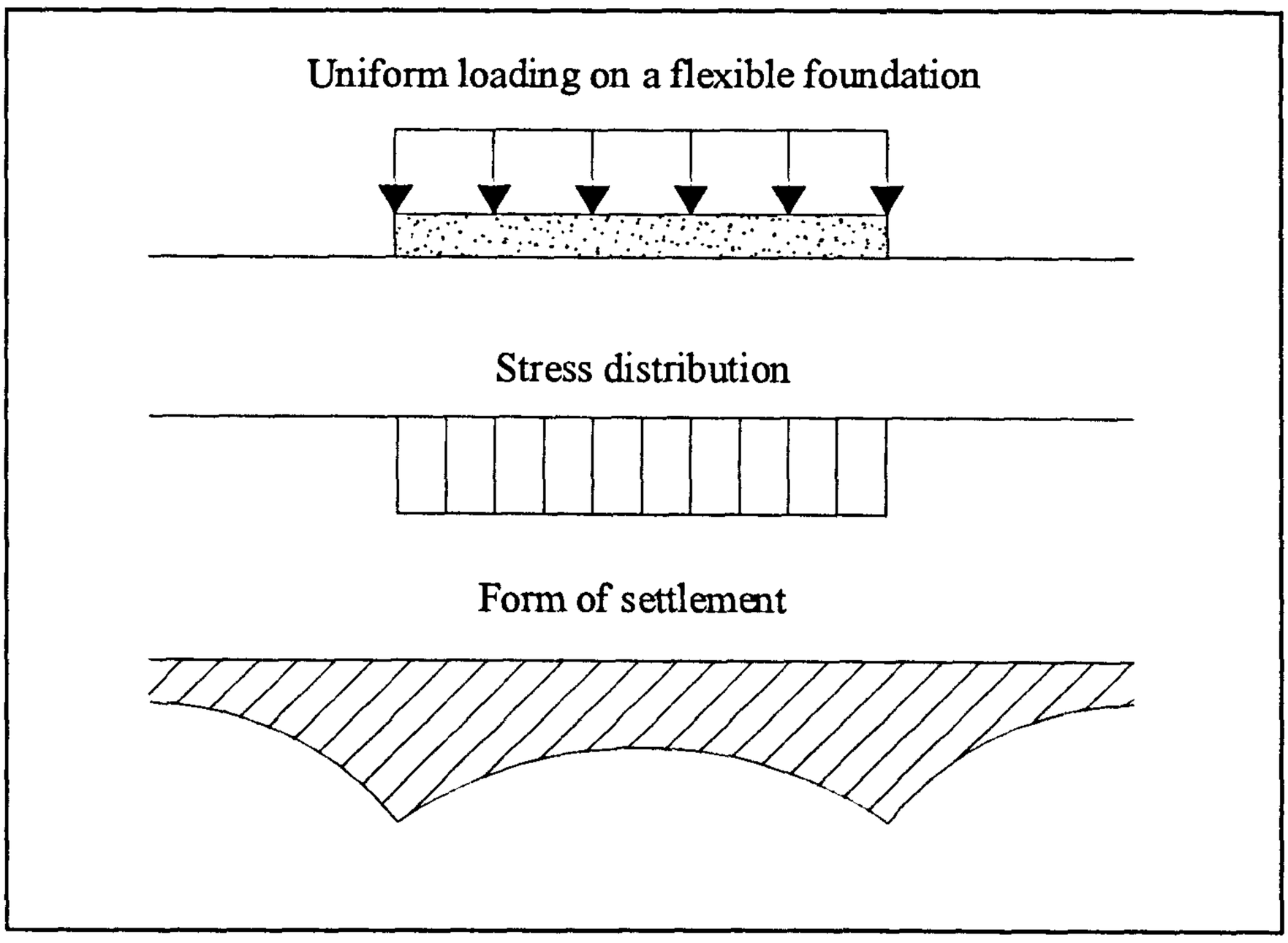

Figure 3.45b Uniform loading on a flexible foundation

CHAPTER 4

Non-Linear Two Dimensional Analysis Of Arch Bridges

4.1 Introduction

National and local road authorities are assessing the arch bridge stock to allow an increase in the maximum allowable gross vehicle weight (GVW) from 38t to 44t and in the maximum axle weight from 10t to 11.5t. Many arch bridges are assessed conservatively by the current assessment method referred to as the MEXE method defined in the Department of Transport's Departmental Standard BD21/97 (1997a) and associated Advice Note BA16/97 (1997b). With the increase of maximum allowable vehicle weight, a more refined assessment method is urgently required for both ultimate and serviceability limit state analyses. This is necessary to prevent heavy vehicles from taking longer trips than would otherwise be required.

In this study, a two dimensional analysis was performed using LUSAS (1997), a commercial available finite element (FE) package. Three full scale single span and one large scale multi-span bridges were modelled. The three full scale single span bridges were Bridgemill (HENDRY *et al.*, 1985), Strathmashie (PAGE, 1989) and Barlae (PAGE, 1989). The large scale multi-span arch bridge, consisted of three equal arch rings and was tested to collapse at Bolton Institute (MELBOURNE *et al.*, 1992a). Results from the single span arch bridges were compared with those obtained from other current arch bridge assessment methods: CTAP, ARCHIE, MEXE and ARCH. Program CTAP, developed by BRIDLE & HUGHES (1989 & 1990), uses Castigliano's elastic strain energy method. Program ARCHIE (SMITH, 1991a) uses the mechanism method to assess the load carrying capacity of arches. The MEXE results were obtained using a computerised version (MINIPONT) developed by the

Department of Transport as defined in BD21/97 (1997a) and BA16/97 (1997b). Program ARCH, another mechanism method based application, was developed by Cascade Software Limited (BA16/97, 1997b). All predictions of the arch collapse loads by ARCHIE, CTAP, ARCH, and MEXE were taken from BA16/97 (1997b).

Parametric studies were carried out using the adopted FE package to study the effect of variations in the arch's elastic modulus, compressive strength, tensile strength and backfill load dispersal angle. The effects of variation in pier material properties were also analysed on the Bolton multi-span bridge.

4.2 LUSAS FE model

Eight-noded quadrilateral elements in conjunction with four Gauss quadrature points were used to model the arch, backfill and extrados interface. Element type QPM8, under plain stress conditions, was used to model the arch; element type QPN8, under plain strain conditions, was used to model the backfill and extrados interface. The strengthening effect from the spandrel walls was not considered in this two dimensional analysis. The backfill above the arch ring was confined by spandrel walls in the transverse dimension and therefore it was assumed to be in a plain strain condition. In contrast, no confinement was applied to the arch ring in the transverse dimension and therefore it was modelled as a plain stress condition. It has been shown in Chapter 3 of this thesis that varying the conditions of the arch and backfill had no significant influence on the predicted arch behaviour. It made no significant difference by assigning plane strain or plane stress to the arch ring, the strongest component of an arch bridge, as a very small Poisson's ratio of 0.2 was used for the arch ring in this study. It is unreasonable to use a high Poisson's ratio for the arch as the material is brittle. More importantly, the condition was chosen in such a way that, when used with realistic material properties, reasonable predictions were made. Similar conditions were used by CRISFIELD *et al.* (1985b). The arch was simulated by a stress dependent von-Mises model, shown in Figure 4.1, enabling different tensile and compressive

material properties to be specified. The behaviour of backfill and interface elements was elasto-plastic with failure defined by Mohr-Coulomb yield criterion, as shown in Figure 4.2.

4.2.1 Loading

The total load on an arch bridge consists of its self-weight, including the backfill above the extrados, plus any imposed live loading. In the current FE analyses the imposed load was applied incrementally after application of the self-weight. The imposed load was applied to the backfill's upper, horizontal surface and distributed over the extrados in accordance with Boussinesq's elastic method (BOUSSINESQ, 1885). Little is known about actual load spreads through arch bridge backfills. PONNIAH *et al.* (1997) recorded a load dispersal angle of 65° during the field test at Kimbolton Butts bridge, Cambridgeshire; previous instrumented load tests (FAIRFIELD *et al.*, 1993a) to collapse have found Boussinesq's method to be surprisingly close to stress states measured on the extrados. BD21/97 (1997a) allows a dispersal angle of 26.6° based on its 1 in 2 side slope for live load stress distribution. A load spread angle of 45° was used in the FE analysis. Parametric studies were carried out by varying the load dispersal angle for each single span arch analysed.

For steep haunched arch bridges with low span to rise ratios, the live load may be distributed beyond the springers; it would be safer to consider the entire live load as being carried by the arch. To this end, it was assumed that sliding could occur along the backfill-extrados interface in regions where the slope of the extrados exceeded the backfill's angle of shearing resistance. In this case, as briefly mentioned in Chapter 3, the relevant friction angle is assumed to be close to the soil-brickwork shearing angle. A similar approach was adopted by GONG (1992).

4.2.2 Boundary conditions

The arch was assumed to be rigidly fixed to its abutments therefore both horizontal and vertical springer displacements were zero. If desired, spring supports can be used to simulate abutment movement; this was not done as abutment movement was not recorded *in situ* for the arch bridges used in this study. All soil elements were rigidly fixed in both horizontal and vertical directions; varying the support condition showed no apparent influence to the prediction. The linear elastic analysis of stress distribution presented in Chapter 3 of this thesis revealed that the variation of backfill's support conditions had no influence on the stress state on the arch extrados.

4.2.3 Backfill material properties

It is difficult to determine the backfill properties as they are inherently variable and subject to the vagaries of compaction, years of dynamic loading, and possible overconsolidation. In some cases, stronger, stiffer backing was found on each side of the arch. No information about the backfill properties was available for all single span arch bridges analysed in this study. The backfill's elastic modulus and cohesion were assumed to be 50MPa and 1MPa respectively for all arch bridges. Assigning zero cohesion of backfill elements is not recommended as it causes numerical instability in the FE model. The angle of shearing resistance for all single span arch bridges was assumed to be 35° and 60.5° for the multi-span arch bridge as obtained from laboratory test (MELBOURNE *et al.*, 1992a).

4.2.4 Arch geometry and material properties

Salient dimensions of the four arch bridges analysed in this study and their material properties used in the FE analyses are presented in Table 4.1. For the multi-span arch bridge, the material properties of the arch and pier were assumed to be similar. Figures

4.3a, 4.4a and 4.5a show Bridgemill (HENDRY *et al.*, 1985), Strathmashie (PAGE, 1989) and Barlae (PAGE, 1989) respectively, before being taken to collapse and Figures 4.3b, 4.4b and 4.5b show their respective idealised meshes used in FE analyses. The idealised mesh for the multi-span arch bridge is shown in Figure 4.7a.

Table 4.1 Arch geometries and material properties

Bridge	Bridgemill	Strathmashie	Barlae	Bolton
Span (m)	18.29	9.425	9.865	3x3
Rise at the crown (m)	2.84	2.99	1.695	0.75
Width (m)	8.30	5.81	9.80	2.88
Ring thickness (m)	0.711	0.60	0.45	0.215
Fill depth at crown (m)	0.203	0.41	0.295	0.30
Arch ring profile	Parabolic	Segmental	Segmental	Segmental
Pier height (m)	N/A	N/A	N/A	1.50
Pier thickness (m)	N/A	N/A	N/A	0.44
Arch elastic modulus (MPa)	5000	5000	5000	6000
Arch tensile strength (MPa)	0.22	0.25	0.33	0.20
Arch compressive strength (MPa)	5	6	7	12

4.3 Numerical results for single span arch bridges

This section presents the numerical results for the three single span arch bridges analysed in this study. A parametric study involving the arch's elastic modulus, its compressive and tensile strength, and the backfill's load dispersal angle was also carried out. The effects of variation of mesh density, support condition and boundary proximity were carried out on Barlae. For each arch analysed, results from *in situ* load tests, program CTAP, program ARCHIE, the MEXE method and program ARCH were compared with the FE output.

4.3.1 Bridgemill

Bridgemill (HENDRY *et al.*, 1985) was a red sandstone masonry arch. The whole structure was in good condition without any significant cracks in the vault and spandrel walls. The bridge was loaded to collapse using a transverse line load over 750mm width located at one ¼-span point. The collapse load recorded was 361kNm^{-1} width perpendicular to the span. The FE result using the arch properties given in Table 4.1 was 362kNm^{-1} width. Comparison was made with the experimental collapse load and those results obtained from other assessment methods: they are presented in Figure 4.3c and discussed later. Results from the parametric study on the effects of arch elastic modulus, compressive strength, tensile strength and backfill load dispersal angle are presented in Figures 4.3d to 4.3g respectively. The hinge locations predicted by FE analysis, crack or hinge development, and compressive stress vectors are presented in Figures 4.3h to 4.3j respectively.

4.3.2 Strathmashie

Strathmashie (PAGE, 1989) was a rubble masonry arch. Dimensionally it was in good condition but there was only a little mortar in parts of the arch and a serious longitudinal crack in the arch ring, as mentioned in the report on its testing (PAGE, 1989). A reduced thickness of 500 mm was used in this study instead of the original thickness of 600 mm due to the aforementioned loss of mortar in the arch ring. Increasing the ring thickness will result in a higher collapse load since a thicker ring can contain the thrustline for a given greater load. However, it is unrealistic, as mentioned by PAGE (1989), to use the original thickness of 600mm due to the scarcity of the ring. The bridge was loaded to collapse using a transverse line load of 750mm width located at one ¼-span point. The ultimate load recorded was 228kNm^{-1} width perpendicular to the span. The FE result using the arch properties given in Table 4.1 was 226kNm^{-1} width. Comparison was made with the experimental collapse load and those results obtained from other assessment methods: they are presented in Figure

4.4c and discussed later. Results from the parametric study on the effects of arch modulus, compressive strength, tensile strength and backfill load dispersal angle are presented in Figures 4.4d to 4.4g respectively. The hinge locations predicted by FE analysis, crack progression and compressive stress vectors are presented in Figures 4.4h to 4.4j respectively.

4.3.3 Barlae

Barlae (PAGE, 1989) was an ashlar masonry arch with a 29° skew. No major defects were found on the bridge which was loaded to collapse using a transverse line load of 750mm width located at one ¼-span point. The ultimate load recorded was 296kNm^{-1} width perpendicular to the span. The FE result using the material properties given in Table 4.1 was 302kNm^{-1} width. Comparison was made with the experimental collapse load and those results obtained from other assessment methods: they are presented in Figure 4.5c and discussed later. Results from the parametric study on the effects of arch elastic modulus, compressive strength, tensile strength and backfill load dispersal angle are presented in Figures 4.5d to 4.5g respectively. The hinge locations predicted by FE analysis, crack progression and compressive stress vectors are presented in Figures 4.5h to 4.5j respectively.

The assumptions made in the FE model such as the mesh density, support condition and boundary proximity were checked on this bridge. All analyses on this bridge were carried out with 90 elements used to discretise the arch ring. The effects of varying the mesh density are presented in Figure 4.5k. The effects of varying the support condition are presented in Figure 4.5l. Case 1 in Figure 4.5l being the standard case of support condition described in Section 4.2.2 (see Figure 3.20c). In Case 2, the backfill elements were restrained horizontally on the lateral side and vertically on the bottom (see Figure 3.20d). Figure 4.5m shows the effects of boundary proximity. Case 1 being the standard case with the length of the wing wall set to quarter of the arch span: Case 2, without the wing wall: Case 3 uses a length of the wing wall equal to half the arch

span: in Case 4 the length of the wing wall was twice the arch span. The dimension of the wing wall in Cases 1 to 4 is shown in Figure 4.5n.

4.4 Analysis of results for single span arch bridges

The results obtained from the FE analyses for single span arch bridges are discussed. Following this, comparisons are made between the capacity as estimated by CTAP, ARCHIE, MEXE and ARCH. References for all these methods are given in Section 4.1. Finally, the influence of arch elastic modulus, compressive strength, tensile strength and backfill load dispersal angle upon the behaviour of arch bridges is discussed and results presented in Figures 4.6a to 4.6d respectively.

4.4.1 FE analysis for single span arch bridges

Results from the FE analyses show close agreement in terms of collapse load and load *versus* deflection characteristics for the three arches analysed here. The percentage difference between test and FE results for Bridgemill, Strathmashie, and Barlae were 0.2%, 0.7%, and 2% respectively. The FE analysis accounted for all major arch and backfill material properties and was able to model material cracking and crushing as well as backfill yielding. Cracking occurs when the principal tensile stress exceeds the ultimate tensile strength. Crushing occurs when the principal compressive stress exceeds the ultimate compressive strength. A full hinge is assumed to occur if all the Gauss points at any section yielded in tension. It will not cover the full depth of the arch ring since a Gauss point is located a certain distance from the boundary of an element (see Figure 3.5). Full hinges were found at both springers for all single span bridges analysed in this study. Crushing was found in Bridgemill at a point under the applied load. Bridgemill was a flat arch with span to rise ratio of 6.44 and this geometry causes higher compressive stress to develop in the arch ring with both

horizontal supports fixed. Information such as the extent of cracking, stress in the arch ring and its deflection at any load are crucial for a serviceability limit state analysis.

Different material properties may be assigned to a single arch ring if it consists of different material due to remedial repairs or if weak spots associated with defects are to be included. The use of two dimensional backfill elements enables the strengthening effects of soil-structure interaction to be modelled realistically. It is common to find stronger, stiffer backings behind the haunches of such bridges: different backfill material with different strengths and stiffness can be assigned to account for the existence of backing.

4.4.2 Results from other assessment methods

It is clear that the collapse loads estimated by four assessment methods used in this study are quite diverse. This is due to different assumptions made and different theoretical models adopted. The author is unaware of the exact material properties used for these bridges analysed by these assessment methods; obviously different arch and backfill material properties and load dispersal angles will result in different behaviour predictions. CTAP is the only method amongst those used here that gives load *versus* deflection information and details of the extent of cracking at any load level. Clearly, different methods will be more suited to different arch geometries, whereas assessment by the FE method will be applicable to any soil-arch system. The drawback of FE assessment is the level of computing power and user time for both data input, mesh generation, and post-processing.

4.4.2.1 The MEXE method

The MEXE method is currently recommended in the Department of Transport Standard, most recently, BD21/97 (1997a) and its associated Advice Note, BA16/97 (1997b). The details of this method are also described in Section 1.2.1 of this thesis. The MEXE method is mainly influenced by modification factors. It is not always conservative; in the case of Barlae the method overestimated the collapse load by 8.1%. For Bridgemill and Strathmashie the MEXE method gave percentage differences of -19.7% and -17.1% respectively. It is unique amongst assessment methods in that different engineers can quite legitimately provide different estimates for a given arch.

4.4.2.2 Program CTAP, a strain energy method

Program CTAP analyses the arch by eliminating the tensile areas of the cross-section. Lateral pressure is modelled with horizontal springs which yield at active and passive limits. The percentage difference between actual and CTAP assessed results for Bridgemill, Strathmashie, and Barlae are -40.2%, -12.7%, and -21.6% respectively. FAIRFIELD *et al.* (1994b) carried out model tests on wooden arches with a dry sand backfill; CTAP was also used to assess their collapse loads with some success (HUGHES, 1997b). Variations between -16% and +6.4% of the actual collapse loads were found indicating the efficacy of CTAP as an assessment method. The one case where CTAP overestimated a collapse load occurred where the weak sand backfill underwent bearing capacity failure resulting in the load point becoming progressively closer to the arch extrados. This was one facet of the structure's behaviour that CTAP does not attempt to model as full scale masonry arch bridges have road pavements above the backfill making bearing capacity failure unlikely.

4.4.2.3 Program ARCHIE & Program ARCH: mechanism methods

Program ARCHIE and ARCH are based on the mechanism method. The mechanism method is based on assumed hinge positions for a given load configuration. Iteration to find a safe line of thrust, the arch ring depth required to contain it, and hence the ultimate load is then carried out. Various different methods of load dispersal through the backfill are used and program ARCHIE is able to assess an arch with some account being taken of the development of passive resistance to deformation of the unloaded side of the span. The mechanism prediction is reliable only when all the forces and their positions are accurately considered. All the currently available arch bridge assessment tools based on the mechanism method do not account for arch deflections. Albeit the actual arch deflection at the moment of collapse is still unknown, it will be shown in Chapter 8 of this thesis that the arch deflection dramatically influences the prediction of arch collapse load based on the mechanism approach. For the three single span bridges assessed here no more than 40% of the full passive pressure was allowed to develop. The percentage differences between actual and ARCHIE assessed results for Bridgemill, Strathmashie, and Barlae were +9.1%, +5.3%, and -27% respectively. The percentage differences between actual and ARCH assessed results for Bridgemill, Strathmashie, and Barlae were -29.1%, +19.3%, and -38.5% respectively. The principal reason for the discrepancies between the assessed and actual collapse loads lay in the way the mechanism method has had to use simplified soil stress distributions on the extrados. The FE results presented earlier were based on more accurate earth pressure distributions not limited by the dictates of any other assessment method.

4.4.3 Analysis of results of the FE parametric study for single span arches

The influence of each quantity considered in the FE based parametric study is discussed separately in the following sections. Four parameters were varied: the arch's

elastic modulus, its compressive and tensile strengths, and the backfill load dispersal angle.

4.4.3.1 The effect of varying the arch's elastic modulus

It was apparent from Figures 4.3d, 4.4d, 4.5d, and 4.6a that the arch's elastic modulus had no significant effect on the system's collapse load. However this may not be true when there is an upper limit to the maximum arch deflection allowed before the onset of buckling. The major influence of arch's elastic modulus comes in the form of its influence on the load *versus* deflection characteristic of an arch. The lower the elastic modulus of the arch ring, the more flexible the system. It is difficult to determine the value of the arch's elastic modulus as it is a composite of mortar and voussoir units. Direct compression tests on this composite material may not give reliable results because replication of the confining stresses pertinent to their *in situ* condition is difficult. The elastic modulus also has its importance diminished because the arches tended to fail with large deformations caused by rotation of segments of arch ring; compression of the material is of lesser importance, provided sufficient gap can open under elastic stresses to allow the first hinge to form. A value of around 5000MPa is found in this study to best simulate the load *versus* deflection characteristics.

4.4.3.2 The effect of varying the arch's compressive strength

Results of the parametric study on the effect of the arch's compressive strength are presented in Figures 4.3e, 4.4e, 4.5e, and 4.6b. The estimated collapse loads were sensitive to variations in arch compressive strength; values ranging from 2MPa to 1×10^{6}MPa were used. A sensible range of 2MPa to 15MPa was contained within this extreme variation; it is not suggested that values as high as 1×10^{6}MPa are used for assessment purposes. Different values of compressive strength did not affect the initial flexibility or deformations. For Bridgemill the FE estimated collapse load increased

from 252kNm^{-1} to 384kNm^{-1} (actual collapse load = 361kNm^{-1}) as the arch's compressive strength increased from 2MPa to 15MPa. For Strathmashie the FE estimated collapse load increased from 157kNm^{-1} to 230kNm^{-1} (actual collapse load = 228kNm^{-1}) as the arch's compressive strength increased from 2MPa to 15MPa. For Barlae the FE estimated collapse load increased from 180kNm^{-1} to 321kNm^{-1} (actual collapse load = 296kNm^{-1}) as the arch's compressive strength increased from 2MPa to 15MPa. A realistic arch compressive strength will obviously be essential for accurate arch assessment by the adopted FE analysis.

4.4.3.3. The effect of varying the arch's tensile strength

Results of the parametric study on the effect of the arch's tensile strength are presented in Figures 4.3f, 4.4f, 4.5f, and 4.6c. The estimated collapse loads were sensitive to variations in arch tensile strength; values ranging from 0.1MPa to 0.5MPa were used. Care must be taken when selecting a value for the arch's tensile strength. On an intact arch, nominally defect free, it is justifiable to use a higher value of arch tensile strength since at no time in the loading history has the tensile stress been large enough to cause full depth discontinuities between the mortar beds and the voussoir units. Full scale tests on arch bridges carried out by DAVEY (1953) recorded a maximum tensile stress of 0.69MPa. Ignoring the tensile strength may lead to conservative results. Non-destructive testing by impact-echo method (BENSALEM *et al.*, 1997a; SIBBALD *et al.*, 1995; ARMSTRONG *et al.*, 1995) can assist an engineer making an assessment of the state of cracking in the arch. Simple visual inspection can also help.

Different values of tensile strength did not affect the initial flexibility or deformations. For Bridgemill the FE estimated collapse load increased from 296kNm^{-1} to 489kNm^{-1} (actual collapse load = 361kNm^{-1}) as the arch's tensile strength increased from 0.1MPa to 0.2MPa. For Strathmashie the FE estimated collapse load increased from 131kNm^{-1} to 314kNm^{-1} (actual collapse load = 228kNm^{-1}) as the arch's tensile strength increased from 0.1MPa to 0.5MPa. For Barlae the FE estimated collapse load increased from

184kNm^{-1} to 360kNm^{-1} (actual collapse load = 296kNm^{-1}) as the arch's tensile strength increased from 0.1MPa to 0.5MPa. Should a test be required to determine the compressive strength as described previously, tensile strength evaluation should also be carried out on as many samples as possible at the same time.

4.4.3.4 The effect of varying the backfill's load dispersal angle

Results of the parametric study on the effect of the backfill's load dispersal angle are presented in Figures 4.3g, 4.4g, 4.5g and 4.6d. An illustration of the load distribution on Barlae is given in Figure 4.6e. Varying the backfill's load dispersal angle had some effect on the estimated collapse loads but little effect on the slope of the initial elastic portion of the load *versus* deformation plot. For Bridgemill the FE estimated collapse load increased from 320kNm^{-1} to 381kNm^{-1} (actual collapse load = 361kNm^{-1}) as the backfill's load dispersal angle increased from the point load case, through 0° to 55°. For Strathmashie the FE estimated collapse load increased from 175kNm^{-1} to 220kNm^{-1} (actual collapse load = 228kNm^{-1}) as the load dispersal angle increased from the point load case through 0° to 70°. For Barlae the FE estimated collapse load increased from 247kNm^{-1} to 310kNm^{-1} (actual collapse load = 296kNm^{-1}) as the backfill's load dispersal angle increased from the point load case, through 0° to 48°. Different ranges of load distribution angle were used because of the geometries of the different arches, at no time was load dispersal beyond the springers permitted.

Given the importance of soil-structure interaction effects upon the assessed capacity of an arch bridge the author recommend selection of a load dispersal angle consistent with the Boussinesq stress distribution's least significant stress increase contour. The use of Boussinesq's method and its variants for stress dispersal above an arch bridge is well documented elsewhere (FAIRFIELD *et al.*, 1994a & b; 1996).

4.5 Bolton multi-span arch bridge

This section presents the numerical results for the Bolton multi-span arch bridge (MELBOURNE *et al.*, 1992a). A parametric study was carried out on the arch's and pier's elastic moduli, compressive strength and tensile strength. This was then followed by a parametric study on the material properties of each component, the arch ring and pier, in order to quantify their individual influence on the ultimate strength of the whole arch bridge. Experimental results were compared with the FE output.

4.5.1 Bolton multi-span arch bridge test results

Salient dimensions and material properties were presented in Table 4.1. The idealised mesh for this bridge is shown in Figure 4.7a. It comprised of three nominally identical segmental arch barrels supported by an abutment at each end and two intermediate piers. Each arch barrel consisted of two brick rings built in stretcher bond with no intimate contact between rings other than the mortar bed joint. There were three multi-span arch bridges tested to collapse but only the one without spandrel walls was analysed in this study as it was more appropriate for the author's two dimensional idealisation.

The model used in the FE analysis for this bridge was similar to that used for the single span arch bridges described in Section 4.2. Springers not supported by piers were rigidly fixed in both horizontal and vertical directions. The piers were also rigidly fixed to the ground in both horizontal and vertical directions. These support conditions were appropriate as no movement of the supports was reported at the springers at either end or at the bases of both piers.

A full width knife edge load was applied to the bridge at one quarter span point on the middle ring. The ultimate load recorded was 111kNm^{-1} associated with the formation of seven hinges which turned the bridge into a global mechanism.

4.5.2 Numerical results for Bolton multi-span arch bridge

The collapse load predicted by the FE method was 111.6kNm^{-1} width perpendicular to the span with the material properties given in Table 4.1. This prediction of the collapse load compared well with the experimental result of 111kNm^{-1} width. Load *versus* deflection relationships under the loading point from the experiment and the FE output are presented in Figure 4.7b. The load *versus* deflection relationships at the crowns of each ring from the FE output are presented in Figure 4.7c. Results from the parametric study on the effects of both arch's and pier's elastic modulus, compressive strength and tensile strength are presented in Figures 4.7d to 4.7f respectively: for the arch ring only these are presented in Figures 4.7g to 4.7i respectively: and for the pier only these are presented in Figures 4.7j to 4.7l respectively. The summaries of the collapse loads from the parametric studies on elastic modulus, compressive strength and tensile strength are presented in Figures 4.7m to 4.7p respectively. The hinge locations predicted by FE analysis and crack development are presented in Figures 4.7q and 4.7r respectively.

4.5.3 FE analysis for Bolton multi-span arch bridge

The FE prediction of the collapse load was 111.6kNm^{-1} which compared well with the experimental result of 111kNm^{-1} width. This yielded a discrepancy of only +0.54%. An excellent prediction of load *versus* deflection relationships was achieved as presented in Figure 4.7b. Figure 4.7c shows the deflections at the crowns of each ring as predicted by the FE analysis. Ring 1 moved upward by about 25mm causing formation of a hinge at the extrados. The crown deflection at ring 2 was so negligible as it may have been close to the segment's instantaneous centre of rotation. The crown deflection at ring 3 was also very small and it remained undamaged after the test.

4.5.4 Analysis of the results of the FE parametric study for Bolton multi-span arch bridge

The influence of material properties of both the arch ring and the pier in the FE based parametric study is discussed. A parametric study was first carried out by varying the material properties of both the arch and pier simultaneously. This was then followed by varying material properties of each component while keeping the material properties of the other component unchanged as given in Table 4.1. Three parameters were investigated: the elastic modulus, compressive strength and tensile strength.

4.5.4.1 The effect of varying the elastic modulus

The effects of varying the elastic modulus of both the arch and pier, arch only, and pier only are presented in Figures 4.7d, 4.7g, and 4.7j respectively. The summary of collapse loads from this parametric study is presented in Figure 4.7m. The range of elastic modulus used in this parametric study was between 2000MPa to 16200MPa. The only major influence of the elastic modulus of the arch ring and pier was the flexibility of load *versus* deflection characteristic. As in the case for single span arches, if there is no limitation of maximum deflection the collapse load will not be affected by elastic modulus. It can be seen from Figure 4.7m that the collapse load increases with the increase of elastic modulus but to a very negligible extent.

The FE estimated collapse load increased from 111kNm^{-1} to 114.4kNm^{-1} (actual collapse load = 111kNm^{-1}) as both the arch and pier elastic moduli increased from 2000MPa to 16200MPa. The difference of collapse load within this range of elastic modulus was only 3.1%. The influence of the elastic modulus of each component the was even more negligible as can be seen in Figure 4.7m.

4.5.4.2 The effect of varying the compressive strength

The effects of varying the compressive strength of both the arch and pier, arch only, and pier only are presented in Figures 4.7e, 4.5h, and 4.7k respectively. The summary of the collapse loads from this parametric study is presented in Figure 4.7n. The initial load *versus* deflection characteristic was not affected by the compressive strength. However, the collapse load was affected by the variations of compressive strength; values ranging from 8MPa to 1×10^{6}MPa were used. As the compressive strength of both the arch and pier increased from 8MPa to 1×10^{6}MPa, the predicted collapse load increased from 107kNm^{-1} to 134kNm^{-1}; the actual collapse load was 111kNm^{-1}. By varying the compressive strength of each individual component from 8MPa to 1×10^{6}MPa the FE predicted collapse load increased from 110.3kNm^{-1} to 129.5kNm^{-1} and from 110.4kNm^{-1} to 124.8kNm^{-1} respectively. A range of compressive strengths between 8MPa to 20MPa is recommended by BS5628 (1992) for the combined compressive strength of masonry work.

4.5.4.3 The effect of varying the tensile strength

The effects of varying the tensile strength of both the arch and pier, arch only, and pier only are presented in Figures 4.7f, 4.7i, and 4.7l respectively. The summary of collapse loads from this parametric study is presented in Figure 4.7p. The estimated collapse loads were very sensitive to variations in both the arch's and pier's tensile strength; values ranging from 0.1MPa to 0.5MPa were used. The FE estimated collapse load increased from 73kNm^{-1} to 231kNm^{-1} (actual collapse load = 111kNm^{-1}) as the tensile strength of both the arch and pier increased from 0.1MPa to 0.5MPa. The influence of the tensile strength of the arch ring was more significant than that of the pier. By increasing the tensile strength of each individual component, the arch and pier, from 0.1MPa to 0.5MPa the FE estimated collapse load increased from 81kNm^{-1} to 203.5kNm^{-1} and from 102kNm^{-1} to 140.4kNm^{-1} respectively.

4.6 Conclusions

A commercially available finite element suite (LUSAS, 1997) has been used successfully to study the behaviour of masonry arch bridges with the following salient findings;

1 The chosen FE analysis could model the load *versus* deflection behaviour extremely well in the cases where the material properties are well known. Unfortunately this is often only the case for bridges where, for research purposes, tests to collapse have been undertaken with associated material testing. Four bridges were assessed: Bridgemill (actual collapse load = 361kNm^{-1}, FE collapse load = 362kNm^{-1}), Strathmashie (actual collapse load = 228kNm^{-1}, FE collapse load = 226kNm^{-1}), Barlae (actual collapse load = 296kNm^{-1}, FE collapse load = 302kNm^{-1}), and Bolton (actual collapse load = 111kNm^{-1}, FE collapse load = 112kNm^{-1}). These results, however, were obtained after carrying out a series of parametric studies to search a combination of input variables which gives good results in terms of the collapse loads and the load *versus* deflection characteristics.

2 The elastic modulus of the arch ring, and pier in the case for the multi-span bridge, had no significant effect on the collapse load but it did affect deformations at lower loads.

3 The compressive strength of the arch ring, and pier in the case for the multi-span bridge, had some effect on the collapse load but did not affect the initial load *versus* deflection characteristic. For Bridgemill the estimated collapse load increased from 252kNm^{-1} to 384kNm^{-1} (actual collapse load, 361kNm^{-1}) as the arch's compressive strength increased from 2MPa to 15MPa. For Strathmashie the estimated collapse load increased from 157kNm^{-1} to 230kNm^{-1} (actual collapse load, 228kNm^{-1}). For Barlae the estimated collapse load increased from 180kNm^{-1} to 321kNm^{-1} (actual collapse load, 296kNm^{-1})

over the same range. For Bolton multi-span bridge the estimated collapse load increased from 107kNm^{-1} to 130kNm^{-1} (actual collapse load, 111kNm^{-1}) as both the arch and pier compressive strength increased from 8MPa to 50MPa.

4 The tensile strength of the arch ring, and pier in the case of the multi-span bridge, significantly affected the collapse load. For Bridgemill the estimated collapse load increased from 296kNm^{-1} to 489kNm^{-1} (actual collapse load, 361kNm^{-1}) as the arch's tensile strength increased from 0.1MPa to 0.5MPa. For Strathmashie the estimated collapse load increased from 131kNm^{-1} to 314kNm^{-1} (actual collapse load, 228kNm^{-1}). For Barlae the estimated collapse load increased from 184kNm^{-1} to 360kNm^{-1} (actual collapse load, 296kNm^{-1}) over the same range. For Bolton multi-span bridge, the estimated collapse load increased from 73kNm^{-1} to 231kNm^{-1} (actual collapse load, 111kNm^{-1}) as both the arch and pier tensile strength increased from 0.1MPa to 0.5MPa. The influence of tensile strength on arch ring was more significant than that on the pier in the case of the Bolton bridge.

5 The load dispersal angle through the backfill had some influence on the collapse load with wider dispersal giving reduced extrados stresses hence lower deformations and higher collapse loads. Wide differences in soil-arch system geometries mean that for full treatment of soil-structure interaction effects such as this, each case may have to be assessed on its own merits.

6 FE results showed that all single span arch bridges failed with the formation of four yielded zones. The plots of compressive stress vectors simulated the position of the thrustline as described in the mechanism method.

7 In the case of the multi-span bridge, FE analysis predicted a total of seven yielded zones. There were three yielded zones on the span remote from the load, three on the span under the load, and one at the base of the pier remote from the load. These locations coincided with the experimental hinge

locations.

8 Failure was not restricted to the loaded span for the multi-span arch bridge. Only the span remote from the load suffered damage but the span closest to the load was undamaged until the final collapse of the bridge.

9 The chosen FE suite performed at least as well as any of the chosen current assessment methods in the three cases presented here. A limitation to the use of FE based assessment would be the time and computer power required for pre-processing and analysis of the data. It is recommended that FE methods are chosen only where the implicit cost merits their use. However, the cost for FE analysis is negligible when compared with the costs of unnecessary replacement and repair as the result of poor assessments.

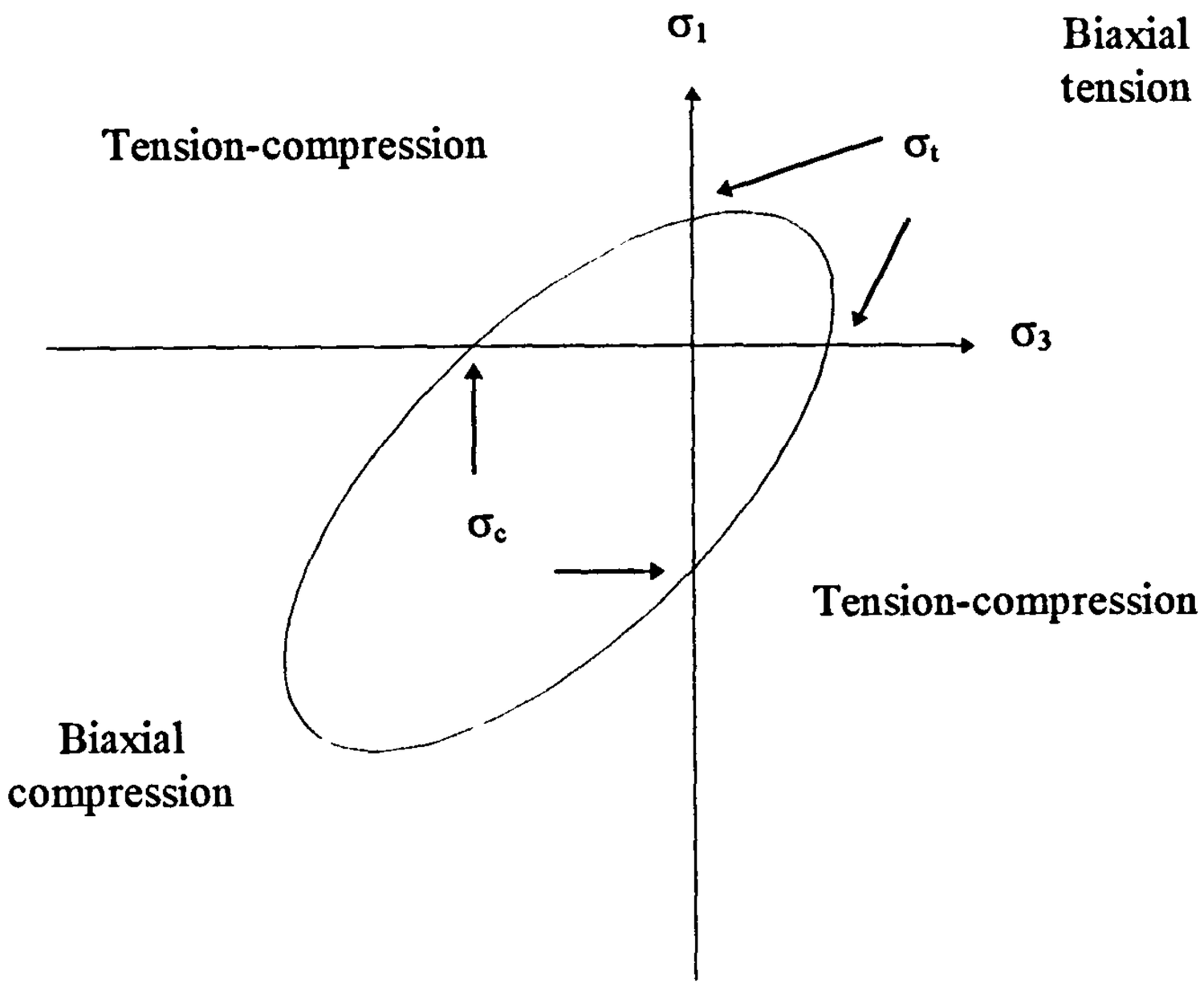

Figure 4.1 Failure envelope for modified von Mises model

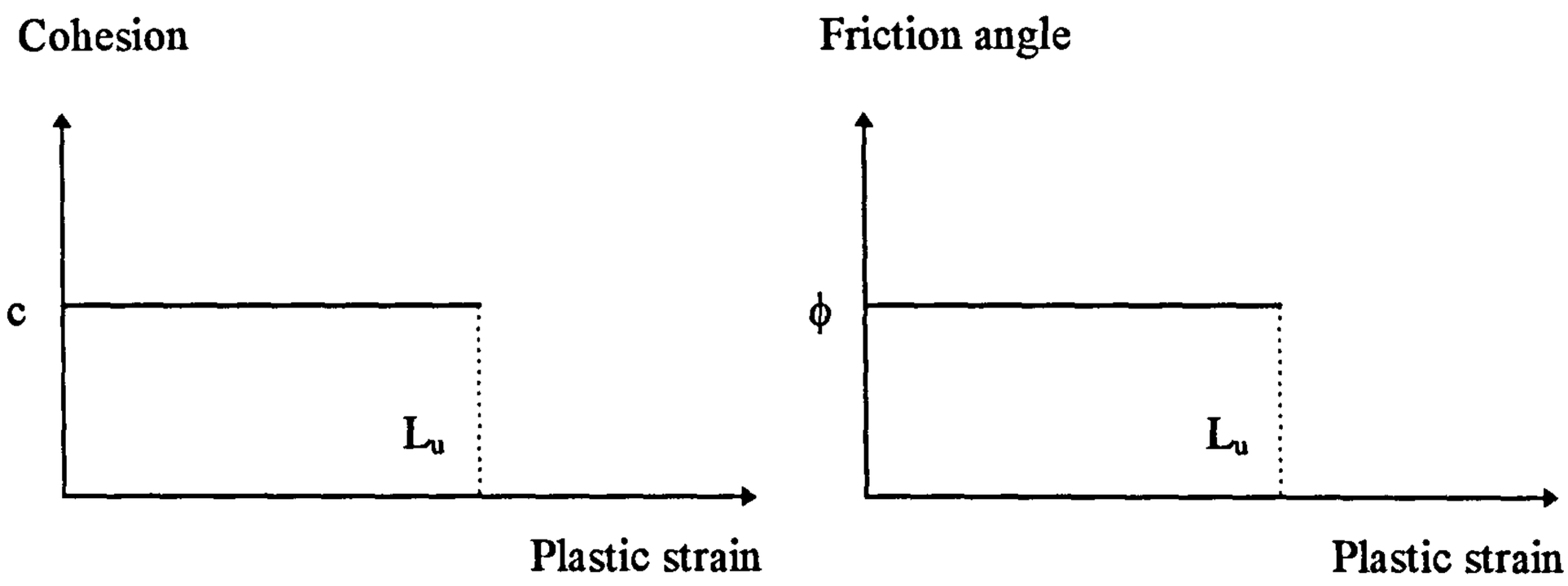

L_u = The limit to which the hardening curve is valid

Figure 4.2 Failure envelope for Mohr-Coulomb model

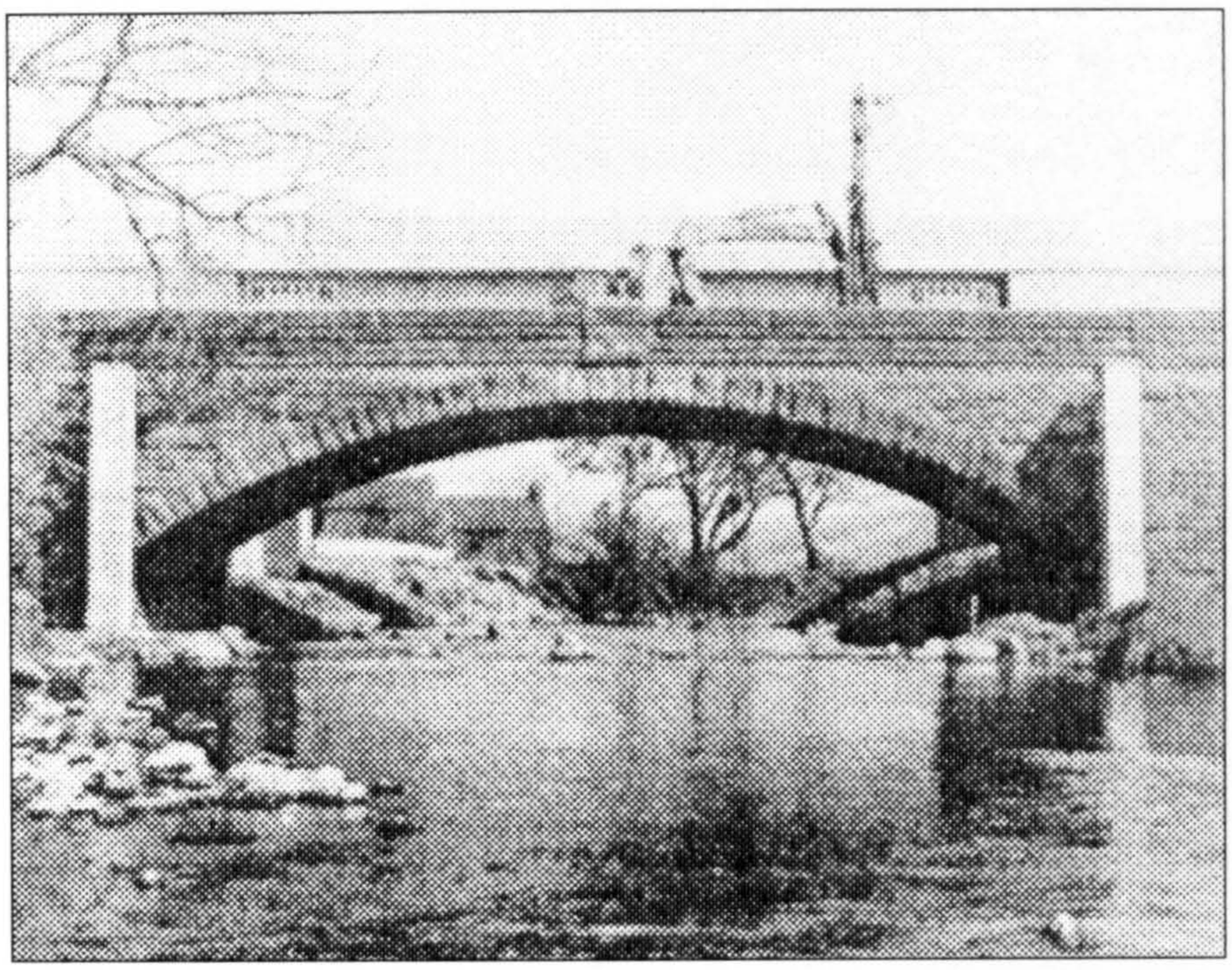

Figure 4.3a Bridgemill bridge (After HENDRY *et al.*, 1985)

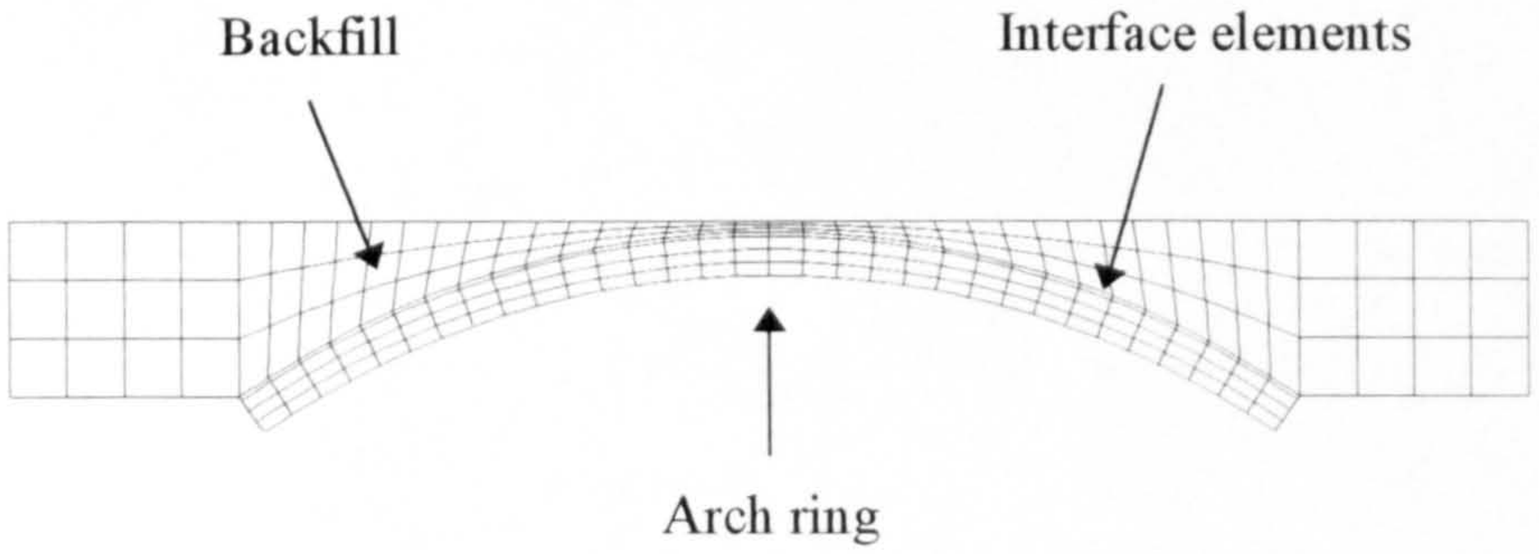

Figure 4.3b Idealised mesh for Bridgemill bridge

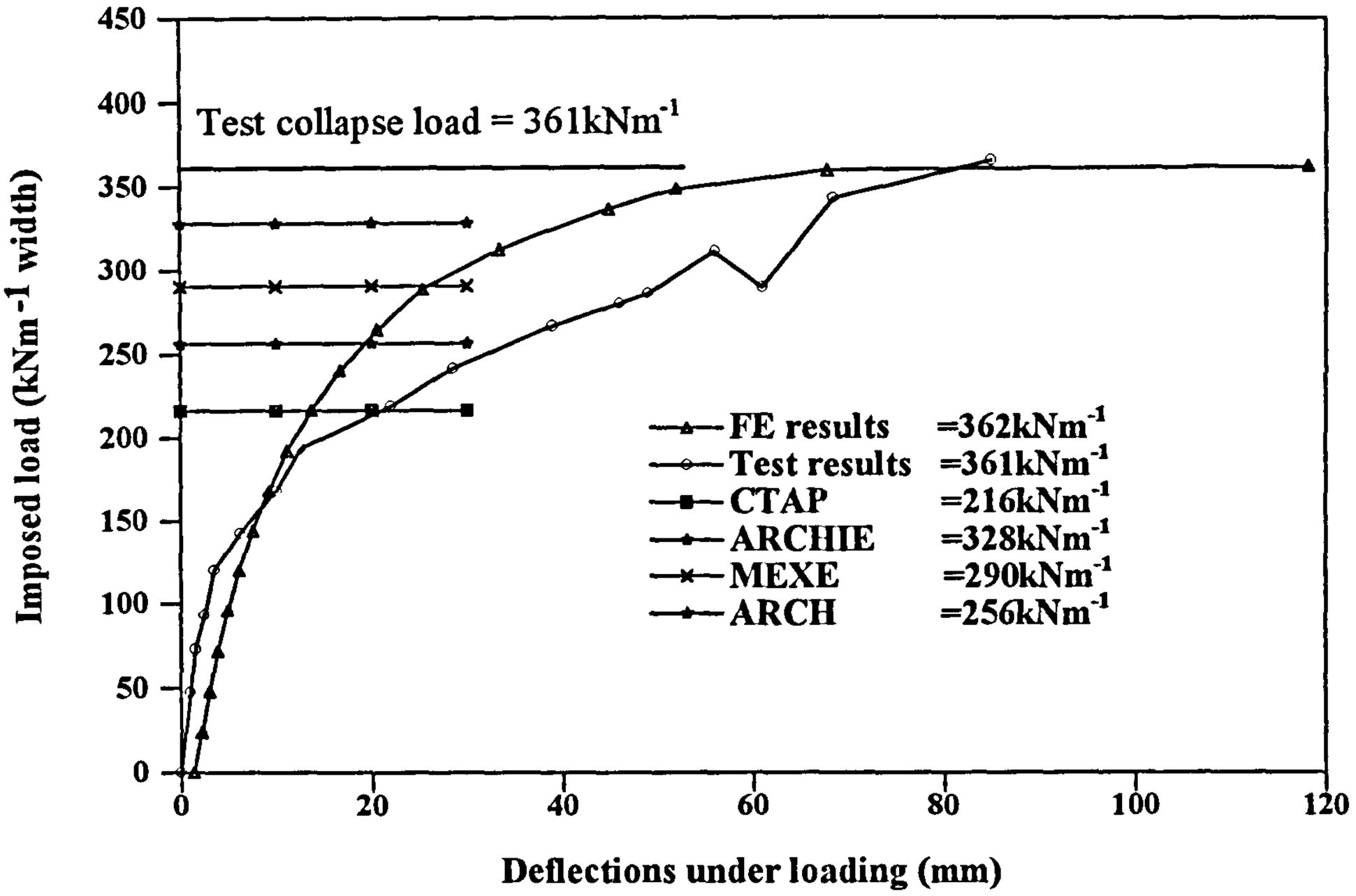

Figure 4.3c Load *versus* deflection relationships for Bridgemill

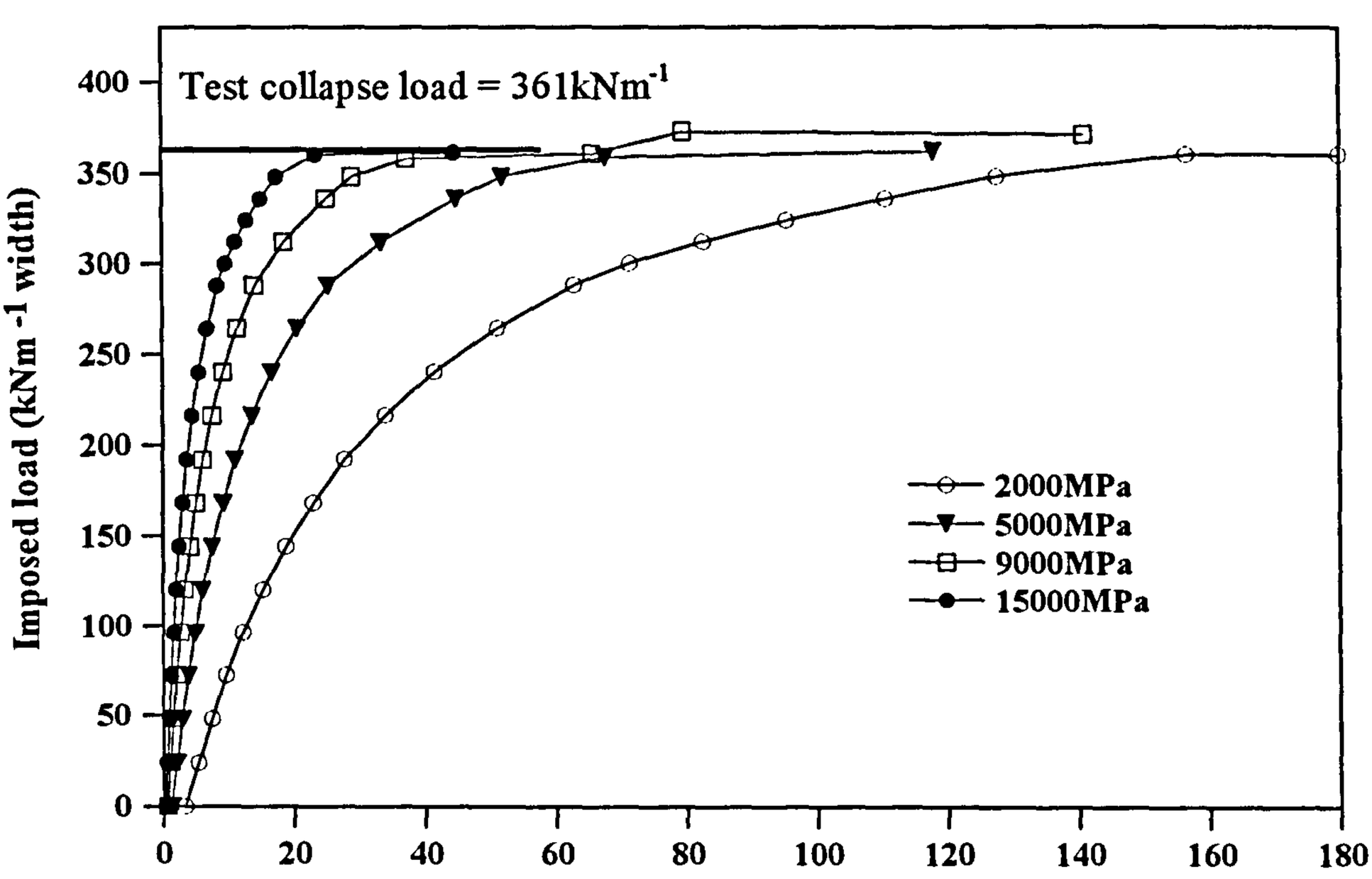

Figure 4.3d Parametric study: the effect of arch elastic modulus on Bridgemill

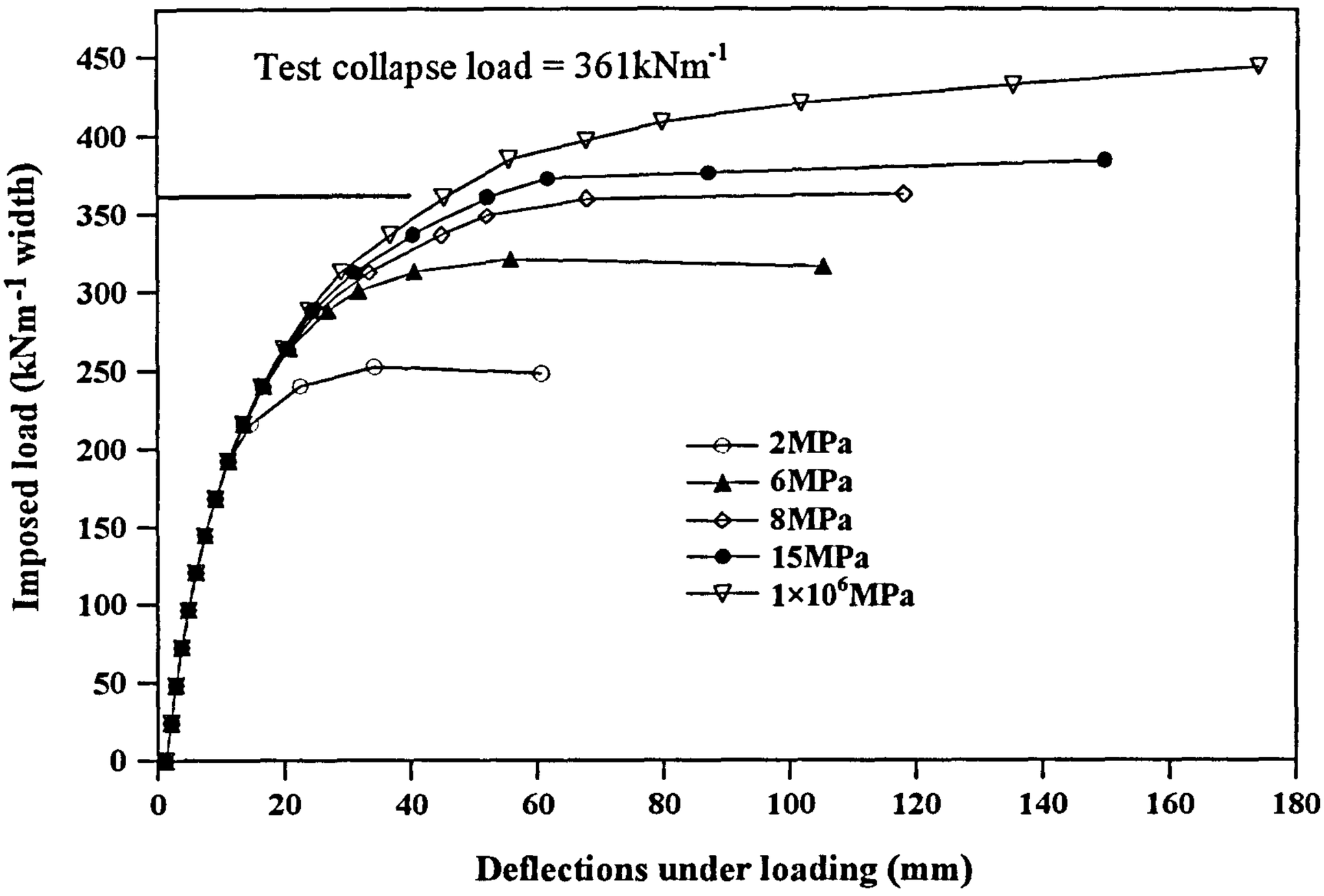

Figure 4.3e Parametric study: the effect of arch compressive strength on Bridgemill

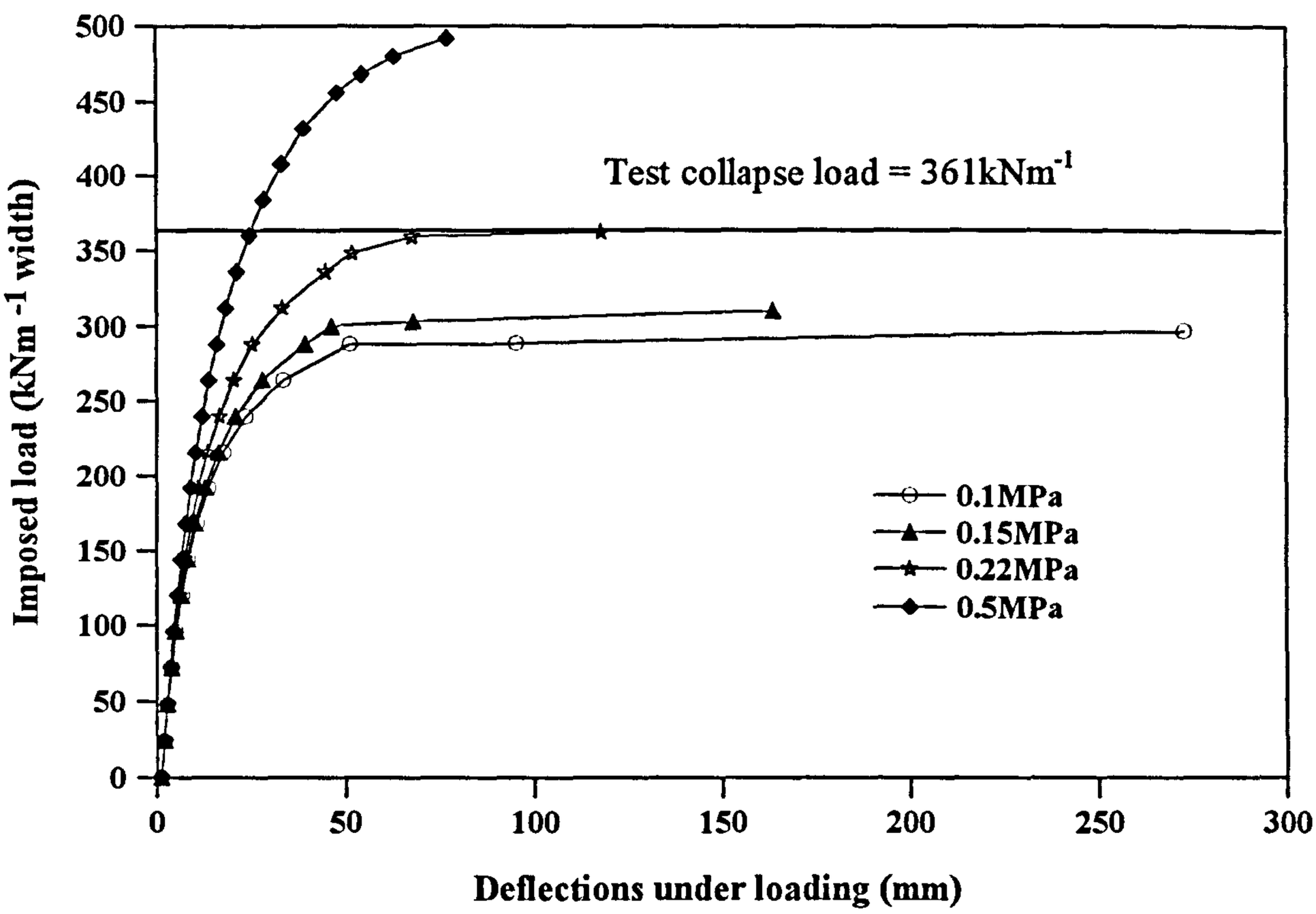

Figure 4.3f Parametric study: the effect of arch tensile strength on Bridgemill

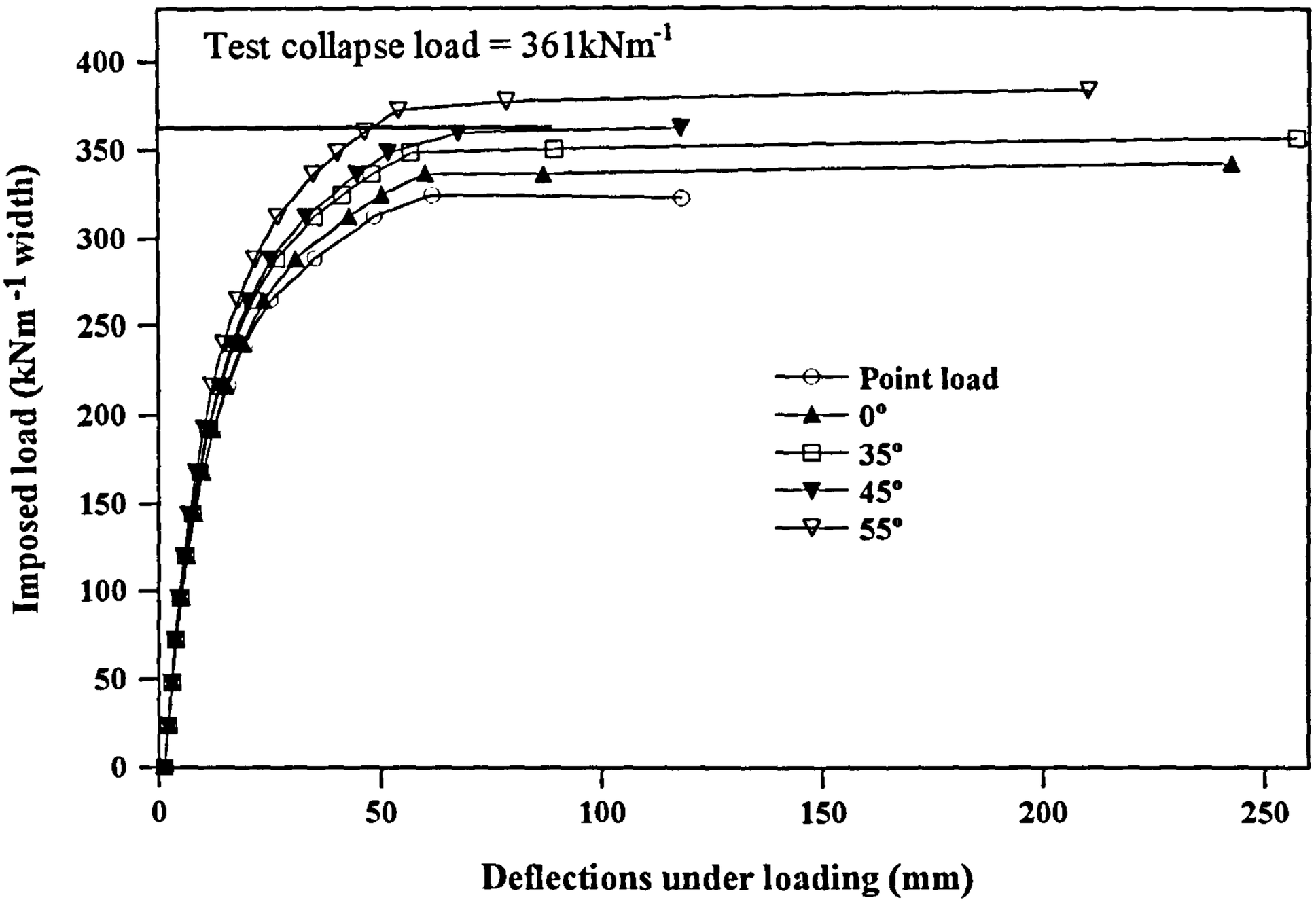

Figure 4.3g Parametric study: the effect of load dispersal angle on Bridgemill

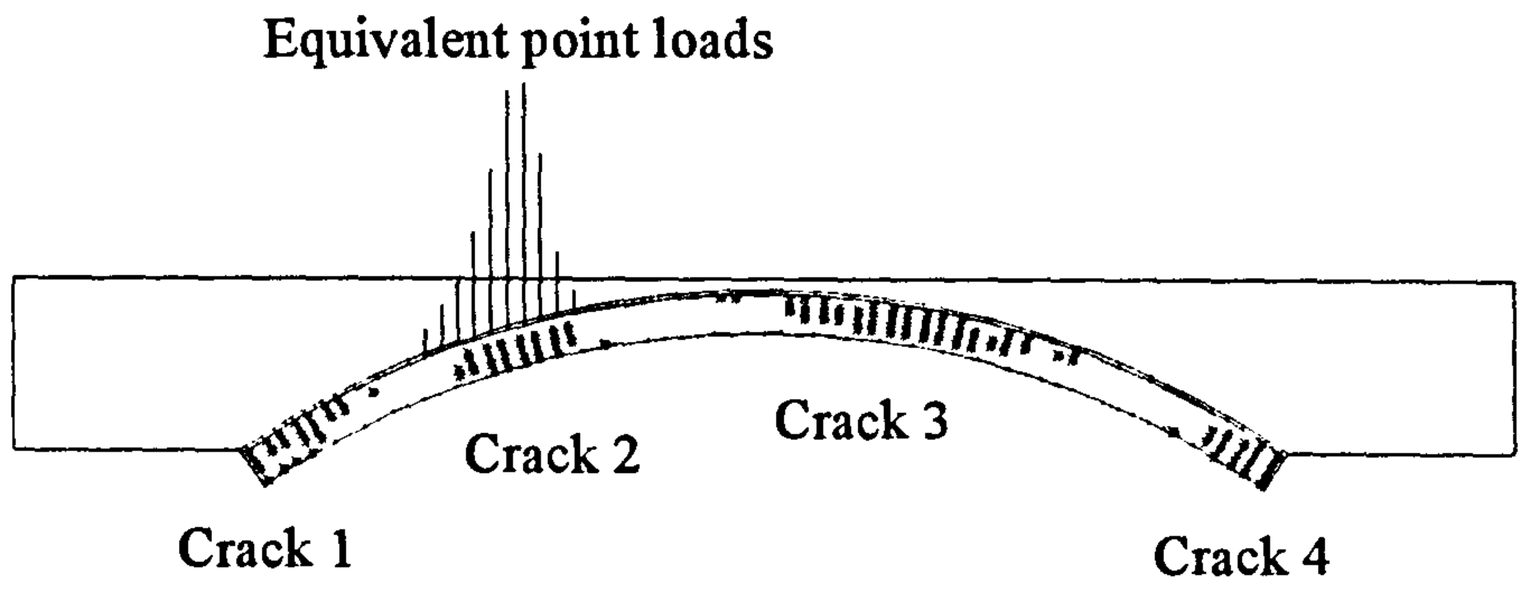

Figure 4.3h Yielded zones at Bridgemill as predicted by FE analysis

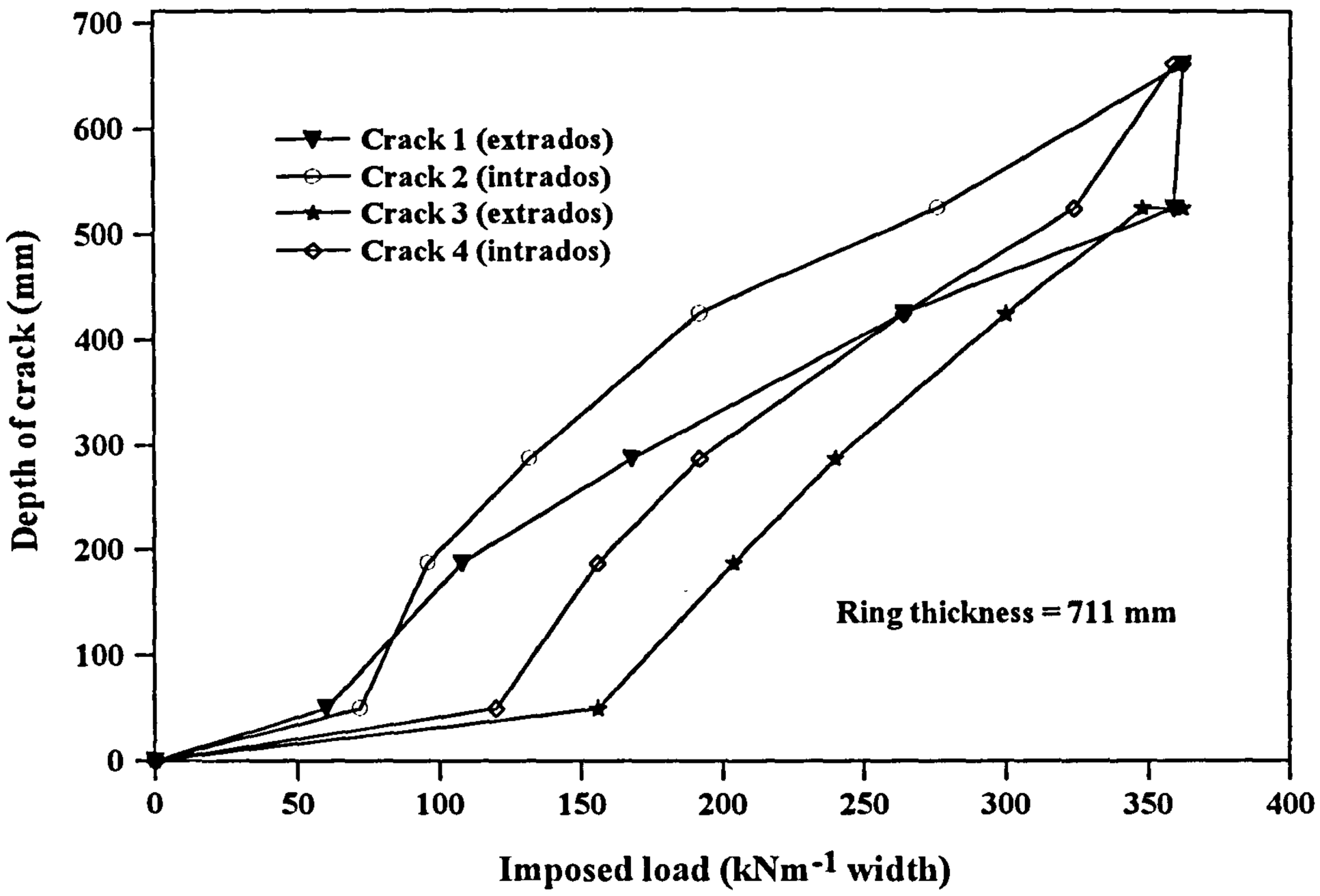

Figure 4.3i Imposed loading and crack development for Bridgemill

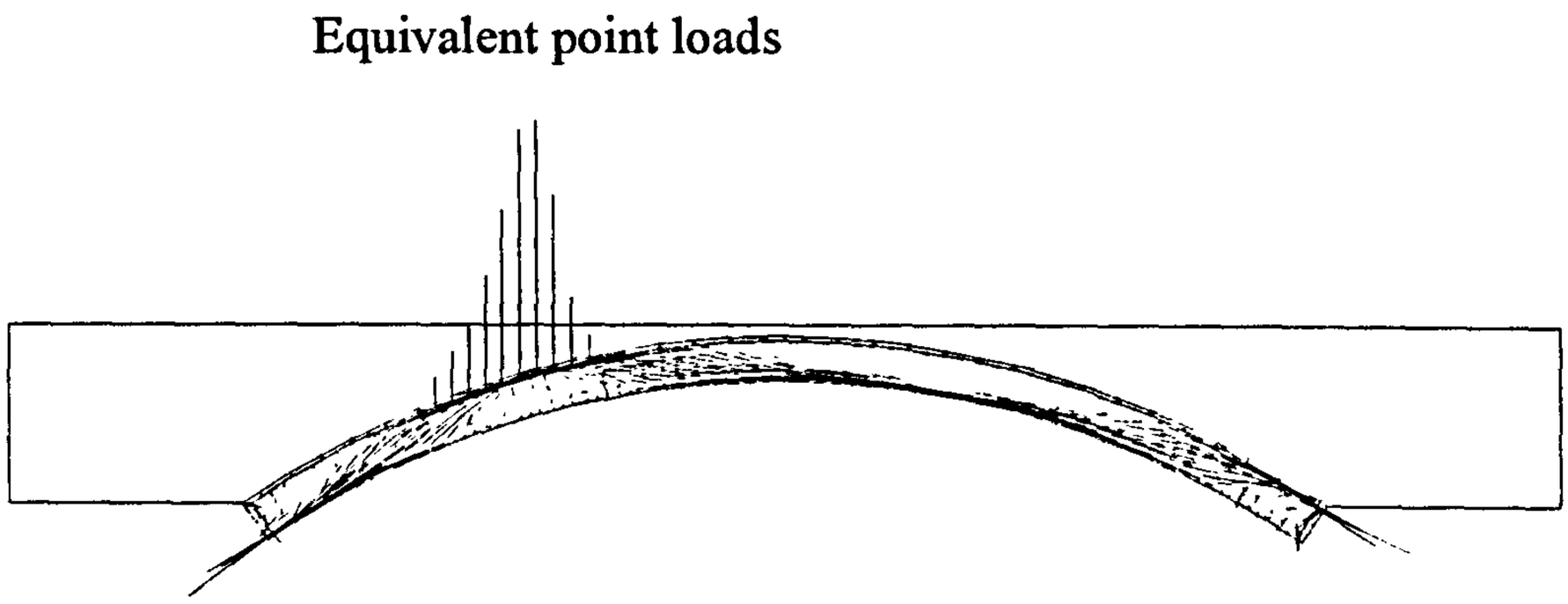

Figure 4.3j Compressive stress vector for Bridgemill

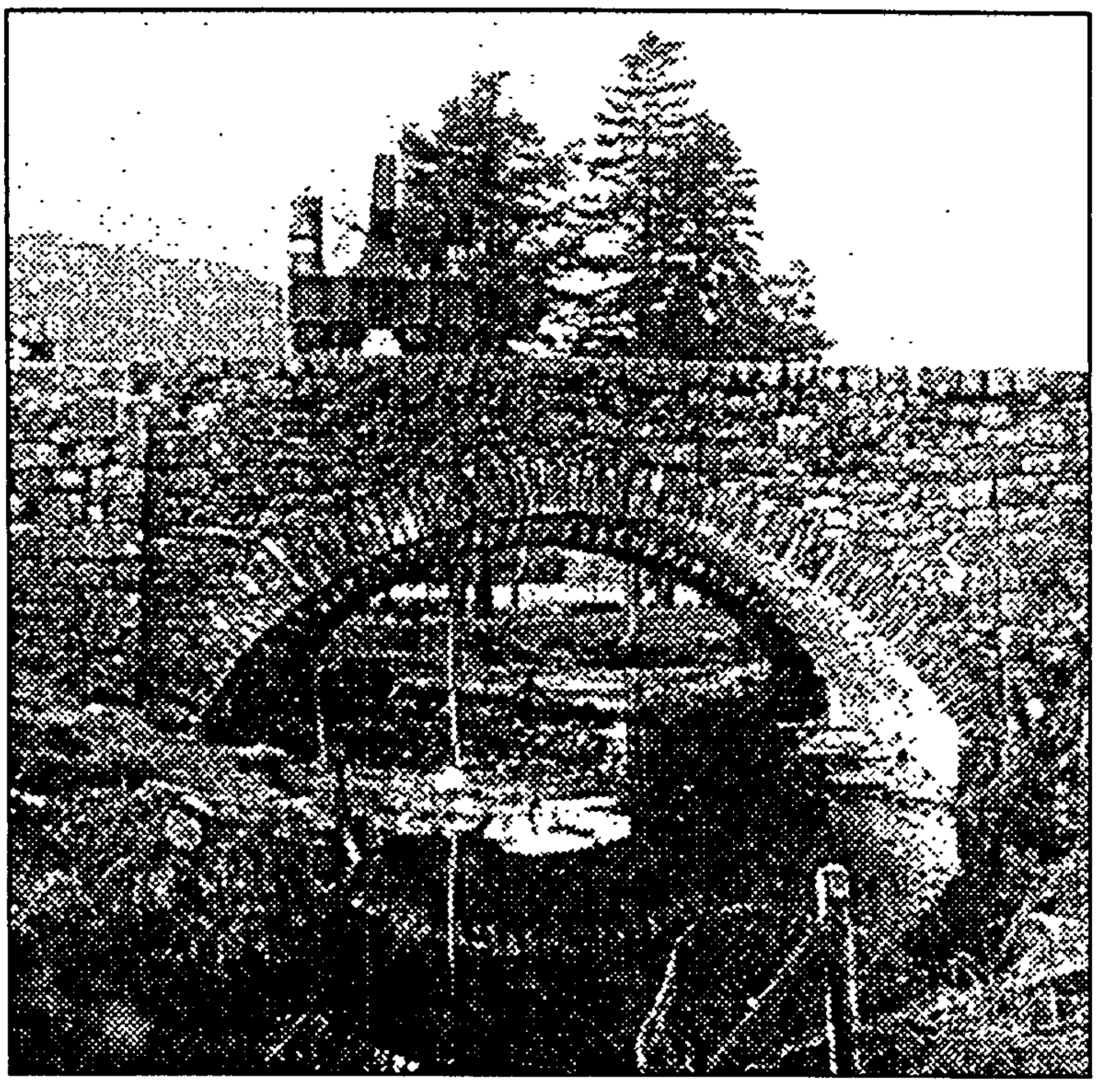

Figure 4.4a Strathmashie bridge (After PAGE, 1989)

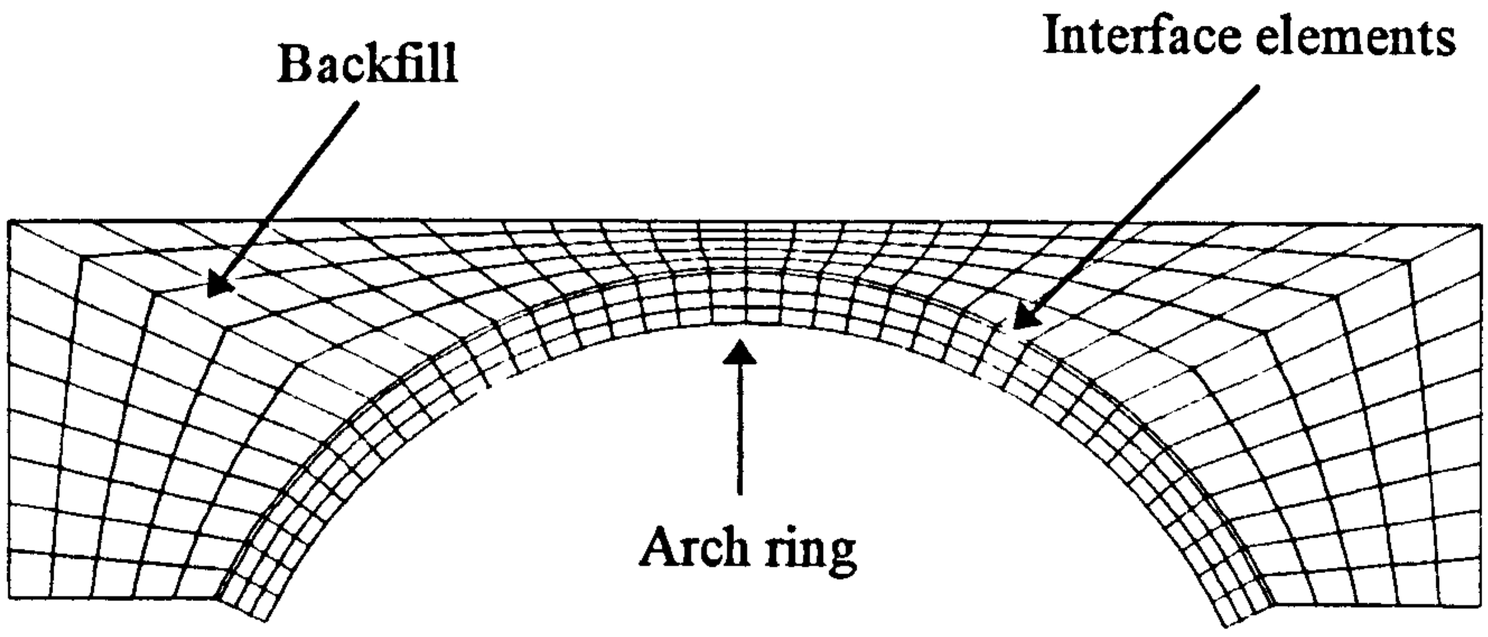

Figure 4.4b Idealised mesh for Strathmashie bridge

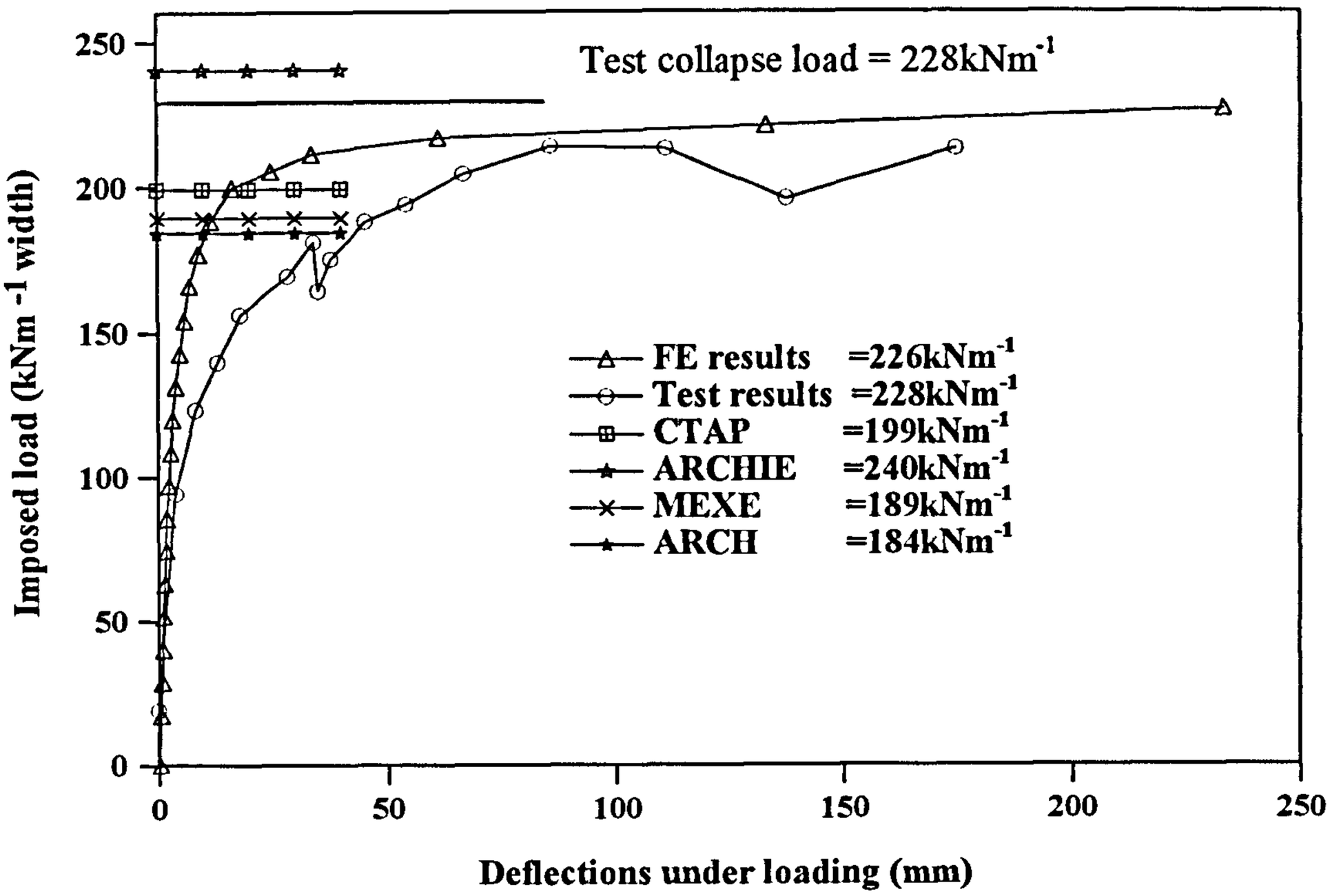

Figure 4.4c Load *versus* deflection relationships for Strathmashie

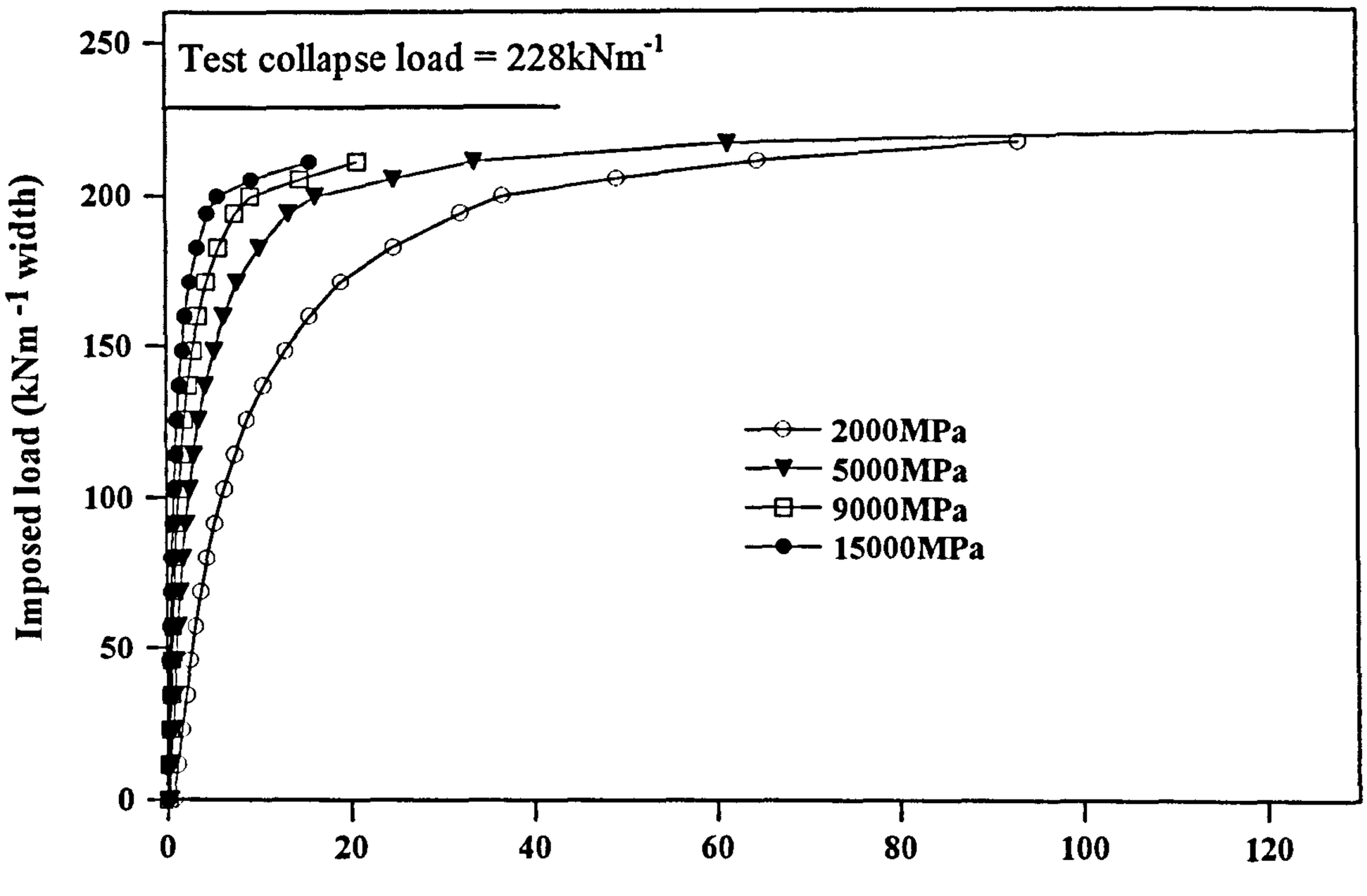

Figure 4.4d Parametric study: the effect of arch elastic modulus on Strathmashie

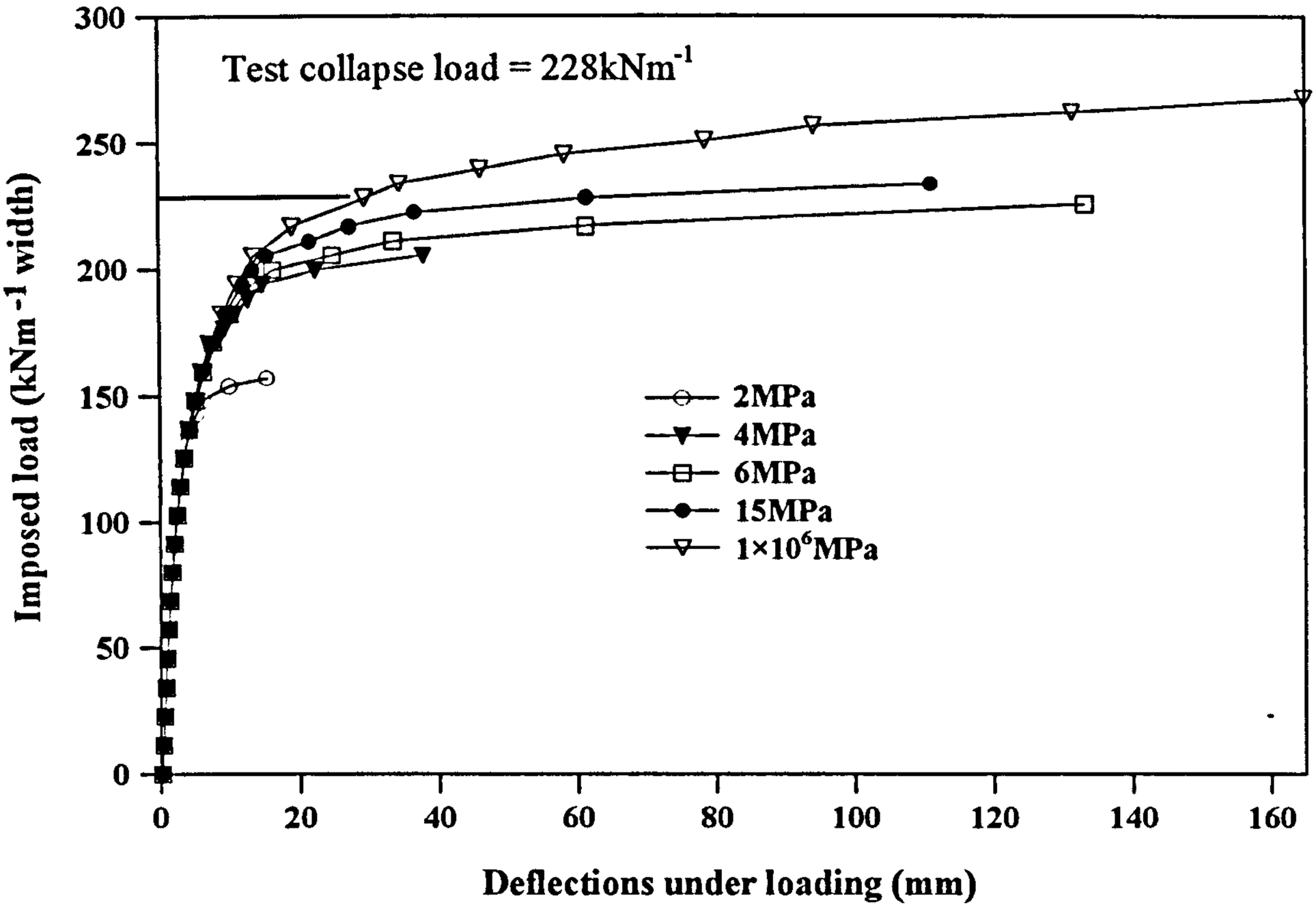

Figure 4.4e Parametric study: the effect of arch compressive strength on Strathmashie

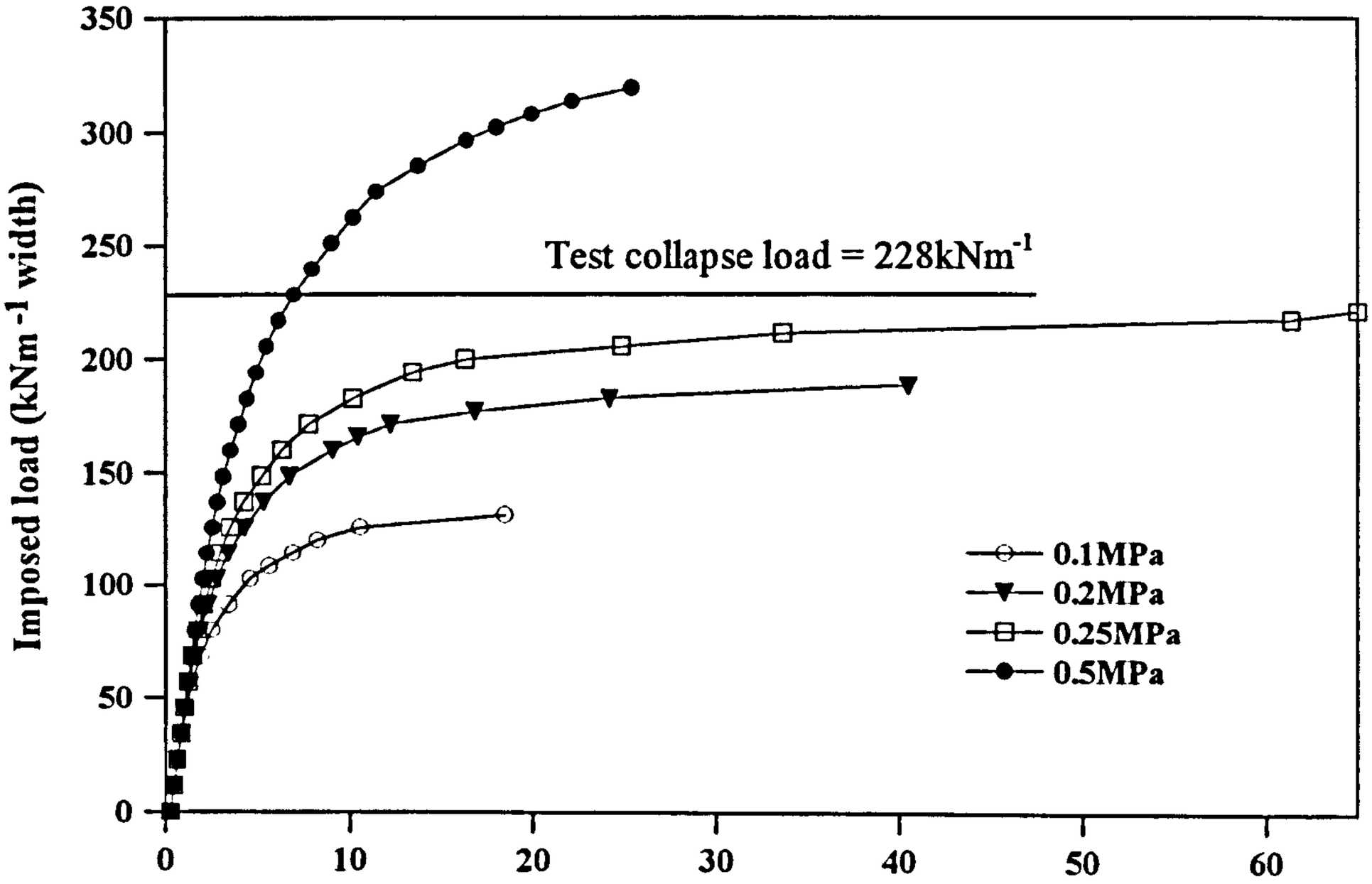

Figure 4.4f Parametric study: the effect of arch tensile strength on Strathmashie

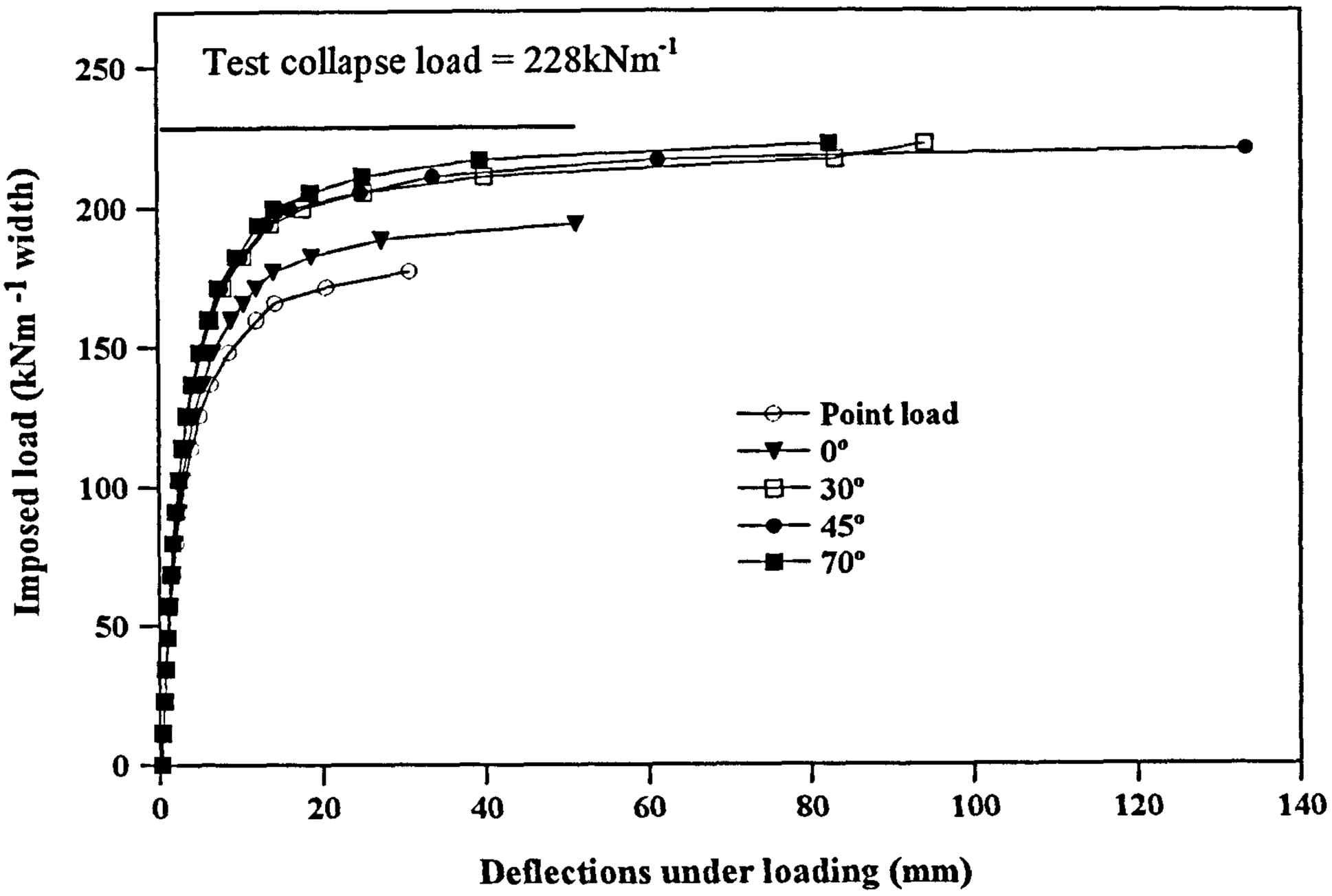

Figure 4.4g Parametric study: the effect of load dispersal angle on Strathmashie

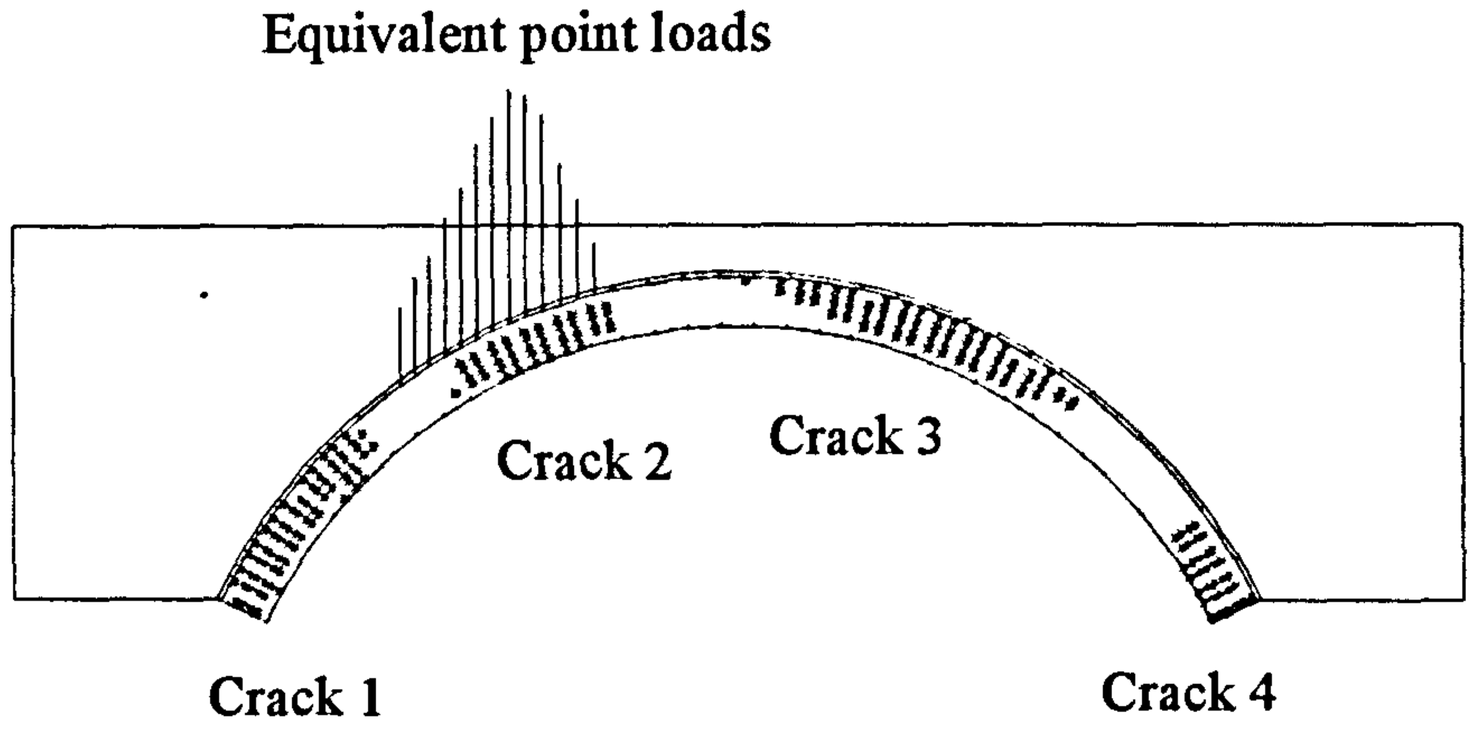

Figure 4.4h Yielded zones at Strathmashie as predicted by FE analysis

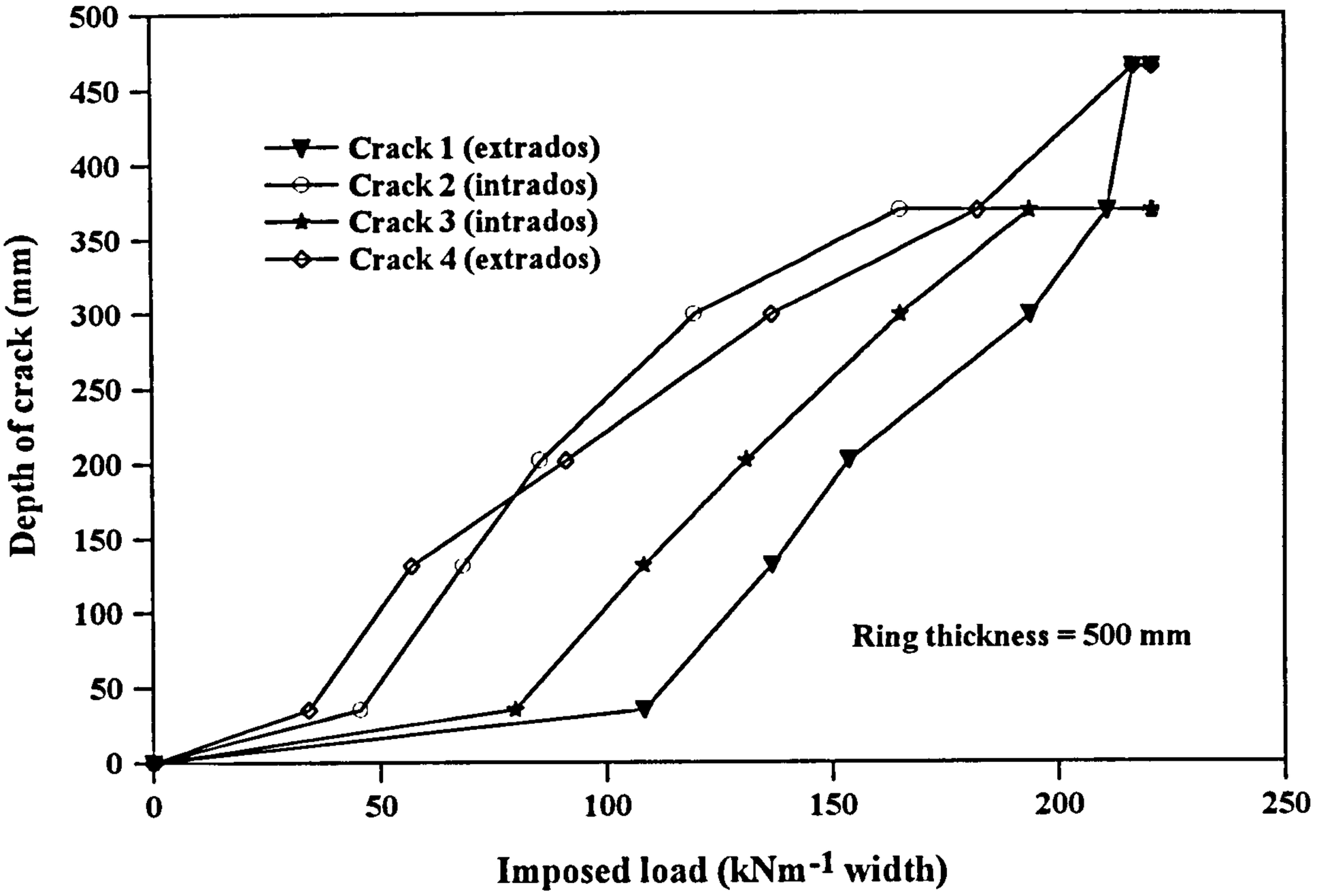

Figure 4.4i Imposed loading and crack development for Strathmashie

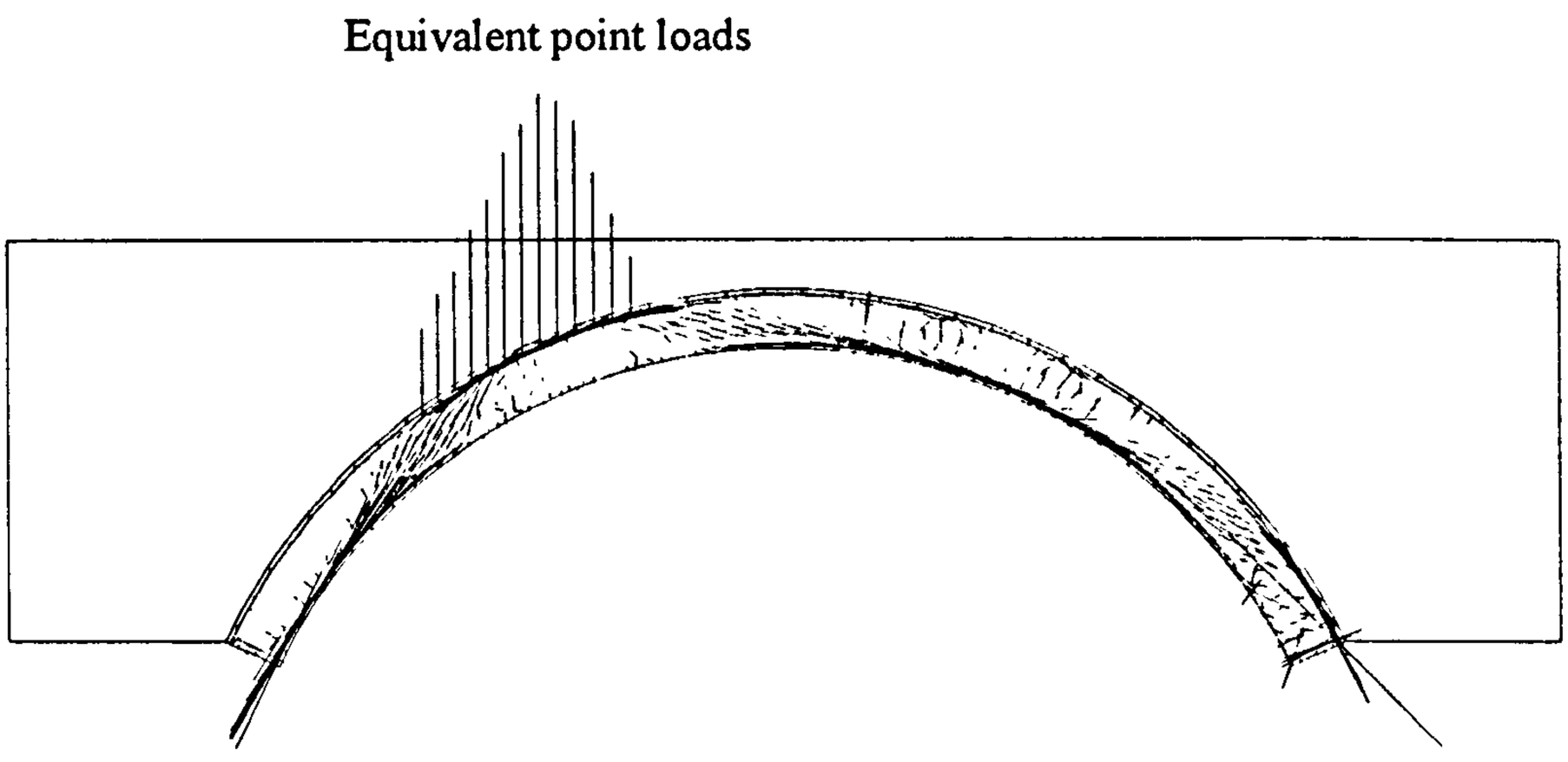

Figure 4.4j Compressive stress vector for Strathmashie

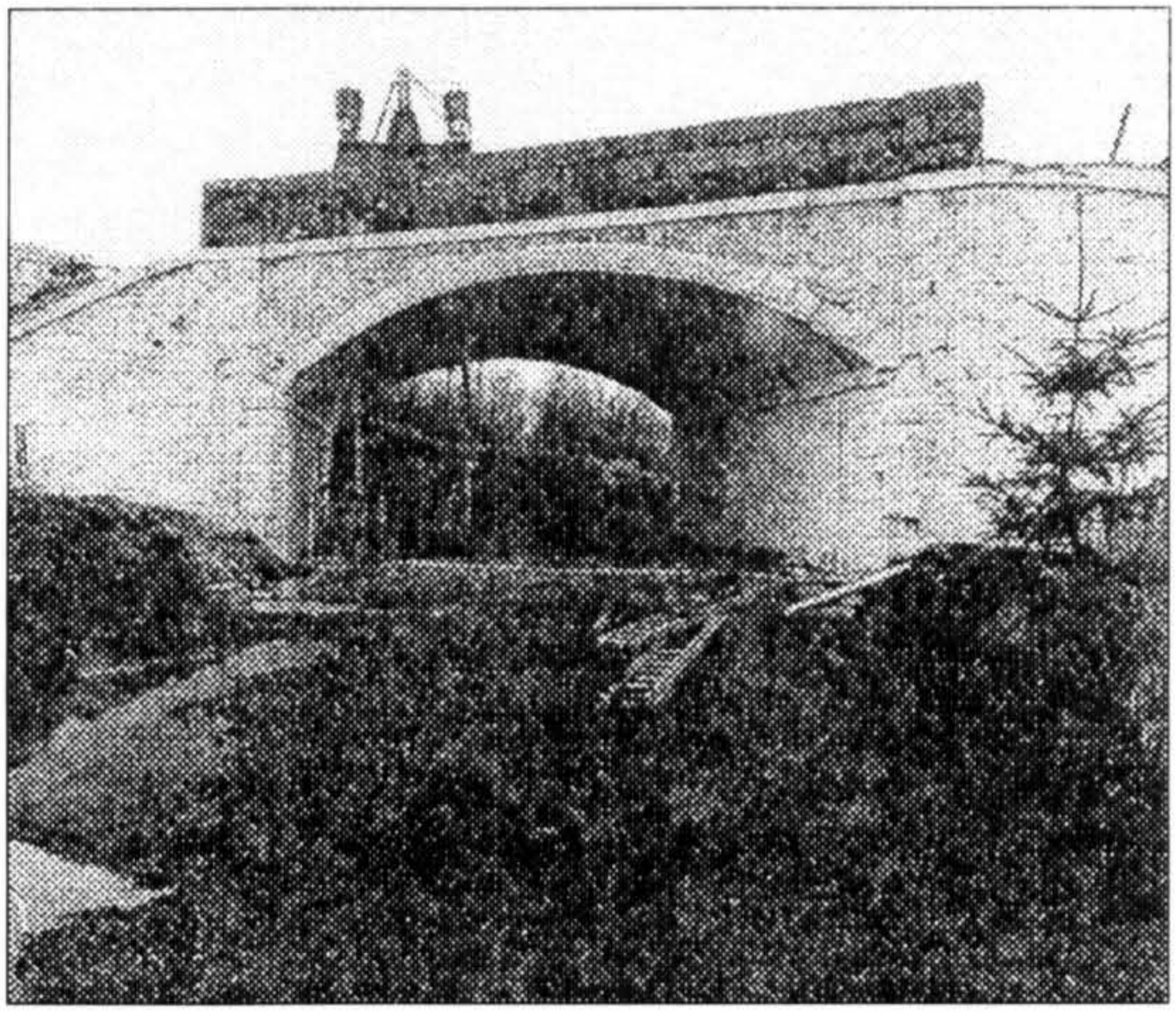

Figure 4.5a Barlae bridge (After PAGE, 1989)

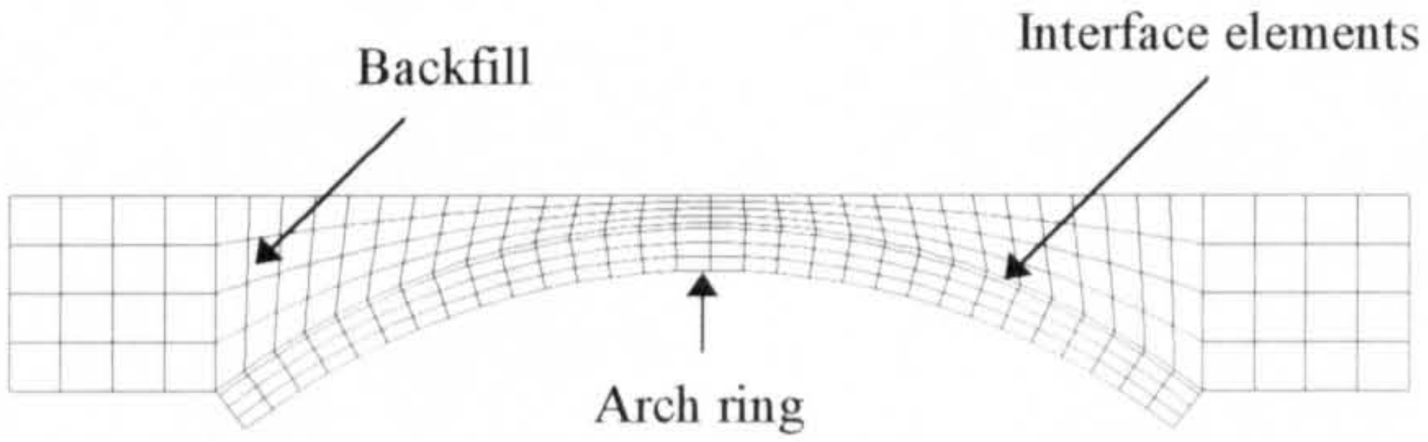

Figure 4.5b Idealised mesh for Barlae bridge

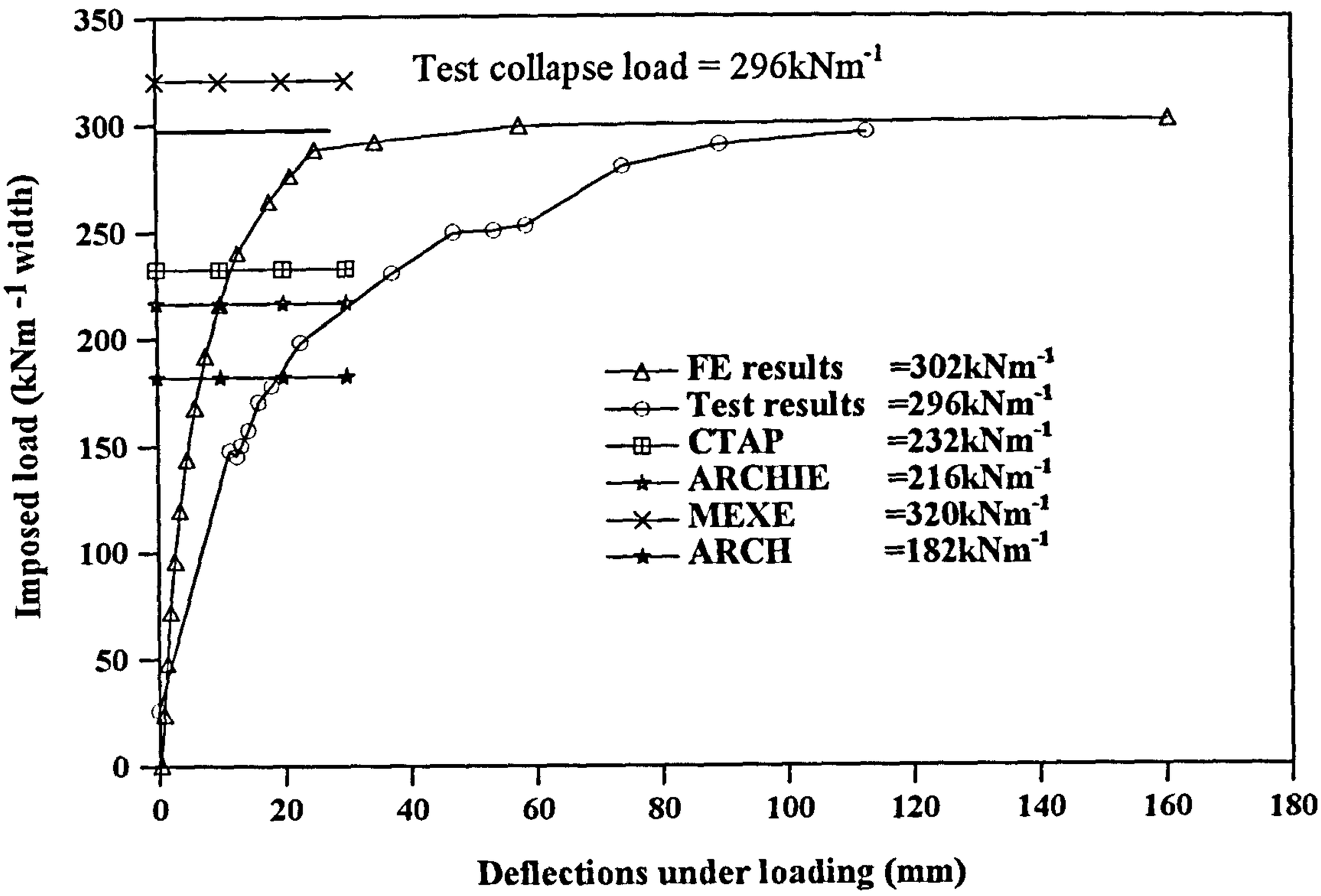

Figure 4.5c Load *versus* deflection relationships for Barlae

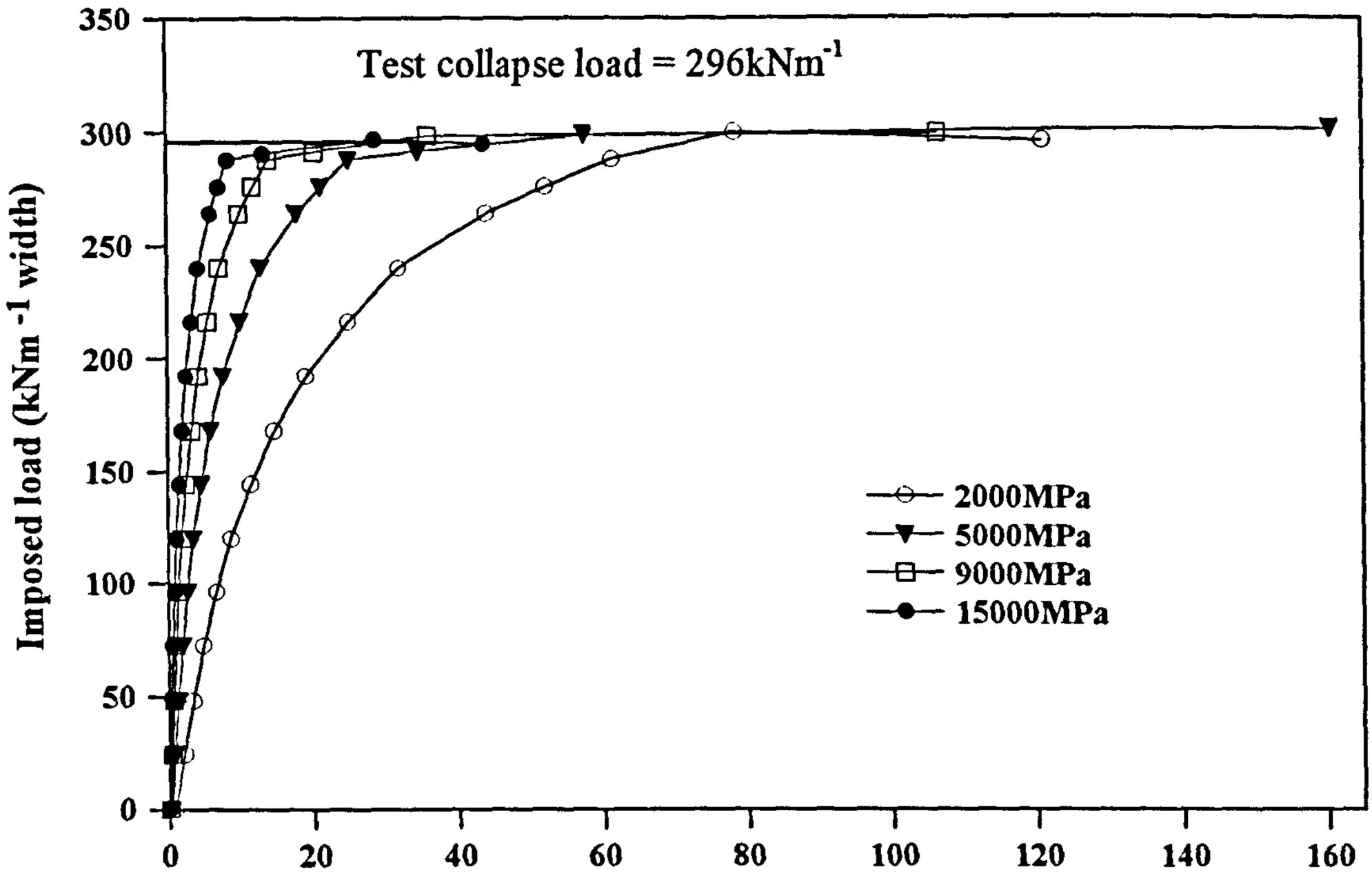

Figure 4.5d Parametric study: the effect of arch elastic modulus on Barlae

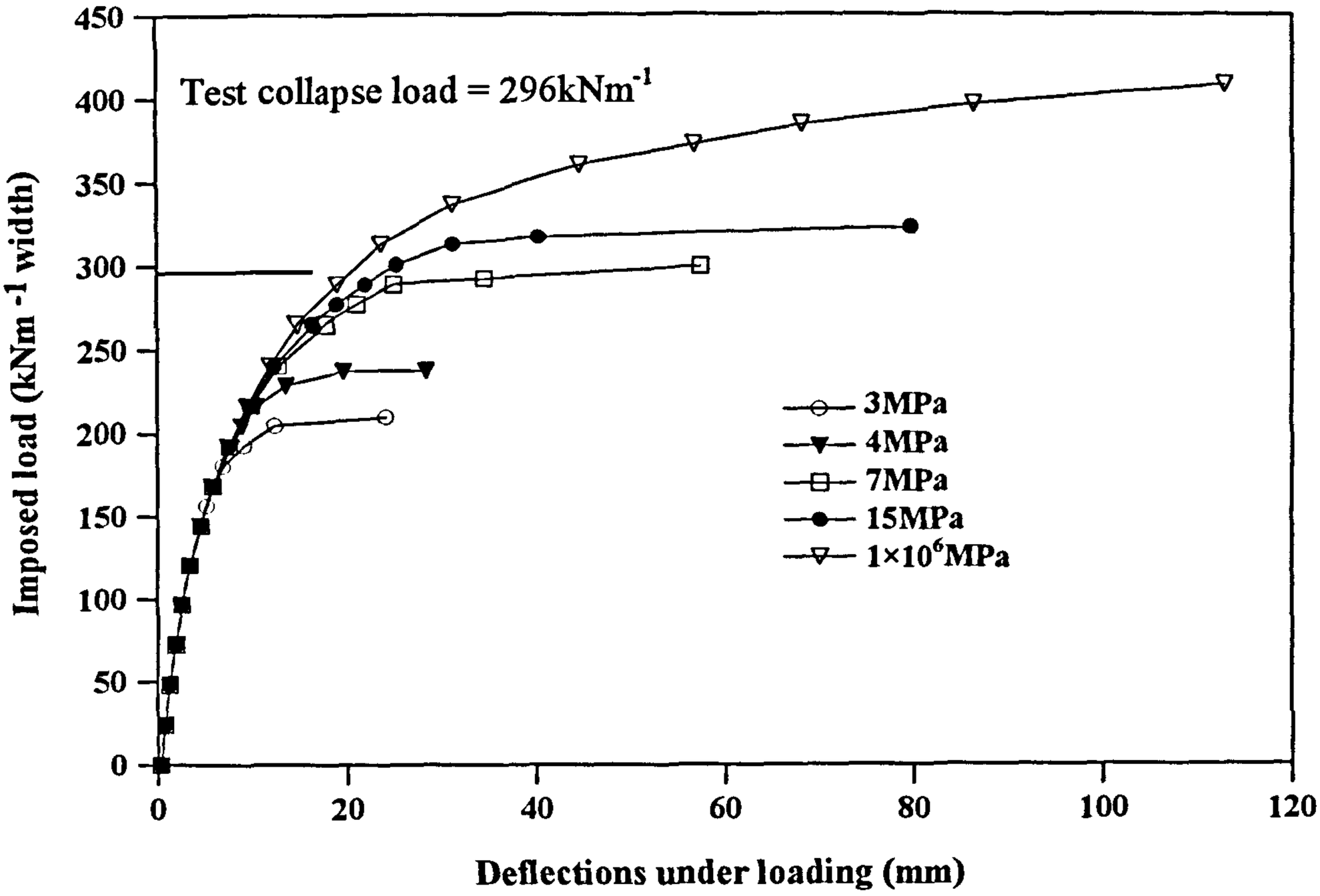

Figure 4.5e Parametric study: the effect of arch compressive strength on Barlae

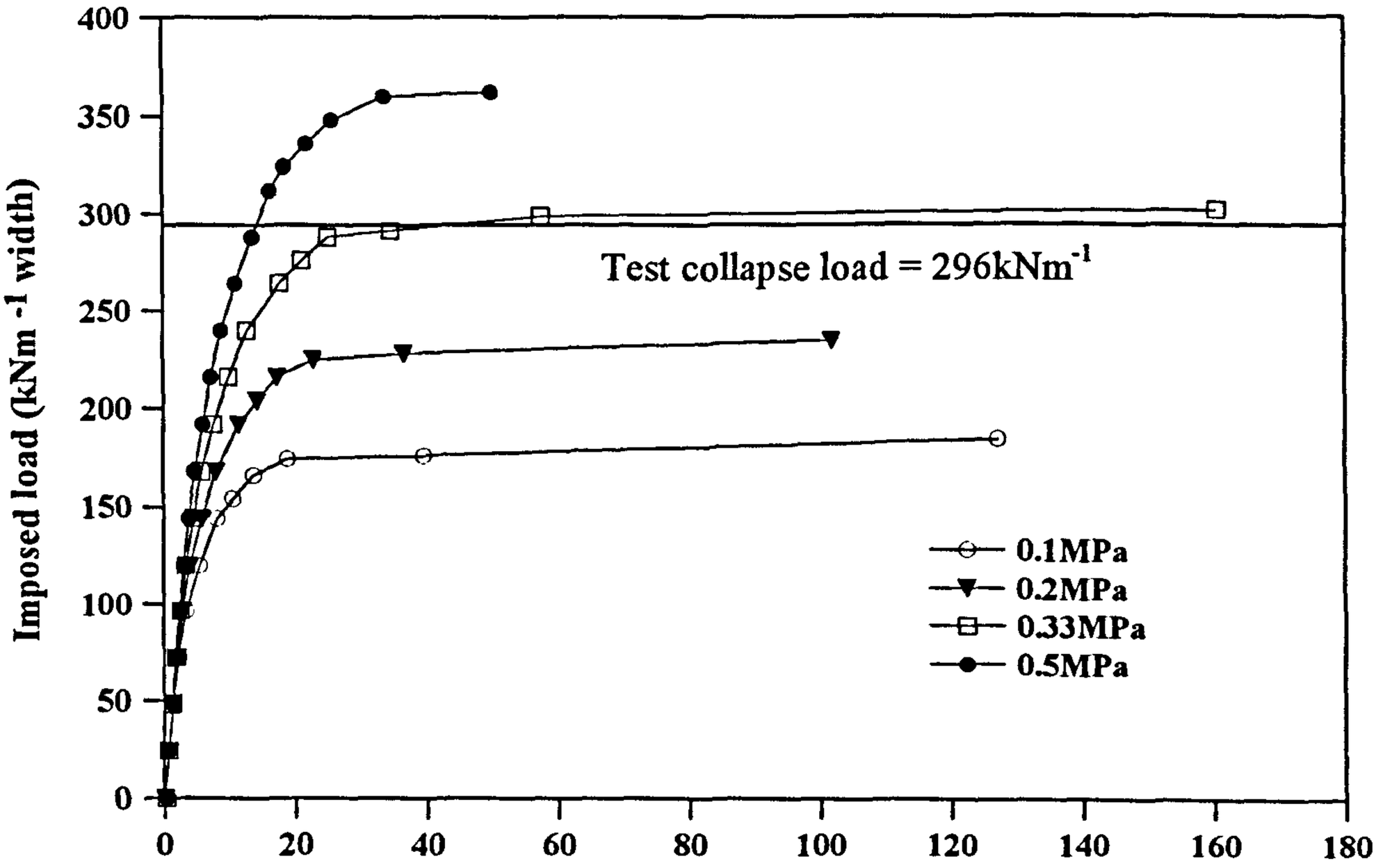

Figure 4.5f Parametric study: the effect of arch tensile strength on Barlae

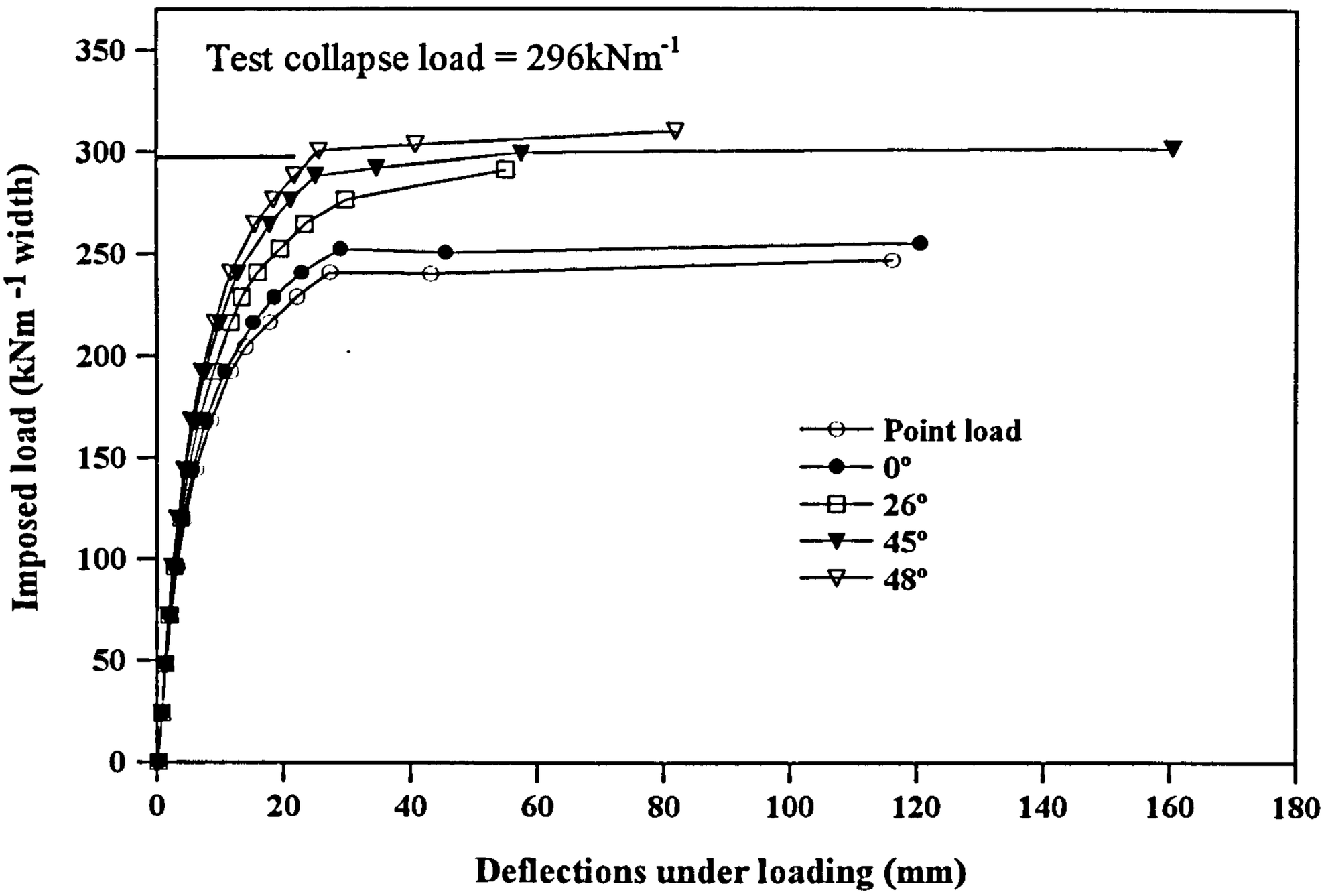

Figure 4.5g Parametric study: the effect of load dispersal angle on Barlae

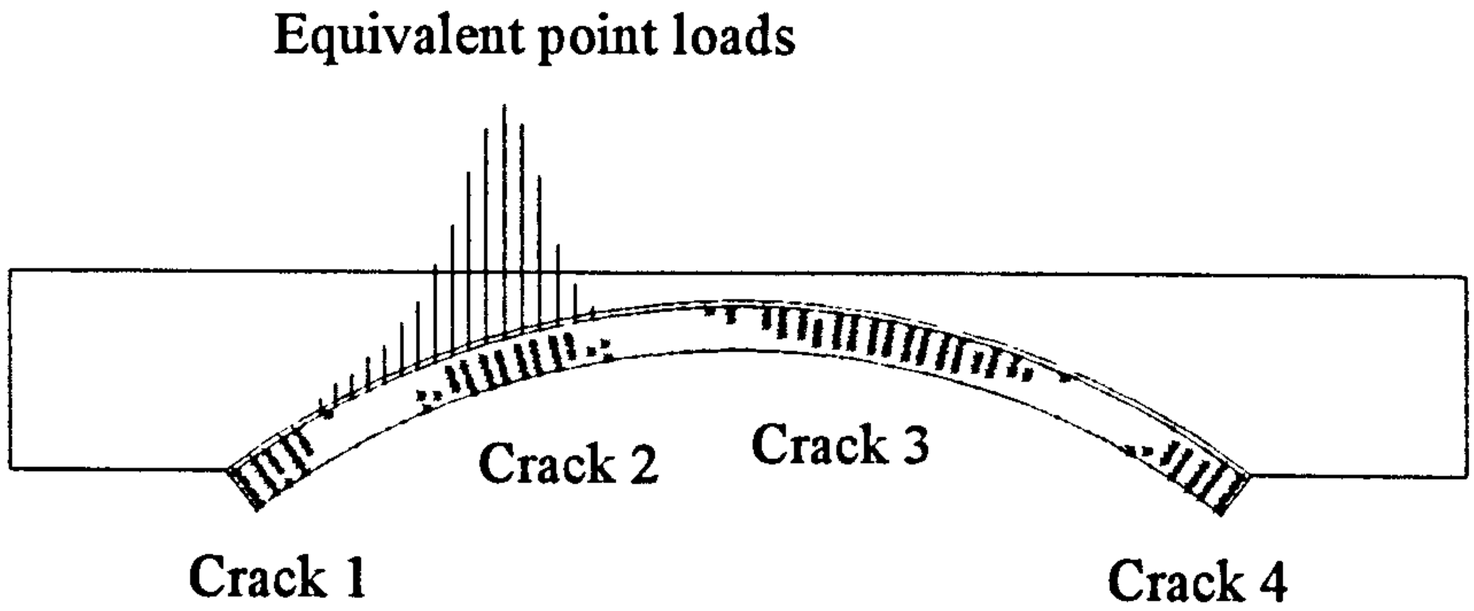

Figure 4.5h Yielded zones at Barlae as predicted by FE analysis

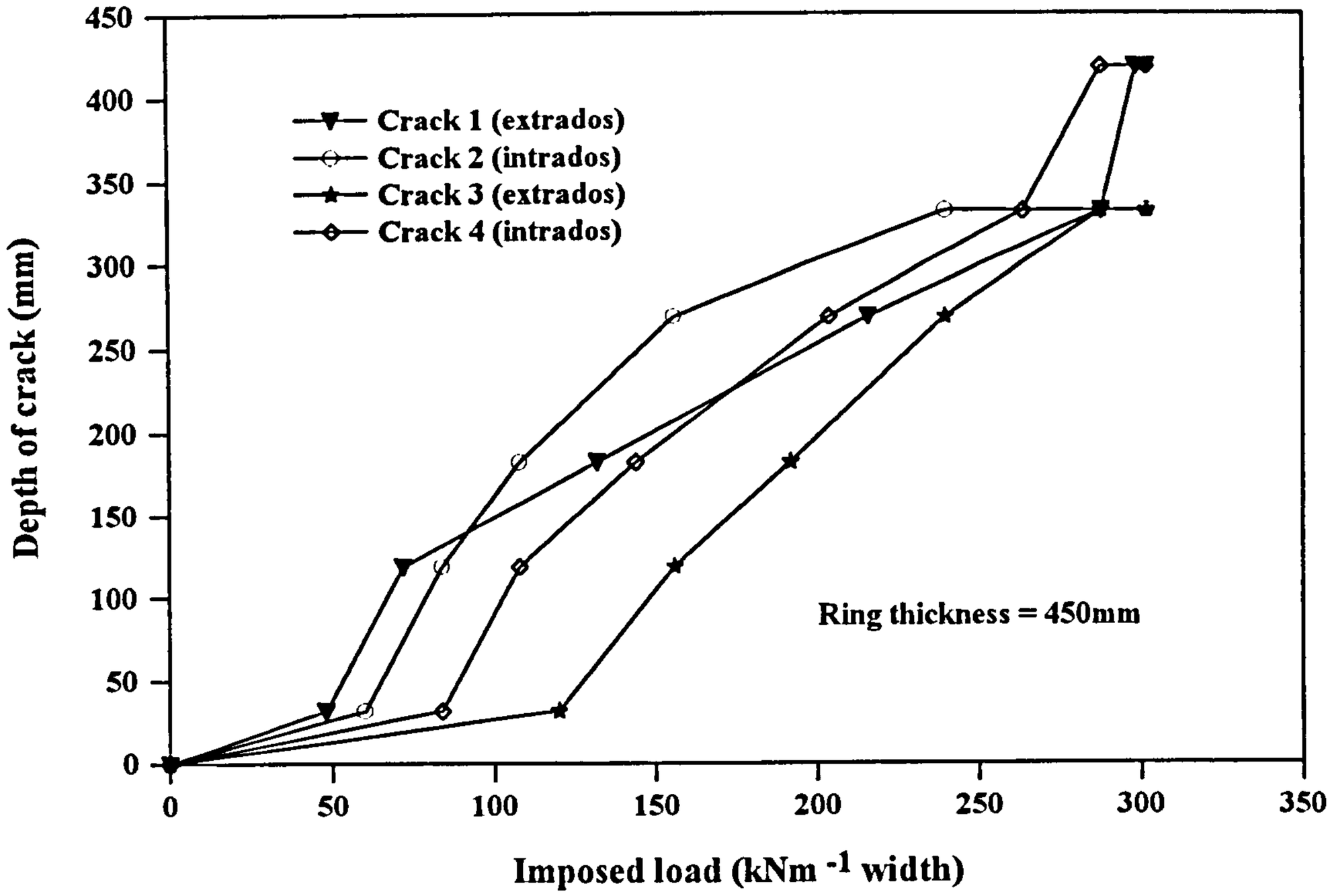

Figure 4.5i Imposed loading and crack development for Barlae

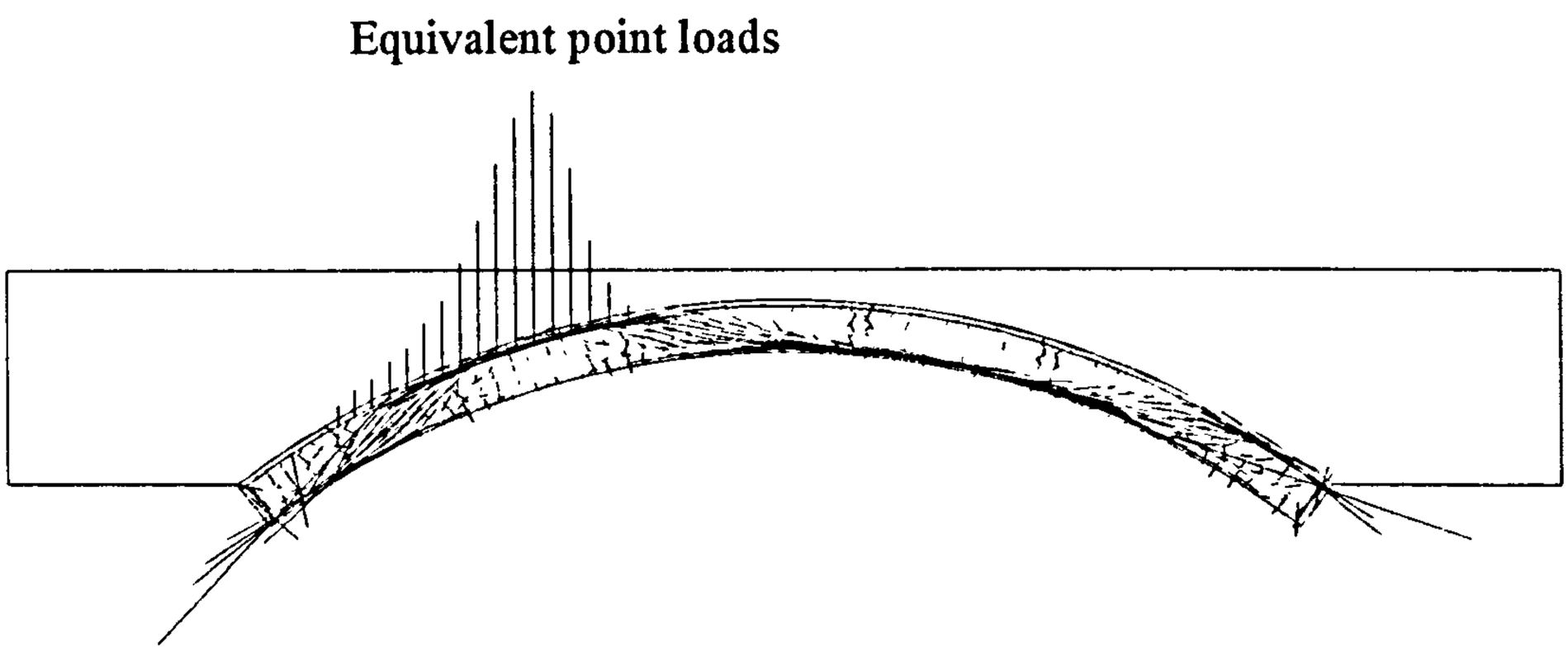

Figure 4.5j Compressive stress vector for Barlae

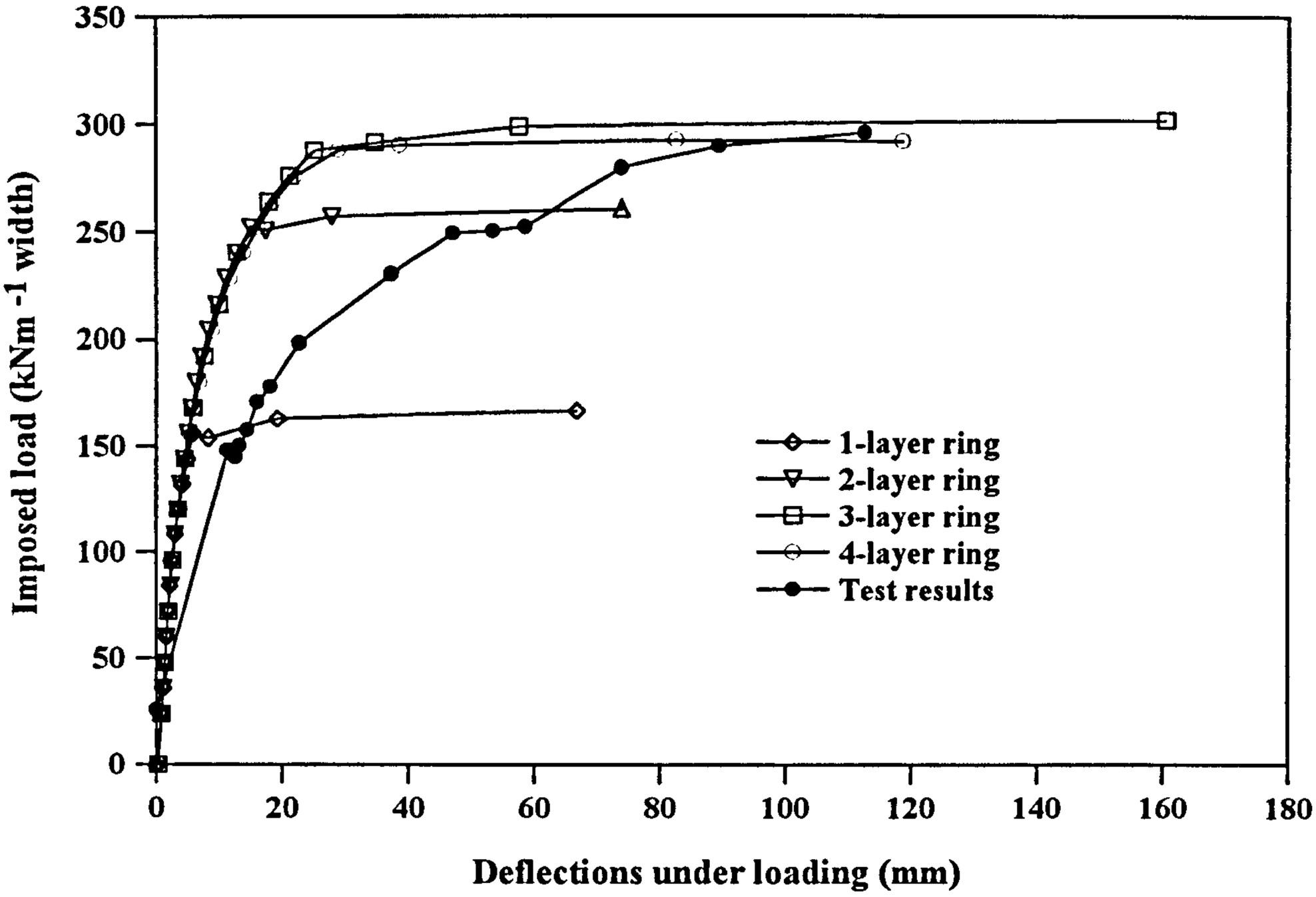

Figure 4.5k The effect of mesh density on Barlae

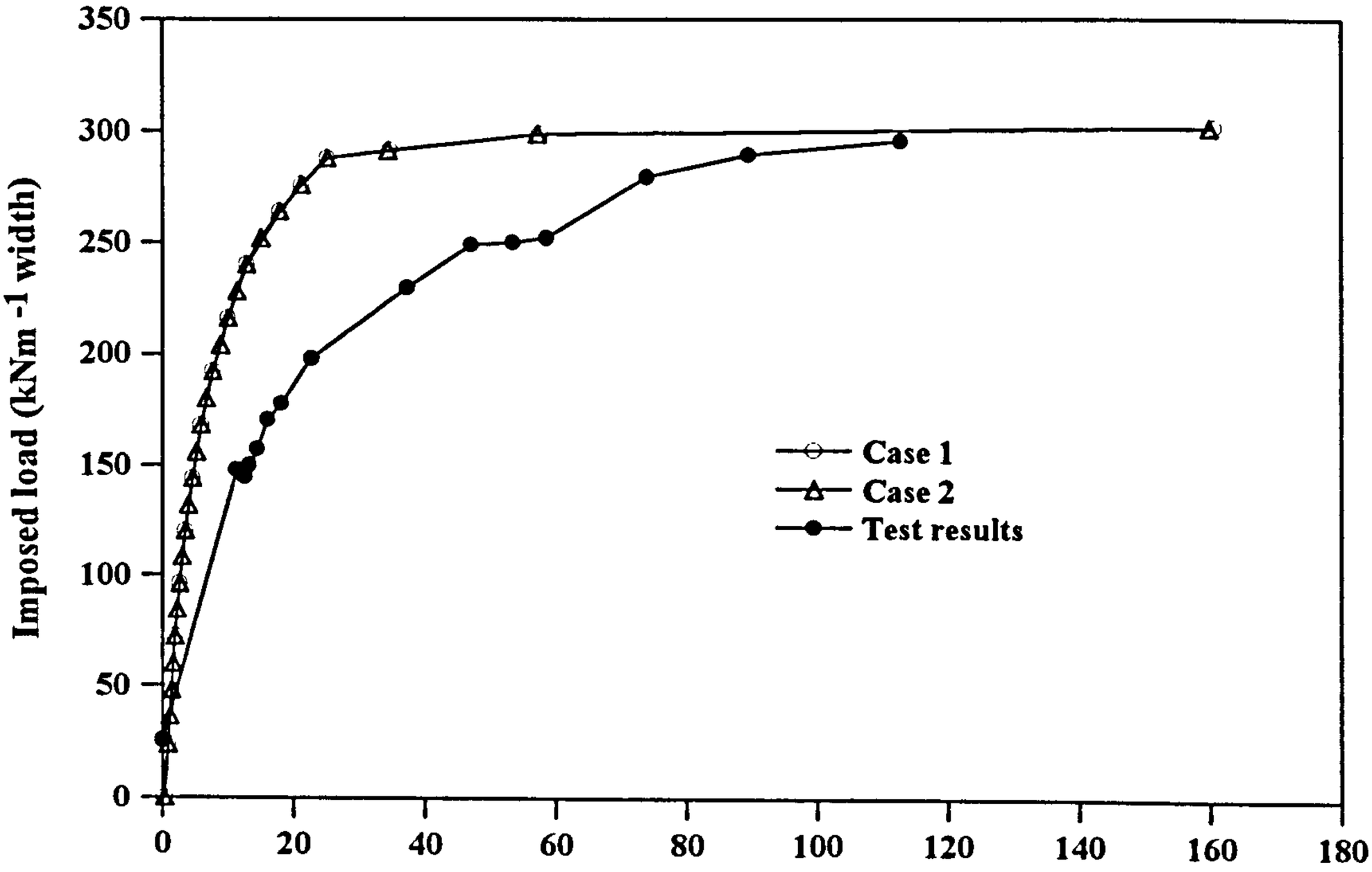

Figure 4.5l The effect of support conditions on Barlae

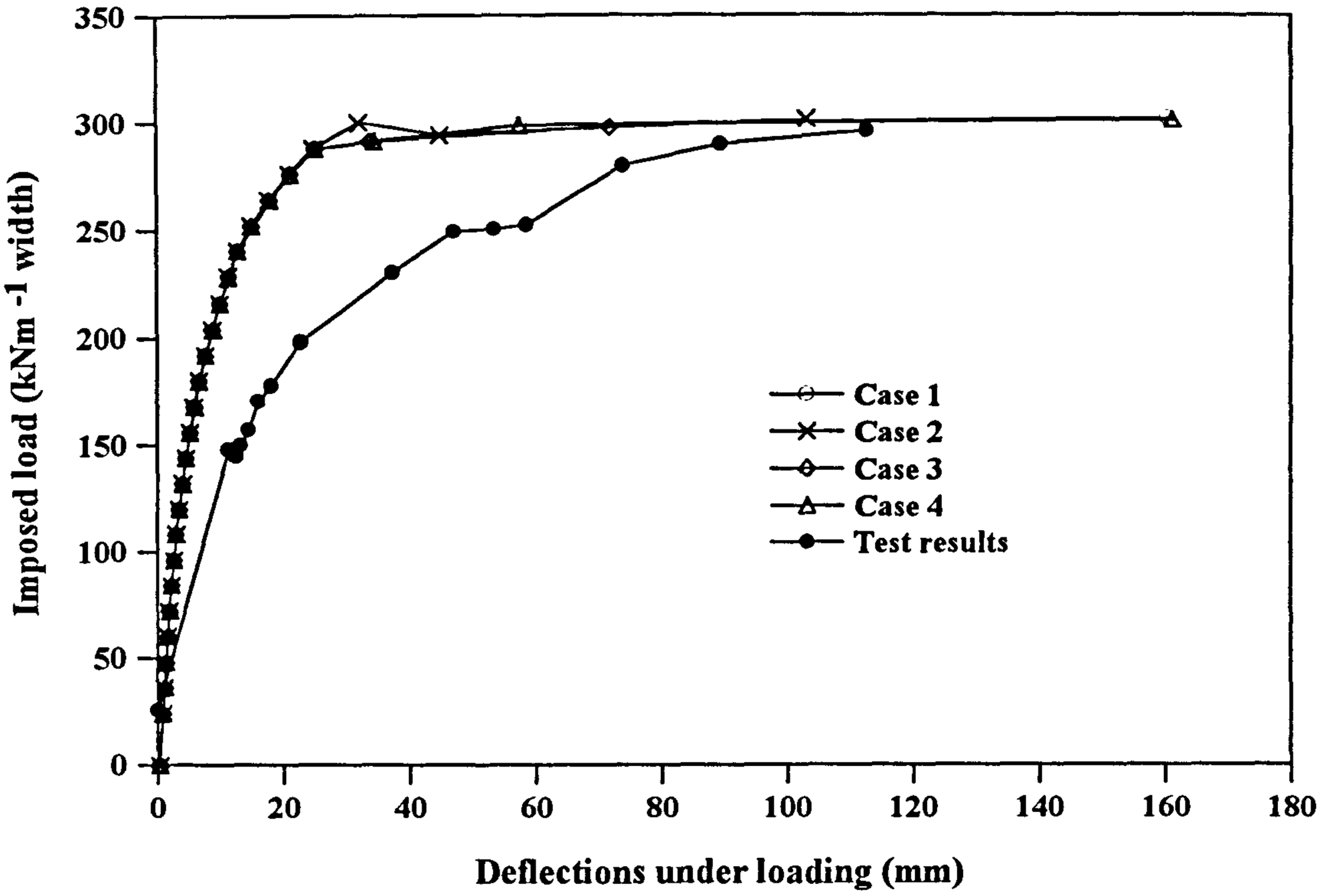

Figure 4.5m The effect of boundary proximity on Barlae

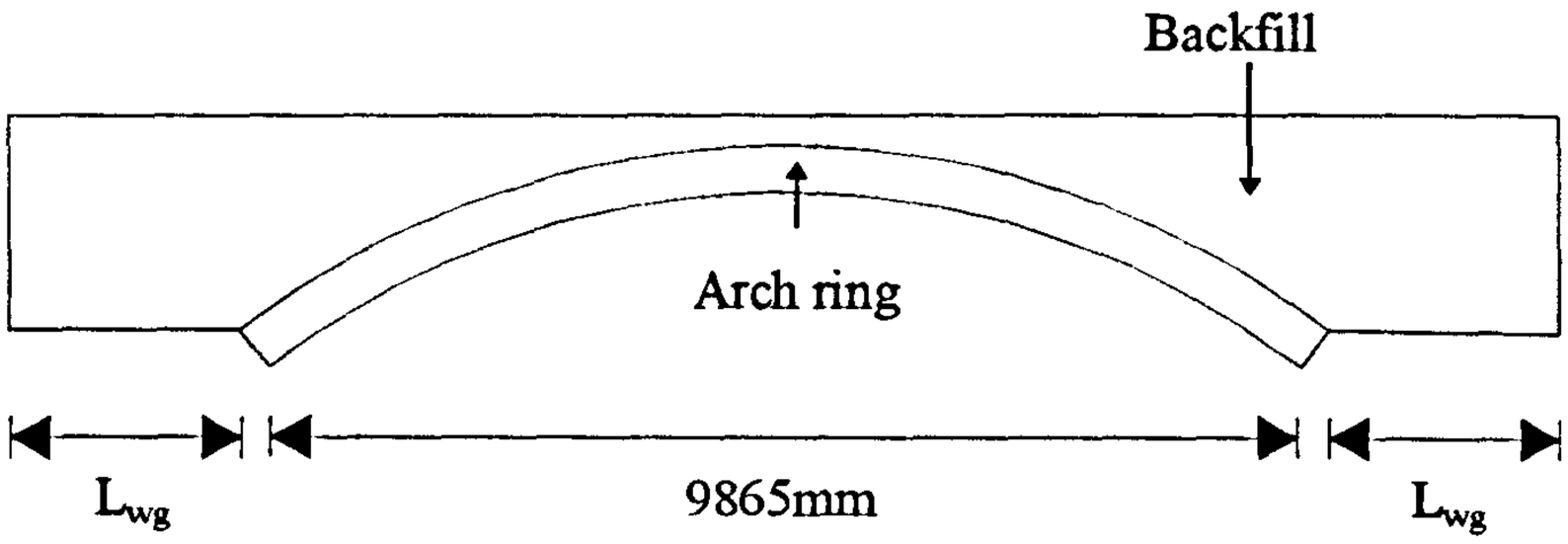

L_{wg} = 2466.25mm (Case 1)
L_{wg} = 0mm (Case 2)
L_{wg} = 4932.5mm (Case 3)
L_{wg} = 19730mm (Case 4)

Figure 4.5n Dimension of the wing wall in Cases 1 to 4

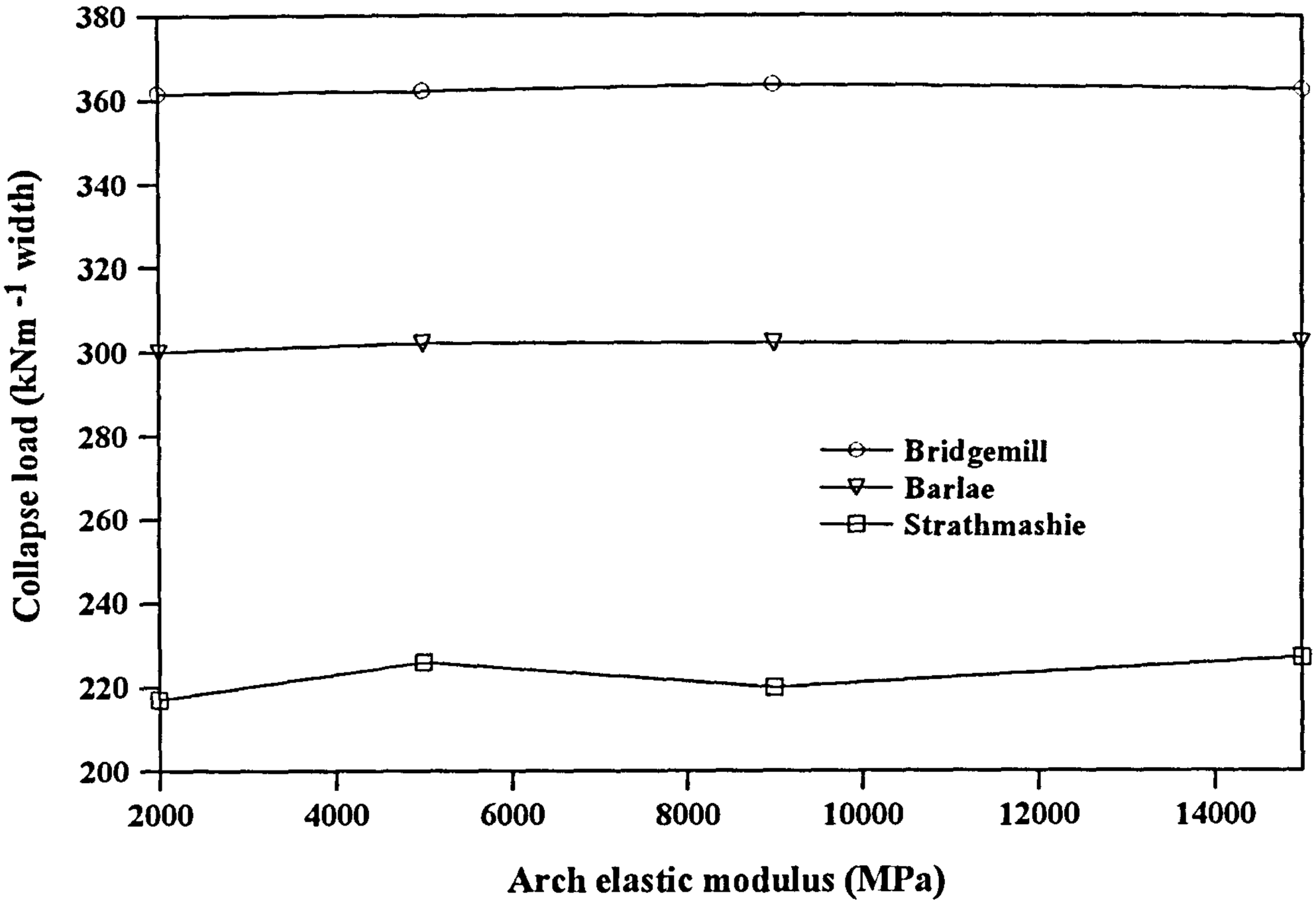

Figure 4.6a Parametric study: the effect of arch elastic modulus on each arch bridge

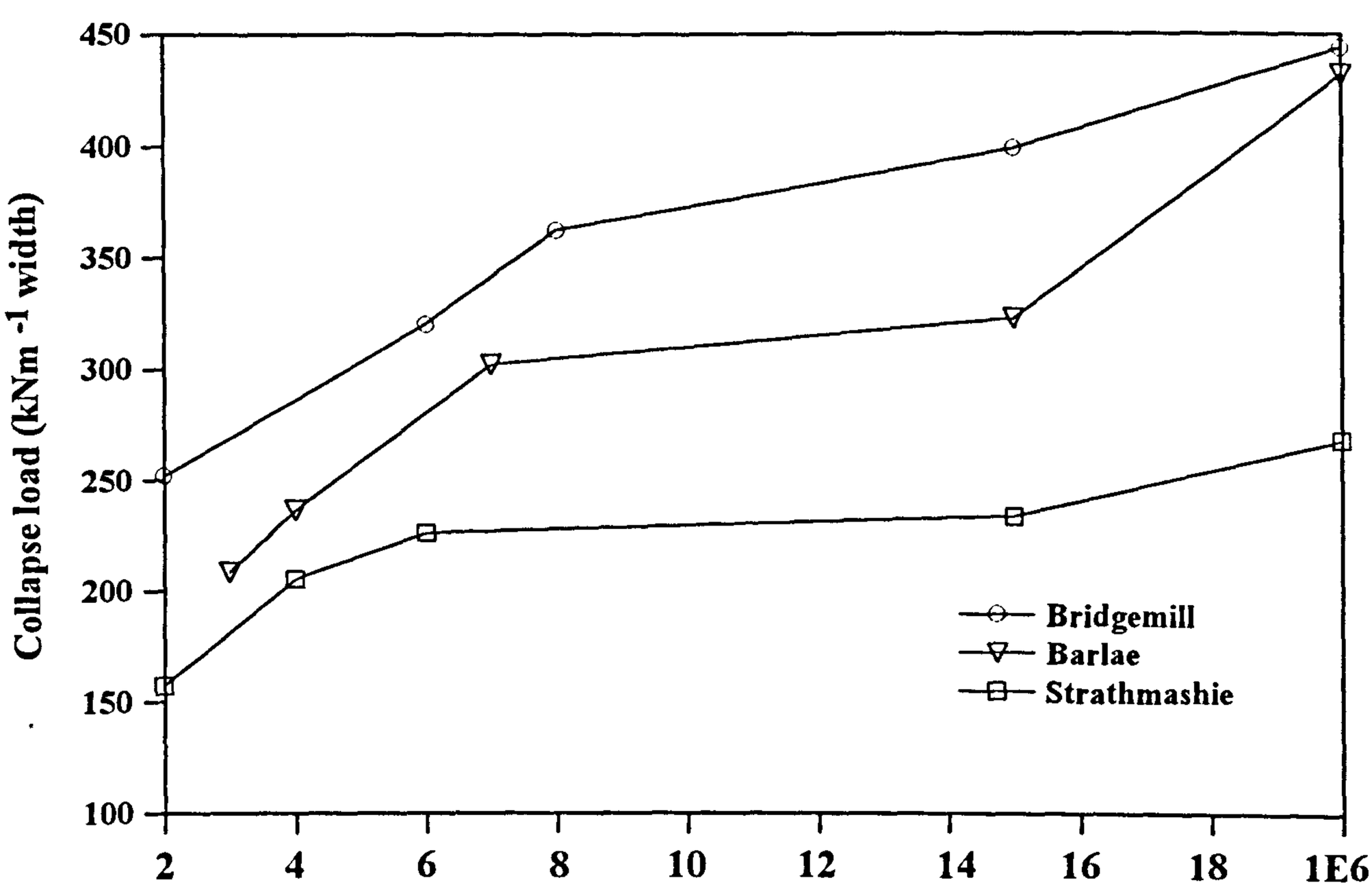

Figure 4.6b Parametric study: the effect of arch compressive strength on each arch bridge

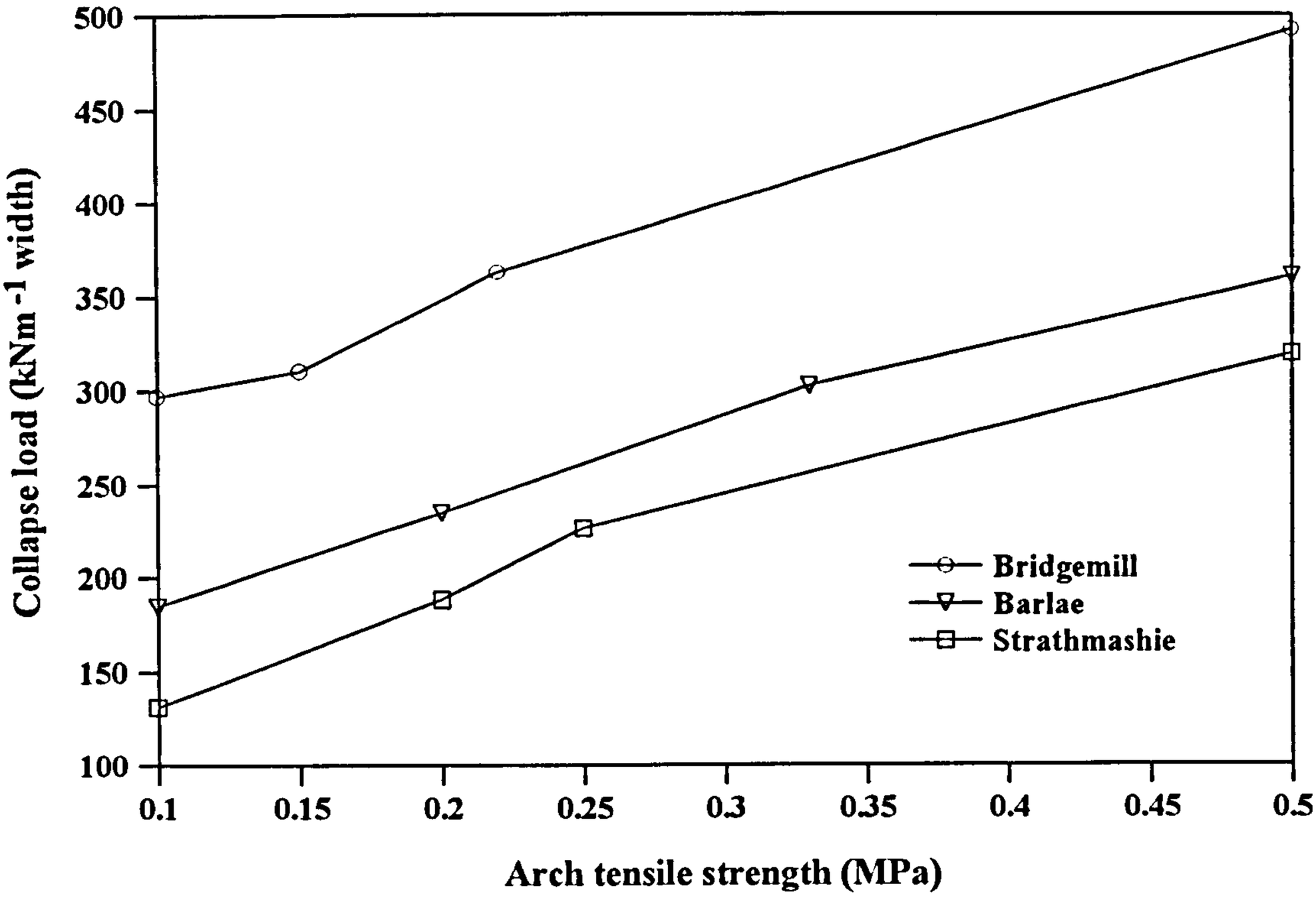

Figure 4.6c Parametric study: the effect of arch tensile strength on each arch bridge

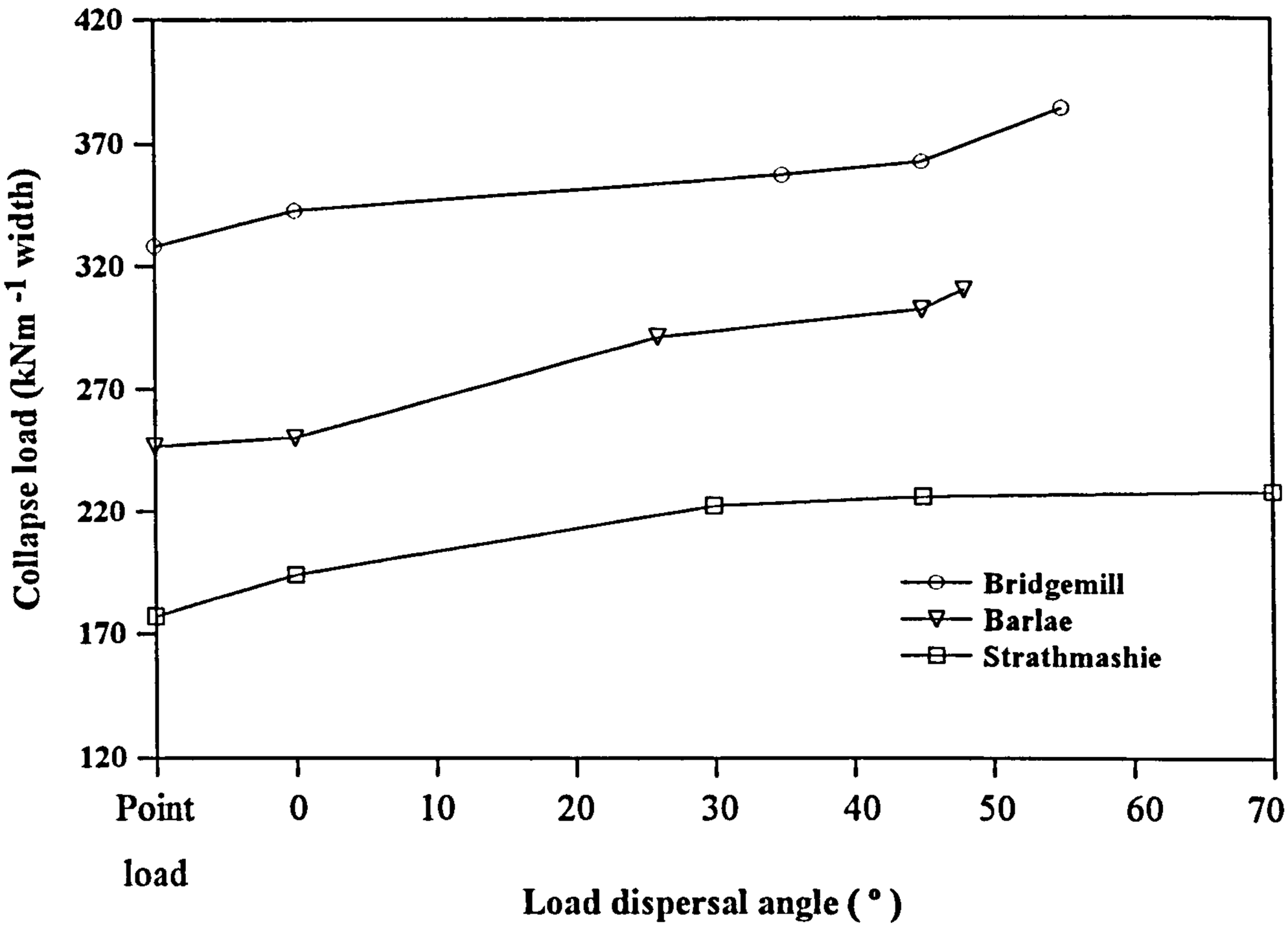

Figure 4.6d Parametric study: the effect of load dispersal angle on each arch bridge

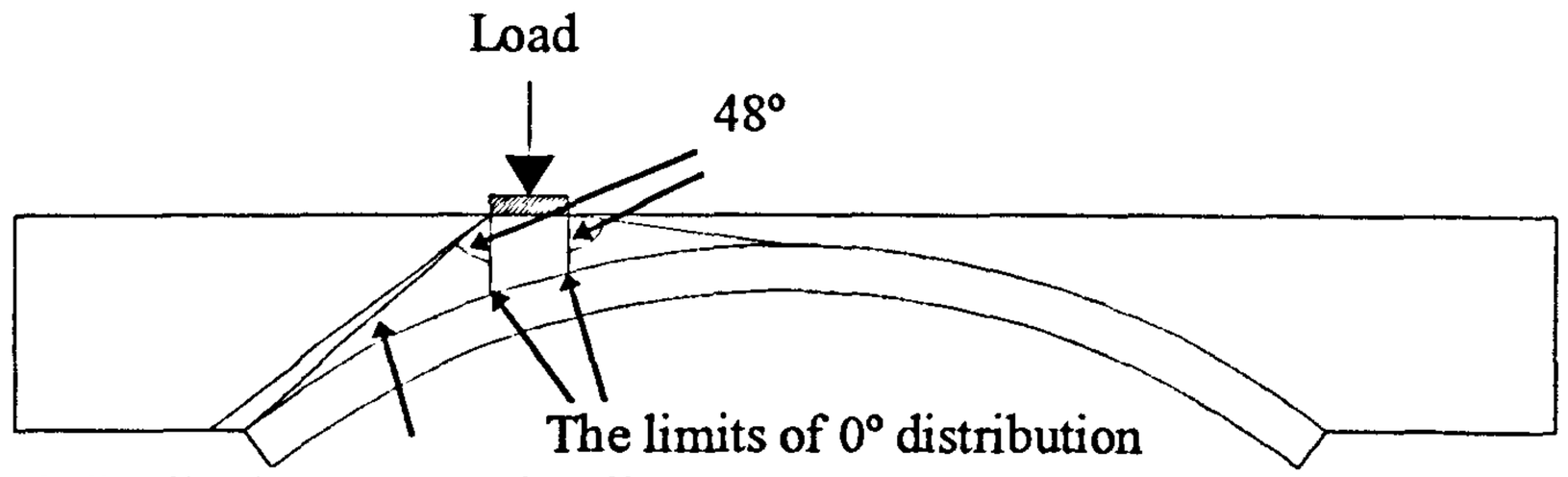

Figure 4.6e An illustration of the load distribution on Barlae from 0° to 48°

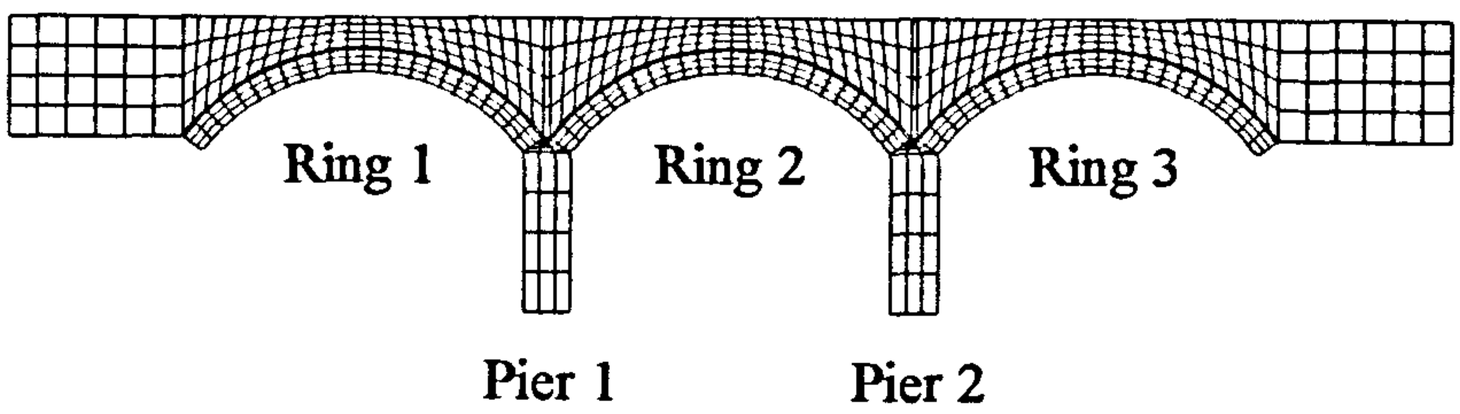

Figure 4.7a Idealised mesh for Bolton multi-span arch bridge

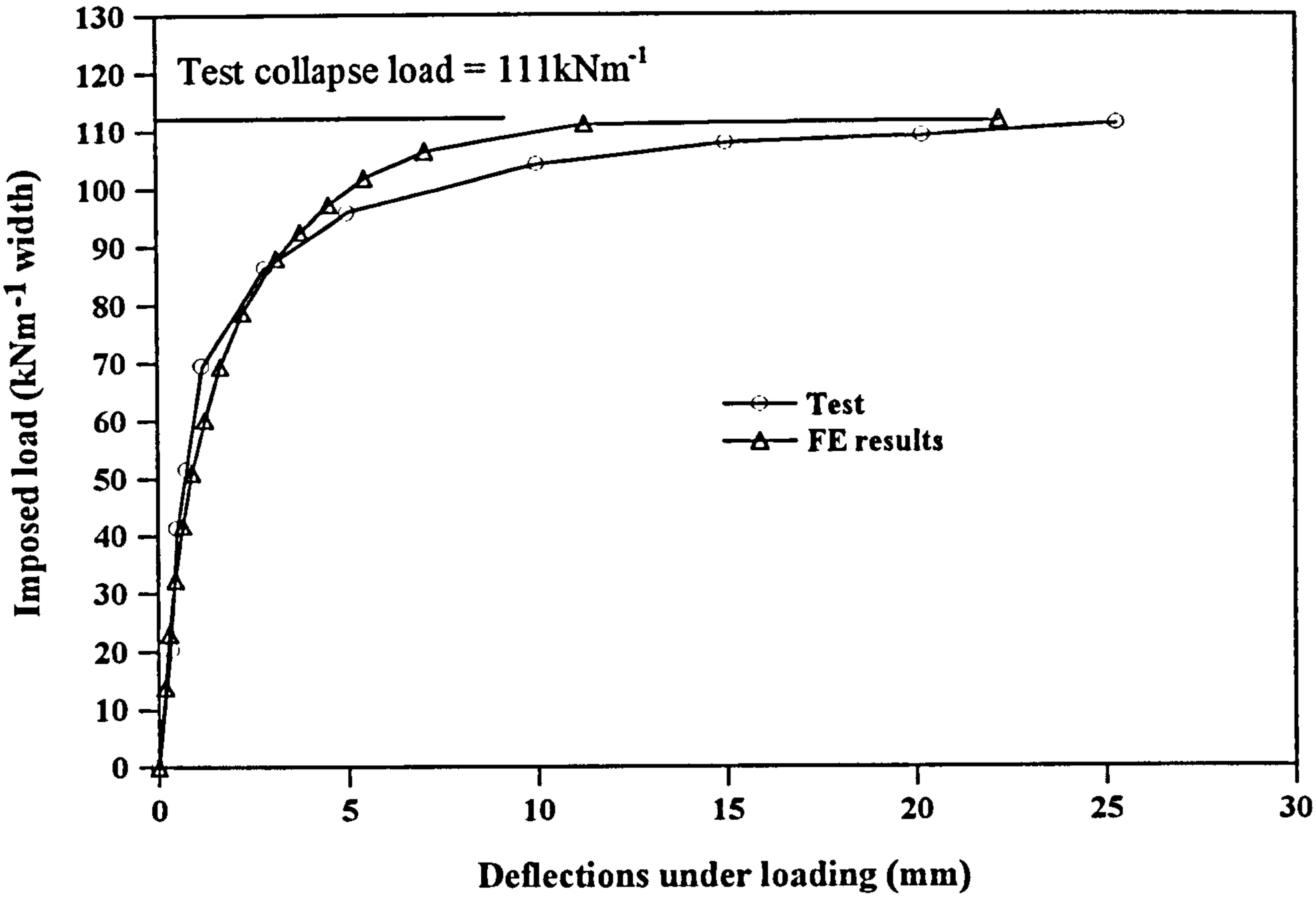

Figure 4.7b Load *versus* deflection relationships under the load point for Bolton

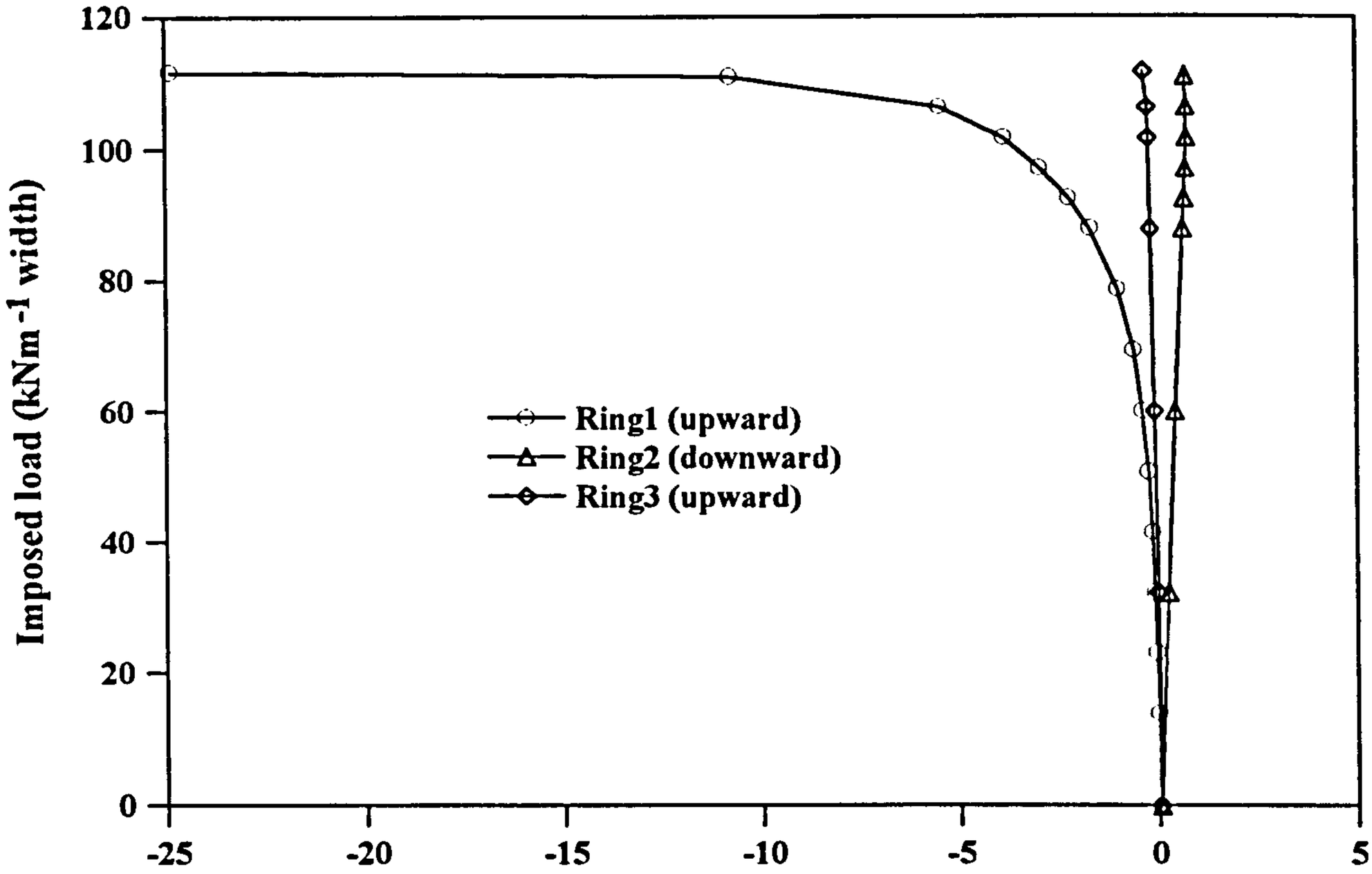

Figure 4.7c Load *versus* deflection relationships at the crown for Bolton

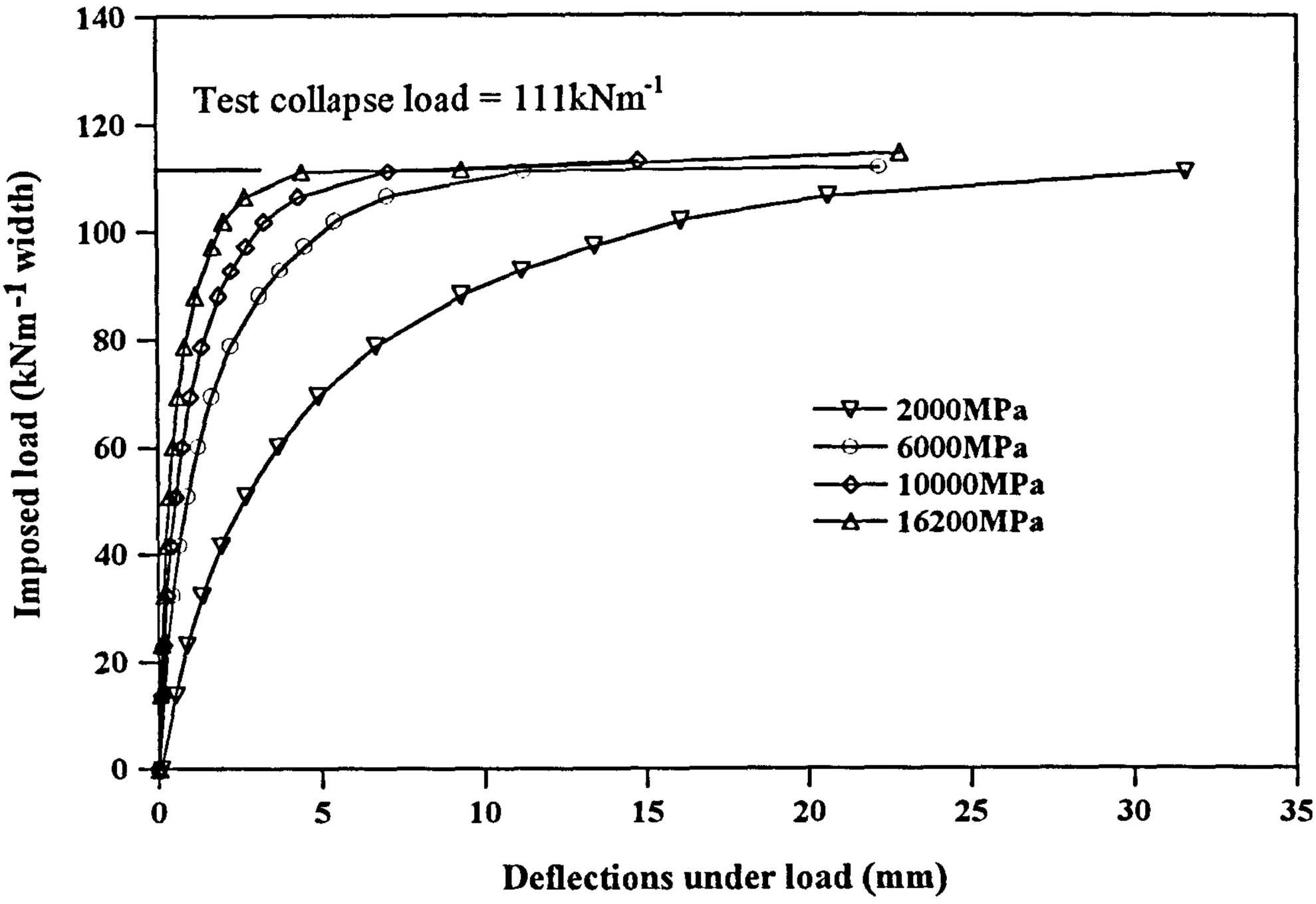

Figure 4.7d Parametric study: Load *versus* deflection relationships with different arch and pier elastic moduli on Bolton

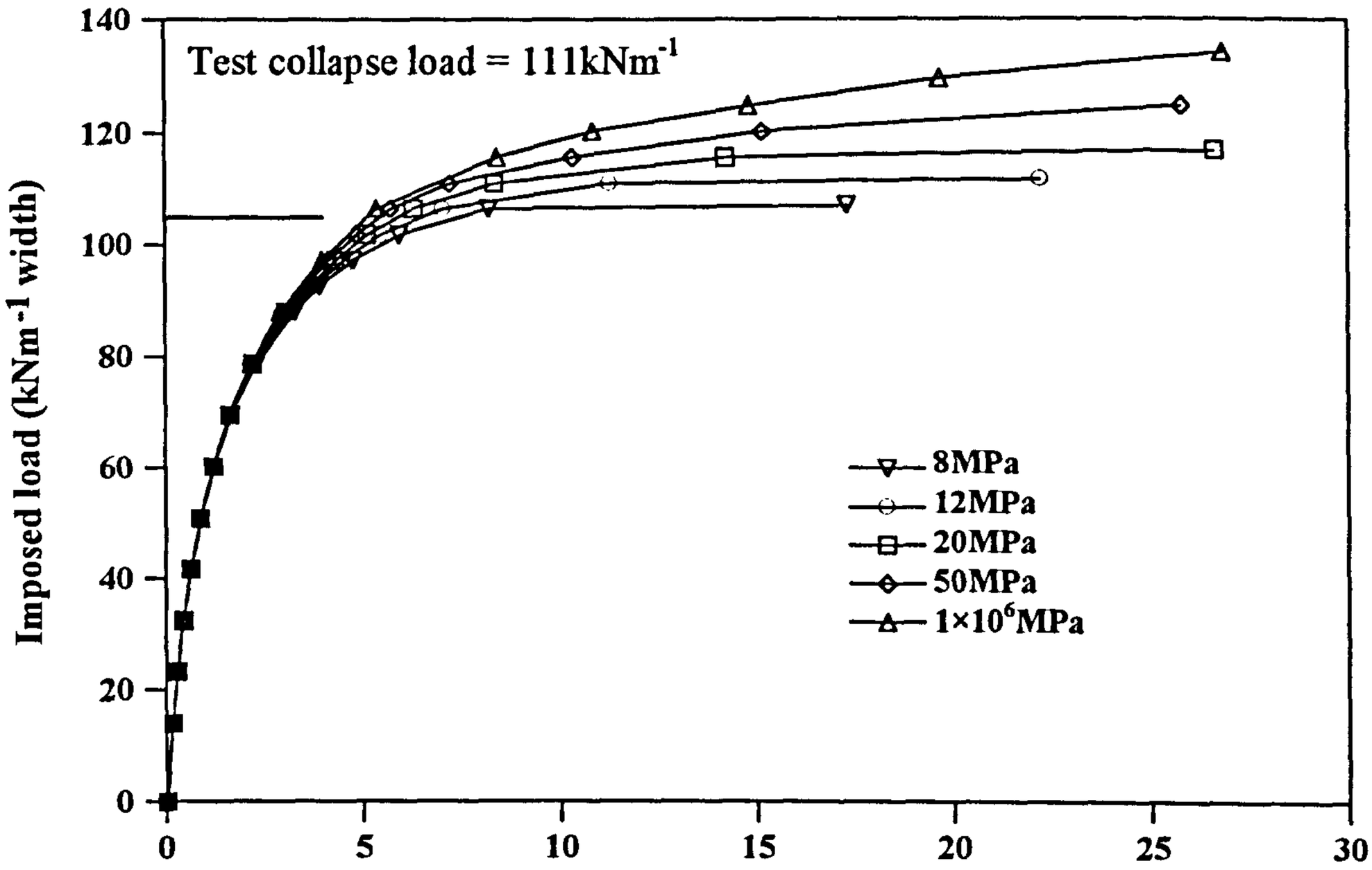

Figure 4.7e Parametric study: Load *versus* deflection relationships with different arch and pier compressive strength on Bolton

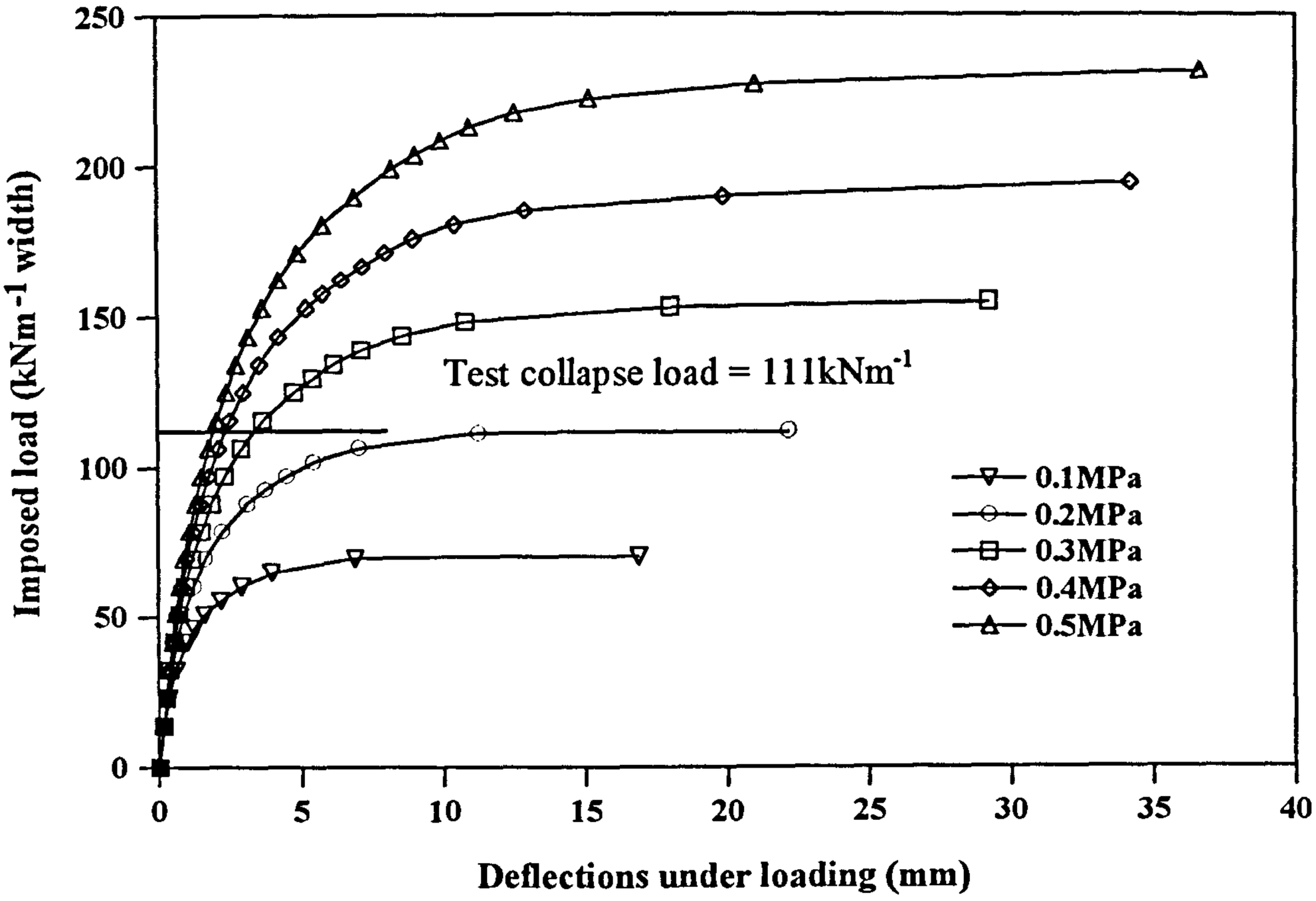

Figure 4.7f Parametric study: Load *versus* deflection relationships with different arch and pier tensile strength on Bolton

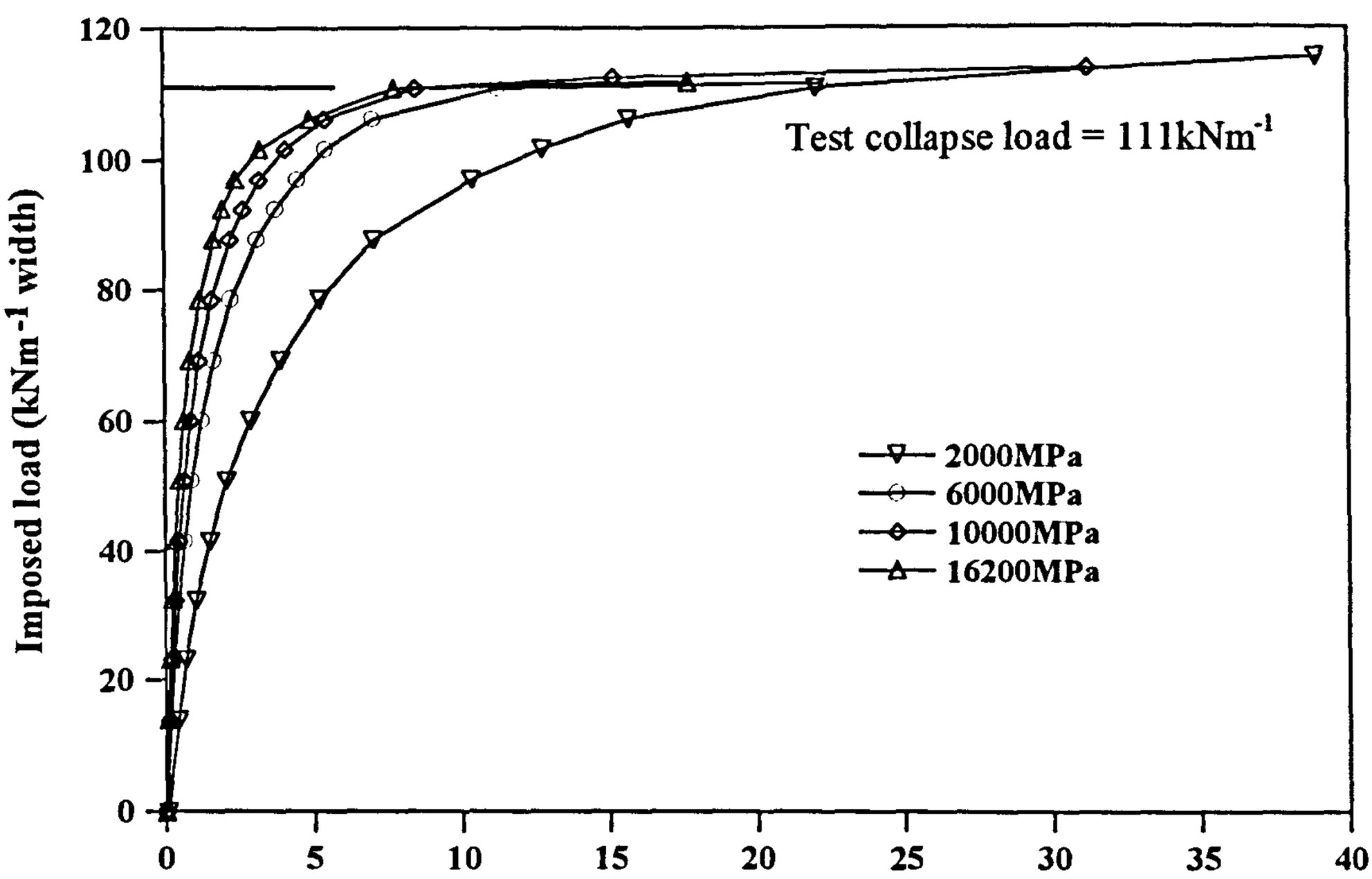

Figure 4.7g Parametric study: the effect of arch elastic modulus on Bolton

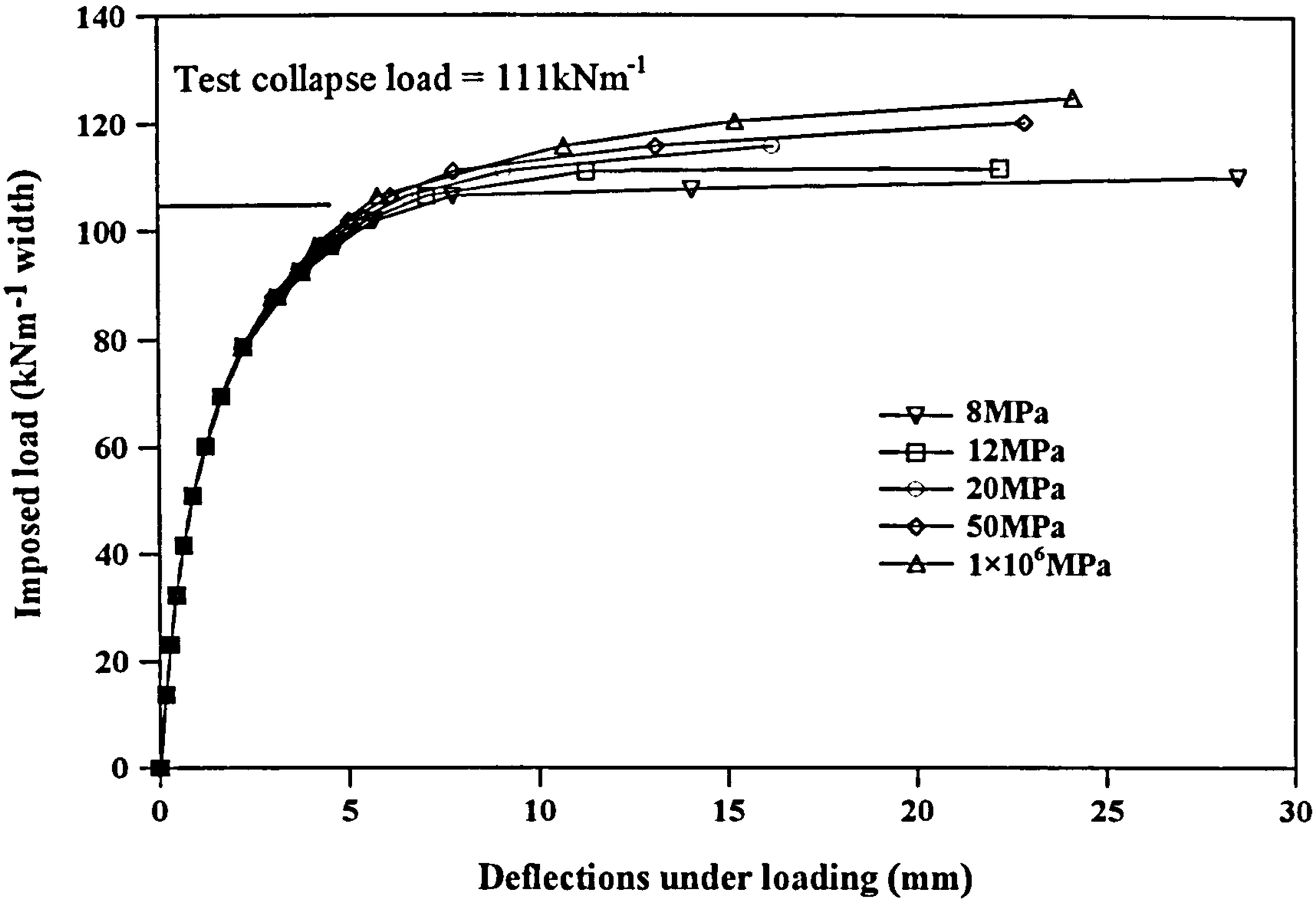

Figure 4.7h Parametric study: the effect of arch compressive strength on Bolton

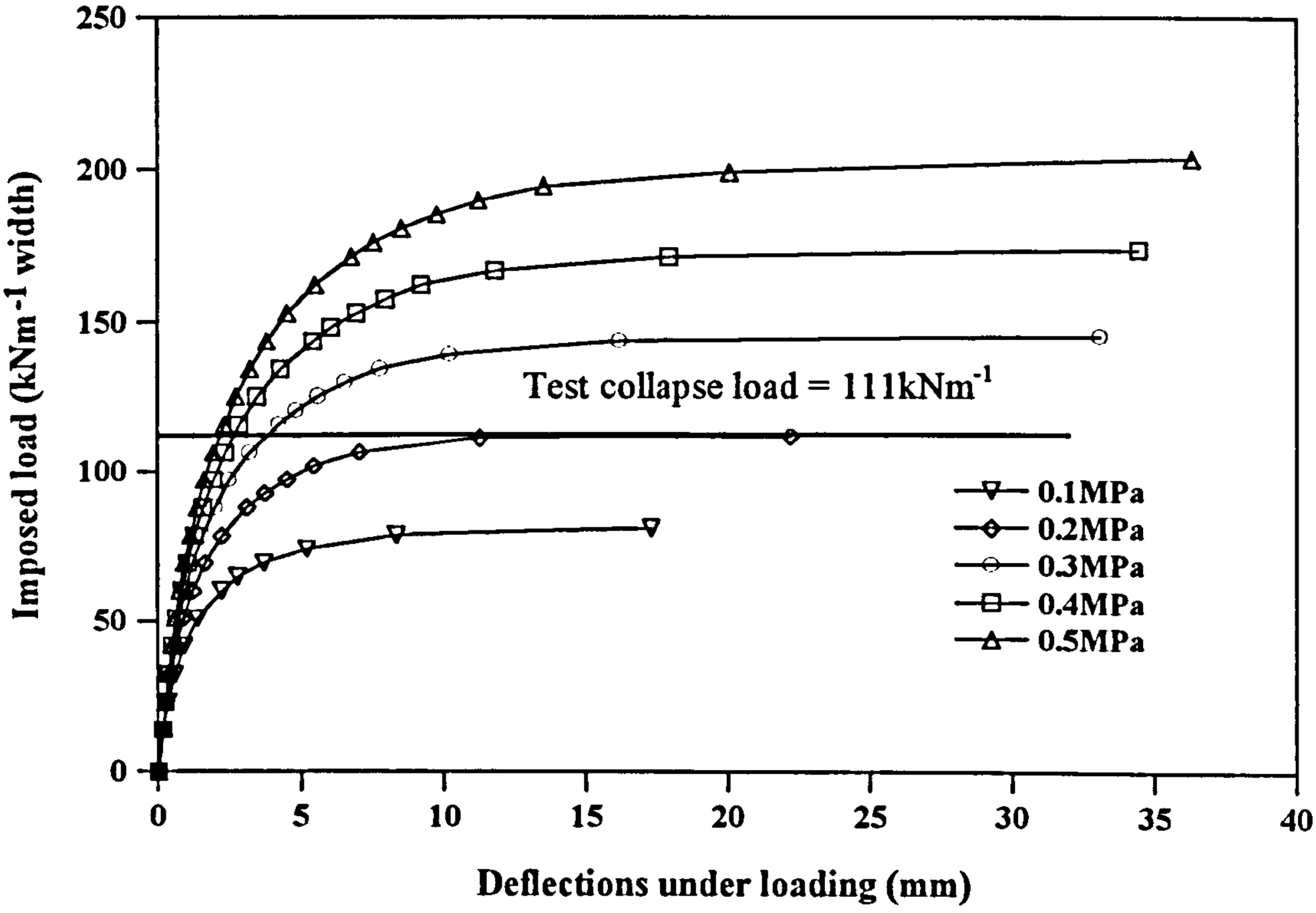

Figure 4.7i Parametric study: the effect of arch tensile strength on Bolton

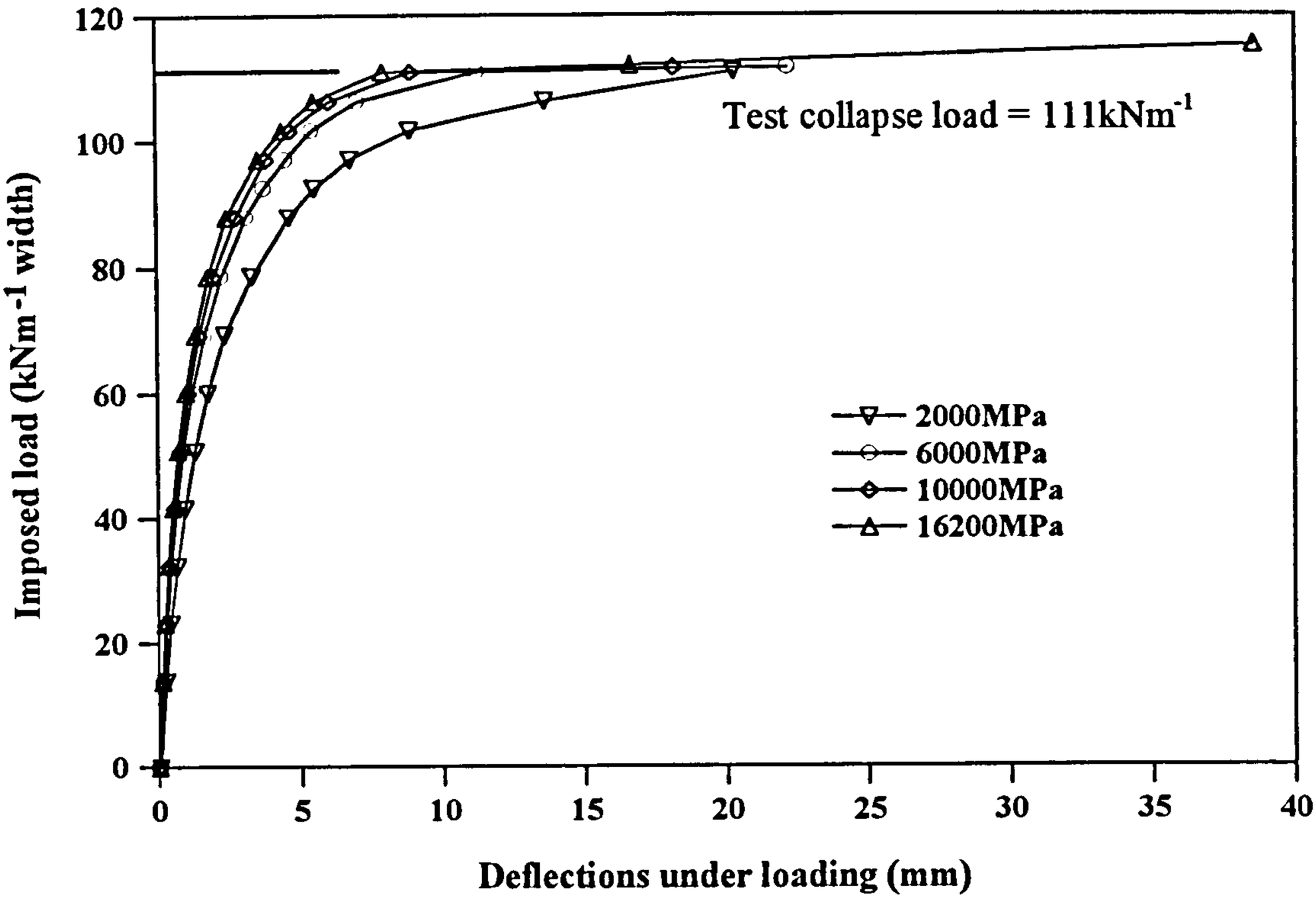

Figure 4.7j Parametric study: the effect of pier elastic modulus on Bolton

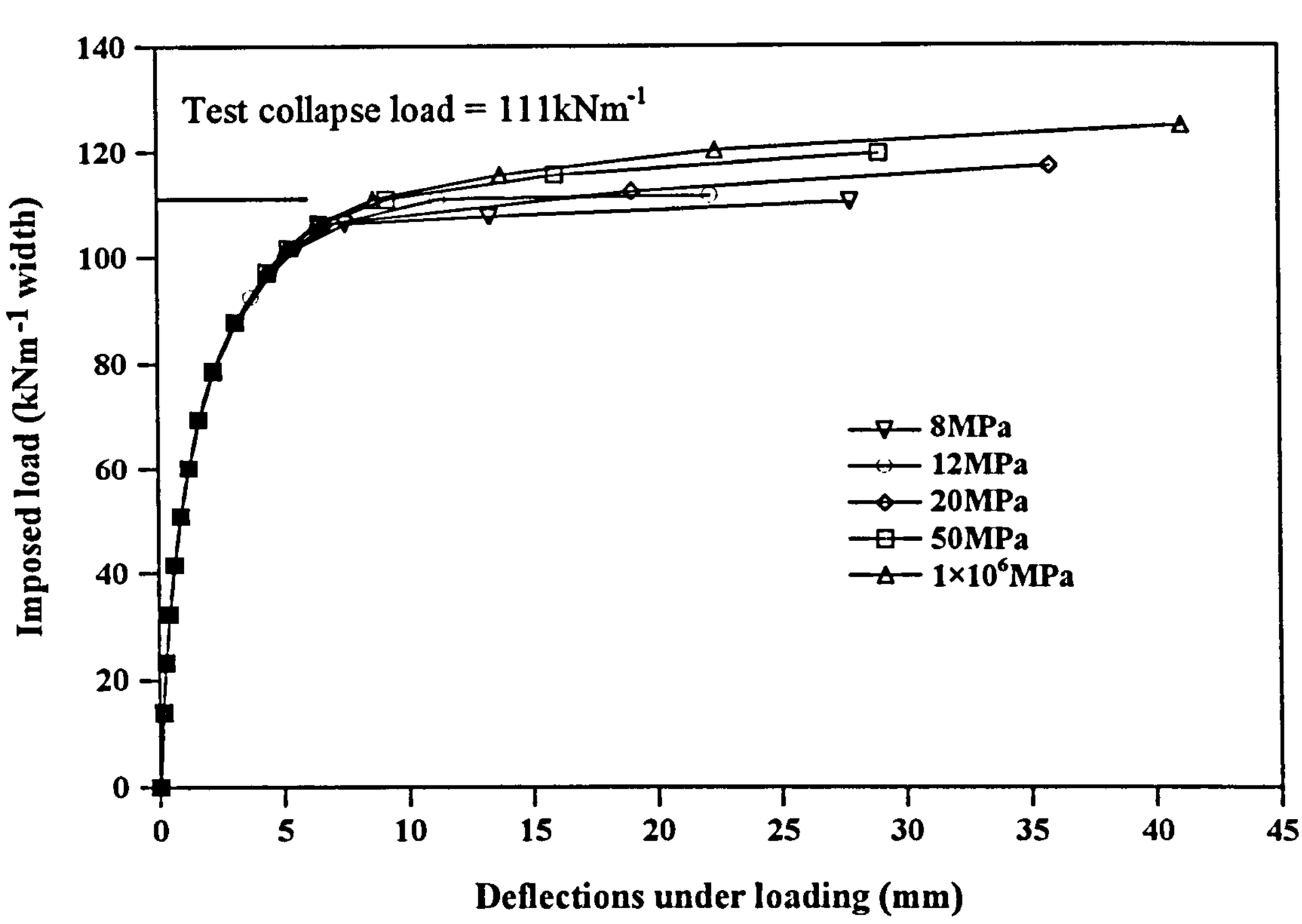

Figure 4.7k Parametric study: the effect of pier compressive strength on Bolton

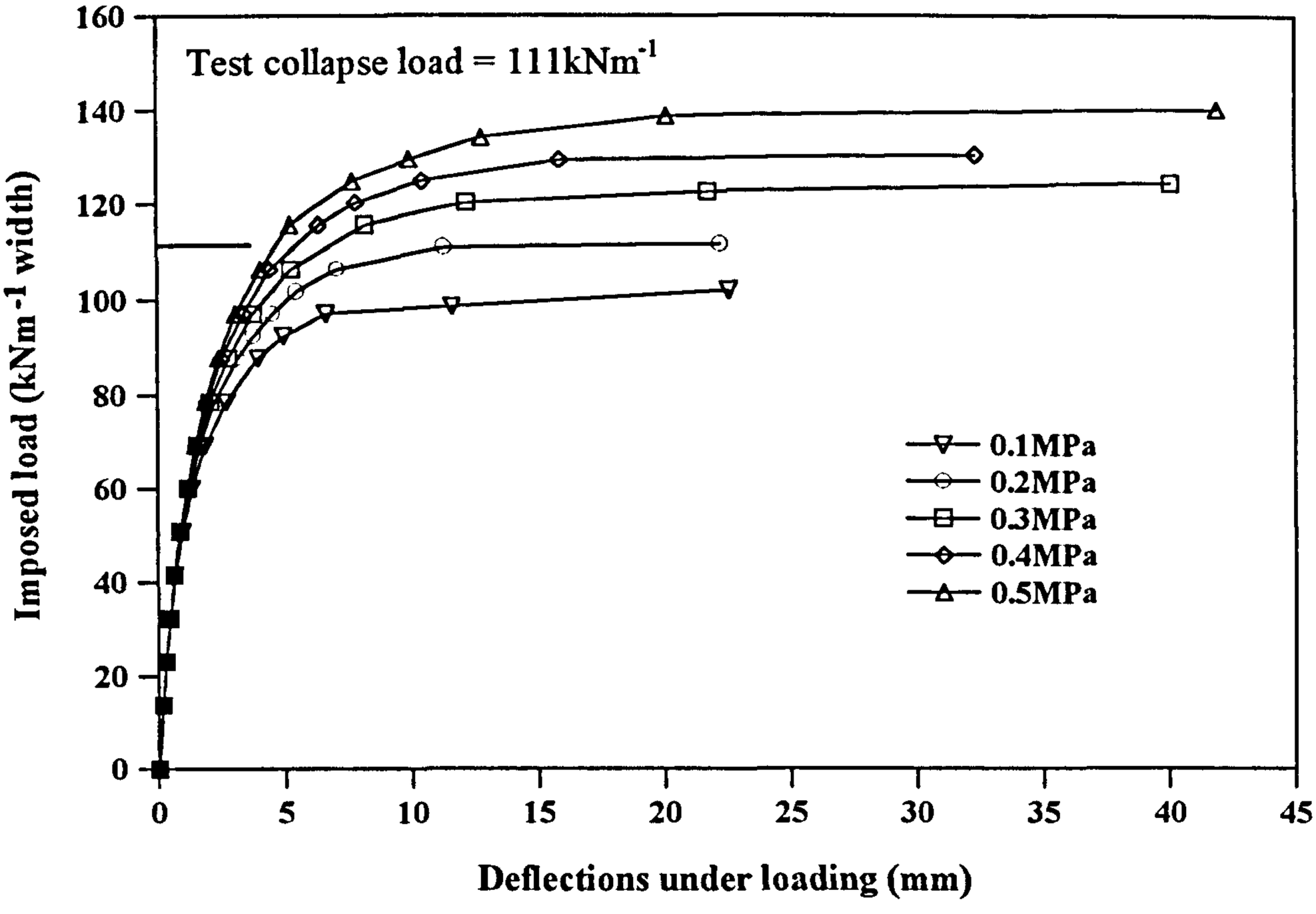

Figure 4.7l Parametric study: the effect of pier tensile strength on Bolton

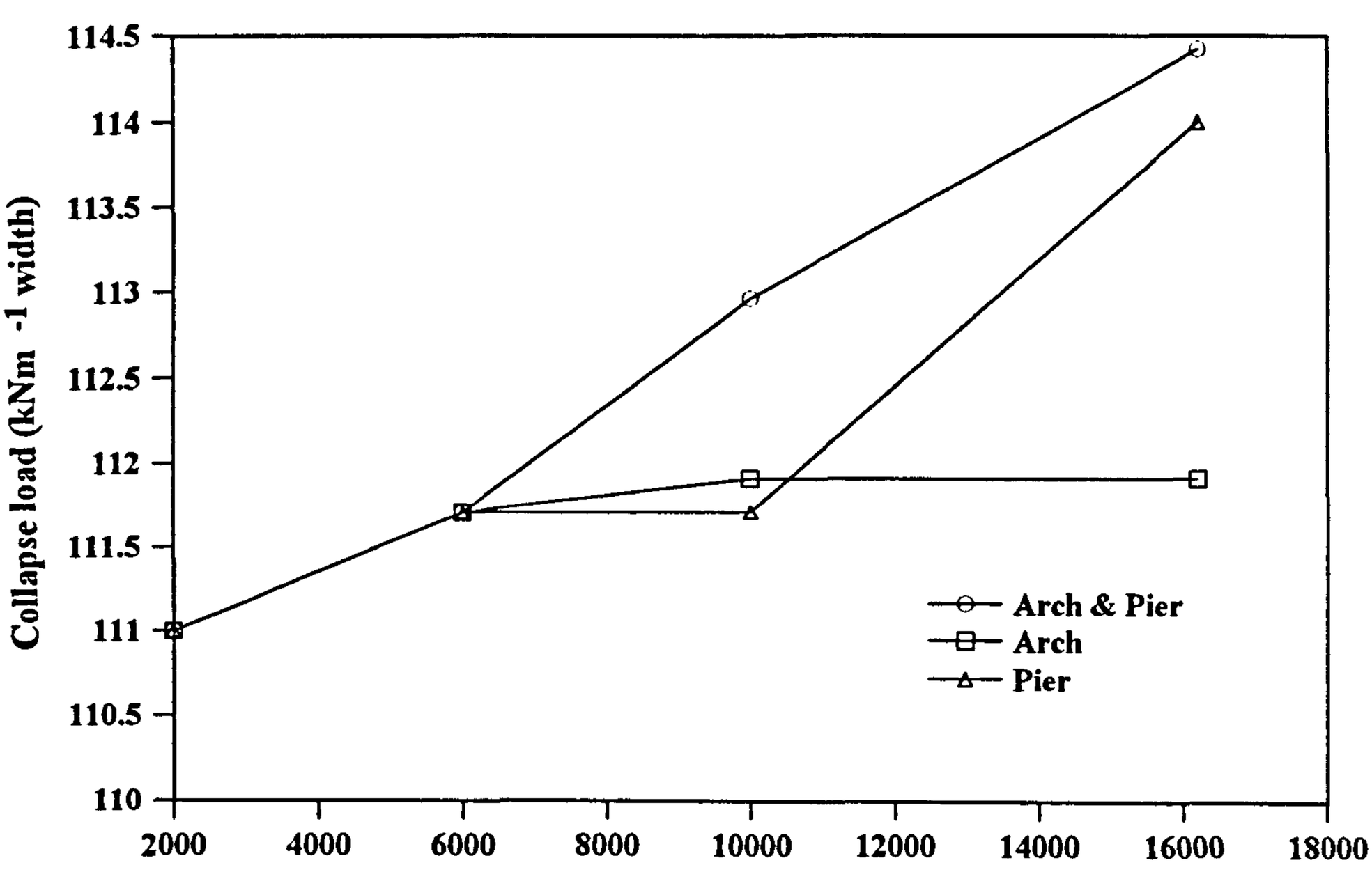

Figure 4.7m Parametric study: the effect of elastic modulus of arch and pier on Bolton

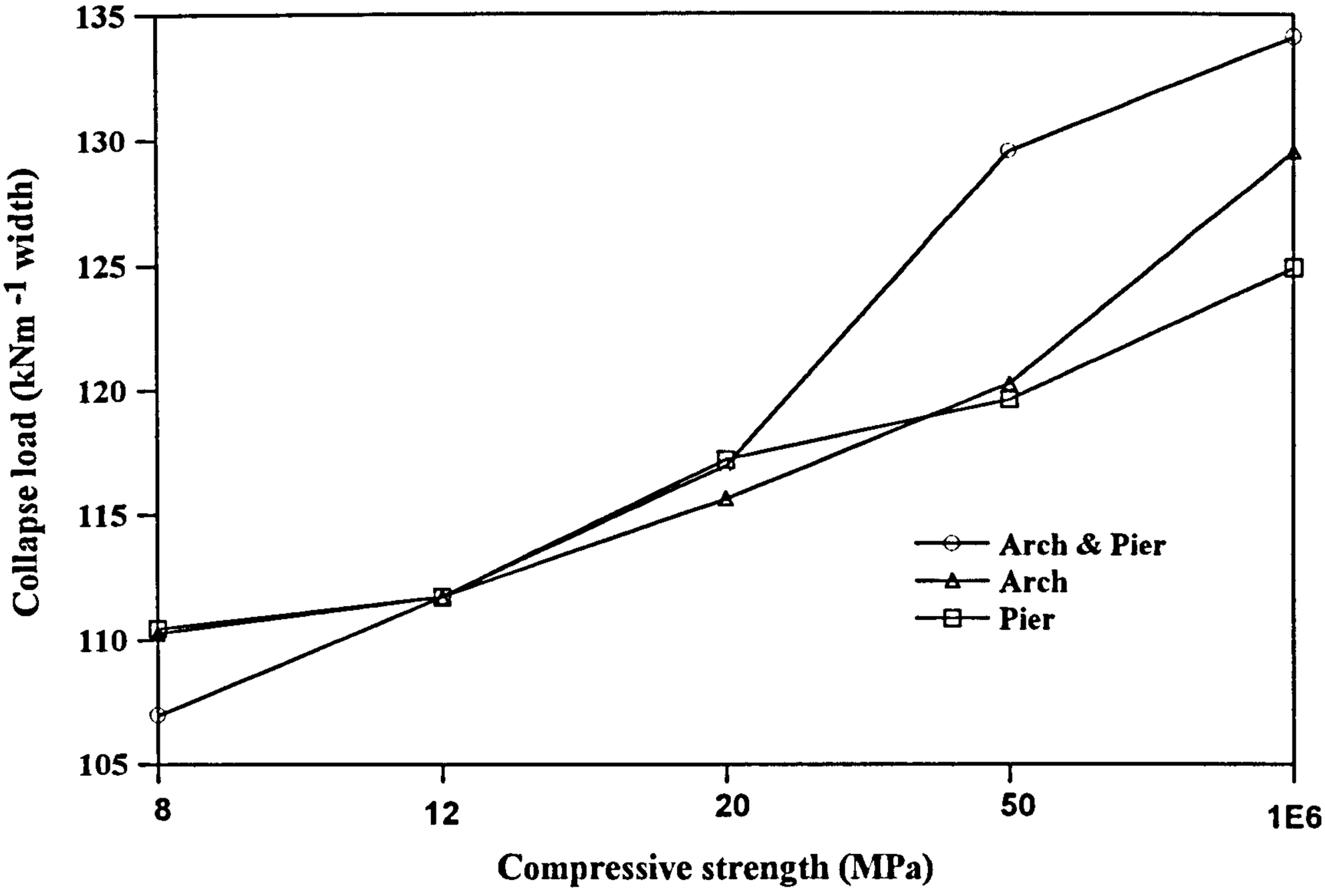

Figure 4.7n Parametric study: the effect of compressive strength of arch and pier on Bolton

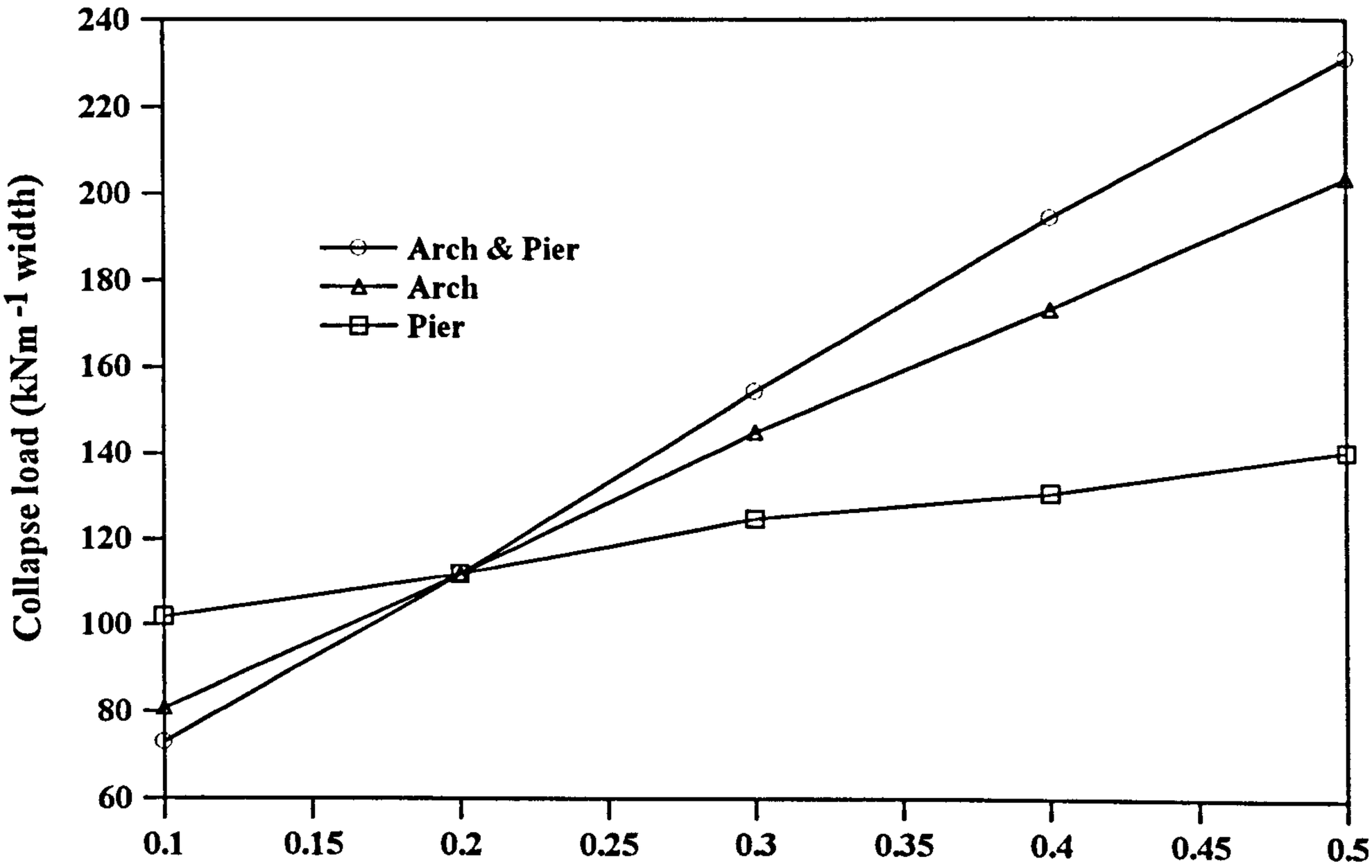

Figure 4.7p Parametric study: the effect of tensile strength of arch and pier on Bolton

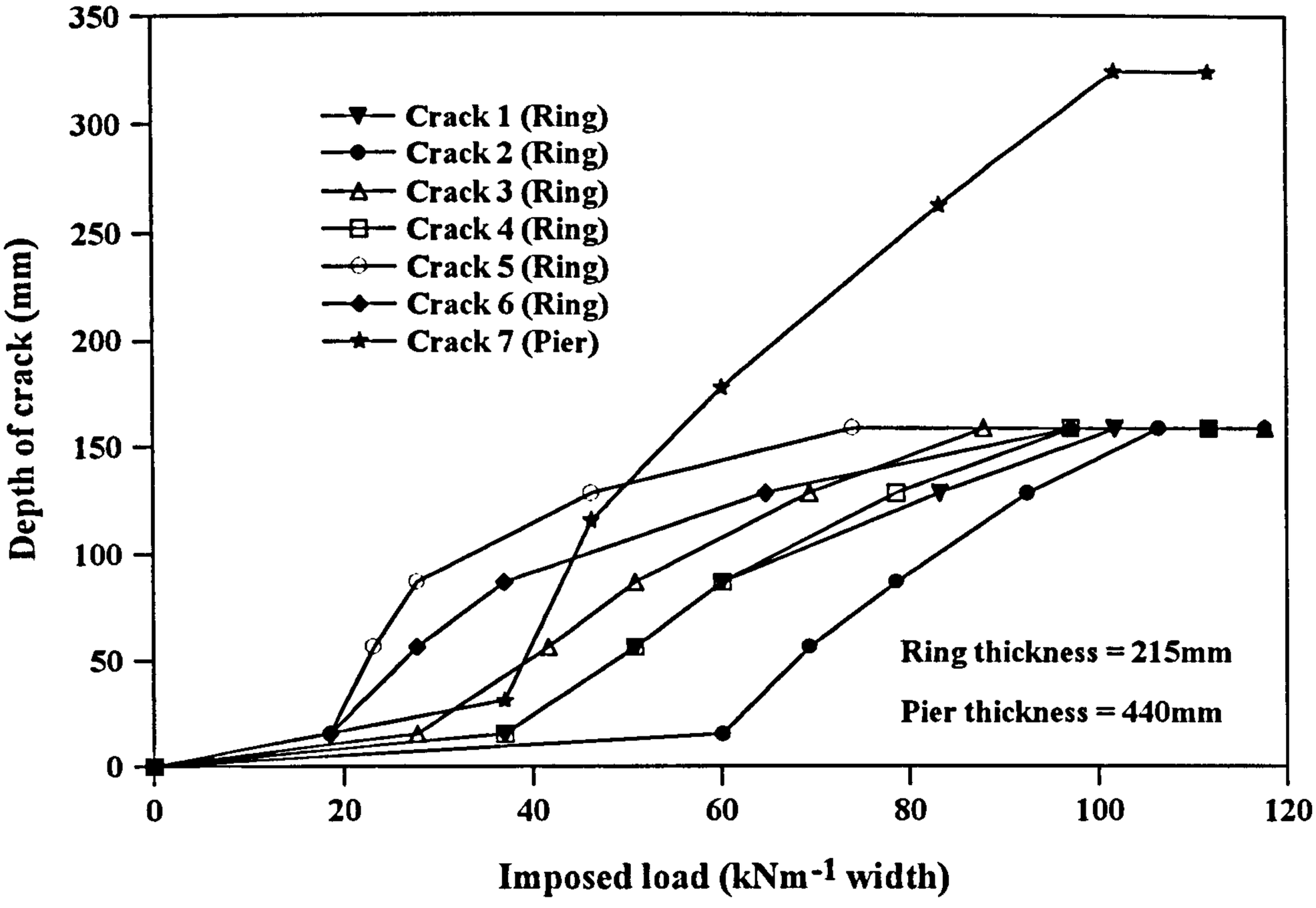

Figure 4.7q Imposed loading and crack development for Bolton

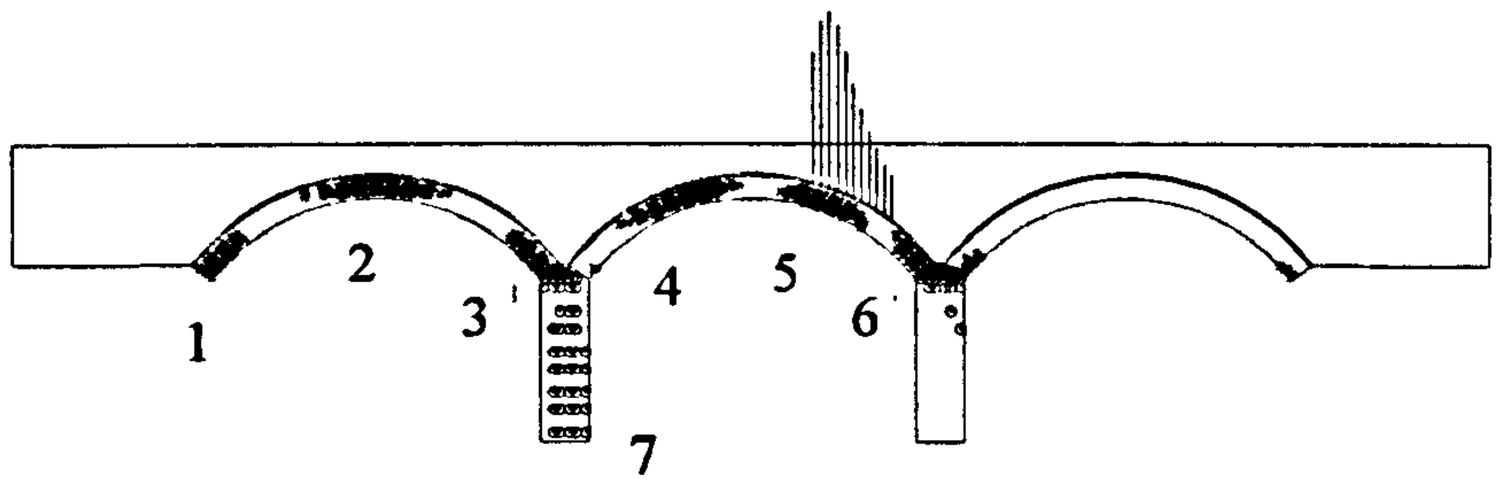

Figure 4.7r Yielded zones at Bolton as predicted by FE analysis

CHAPTER 5

Material Testing

5.1 Introduction

It has been shown in Chapter 4 that the material properties of the arch ring had a significant influence on the FE predictions. Experimental evaluation of the material properties of the arch was therefore essential to obtain greater accuracy in analyses which depend on input arch material properties. This chapter describes the evaluation of material properties of the mortar and brick batches which were used by the author for constructing three large-scale arch bridges. Full details of these arch bridges and the relevant test procedures will be presented in Chapter 6 of this thesis.

The brick and mortar were first tested separately to evaluate their elastic moduli, Poisson's ratios and compressive strengths. Similar tests were also carried out on masonry prisms of bricks jointed by mortar so that the combined material properties could be evaluated. Further tests involved the evaluation of brick-mortar bond strength of brickwork prisms.

5.2 Loading frame

All compressive tests were carried out under an Avery Denison 1000kN capacity hydraulic rig. A microcomputer was attached to the loading frame to control the load rate. Figure 5.1 shows the Avery Denison testing rig with a specimen under load. Specimens tested for flexural bond strength were loaded using a small-scale testing machine, the Lloyd 30kN universal test machine. The Lloyd testing machine was also

attached to a microcomputer enabling the load *versus* deflection curves to be displayed on a monitor at every load increment. Figure 5.2 shows the Lloyd testing machine with a specimen about to be loaded. Both machines were calibrated to a traceable load standard based at the National Physical Laboratory. The derived machine extension curves were tared into the machine's control program settings. All specimens were tested at between 20°C to 23°C (both load frames calibrated at the same temperature range).

5.3 Foil electrical strain gauges and datalogger

Electrical strain gauges manufactured by Micro-Measurement Division, USA, with a gauge length of 10mm were used for measuring strains in all specimens, with the exception of those specimens for flexural tensile tests. Strain gauges were attached to each specimen in a different configuration to replicate the strain rosette. All prisms subjected to compressive tests were fitted with strain gauges arranged in the form of an ' L ' or ' T ' strain rosette with one strain gauge parallel to the direction of loading. This enabled the strains in both horizontal and vertical directions to be measured. A dummy gauge was also attached to an unstressed specimen in each test. This was to ensure that the change in strain due to atmospheric change in temperature and heat induced in the strain gauge due to electrical current flow were automatically compensated.

Before attaching strain gauges to a specimen the face where the gauges were to be attached was treated. The first step involved the application of degreaser to the specimen's face to remove oils, grease and organic contaminants. The specimen's face was then smoothed with fine grained sand paper and a small amount of dilute phosphoric acid in aqueous solution. A thin layer of neutraliser was then applied onto the sanded area to neutralise any chemical reaction introduced by the phosphoric acid. A very thin layer of catalyst was then applied onto the surface of a strain gauge and a small amount of adhesive was used to attach the strain gauge to the specimen. Finally, a protective coating (polyurethane) was applied to provide mechanical protection to

the attached strain gauges. All gauges were then cured for at least six days. Each strain gauge was soldered wired and connected to a System 5000 (Measurement Group) datalogger. The datalogger was connected to a personal computer enabling the strains at each load increment to be viewed and recorded.

5.4 Test specimens

Four types of specimens were considered in this study; mortar cubes, solid engineering bricks and masonry prisms for both compressive and flexural tensile tests. To match the material used for constructing the three large scale arches, a mortar of 1: 1: 6 (cement: lime: sand) mix and Class B solid engineering bricks (BS3921, 1985) were used. All mortar cubes and masonry prisms were cured under a plastic sheet for 28 days. A similar curing method was also applied to the author's large scale arches immediately after construction. Plywood capping was used on all specimens, the exception being those specimens for flexural tensile tests, to ensure better contact between the load platen and the specimen's face. All specimens for compression tests were tested following the method outlined in BS1881 (1993). According to this method, a cyclic load is applied to the specimen at least three times. This load should be approximately one third of the previously established compressive strength of similar samples. This eliminates any slack in the specimen from capping materials and eliminates any hysteresis therein.

5.4.1 Compression tests for mortar cubes

Three mortar cubes with 100mm sides were cast from a 1: 1: 6 (cement: lime: sand) mix. An average moisture content of 11.35% was recorded. Four samples were taken from the mortar mix which were then weighted to obtain the total mass of each sample and then oven dried to obtain the solid mass and hence the mass of water evaporated. The moisture content is a ratio of the mass of water to the mass of solid. Each mortar cube was fitted with two strain gauges in an ' L ' configuration strain rosette in such a

way that one of these gauges was parallel to the direction of the applied load. This was to ensure that both the vertical and horizontal strains were measured. A diagrammatic illustration of the specimen with attached strain gauges is shown in Figure 5.3. Tests were carried out according to BS1881 (1993). The elastic modulus, compressive strength and Poisson's ratio for the mortar cubes were established from these tests.

5.4.2 Compression tests for bricks

Three Class B solid engineering bricks were tested in compression to determine the elastic modulus, compressive strength and Poisson's ratio. Half bricks with dimensions 107.5mm × 102.5mm × 65mm were used instead of full bricks because it was beyond the capacity of the Avery Denison machine to crush a full brick with similar properties. As illustrated in Figure 5.4, an ' L ' configuration strain was attached to each specimen. Tests were carried out in accordance with BS1881 (1993).

5.4.3 Compression tests for brickwork masonry prisms

Three masonry prisms were prepared to establish the combined properties of brick and mortar. Figure 5.5 illustrates a masonry prism with attached strain gauges on the middle mortar joint. Only half bricks were used for these prisms. These tests enabled the compressive strength of those masonry prisms and the material properties of the confined mortar joints to be established. Tests were carried out in accordance with BS1881 (1993).

5.4.3.1 Elastic analysis of brickwork strength

It is possible to derive a formula for establishing the combined strength of a brickwork masonry prism based on elastic analysis. However, certain assumptions have to be made such as slip at the interface does not occur and load is applied uniformly over the

whole loaded area. The former is justifiable since the load is applied normal to the interface. However, the application of uniform load is only a hypothesis since the load platen imposes a different degree of confinement to the loaded area rendering the stress distribution under the platen non-uniform (see Figure 3.45a).

We now consider a brickwork masonry prism acted on by a compressive uniformly distributed load and with the mortar's Poisson's ratio higher than that of the brick. The lateral movement of the mortar is restrained by the brick putting the mortar in a state of compression while the brick is in tension. The directions of the stresses in both the brick and mortar are illustrated in Figure 5.6. Using the constitutive laws of the materials, the horizontal strain in the mortar can be derived as shown in Eqn 5.1.

$$\varepsilon_m = -\frac{\sigma_m}{E_m} + \nu_m \frac{\sigma_c}{E_m} \qquad 5.1$$

Similarly, the horizontal strain in the brick would be;

$$\varepsilon_b = -\frac{\sigma_b}{E_b} + \nu_b \frac{\sigma_c}{E_b} \qquad 5.2$$

By considering the system's static equilibrium, the total lateral forces in the mortar and brick are equal and opposite. Let the thicknesses of the brick and mortar be d_b and t_m respectively. A relationship between the stresses in the mortar and brick could be derived as shown in Eqn 5.3

$$\sigma_m = \frac{d_b}{t_m} \times \sigma_b \qquad 5.3$$

Substituting Eqn 5.3 into Eqn 5.1 gives

$$\varepsilon_m = \frac{-\frac{d_b}{t_m}\sigma_b}{E_m} + \nu_m \frac{\sigma_c}{E_m} \qquad 5.4$$

Equating Eqn 5.2 and Eqn 5.4 gives,

$$\sigma_c = \frac{\sigma_b\left[\frac{1}{E_b} + \frac{d_b}{t_m} \times \frac{1}{E_m}\right]}{\frac{\nu_m}{E_m} - \frac{\nu_b}{E_b}} \qquad 5.5$$

A failure criterion based on the limiting tensile strain in the brick is applied as shown in Eqn 5.6. The ultimate horizontal strain in the brick is denoted by ε_{ult}.

$$\varepsilon_{ult} = \frac{\sigma_b}{E_b} + \nu_b \frac{\sigma_c}{E_b} \qquad 5.6$$

The corresponding limiting tensile stress in the brick could be expressed as shown in Eqn 5.7.

$$\sigma_t = E_b \times \varepsilon_{ult} \qquad 5.7$$

Substituting Eqn 5.7 into Eqn 5.6 and rearranging gives,

$$\sigma_b = \sigma_t - \nu_b \sigma_c \qquad 5.8$$

Substituting Eqn 5.8 into Eqn 5.5 and rearranging gives,

$$\sigma_c = \frac{\sigma_t\left[\frac{1}{E_b} + \frac{d_b}{t_m \times E_m}\right]}{\frac{\nu_m}{E_m} - \frac{\nu_b}{E_b} + \nu_b\left[\frac{1}{E_m} + \frac{d_b}{t_m \times E_m}\right]} \qquad 5.9$$

Using Eqn 5.9, the maximum compressive stress that is required to cause a tensile failure in the brick can be calculated. A numerical example using Eqn 5.9 will be given in Section 5.6.3 and a comparison will also be made with the experimental results.

5.4.4 Brick-mortar flexural bond strength

Figure 5.7 shows a specimen and the set-up for a test to establish the brick-mortar flexural bond strength. In order to reflect the bond strength in the three large scale arches as described in Chapter 6 of this thesis, a total of twelve specimens were built during the construction of each arch using the same batches of bricks and mortar. The first, second and third arches were subsequently referred to as SR4-A, SR4-B and SR4-C respectively. The thickness of mortar adopted for these specimens was 10mm and a lapped length of 95mm as indicated in Figure 5.7. Each specimen was loaded and supported by a 10mm square steel bar at each support and at the load point. In order to provide better contact, a layer of dental plaster was applied to each steel bar before attaching it to the specimen. The Lloyd universal testing machine was used for testing these specimens as shown in Figure 5.2.

5.4.4.1 Theoretical derivation of the flexural bond strength

This method is previously described by TAYLOR (1997). However, it was found that his theoretical derivation to establish the flexural bond strength was based on the assumption that the weight of each brick was acting directly under the centre line of the applied load. Such an idealisation had little influence on the prediction of the flexural tensile strength in this case because the self-weight of the brick is small compared with the maximum applied load. However, such an assumption is unnecessary and its absence does not render the derivation impossible or more difficult. The following paragraphs present the derivation of the brick-mortar flexural bond strength with the weight of each brick acting at its centre of gravity.

Let P and W be the applied loads required to overcome the flexural tensile strength and the self-weight of each brick respectively. The self-weight of the mortar is not considered in the derivation as it is negligible compared to the weight of the brick. Referring to Figure 5.7, by taking moments about point B and assuming that both ends

of the specimen are simply supported, the reaction at point A can be expressed as shown in Eqn 5.10.

$$R_a = \frac{P\left[L_b - L_m\right] + W\left[2L_b - W_p - L_m\right]}{2L_b - L_m - W_p} \qquad 5.10$$

Let W_b be the width of the brick and assuming that the distribution of tensile stress along the lapped length is linear as shown in Figure 5.8, the total bonding force could be obtained as shown in Eqn 5.11. The flexural bond strength is denoted by f_{tb}.

$$F_{tb} = \frac{1}{2} L_m W_b f_{tb} \qquad 5.11$$

From Figure 5.8a, by taking moments about point C and considering the equilibrium of the whole system, another expression could be derived as shown in Eqn 5.12.

$$\frac{2}{3} L_m F_{tb} = R_a \left[L_b - \frac{1}{2} W_p\right] - \frac{1}{2} W_p P - \frac{1}{2} W L_b \qquad 5.12$$

Substituting Eqn 5.11 into Eqn 5.12 gives,

$$f_{tb} = \frac{3}{W_b L_m^2}\left[R_a \left(L_b - \frac{1}{2} W_p\right) - \frac{1}{2} P W_p - \frac{1}{2} W L_b\right] \qquad 5.13$$

Substituting Eqn 5.10 into Eqn 5.13 gives,

$$f_{tb} = \frac{3}{W_b L_m^2}\left[\frac{P\left(L_b - L_m\right) + W\left(2L_b - W_p - L_m\right)}{2L_b - L_m - W_p} \times \left(L_b - \frac{1}{2} W_p\right) - \frac{1}{2} P W_p - \frac{1}{2} W L_b\right] \qquad 5.14$$

Substituting the geometrical dimensions of the specimens as shown in Figure 5.7 and the weight of a brick is 31N (average weight of ten bricks), implies Eqn 5.14 could be simplified as shown in Eqn 5.15 in units of Nmm^{-2} or MPa.

$$f_{tb} = \frac{P}{4251} + 0.0103 \qquad 5.15$$

From Eqn 5.14, it can be seen that the flexural bond strength can be established by knowing the applied load required to overcome the tensile bond strength and all other geometrical properties of the specimen. If a parabolic distribution of tensile stress on the brick-mortar interface is assumed, a slight change has to be made in the evaluation of total force as shown in Eqn 5.16; the resultant now acts at a horizontal distance of $5\,L_m\,/\,8$ from point C as shown in Figure 5.8b.

$$F_{tb} = \frac{2}{3} L_m\, W_b\, f_{tb} \qquad 5.16$$

Similarly the flexural tensile strength can be derived from a parabolic stress distribution as shown in Eqn 5.17.

$$f_{tb} = \frac{12}{5\,W_b\,L_m^2}\left[\frac{P\left(L_b - L_m\right) + W\left(2L_b - W_p - L_m\right)}{2L_b - L_m - W_p} \times \left(L_b - \frac{1}{2}W_p\right) - \frac{1}{2}P\,W_p - \frac{1}{2}W\,L_b\right] \qquad 5.17$$

The flexural tensile strength evaluated by Eqn 5.17 is 20% lower than that evaluated by Eqn 5.14. The author is unaware of the actual stress distribution of the brick-mortar interface. The experimental flexural tensile strength will be evaluated using Eqn 5.14 assuming a linear stress distribution in this study: the result is 20% lower if a parabolic stress distribution is assumed.

5.5 Results

The results from the tests described in Sections 5.4.1 to 5.4.4 inclusive are now presented. The material properties such as the elastic modulus, Poisson's ratio and compressive strength were established from those tests carried out on mortar cubes, bricks and brickwork masonry prisms. The brick-mortar flexural tensile strength was evaluated using Eqn 5.14.

5.5.1 Compression tests for mortar cubes

The vertical and horizontal strains recorded by electrical strain gauges attached to three mortar cubes are presented in Figures 5.9 and 5.10 respectively. The stress *versus* strain curves were approximately linear up to a vertical applied stress of 4MPa for the three specimens. Linear regression analyses were performed up to an applied stress of 4MPa which revealed that the elastic moduli of specimens 1, 2 and 3 were 7400MPa, 6200MPa and 7000MPa respectively. Similarly, the Poisson's ratios were found to be 0.262, 0.272 and 0.256 for specimens 1, 2 and 3 respectively. The maximum compressive strengths of specimens 1, 2 and 3 were 4.66MPa, 5.20MPa and 4.85MPa respectively.

5.5.2 Compression tests for bricks

Figures 5.11 and 5.12 shows the vertical and horizontal strains, respectively, recorded by electrical strain gauges attached to three brick specimens. A similar maximum applied stress of 92MPa was recorded in these tests. It could be seen from Figures 5.11 and 5.12 that the stress *versus* strain curves were approximately linear up to the maximum applied stress. Linear regression analyses were performed up to an applied stress of 92MPa which revealed that the elastic moduli were 38300MPa, 36600MPa and 39200MPa for specimens 1, 2 and 3 respectively. Similarly the Poisson's ratios were 0.153, 0.156 and 0.153 for specimens 1, 2 and 3 respectively. The compressive strength for the three specimens was 92MPa.

5.5.3 Compression tests for masonry prisms

The vertical and horizontal strains recorded by electrical strain gauges attached to the confined mortar joints were presented in Figures 5.13 and 5.14 respectively. The maximum compressive strengths of specimens 1, 2 and 3 were 32.1MPa, 31.3MPa and 29.5MPa respectively. It could be seen from Figures 5.13 and 5.14 that the stress

versus strain curves were approximately linear up to an applied stress of about 25MPa. Linear regression analyses were performed up to an applied stress of 25MPa which revealed that the elastic moduli of the confined joints of specimens 1, 2 and 3 were 4702MPa, 5001MPa and 5100MPa respectively. Similarly the Poisson's ratios were found to be 0.129, 0.142 and 0.134 for specimens 1, 2 and 3 respectively.

5.5.4 Brick-mortar flexural tensile strength

A total of 36 specimens for establishing the brick-mortar flexural tensile strength were tested during three different periods. Twelve specimens were built at one time during the construction of each large scale arch, as described in Chapter 6, using the same batches of bricks and mortar. For the sake of clarity, the first, second and third groups of specimens are subsequently referred to as Groups A, B and C, respectively, representing the flexural tensile strengths of arches SR4-A, SR4-B and SR4-C respectively. Equation 5.14 was used to evaluate the tensile strength of each specimen. However, if a parabolic distribution of the flexural tensile stress at the brick-mortar interface was assumed, the flexural tensile strength would be 20% lower than that evaluated by Eqn 5.14 which assumed a linear distribution of tensile stress. The results of the brick-mortar flexural tensile strength from Groups A, B and C are presented in Figures 5.15, 5.16 and 5.17 respectively. A summary of the statistical properties of the flexural tensile strength is presented in Table 5.1. Figure 5.18 shows the distribution of the flexural tensile strength considering 36 specimens. The mean, standard deviation (S.D.) and coefficient of variation (C.V.) of all specimens were 0.521MPa, 0.244MPa and 42.97% respectively.

Table 5.1 Flexural tensile strength

Arch	Mean (MPa)	S.D. (MPa)	C.V. (%)
SR4 - A	0.542	0.266	49.16
SR4 - B	0.471	0.121	25.74
SR4 - C	0.550	0.264	48.06
36 Specimens	0.521	0.224	42.97

5.6 Discussion

The results presented in Section 5.5 are discussed here. Comparisons were made between the material properties obtained from the author's experiments and those established by others.

5.6.1 Compression tests for mortar cubes

The average compressive strength, elastic modulus and Poisson's ratio of the mortar cubes tested were 4.90MPa, 6867MPa and 0.263 respectively. Similar tests performed by TAYLOR (1997) revealed that the compressive strength, elastic modulus and Poisson's ratio were 4.51MPa, 8100MPa and 0.27 respectively which are in good agreement with those obtained by the author. A compressive strength of 3.60MPa is recommended in BS5628 (1992), for a similar mix, which is 26.5% lower than that obtained by the author. Such a compressive strength recommended in BS5628 is purely based on the proportion of cement, lime and sand without considering the moisture content of the mix. In this study, an average moisture content of 21.5% was used to obtain a workable mix.

5.6.2 Compression tests for bricks

The average compressive strength, elastic modulus and Poisson's ratio of the bricks tested in this study were 92MPa, 38033MPa and 0.154 respectively. These results were based on tests on half bricks with a shape factor (ratio of height to least horizontal length of the block) of 0.63. However, if a full brick was used, there would be no change in shape factor provided the load was applied to the largest area of the specimen.

The average compressive strengths of Class B and Class A engineering bricks recommended in BS3921 (1985) are not less than 50MPa and 70MPa respectively.

Surprisingly, the average compressive strength of those Class B engineering bricks tested by the author was 31.4% higher than the compressive strength of Class A engineering brick recommended in BS3921. Such a high discrepancy may be due to the inconsistency in the brick material and also the manufacturing process which are out of the author's reach to make further comments.

5.6.3 Compression tests for brickwork masonry prisms

The average compressive strength of the brickwork masonry prisms tested by the author was 31MPa. For a similar mortar mix, a mean compressive strength of 15.5MPa is recommended in BS5628 (1992) assuming the compressive strength of the unit is 100MPa. The recommended compressive strength is 50% lower than that obtained by the author. This might be because the mortar used by the author had a higher compressive strength than that recommended in BS5628 (1992).

It was noticed during testing that all the prisms failed by tensile splitting of the bricks which indicated that the horizontal strain in the mortar joint was sufficiently large to split the brick. Such a mechanism is a fundamental assumption made to derive the combined compressive strength of a masonry prism, as shown in Eqn 5.9, which fails by tensile splitting of the bricks. The ratio of tensile to compressive strengths of a brick is usually within the region of 1:20 to 1:10. Assuming that the compressive strength of the brick is fifteen times the tensile strength and using the average values of elastic moduli and Poisson's ratios obtained by the author, Eqn 5.9 gives a combined compressive strength of 29.5MPa which was only 4.8% lower than the experimental compressive strength of 31MPa.

The average elastic modulus and Poisson's ratio of the confined mortar joint were 4934MPa and 0.135 respectively. Referring to Section 5.5.1, it could be seen that the elastic modulus and Poisson's ratio of a mortar cube were higher than those for a mortar joint. This was because the plasticity of the mortar joint was increased due to the higher degree of confinement afforded to the joint by the neighbouring bricks.

5.6.4 Brick-mortar flexural tensile strength

The average flexural tensile strength obtained from the author's tests was 0.521MPa with a coefficient of variation of 42.97%. Similar tests were also carried out by TAYLOR (1997) which yielded an average flexural tensile strength of 0.61MPa. A lower flexural tensile strength of 0.5MPa is recommended in BS5628 (1992). The author's result is in good agreement with that recommended by BS5628 but is 14.6% lower than that by TAYLOR (1997). Possible reasons are given in the following paragraphs.

The experimental flexural tensile strength established by the author suffered a high degree of variation with a coefficient of variation of 42.97%. The maximum and minimum flexural tensile strengths recorded from the tests were 1.179MPa and 0.127MPa respectively. It has been shown by KAMF (1963) and DE GROOT (1987) that both the moisture content and workmanship are the most important factors affecting the bond strength. GRANDET (1975) found that the brick-mortar bond was due to penetration of hydration products such as calcium silicate hydrate and ettringite into brick pores. This indicated that surface roughness plays an important role in influencing the bond properties.

It is not the purpose of the current tests to generalise the brick-mortar flexural tensile strength. They were carried out in an attempt to get an idea of the bond properties in those large scale arches built by the author. Unfortunately, such a high degree of variability in the evaluation of the flexural tensile strength has widened the gap in the relationship between the evaluated flexural tensile strength and that of the arch. It should perhaps be noted here that problems like this gave rise to the author's work on risk analysis which will be presented in Chapter 7.

5.7 Limitations of the evaluated material strengths

The elastic moduli of both the brick and mortar were established in this study. However, there is still a difficulty in relating the evaluated elastic moduli of both the brick and mortar to that of the arch since the load regime experienced by an arch is different from those in the current tests. An elastic modulus of the arch is suggested to be lower than that of the brick since the elasticity of the arch is very much influenced by mortar joints of a comparatively low elastic modulus. However, the arch deflection is very much influenced by the rotation of arch segments about hinges formed in the arch. Replication of this large deflection effect due to arch rotation can only be considered by assigning an arch elastic modulus which is much lower than that of the brick in an arbitrary manner.

The reliability of the established material properties such as elastic modulus and Poisson's ratio depends on the effectiveness of the strain gauges used in this study. Whilst every precaution was taken during their installation, it was not an easy task to achieve a perfect installation unless they were installed by persons who have been trained in this art. Although dummy gauges were used to account for the change in strain due to change in temperature, strain readings were also affected by other factors such as the length and type of the cable used to connect the strain gauge to the datalogger. These factors are listed here to summarise other non-quantifiable sources of possible error in the author's material properties.

5.8 Conclusions

1. The average compressive strength, elastic modulus and Poisson's ratio of the mortar cubes in a 1: 1: 6 (cement: lime: sand) mix were 4.90MPa, 6867MPa and 0.263 respectively.

2. The average compressive strength, elastic modulus and Poisson's ratio of the Class B engineering bricks were 92MPa, 38033MPa and 0.154 respectively.

3. The compressive strength of the brickwork masonry prisms was 31MPa.

4. The average elastic modulus and Poisson's ratio of the confined mortar joints were 4934MPa and 0.135 respectively.

5. The average brick-mortar flexural tensile strength was 0.521MPa with a coefficient of variation of 42.97%.

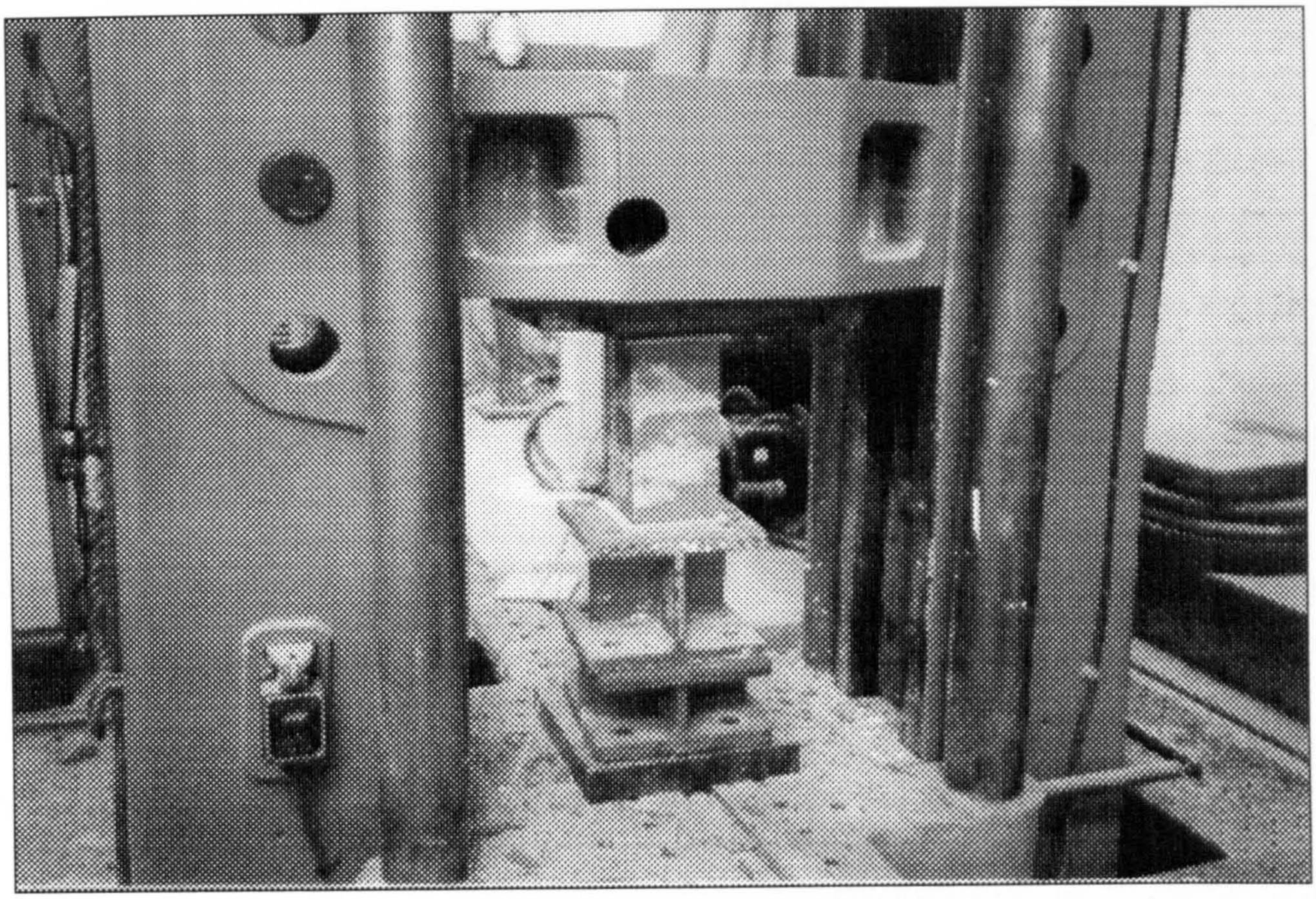

Figure 5.1 The Avery Denison hydraulic testing rig

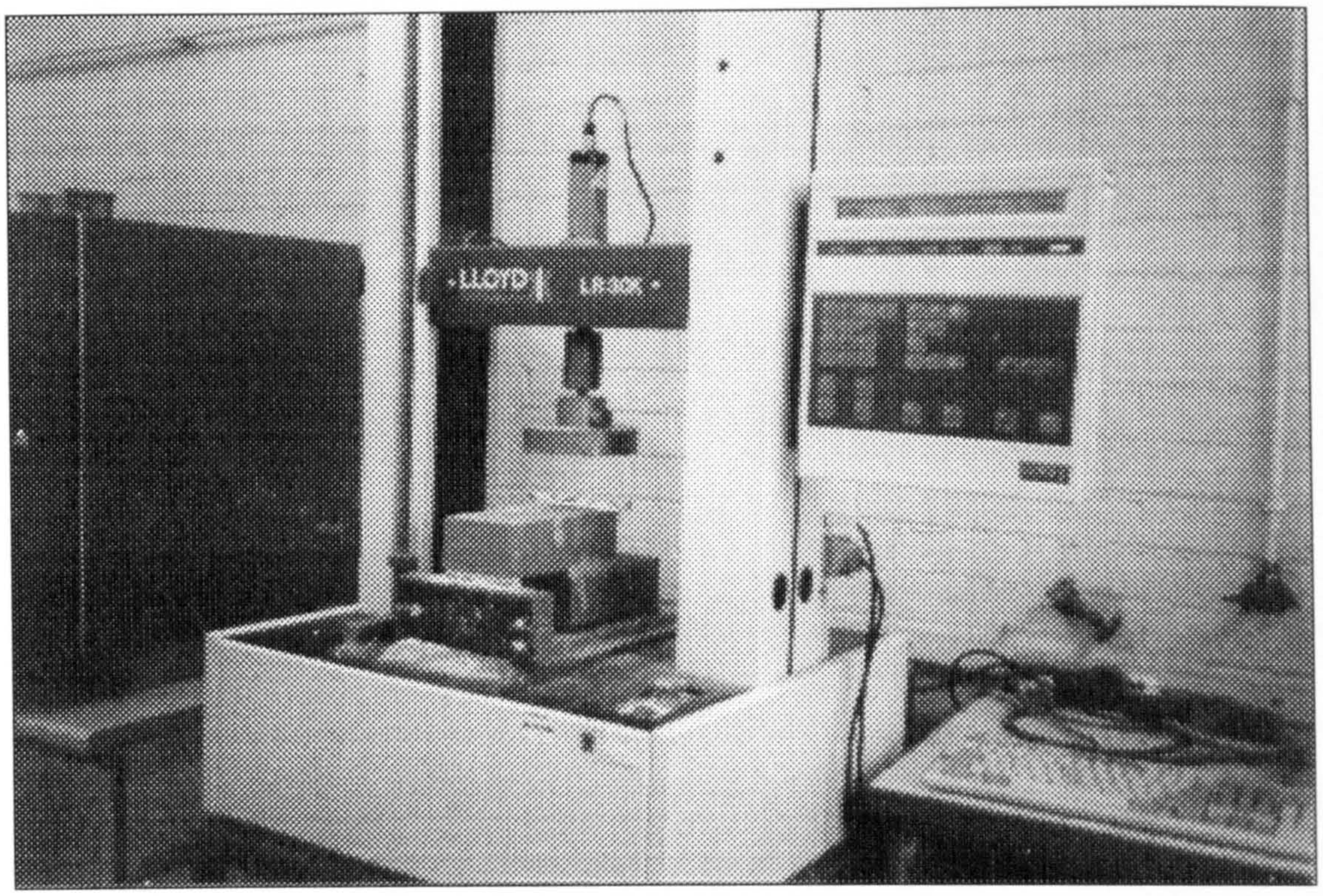

Figure 5.2 The Lloyd universal testing machine

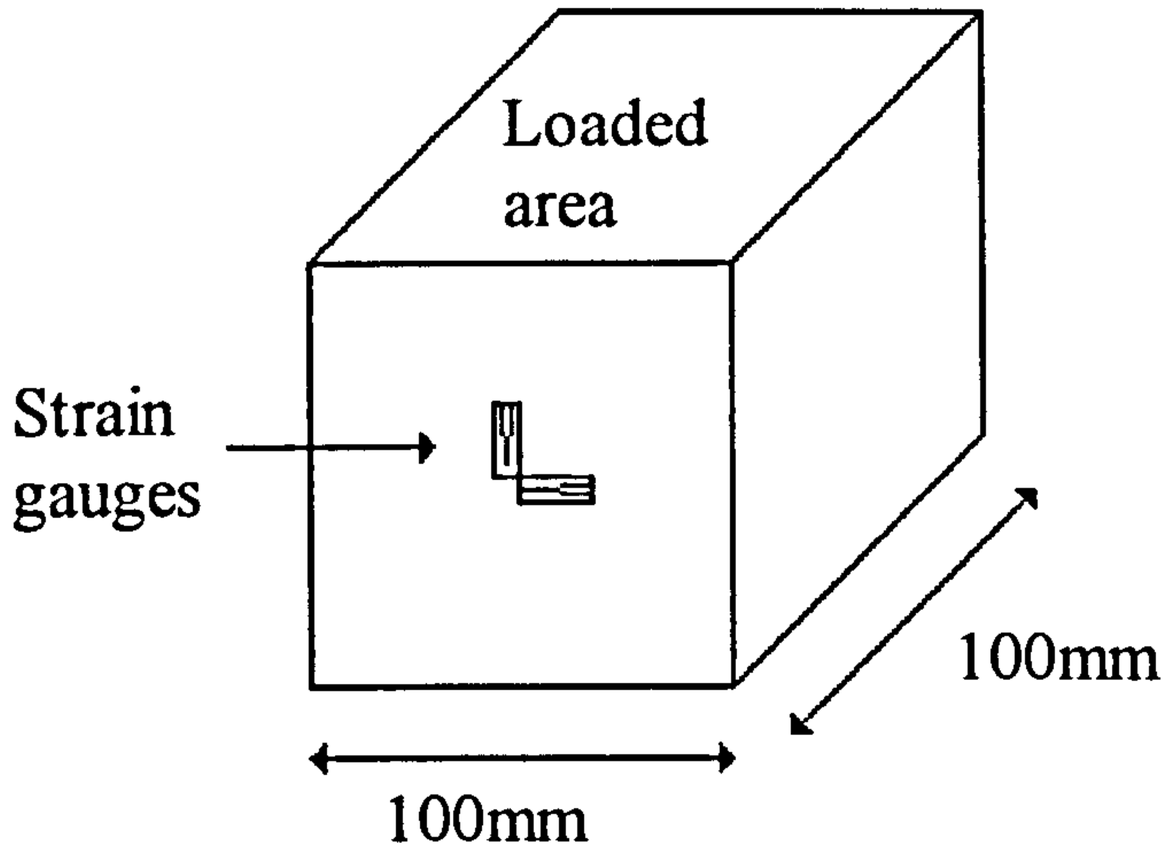

Figure 5.3 A mortar cube with attached strain gauges

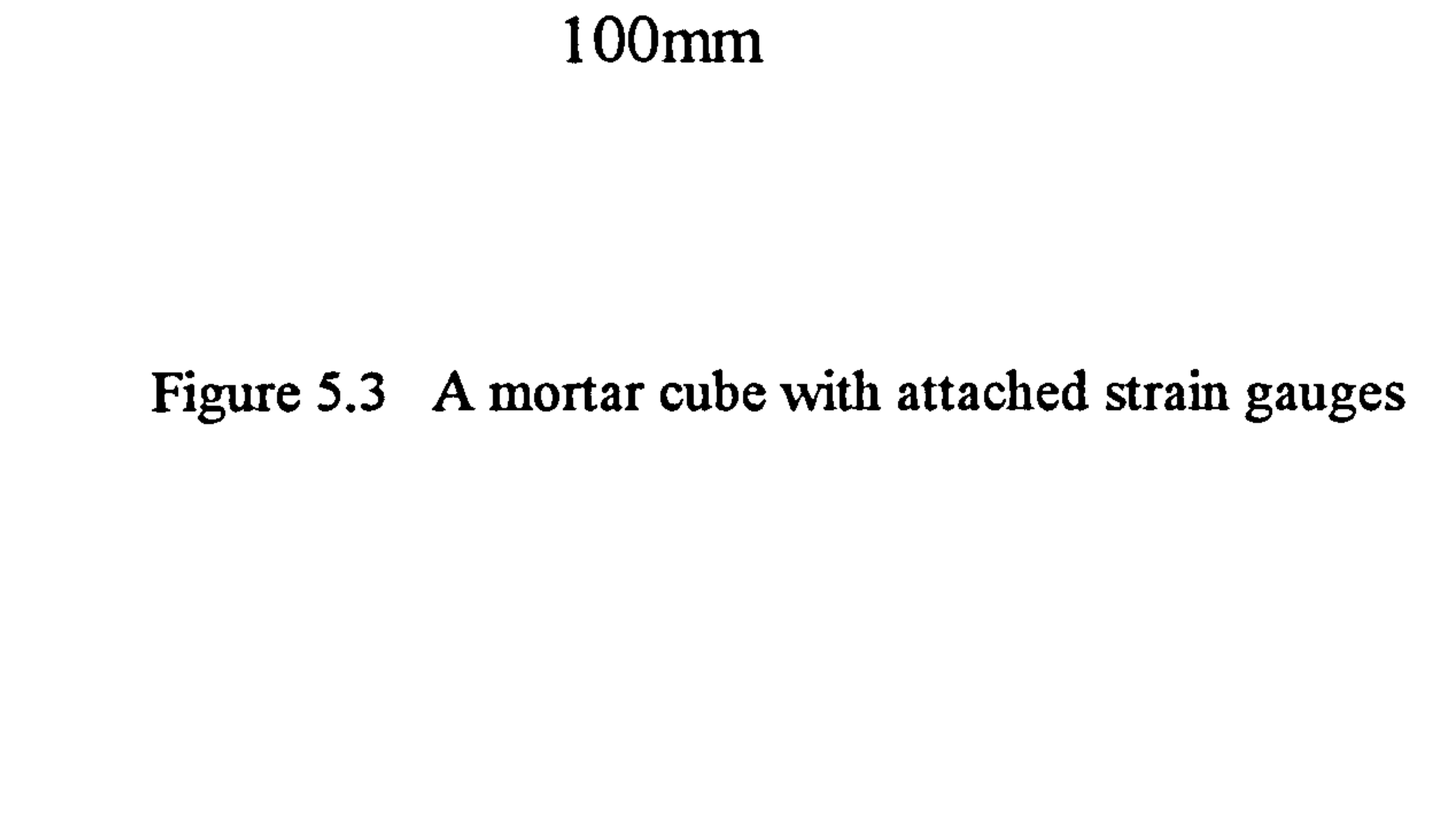

Figure 5.4 A brick specimen with attached strain gauges

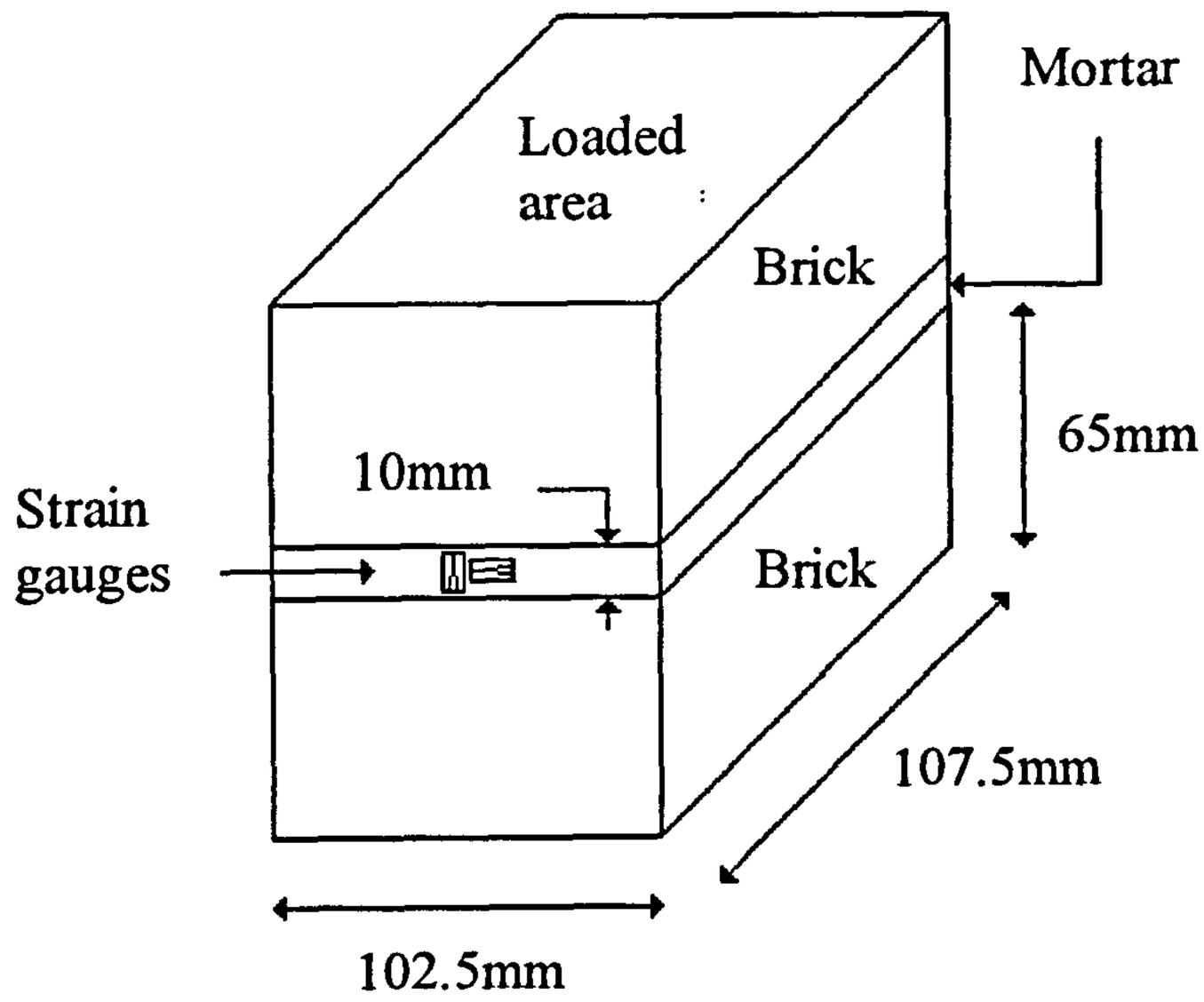

Figure 5.5 A brickwork masonry prism with attached strain gauges

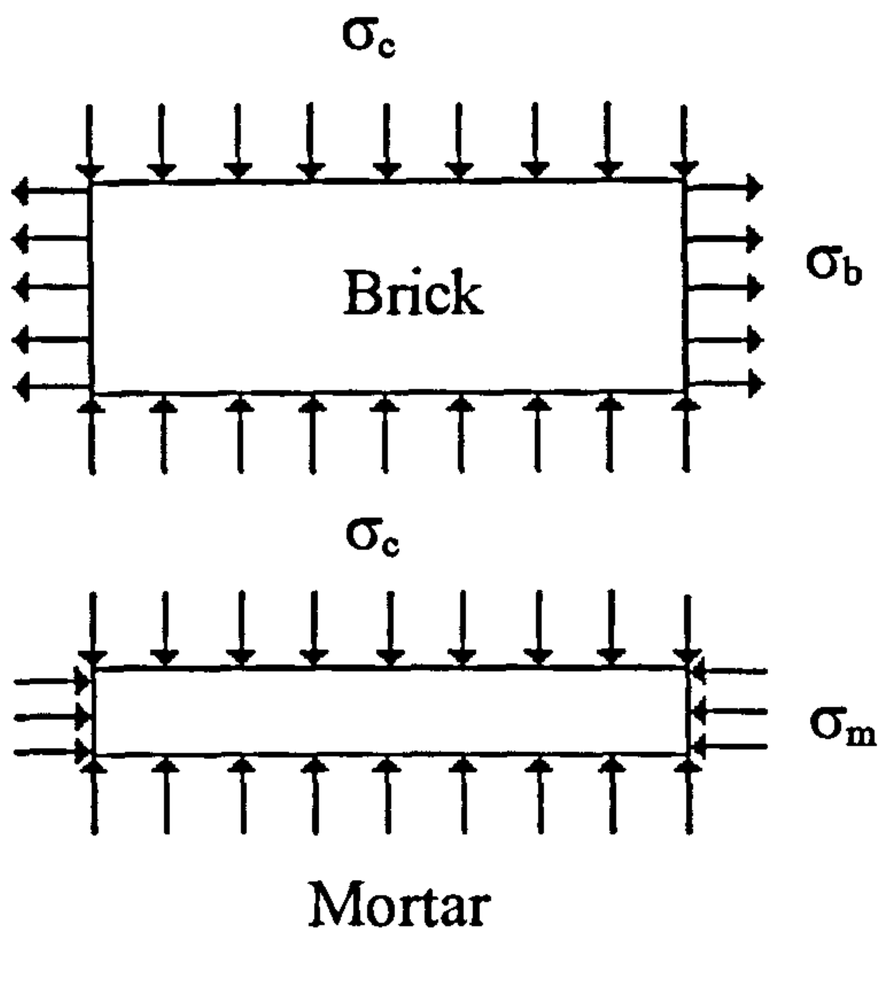

Figure 5.6 Direction of stresses on brick and mortar

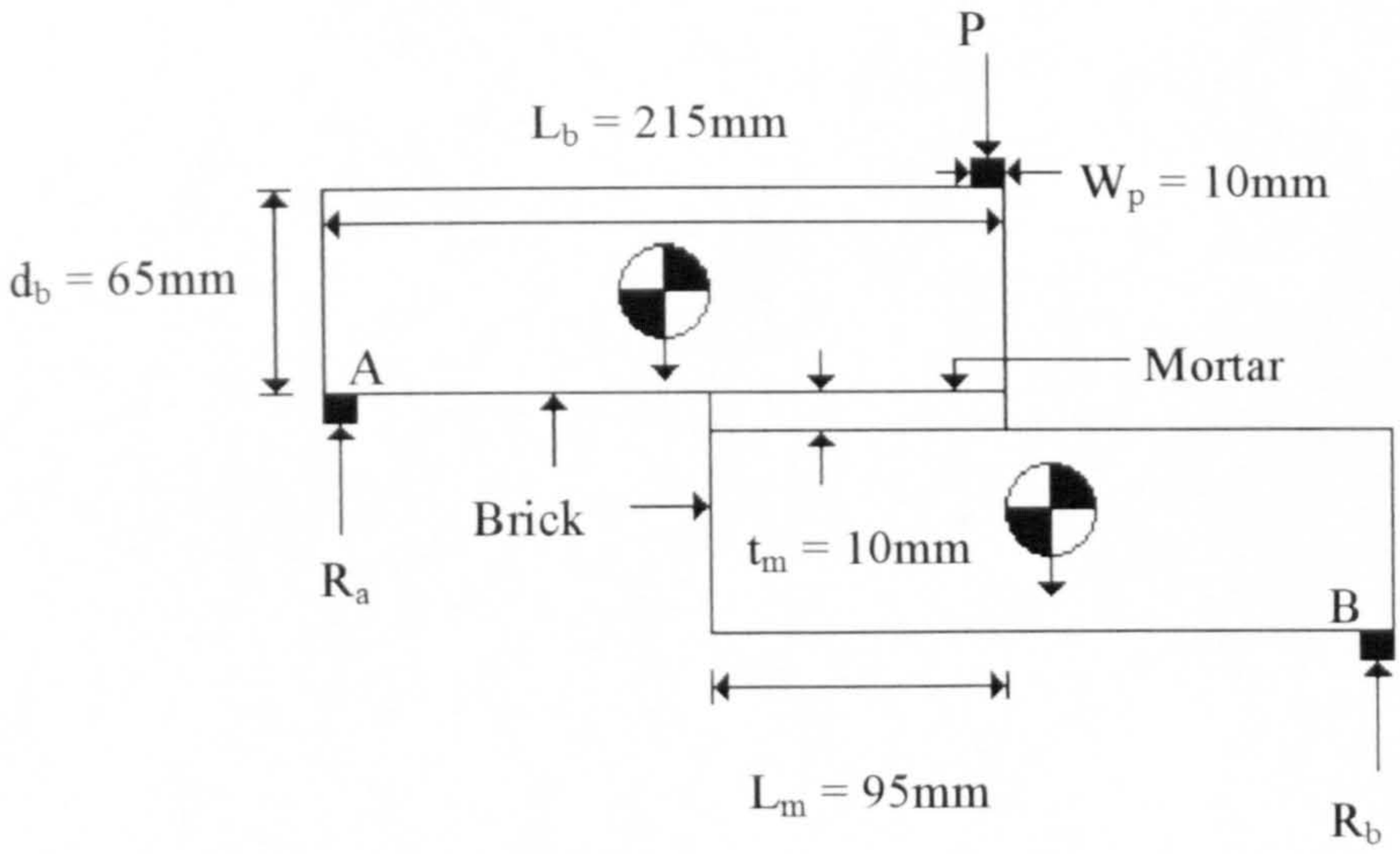

Figure 5.7 A brickwork-mortar specimen for the flexural tensile test

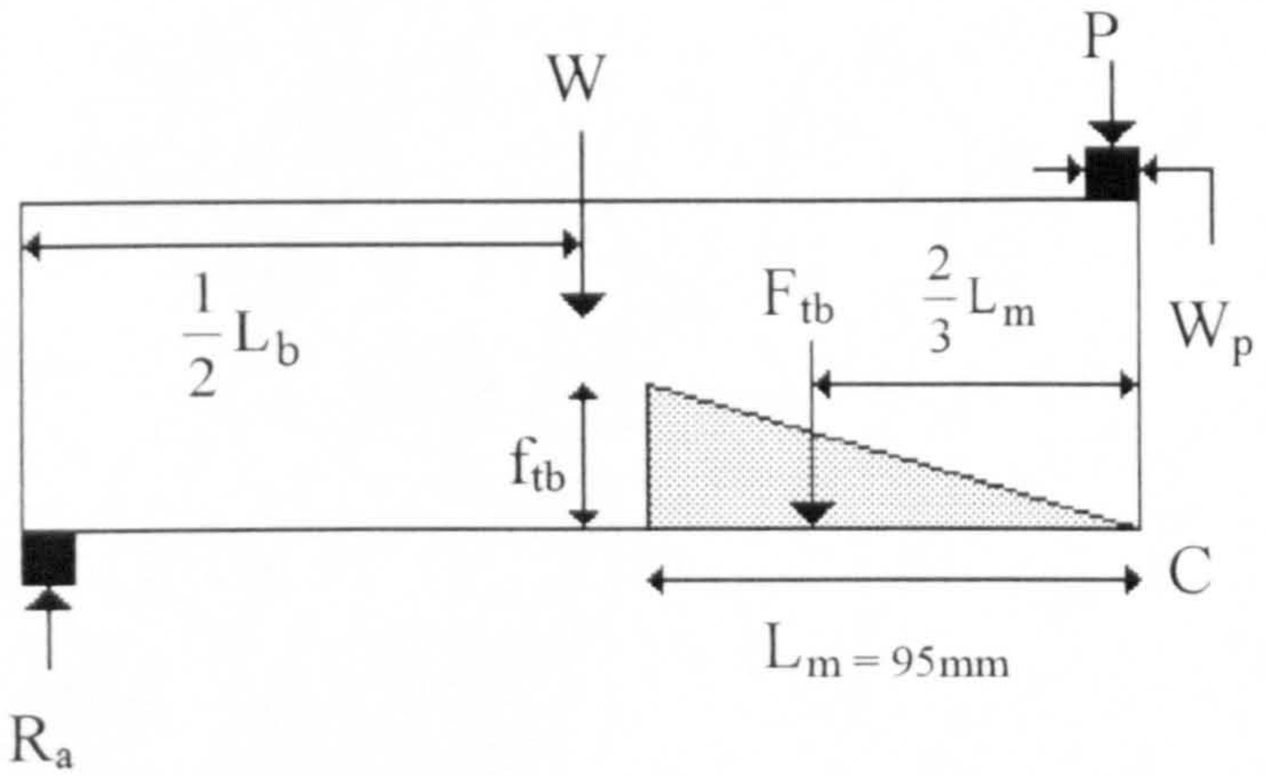

Figure 5.8a Linear distribution of tensile stress

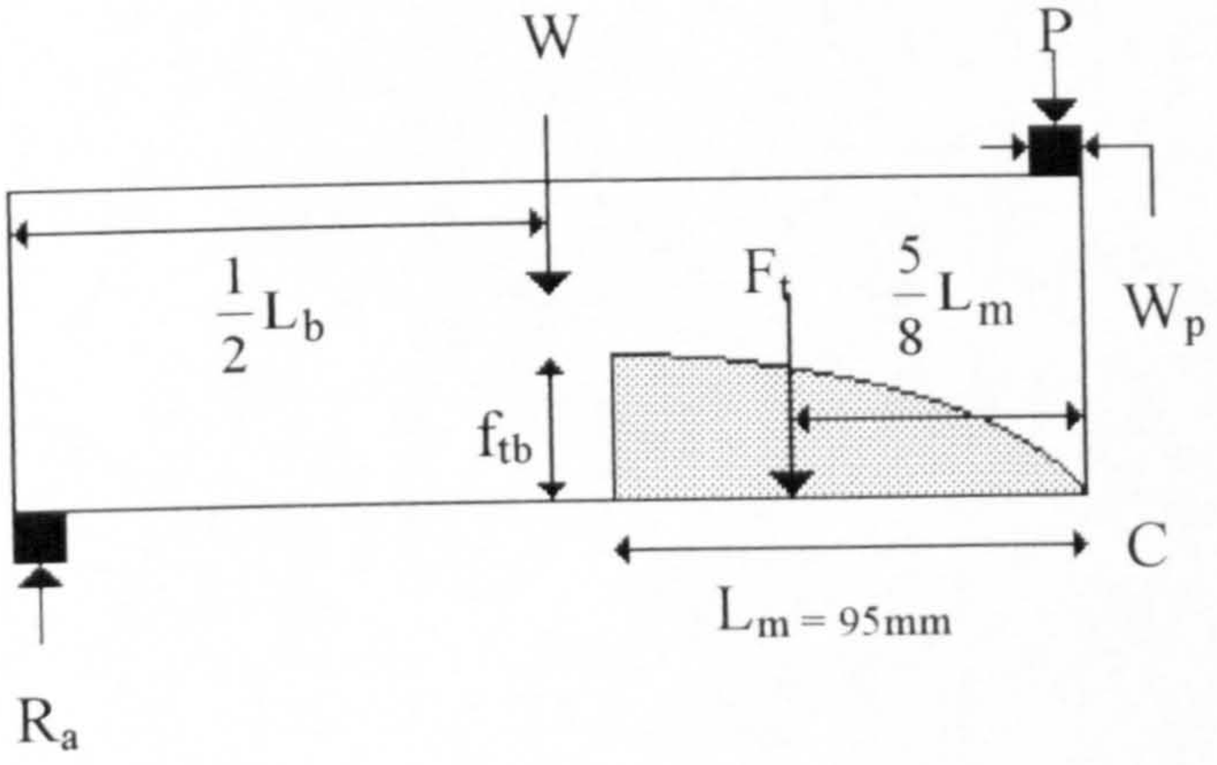

Figure 5.8b Parabolic distribution of tensile stress

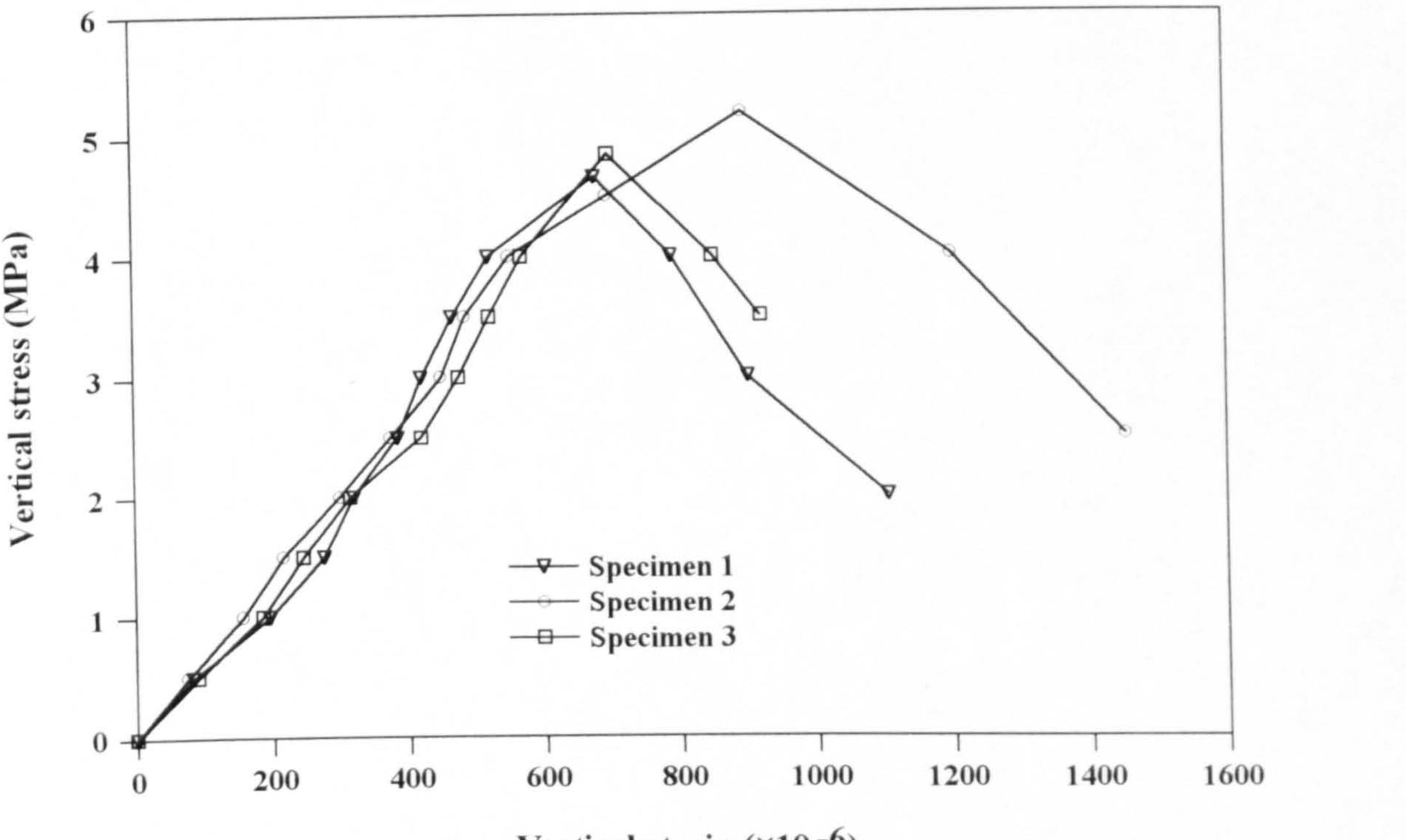

Figure 5.9 Vertical stress *versus* vertical strain curves for mortars

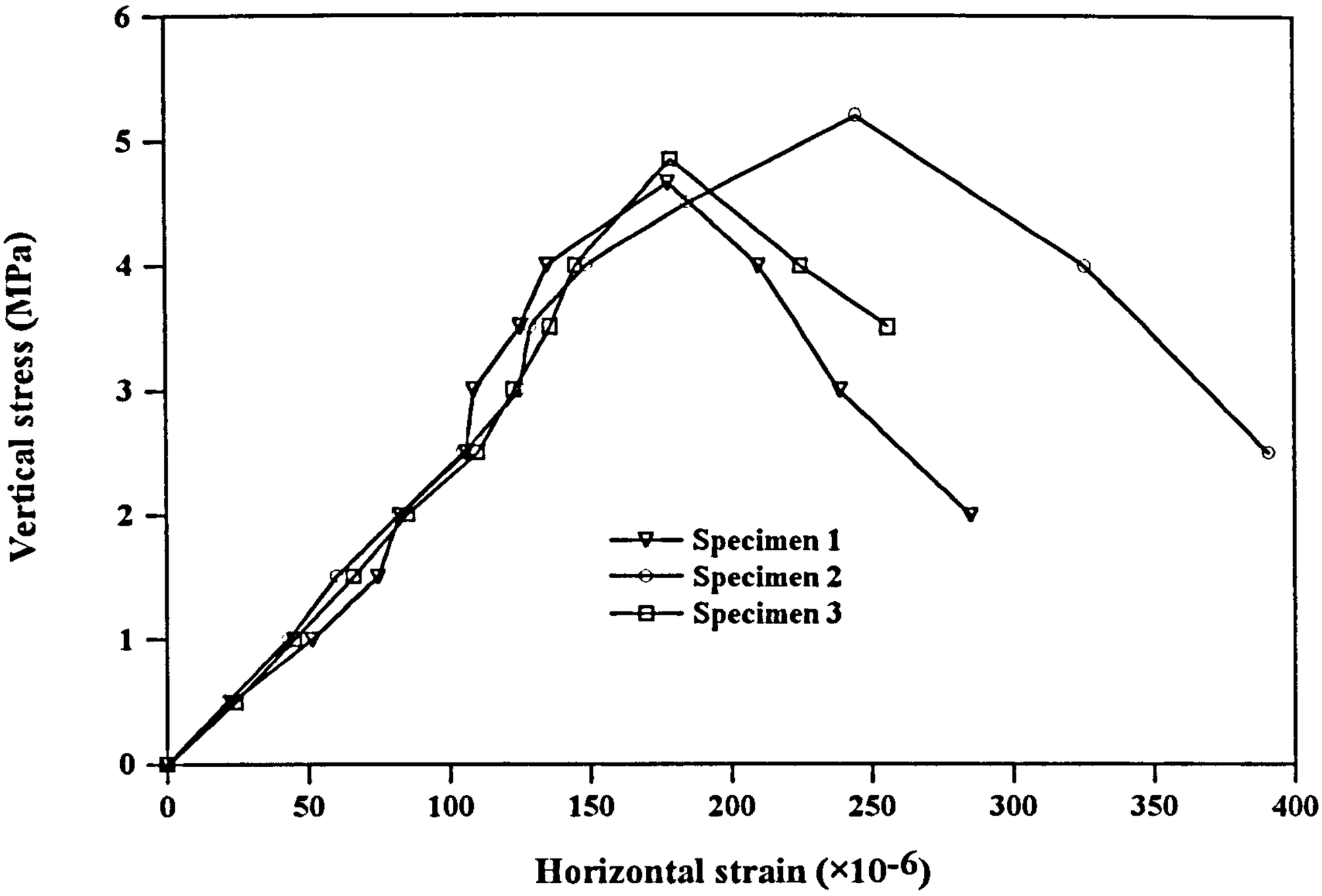

Figure 5.10 Vertical stress *versus* horizontal strain curves for mortars

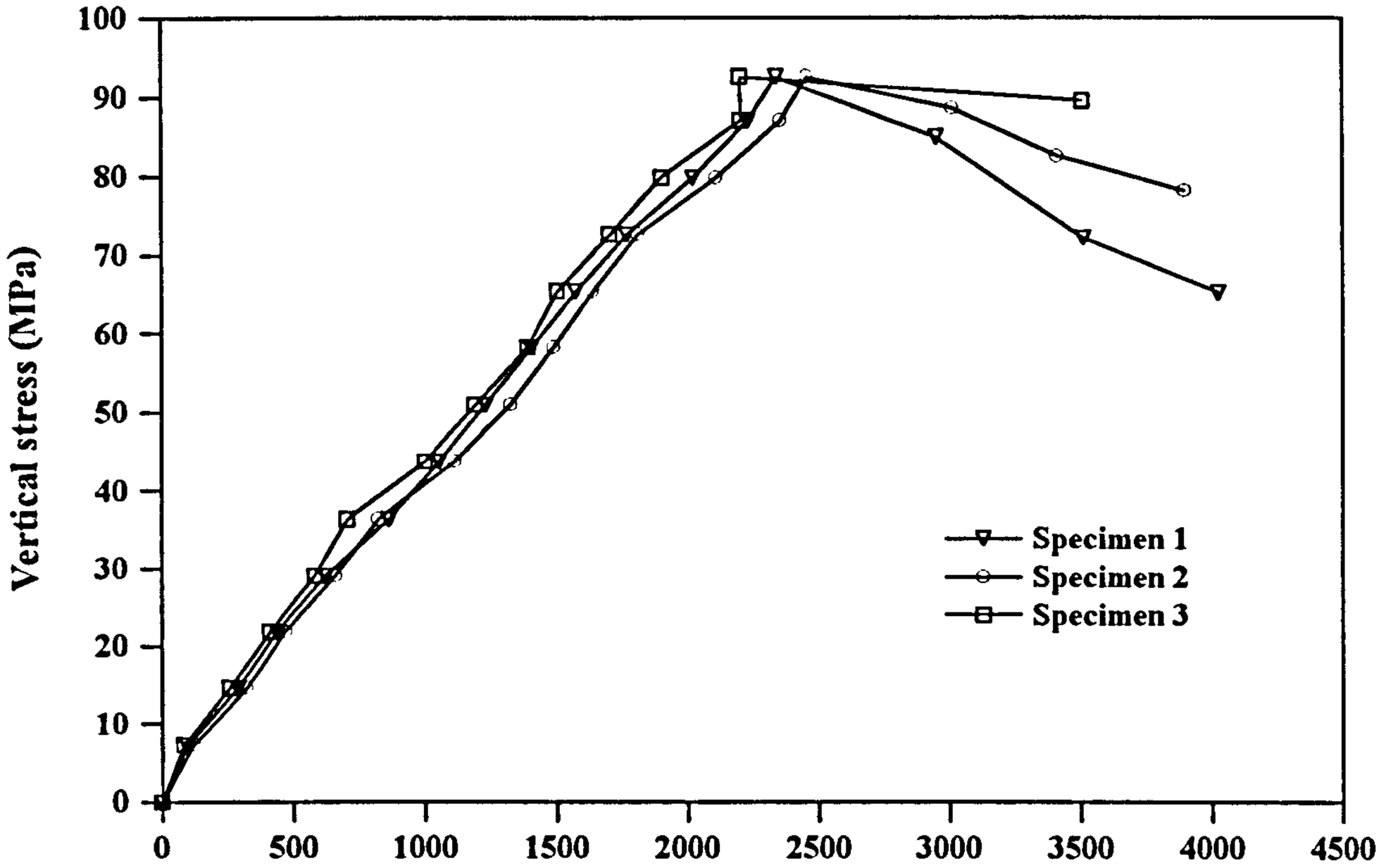

Figure 5.11 Vertical stress *versus* vertical strain curves for brick specimens

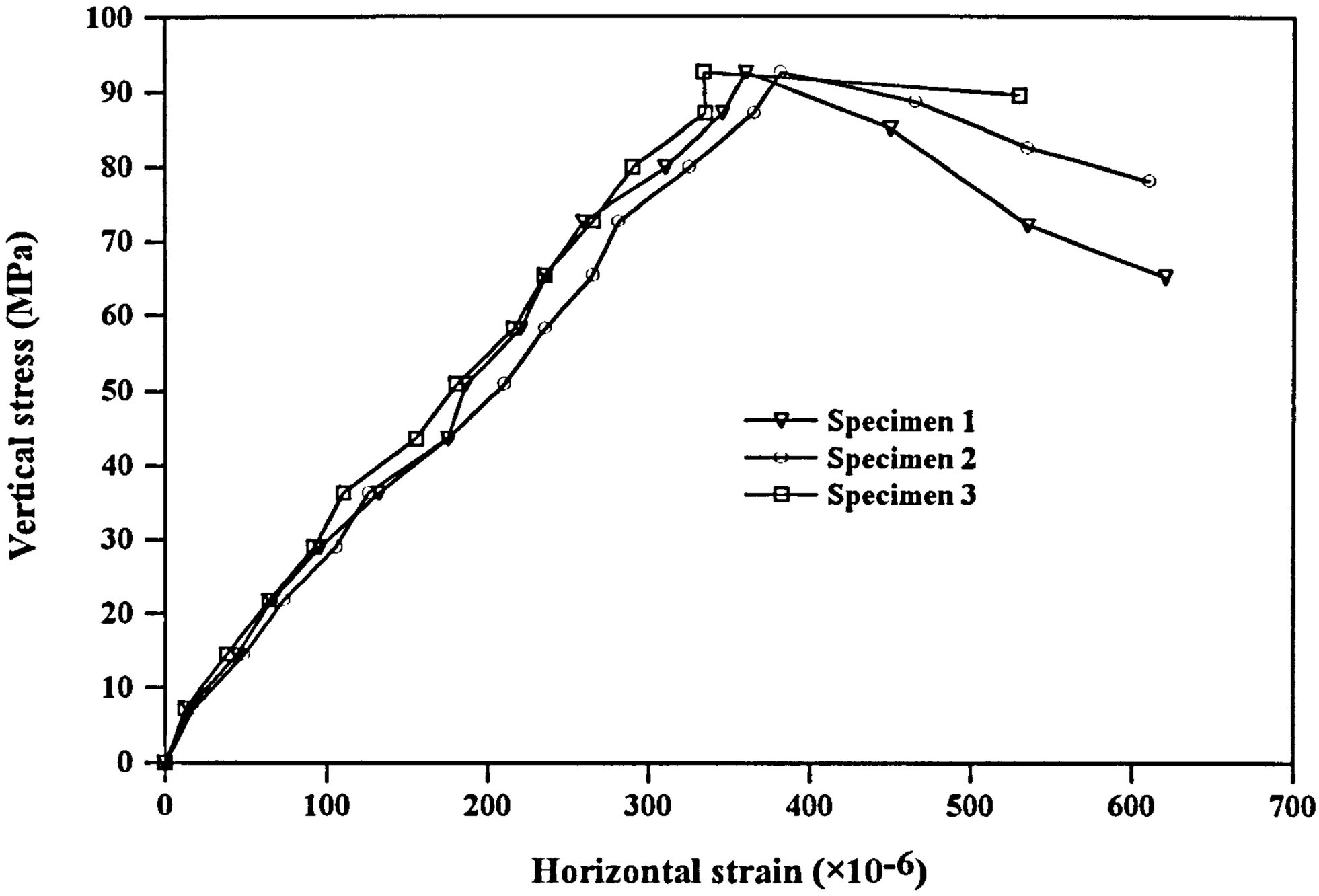

Figure 5.12 Vertical stress *versus* horizontal strain curves for brick specimens

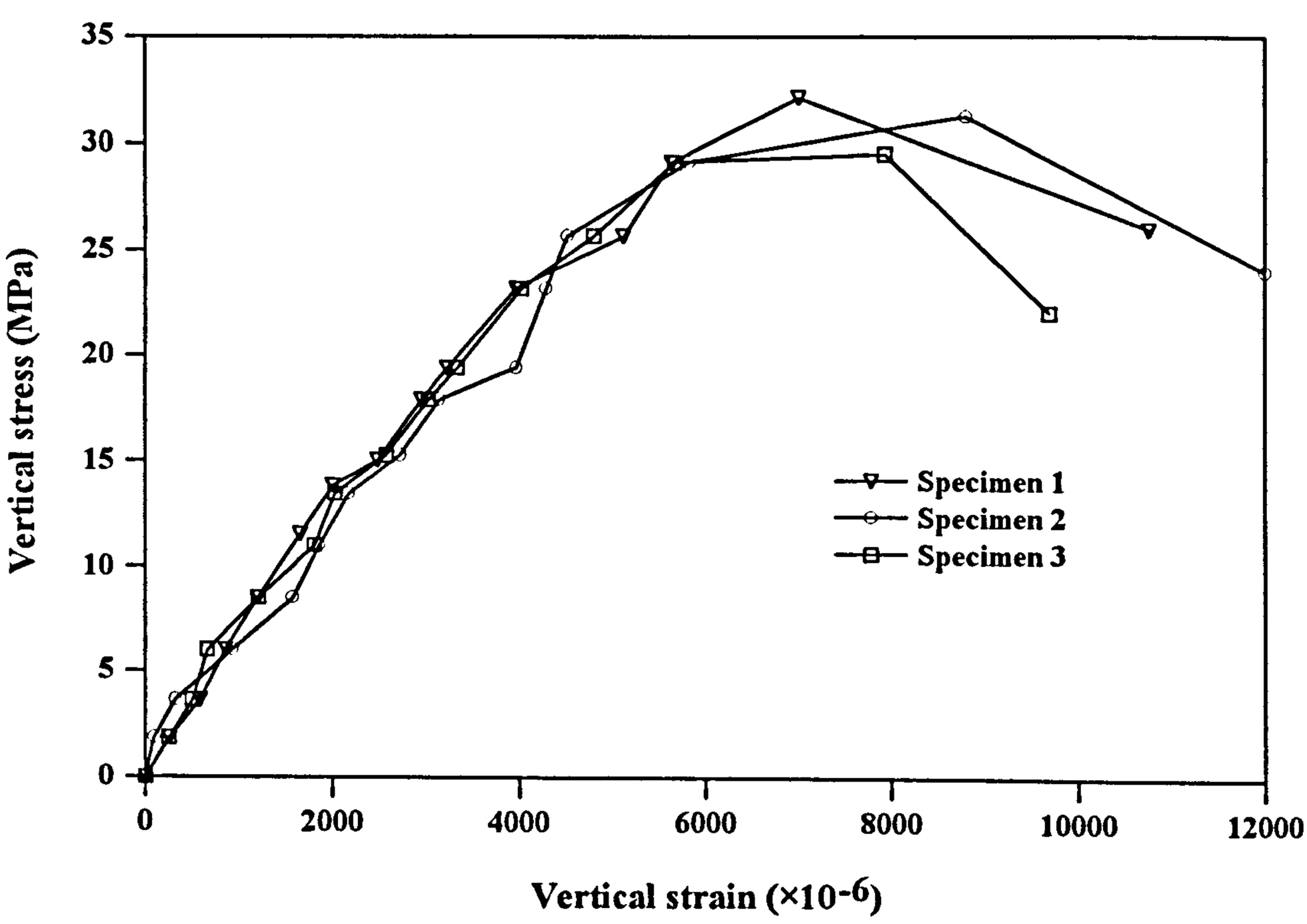

Figure 5.13 Vertical stress *versus* vertical strain curves for confined mortar joints

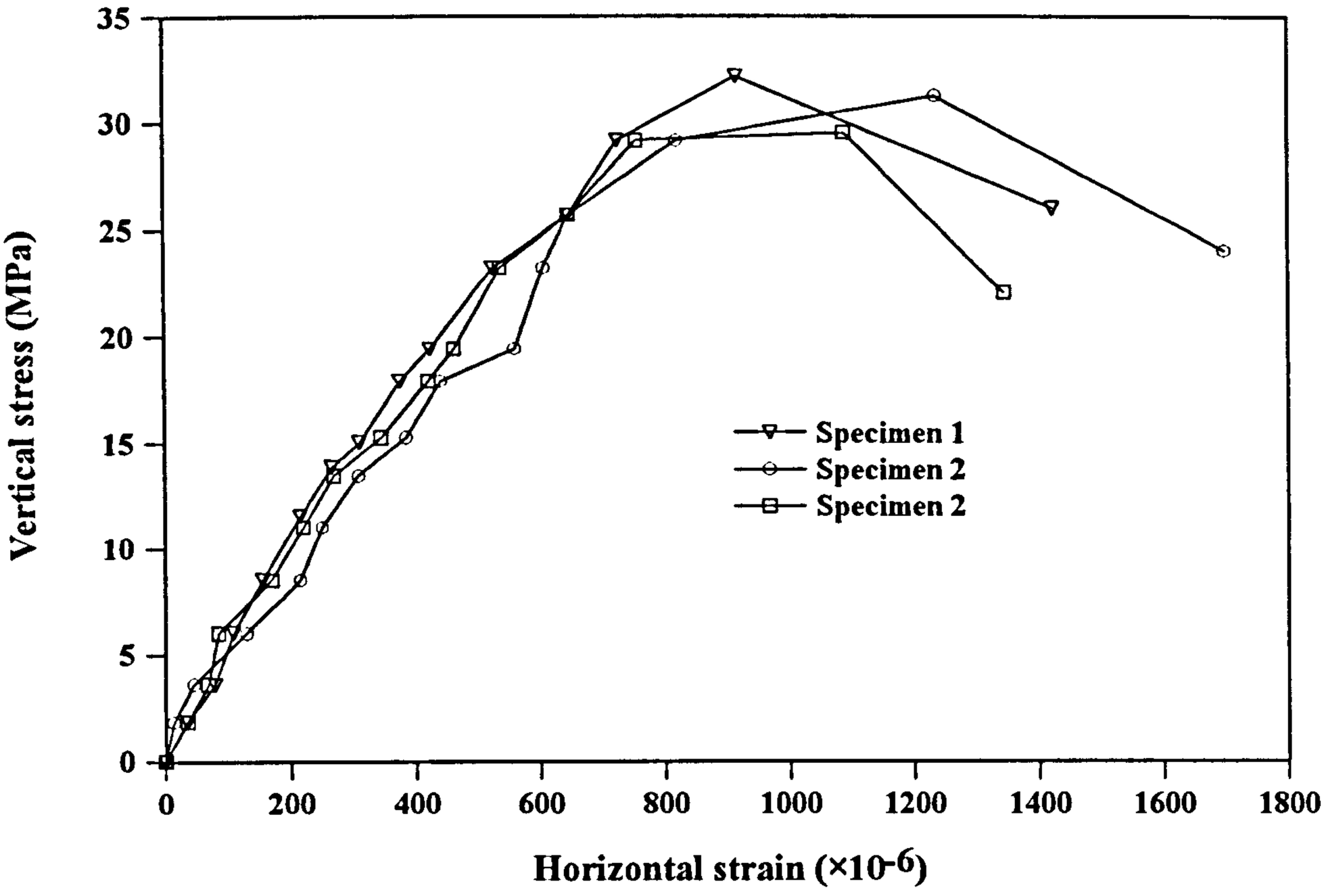

Figure 5.14 Vertical stress *versus* horizontal strain curves for confined mortar joints

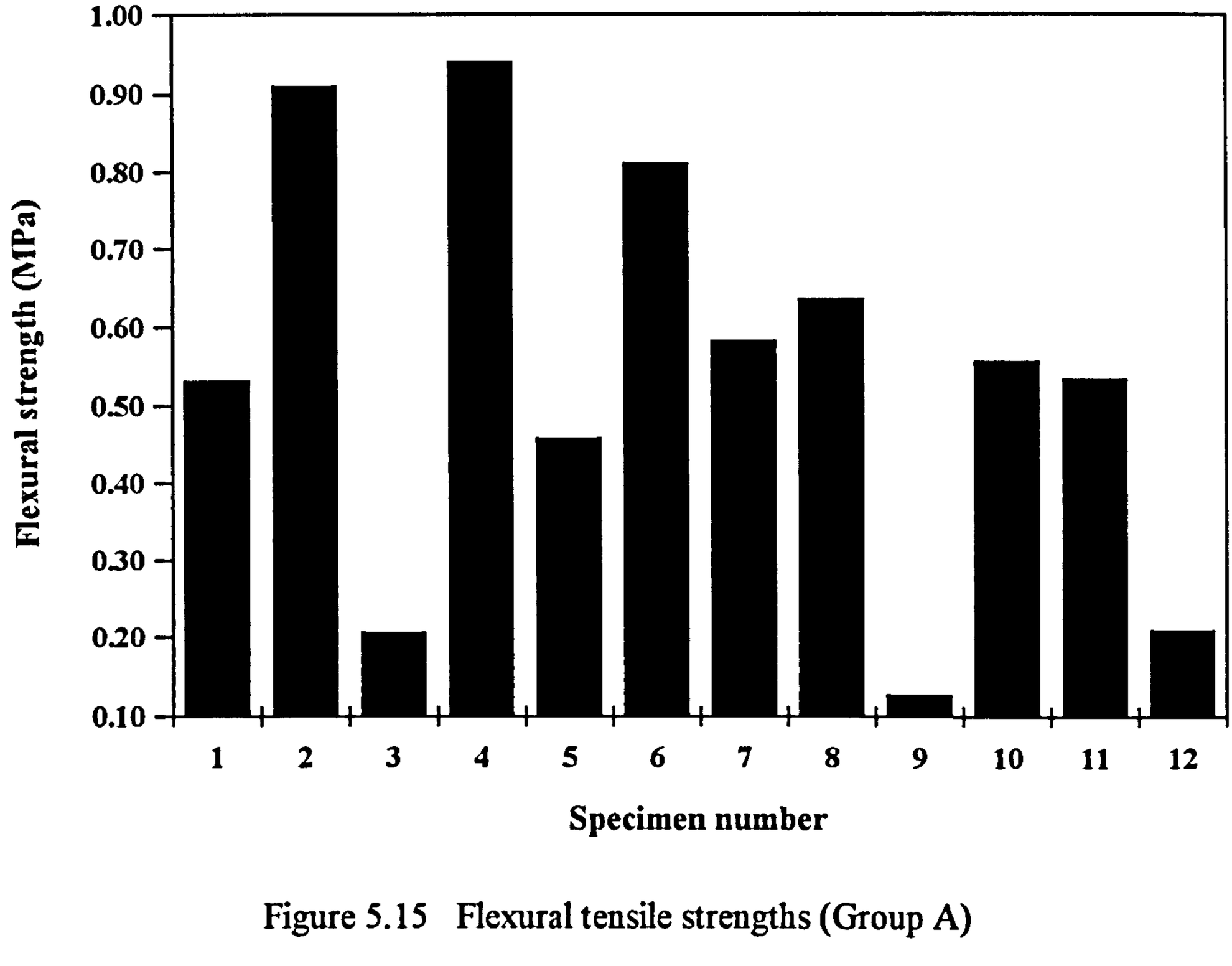

Figure 5.15 Flexural tensile strengths (Group A)

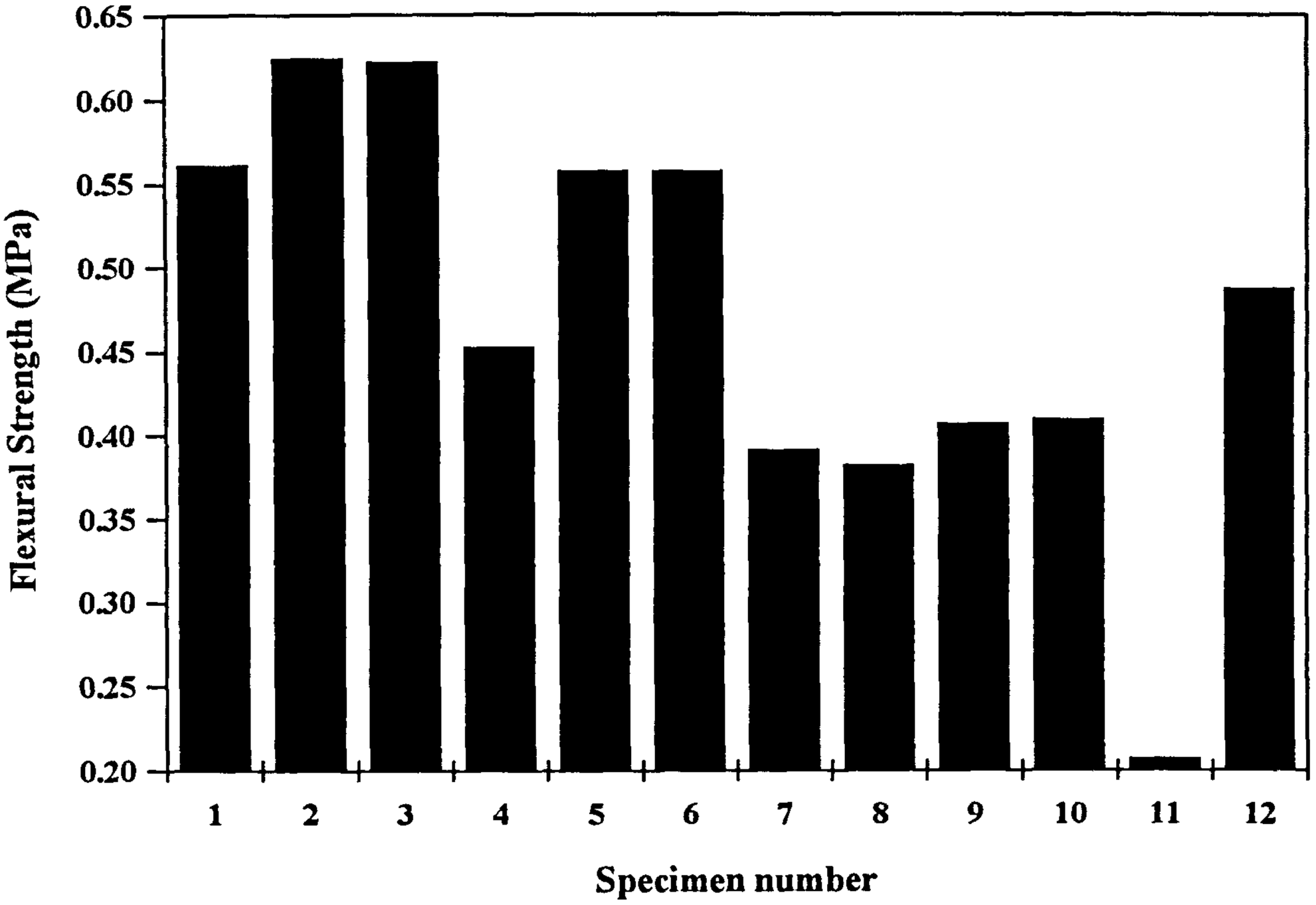

Figure 5.16 Flexural tensile strengths (Group B)

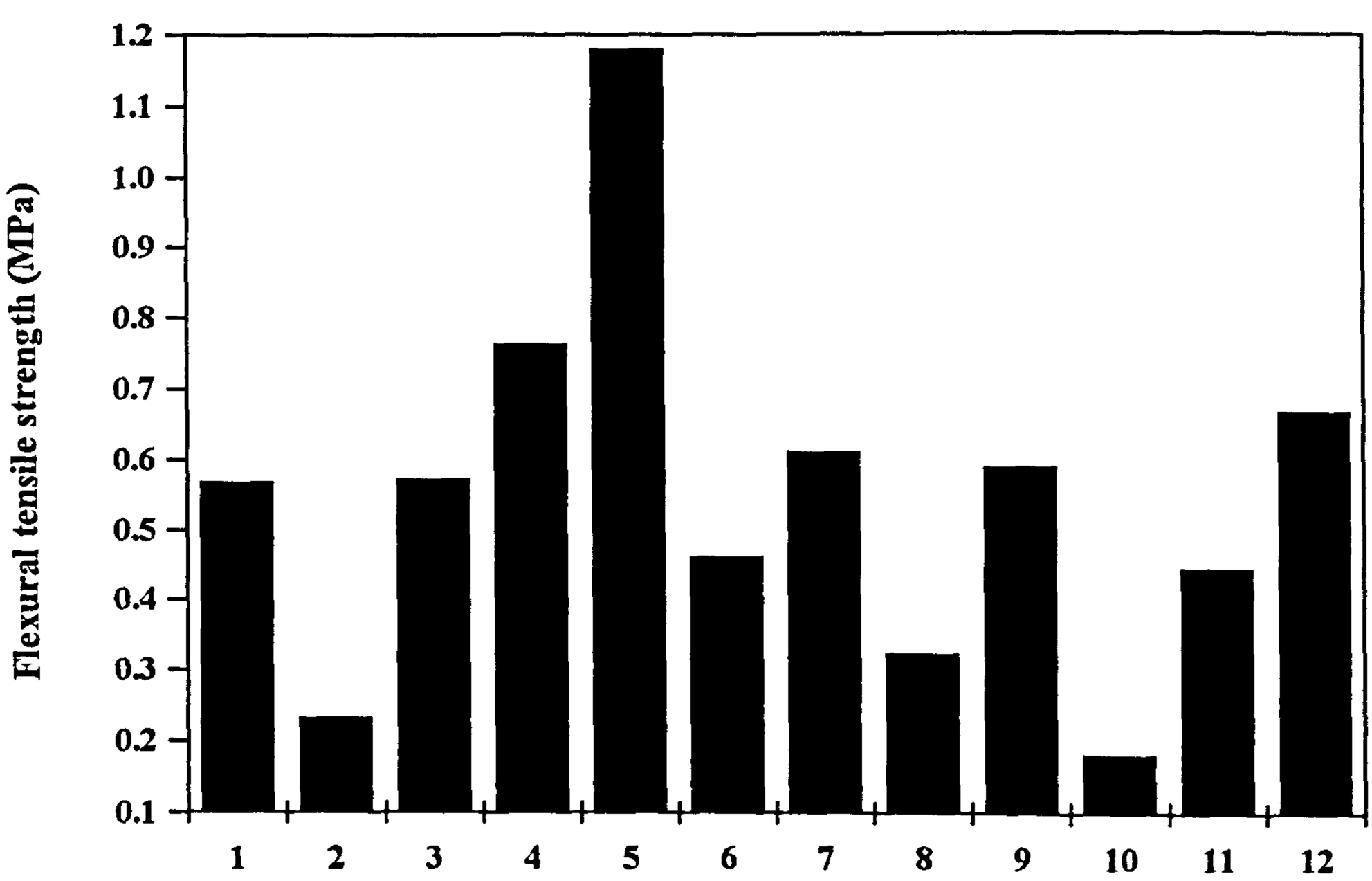

Figure 5.17 Flexural tensile strengths (Group C)

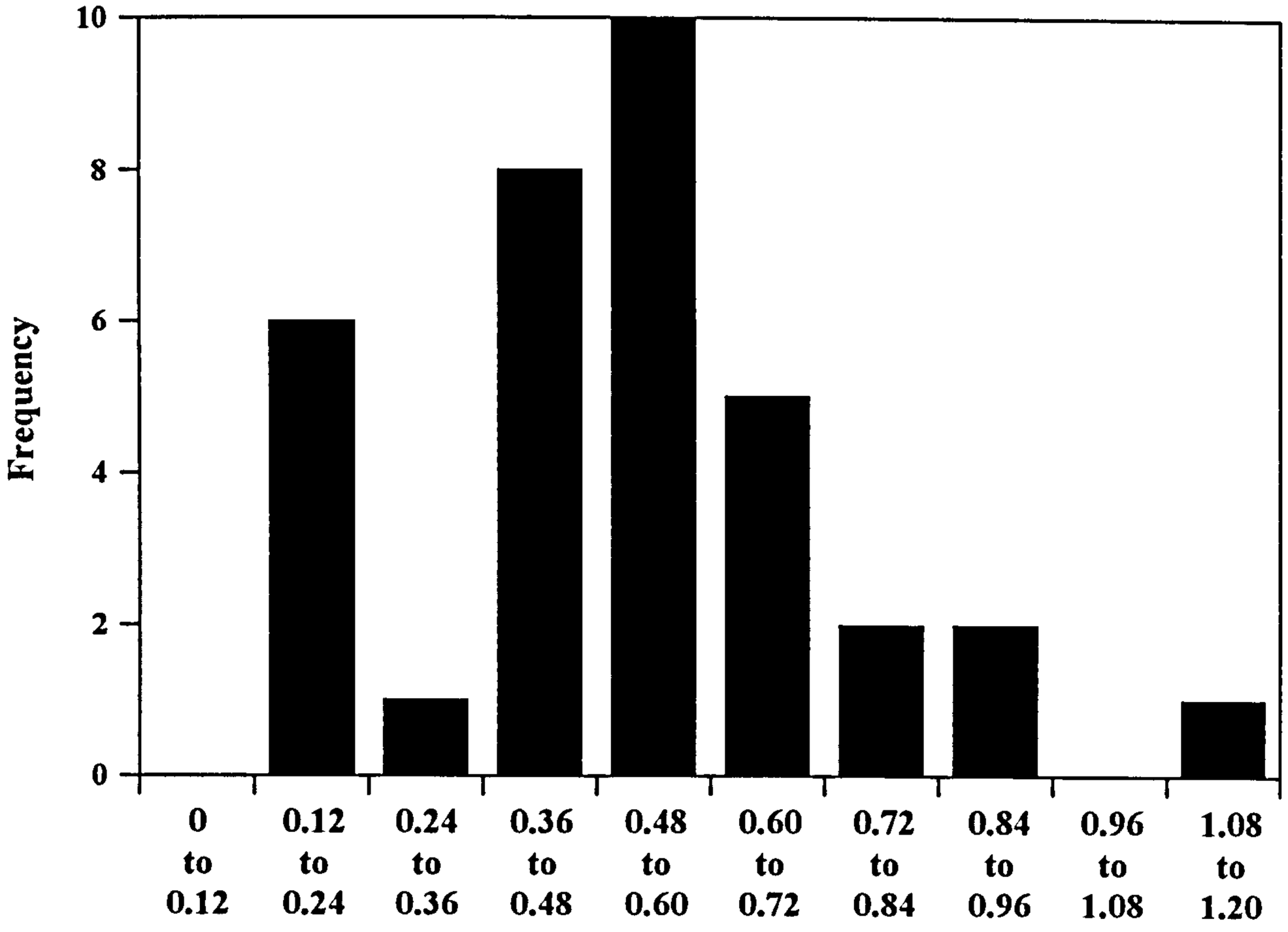

Figure 5.18 Distribution of the brickwork's flexural tensile strength

CHAPTER 6

Repeatability Tests On Large Scale Arch Bridges

6.1 Introduction

In recent years, arch bridges have been a subject of active research. Engineers have come to the view that they are underestimating the capacity of these arched structures as many vehicles with weights far beyond the allowable limit have been crossing arch bridges without causing any significant distress or damage. It is now economically important to search for a more reliable assessment which eliminates the possibility of abandoning or repairing arch bridges which are perfectly adequate.

Recently, many numerical methods have been proposed (CHOO *et al.*, 1990a; 1990b; 1991; CRISFIELD *et al.*, 1984; 1985a & b; 1988; HARVEY *et al.*, 1987; 1988a; BRIDLE *et al.*, 1989; 1990; LOO *et al.*, 1991a; 1991b; 1995) to study the behaviour of arch bridges using different approaches. With assumed material properties and idealised geometries of the arch and backfill, results predicted by these methods bear considerable resemblance to those observed in recent full scale tests. However, arch bridges are complex three dimensional structures and are subjected to a wide range of material variability and geometrical imperfections. The question has to be asked about whether nominally identical arches will have the same collapse load. This is particularly important as the geometry of an arch bridge is a dominant parameter in determining its capacity in many arch bridge assessment methods.

A pilot experimental study was carried out by the author at Napier University by building three nominally identical large scale arch bridges with a span to rise ratio of four. These were tested to collapse to investigate the repeatability of large scale tests.

Although large scale tests have been carried out by various researchers (FAIRFIELD, 1994a; ROYLES *et al.*, 1991; HARVEY *et al.*, 1989; TOWLER, 1981; PENG *et al.*, 1997a & b), repeatability tests on large scale arches have not been carried out mainly because of financial reasons. It is therefore deemed necessary to conduct a series of repeatability tests on large scale arches to give engineers an idea of the reliability of their analyses.

Before testing the first arch, analytical studies were performed to predict the behaviour of the arch up to its ultimate limit state using various arch bridge assessment methods: LUSAS FE analysis, ARCHIE, CTAP-elastic cracking method, the MEXE method and Heyman's plastic analysis. This helped examine their abilities when assessing large scale laboratory arches. With the exception of the 2-D FE analysis and SOILARCH.FOR (a mechanism based analysis coded by the author), relevant literature about these methods was presented in Chapter 2 of this thesis. It was found that the predicted results by all these analytical methods covered a significant range. This was mainly because of the many different assumptions and idealisations incorporated in each assessment method.

Results from current experimental studies were also compared with those large scale tests conducted by FAIRFIELD (1994a), who used a semicircular arch, and PENG (1997a & b), who used a flat arch with a span to rise ratio of ten. These two bridges were chosen for comparisons because of the similarity in span and arch ring thickness. Although subjected to small variations in fill depth, workmanship, platen width, and ring and fill materials, qualitative understanding of the arch behaviour with different span to rise ratios can be demonstrated.

6.2 Design and construction of the arch

Three nominally identical arch bridges with a span to rise ratio of four were built in the laboratory. The brick, backfill, mortar mix and construction method were kept

unchanged throughout the construction of these arches. The first, second and third arches were subsequently referred to as SR4-A, SR4-B and SR4-C respectively. Unless otherwise stated, the material properties, geometries and conditions of these arches were considered to be identical. A diagrammatic illustration of the arch together with its salient dimensions is shown in Figure 6.1.

6.2.1 The arch ring

All arches were circular segmental with a span of 2000mm, span to rise ratio of four and a width of 1000mm. The arch ring consisted of a single course of brickwork 102.5mm thick. Each arch ring was supported by a strong abutment at each end in such a way that a layer of mortar joint lay between the far-end voussoir and the abutment. Figure 6.2 shows a photograph of a bare arch (SR4-A), supported by timber centring and concrete piers.

6.2.2 Voussoirs

The voussoirs used for constructing the arch ring were Class B solid engineering bricks. Each arch ring consisted of 32 rows of bricks along the direction of the curve. Each arch ring was constructed in such a way that only 12 rows of voussoir were laid from each end of the arch ring leaving a space of 8 rows to be completed after three days. This measure was necessary to ensure that sufficient time was allowed for wet mortar joints to settle and harden thus preventing the formation of contraction cracks. Tests carried out in Chapter 5 of this thesis revealed that the average elastic modulus, Poisson's ratio and compressive strength of the brick were 38033MPa, 0.154 and 92MPa respectively.

6.2.3 Mortar

The mortar used for all arches was a 1:1:6 (cement: lime: sand) mix. Mortar cubes with similar mix design were cast and tested for Chapter 5 of this thesis which revealed that the average elastic modulus, Poisson's ratio and uniaxial compressive strength were 6867MPa, 0.263 and 4.90MPa respectively. For every arch built, four mortar cubes were also cast from the same batch of mortar. These mortar cubes were cured under plastic sheeting for 7 days and air dried for a further 21 days. The results of crushing tests on the mortar cubes are summarised in Table 6.1. All units of compressive strength in Table 6.1 are in MPa.

Table 6.1 Compressive strength and moisture content of mortars

Arch	7 day	28 day			Moisture content (%)
SR4 - A	8.25	8.46	8.77	9.23	24.2
SR4 - B	7.17	7.89	7.31	7.88	24.5
SR4 - C	5.89	9.57	9.38	9.51	25.6

The average compressive strength of mortars for SR4-A, SR4-B and SR4-C were 8.82MPa, 7.69MPa and 9.49MPa respectively with a small variation in moisture content. It has been concluded by LENCZNER (1966) that the water/cement ratio and subsequent workability of mortar do not affect the mortar strength. Therefore, the water/cement ratio was left to the discretion of the brick layer to produce a required workable mix.

It is always difficult to maintain a constant thickness of all mortar joints along the whole arch ring. Figures 6.3a, 6.3b, and 6.3c show the distributions of mortar joint thickness for SR4-A, SR4-B, and SR4-C respectively. It was apparent that the fluctuation of mortar thickness was severe in the transverse direction and also along the arch ring. FRANCIS *et al.*, (1971) investigated the relationship between mortar/brick-thickness ratio (φ) and brickwork prism/brick compressive strength ratio and found that the mortar thickness is influential in determining the compressive strength of the brickwork prism. A numerical example from FRANCIS *et al.*, (1971),

shows an increase in the mortar/brick-thickness ratio from 0.1 to 0.3 causes a brickwork prism/brick compressive strength ratio to increase from 0.3 to 0.5. It is beyond the scope of this study to further investigate the influence of the mortar thickness upon the combined compressive brickwork strength. However, the mortar thickness distributions indicated that the compressive strength might vary along each arch ring and therefore a range of compressive strengths was considered in the subsequent analyses. Table 6.2 gives the statistical dimensional properties of the mortar joint of each arch.

Table 6.2 Dimensions of the mortar joints

ARCH	Mean mortar thickness (mm)	Standard deviation of mortar thickness (mm)	Mean φ	Minimum φ	Maximum φ
SR4-A	14.2	3.03	0.22	0.12	0.34
SR4-B	11.3	1.40	0.17	0.11	0.23
SR4-C	12.7	1.26	0.20	0.15	0.25

6.2.4 Brick-mortar bond strength

The brick-mortar bond strength was investigated as described in Chapter 5 of this thesis. A total of twelve specimens were built during the construction of each arch using the same batch of mortar. Results revealed that the average brick-mortar bond strengths for SR4-A, SR4-B, and SR4-C were 0.542MPa, 0.471MPa, and 0.55MPa respectively. However, as shown in Table 5.1, the standard deviations and coefficients of variation for these samples were too significant and subjective judgement still has to be made when deciding the tensile strength of the arch.

6.2.5 Abutment

The arch ring was supported by two strong concrete piers (Figure 6.1). Each concrete pier had a length, height and width of 790mm, 700mm and 1000mm respectively. They

rested on a base slab of equal width, 300mm height and 1400mm width. Previous tests (PENG, 1997a) on flat arches, with a span to rise ratio of ten, supported by these two concrete piers revealed no signs of horizontal movement of the supports. The author's arches, with a span to rise ratio of four, would induce even less horizontal thrust thus supporting the assumption of rigid abutments for subsequent theoretical analyses.

6.2.6 Centring

Softwood timber 18mm thick was used for the centring. Two centring pieces were cut to the required profile and nailed to the concrete piers parallel to the spandrel walls. Smaller timber pieces, 70mm wide, cut to an appropriate angle, were fixed to the outer curved surface to give the required arch profile. To ensure all arches of identical profiles were built, the same set of centring was reused for the construction of all arches. All centring pieces were measured each time shortly before laying the voussoirs to ensure no distortions of the curved profile due to inadequate fixing or contraction of these timber pieces due to moisture evaporation had occurred.

6.2.7 Spandrel, wing and end walls

For consistency with the tests carried out by FAIRFIELD (1994a) and PENG (1997a), the spandrel, wing and end walls were made of softwood timber. The spandrel and wing walls were not structural and only served the purpose of retaining the fill. To avoid interference with the arch ring, a gap of 10mm was provided between the arch ring and the spandrel walls. Heavy duty polythene strips were lapped 100mm over the arch extrados and fixed to the inner surface of the timber spandrel wall up to a height of 100mm above the arch. The spandrel and wing walls were held in place by three steel rods running through the backfill. This was to reduce lateral deformations of the spandrels during testing. Both end walls were fixed to the end of wing walls with no extra support given to them as it was felt that both end walls were at a considerable

distance from the arch and no interference was expected from the arch deformations. Figure 6.4 shows a photograph of an arch (SR4-B) with spandrel, wing and end walls before being filled with sand.

6.2.8 Backfill

The backfill bulk unit weight and the depth of backfill over the crown were 14.86kNm^{-3} and 150mm respectively. These parameters were consistent with those used by FAIRFIELD (1994a) in his large scale semicircular arch test. The fill was placed from zero drop height in 200mm layers. The required weight of fill to achieve the required bulk unit weight for each 200mm fill layer was determined prior to backfilling. By compacting an appropriate amount of fill into each layer, a constant bulk unit weight was achieved.

A series of tests were carried out, in accordance with BS1377 (1990), to determine the fill's moisture content, apparent cohesion, angle of shearing resistance, particle size distribution and elastic modulus. The moisture contents of the fill in the tests for SR4-A, SR4-B and SR4-C were 12.6%, 12.4% and 12.0% respectively. Although a similar batch of fill was reused for each test which was covered with plastic sheeting when it was not being used, total prevention of moisture evaporation can not be guaranteed. However, given such a small magnitude of moisture variation, the fill properties should not vary significantly between tests.

A mass of 200g of the fill was oven dried and subsequently used to determine the particle size distribution by dry sieving. Results are presented in Figure 6.5 on a semi-logarithmic scale. The fill was classified as uniformly graded with a uniformity coefficient of 11.

A series of direct shear box tests was carried out to determine the apparent cohesion and angle of shearing resistance. Since the particle size was always less than 1mm and

the fill uniformly graded, a small scale (60mm × 60mm) direct shear box was used. All samples were compacted in the shear box to a bulk unit weight of 14.86kNm^{-3}. Results are presented in Figure 6.6 showing that the fill's apparent cohesion and angle of shearing resistance were 0.1kPa and 28.6 ° respectively. The apparent cohesion was therefore negligible and was taken as zero for all analyses.

The fill was then subjected to a series of triaxial tests. Each fill sample was placed in a 100mm diameter cylinder compacted to a bulk unit weight of 14.86kNm^{-3}, and tested in an undrained condition. Results are presented in Figure 6.7 which revealed that the fill's apparent cohesion and angle of shearing resistance was zero and 30.5° respectively. These results were quite close to those obtained from the direct shear box test. The stress *versus* strain relationship, with cell pressures of 100kPa, 150kPa, and 200kPa is shown in Figure 6.8. from which the average elastic modulus was found to be approximately 10MPa.

6.2.9 Loading system

A 100t capacity hydraulic jack was used to impose live loads on the arches. Two steel reaction frames were bolted to the floor aligned with the quarter span of the arch. The pair of reaction frames was held in position by a steel channel section to which the jack was attached. The imposed load from the jack was applied to the surface of backfill at the ¼-span point through a 180mm wide spreader beam covering the whole width of the arch. A calibrated load cell was placed between the jack and spreader beam to enable the imposed load to be measured. Figure 6.9 shows a photograph of the spreader beam resting on the backfill's surface with a load cell between the I-beam and the jack. To prevent foundation bearing failure under the load platen, a geotextile strip (380mm × 1000mm) was placed right under the load platen.

6.3 Instrumentation

The following sections describe the displacement transducers, datalogging system, and crack monitors, used in the author's tests. Although strain gauges were used to measure the variation of strain across the arch ring during the first arch test, it was found that the variation of strain was imperceptible. Neither the results from the strain measurements nor the relevant experimental details are discussed here.

6.3.1 Displacement measurements

Linear variable differential transducers (LVDTs), manufactured by Measurement Group UK Ltd, were used to measure arch deflections. The LVDTs were connected to a datalogging machine (the System 5000) for reading and storing the output from the LVDTs. All LVDTs were calibrated using the same datalogger over the entire travel of the transducer. Each LVDT was held in position for 30 minutes and no significant variation to the output was recorded by the datalogger.

Twelve LVDTs, eight of long (100mm) and four of short (50mm) travel type, were used in each test to measure arch deflections at positions shown in Figure 6.10. Eight long LVDTs were connected to channels 1, 2, 5, 6, 7, 8, 11, and 12; four short LVDTs to channels 3, 4, 9, and 10. The LVDTs were not mounted directly around the arch intrados. The arch deflections were measured using the LVDTs through wooden platforms attached to the arch intrados at locations to be monitored. This measure was taken so that the LVDTs were not positioned under the arch intrados rendering early removal of the LVDTs, to avoid damage, unnecessary.

Figure 6.11 shows the wooden platforms attached to the arch intrados and the positions of the LVDTs. The wooden platforms were constructed in such a way that a wooden column, approximately 150mm long, was attached to a point of interest on the intrados and a wooden slab, approximately 150mm × 150mm, was attached to the

other end of the wooden column. Each edge of the wooden column was cut to an accurate slope so that the wooden slab remained horizontal before the arch was loaded. An LVDT was positioned vertically on the slab's surface to measure arch's vertical deflections. A small piece of wooden slab was also attached vertically to the flat wooden slab and a LVDT was mounted horizontally to this vertical slab for the measurement of horizontal deflections.

The LVDTs were held in positions on a scaffold frame. This enabled easy removal of the LVDTs shortly before the onset of collapse. Despite this, the wooden platforms were still used so that deflection measurements could be made until the arch collapsed, all LVDTs were removed when the arch was deemed to be close to collapse to prevent any drastic impact between the wooden platforms and the LVDTs.

6.3.2 Crack monitors

Crack monitoring devices known as "Scratch-A-Track", manufactured by Hammond Concrete Services, were used to monitor cracks formed in the arch ring in each test. The device consists of a steel scriber and a record card attached across a mortar joint, as shown in Figure 6.12. A pair of the crack measuring devices was used to monitor one mortar joint. One of which was attached near to the extrados and the other near to the intrados. A total of four mortar joints, on each side of the arch, were fitted with crack measuring devices: one at each abutment, one at the ¼-span point, and one at the ¾-span point.

6.4 Experimental results

This section presents the experimental results from three large-scale identical arches (Figure 6.1). Loading was applied to each arch using a hand pumped hydraulic jack, as mentioned in Section 6.2.9. The magnitude of the applied load was measured by a load

cell between the hydraulic jack and the load platen. The arrangement of LVDTs for each test was identical, as shown in Figure 6.10, and the System 5000 was used to scan and record information obtained from those LVDTs.

A load increment of 0.5kNm^{-1} width, perpendicular to the arch span, was adopted followed by inspection of the arch ring for the formation of cracks. The loading system was monitored after each load increment to ensure that no tilting of the loading system had occurred. If the loading system had tilted, as happened in SR4-C, the loading system was levelled and adjusted before re-loading started.

The experimental phenomena observed during each load test are described in the following sections. As a summary of the experimental results, Table 6.3 gives the experimental collapse loads and the hinge locations for the three tests. The hinge locations are represented by their mortar numbers. Each mortar was numbered in such a way that the sequence started from the mortar joint adjacent to the left abutment (Figure 6.1) to the one next to the right abutment. There were 33 mortar joints along each arch ring. The order in which the locations of hinges are presented in Table 6.3 do not represent the order in which the hinges were formed. The load *versus* deflection curves recorded by LVDTs, position at channels 1 to 12 inclusive, are presented in Figures 6.13 to 6.24 inclusive, respectively. All downward deflections and deflections towards the right-hand abutment are positive.

Table 6.3 Experimental collapse loads and hinge locations

Arch	Collapse load (kNm^{-1} width)	Hinge location (joint number)
SR4-A	21	1, 12, 22, 33
SR4-B	16	3, 10, 21, 33
SR4-C	25	1, 9, 19, 33

6.4.1 Experimental behaviour of SR4-A

The arch was loaded to collapse at a maximum applied live load of 21kNm^{-1} width perpendicular to the arch span at the ¼-span point. The arch finally collapsed with four hinges at joint numbers 1, 12, 22, and 33. Deflections of the arch were taken at twelve channels as shown in Figure 6.10 using LVDTs and their resulting load *versus* deflection curves presented in Figures 6.13 to 6.24 inclusive.

No signs of damage to the arch were observed before application of live load. A load increment of 0.5kNm^{-1} width was applied to the surface of backfill, through a load platen of 180mm width, which was then followed by an inspection of the arch for the formation of tensile cracks in the arch ring. With an imposed load of 10kNm^{-1}, the arch vertical deflection at the ¼-span point was only 0.102mm. No signs of the formation of hinges were noticed at this load. When loaded to 17kNm^{-1} width, a foundation bearing failure occurred directly beneath the load platen but its effect was not significant as the load platen was restrained by the geotextile strip. A small soil tensile crack also occurred near the load platen. The formation of tensile cracks in the arch ring was neither obvious to the naked eye nor recorded by crack monitors at this load.

The arch showed no signs of distress at a load of 20kNm^{-1}. Referring to Figures 6.13 to 6.24 inclusive, the load *versus* deflection curves for SR4-A until this load level were approximately linear. However, a more obvious foundation settlement was noticed at this load level but no adjustment was made to the loading system as it remained in a vertical position.

When the load increased to 21kNm^{-1}, an obvious hinge was formed in the arch ring at an interface near to the ¼-span point (joint 12). This was followed by an immediate loss of arch stiffness and a rapid increase in the deflection. The load fell rapidly from 21kNm^{-1} to 16kNm^{-1} resulting in an increase in the arch vertical deflection, at the ¼-span point, from 0.752mm to 10.097mm. Such a significant arch deflection caused the formation of another three hinges in the arch ring at joints 1, 22, and 33. Further

application of live loads accompanied by a rapid increase in the arch deflection meant that no loads higher than the previous maximum could be applied to the arch. A large tensile crack was observed on the surface of backfill at about the ¾-span point remote from the load as shown in Figure 6.25. This was caused by large rotation of three arch segments about the four hinges in the arch ring.

With the load reduced to 13.3kNm^{-1}, collapse of the arch was deemed imminent and all LVDTs were removed to avoid damage. On re-loading, the arch deflection increased further and the arch finally collapsed in a mechanism. No signs of compressive failure of the arch material were noticed throughout the whole loading regime.

6.4.2 Experimental behaviour of SR4-B

The arch was loaded to collapse at a maximum applied live load of 16kNm^{-1} width perpendicular to the arch span at the ¼-span point. The arch finally collapsed with four hinges (joints 3, 10, 21, and 33) in the arch ring. Figure 6.26 shows one arch (SR4-B) shortly before collapse. Figures 6.13 to 6.24 inclusive show the load *versus* deflection curves recorded by LVDTs positioned at the twelve channels as shown in Figure 6.10.

The arch was intact before the application of live load. As for the first arch (SR4-A), a load increment of 0.5kNm^{-1} width was applied through a 180mm wide load platen located on the backfill's surface at the ¼-span point. The live load was applied to the arch incrementally followed by visual inspection for the formation of tensile cracks or hinges in the arch ring after each load increment. When loaded to 9kNm^{-1}, settlement at the load platen was noted. No adjustment to the loading system was made as it remained perpendicular to the surface of backfill. Careful inspection of the arch revealed no cracks had formed in the arch ring at this load.

When the arch was loaded to 16kNm^{-1}, an apparent hinge was formed in the arch ring somewhere near the ¼-span point (joint 10). The applied load quickly dropped from

16kNm^{-1} to 14.5kNm^{-1} resulting in an increase in the arch vertical deflection, at the ¼-span point, from 0.709mm to 5.03mm. When the load was being decreased, due to the arch deflection, three more hinges were formed in the arch ring (joints 3, 21, and 33). All LVDTs were then removed as previous test (SR4-A) revealed that the arch was not far from total collapse after the load was decreased from its maximum to 13kNm^{-1}.

On re-loading, no loads higher than 16kNm^{-1} could be applied to the arch. The arch's deflection increased substantially resulting in a large tensile crack on the surface of backfill at about the ¾-span point remote from the load. The arch finally collapsed in a mechanism with no signs of material compressive failure.

6.4.3 Experimental behaviour of SR4-C

The arch was loaded to collapse at a maximum applied live load of 25kNm^{-1} width perpendicular to the span at the ¼-span point. The arch finally collapsed with four hinges in the arch ring at joints 1, 9, 19, and 33. Twelve LVDTs were used to record arch deflections at various positions as shown in Figure 6.10 and the resulting load *versus* deflection curves are presented in Figures 6.13 to 6.24 inclusive.

No signs of damage to any part of the structure were noticed before the application of live loads. As in the case of the two previously tested arches (SR4-A and SR4-B), a load increment of 0.5kNm^{-1} was applied to the arch through a load platen of 180mm width, covering the full transverse width of the span, positioned at the ¼-span point. No obvious signs of distress to the whole structure were observed until the live load reached 12kNm^{-1} at which a settlement of the load platen occurred. However, no hinges or cracks were observed in the arch ring. Since the loading system was still in its original alignment no adjustment to the load platen was made and further live loads were applied to the arch with careful attention being paid to the orientation of the load platen.

At a load of 18kNm^{-1}, the load platen tilted slightly as its base moved towards the crown. However, further loads were still being applied to the arch. When loaded to 20kNm^{-1}, the tilting of the load platen was significant and any further increase in live load would have caused it to become unstable. The applied load was removed and the whole loading system re-adjusted and the surface of backfill, on which the load platen was placed, re-levelled. On re-loading, an increment of 5kNm^{-1} was used until the load reached its previous maximum of 20kNm^{-1}. The load *versus* deflection results show that the arch did not fully recover its original shape before re-loading. At a live load of 20kNm^{-1} after the re-loading, the arch vertical deflection at the ¼-span point was 0.324mm which was higher than 0.316mm recorded at the same load before adjustment of the loading system was carried out.

After the load was increased to 20kNm^{-1}, the load increment was restored to its previous value of 0.5kNm^{-1}. When loaded to 24kNm^{-1}, once again, the loading system was adjusted due to tilting of the load platen. As before, the hydraulic jack was fully relaxed and the whole loading system adjusted. The arch was then re-loaded with a load increment of 5kNm^{-1} until it reached its previous maximum at 24kNm^{-1}. Following load increments were reduced to 0.5kNm^{-1}.

When the live load reached 25kNm^{-1}, the first hinge formed at joint 9, near the ¼-span point. As happened previously for SR4-A and SR4-B, the arch lost most of its stiffness immediately after the formation of the first hinge. The formation of three more hinges at joints 1, 19, and 33 occurred soon after the first one. Further application of live loads, albeit not enough to exceed the previous maximum of 25kNm^{-1}, substantially increased the arch deflection. An obvious tensile crack was formed on the surface of backfill at about the ¾-span point remote from the loaded point. With the applied live load being reduced to 9kNm^{-1}, the arch vertical deflection at the ¼-span was 37.297mm. All LVDTs were then removed as a complete collapse of the arch was deemed imminent. Further increases in the deflection caused the arch to collapse in a mechanism. Material compressive failure was not noticed over the whole loading period.

6.5 Analytical studies on the tested arches

This section presents the predictions obtained from various arch bridge assessment tools as described in the following sections.

6.5.1 Analytical methods

As mentioned in Section 6.1, six assessment methods were used in this study and they were, ARCHIE, CTAP-elastic cracking, the MEXE, SOILARCH.FOR, Heyman's plastic analysis and 2-D non-linear finite element methods. For the sake of completeness, the principles inherent in each method are briefly discussed in the following sections. In addition to the arch geometry, any additional input variables required by any assessment method are given in their respective sections.

6.5.1.1 ARCHIE

ARCHIE (SMITH, 1991a) is a computer program based on the mechanism method. The thrustline for a given applied load acting on an arch is calculated. By specifying the compressive yield strength of the arch, the zone of thrust is obtained by dividing the thrust by the yield strength. Minimum arch thickness can then be defined based on this zone of thrust. It considers most of the soil-arch interactions such as load distribution and lateral soil resistance. The mobilisation of backfill passive resistance and the arch compressive strength were assumed to be 80% of the full Rankine value and 30MPa respectively. Parametric studies were carried out to investigate the influence of the backfill passive pressure on the prediction of arch collapse load.

6.5.1.2 CTAP - elastic cracking method

CTAP (BRIDLE *et al.*, 1989; 1990) is a computer program based on Castigliano's strain energy principles. The principle of this program is to ignore tensile zones in the arch ring which appear due to cracking. A hinge is defined at a particular section where the tensile zone covers almost the whole section. Compared with the mechanism method, this method has extra options to allow the user to vary the arch elastic modulus, thereby monitoring or controlling the stresses and modulus of subgrade reaction. The live load dispersal angle, the mobilisation of backfill active and passive resistance, and the arch elastic modulus were assumed to be 45°, 80% of the full Rankine value and 8000MPa respectively. The influence of the live load dispersal angle and the backfill passive pressure coefficient were investigated in a series of parametric studies.

6.5.1.3 The MEXE method

This method was derived by the Military Engineering Experimental Establishment based on the work done by PIPPARD *et al.* (1938, 1941, 1948 & 1951) and is currently recommended by the Department of Transport (BD21/97, 1997a) for the assessment of arch bridges. An empirical equation is used to calculate the provisional axle load involving only the span, ring thickness and the depth of fill at the crown. The provisional axle load is then modified by various modification factors for span to rise ratios other than four, material factors for fill, joints and arch ring, factors for depth and thickness of mortar, and the condition factor for the overall condition of the arch. The product of the provisional axle load and all these modification factors gives the allowable double axle load which is then converted to an allowable single axle load based on the span of the arch. The span to rise ratio factor, profile factor, material factor, joint factor and condition factor were 1.000, 0.898, 0.822, 0.770 and 0.600 respectively. A low value of condition factor was used to account for the absence of structural spandrel walls.

6.5.1.4 SOILARCH.FOR

SOILARCH.FOR is a computer program coded by the authors (NG *et al.*, 1998) based on the mechanism method. This method considers a wide range of options such as the backfill lateral active and passive resistance, width of load platen, weight of backfill and voussoirs, and also the live load distribution. The live load dispersal angle, the mobilisation of backfill active and passive resistance were assumed to be 45° and 80% of the full Rankine value respectively. Parametric studies were carried out for the live load dispersal angle and the backfill passive pressure mobilisation.

6.5.1.5 Heyman's plastic method

The prediction of the arch collapse load by this method is made using an equation which was derived based on the simplified mechanism method (HEYMAN, 1982). The backfill was treated as a series of vertical loads. Neither the backfill lateral resistance nor the live load distribution was considered in this method. The arch was divided equally into four large segments and the thrustline was supposed to touch the intrados or the extrados of the arch at each section. Furthermore, the arch and backfill bulk unit weights were assumed to be identical. Apart from the arch geometry, a combined bulk unit weight was required. In this analysis, the material bulk unit weight was assumed to be 15kNm^{-3}. This was slightly higher than the backfill bulk unit weight of 14.86kNm^{-3} but lower than the arch's bulk unit weight of 21kNm^{-3} since the volume of the backfill was comparatively large compared with that of the arch.

6.5.1.6 2-D FE analysis

Eight-noded quadrilateral elements in conjunction with nine Gauss quadrature points were used to model the arch and the backfill. The analysis was performed using commercially available software (LUSAS Version 11_46). A total of 96 elements were

used for the arch ring, 128 for the backfill, and 32 for the interface. The concrete model was used to govern failure of the arch material. Figure 6.27 shows the failure envelope for the biaxial concrete model. This model was justified, although being unable to consider material failure when subjected to biaxial compression, because no compressive failure of the arch material was noticed. LOO (1995) revealed that the arch collapse load was insensitive to the variation of arch compressive strength from his FE analyses which considered failures in both biaxial compression and tension. The strain softening model used in the current concrete model is depicted in Figure 6.28. A thin layer interface element was incorporated in between the arch ring and backfill enabling more flexible movement between these two components of the structure. The behaviour of the backfill and interface elements was elasto-plastic with failure defined by Mohr-Coulomb yield criterion. All elements were assumed to be in a plane stress condition. Results revealed that the predictions were not significantly affected by using different conditions; plane strain or plane stress.

Table 6.4 Benchmark input variables for the FE analyses

Property	Arch	Backfill
Elastic modulus (MPa)	8000	15
Poisson's ratio	0.2	0.4
Bulk unit weight kNm^{-3}	21	14.86
Compressive strength (MPa)	30	N/A
Tensile strength (MPa)	0.3	N/A
Strain softening factor	8	N/A
Angle of shearing resistance (Degrees)	N/A	30.5

Table 6.4 gives the material properties used as benchmark values in the FE analyses. A series of parametric studies was performed by varying the arch compressive and tensile strengths, arch elastic modulus, tension softening factor, backfill elastic modulus, and live load dispersal angle. Analyses were also carried out ignoring interface elements and assigning a plane strain condition to the backfill.

6.5.2 Results

This section presents the analytical results predicted by those assessment tools mentioned in Sections 6.5.1.1 to 6.5.1.6 inclusive. Figure 6.29 shows the results from the parametric studies on the backfill passive pressure mobilisation by ARCHIE, CTAP, and SOILARCH.FOR. Results for the parametric study on the live load dispersal angle by CTAP and SOILARCH.FOR are presented in Figure 6.30. All results by other assessment methods are presented in their respective sections.

6.5.2.1 ARCHIE

The backfill passive pressure mobilisation was varied in a parametric study and results presented in Figure 6.29. By increasing the mobilisation of backfill passive resistance from 10% to 100%, the predicted arch collapse load increased from 11kNm^{-1} to 17.4kNm^{-1}. Such an increase was approximately linear. As can be seen from Figure 6.29, the arch collapse loads predicted by ARCHIE were lower than those by SOILARCH.FOR and CTAP. The live load dispersal angle was not allowed to be varied in this method and therefore it was not included in the parametric study.

6.5.2.2 CTAP

The backfill passive pressure mobilisation and the live load dispersal angle were varied in the parametric studies and results presented in Figures 6.29 and 6.30. By increasing the mobilisation of backfill passive resistance from 10% to 100%, CTAP predicted an increase in the arch collapse load from 13.62kNm^{-1} to 19.12kNm^{-1}. The predicted collapse loads were higher than those predicted by ARCHIE. However, its predictions are only higher than those by SOILARCH.FOR for mobilisation of backfill passive resistance within the range 10% to 70%.

The live load dispersal angle was increased from 10° to 60° resulting in an increase in the collapse load from 10.31kNm^{-1} to 36kNm^{-1}. Such an increase was approximately quadratic. CTAP's predictions were lower than those by SOILARCH.FOR for dispersal angles from 10° to 45° and higher for dispersal angles from 50° to 60°.

6.5.2.3 MEXE

The allowable single axle load predicted by the MEXE method was 18.98kNm^{-1}. This figure lay between the maximum and minimum arch collapse loads from the experiments. However, it must be emphasised that MEXE only gives allowable axle loads, not the predicted collapse load. If a factor of safety of 3.4 is applied, as recommended by the Department of Transport (BA16/97, 1997b), then the predicted arch collapse load would be 64.55kNm^{-1}. Although the derivation of the MEXE method was conservative as it ignored lateral soil forces and used limited load distribution, the MEXE method still predicted a load above the actual arch collapse loads. The MEXE method was derived particularly for full scale arches and might not be applicable to these laboratory arches with small spans and without structural spandrel walls. However, if a large value of load partial factor of safety is used, the MEXE method can give a conservative result.

6.5.2.4 SOILARCH.FOR

Parametric studies were carried out by varying the backfill passive pressure coefficient and the live load dispersal angle; results are presented in Figures 6.29 and 6.30 respectively. By increasing the mobilisation of backfill passive resistance from 10% to 100%, SOILARCH.FOR predicted an increase in the collapse load from 12.76kNm^{-1} to 23.23kNm^{-1}. Similarly, increasing the load dispersal angle from 10° to 60° increased the collapse load from 12.80kNm^{-1} to 22.31kNm^{-1}. However, the maximum arch collapse load from these parametric studies was still below the maximum experimental

collapse load of 25kNm^{-1}. This might be because the mechanism method ignores the contribution of tensile strength and yields a lower arch collapse load.

6.5.2.5 Heyman's plastic method

Heyman's plastic method predicted a collapse load of just 10.13kNm^{-1}. This is far below the experimental collapse loads. The neglect of arch tensile strength, live load distribution, and the contribution of backfill lateral resistance rendered the prediction conservative.

6.5.2.6 2-D FE analysis

Figure 6.31 shows the predicted collapse mode by 2-D FE model with a predicted collapse load of 26kNm^{-1} using the benchmark input variables given in Table 6.4. No load *versus* deflection results are presented from this analysis as they were found to be even more brittle than those recorded in the experiments. The arch deflections given by this FE analyses were due to the bending of the arch rendering them comparatively small. In reality, a large arch deflection is possible due to the rotation of arch segments about hinges formed in the arch ring. The failure of the arch in the current FE analysis was defined by full propagation of a crack along a section in the arch. Table 6.5 gives the results of the parametric studies. Only one variable was varied in each parametric study and the other input variables were kept constant as given in Table 6.4.

The FE prediction of the arch collapse load without interface elements was found to be 25kNm^{-1} which was only 1kNm^{-1} lower than that with interface elements. A more rigid connection between the arch and the backfill might have concentrated the stress over the loaded area resulting in a lower collapse load. A similar prediction of the arch collapse load was found by assuming the backfill was in a condition of plane strain. The arch was assumed to be under plane stress conditions in all parametric studies

since the concrete model used in this study was incompatible with plane strain conditions. It made little difference assigning a plane strain condition to the arch as its Poisson's ratio, as used in the FE analysis, was only 0.2.

Table 6.5 Results of the FE parametric studies

Arch tensile strength (MPa)	Collapse load (kNm^{-1})	Arch compressive strength (MPa)	Collapse load (kNm^{-1})
0.1	18	10	26
0.2	21	20	26
0.3	26	30	26
0.4	31	40	26
0.5	35	80	26
0.6	39	1×10^6	26
Tension softening factor	Collapse load (kNm^{-1})	Arch elastic modulus (MPa)	Collapse load (kNm^{-1})
5	24	6000	26
8	26	7000	26
15	29	8000	26
20	31	9000	26
Live load dispersal angle (Degrees)	Collapse load (kNm^{-1})	Backfill elastic modulus	Collapse load (kNm^{-1})
27	23	10	25
35	24	15	26
45	26	20	26
60	26	25	26

6.5.3 Discussion of the experimental and analytical results

This section presents discussion of both the experimental results and those predicted by ARCHIE, CTAP, MEXE, SOILARCH.FOR, Heyman's plastic method and 2-D FE analyses. The experimental and analytical results are discussed in the following separate sections.

6.5.3.1 Discussion of the experimental results

The main finding of this study was that nominally identical arches may yield a significantly different collapse load. The collapse loads for SR4-A, SR4-B, and SR4-C were 21kNm^{-1}, 16kNm^{-1}, and 25kNm^{-1} respectively. Such a significant discrepancy in the collapse load was believed to be due to the variation of arch tensile strength as it was the only property of the whole structure that was most unlikely to be kept uniform for the three arches. As presented in Chapter 5 of this thesis, the brick-mortar bond strength was found to be between 0.13MPa and 1.18MPa with a mean, standard deviation, and coefficient of variation of 0.52MPa, 0.22MPa, and 42.97% respectively. Such a high coefficient of variation rose concerns as to whether the mean brick-mortar bond strength should be used to represent the arch tensile strength. A more sensible question would be; what was the arch tensile strength at the region under the loaded point? If the arch tensile strength at a brick-mortar interface where the first hinge occurred was low, the arch could yield a much lower collapse load. However, this is only true when the arch tensile strength dominates the behaviour of the arch as was the case for those arches tested in this study.

Referring to Figures 6.13 to 6.24 inclusive, it could be seen that the load *versus* deflection relationships for those arches were brittle. Each arch lost much of its stiffness immediately after formation of the first hinge. The maximum applied live load was that to cause formation of the first hinge. The failure of these arches was due to material failure (tensile failure) although they finally collapsed in the form of a mechanism.

Any arch bridge assessment method which ignores the contribution of arch tensile strength would underestimate the capacity of these arches. The mechanism method was deemed to be inappropriate in this case, apart from ignoring the arch tensile strength, since the maximum applied load on each arch did not occur with the formation of a mechanism but it was the load needed to overcome the tensile strength at the first hinge. The 2-D FE concrete model would be more realistic in this case since

it simulates the propagation of cracks in the arch ring and failure of the arch is defined by tensile failure of the arch material.

6.5.3.2 Discussion of the analytical results

ARCHIE, CTAP, SOILARCH.FOR, and Heyman's plastic method are likely to underestimate the arch collapse load in this study since arch tensile strength is excluded in these methods. However, with the exception of Heyman's plastic method, the prediction of arch collapse load by these methods could be arbitrarily increased by increasing the mobilisation of backfill passive resistance. By increasing the mobilisation of backfill passive resistance from 10% to 100%, ARCHIE, CTAP, and SOILARCH.FOR predicted an increase in the arch collapse load from 11kNm^{-1} to 17.4kNm^{-1}, 13.62kNm^{-1} to 19.12kNm^{-1}, and 12.76kNm^{-1} to 23.23kNm^{-1} respectively. However, the use of a high percentage of backfill passive resistance is unjustifiable, other than to indirectly compensate for the neglect of arch tensile strength, since each arch achieved its maximum applied live load with only a small arch deflection at which the backfill passive resistance mobilised would be slightly higher than that in the at-rest state.

As expected, Heyman's plastic method predicted a collapse load of 10.13kNm^{-1} which lay far below the experimental collapse loads. However, Heyman's plastic method might not always be conservative as it assumes that the arch has an infinite compressive strength and elastic modulus. The influence of the arch deflection has been shown to significantly affect the mechanism prediction of the arch collapse load in Chapter 8 of this thesis.

The MEXE method, albeit claimed as conservative by ignoring the backfill lateral resistance and considering a limited live load distribution, actually predicted a reasonable allowable single axle load of 18.98kNm^{-1}. The author is unaware of the range over which the arch geometry was considered in the derivation of the MEXE

method. It might not be suitable for assessing the current arches with their 2m span. No further comment on the MEXE method could be made as the provisional axle load and all the modification factors are purely empirical and might be subjected to subjective manipulations by those who derived it.

Among all the input variables used in the parametric studies by the 2-D FE method, the arch tensile strength and the tension softening factor were the most influential. The arch compressive strength, arch and backfill elastic moduli, and live load dispersal angle were insignificant over the range of each parametric study. By increasing the arch tensile strength from 0.1MPa to 0.6MPa, the FE method predicted an increase in the arch collapse load from 18kNm^{-1} to 39kNm^{-1}. Increasing the tension softening factor from 5 to 20 resulted in an increase in predicted collapse load from 24kNm^{-1} to 31kNm^{-1}. It was expected that the arch tensile strength and its inherent tension softening factor were likely to have a great influence in the prediction of the arch collapse load since collapse in the FE analysis was defined by tensile failure of the arch. The predicted arch collapse load using the benchmark input variables given in Table 6.4 was 26kNm^{-1}. This prediction was still higher than all the experimental collapse loads even with a low arch tensile strength of 0.3MPa. However, if an arch tensile strength of 0.5MPa (approximately the mean brick-mortar bond strength obtained in Chapter 5 of this thesis) was used, the predicted arch collapse load would be much higher at 35kNm^{-1}. For this study, the arch tensile strength was recommended to lie between 0.2MPa to 0.3MPa and the tension softening factor between 5 to 8 for a reasonable prediction of the arch collapse load.

6.6 Comparison with other large scale arch bridge tests

Table 6.6 gives the details of the geometry, material properties and the experimental arch collapse loads from the author, FAIRFIELD (1994a), and PENG (1997a). From Table 6.6, it could be seen that the arch with a span to rise ratio of ten achieved the highest collapse load at 45.5kNm^{-1}. The semicircular arch yielded a maximum load at

21kNm^{-1} which was reasonably close to those collapse loads found by the author. Although Peng's flat arch was built with solid Engineering Class A bricks which were most likely to have a higher compressive strength, the high collapse load was deemed to be insignificantly affected by the compressive strength but was largely due to a flatter profile of the arch which induced a greater compressive zone in the arch ring. This resulted in a greater load needed to deform the arch in order to develop tensile zones to form a mechanism. Besides, the flat arch was backfilled to a greater depth, resulting in a greater load distribution, which enhanced the arch capacity.

It must be noted that the MEXE method recommended by the Department of Transport (BD21/97, 1997a; BA16/97, 1997b), albeit not considering arches with span to rise ratios greater than eight, imposes a lower span/rise factor for arches with span to rise ratios greater than four. This was because the method was derived based on a limiting compressive stress allowed to develop in the arch ring. Undoubtedly, a flat arch would be subjected to a greater compressive stress than a deep arch for a given live load. However, using the limiting compressive stress as a criterion to assess arch bridges might be totally unacceptable unless the compressive failure of the arch material dominates the collapse mechanism of the arch. Confined to this comparison only, the arch's capacity increases with the span to rise ratio.

Table 6.6 Properties of different arches and their collapse loads

Property	Author	FAIRFIELD	PENG
Span (mm)	2000	2000	2000
Rise (mm)	500	1000	200
Ring thickness (mm)	102.5	102.5	102.5
Depth of backfill (mm)	150	150	229
Backfill bulk unit weight (kNm^{-3})	14.86	14.86	15.20
Loaded point	1/4-span point	1/3-span point	1/4-span point
Platen width (mm)	180	180	150
Voussoir type	Class B Engineering bricks	Class B Engineering bricks	Class A Engineering bricks
Mortar mix (cement: lime: sand)	1: 1: 6	1: 1: 6	1: 2: 9
Collapse load (kNm^{-1})	21, 16, and 25	21	45.5

6.7 Conclusions

1 Three nominally identical arches, SR4-A, SR4-B, and SR4-C, yielded significantly different collapse loads of 21kNm^{-1}, 16kNm^{-1}, and 25kNm^{-1} respectively.

2 The load *versus* deflection relationships for all arches tested in this study were brittle. This was due to a sudden release of tensile energy at brick-mortar interfaces where hinges were formed.

3 The maximum applied live load required to overcome the tensile strength at the first hinge in each arch was higher than that required to form a mechanism.

4 Each arch lost its stiffness immediately after formation of the first hinge.

5 No compressive failure of the arch material was noticed in each test over the whole loading regime.

6 Using an arbitrarily high mobilisation of backfill passive resistance, ARCHIE, CTAP, and SOILARCH.FOR predicted a reasonable arch collapse load for these arches.

7 Heyman's plastic method predicted a collapse load of 10.13kNm^{-1} which was far below experimental collapse loads.

8 The MEXE method predicted an allowable single axle load of 18.98kNm^{-1}.

9 The 2-D FE concrete model has been successfully used in this study to predict both the collapse mode and collapse load for these arches.

10 The arch tensile strength and the tension softening factor were found to be

influential in the FE prediction of the arch collapse load.

11 An arch tensile strength of between 0.2MPa to 0.3MPa was recommended for this study whilst 5 to 8 was recommended for the tension softening factor.

12 The arch compressive strength, arch and backfill elastic moduli, and the live load dispersal angle had no significant influence on the FE prediction of the arch collapse load for these arches.

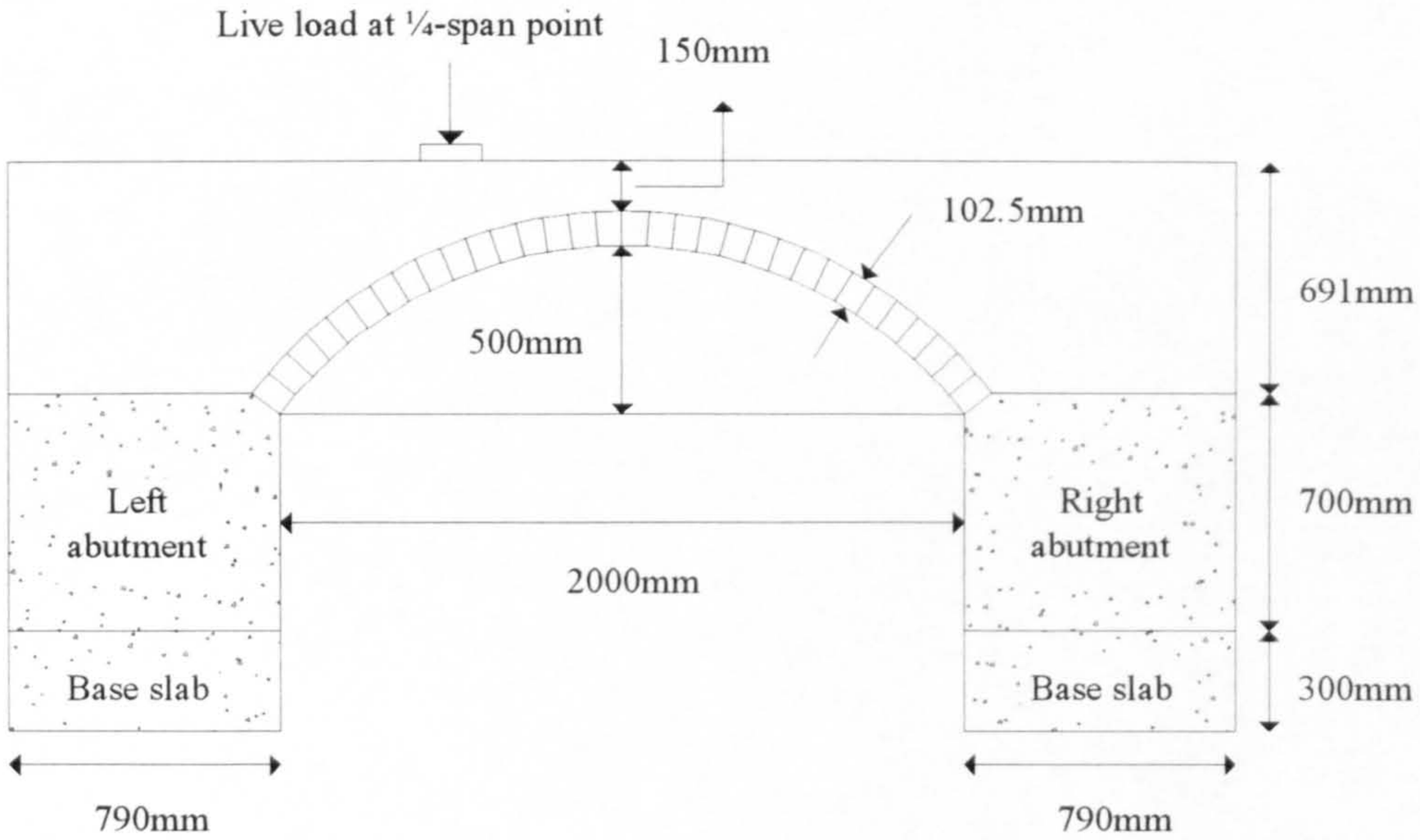

Figure 6.1 Salient dimensions of the arch bridge

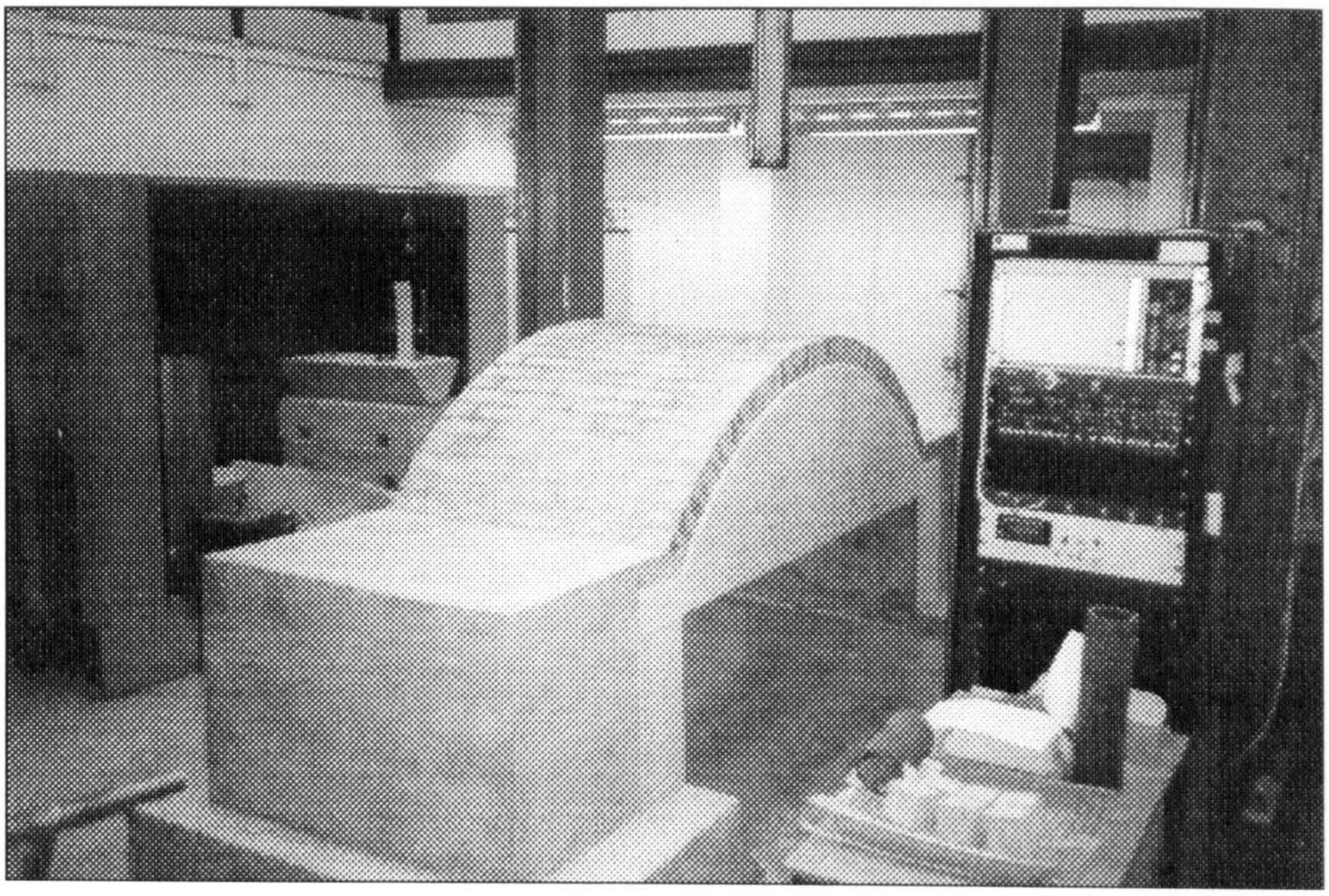

Figure 6.2 The bare arch ring supported by its timber centring

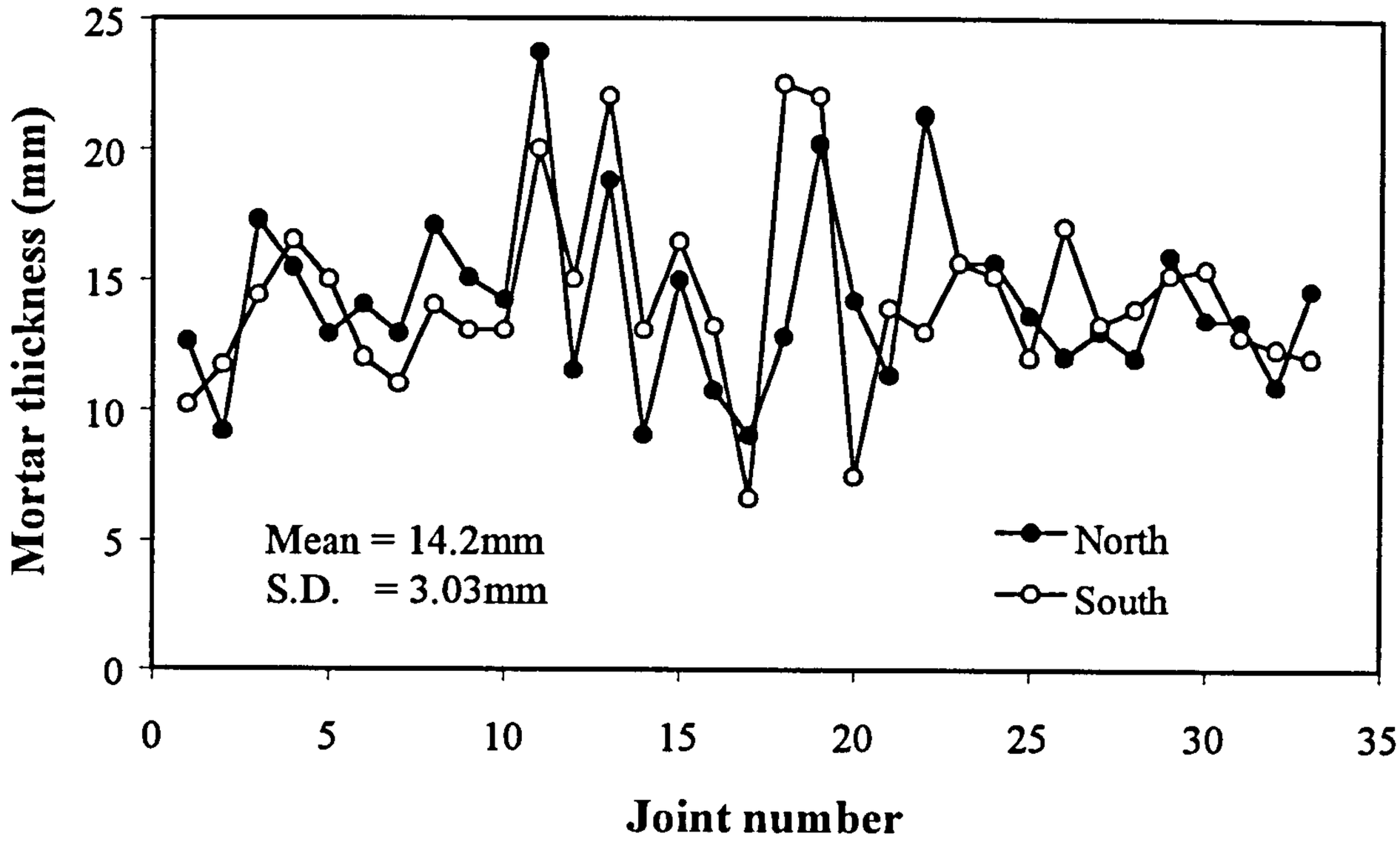

Figure 6.3a Distribution of mortar thickness for SR4-A

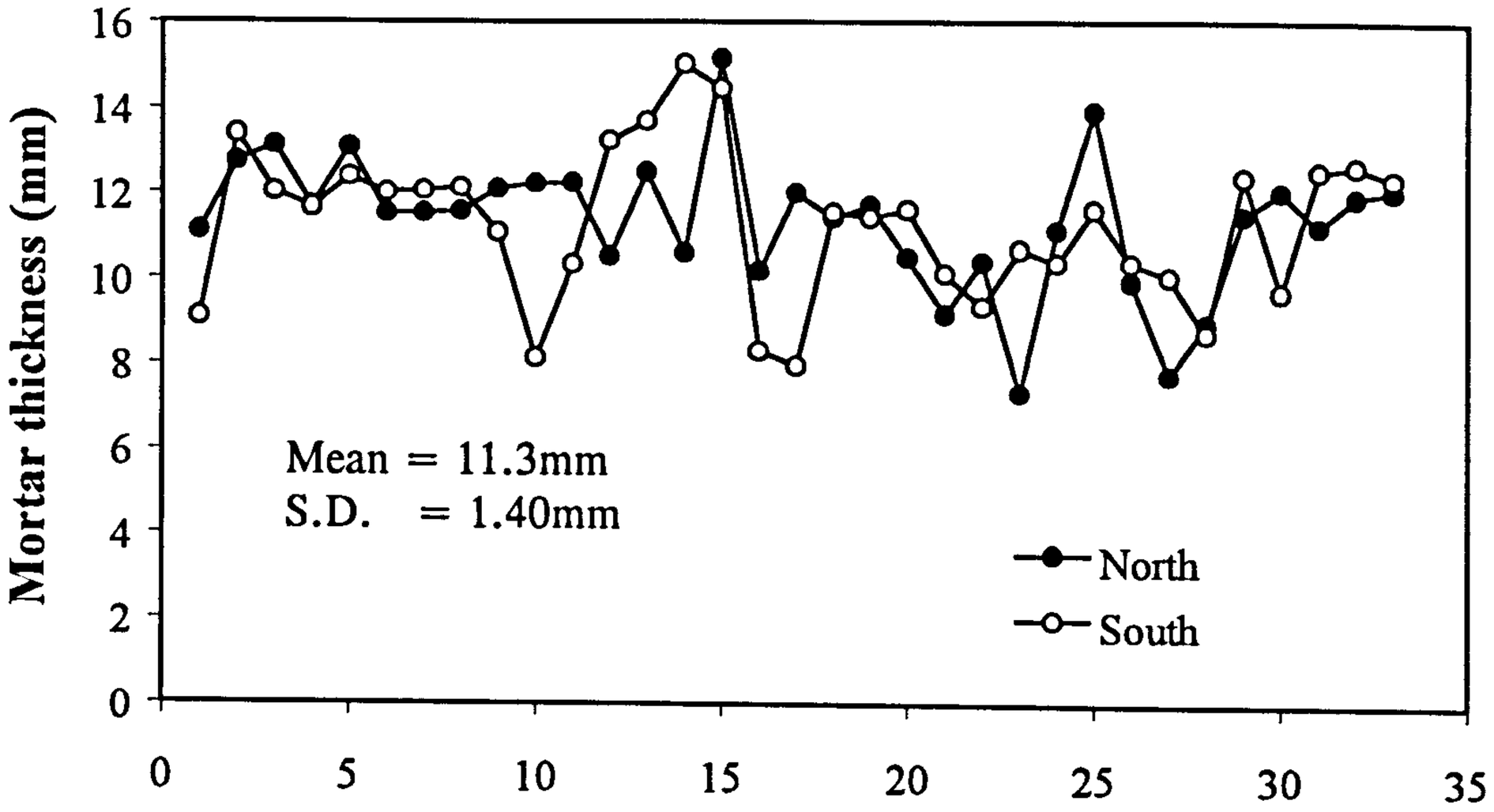

Figure 6.3b Distribution of mortar thickness for SR4-B

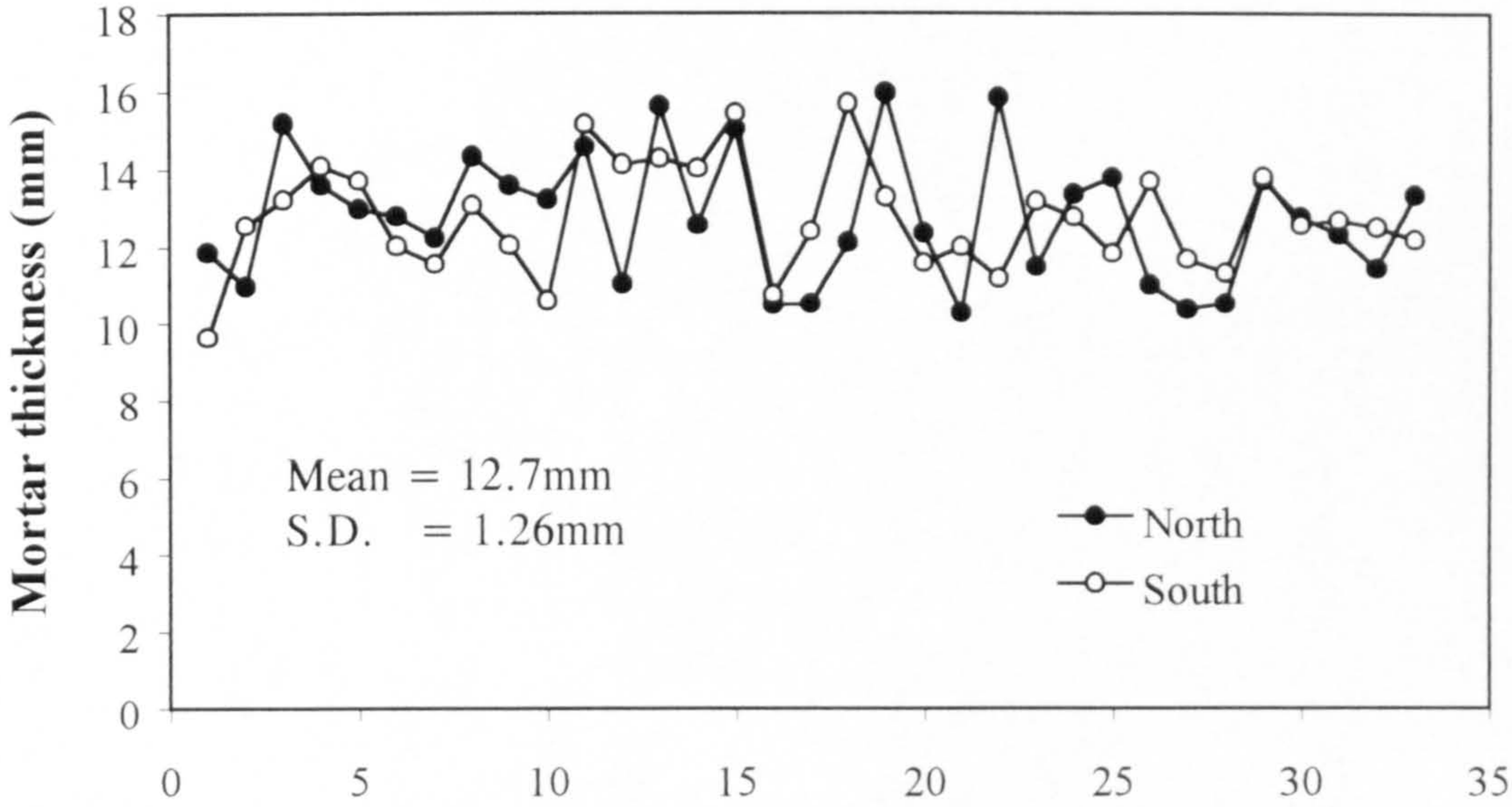

Figure 6.3c Distribution of mortar thickness for SR4-C

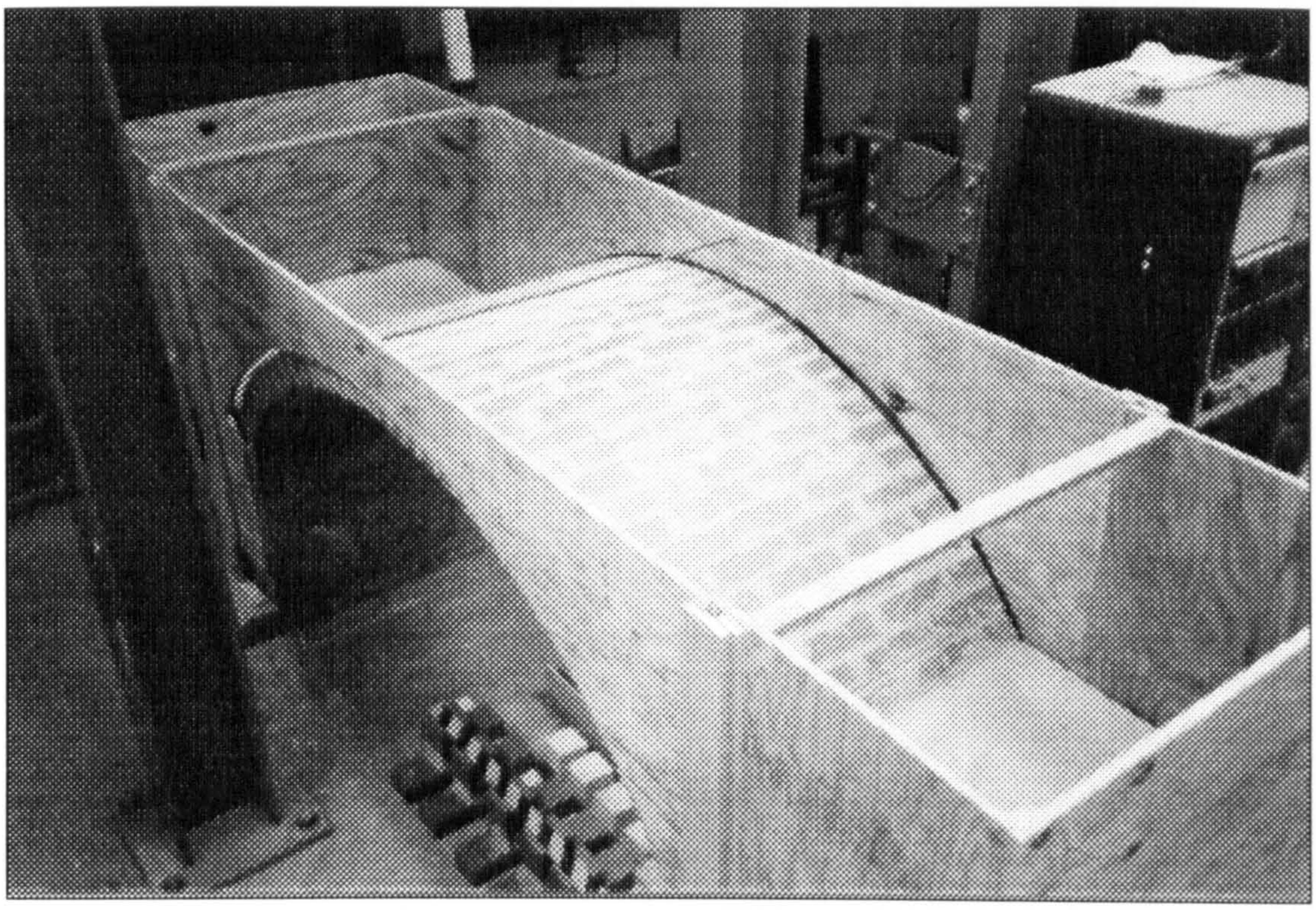

Figure 6.4 A bare arch with timber spandrel, wing and end walls

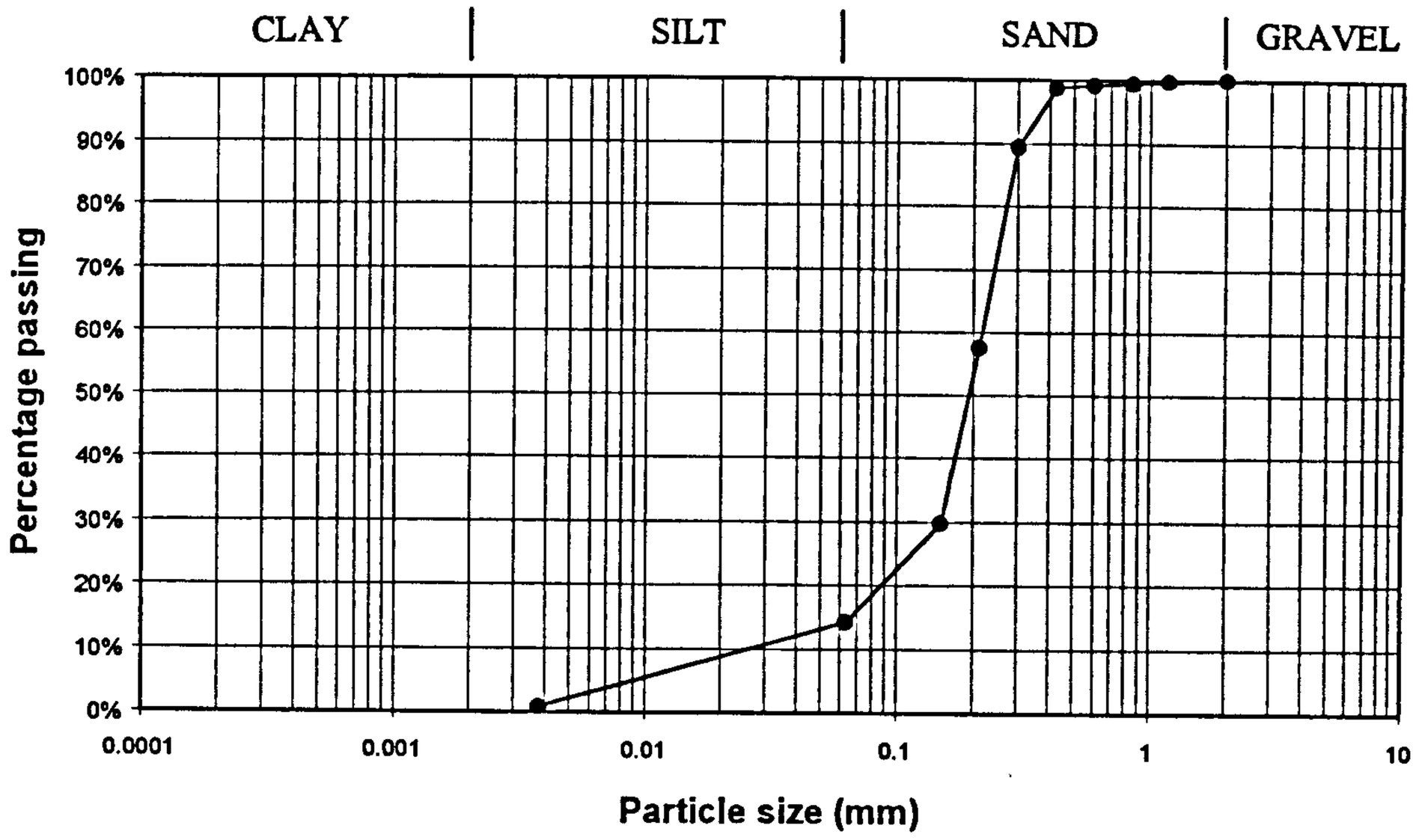

Figure 6.5 Particle size distribution of the backfill material

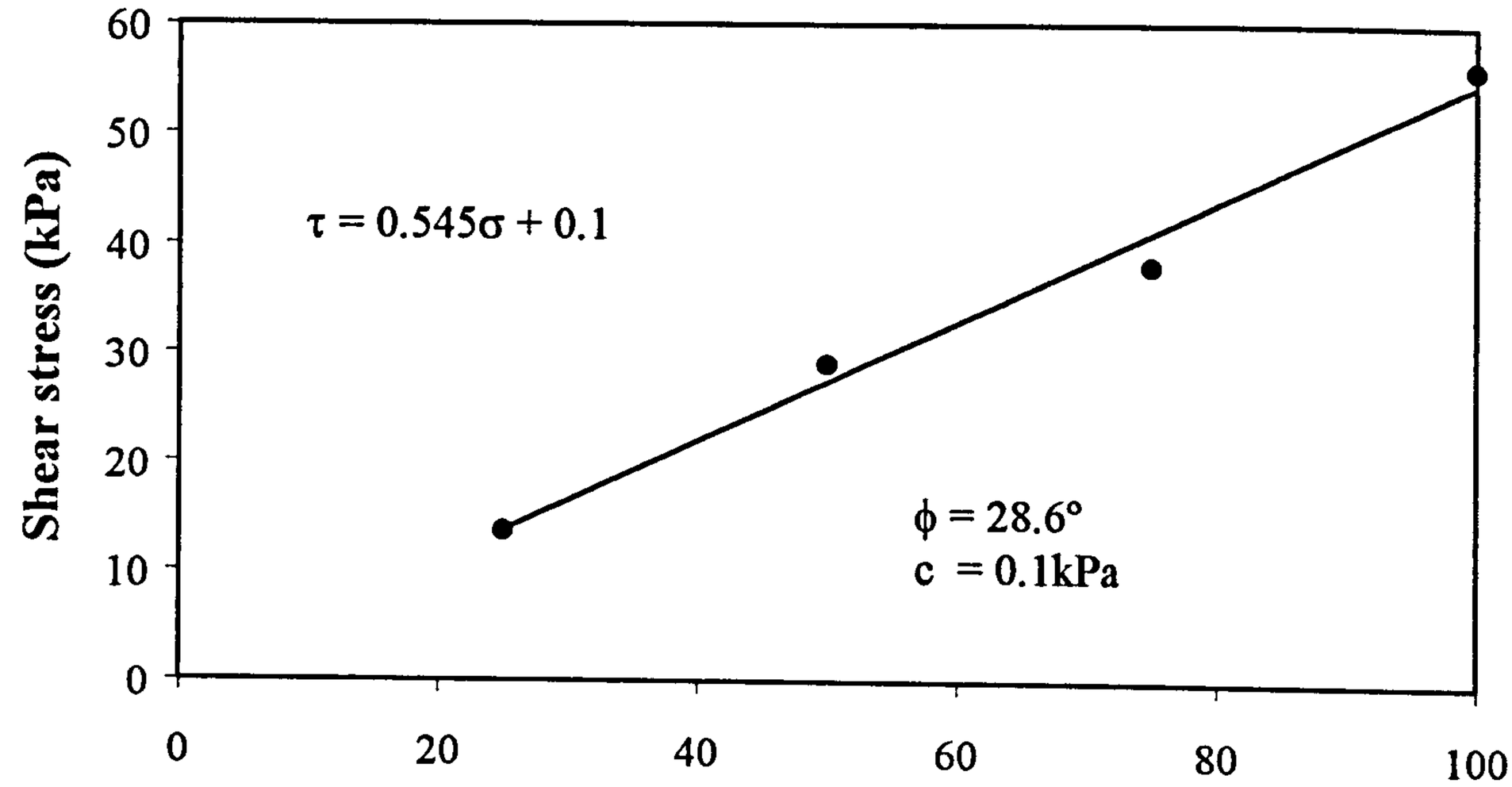

Figure 6.6 Shear strength of the backfill material from shear box tests

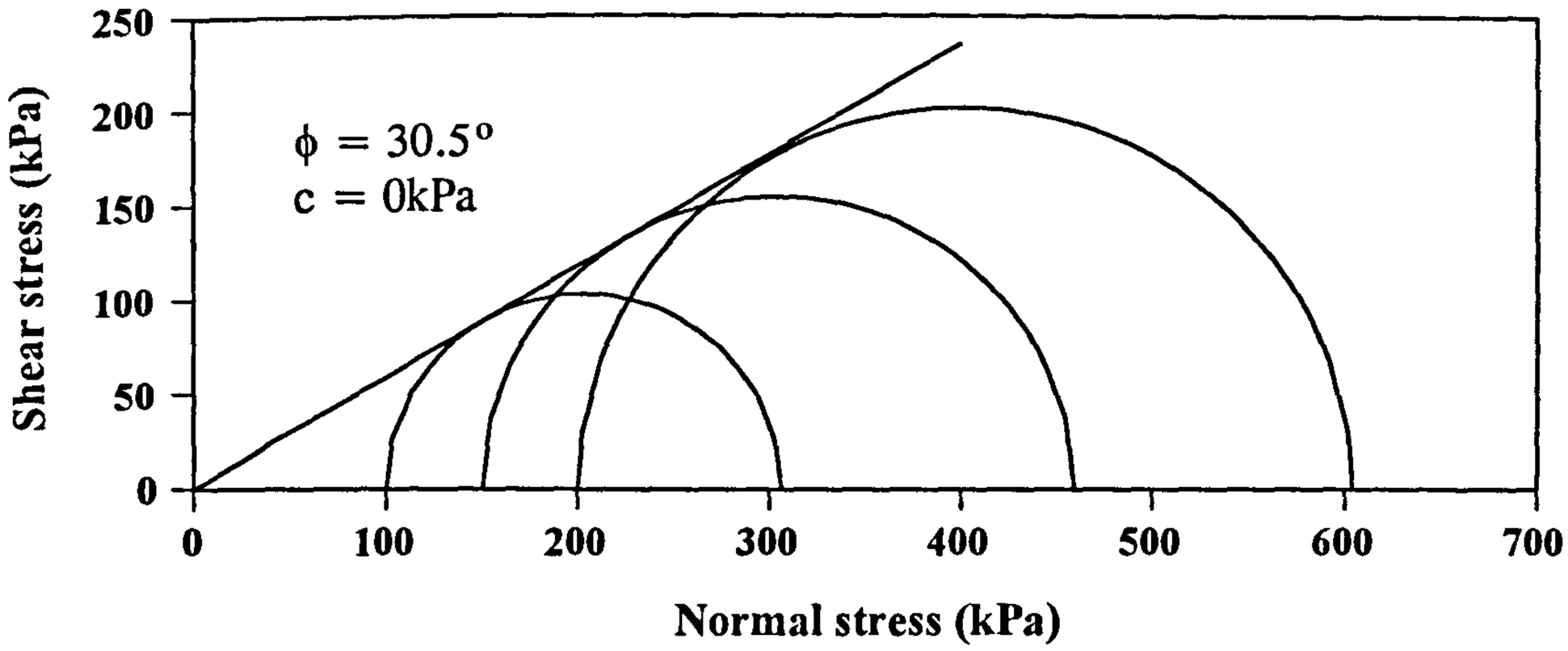

Figure 6.7 Shear strength of the backfill material from triaxial tests

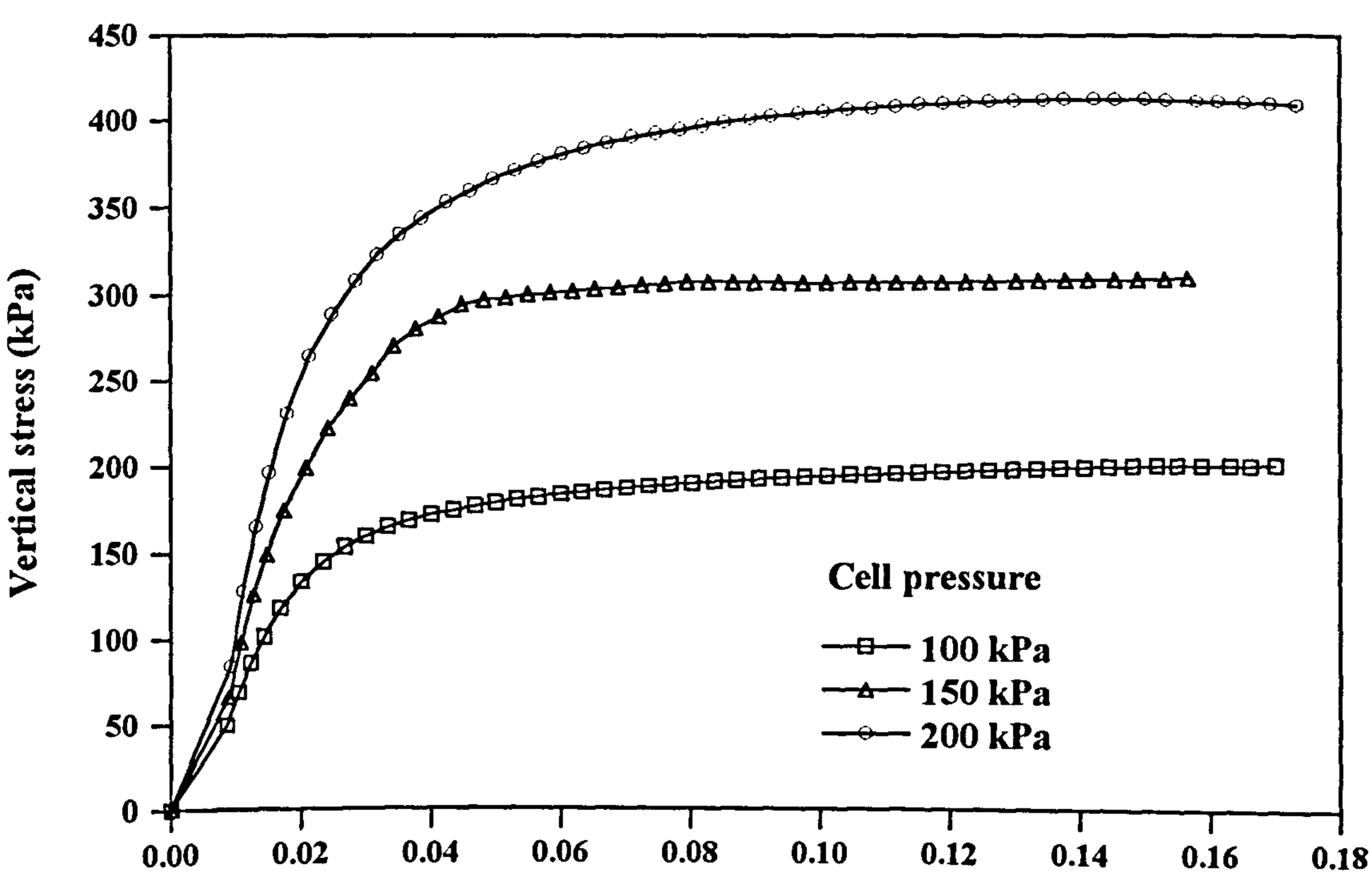

Figure 6.8 Vertical stress *versus* vertical strain curves for the backfill material

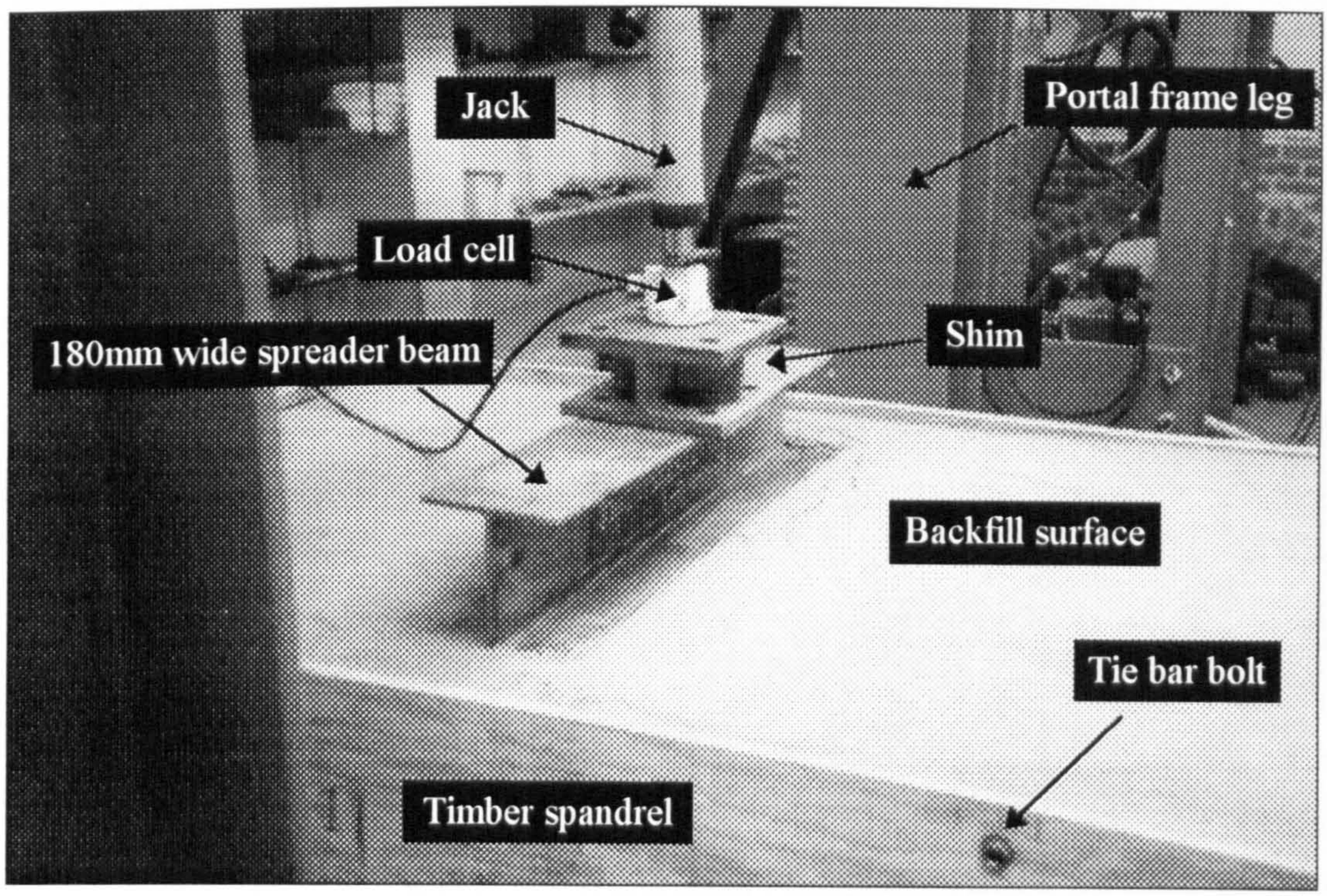

Figure 6.9 The spreader beam and the loading system

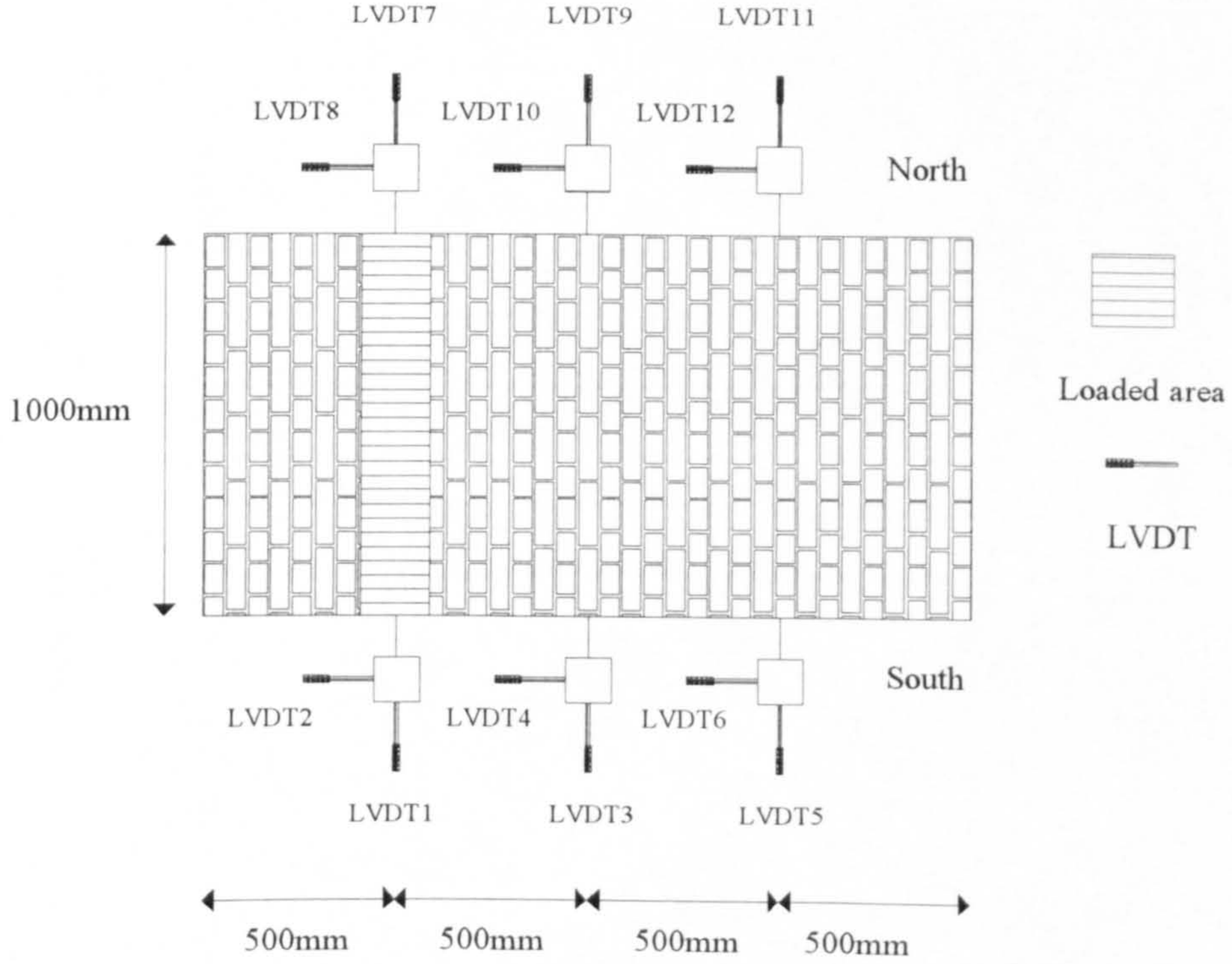

Figure 6.10 Locations for the LVDTs (plan view)

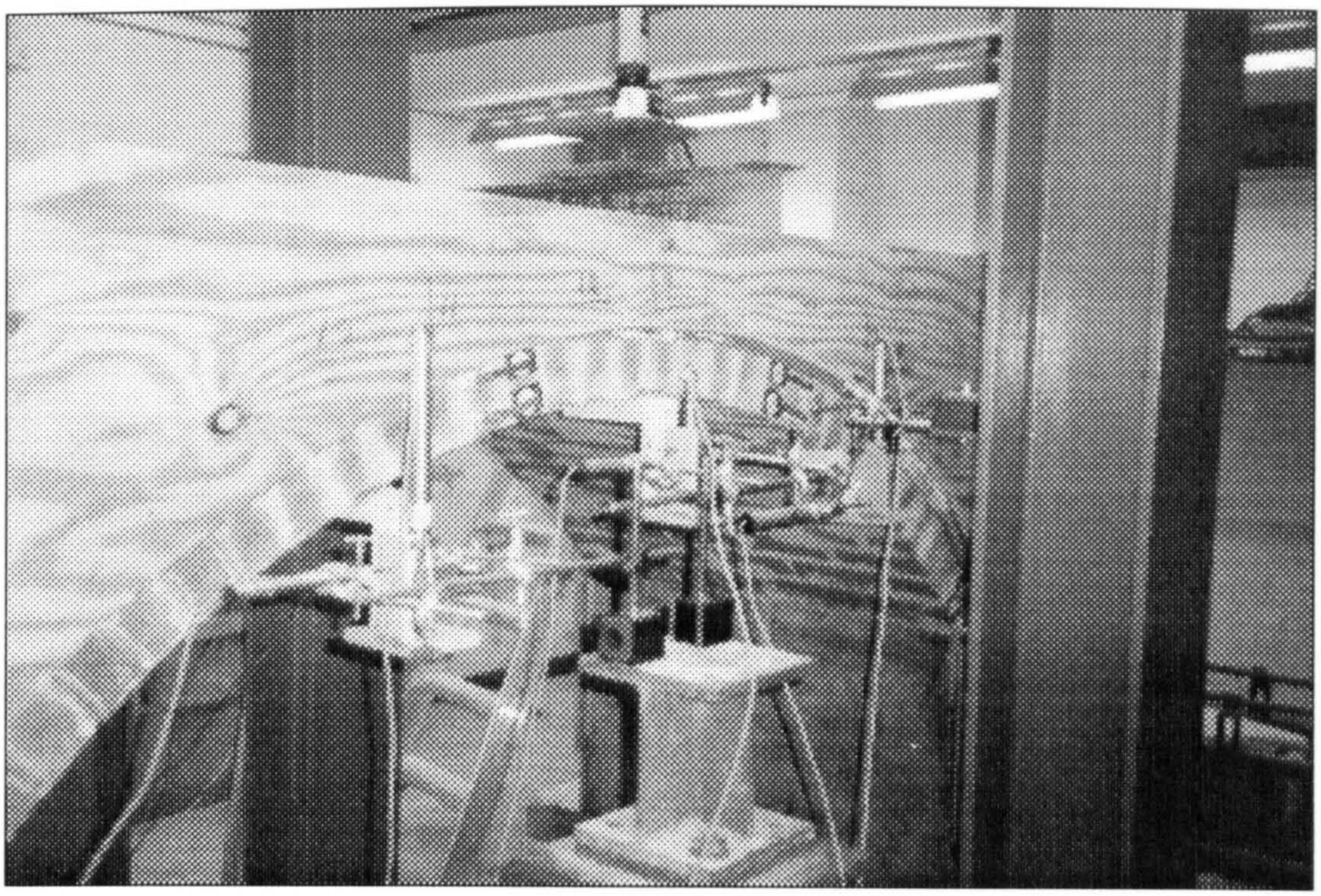

Figure 6.11 Wooden platforms and the positions of the LVDTs

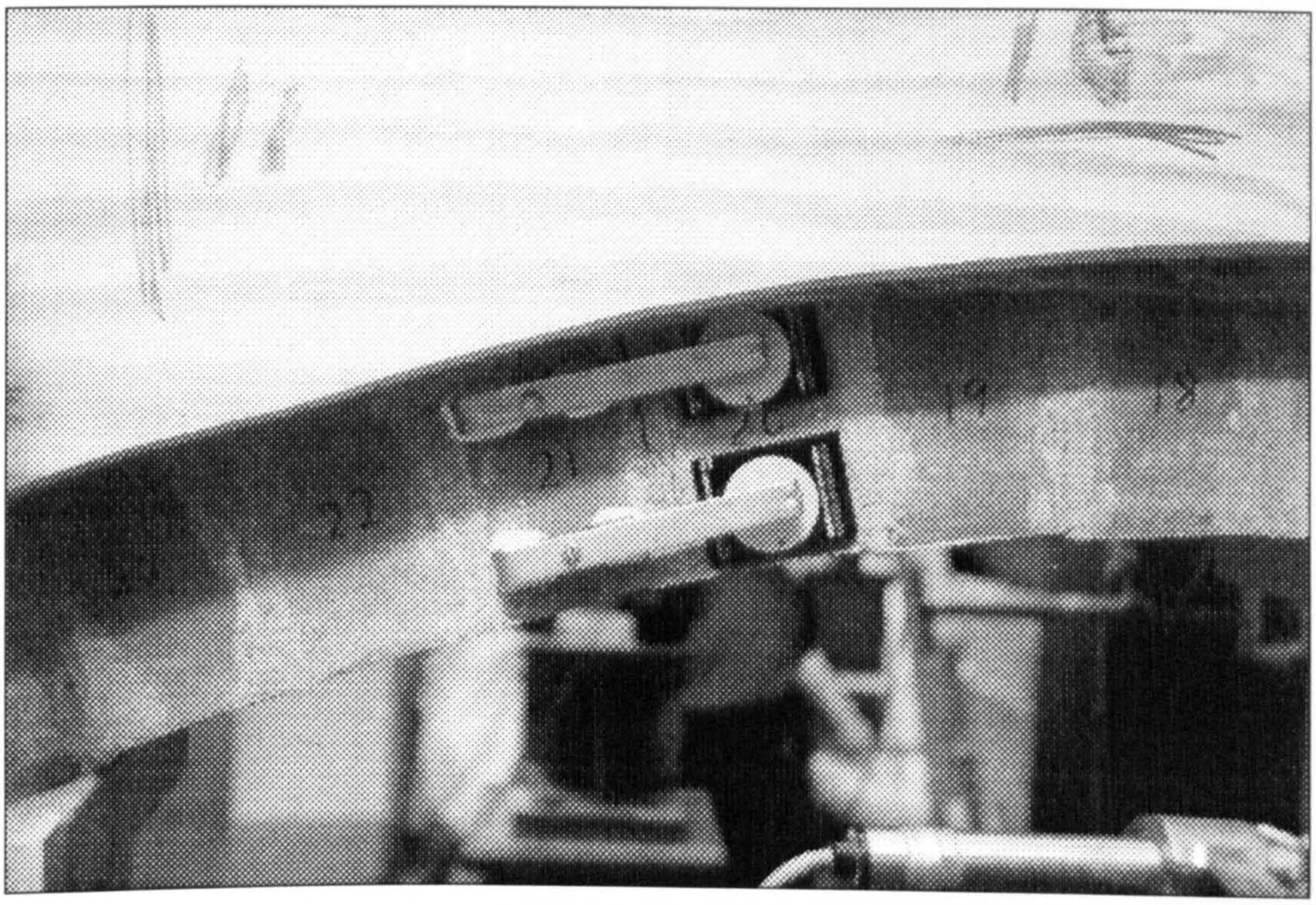

Figure 6.12 Crack monitoring devices

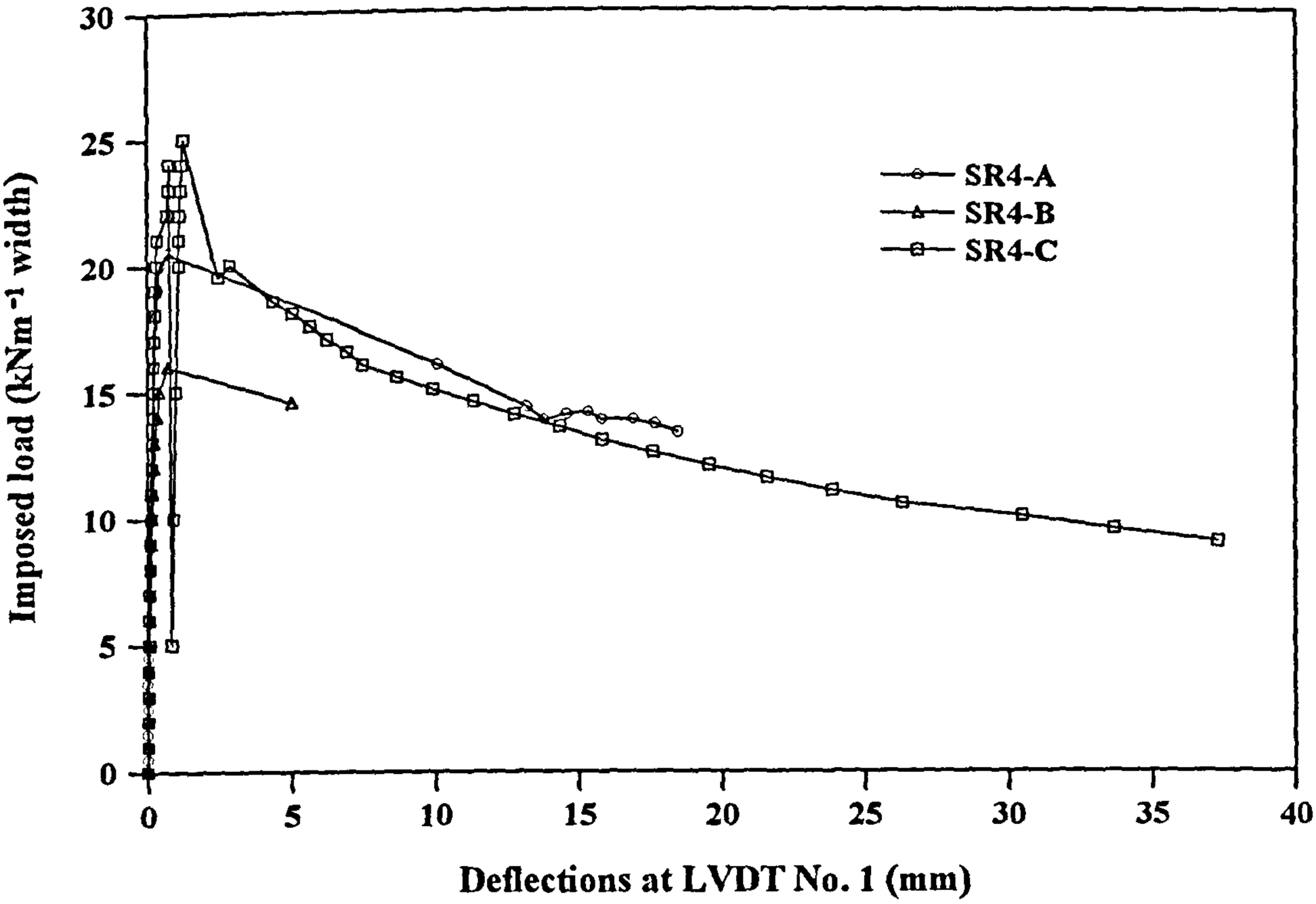

Figure 6.13 Load *versus* vertical deflection curve at channel 1

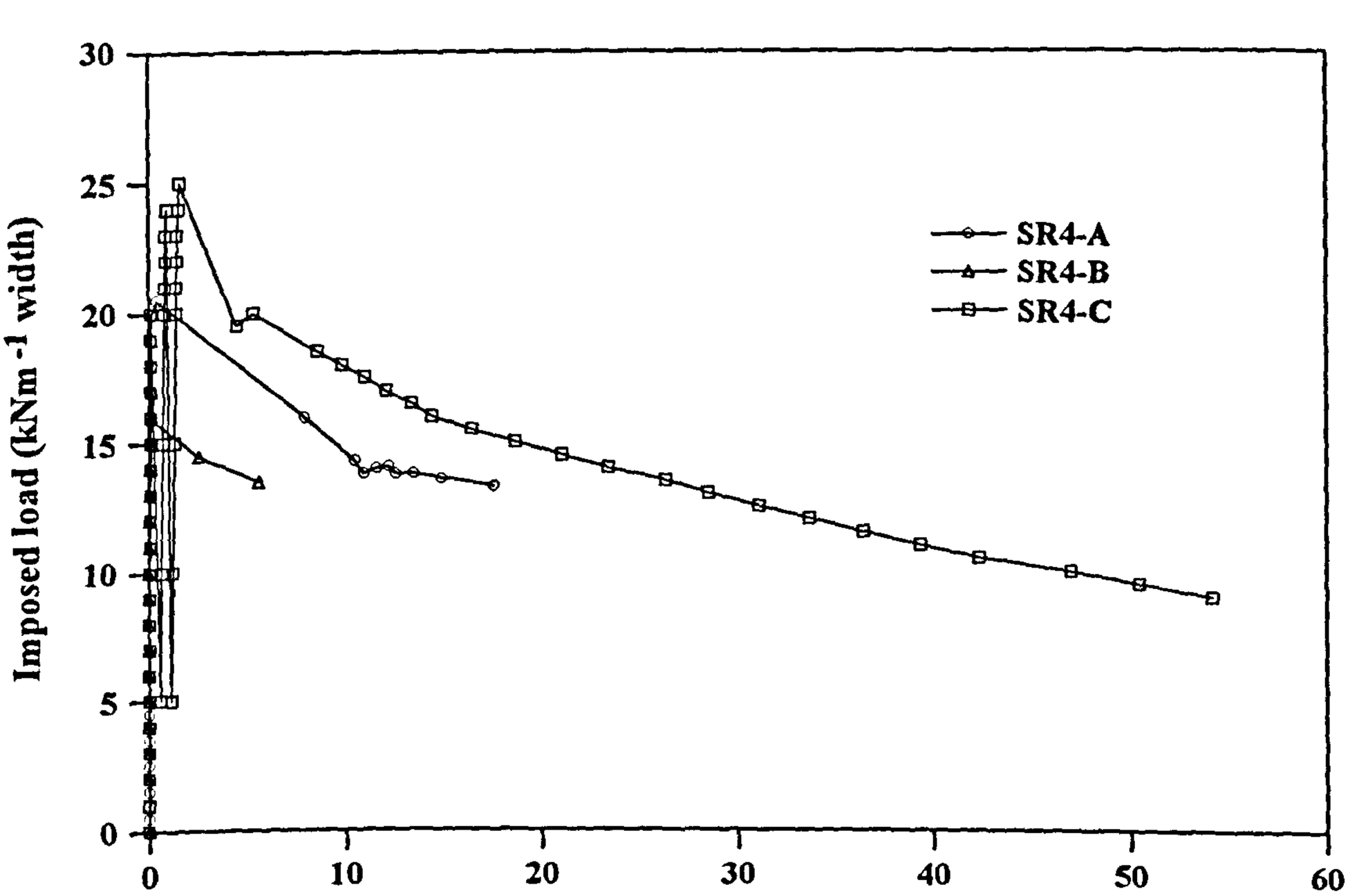

Figure 6.14 Load *versus* horizontal deflection curve at channel 2

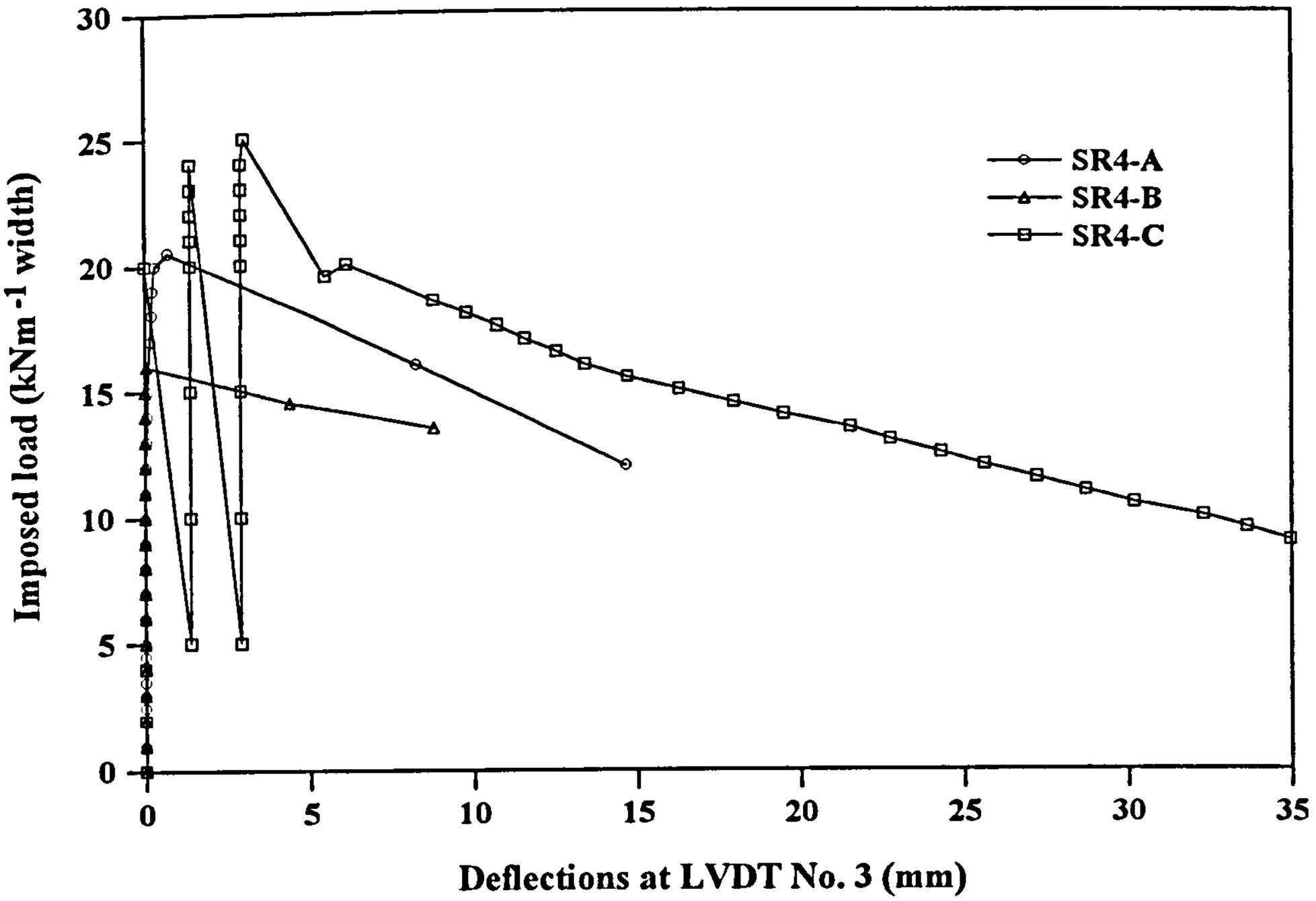

Figure 6.15 Load *versus* vertical deflection curve at channel 3

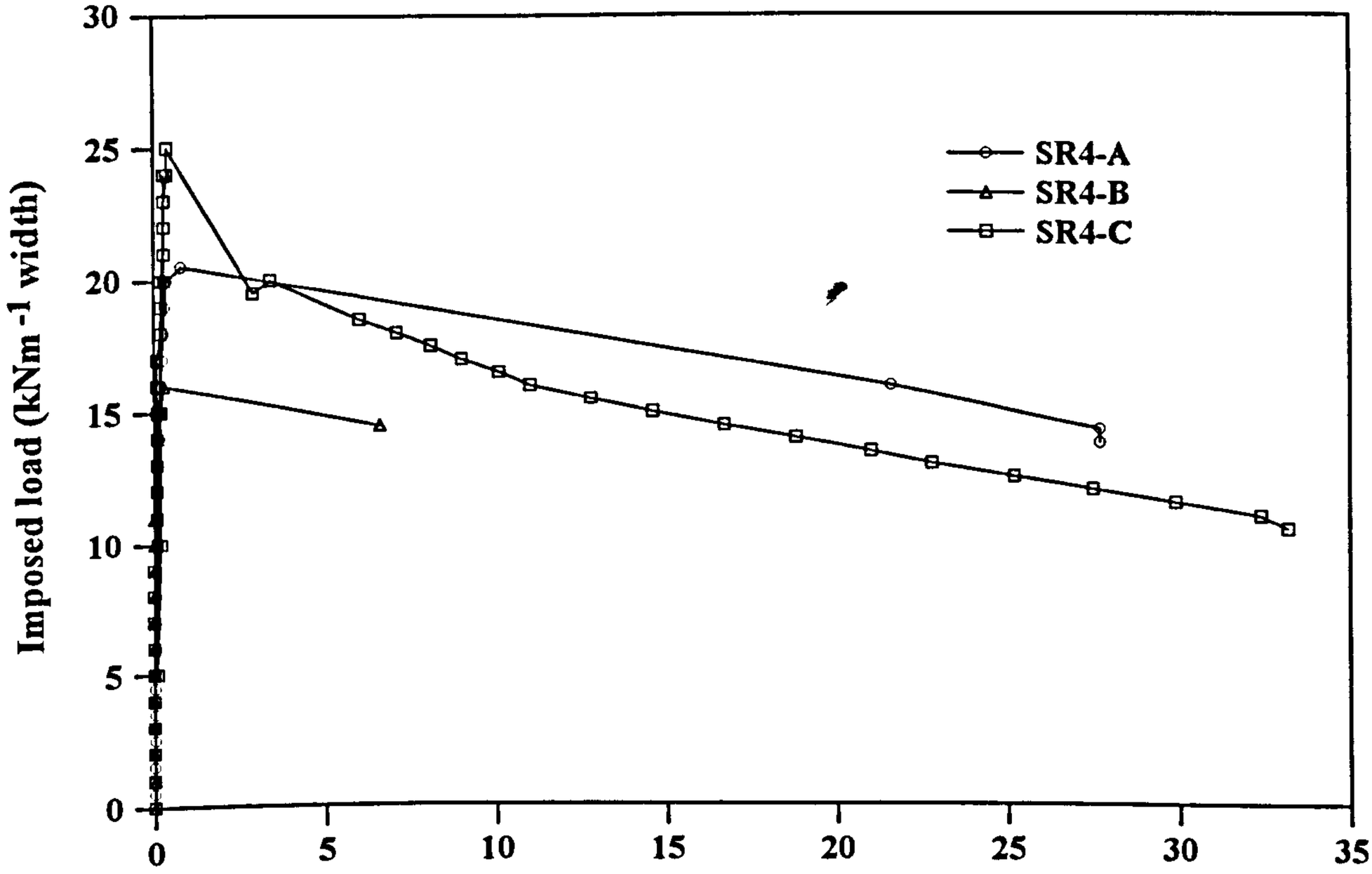

Figure 6.16 Load *versus* horizontal deflection curve at channel 4

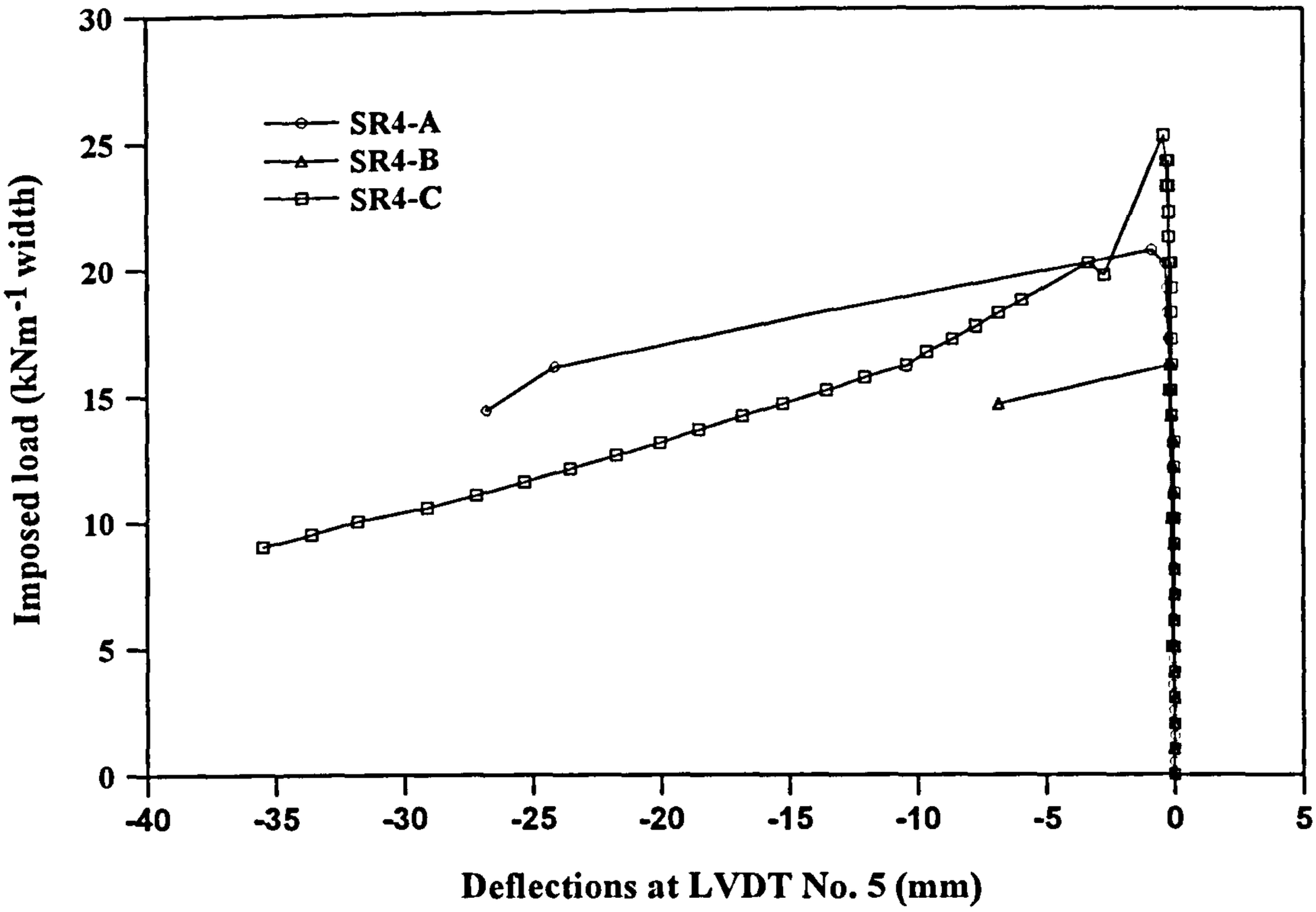

Figure 6.17 Load *versus* vertical deflection curve at channel 5

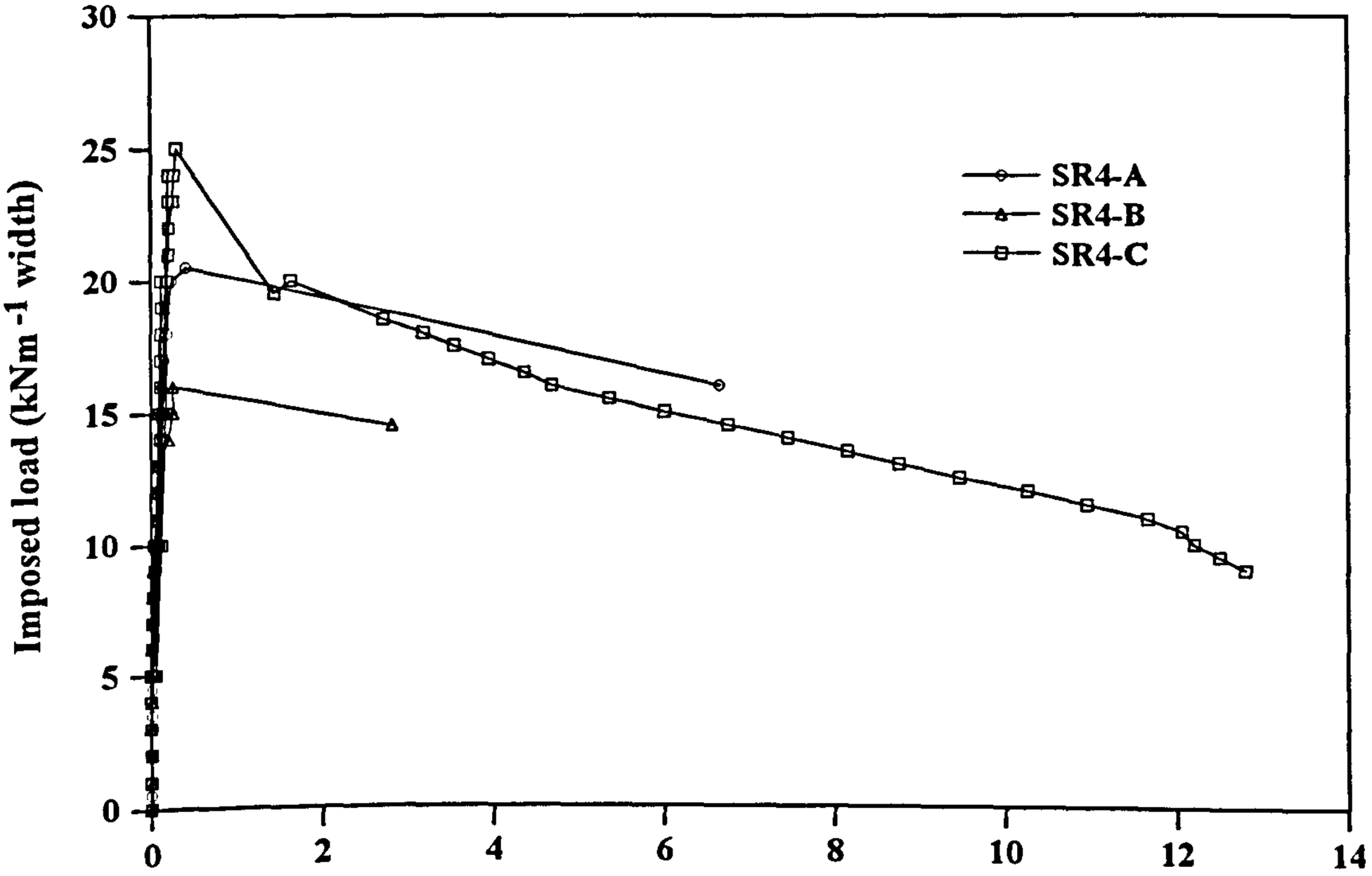

Figure 6.18 Load *versus* horizontal deflection curve at channel 6

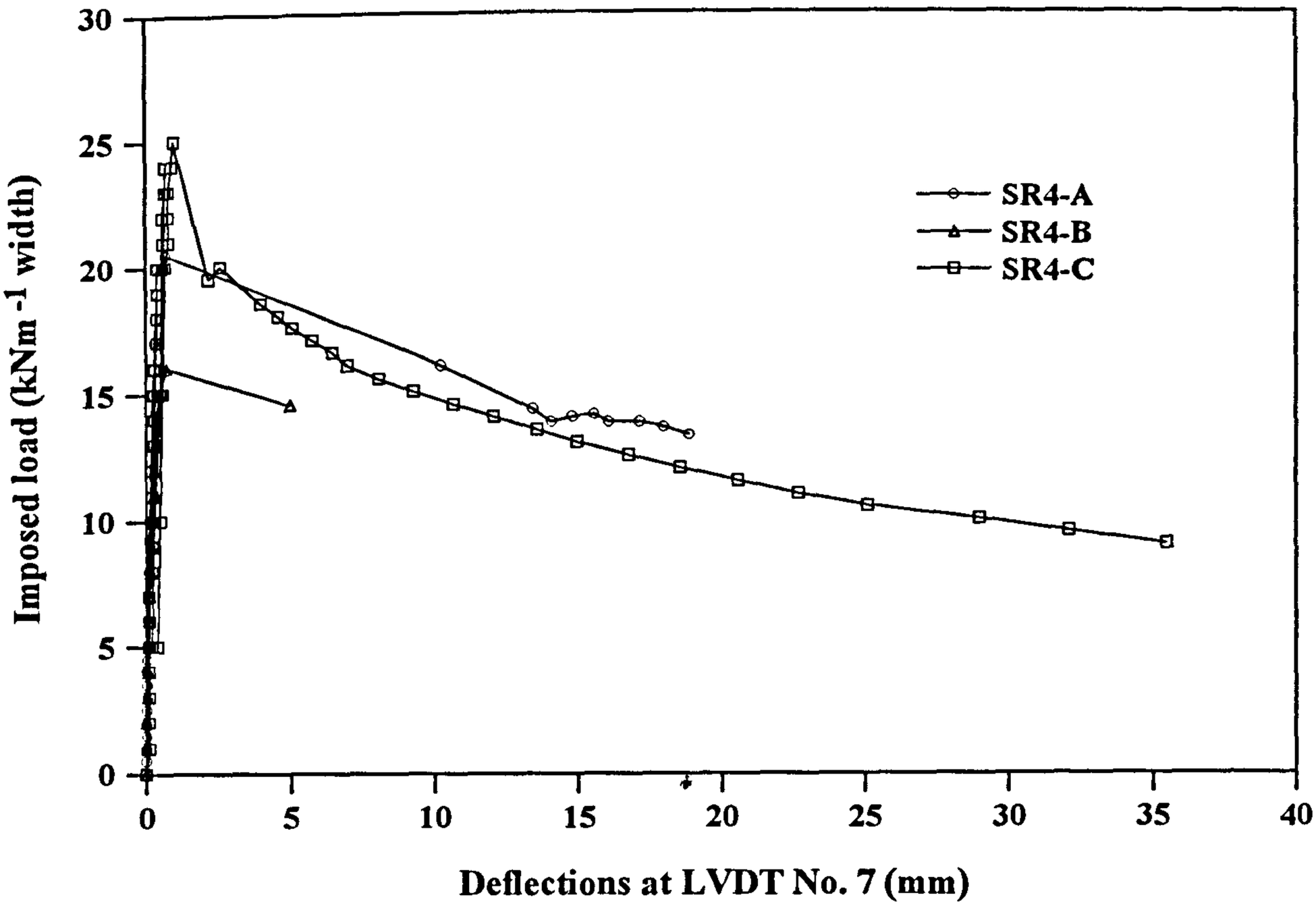

Figure 6.19 Load *versus* vertical deflection curve at channel 7

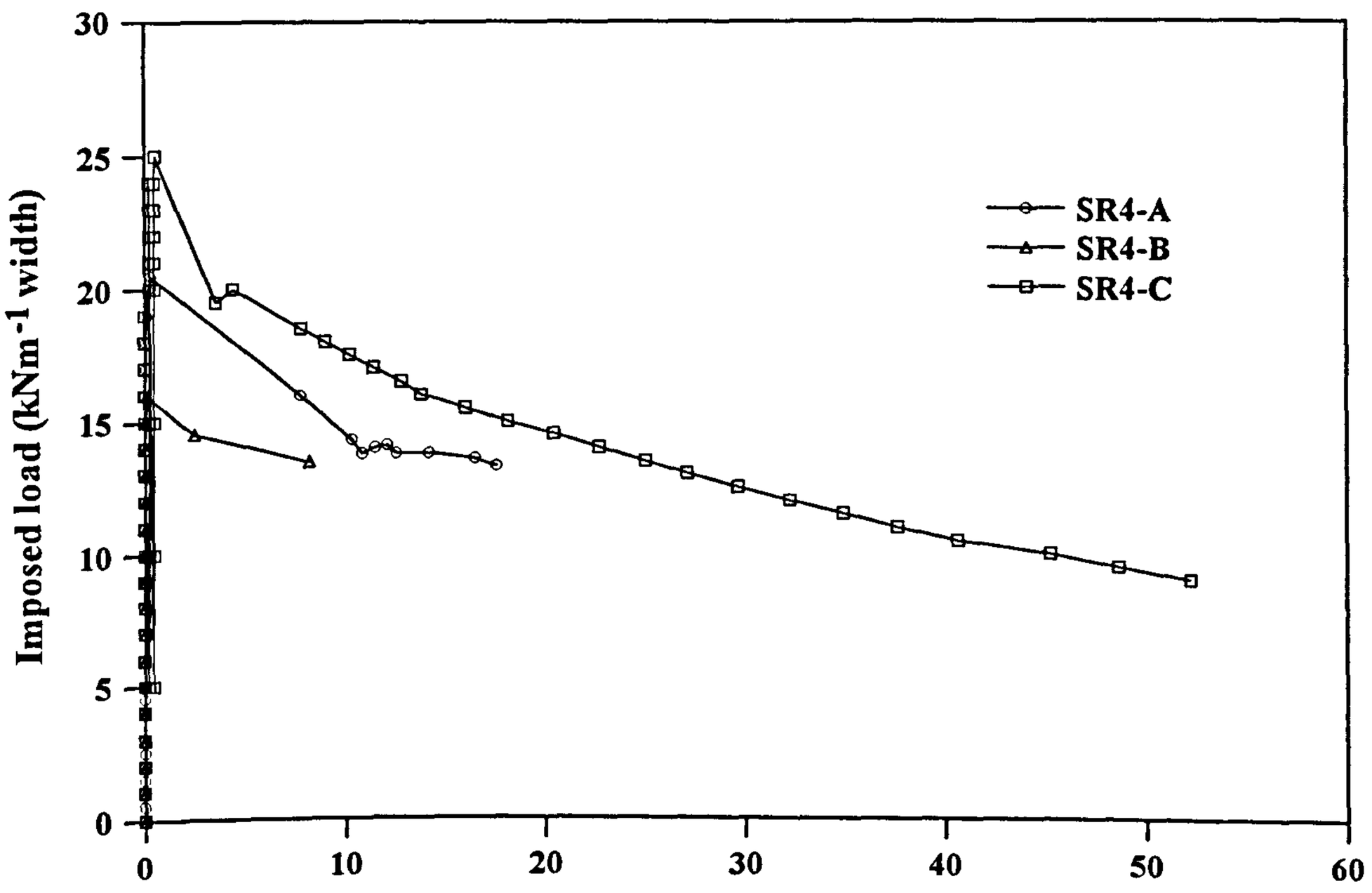

Figure 6.20 Load *versus* horizontal deflection curve at channel 8

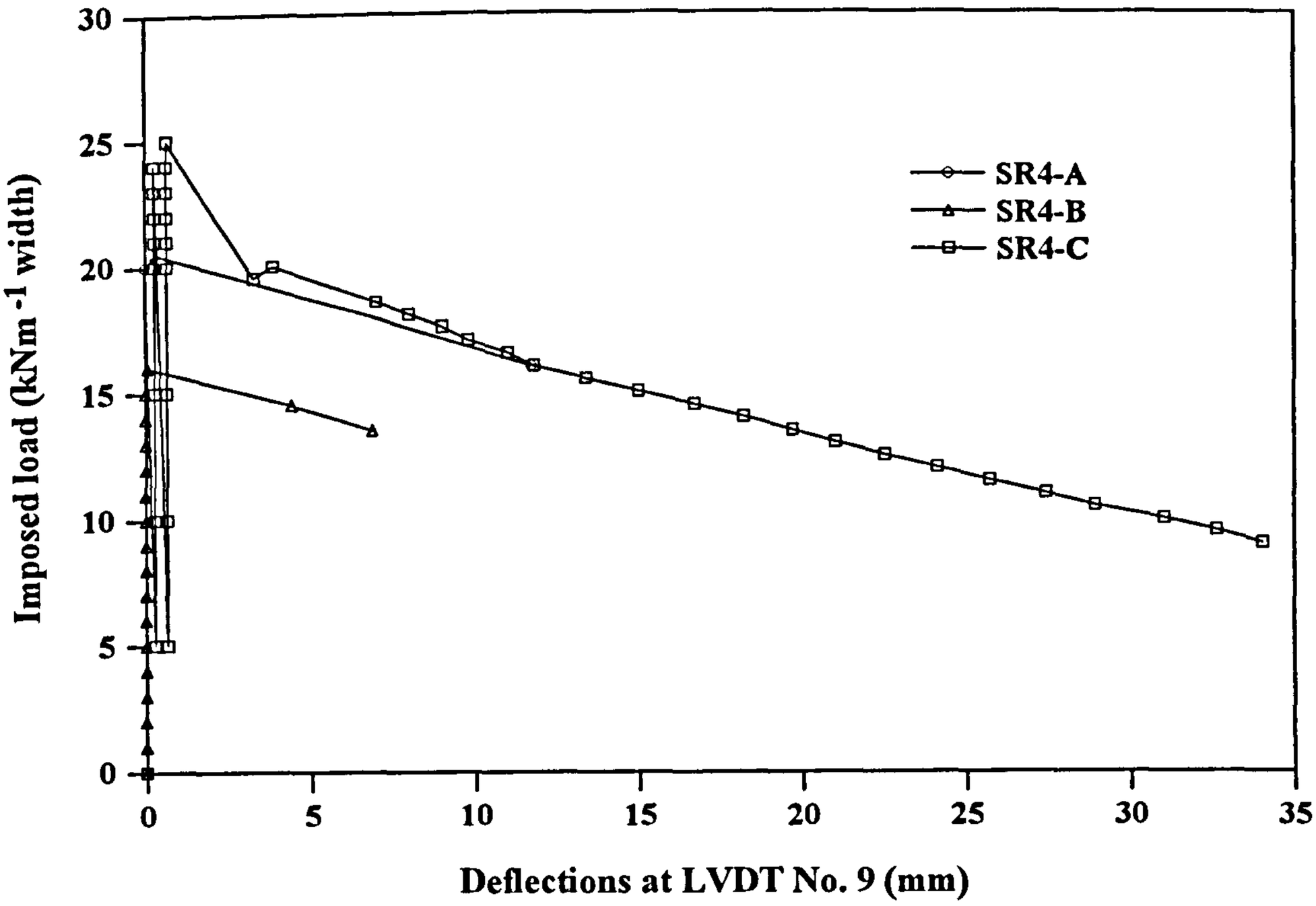

Figure 6.21 Load *versus* vertical deflection curve at channel 9

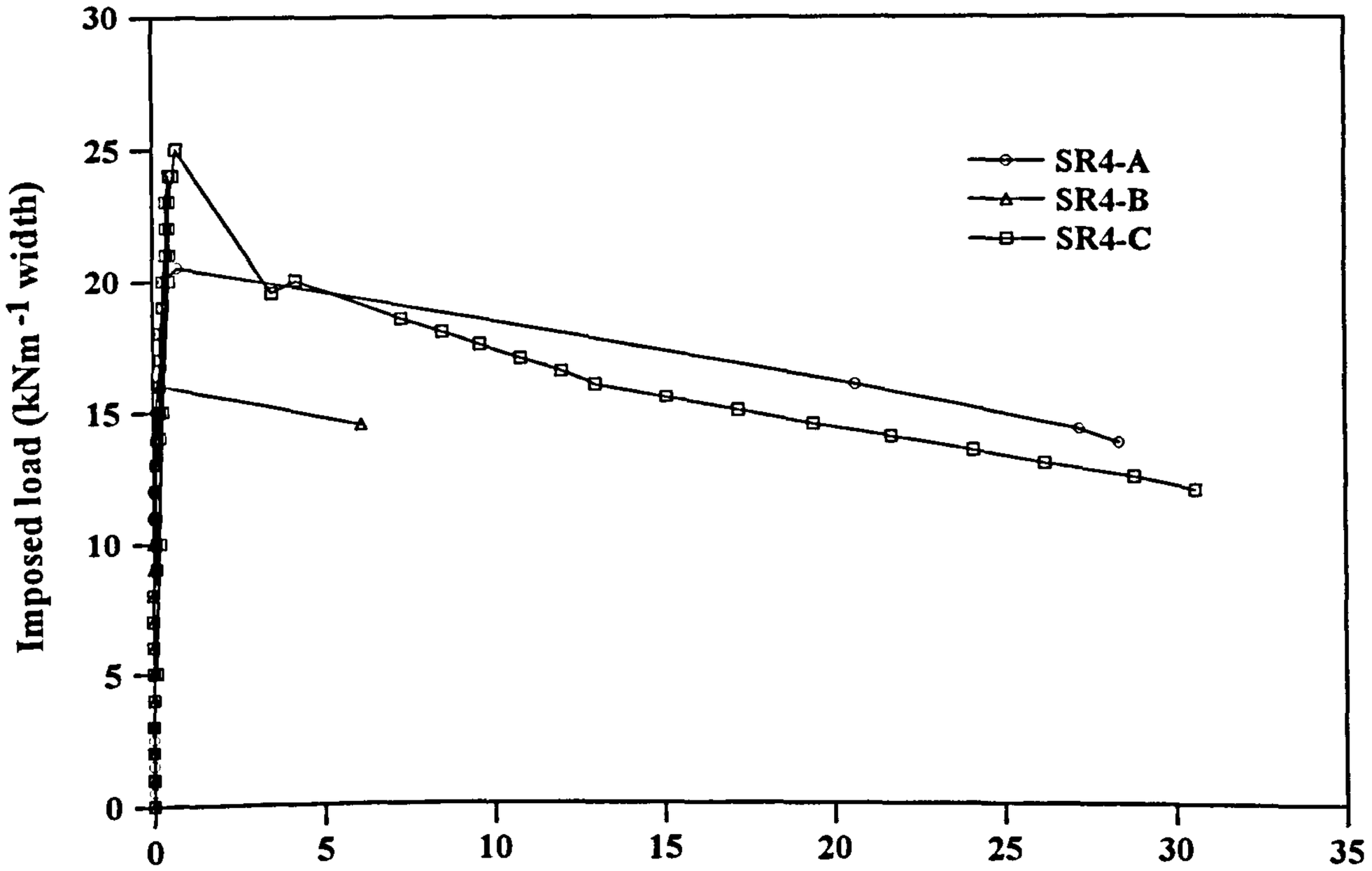

Figure 6.22 Load *versus* horizontal deflection curve at channel 10

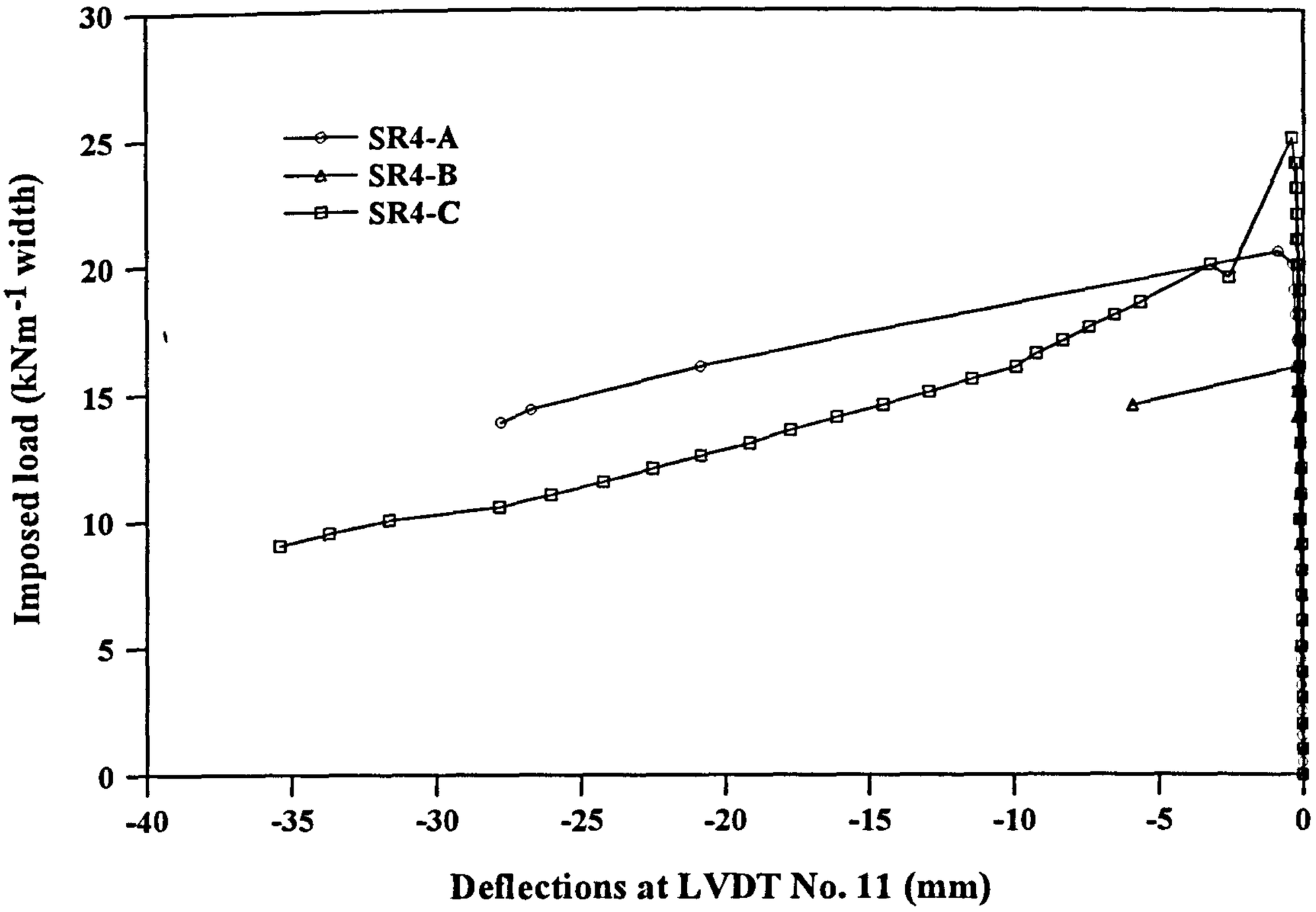

Figure 6.23 Load *versus* vertical deflection curve at channel 11

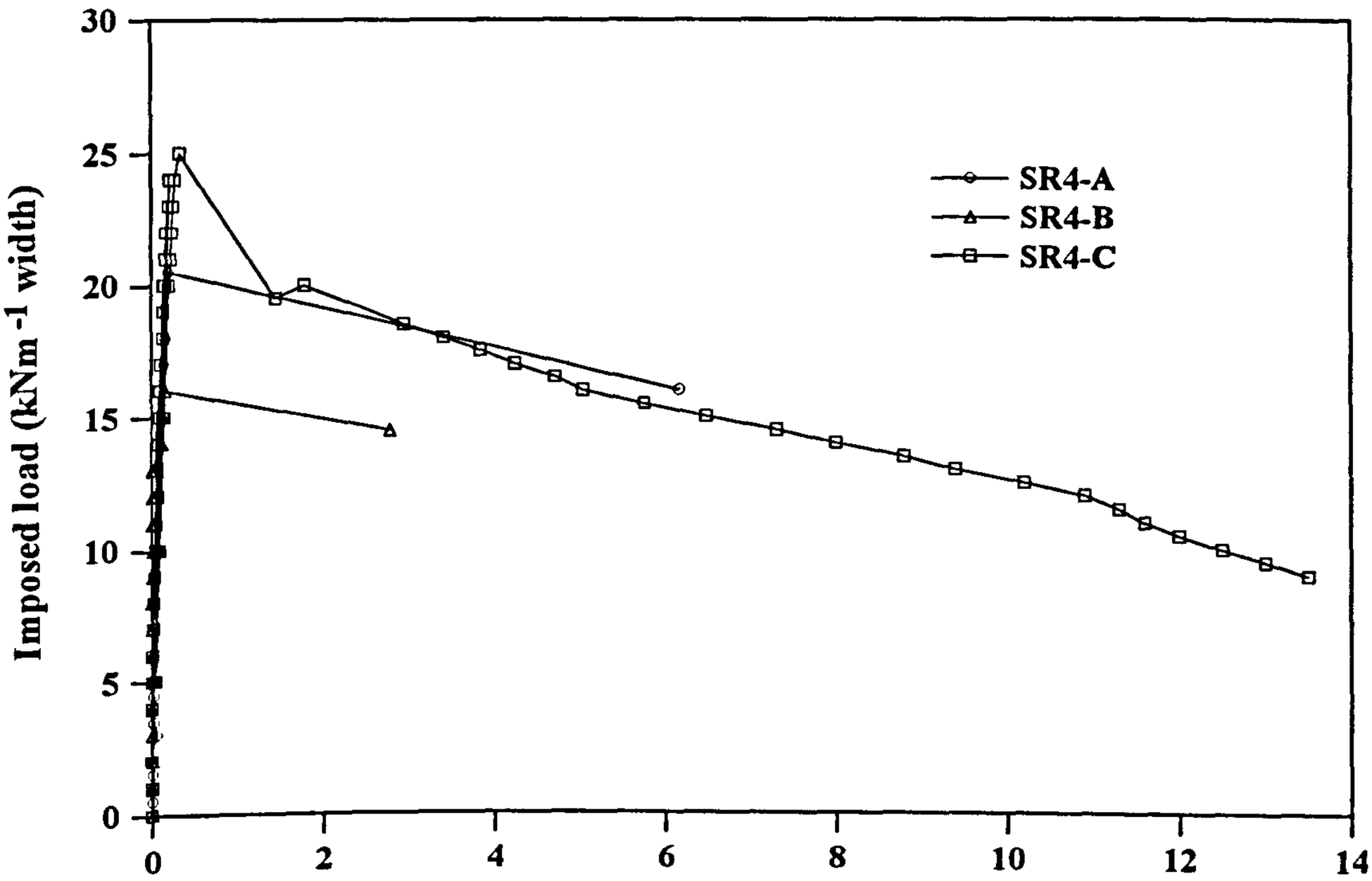

Figure 6.24 Load *versus* horizontal deflection curve at channel 12

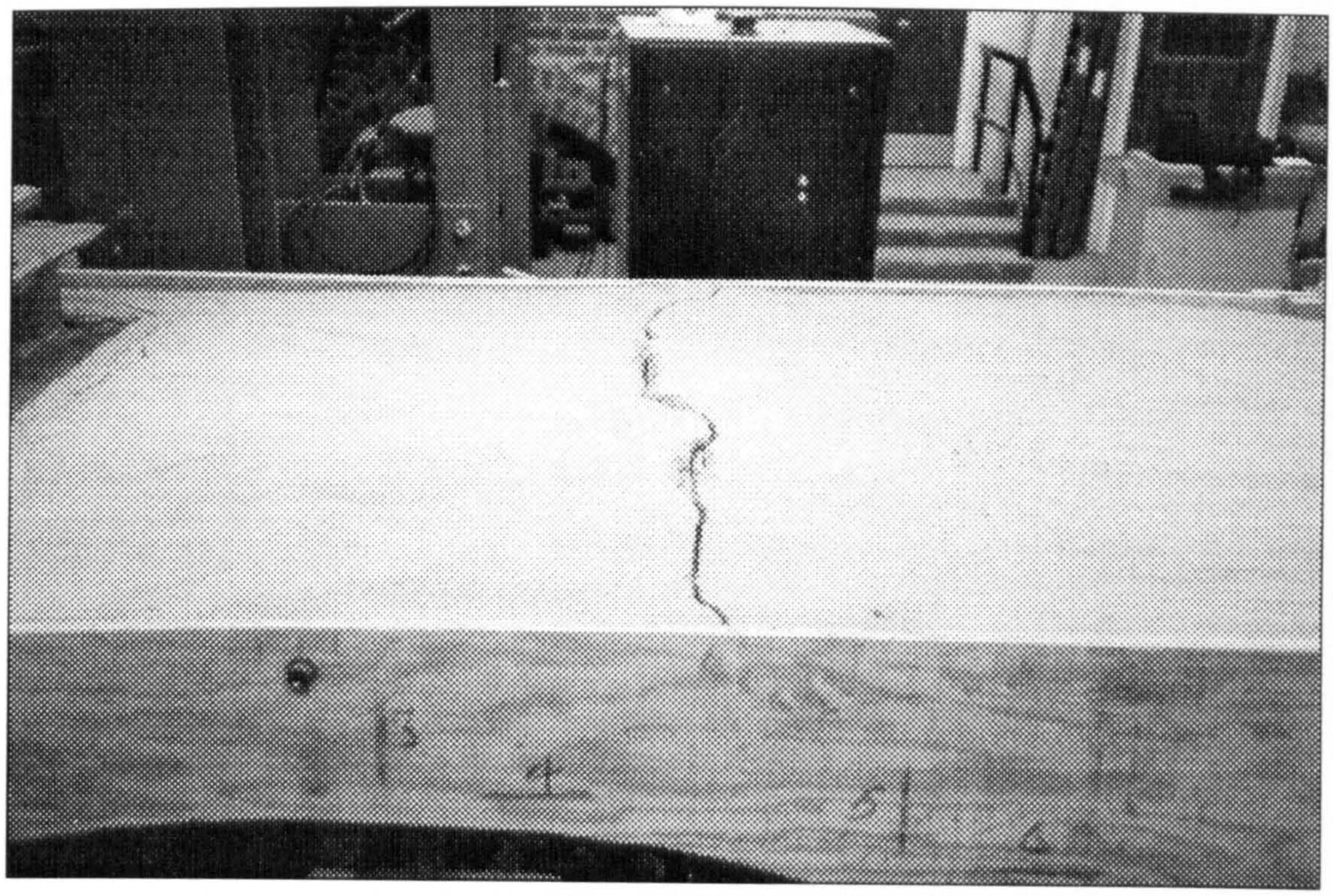

Figure 6.25 Tensile crack on the backfill's surface at 21kNm^{-1} on SR4-A

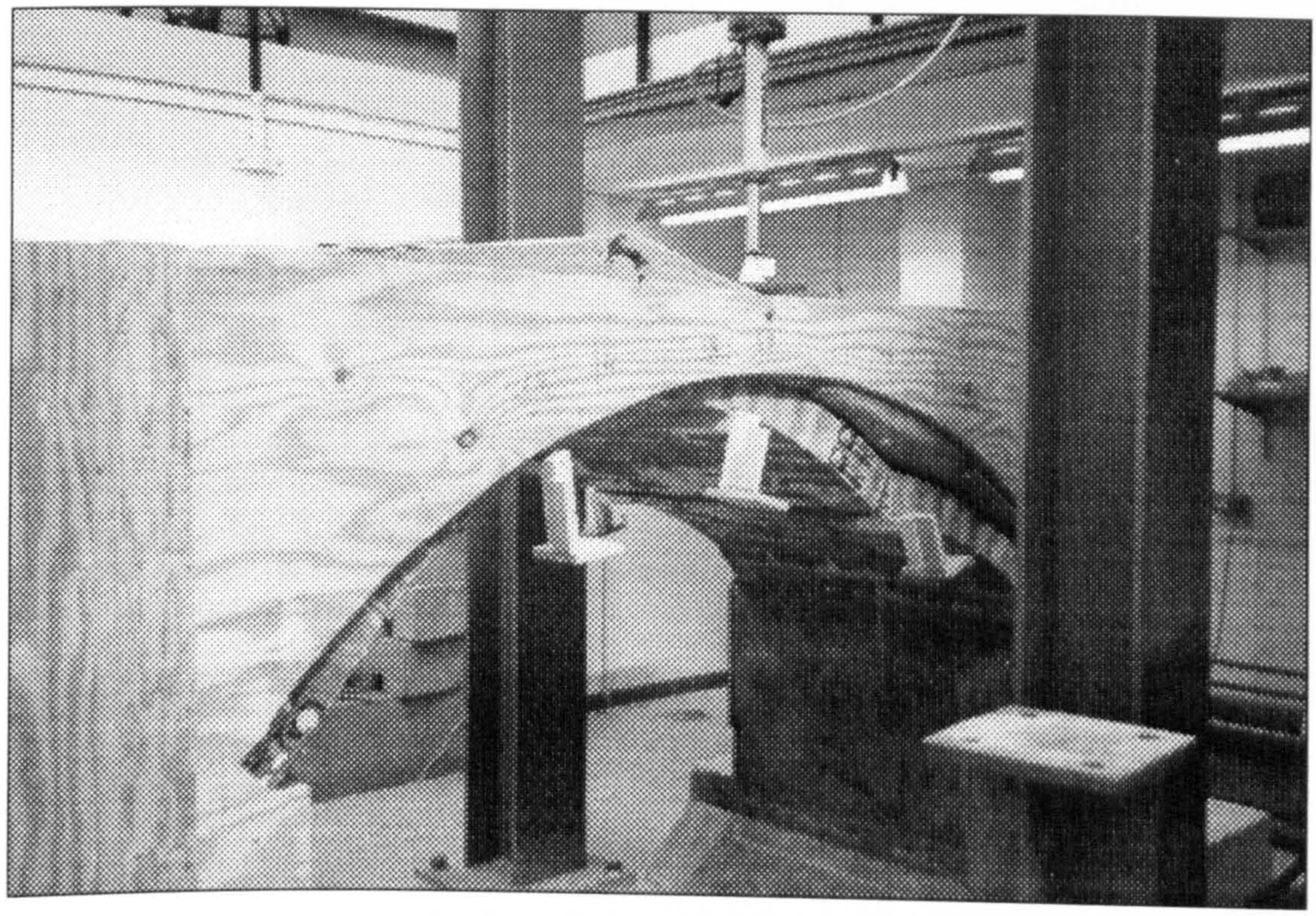

Figure 6.26 Arch SR4-B shortly before collapse

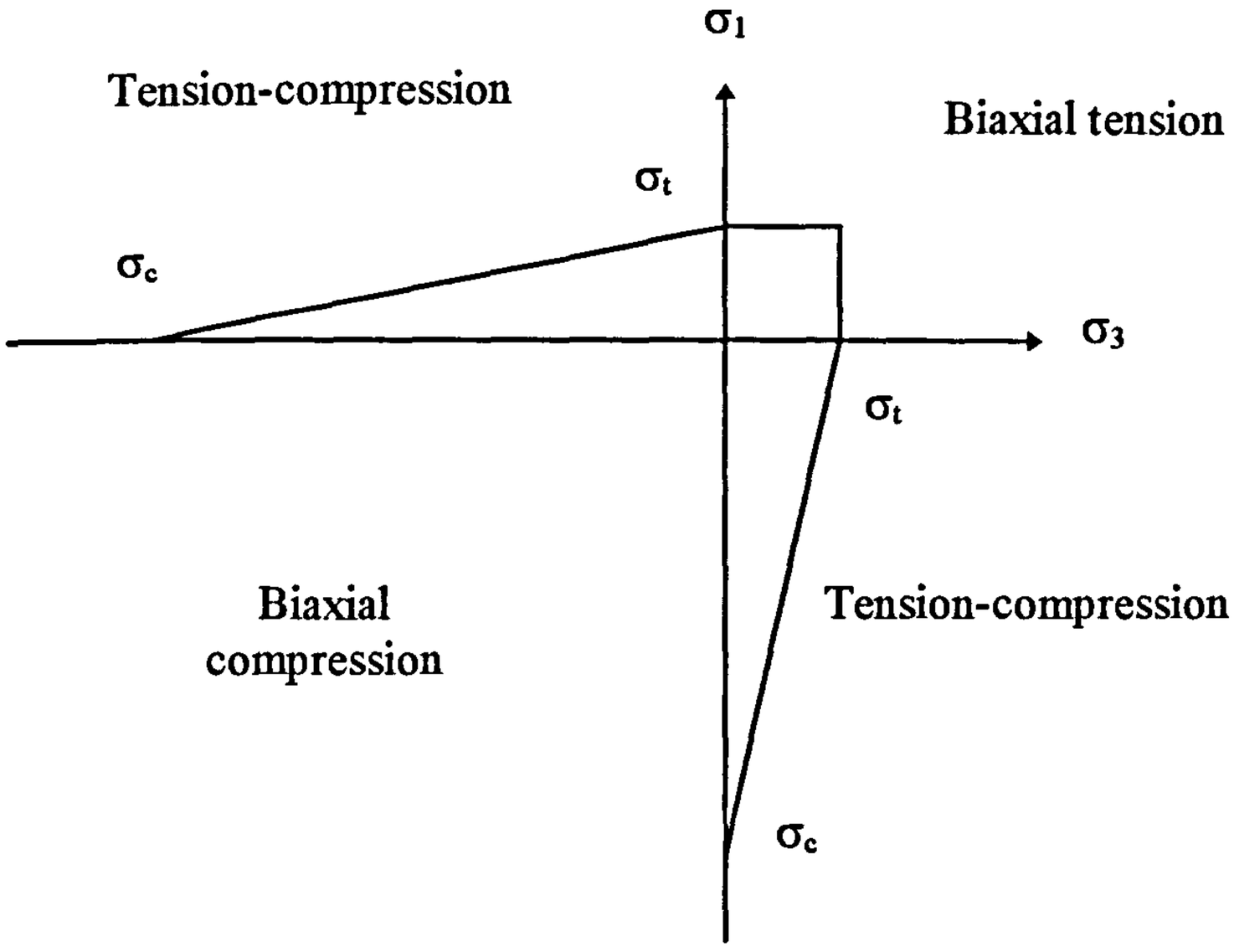

Figure 6.27 Failure envelope for biaxial concrete constitutive model

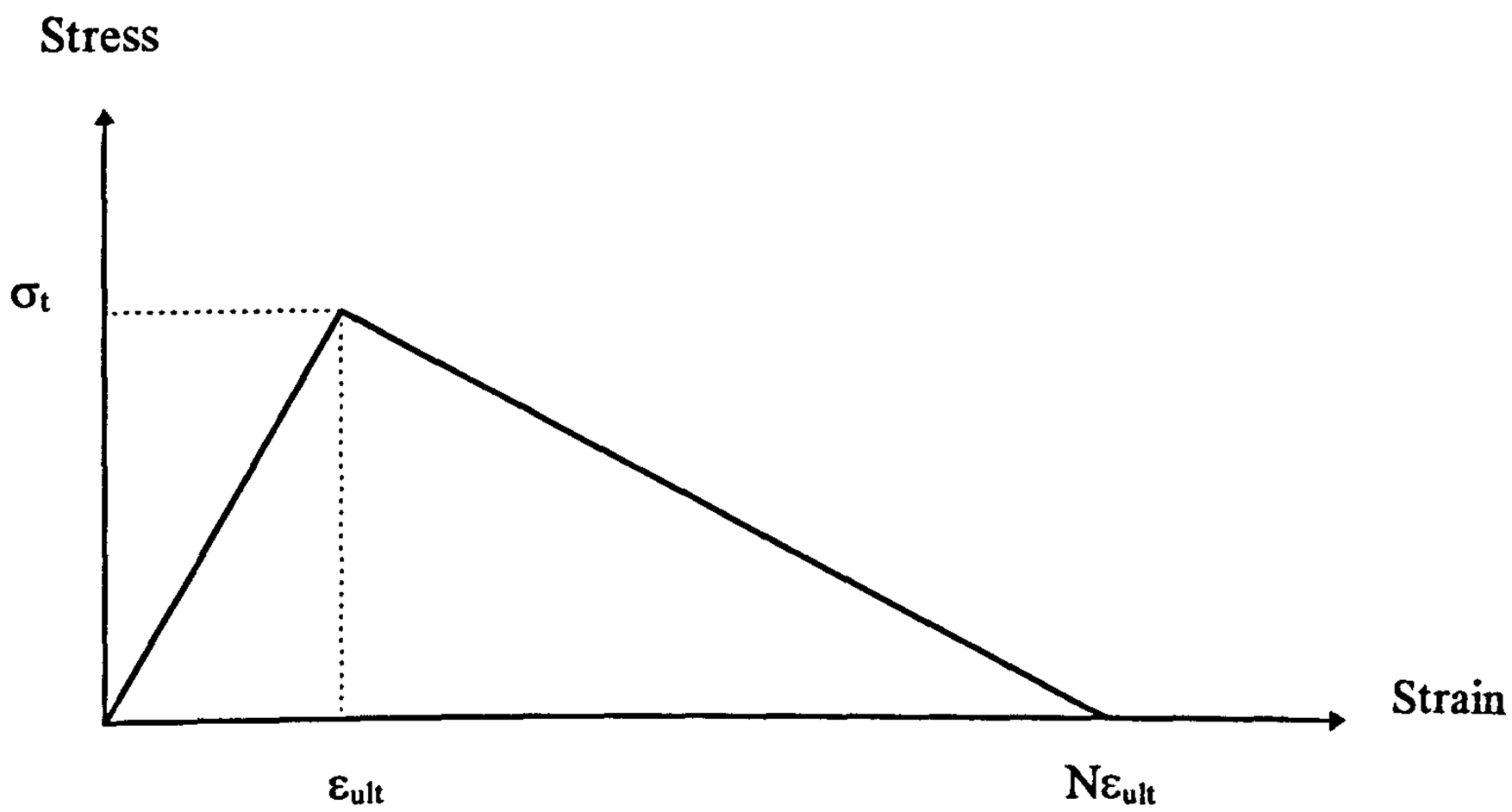

Figure 6.28 Stress-strain curve for arch material

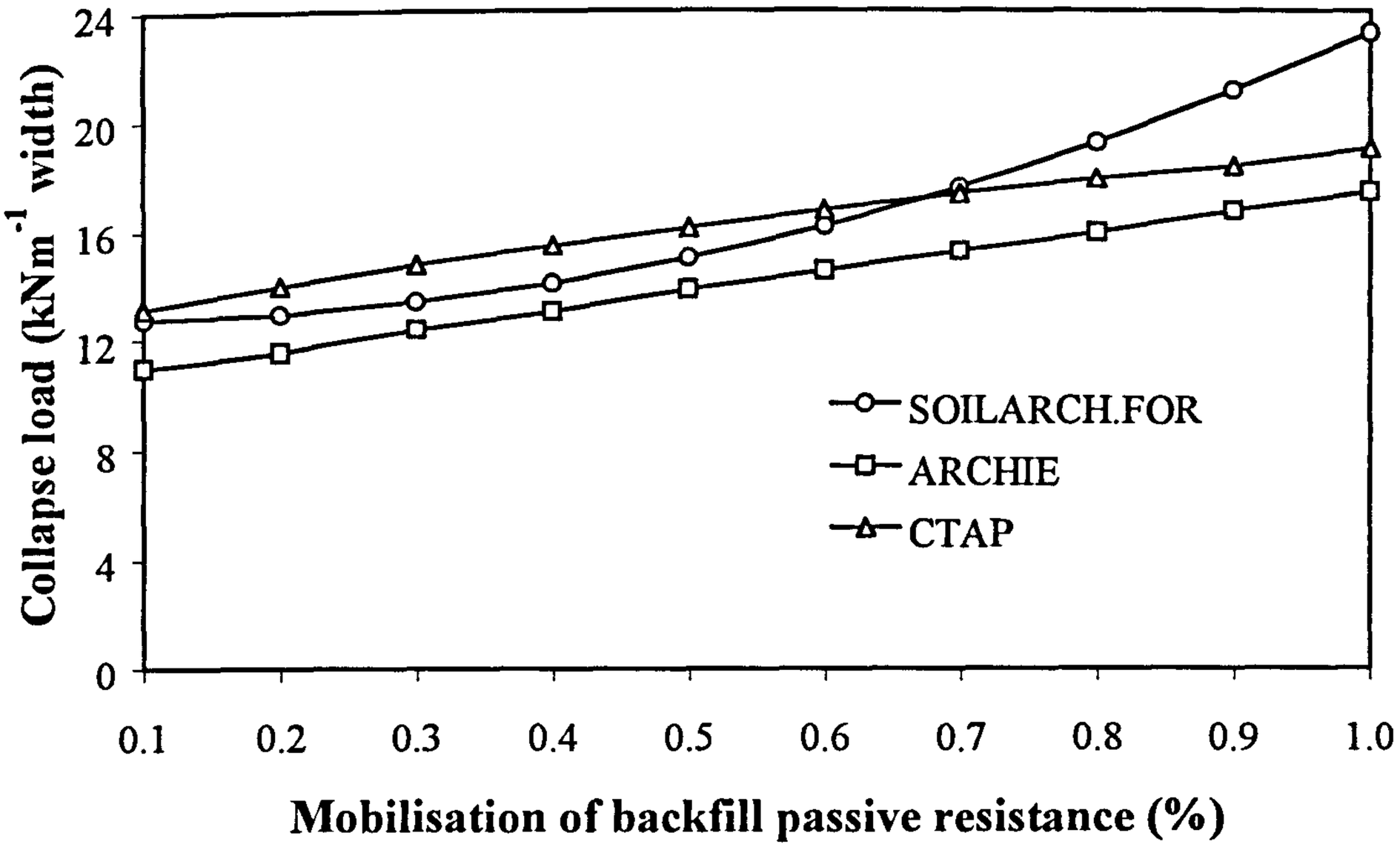

Figure 6.29 The influence of the mobilisation of backfill passive resistance

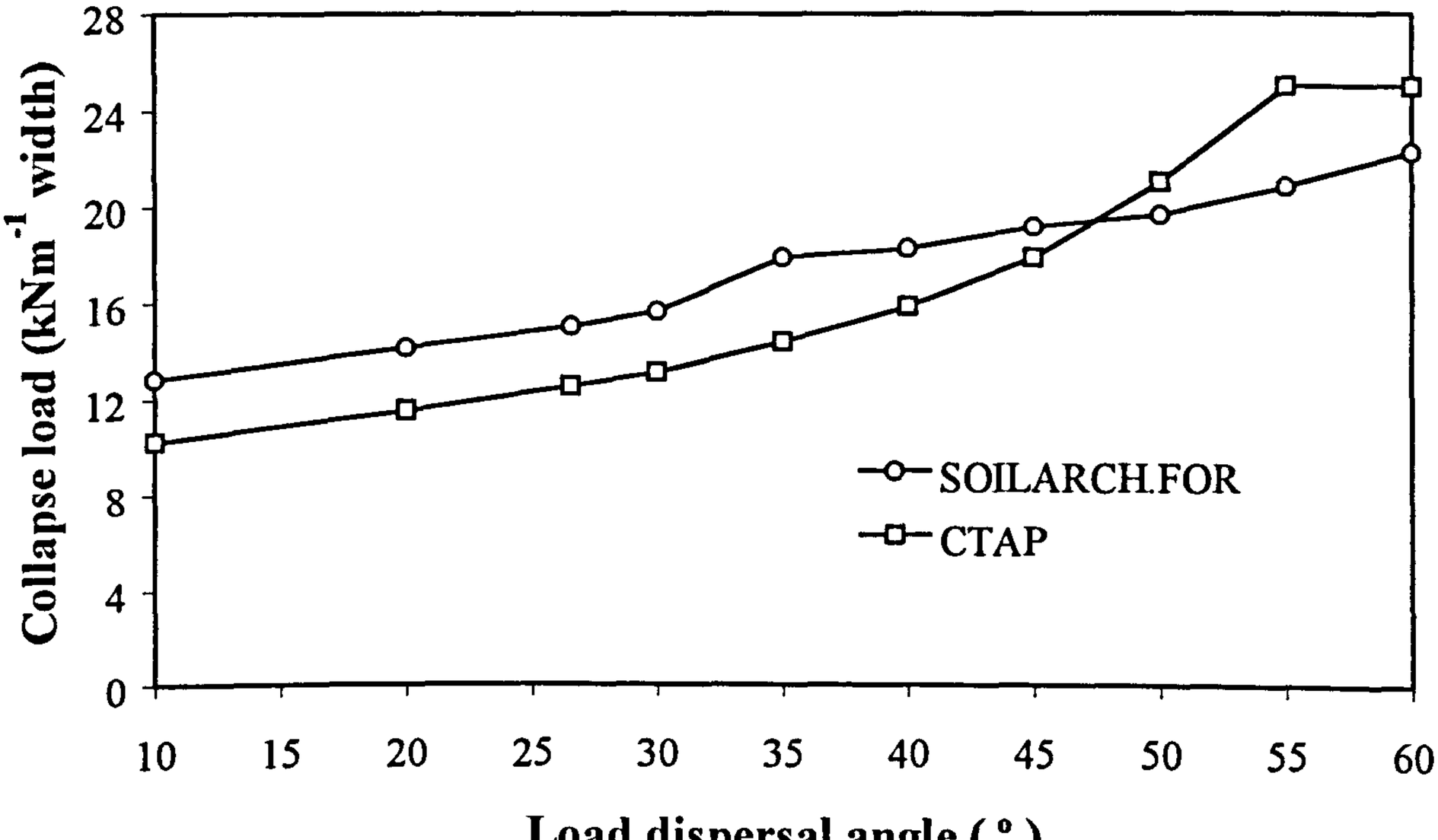

Figure 6.30 The influence of live load dispersal angle

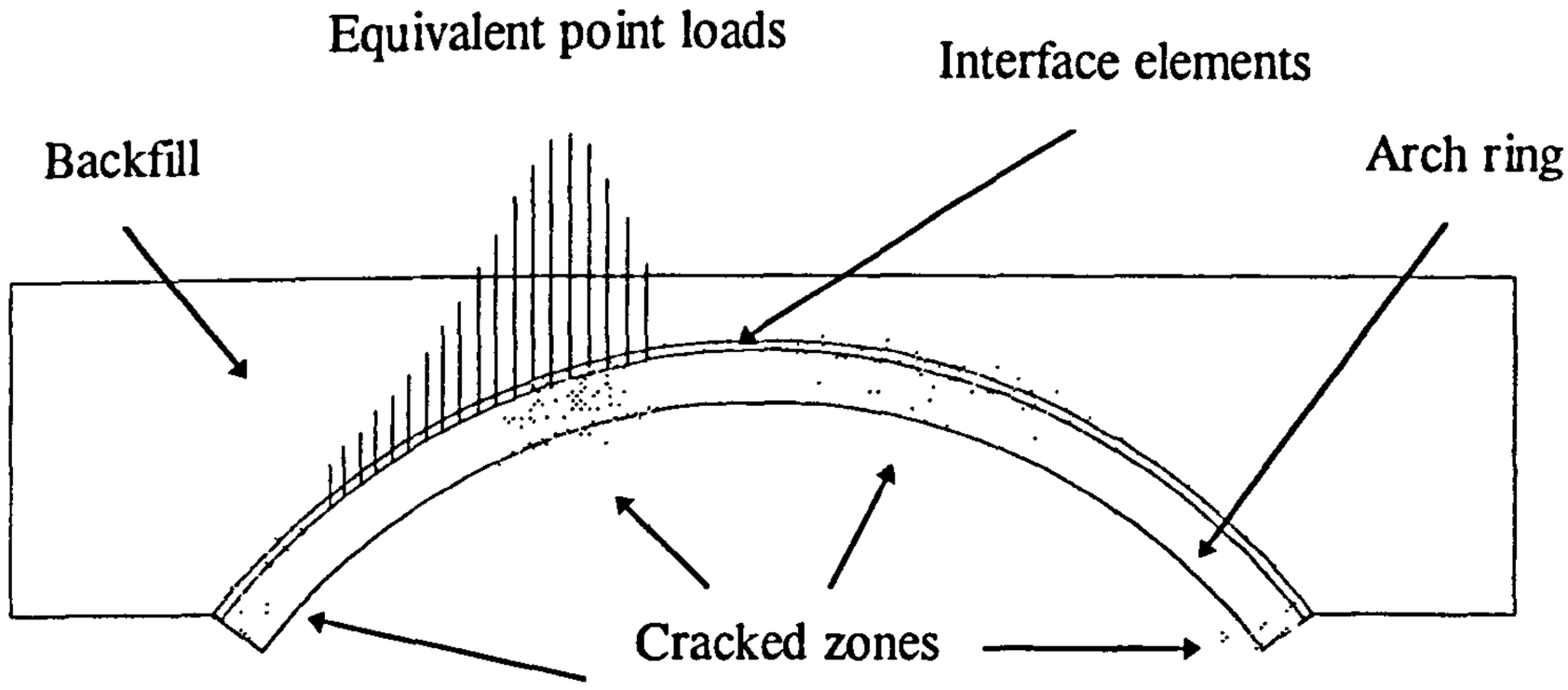

Figure 6.31 Predicted collapse mode by the FE analysis

CHAPTER 7

Risk Analysis Using Monte Carlo Simulation

7.1 Introduction

During the past few decades, many arch bridge assessment tools have been developed such as the MEXE method (BD21/97, 1997a & BA16/97, 1997b), the plastic method (HEYMAN, 1982), ARCHIE (SMITH, 1991a), CTAP (BRIDLE *et al.*, 1989) and MAFEA (CHOO *et al.*, 1990a). With the exception of the plastic method, results obtained from these methods have been used in comparison with a range of full scale arch bridge tests (BA16/97, 1997b). Reasonable correlations were achieved between the predicted and experimental results. Among all the assessment methods, MEXE and ARCHIE, a mechanism based method, have been widely used for routine assessments of arch bridges because of their ease of use.

The masonry arch bridge is a complex three dimensional structure. The complexity is mainly contributed to by soil-arch interactions and the existence of spandrel, parapet and wing walls. In most arch bridge assessment methods, the structure is idealised in a simple two dimensional plane strain condition. Soil-structure interactions are also considered in a speculative manner such as the live load dispersal angle and the lateral soil forces acting on the arch. These idealisations and assumptions have rendered the predicted results no better than educated guesses based largely on engineering judgement.

Undoubtedly, all the currently available arch bridge assessment models are idealised representations of reality and those models are therefore imperfect representations of

the real world. Furthermore, subjective judgements have to be made when determining the parameters to be used in any assessment model since arch bridges are normally imperfect in their shapes and materials are rarely homogeneous and isotropic.

All uncertainties, whether they are associated with inherent variabilities or with prediction error, may be assessed in statistical terms. The significance of such uncertainties on the assessment of these old structures can be evaluated using the concept of risk analysis.

The Monte Carlo simulation (HENLEY *et al.*, 1981) was incorporated with the mechanism and MEXE methods in this study to perform risk assessments on arch bridges. Full details of the Monte Carlo simulation are given in Section 7.3.3. All random variables used in the simulation were generated by a computer based random number generator. The Monte Carlo simulation is particularly suited to simulating complicated problems such as the mechanism method where the problem can not be reduced to a single expression unless subjected to a gross idealisation. One drawback of the Monte Carlo simulation is the processing time if a large number of iterations is required. However, with the advent of modern processors, the simulation time is significantly reduced or even made possible for more complicated problems.

Parametric studies were carried out on Barlae bridge (PAGE, 1989) using two of the author's novel risk assessment programs to study the influence of each parameter on the prediction of arch collapse load (by the mechanism method) and the allowable axle load (by the MEXE method). Besides Barlae bridge, these two assessment programs were also used to evaluate the distribution of predicted arch collapse loads or allowable axle loads for another eight bridges namely; Bridgemill (HENDRY *et al.*, 1985), Kimbolton Butts (FAIRFIELD *et al.*, 1993b), Bolton (MELBOURNE *et al.*, 1995e), Prestwood (PAGE, 1987), Bargower (HENDRY *et al.*, 1986) , Shinafoot (PAGE, 1988), Strathmashie (PAGE, 1989) and the author's large scale arch presented in Chapter 6 of this thesis. Comparisons were made with the predicted

collapse loads by the CTAP mechanism and elastic cracking methods (BRIDLE *et al.*, 1989), ARCHIE (SMITH, 1991a) and Heyman's plastic method (HEYMAN, 1982).

7.2 Statistical tests for the generated random variables

As mentioned in the introduction to this chapter, all random variables used in the Monte Carlo simulation were generated by a computer based random number generator. It is necessary to perform statistical checks on these generated random variables to determine the ability of the number generator used in this study to generate random numbers.

7.2.1 Method; statistical tests for the generated random variables

The random numbers generated in this study were based on a prescribed mean, standard deviation and the assumption that they were normally distributed. A seed number is required to determine the sequence in which the random numbers are to be generated. An identical set of random variables will then be generated if a similar seed number is used. These random numbers are therefore referred to as pseudo random numbers. It is shown later in this chapter that, provided a sufficient number of iterations is used, the statistical properties of the generated random variables remain imperceptibly changed with the use of different seed numbers.

Statistical tests, which are discussed in the following sections, were used to asses the degree of consistency between those numbers generated and those described by a theoretical normal distribution. The mean, standard deviation (S.D.), skewness and kurtosis of generated random variables were evaluated using Eqns 7.1, 7.2, 7.3 and 7.4 respectively. The term X_i refers to a random number generated at the i^{th} iteration and px_i is the probability of getting X_i which is equal to the inverse of the total number of iterations.

$$\mu = \sum_{\text{all } x_i} x_i \,.\, px_i \qquad 7.1$$

$$\sigma = \sqrt{\sum_{\text{all } x_i} (x_i - \mu)^2 \,.\, px_i} \qquad 7.2$$

$$\text{Skewness} = \sum_{\text{all } x_i} \left(\frac{x_i - \mu}{\sigma} \right)^3 \,.\, px_i \qquad 7.3$$

$$\text{Kurtosis} = \sum_{\text{all } x_i} \left(\frac{x_i - \mu}{\sigma} \right)^4 \,.\, px_i \qquad 7.4$$

Eight distributions were generated with the means, standard deviations and seeds as shown in Table 7.1. A designation was given to each distribution for later reference. Each distribution was generated with 30000 random variables.

Table 7.1 Property of each distribution

Designation	Mean	Standard deviation	Seed
A	8	2	6227269
B	40	8	1234567
C	100	12	8
D	8	2	8313
E	40	8	246810
F	100	12	875148
G	150	20	4552232
H	120	10	874000

7.2.1.1 Area under a standard normal distribution curve

A normal distribution curve can be defined using Eqn 7.5. The term $(x-\mu)/\sigma$ is called the standardised normal variate. The total area under the curve defined by Eqn 7.5 is one which refers to the total probability. The area under a standard normal distribution curve for a given value of standard normal variate can be obtained from a standard normal distribution table which can be found in most statistical text books.

$$y = \frac{1}{\sigma\sqrt{2\pi}} e^{-\frac{1}{2}\left(\frac{x-\mu}{\sigma}\right)^2} \qquad 7.5$$

How identical the distribution of the generated random variables is compared with the normal distribution can be examined by comparing the probability of obtaining a range of generated random variables with the area under the standard normal curve for a similar range of standard normal variate. The probabilities shown in Table 7.2 were those obtained from a standard normal distribution table for their respective boundaries and were used in this study for comparisons.

Table 7.2 Probability under enclosed boundaries

Boundaries	Probability
$\mu - 1.96\sigma < x \leq \mu + 1.96\sigma$	95%
$\mu - 2.58\sigma < x \leq \mu + 2.58\sigma$	99%
$\mu - 3.29\sigma < x \leq \mu + 3.29\sigma$	99.9%

7.2.1.2 Goodness-of-fit method

Another method used in this study to test the normality of the distribution of generated random variables is known as the goodness-of-fit method (DEVORE *et al.*, 1993). This method is carried out by evaluating the magnitude of the discrepancies between generated random variables and those expected according to a particular distribution. The magnitude of discrepancy is defined in Eqn 7.6 and is called the goodness-of-fit statistic denoted by χ^2.

$$\chi^2 = \frac{(\text{Generated count} - \text{Expected count})^2}{\text{Expected count}} \qquad 7.6$$

In general, with the number of observations in each interval of a distribution not less than five, the goodness-of-fit statistic has approximately a chi-squared distribution with K - 1 degrees of freedom (D.O.F); K denotes the total number of intervals. If the

number of observations in an interval is less than five, the adjacent interval should be combined resulting in the loss of a D.O.F. The next step involves formulation of hypotheses. In this case the null hypothesis (H_o) is;

"the generated random variables are normally distributed with specified values of mean and standard deviation"

The alternative hypothesis is that H_o is false. A significance level is then chosen and the critical chi-squared value corresponding to the degree of freedom for a test can be obtained from a chi-squared distribution table (available in most statistics text books). The null hypothesis is accepted if the sum of the chi-squared values evaluated from Eqn 7.6 is less than the critical chi-squared value. It is generally assumed that a significance level lies between 0.01 to 0.05. In this study, a significance level of 0.025 is chosen for all tests described in this section.

7.2.1.3 First-order second-moment (FOSM) method

This method has been widely used in reliability analyses to determine the probability of failure and was first described by CORNELL (1969). For a given distribution of resistance R with a mean (μ_R) and standard deviation (σ_R), and a distribution of stress S with a mean (μ_S) and standard deviation (σ_S), a limit state function can be defined as shown in Eqn 7.7

$$Z = R - S \qquad 7.7$$

If R and S are normally distributed, then Z will also be normally distributed with the mean (μ_Z) and standard deviation (σ_Z) as shown in Eqns 7.8 and 7.9 respectively.

$$\mu_Z = \mu_R - \mu_S \qquad 7.8$$

$$\sigma_Z = \sqrt{\sigma_R^2 + \sigma_S^2} \qquad 7.9$$

The probability of failure is the overlapped area between the distribution of R and S and could be evaluated using Eqn 7.10.

$$P_F = 1 - \Phi\left(\frac{\mu_R - \mu_S}{\sqrt{\sigma_R^2 + \sigma_S^2}}\right) \qquad 7.10$$

In order to perform this test, two sets of random variables (data G & H) were generated as shown in Section 7.2. The normality of each distribution was examined using the procedures described in Sections 7.2.1 and 7.2.2. This was then followed by the evaluation of G - H which represented the probability of failure. If G & H are normally distributed, the generated distribution of G - H will also have a mean and standard deviation similar to those evaluated using Eqns 7.8 & 7.9 respectively. Furthermore, the distribution of generated G - H data should also be normal.

7.2.2 Results; statistical tests for the generated random variables

Eight proposed normal distributions, with their properties as shown in Table 7.1, were generated. The test procedures described in Sections 7.2.1.1 and 7.2.1.2 were used to check the normality of these generated distributions. The FOSM method was performed by subtracting data H from G. The resulting distribution (G - H) was again checked for normality under the procedures described in Sections 7.2.1.1 and 7.2.1.2. Table 7.3 shows the properties of the generated distributions with designations from A to H.

Referring to Table 7.3 and 7.1, it can be seen that those generated means and standard deviations of all distributions were almost identical to those proposed. The skewness of all generated distributions were found to be very small which indicated a symmetrical distribution. The influence of the seed number on the generation of random variables is shown in Figures 7.1 and 7.2. Only the first 1000 iterations from each distribution (A to F) were plotted so as to clearly demonstrate the variation in the sequence in which those random variables were generated. It could be seen from

Figures 7.1 and 7.2 that the random patterns of all distributions, generated with different seed numbers, were not identical to each other. However, since the number of iterations used to define each distribution was sufficiently large (30000 iterations in this case), the generated means and standard deviations appeared to have been insignificantly influenced by the use of different seed numbers as can be seen from Table 7.3.

Table 7.3 Properties of the generated random variables

Designation	Generated μ	Generated σ	Skewness	Kurtosis
A	8.003	2.010	-0.04182	2.953
B	40.015	8.072	0.00083	2.918
C	100.020	12.053	0.01332	2.932
D	8.003	2.005	-0.00615	2.922
E	40.011	8.005	-0.00248	2.919
F	99.935	12.057	-0.01268	2.946
G	150.076	20.109	0.02512	2.950
H	119.996	9.986	-0.02446	2.948

For a qualitative check on the normality of those generated distributions (A to F), each distribution is presented. Figures 7.3, 7.4 and 7.5 present the generated distributions with designations A & D, B & E, and C & F respectively. Each plot consists of two generated distributions with different seed numbers each with a similar proposed mean and standard deviation. For ease of comparison, a theoretical normal distribution was also included. At no point in Figures 7.3 to 7.5 inclusive did any discrepancy seem to be perceptible. Table 7.4 shows the results of the test, described in Section 7.2.1.1, for all generated distributions.

Results shown in Table 7.4 revealed that the probabilities within prescribed boundaries from those generated distributions were reasonably close to those obtained from a theoretical normal distribution. This suggested that those generated distributions were close to a normal distribution.

Table 7.4 Probabilities within confined boundaries

Designation	$\mu-1.96\sigma < x \leq \mu+1.96\sigma$	$\mu-2.58\sigma < x \leq \mu+2.58\sigma$	$\mu-3.29\sigma < x \leq \mu+3.29\sigma$
A	95.070	98.923	99.920
B	94.927	99.023	99.903
C	94.974	99.044	99.913
D	95.007	99.070	99.930
E	95.207	99.090	99.920
F	94.924	99.070	99.906
G	94.907	99.030	99.920
H	95.070	99.080	99.923

Table 7.5 presents the results from the goodness-of-fit method performed on all generated distributions. The critical χ^2 is obtained from a standard chi-squared distribution table with a significance level of 0.025. The D.O.F is defined as K - 1 where K is the total number of intervals where each interval consists of at least five observations.

Table 7.5 Results from the goodness-of-fit method

Designation	D.O.F	Critical χ^2	Generated χ^2	Null hypothesis
A	18	31.500	25.722	Accepted
B	18	31.500	28.953	Accepted
C	18	31.500	29.196	Accepted
D	19	32.900	25.871	Accepted
E	19	32.900	21.041	Accepted
F	19	32.900	24.616	Accepted
G	19	32.900	25.975	Accepted
H	19	32.900	12.282	Accepted

Referring to Table 7.5, it can be seen that the null hypothesis for each test was accepted which indicated that those generated random variables were normally distributed at a significance level of 0.025.

Figure 7.6 shows the distributions of G and H. The overlapped area represents the probability of failure. However, since the interval width of each distribution is not identical, a quantitative evaluation of the probability of failure could not be performed directly by calculating the area of the overlapped zone. The generated probability of

failure was obtained by dividing the total negative observations by the total number of iterations. Figure 7.7 shows the distribution of G - H. The area below the vertical line located at zero, on the horizontal axis, represents the probability of failure. The properties of the generated G - H distribution and the results from all statistical tests for normality, described in Sections 7.2.1.1 to 7.2.1.3 inclusive, are presented in Table 7.6.

Table 7.6 Properties of the G - H distribution

Properties	Generated	Theoretical
Mean	30.079	30.000
Standard deviation	22.465	22.361
Probability of failure	9.09%	9.010%
$\mu - 1.96\sigma < x \leq \mu + 1.96\sigma$	95.024%	95%
$\mu - 2.58\sigma < x \leq \mu + 2.58\sigma$	99.103%	99%
$\mu - 3.29\sigma < x \leq \mu + 3.29\sigma$	99.910%	99.9%
Properties	Generated	
D.O.F	17	
χ^2	27.943	
Critical χ^2	30.200	
Null hypothesis	Accepted	

Table 7.6 shows the results of the tests carried out on the G - H distribution. The theoretical mean, standard deviation and the probability of failure were evaluated using Eqns 7.8, 7.9 and 7.10 respectively. The generated probability of failure is found to be only 0.888% higher than that evaluated theoretically. The null hypothesis, that the distribution is normal, was also accepted from the goodness-of-fit at a significance level of 0.025.

7.2.3 Discussion; statistical tests for the generated random variables

The tests described in Sections 7.2.1.1 to 7.2.1.3 inclusive were used to test the normality of each generated distribution. All tests confirmed that the author's

generated distributions were in close agreement with the normal distribution. The use of different seed numbers for the random number generator was found to have only varied the sequence in which the random variables were generated without significantly affecting the global parameters of the generated distribution such as the mean and standard deviation.

The goodness-of-fit tests performed on all generated distributions revealed that all distributions were normally distributed at a significance level of 0.025. If a larger value of significance level was adopted, some distributions might eventually fail to be accepted as normally distributed. However, as can be seen from the results of the tests, described in Sections 7.2.1.1 and 7.2.1.3, all generated distributions were in good agreement with a normal distribution.

In real life, it is highly unlikely to have a distribution which is exactly normally distributed with a χ^2 of zero. It is more appropriate to say that the distribution, such as the one associated with measurement errors, is 'somewhat' normal from a practical point of view. It is neither the purpose of this study nor is it necessary to generate a perfect normal distribution. The Monte Carlo simulation requires random variables which are 'randomly' generated with the generated mean, standard deviation and shape of the distribution being in reasonable agreement with those proposed. It has been clearly shown in Section 7.2 that the current adopted random number generator has met this requirement.

7.3 Methods; arch bridge assessment

Two arch bridge assessment methods namely the mechanism and MEXE methods were integrated with the Monte Carlo simulation to perform risk analysis on arch bridges. These two methods have been coded by the author (MCMECH.FOR, for the mechanism method, and MCMEXE.FOR, for the MEXE method) in FORTRAN 77. These programs start by generating the random variables, followed by the evaluation of

arch collapse loads or allowable axle loads. Finally the programs carry out statistical analyses on the derived results. A brief derivation of the mechanism method is given in Section 7.3.1 and the MEXE method, although introduced in the literature review of this thesis, is discussed in more detail in Section 7.3.2 for the sake of completeness.

7.3.1 The mechanism method

Masonry arches are statically indeterminate structures which become determinate when three hinges are formed in the arch ring due to cracking. In this method, the arch was assumed to be on the verge of collapse under a single axle load located at somewhere near the quarter span of the arch. Four hinge positions were selected iteratively to search for the minimum collapse load whilst still fully containing the thrustline within the arch ring. Referring to Figure 7.8, the arch is at its ultimate limit state and there are four hinges in the arch ring at points A, B, C and D. There are three unknowns in this case; the collapse load, and the vertical and horizontal support reactions. By taking moments about points A, B and C, three equilibrium equations (Eqns 7.11 to 7.13) can be derived.

$$R_{RV}\left[X^{D}-X^{C}\right]=R_{RH}\left[Y_{IN}^{C}-Y_{EX}^{D}\right]+\sum_{n=C}^{D}\left[W_{FILL}^{n}+W_{V}^{n}\right]\left[X^{n}-X^{C}\right]+\sum_{n=C}^{D}W_{PAS}^{n}\left[Y_{IN}^{C}-Y_{EX}^{n}\right] \qquad 7.11$$

$$R_{RV}\left[X^{D}-X^{B}\right]=R_{RH}\left[Y_{EX}^{B}-Y_{EX}^{D}\right]+\sum_{n=B}^{D}\left[W_{FILL}^{n}+W_{V}^{n}+W_{PL}^{n}\right]\left[X^{n}-X^{B}\right]+\sum_{n=B}^{D}\left[W_{PAS}^{n}-W_{ACT}^{n}\right]\left[Y_{EX}^{B}-Y_{EX}^{n}\right] \qquad 7.12$$

$$R_{RV}\left[X^{D}-X^{A}\right]=-R_{RH}\left[Y_{EX}^{D}-Y_{IN}^{A}\right]+\sum_{n=A}^{D}\left[W_{FILL}^{n}+W_{V}^{n}+W_{PL}^{n}\right]\left[X^{n}-X^{A}\right]+\sum_{n=A}^{D}\left[W_{ACT}^{n}-W_{PAS}^{n}\right]\left[Y_{EX}^{n}-Y_{IN}^{A}\right] \qquad 7.13$$

By introducing Eqn 7.14 and Eqn 7.15, Eqns 7.11 to 7.13 can be simplified to the matrix form shown in Eqn 7.16. The three unknowns can then be found explicitly by solving the matrix. The thrustline is then drawn along the arch ring using the conventional static equilibrium method.

$$\sum_{n=A}^{D} \left| I_n \right|_{\theta^n \le \theta} = I_p \qquad 7.14$$

$$W_{PL}^{n} = F \times \sum_{n=B}^{D} \frac{\left| I_n \right|_{\theta^n \le \theta}}{I_p} \times \left[X^n - X^B \right] \qquad 7.15$$

$$\begin{bmatrix} R_{RV} \\ R_{RH} \\ F \end{bmatrix} \begin{bmatrix} \left[X^D - X^A \right] & \left[Y_{EX}^D - Y_{IN}^A \right] & -\sum_{n=A}^{D} \frac{\left| I_n \right|_{\theta^n \le \theta}}{I_p} \left[X^n - X^A \right] \\ \left[X^D - X^C \right] & -\left[Y_{IN}^C - Y_{EX}^D \right] & 0 \\ \left[X^D - X^B \right] & -\left[Y_{EX}^B - Y_{EX}^D \right] & -\sum_{n=B}^{D} \frac{\left| I_n \right|_{\theta^n \le \theta}}{I_p} \left[X^n - X^B \right] \end{bmatrix}$$

$$= \begin{bmatrix} \sum_{n=A}^{D} \left[W_{FILL}^n + W_V^n \right] \left[X^n - X^A \right] + \sum_{n=A}^{D} \left[W_{ACT}^n - W_{PAS}^n \right] \left[Y_{EX}^n - Y_{IN}^A \right] \\ \sum_{n=C}^{D} \left[W_{FILL}^n + W_V^n \right] \left[X^n - X^C \right] + \sum_{n=C}^{D} W_{PAS}^n \left[Y_{IN}^C - Y_{EX}^n \right] \\ \sum_{n=B}^{D} \left[W_{FILL}^n + W_V^n \right] \left[X^n - X^B \right] + \sum_{n=B}^{D} \left[W_{PAS}^n - W_{ACT}^n \right] \left[Y_{EX}^B - Y_{EX}^n \right] \end{bmatrix} \qquad 7.16$$

There are thirteen variables in the mechanism method. They are the arch's span, rise, ring thickness, fill depth over the crown, centreline co-ordinate of the load platen, width of load platen, backfill and arch bulk unit weights, backfill active and passive pressure coefficients, backfill angle of shearing resistance, number of arch segments, and the live load dispersal angle or Boussinesq's limiting live load influence factor.

7.3.2 The MEXE method

This method was derived by the Military Engineering Experimental Establishment based on the work done by PIPPARD *et al.* (1936) and is currently recommended by the Department of Transport for the assessment of arch bridges. An empirical equation is used to calculate the provisional axle load involving only the span, ring thickness and the depth of fill at the crown. The provisional axle load is then to be modified by various modification factors for span to rise ratios other than four, material factors for fill, joints and arch ring, factors for depth and thickness of mortar, and a condition factor for the overall condition of the arch. The empirical equation together with its modification factors is expressed in Eqn 7.17. The product of the provisional axle load and the modification factors gives the modified double axle load which is converted to an allowable single axle load based on the span of the arch.

$$\text{Modified axle load} = \frac{740(d+h)^2}{L^{1.3}} \times F_{sr} \times F_p \times F_m \times F_j \times F_o \qquad 7.17$$

The material and joint factors are evaluated using Eqns 7.18 and 7.19 respectively.

$$F_m = \frac{F_b \times d + F_f \times h}{d + h} \qquad 7.18$$

$$F_j = F_w \times F_d \times F_{mo} \qquad 7.19$$

7.3.3 The Monte Carlo simulation

In the current Monte Carlo simulation, all or part of the input variables were generated randomly and subsequently used as input variables for the mechanism or the MEXE method. As the result, the evaluated arch collapse loads or the allowable axle loads can also be expressed in the form of a distribution. In this study, each variable was

generated from a Gaussian or normal distribution with a prescribed mean and coefficient of variation. It will be shown later in this chapter that 5000 iterations are normally sufficient to achieve a converged result. The coefficient of variations of all input variables were assumed to be the same at any one time. However, it is possible to use different coefficient of variation for each input variable in the author's Monte Carlo programs.

Measures were also taken to prevent the random variables being generated beyond reasonable practical ranges. Referring to Figure 7.9, two limits were set in such a way that the probability of the shaded area on each side was equal to a prescribed limit. This limit was subsequently referred to as the variable end limit.

The final part of the analysis consists of a series of statistical evaluations of the generated results in terms of mean, standard deviation, skewness, kurtosis, maximum and minimum. The probability of failure or the probability of over estimating the arch collapse load was also evaluated in this analysis.

Unless otherwise stated in the text, the number of iterations, seed number, coefficient of variation and variable end limit used in all analyses were 30000, 773311, 3% and 3% respectively. Apart from all the variables considered in this simulation, parametric studies were also carried out to determine the influence of the seed for random number generation, the number of iterations and also the variable end limit.

7.4 Barlae bridge

Barlae was an ashlar masonry arch with a 29° skew angle which was tested to collapse by the Transport Research Laboratory (PAGE, 1989). No major defects were found on the bridge before applying load by a transverse, 750mm width, line load at the ¼-span. The ultimate load recorded was 296kNm^{-1} width perpendicular to the span. The arch span, rise at the crown, ring thickness and fill depth over the crown were

9197.5mm, 1695mm, 450mm and 295mm respectively. Since the arch was skewed, there was no clear indication as to how the arch span is to be considered in the current two dimensional analysis. In this study the arch span was taken as 9197.5mm which is the average of the shortest and longest distances measured square along the bridge. A parametric study was also carried out by considering the shortest and longest spans of the arch. Apart from the arch geometry just mentioned, additional mean input variables for the mechanism and MEXE methods are given in Tables 7.7 and 7.8 respectively.

Table 7.7 Mean input variables for the mechanism method (Barlae)

Width of the load platen	750mm
Centre line of the load platen	2299mm
Backfill active pressure coefficient	0.8
Backfill passive pressure coefficient	0.5
Backfill bulk unit weight	20 kNm^{-3}
Arch bulk unit weight	23 kNm^{-3}
Backfill angle of shearing resistance	35°
Load dispersal angle	35°

Table 7.8 Mean input variables for the MEXE method (Barlae)

Barrel factor	1.30
Fill factor	0.70
Width factor	0.90
Depth factor	0.85
Mortar factor	0.95
Condition factor	0.80

7.5 Results; Barlae bridge

This section presents the results obtained from the computer programs MCMECH.FOR and MCMEXE.FOR on Barlae bridge. For the sake of clarity, the results from each method are presented in separate sections. Statistical tests on the normality of the generated results from both methods are presented in Section 7.6.

7.5.1 Monte Carlo simulation; the mechanism method

This section presents results from the Monte Carlo simulation with the mechanism method. Data from each parametric study is presented in separate subsections. A total of thirteen variables were investigated and they were the coefficient of variation, seed for random number generator, arch span, number of segments, live load dispersal angle, number of iterations, backfill and arch bulk unit weights, backfill active and passive pressure coefficients, backfill angle of shearing resistance, variable end limit and Boussinesq's limiting live load influence factor.

A summary of statistical properties of the predicted arch collapse load such as the mean, standard deviation, skewness, kurtosis, maximum and minimum, and also the probability of failure will be given in Table 7.9.

7.5.1.1 Standard results

Figure 7.10 shows the result obtained from the Monte Carlo simulation for the mechanism method using variables stated in Table 7.7. A classical bell shaped distribution was obtained. The full scale test on Barlae arch revealed that the arch collapsed at 296kNm^{-1}. Referring to Figure 7.10, the shaded region represents the probability of overestimating the arch collapse load; here this amounted to 11.8%.

For the statistical properties of the predicted arch collapse load, the mean, standard deviation, skewness, kurtosis, maximum and minimum were 265.1kNm^{-1}, 18.2kNm^{-1}, 0.211, 2.754, 332.4kNm^{-1} and 213.1kNm^{-1} respectively.

Figure 7.11 shows the results obtained from current Monte Carlo simulation for the mechanism method. Comparisons were also made with the actual arch collapse load and that predicted by CTAP mechanism, CTAP elastic cracking, ARCHIE and Heyman's plastic methods. A compressive strength of 8MPa was assigned to the arch

ring in the CTAP mechanism method and ARCHIE. The actual arch collapse load was also included for comparison. The mean arch collapse load for the current Monte Carlo simulation was 265.6kNm^{-1} which was 10.3% lower than the actual arch collapse load of 296kNm^{-1}. The CTAP mechanism, CTAP elastic cracking, ARCHIE and Heyman's plastic methods predicted a collapse load of 308kNm^{-1}, 235kNm^{-1}, 190kNm^{-1} and 230kNm^{-1} respectively.

Figures 7.12 to 7.15 show the distribution of left abutment vertical reaction (mean = 348.0kNm^{-1}, standard deviation = 21.6kNm^{-1}), right abutment vertical reaction (mean = 166.7kNm^{-1}, standard deviation = 7.3kNm^{-1}), left abutment horizontal reaction (mean = 346.8kNm^{-1}, standard deviation = 27.8kNm^{-1}), and right abutment horizontal reaction (mean = 317.0kNm^{-1}, standard deviation = 28.1kNm^{-1}) respectively.

7.5.1.2. The effect of varying the coefficient of variation of the input variables

Figure 7.16 shows the effect of varying the coefficient of variation of every input parameter stated in Section 7.3.1 on the prediction of arch collapse load. The analysis was carried out with coefficient of variation of 2%, 3%, 4% and 5%. It is clear from Figure 7.16 that the larger the coefficient of variation, the wider the spread in predicted capacity distribution. By increasing the coefficient of variation from 2% to 5% the predicted mean collapse load rose from 265.1kNm^{-1} to 270.2kNm^{-1}. Similarly, the standard deviation of the predicted arch collapse load increased from 18.2kNm^{-1} to 41.5kNm^{-1}. The probability of failure also increased from 5.13% to 24.7% due to a wider spread of predicted collapse loads.

7.5.1.3 The effect of varying the seed for the random number generator

Figure 7.17 shows the results from the Monte Carlo simulation for the mechanism method by varying the seed for the random number generator. The seeds adopted for this parametric study were 819, 773311 and 4552466. Referring to Figure 7.17, it is clear that at no point did the results seem to be different from each other. From Table 7.9, it is also apparent that the statistical properties of the predicted arch collapse load remain practically unchanged.

7.5.1.4 The effect of varying the arch span

As mentioned in Section 7.4, Barlae bridge had a 29° skew. This study assumed that the arch was under two dimensional plane strain conditions. The arch span was undefined for such an idealisation. The longest and shortest longitudinal distances measured along the arch span were 9865mm and 8530mm respectively. A parametric study was carried out with the spans of 8530mm, 9197.5mm and 9865mm, and the results are presented in Figure 7.18. By increasing the arch span from 8530mm to 9865mm, the predicted mean collapse load reduced from 275.9kNm^{-1} to 260.3kNm^{-1}. Similarly, the predicted standard deviation of the collapse load fell from 27.6kNm^{-1} to 23.1kNm^{-1}. Such an increase in span also reduced the probability of failure from 22.6% to 6.90%.

7.5.1.5 The effect of varying the number of arch segments

Figure 7.19 shows the effect of varying the number of arch segments on the prediction of arch collapse load. The numbers of arch segments used in this parametric study were; 20, 40, 60, 80 and 100. From Figure 7.19, it can be seen that the results

converged when the number of arch segments was 40 or greater. By increasing the number of arch segments from 20 to 100, the predicted mean collapse load increased from 257.3kNm^{-1} to 268.2kNm^{-1}. Similarly, the predicted standard deviation of the arch collapse load increased from 22.9kNm^{-1} to 23.9kNm^{-1}. The probability of failure increased from 5.30% to 12.8% for same increase in the number of arch segments.

Increasing the number of arch segment had a significant influence on the processing time as shown by Figure 7.20. Increasing the number of arch segments from 20 to 100 increased the processing time *per* 100 iterations from 3.2 seconds to 200 seconds on a 100MHz Pentium based computer.

7.5.1.6 The effect of varying the live load dispersal angle

Figure 7.21 shows the effect of varying the live load dispersal angle on the collapse load prediction. The live load dispersal angles used in this parametric study were 30°, 35° and 40° from each side of the loaded area's edge. By increasing the load dispersal angle from 30° to 40°, the predicted mean collapse load increased from 254.2kNm^{-1} to 282.9kNm^{-1}. Similarly, the standard deviation of the predicted collapse load increased from 23.4kNm^{-1} to 26.7kNm^{-1}. The same increase in load dispersal angle increased the probability of failure from 4.69% to 30.2%.

7.5.1.7 The effect of varying the number of iterations

Figure 7.22 shows the effect of varying the number of iterations on the prediction of arch collapse load. The numbers of iteration used in this parametric study were 50, 100, 500, 5000, 30000 and 50000. Referring to Figure 7.22, it can be seen that the influence of the number of iteration becomes insignificant for 500 or more iterations. For the sake of clarity, the distributions of the predicted collapse load associated with 50, 500, 30000 and 50000 iterations are shown in Figures 7.23 to 7.26. It is clear from

these figures that the larger the number of iterations, the better will be the shape of the distribution.

By increasing the number of iterations from 50 to 50000, the predicted mean collapse load fell from 276.2kNm^{-1} to 265.7kNm^{-1}. Similarly, the standard deviation of the predicted collapse load fell from 32.2kNm^{-1} to 24.8kNm^{-1}. The probability of failure fell from 26.0% to 11.9%.

7.5.1.8 The effect of varying the backfill bulk unit weight

Figure 7.27 shows the effect of varying the backfill bulk unit weight on the prediction of arch collapse load. The parametric study was carried out with backfill bulk unit weights of 18kNm^{-3}, 20kNm^{-3} and 22kNm^{-3}. It is clear from Figure 7.27 that the backfill bulk unit weight had a significant influence on the prediction of arch collapse load. With an increase in backfill bulk unit weight from 18kNm^{-3} to 22kNm^{-3}, the predicted mean collapse load rose from 250.7kNm^{-1} to 280.5kNm^{-1}. Similarly, the predicted standard deviation of the arch collapse load increased from 23.5kNm^{-1} to 26.2kNm^{-1} whilst the failure probability increased from 3.55% to 27.0%.

7.5.1.9 The effect of varying the arch bulk unit weight

Figure 7.28 shows the effect of varying the arch bulk unit weight on the prediction of arch collapse load. Three different arch bulk unit weights were used in this parametric study: 21kNm^{-3}, 23kNm^{-3} and 25kNm^{-3}. Referring to Figure 7.28, it is apparent that the arch bulk unit weight had a significant influence on the prediction of arch collapse load. By increasing the arch bulk unit weight from 21kNm^{-3} to 25kNm^{-3}, the predicted mean collapse load was found to increase from 255.5kNm^{-1} to 275.8kNm^{-1}. The standard deviation of the predicted collapse load also increased from 23.9kNm^{-1} to

25.9kNm^{-1}. The same increase caused the failure probability to rise from 5.44% to 21.6%.

7.5.1.10 The effect of varying the backfill active pressure mobilisation

Figure 7.29 shows the effect of varying the backfill active pressure mobilisation on the prediction of arch collapse load. The backfill active pressure coefficients used in this parametric study were the traditional Rankine coefficients. The percentages of this active pressure which were permitted to be mobilised were 60%, 80%, and 90%. There was no noticeable influence on the predicted results. The mean, standard deviation, and failure probability remained unchanged throughout this part of the parametric study.

7.5.1.11 The effect of varying backfill passive pressure mobilisation

Figure 7.30 shows the effect of varying the backfill passive pressure mobilisation on the prediction of arch collapse load. The passive pressure coefficients used in this parametric study were Rankine's values given by the reciprocal of his active pressure coefficients as described in Section 7.5.1.10. The percentages of full passive pressure permitted to be mobilised were 30%, 50%, and 70%. The backfill passive pressure significantly influenced the capacity predictions. Increasing the percentage of full backfill passive pressure mobilised from 30% to 70% caused the predicted mean collapse load to increase from 248.1kNm^{-1} to 293.3kNm^{-1}. Its standard deviation increased from 23.7kNm^{-1} to 27.2kNm^{-1}. This increase in the backfill passive pressure significantly increased the probability of failure from 2.97% to 44.0%.

7.5.1.12 The effect of varying the backfill angle of shearing resistance

Figure 7.31 shows the effect of varying the backfill angle of shearing resistance on the prediction of arch collapse load. The backfill angles of shearing resistance used in this parametric study were 30°, 35°, 40° and 50°. It could be seen from Figure 7.31 that the backfill angle of shearing resistance had an influence on the predicted arch collapse load especially at higher angles. By increasing the backfill angle of shearing resistance from 30° to 50°, the predicted mean collapse load increased from 259.7kNm^{-1} to 298.9kNm^{-1}. Similarly, the standard deviation of the predicted collapse load increased from 24.7kNm^{-1} to 28.3kNm^{-1}. The probability of failure was also significantly increased from 7.75% to 52.0% for such an increase in the backfill angle of shearing resistance.

7.5.1.13 The effect of varying the variable end limit

Figure 7.32 shows the effect of varying the variable end limit on the prediction of arch collapse load. Four different variable end limits were used in this parametric study: 1%, 3%, 5% and 7%. Referring to Figure 7.32, it could be seen that no significant difference in the prediction of collapse load was found over the range of variable end limits used. The influence of the variable end limit on the collapse load prediction was imperceptible.

7.5.1.14 The effect of varying Boussinesq's limiting live load influence factor

Figure 7.33 shows the effect of varying Boussinesq's limiting live load influence factor on the prediction of arch collapse load. Five different load influence factors were used

in this parametric study: 0.5, 0.1, 0.05, 0.01, and 0.001. It is apparent from Figure 7.33 that the load influence factor had a significant influence on the prediction of arch collapse load especially for higher influence factors. By reducing the load influence factor from 0.5 to 0.001, the predicted mean collapse load increased from 210.5kNm^{-1} to 269.8kNm^{-1}. The standard deviation of the predicted collapse load also increased from 21.1kNm^{-1} to 23.4kNm^{-1}. For a similar reduction in the load influence factor, the probability of failure increased from 0.12% to 13.7%.

Table 7.9 Statistical properties of the generated arch collapse load (Barlae)

Property	Unit	Coefficient of variation			
		2%	3%	4%	5%
Mean collapse load	kNm^{-1}	265.1	265.6	267.6	270.2
S.D. of collapse load		18.2	24.9	32.8	41.5
Skewness of collapse load		0.211	0.328	0.452	0.589
Kurtosis of collapse load		2.75	2.92	3.14	3.45
Maximum collapse load		332.4	366.9	433.8	482.5
Minimum collapse load		213.1	194.3	180.1	167.1
Probability of failure	%	5.13	11.8	19.0	24.7

Property	Unit	Seed number		
		819	773311	4552466
Mean collapse load	kNm^{-1}	265.7	265.6	265.5
S.D. of collapse load		24.9	24.9	24.8
Skewness of collapse load		0.35	0.33	0.35
Kurtosis of collapse load		3.02	2.92	2.99
Maximum collapse load		386.3	366.9	395.5
Minimum collapse load		194.7	194.3	196.6
Probability of failure	%	11.7	11.8	11.6

Property	Unit	Arch span		
		8530mm	9197.5mm	9865mm
Mean collapse load	kNm^{-1}	275.9	265.6	260.3
S.D. of collapse load		27.6	24.9	23.1
Skewness of collapse load		0.42	0.33	0.29
Kurtosis of collapse load		3.08	2.92	2.87
Maximum collapse load		400.5	366.9	364.0
Minimum collapse load		197.4	194.3	190.7
Probability of failure	%	22.6	11.8	6.90

Table 7.9 Statistical properties of the generated arch collapse load (Barlae): cont'

Property	Unit	Number of arch segments				
		20	40	60	80	100
Mean collapse load	kNm^{-1}	257.3	265.6	267.5	268.1	268.2
S.D. of collapse load		22.9	24.9	24.2	24.0	23.9
Skewness of collapse load		0.42	0.33	0.32	0.31	0.32
Kurtosis of collapse load		3.32	2.92	2.90	2.87	2.89
Maximum collapse load		388.1	366.9	371.8	365.0	369.8
Minimum collapse load		194.4	194.3	199.8	201.4	202.2
Probability of failure	%	5.30	11.8	12.7	12.9	12.8

Property	Unit	Load dispersal angle		
		30°	35°	40°
Mean collapse load	kNm^{-1}	254.2	265.6	282.9
S.D. of collapse load		23.4	24.9	26.7
Skewness of collapse load		0.36	0.33	0.33
Kurtosis of collapse load		2.99	2.92	2.96
Maximum collapse load		356.2	366.9	410.5
Minimum collapse load		186.9	194.3	205.7
Probability of failure	%	4.69	11.8	30.2

Property	Unit	Number of iterations					
		50	100	500	5000	30000	50000
Mean collapse load	kNm^{-1}	276.2	273.9	265.2	265.6	265.6	265.7
S.D. of collapse load		32.21	28.11	24.58	24.87	24.86	24.85
Skewness of collapse load		0.30	0.41	0.16	0.34	0.33	0.34
Kurtosis of collapse load		3.26	3.91	2.90	2.99	2.92	2.94
Maximum collapse load		361.3	361.3	354.4	356.2	366.9	389.1
Minimum collapse load		206.0	206.0	202.4	199.0	194.3	192.1
Probability of failure	%	26.0	17.0	11.8	11.5	11.8	11.9

Property	Unit	Backfill bulk unit weight		
		$18\,kNm^{-3}$	$20\,kNm^{-3}$	$22\,kNm^{-3}$
Mean collapse load	kNm^{-1}	250.7	265.6	280.5
S.D. of collapse load		23.5	24.9	26.2
Skewness of collapse load		0.33	0.33	0.33
Kurtosis of collapse load		2.92	2.92	2.92
Maximum collapse load		345.5	366.9	388.4
Minimum collapse load		183.5	194.3	205.2
Probability of failure	%	3.55	11.8	27.0

Table 7.9 Statistical properties of the generated arch collapse load (Barlae): cont'

Property	Unit	Arch bulk unit weight		
		21 kNm^{-3}	23 kNm^{-3}	25 kNm^{-3}
Mean collapse load	kNm^{-1}	255.5	265.6	275.8
S.D. of collapse load		23.9	24.9	25.9
Skewness of collapse load		0.33	0.33	0.33
Kurtosis of collapse load		2.91	2.92	2.92
Maximum collapse load		353.7	366.9	380.2
Minimum collapse load		186.9	194.3	201.8
Probability of failure	%	5.44	11.8	21.6

Property	Unit	Backfill active pressure mobilisation		
		60%	80%	90%
Mean collapse load	kNm^{-1}	265.4	265.6	265.6
S.D. of collapse load		24.9	24.9	24.9
Skewness of collapse load		0.33	0.33	0.33
Kurtosis of collapse load		2.91	2.92	2.92
Maximum collapse load		366.8	366.9	366.8
Minimum collapse load		194.1	194.3	194.3
Probability of failure	%	11.7	11.8	11.8

Property	Unit	Backfill passive pressure mobilisation		
		30%	50%	70%
Mean collapse load	kNm^{-1}	248.1	265.6	293.3
S.D. of collapse load		23.7	24.9	27.2
Skewness of collapse load		0.34	0.33	0.32
Kurtosis of collapse load		2.92	2.92	2.92
Maximum collapse load		344.1	366.9	406.8
Minimum collapse load		181.2	194.3	215.4
Probability of failure	%	2.97	11.8	44.0

Property	Unit	Backfill angle of shearing resistance			
		30°	35°	40°	50°
Mean collapse load	kNm^{-1}	259.7	265.6	273.4	298.9
S.D. of collapse load		24.5	24.9	25.5	28.3
Skewness of collapse load		0.33	0.33	0.32	0.32
Kurtosis of collapse load		2.92	2.92	2.92	2.95
Maximum collapse load		358.6	366.9	378.1	415.8
Minimum collapse load		189.8	194.3	200.1	218.1
Probability of failure	%	7.75	11.8	18.9	52.0

Table 7.9 Statistical properties of the generated arch collapse load (Barlae): cont'

Property	Unit	Variable end limit			
		1%	3%	5%	7%
Mean collapse load	kNm^{-1}	265.9	265.6	265.5	265.2
S.D. of collapse load		25.8	24.9	24.0	23.2
Skewness of collapse load		0.37	0.33	0.30	0.28
Kurtosis of collapse load		3.10	2.92	2.80	2.73
Maximum collapse load		376.4	366.9	357.1	352.5
Minimum collapse load		189.3	194.3	197.7	200.1
Probability of failure	%	12.5	11.8	11.1	10.2

Property	Unit	Boussinesq's limiting live load influence factor				
		0.5	0.1	0.05	0.01	0.001
Mean collapse load	kNm^{-1}	210.5	245.4	258.6	268.3	269.8
S.D. of collapse load		21.1	21.2	21.8	23.1	23.4
Skewness of collapse load		0.67	0.38	0.33	0.36	0.36
Kurtosis of collapse load		3.80	3.03	2.89	2.98	2.96
Maximum collapse load		320.1	348.9	356.7	376.9	379.8
Minimum collapse load		153.4	188.9	200.1	207.6	208.5
Probability of failure	%	0.12	1.45	5.23	12.24	13.70

7.5.2 Monte Carlo simulation applied to the MEXE method

This section presents the results from the Monte Carlo simulation for the MEXE method. The results obtained by using the input variables given in Table 7.8 are presented first and are referred to as the standard results. This is then followed by the presentation of results from all parametric studies. There were five parameters used: the coefficient of variation, the number of iterations, seed number for the random number generator, condition factor and the arch span. The width of Barlae bridge was 9.8m which was enough to accommodate two vehicles in parallel in the transverse direction. All results were given in tonnes which represented the allowable load for the entire bridge.

7.5.2.1 Standard results

Figure 7.34 shows the predicted distribution of the allowable single axle load (A.S.A.L) using standard input variables as shown in Table 7.8. The predicted mean and standard deviation of the A.S.A.L were 34.1t and 3.08t respectively. This gave a factor of safety of 8.69 when compared with the actual collapse load of 296t. However, if a load partial factor of safety of 3.4, as recommended by BD21/97 (1997a) for calculating the ultimate load, was used the resulting safety factor against collapse was only 2.56.

The predicted distribution for the allowable double axle load is shown in Figure 7.35. The mean and standard deviation of the allowable double axle load were 21.8t and 2.04t respectively. Without performing the Monte Carlo simulation, the allowable single and double axle loads, evaluated directly from Eqn 7.17 using the input variables given in Table 7.8, were 34.0t and 21.7t respectively which were almost identical to the mean values generated from the Monte Carlo simulation.

7.5.2.2 The effect of varying the coefficient of variation of input variables

Figures 7.36 shows the effect of varying the coefficient of variations of all input variables on the prediction of A.S.A.L. The coefficient of variations of all input variables were varied from 2% to 5% resulting in an increase in the A.S.A.L from 34.0t to 34.1t. Simultaneously, the mean load factor of safety reduced from 8.68 to 8.67. No significant changes of A.S.A.L were noticed. This was because the change in the coefficient of variations of all input variables varied the spread of the distribution of each input variable without influencing their means. By increasing the coefficient of variation of all input variables from 2% to 5%, the standard deviation of the predicted A.S.A.L rose from 2.048t to 5.016t due to a wider spread of the distribution of each input variable.

7.5.2.3 The effect of varying the number of iterations

The results of the parametric study on the number of iterations were shown in Figure 7.37. Six different numbers of iterations were used in this parametric study: 50, 100, 500, 5000, 30000 and 50000. There was no noticeable influence on the predicted A.S.A.L over the range of this parametric study. The distributions of A.S.A.L for 50, 500, 5000 and 50000 were presented in Figures 7.38 to 7.41 respectively. From Figures 7.38 to 7.41, it could be seen that distributions with 5000 iterations and above seemed to be satisfactory with a smooth bell-shaped profile. However, from Figure 7.37, convergence was achieved only with 500 and above iterations.

7.5.2.4 The effect of varying the seed for the random number generator

Figure 7.42 shows the results from the parametric study involving three different seed numbers for the random number generator. As can be seen from Figure 7.42 the change in the seed number had no influence on the prediction of A.S.A.L. The use of different seed numbers will only result in a different sequence in which the random variables are generated. If many iterations used, the overall mean and standard deviation of a proposed distribution are not affected by the use of different seed numbers.

7.5.2.5 The effect of varying the condition factor

Figure 7.43 shows the results from the parametric study using different condition factors. The condition factor was varied from 0.6 to 0.9 resulting in an increase in the mean A.S.A.L from 25.6t to 38.3t. Such an increase in the condition factor has also resulted in a reduced factor of safety from 11.6 to 7.7. Simultaneously, the standard deviation of the A.S.A.L increased from 2.31t to 3.47t.

7.5.2.6 The effect of varying the arch span

Figure 7.44 shows the results from the parametric study involving three different arch spans. By increasing the arch span from 8530mm to 9865mm, the predicted mean A.S.A.L decreased from 38.6t to 30.4t. With a similar increase in the arch span, the standard deviation of the A.S.A.L decreased from 3.48t to 2.73. Simultaneously the load factor of safety was found to increase from 7.66 to 9.74.

Table 7.10 Statistical properties of the generated allowable single axle load (Barlae)

Property	Unit	Coefficient of variation			
		2%	3%	4%	5%
Mean A.S.A.L	tonnes	34.0	34.1	34.1	34.1
S.D. of A.S.A.L		2.05	3.08	4.05	5.02
Skewness of A.S.A.L		0.18	0.27	0.35	0.42
Kurtosis of A.S.A.L		3.02	3.09	3.16	3.26
Maximum A.S.A.L		43.5	48.9	54.4	60.0
Minimum A.S.A.L		27.1	24.3	21.6	19.3
Load factor of safety		8.69	8.68	8.67	8.67

Property	Unit	Number of iterations					
		50	100	500	5000	30000	50000
Mean A.S.A.L	tonnes	34.4	34.7	34.0	34.1	34.1	34.1
S.D. of A.S.A.L		3.45	3.25	3.18	3.13	3.08	3.08
Skewness of A.S.A.L		-0.19	-0.17	0.30	0.33	0.27	0.27
Kurtosis of A.S.A.L		2.52	2.56	3.13	3.10	3.09	3.08
Maximum A.S.A.L		40.9	41.1	44.8	46.8	48.9	48.9
Minimum A.S.A.L		25.8	25.8	25.8	24.9	24.3	24.3
Load factor of safety		8.60	8.53	8.70	8.67	8.68	8.68

Property	Unit	Seed number		
		365	773311	1451972
Mean A.S.A.L	tonnes	34.1	34.1	34.1
S.D. of A.S.A.L		3.14	3.08	3.09
Skewness of A.S.A.L		0.27	0.27	0.28
Kurtosis of A.S.A.L		3.10	3.09	3.07
Maximum A.S.A.L		47.5	48.9	48.6
Minimum A.S.A.L		23.4	24.3	24.2
Load factor of safety		8.67	8.68	8.68

Table 7.10 Statistical properties of the generated allowable single axle load (Barlae): cont'

Property	Unit	Condition factor			
		0.6	0.7	0.8	0.9
Mean A.S.A.L	tonnes	25.6	29.8	34.1	38.3
S.D. of A.S.A.L		2.31	2.70	3.08	3.47
Skewness of A.S.A.L		0.27	0.27	0.27	0.27
Kurtosis of A.S.A.L		3.09	3.09	3.09	3.09
Maximum A.S.A.L		36.7	42.8	48.9	55.0
Minimum A.S.A.L		18.2	21.2	24.3	27.3
Load factor of safety		11.6	9.92	8.68	7.71

Property	Unit	Arch span		
		8530mm	9197.5mm	9865mm
Mean A.S.A.L	tonnes	38.6	34.1	30.4
S.D. of A.S.A.L		3.48	3.08	2.73
Skewness of A.S.A.L		0.27	0.27	0.27
Kurtosis of A.S.A.L		3.08	3.09	3.09
Maximum A.S.A.L		55.3	48.9	43.6
Minimum A.S.A.L		27.5	24.3	21.6
Load factor of safety		7.66	8.68	9.74

7.6 Shape of the predicted distribution of collapse load and allowable axle load

This section presents a study of the shape of the predicted distribution of the arch collapse load and the allowable axle load from the Monte Carlo simulation. The predicted distributions of the collapse load and the A.S.A.L presented in Sections 7.5.1.1 and 7.5.2.1 respectively were used in this study. As can be seen from Tables 7.9 and 7.10, the skewness of the predicted distribution from each parametric study is not near to zero suggesting that the predicted distribution for both collapse load and allowable axle load could not be well represented by a normal distribution.

Four analytical distributions namely the normal, log-normal, beta and gamma were used in the chi-squared test to determine which analytical distribution was most suited to represent the predicted distribution of collapse load and allowable axle load. The chi-square in this study was presented in terms of the probability, rather than the frequency, of each interval.

Figure 7.45 shows the distribution of the predicted collapse load together with four analytical distributions. The chi-square values for the normal, log-normal, beta and gamma distributions, when compared with the predicted distribution from the Monte Carlo simulation, were 0.019577, 0.004077, 0.078458 and 0.006871 respectively. This showed that the log-normal distribution was the best, amongst these analytical distributions, to represent the distribution of the predicted arch collapse load presented in Section 7.5.1.1.

Figure 7.46 shows the distribution of the A.S.A.L together with four analytical distributions. The chi-square values for the normal, log-normal, beta and gamma distributions, when compared with the predicted distribution from the Monte Carlo simulation, were 0.014332, 0.000522, 1.628722 and 0.001950 respectively. Again, the log-normal distribution was the best amongst all these analytical distributions at representing the predicted distribution of A.S.A.L presented in Section 7.5.2.1.

7.7 Discussion

The results obtained from the Monte Carlo simulation with the mechanism and MEXE methods are discussed. The influence of each input parameter in each method is also discussed. Following this, some limitations of the author's Monte Carlo simulations are discussed.

7.7.1 Discussion; Monte Carlo simulation and the mechanism method

A Monte Carlo simulation has been successfully incorporated into the mechanism method for the analysis of Barlae bridge. Unlike other arch bridge assessment methods, the current Monte Carlo simulation gives statistical information about the predicted arch collapse load such as its mean, standard deviation, skewness, kurtosis, and range. The risk involved in assessing an arch bridge can be measured by analysing the standard deviation of the predicted collapse load. The larger this is the greater the risk involved: such information can help an engineer to have some idea of the reliability of their assessment. The parametric studies carried out showed that some variables had a significant influence on the prediction of arch collapse load most notably: the variable's coefficient of variation, the arch's span, the live load dispersal angle, the arch and backfill unit weights, the permitted mobilisation of backfill passive pressure, the backfill's angle of shearing resistance, and Boussinesq's limiting live load influence value. Other parameters did not influence the predicted results such as: the seed for the random number generator, the mobilisation of backfill active pressure and the individual variable end limits.

The influence of the number of arch segments and the number of iterations depended on their magnitudes. Parametric studies have to be carried out to search for a minimal number of arch segments and the number of iterations in such a way that any increase in their magnitudes does not significantly affect the collapse load prediction. In this study, 40 arch segments and 30000 iterations were found to be appropriate. As presented in Figure 7.20 the processing time increased dramatically with an increase in the number of arch segments. Care must be taken to obtain an optimal number of arch segments for the sake of saving time whilst still getting good results.

The coefficient of variations of the input variables have been shown to affect the predicted results. In this study, the coefficient of variations of all input variables were set to be similar at any one time. However, the program also allows the user to specify

different coefficient of variations for each input variable. The range of coefficient of variations used in this parametric study was between 2% to 5%. This was deemed appropriate since most of the geometrical properties of the arch bridge are unlikely to be unduly dispersed about their respective means. However, individual analyses should be done for parameters such as load dispersal angle, arch and backfill unit weights, backfill lateral pressures, angle of shearing resistance and Boussinesq's limiting live load influence value which are difficult to find from what may only be a cursory survey and visual inspection of a bridge.

The influence of the seed for the random number generator was insignificant because different values of this seed only varied the sequence in which random numbers were generated. Provided a sufficient number of iterations is used, the statistical properties of the random numbers will not differ significantly.

Two types of load distribution methods were used in this study. The first was based on a specified distribution angle from each side of the loaded area as recommended by the Department of Transport (BD21/97, 1997a). The second method was Boussinesq's distribution (TERZAGHI, 1943). Research on the distribution of live load for masonry arch bridges finds that the load dispersal angle can reach 65° in a full scale test (FAIRFIELD, 1993b). Although a subject of many years' research, the actual live load distribution in a complex soil-arch system is still unknown. Parametric studies carried out here showed that the influence of both live load dispersal angle and Boussinesq's limiting live load influence value were significant.

Parametric studies carried out on both the arch and backfill bulk unit weights revealed that both parameters significantly influenced the capacity predictions. This was expected as the failure of an arch bridge is usually a mechanism involving rotation of several (usually three) sections of the ring against gravitational attraction and restraining pressure from the backfill. The higher the arch and backfill unit weights, the larger the live load required to form the failure mechanism.

A parametric study on the mobilisation of backfill passive pressure showed it significantly influenced the capacity predictions. In contrast, the backfill active pressure mobilisation was found to have no influence on the predicted results. Both Rankine's active and passive earth pressure coefficients involve the backfill's angle of shearing resistance. A maximum of 70% passive pressure mobilisation was used here because it was thought unlikely that full passive resistance could be mobilised in such a soil-arch system. Alternatively full mobilisation of the active state would be possible but as active pressures are so much lower than their passive counterparts they were still unable to influence the collapse load predictions.

The parametric study carried out on the variables' end limits revealed that they were insignificant over the range tested. It must be emphasised that the use of this limit is to prevent random variables being generated so many standard deviations away from the mean as to be unfeasible. The range from 1% to 7% is recommended for future use.

7.7.2 Discussion; Monte Carlo simulation and the MEXE method

A Monte Carlo simulation has been successfully integrated into the MEXE method to perform risk analysis on Barlae bridge. This Monte Carlo simulation gives additional information about the evaluated allowable axle loads such as the mean, standard deviation, skewness, kurtosis, and range. This information can help an engineer to gauge the reliability of MEXE assessments of arch bridges.

The results from parametric studies showed that the coefficient of variation of all input variables, the condition factor and the arch span had a significant influence on the prediction of the allowable axle load. Coefficient of variations of the input variables between 2% to 5% of their means are recommended. However, it is up to the engineer to chose the coefficient of variations of all input variables based on their experience or the reliability of available information about an arch bridge.

The influence of condition factor on the prediction of the allowable axle load was found to be significant as shown in Figure 7.43. This might be a drawback of using the MEXE method as the condition factor is always selected by an engineer based largely on how he feels about the arch and the decision is made in a subjective manner. The arch span was also found to have a dramatic influence on the prediction of the allowable axle load. The shorter the arch span, with all other geometrical properties unchanged, the stronger will be the evaluated capacity. This is because reducing the arch span would result in an increase in the ring thickness to arch span ratio rendering the arch more stocky. Further research is still needed to find out the effective span of skewed arches if the analysis is to be performed in two dimensions.

A total of thirty seconds was required to perform 30000 iterations by the Monte Carlo simulation with the MEXE method. Such a short processing time and the ease of use should make this a cost effective method suitable for incorporation into routine arch bridge assessment programs.

7.7.3 Limitations

The mechanism and MEXE methods have been widely used for analysing arch bridges because no complicated computations are required and they are quick. However, these methods were based on many unrealistic assumptions such as the arch having no spandrels, wing walls and parapet. Many subjective judgements have to be made relating to the live load dispersal angle, active and passive pressure coefficients, when performing the mechanism method, and condition factor, when using the MEXE method. These drawbacks are themselves the very reason for incorporating Monte Carlo simulation as a risk analysis tool into traditional mechanism and MEXE methods for arch assessments.

A major drawback arising from this Monte Carlo simulation is the processing time required for a sufficient number of iterations. However, most of the processing time

was occupied with the evaluation of collapse load distributions and not spent generating random variables. The coefficient of variations of all the input variables can only be assumed subjectively because there is no such information available and it is highly unlikely that cursory site investigation will provide such data from field measurements. Over the wide range of bridges built in any one Local Authority area a database of experience will gradually have been built up concerning the likely variability in some of the more common material properties. Local building stones are generally used and their properties can often be assessed in similar modern quarries. One of the benefits of this type of risk based assessment is that it allows an engineer faced with a complex problem to examine the possibilities previously unavailable through use of any of the other traditional or modern arch assessment methods in isolation.

7.8 Monte Carlo simulation for selected arch bridges

Both Monte Carlo simulation programs, MCMECH.FOR and MCMEXE.FOR, were tried on eight selected arch bridges: Bridgemill (HENDRY *et al.*, 1985), Kimbolton Butts (FAIRFIELD *et al.*, 1993b), Bolton (MELBOURNE *et al.*, 1995e), Prestwood (PAGE, 1987), Bargower (HENDRY *et al.*, 1986) , Shinafoot (PAGE, 1988), Strathmashie (PAGE, 1989), and the author's large scale arch presented in Chapter 6 of this thesis. Comparisons were made with the results predicted by the CTAP mechanism and elastic cracking methods (BRIDLE *et al.*, 1989), ARCHIE (SMITH, 1991a) and Heyman's plastic method (HEYMAN, 1982). With the exception of Kimbolton Butts bridge, the collapse load for each bridge was included for comparisons. The geometrical and material properties of the selected arch bridges to be analysed in this section are presented in Tables 7.11 and 7.12 for the collapse analysis and the MEXE method respectively.

The backfill bulk unit weight was used to represent the bulk unit weight of the bridge in Heyman's plastic method. No other material properties, except the backfill bulk unit

weight, presented in Table 7.11 were used in Heyman's plastic method. For the Monte Carlo simulation, a coefficient of variation of 3% and a variable end limit of 3% were used for all input variables. A total of 30000 iterations was used in each analysis.

Table 7.11 Input variables for the collapse analysis applied to selected arch bridges

Properties	Bridgemill	Kimbolton	Bolton	Prestwood	Author
Span (m)	18.29	8.000	3.000	6.550	2.000
Rise (m)	2.840	2.000	0.750	1.428	0.500
Ring thickness (m)	0.711	0.440	0.215	0.220	0.1025
Depth of fill (m)	0.203	0.450	0.300	0.165	0.150
Arch bulk unit weight (kNm^{-3})	21	22	22.7	21	21
Backfill bulk unit weight (kNm^{-3})	20	21.8	22.2	20	14.86
Backfill angle of shearing resistance	35°	35°	60°	35°	30.5°
Load dispersal angle (except ARCHIE)	45°	45°	45°	45°	45°
Arch compressive strength (MPa) (CTAP mechanism & ARCHIE only)	8	15.5	18.1	8	30
Percentage of active pressure mobilised (except ARCHIE)	80%	80%	80%	80%	80%
Percentage of passive pressure mobilised	20%	50%	50%	50%	80%
Platen width (m) (except ARCHIE)	0.75	0.75	0.21	0.75	0.18
Arch elastic modulus (MPa) (Elastic cracking only)	5000	5000	8000	8000	8000
Modulus of subgrade reaction (kNm^{-3}) (Elastic cracking only)	10000	10000	10000	10000	10000

Table 7.12 Input variables for the MEXE method applied to selected arch bridges

	Bargower	Shinafoot	Strathmashie	Author
Span (m)	10.36	6.160	9.425	2.000
Rise (m)	5.180	1.180	2.990	0.500
Ring thickness (m)	0.558	0.542	0.600	0.1025
Depth of fill (m)	1.200	0.215	0.410	0.150
Barrel factor	1.200	1.400	1.400	1.000
Fill factor	0.700	0.700	0.700	0.700
Width factor	0.850	0.850	0.850	0.900
Depth factor	0.800	0.800	0.800	0.800
Mortar factor	0.950	0.950	0.950	0.950
Condition factor	0.700	0.700	0.600	0.500

7.8.1 Results; Monte Carlo simulation with the mechanism method for selected arch bridges

The results from the Monte Carlo simulation, CTAP mechanism, CTAP elastic cracking, ARCHIE and Heyman's plastic methods for Bridgemill, Kimbolton Butts, Bolton, Prestwood and the author's large scale arches are presented in Figures 7.47 to 7.51 respectively. All input variables for these analyses are given in Table 7.11. With the exception of Kimbolton Butts, the collapse load of each arch bridge is also presented in its respective figure for comparison.

Table 7.13 Predicted arch collapse loads (all values in kNm^{-1})

Methods	Bridgemill	Kimbolton	Bolton	Prestwood	Author
Test	361.00	N/A	190.00	60.00	21, 16, 25
CTAP mechanism	425.71	443.02	375.19	71.84	26.95
CTAP elastic cracking	329.68	314.37	173.12	45.62	18.18
ARCHIE	330.00	200.00	190.00	37.00	14.00
Heyman	459.22	222.46	103.78	33.71	8.58
Monte Carlo simulation	458.55	325.83	187.99	61.45	19.13

A summary of the predicted collapse loads from all methods is given in Table 7.13. The predicted collapse load from the Monte Carlo simulation presented in Table 7.13 is represented by the predicted mean collapse load.

7.8.2 Results; Monte Carlo simulation with the MEXE method for selected arch bridges

The results from the Monte Carlo simulation with the MEXE method performed on Bargower, Shinafoot, Strathmashie and the author's large scale arches are presented in Figures 7.52 to 7.55 respectively. The input variables for these analyses are given in Table 7.12. The collapse load of each bridge is also presented in its respective figure for comparison. With the exception of the author's large scale arches, the predicted A.S.A.L represents the total allowable load based on the number of lanes on each arch bridge. The width of the author's large scale arches was one metre and this was unable to accommodate one vehicle. The A.S.A.L for the author's arch was obtained by dividing the MEXE prediction by a factor of 2.5, assuming that the width of each lane is 2.5m.

7.9 Discussion; Monte Carlo simulation for selected arch bridges

The Monte Carlo simulation has been performed on selected arch bridges to predict their collapse loads, by MCMECH.FOR, and allowable axle loads, by MCMEXE.FOR. Comparisons were made between the predicted arch collapse loads with Monte Carlo simulation, CTAP mechanism, CTAP elastic cracking, ARCHIE and Heyman's plastic methods. Where available, the actual collapse load of each arch was also included for comparison. The prediction of the A.S.A.L on four arches was also performed enabling the mean load factor of safety to be evaluated.

Referring to Figures 7.47 to 7.51, it could be seen that no general comment could be made as to whether any of the analytical assessment methods including the author's Monte Carlo simulation was the best for achieving the highest accuracy in the prediction of collapse loads on those selected arch bridges. As every attempt has been made to use similar input variables in all assessment methods, it could not be done so since some of the input variables were fixed as default values whilst some were ignored. This might also lead to the discrepancies as shown in Figures 7.47 to 7.51.

With the exception of the Bolton arch, all ARCHIE's predictions were lower than those mean collapse loads generated by MCMECH.FOR. This might be because ARCHIE adopts a limited live load distribution, a sine wave distribution, a smaller platen width of 300mm, and a reduced ring thickness due to compressive failure. From the author's point of view, it might not be sensible to consider compressive failure in the arch as this might happen only when the arch is locked by strong backings or the arch is too stocky for a mechanism failure to take place. The use of a limiting compressive strength in the arch would, especially for those large or flat arches, result in the arch ring being arbitrarily reduced because the arch ring of a large or flat arch could sustain a comparatively large thrust. A compressive or explosive type of failure does not seems to be a common failure mode for masonry arch bridges. If it does happen, the mechanism method is no longer suitable.

Heyman's plastic method, albeit being criticised as too conservative for ignoring the lateral soil resistance and the live load distribution, yielded a satisfactory result on Bridgemill. However, its predictions were found to be the lowest amongst all other assessment methods on Bolton, Prestwood and the author's large scale arches. It must be emphasised that Heyman's plastic method does not always give conservative results, when compared with those predictions by other assessment methods, since arch compressive failure is ignored in Heyman's plastic method. In cases such as Bridgemill, Heyman's prediction is greater than those assessed by ARCHIE and CTAP mechanism method. This was due to the ring thickness being reduced in both ARCHIE and CTAP with the use of a limiting arch compressive strength.

The distributions of the allowable single axle loads generated by the Monte Carlo simulation, MCMEXE.FOR, performed on four selected arch bridges are shown in Figures 7.52 to 7.55 inclusive. The mean factors of safety on Bargower, Shinafoot and Strathmashie were found to be 5.14, 5.62 and 5.61 respectively. For the author's three large scale arches, the mean factors of safety were 1.11, 0.849 and 1.33 for SR4-A, SR4-B and SR4-C respectively.

The main conclusions derived from this study are presented as follow.

7.10 Conclusions

1 Monte Carlo simulation has been successfully incorporated into the mechanism and MEXE methods to perform risk analysis based arch bridge assessment.

2 A series of statistical tests, performed on generated random variables, showed that the currently adopted random number generator was appropriate.

3 The seed for the random number generator had no influence on the prediction of arch collapse load and allowable axle load.

4 The coefficient of variations of input variables had affected the prediction of arch collapse load and allowable axle load. A range between 2% to 5% is recommended.

5 The arch span had significantly affected the prediction of arch collapse load and allowable axle load.

6 A total of forty arch segments or above is recommended for the Monte Carlo simulation with the mechanism method in this study. Increasing the number of arch segments had been shown to increase the processing time significantly.

7 The live load dispersal angle had a significant influence on the prediction of arch collapse load.

8 A total of 30000 iterations was shown to be sufficient for both the MCMECH.FOR and MCMEXE.FOR programs to achieve a converged result.

9 The backfill and arch bulk unit weights had a significant influence on the prediction of arch collapse load.

10 The backfill active pressure coefficient had no influence on the prediction of arch collapse load.

11 The backfill passive pressure coefficient had a significant influence on the prediction of arch collapse load.

12 The backfill angle of shearing resistance had an influence on the prediction of arch collapse load.

13 The variable end limit had no significant influence on the prediction of arch collapse load and allowable axle load. A range of between 1% to 7% is recommended in this study.

14 The condition factor had a significant influence on the prediction of allowable axle load.

15 The log-normal distribution, amongst the normal, log-normal, beta and gamma distributions, was found to be the best to represent the predicted distribution of the arch collapse load and allowable single axle load for Barlae.

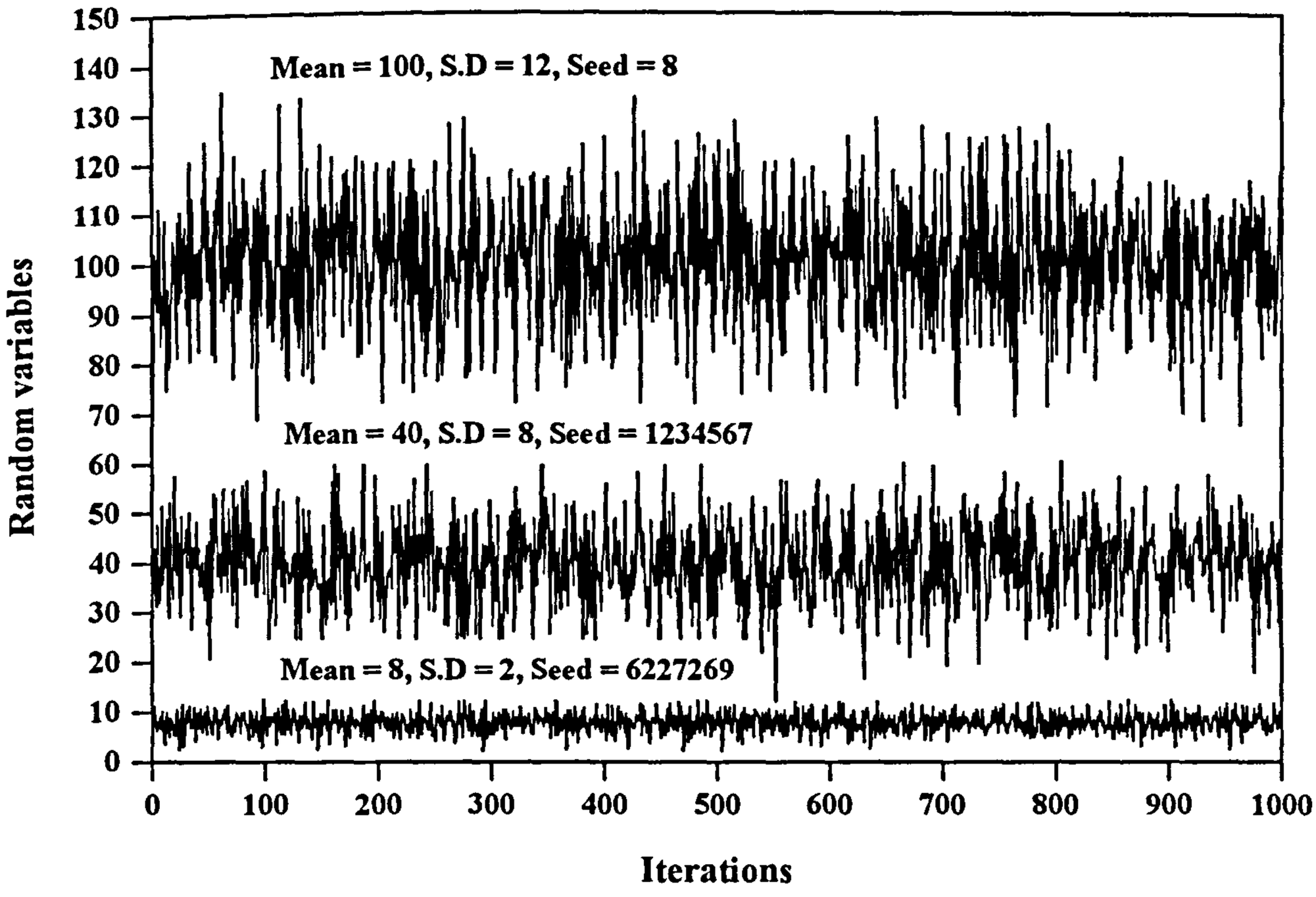

Figure 7.1 Random variables (A, B & C)

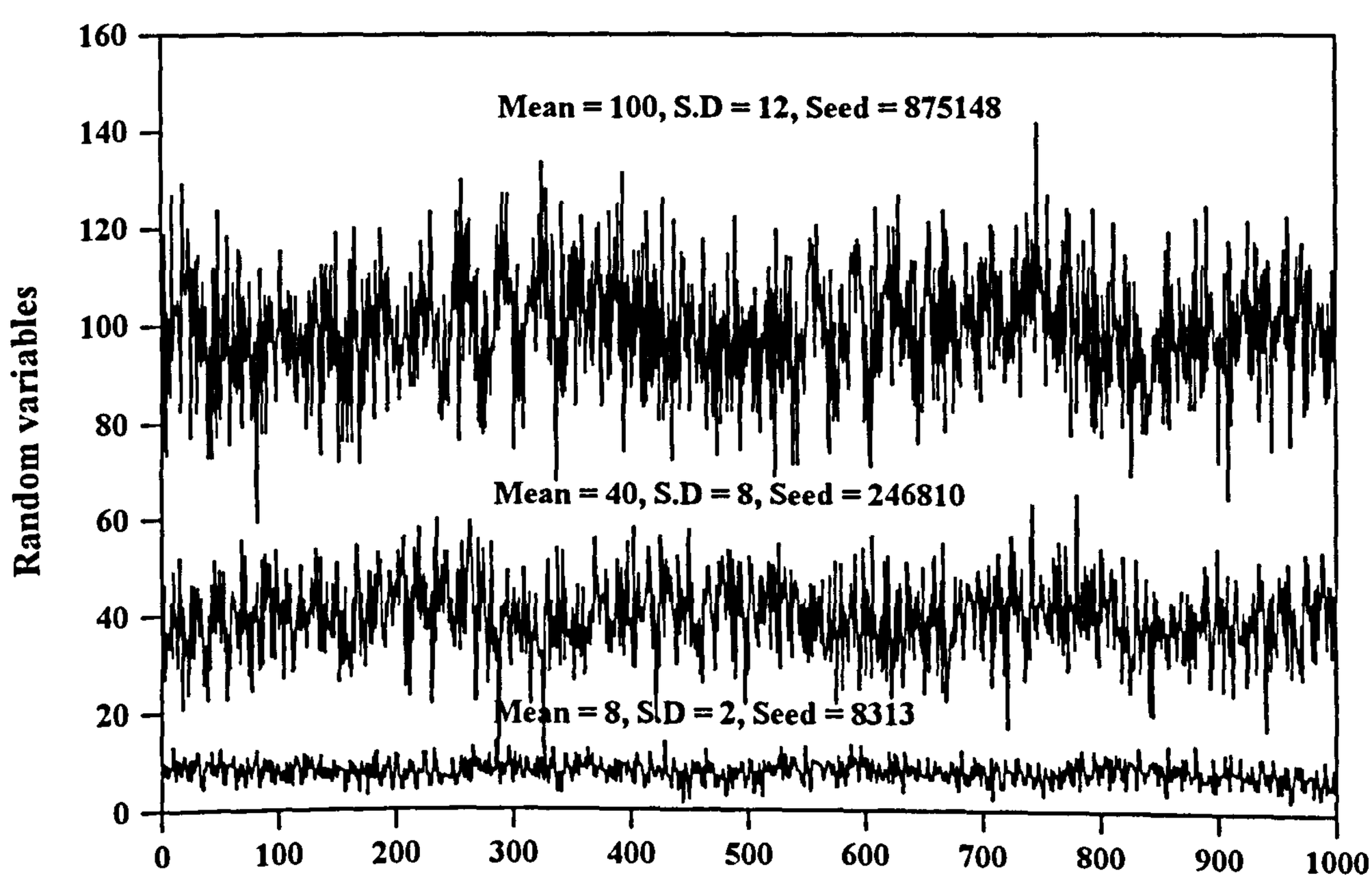

Figure 7.2 Random variables (D, E & F)

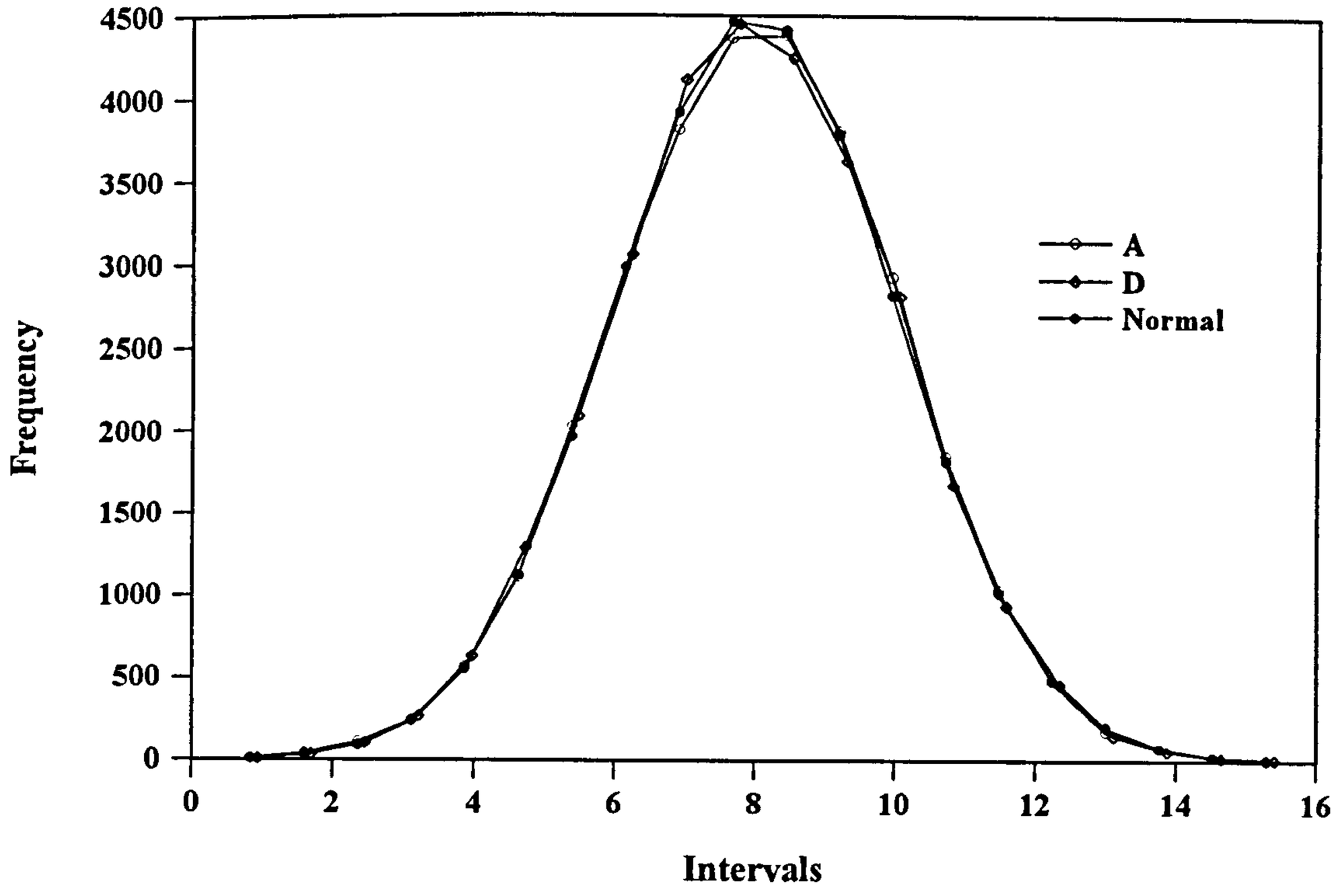

Figure 7.3 A, D and the normal distributions

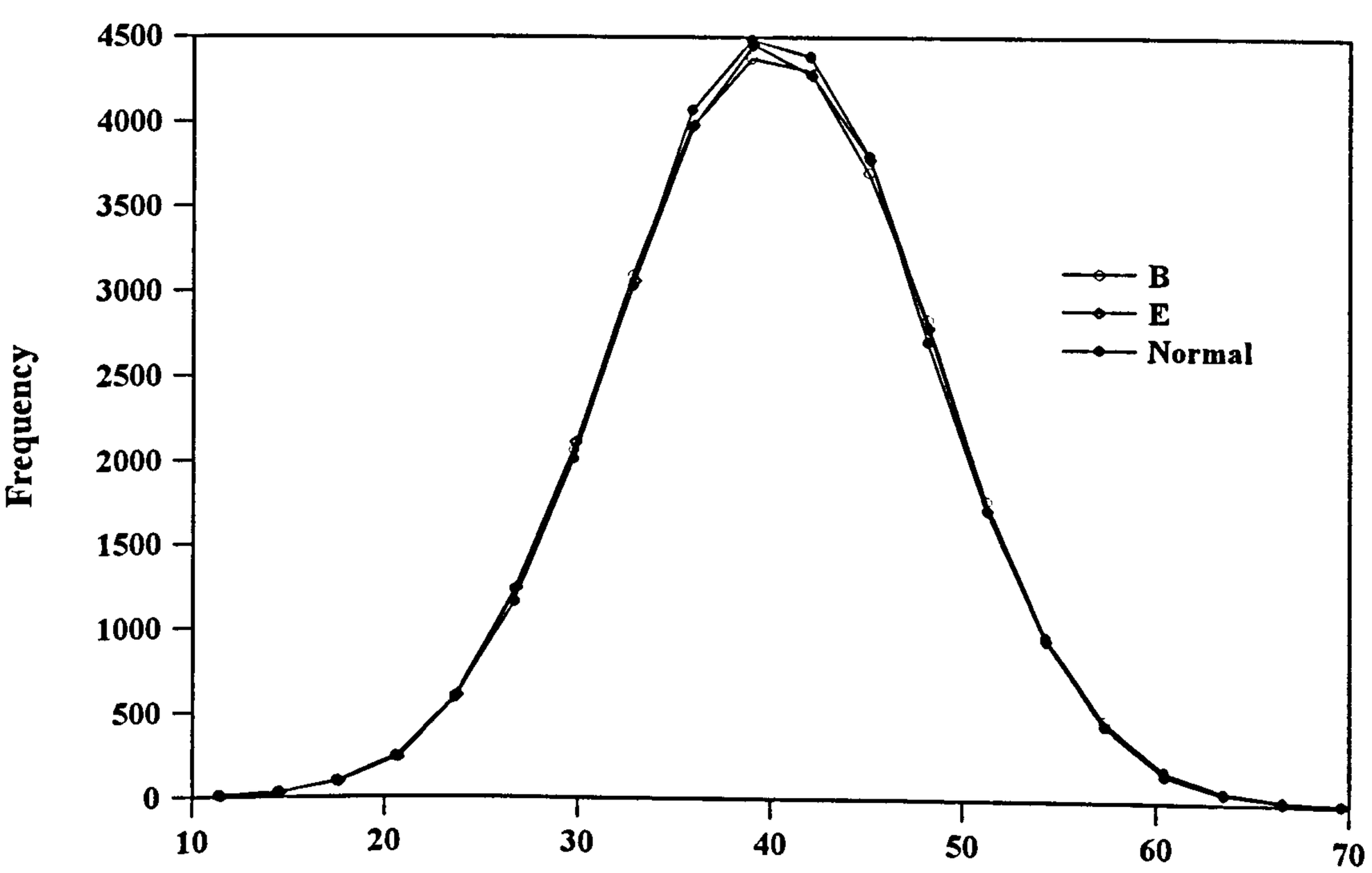

Figure 7.4 B, E and the normal distributions

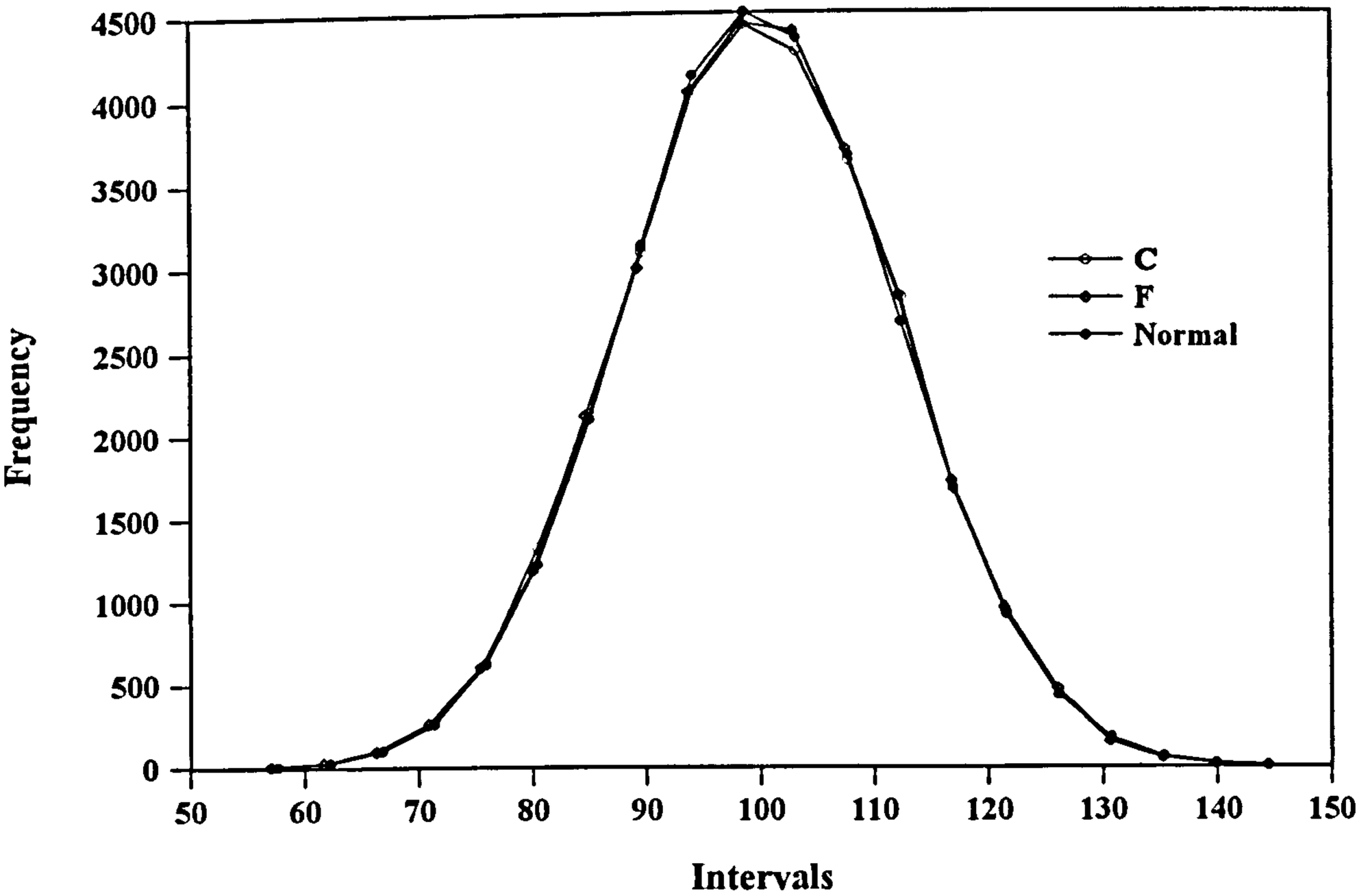

Figure 7.5 C, F and the normal distributions

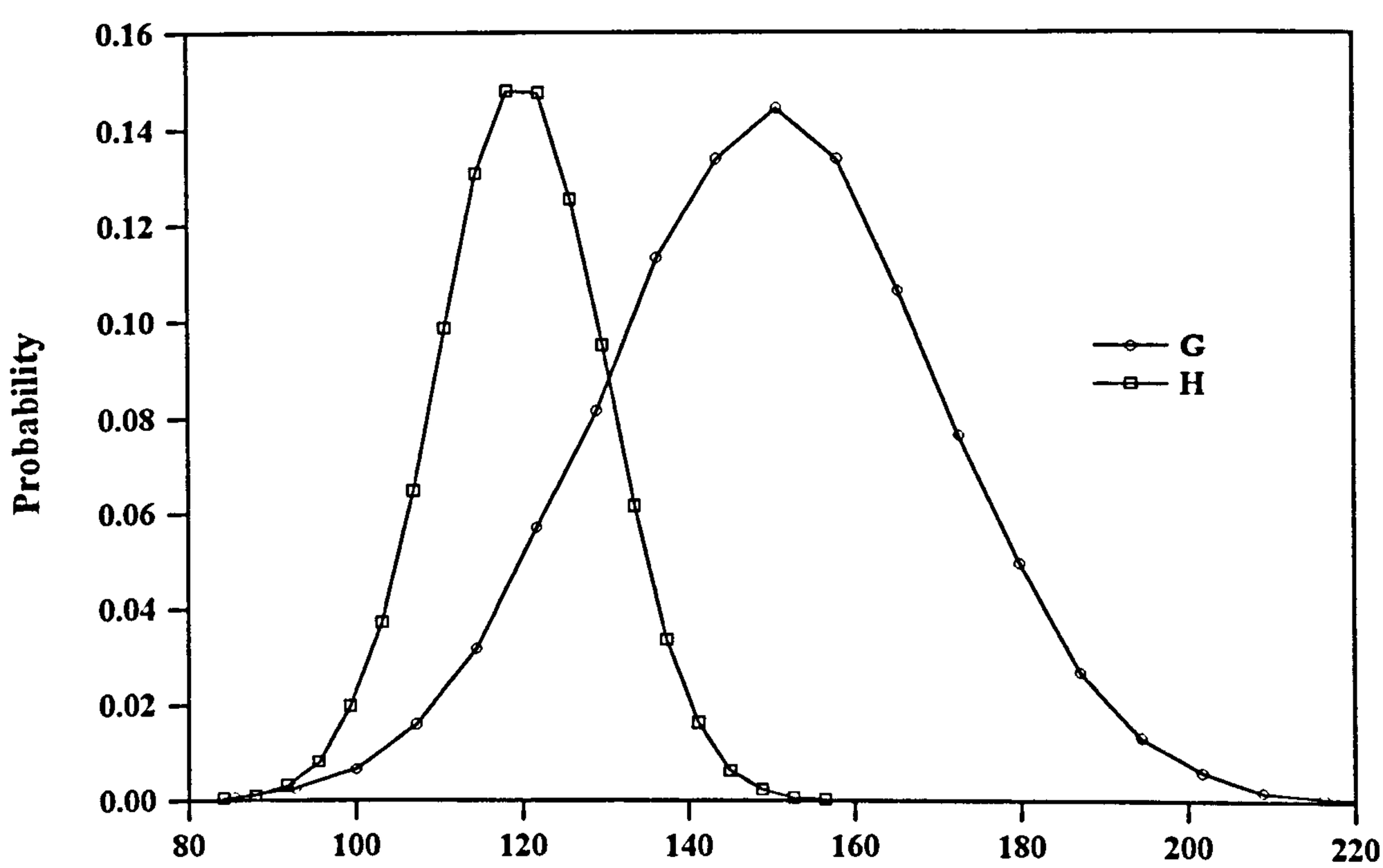

Figure 7.6 G & H distributions

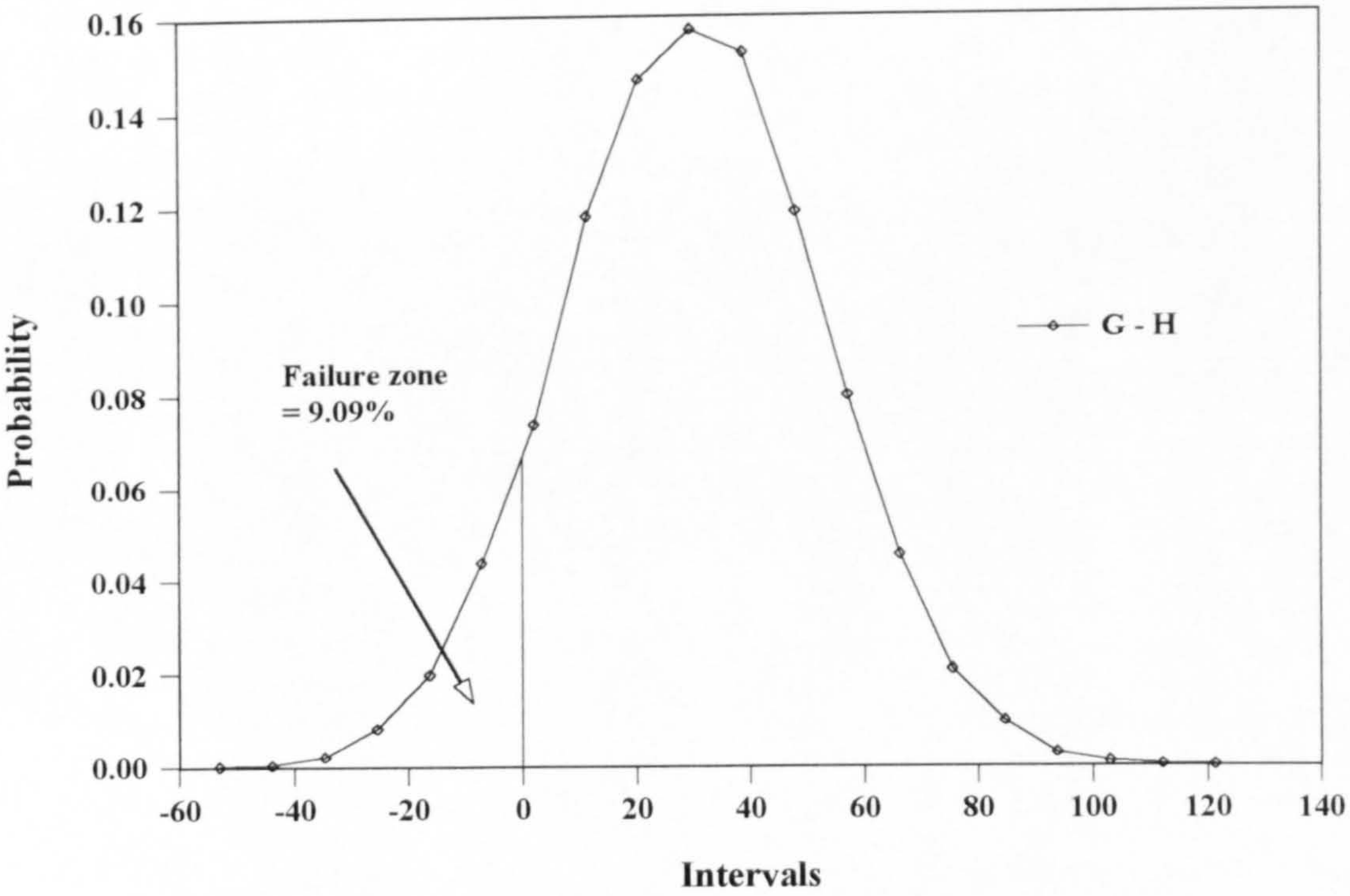

Figure 7.7 Distribution of G - H

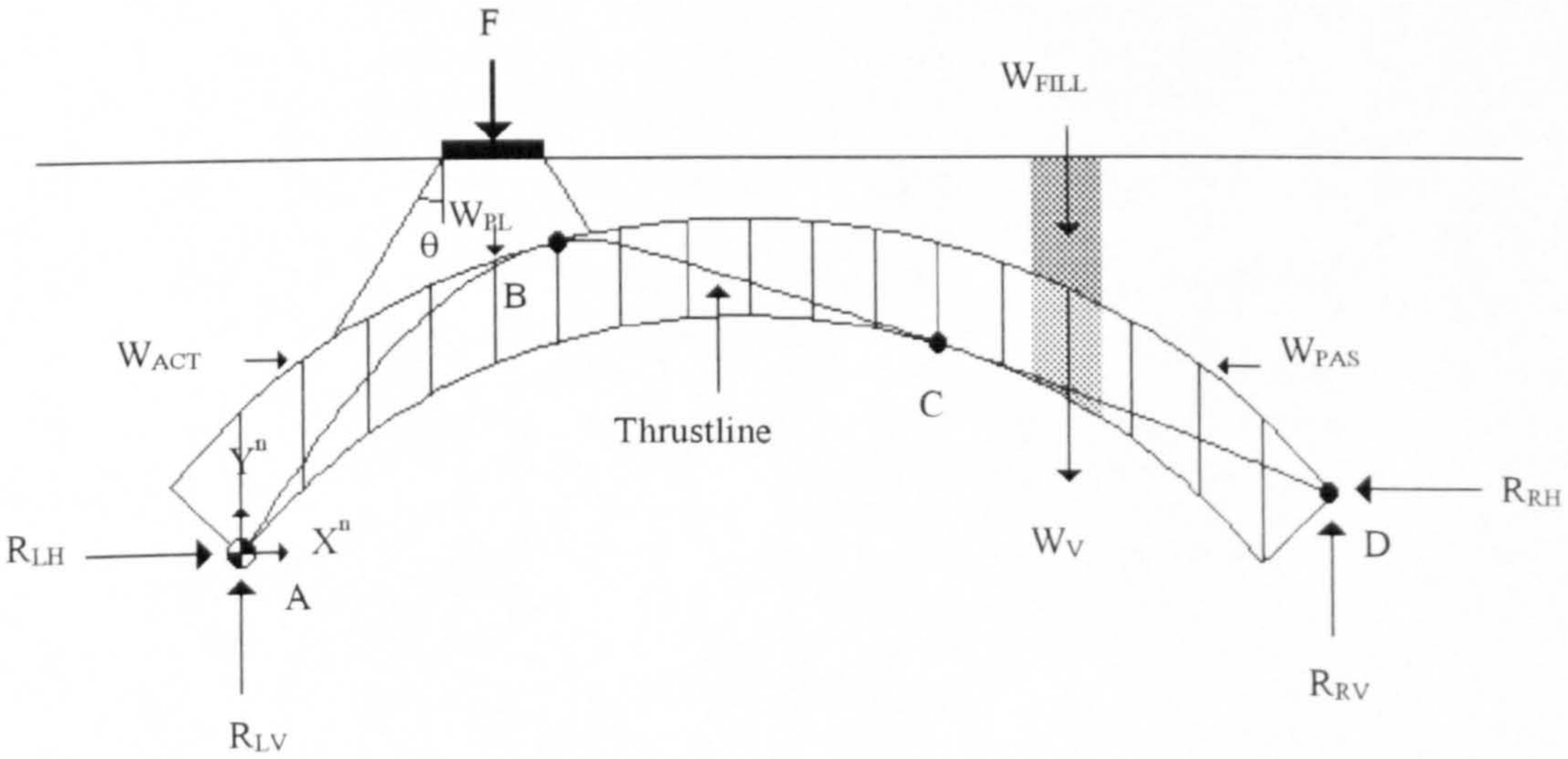

Figure 7.8 Idealisation of an arch bridge with its typical failure mechanism

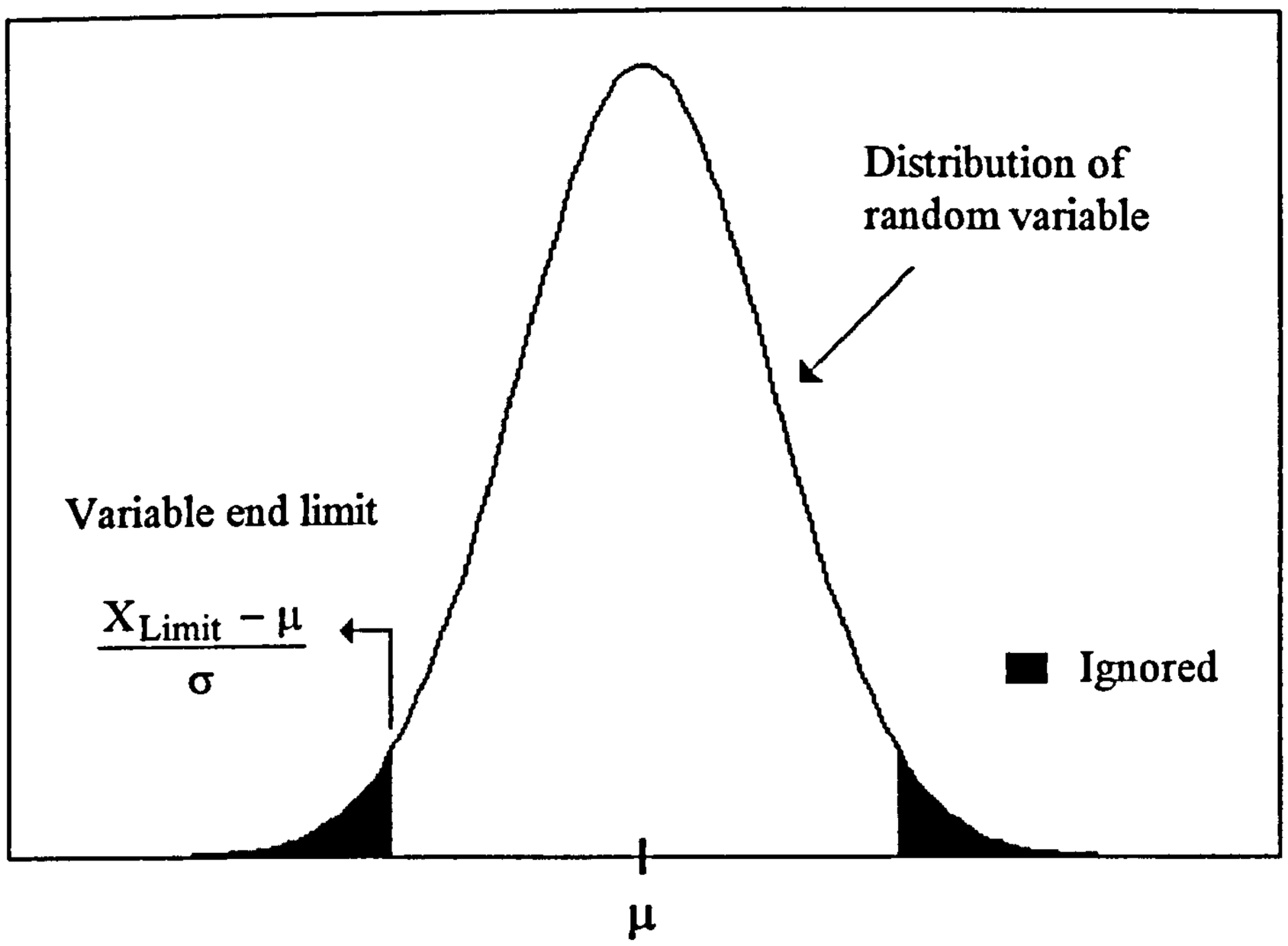

Figure 7.9 The distribution of random variables and the variable end limits

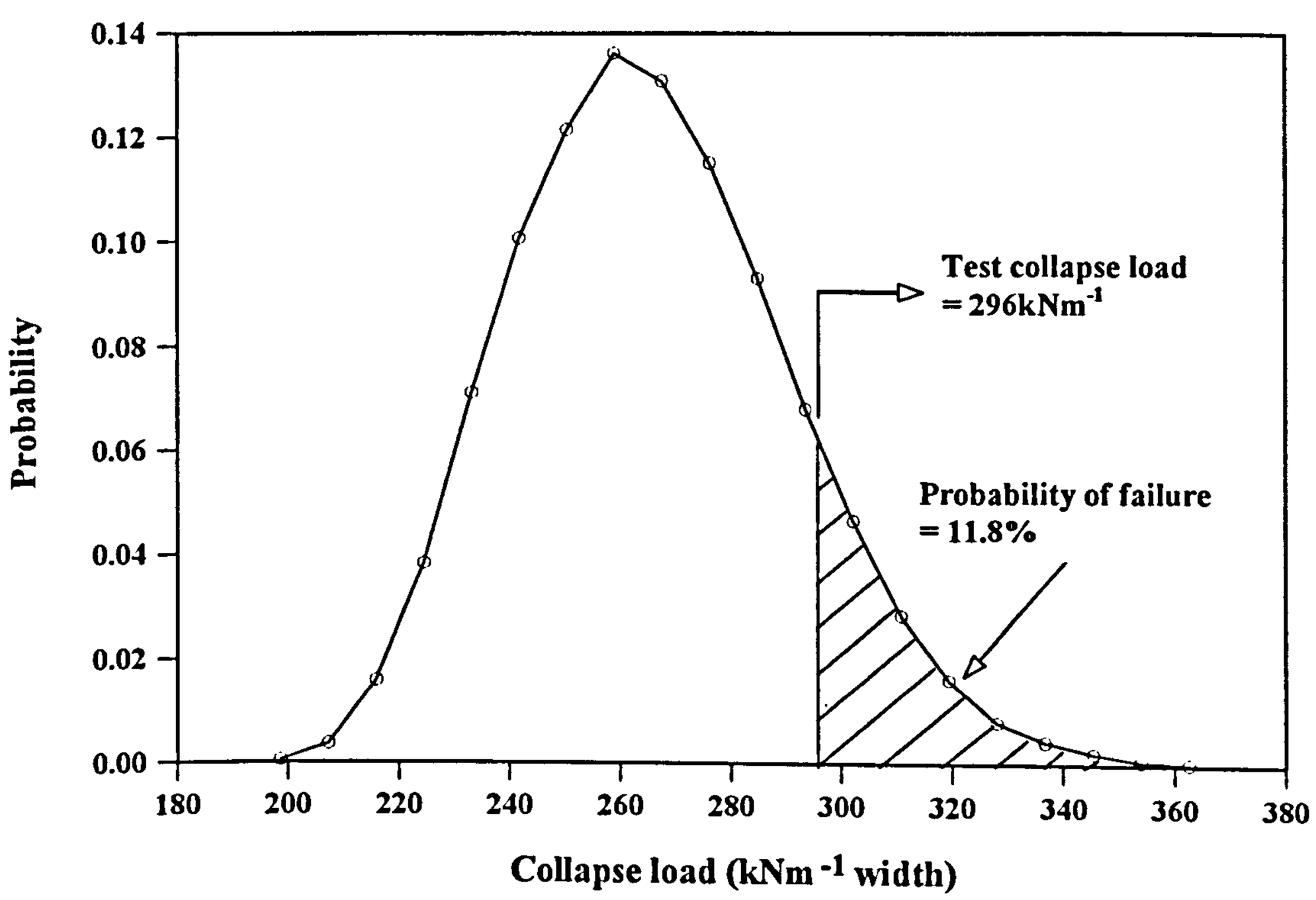

Figure 7.10 Distribution of predicted arch collapse load for Barlae bridge

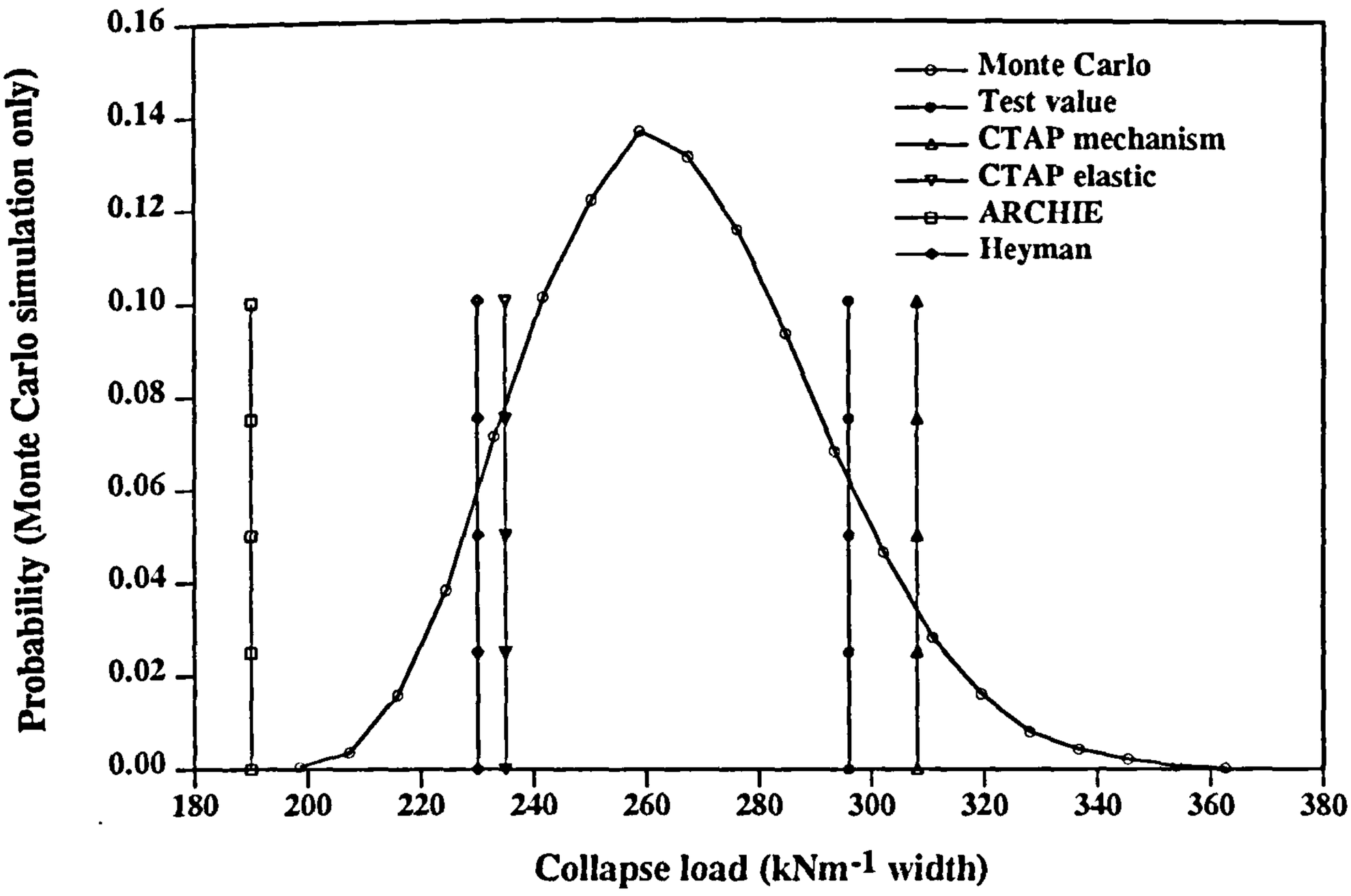

Figure 7.11 Comparison with other assessment methods

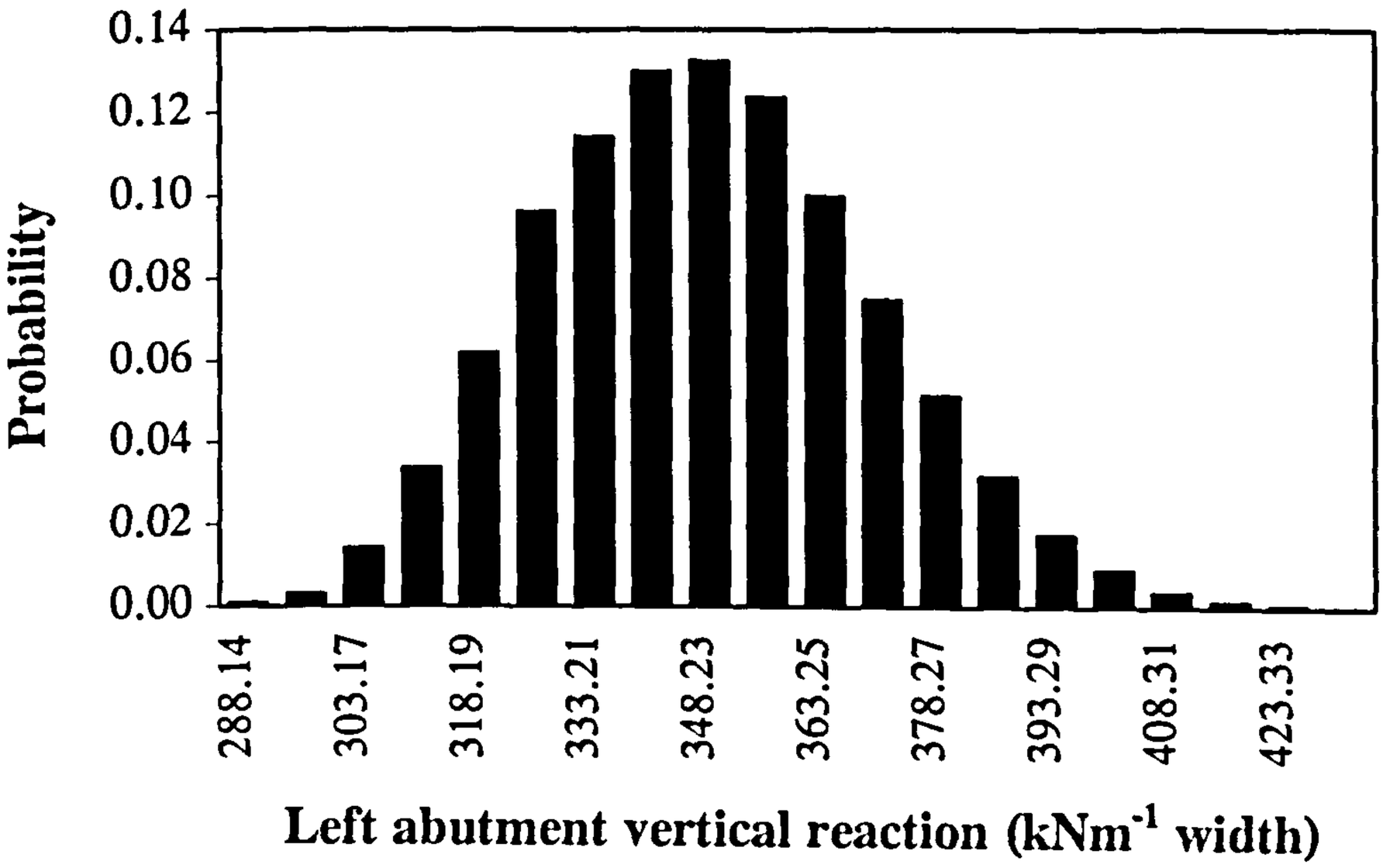

Figure 7.12 Probability distribution of left abutment vertical reaction

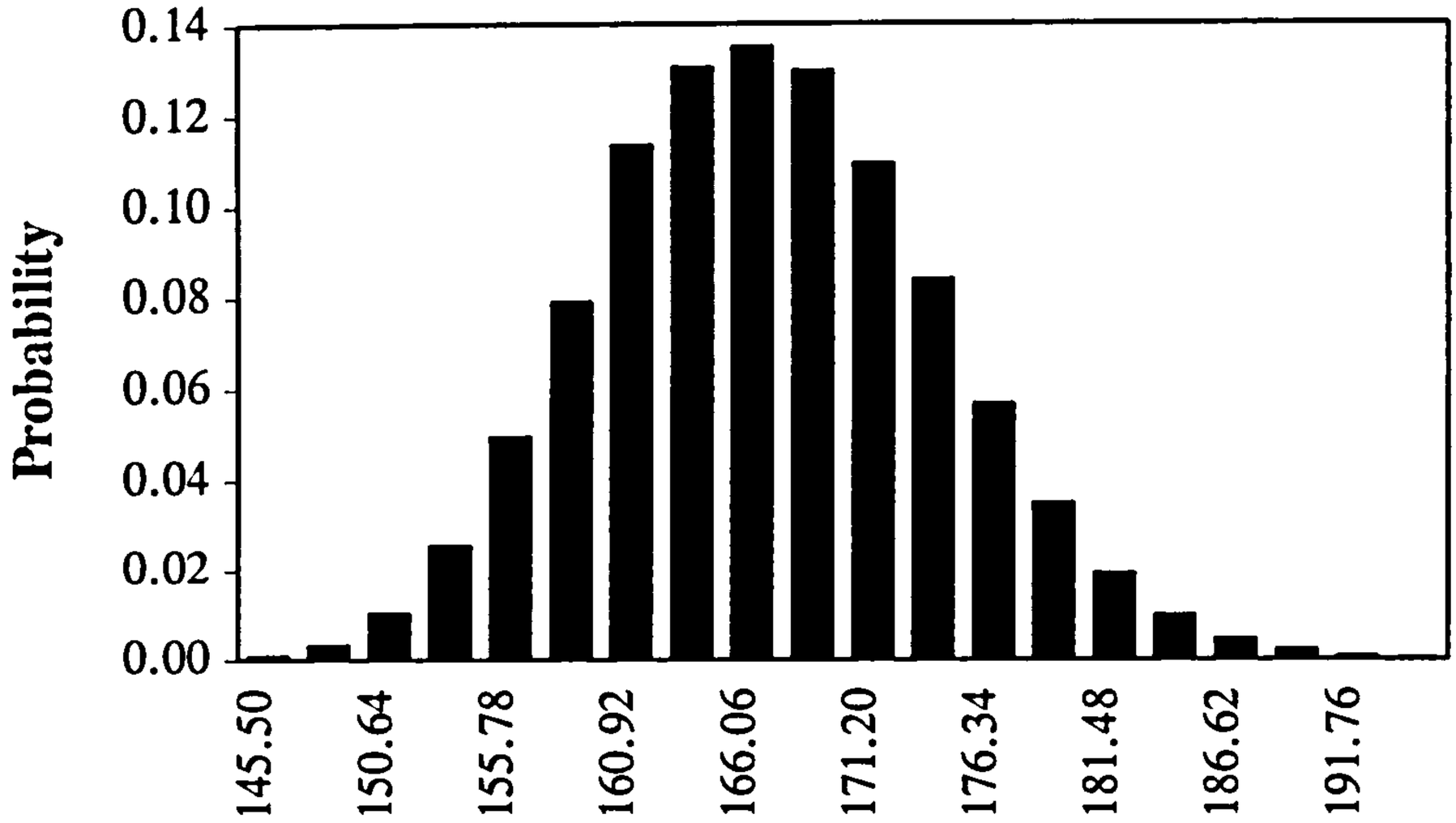

Figure 7.13 Probability distribution of right abutment vertical reaction

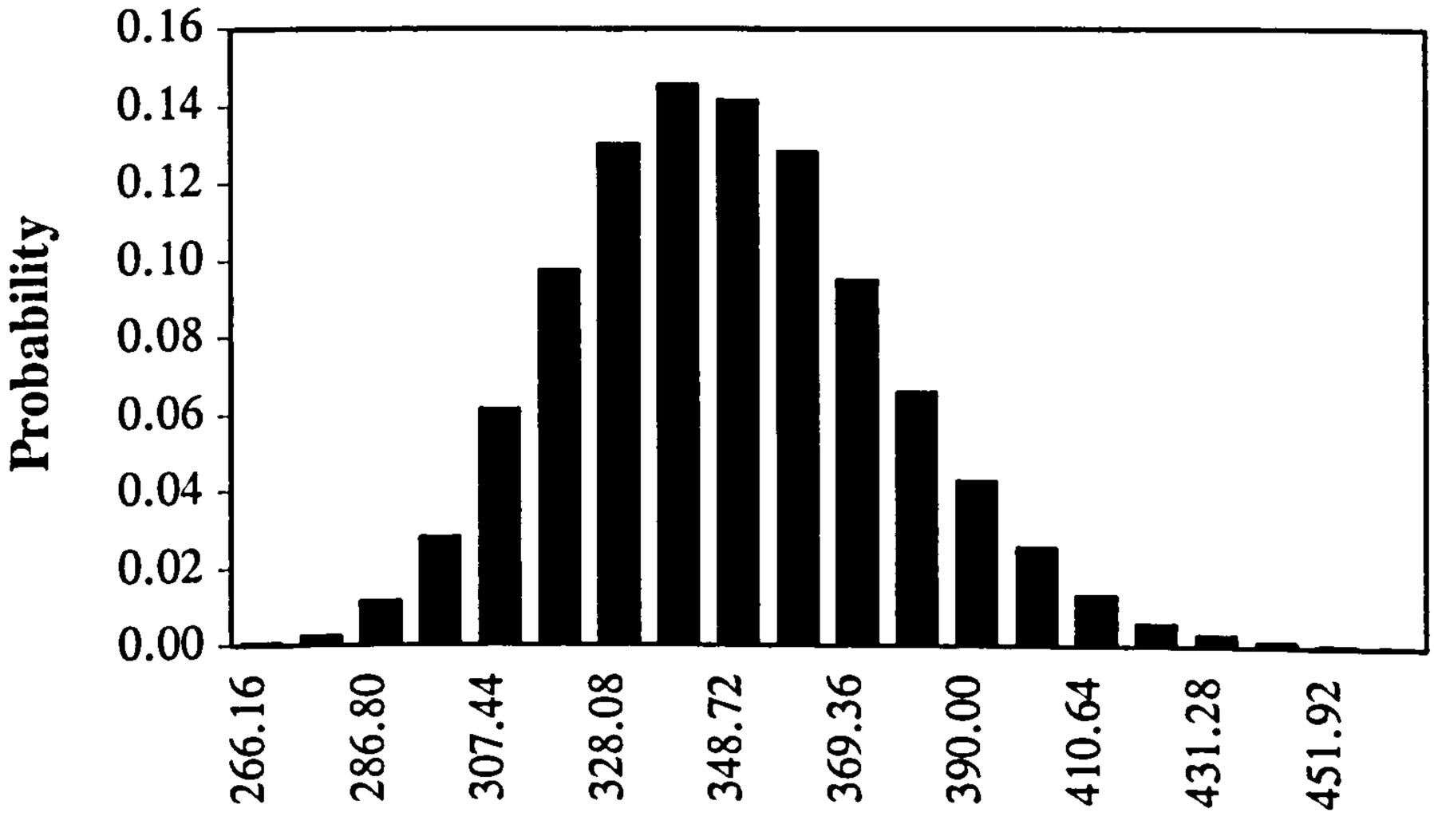

Figure 7.14 Probability distribution of left abutment horizontal reaction

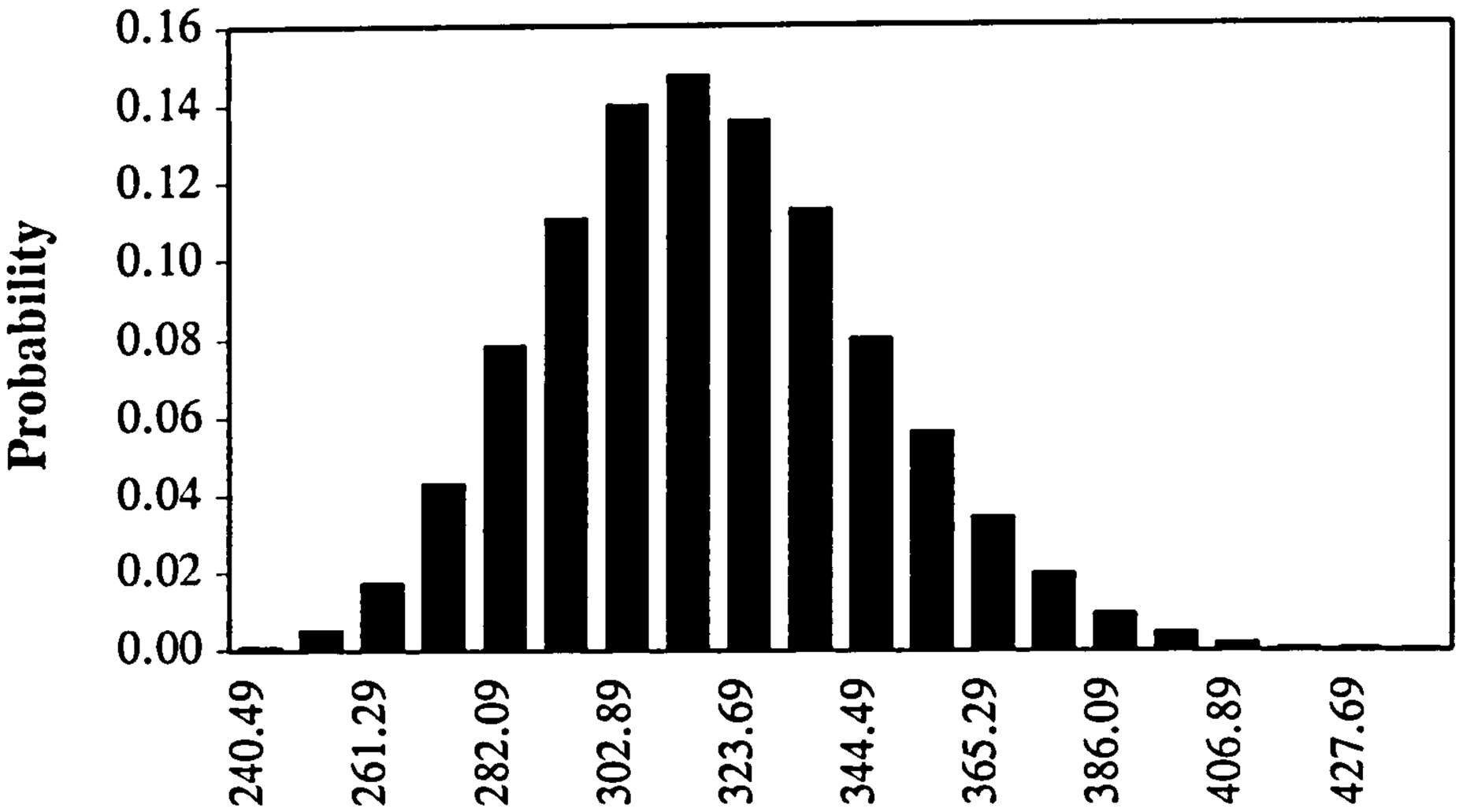

Figure 7.15 Probability distribution of right abutment horizontal reaction

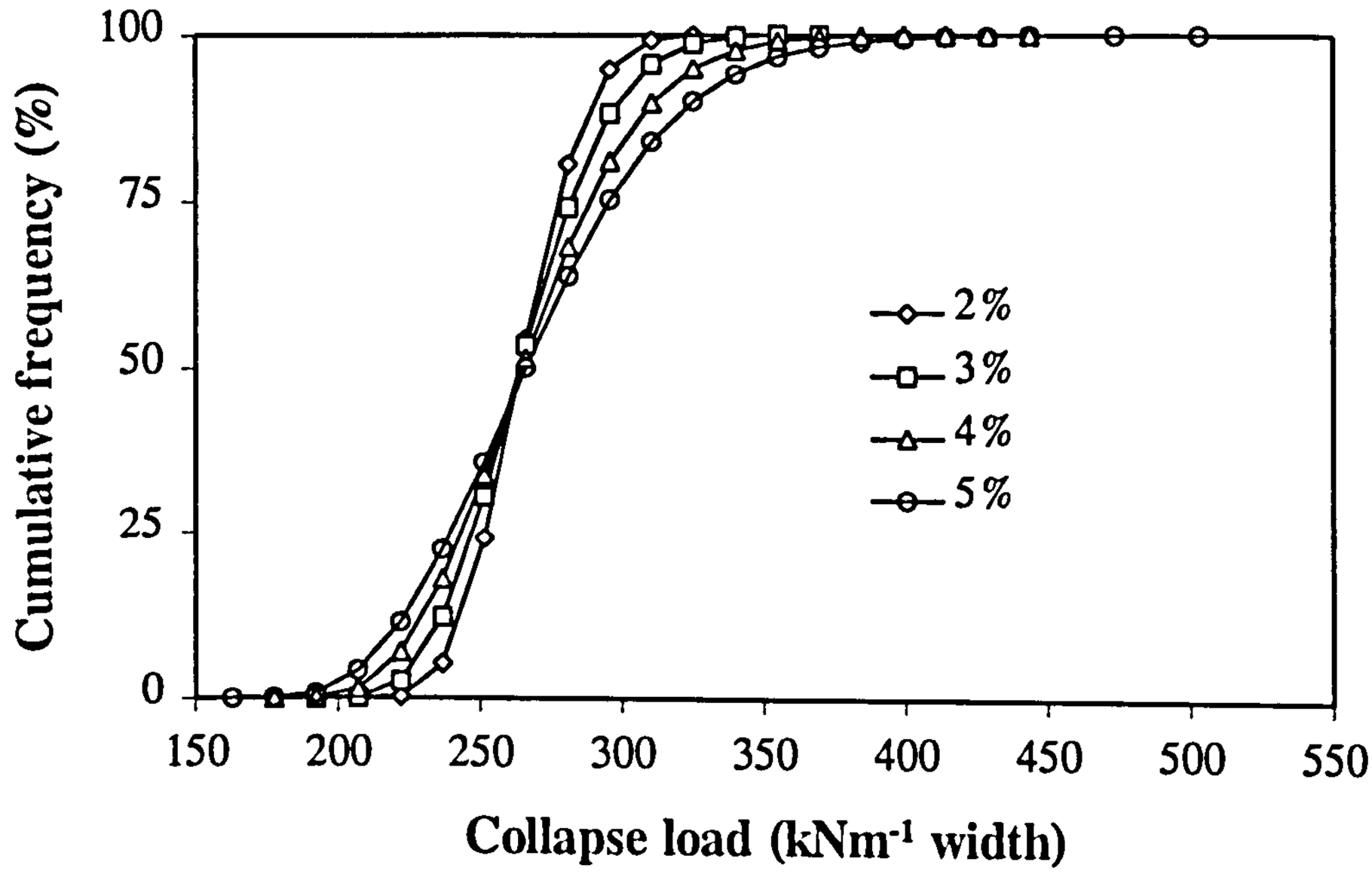

Figure 7.16 The effect of changing coefficient of variation of variables

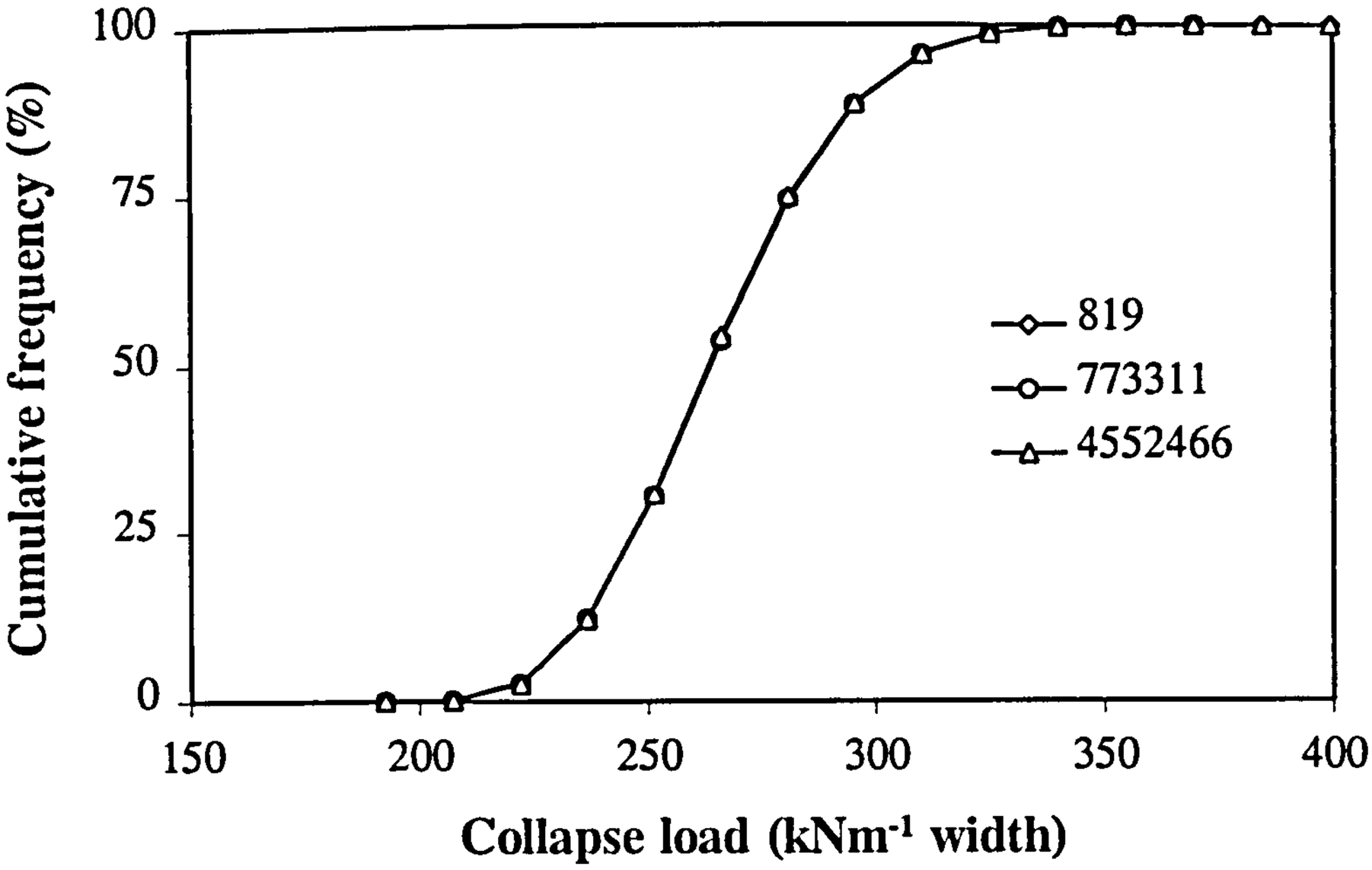

Figure 7.17 The effect of the seed for the random number generator

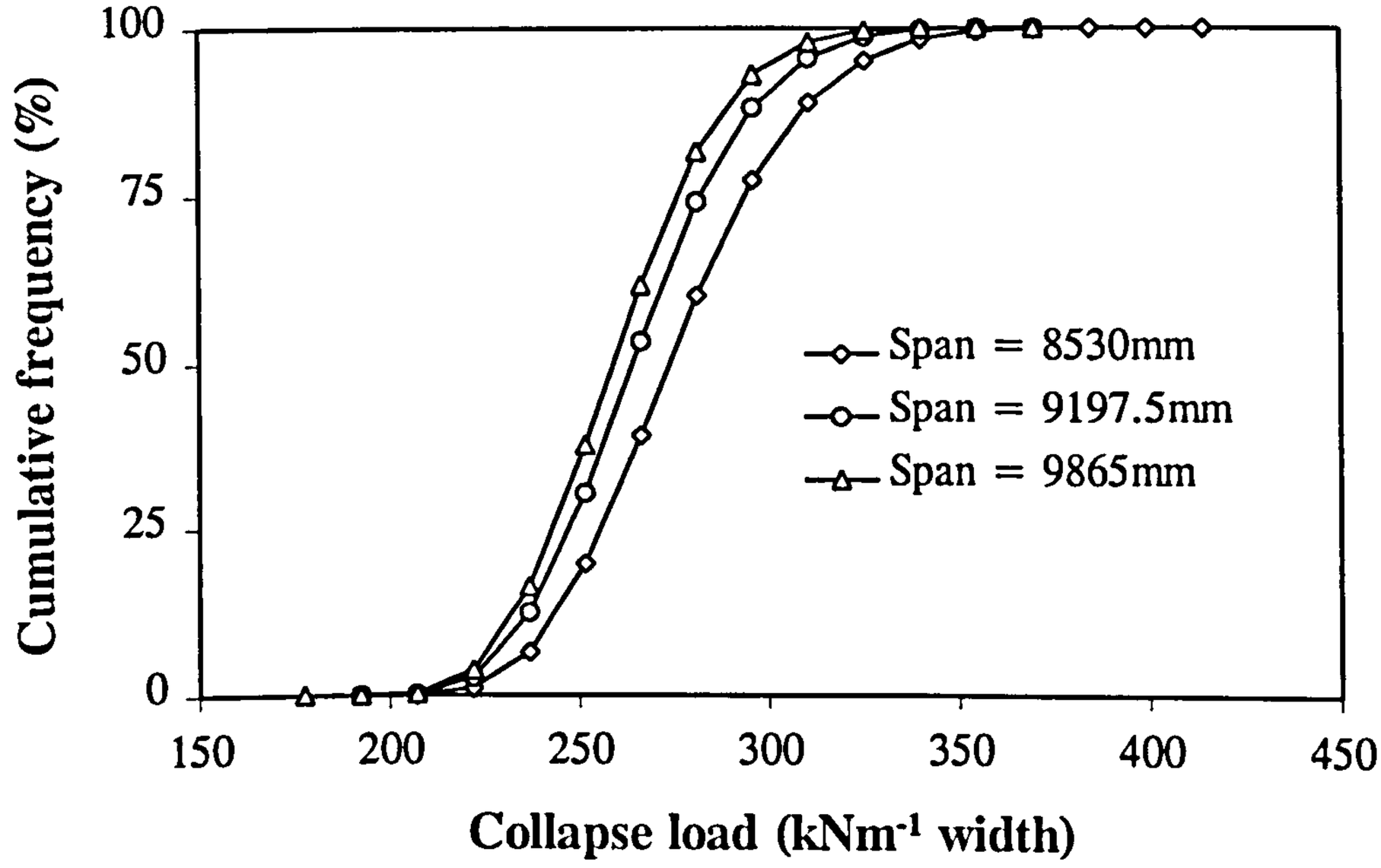

Figure 7.18 The effect of arch span upon the collapse load

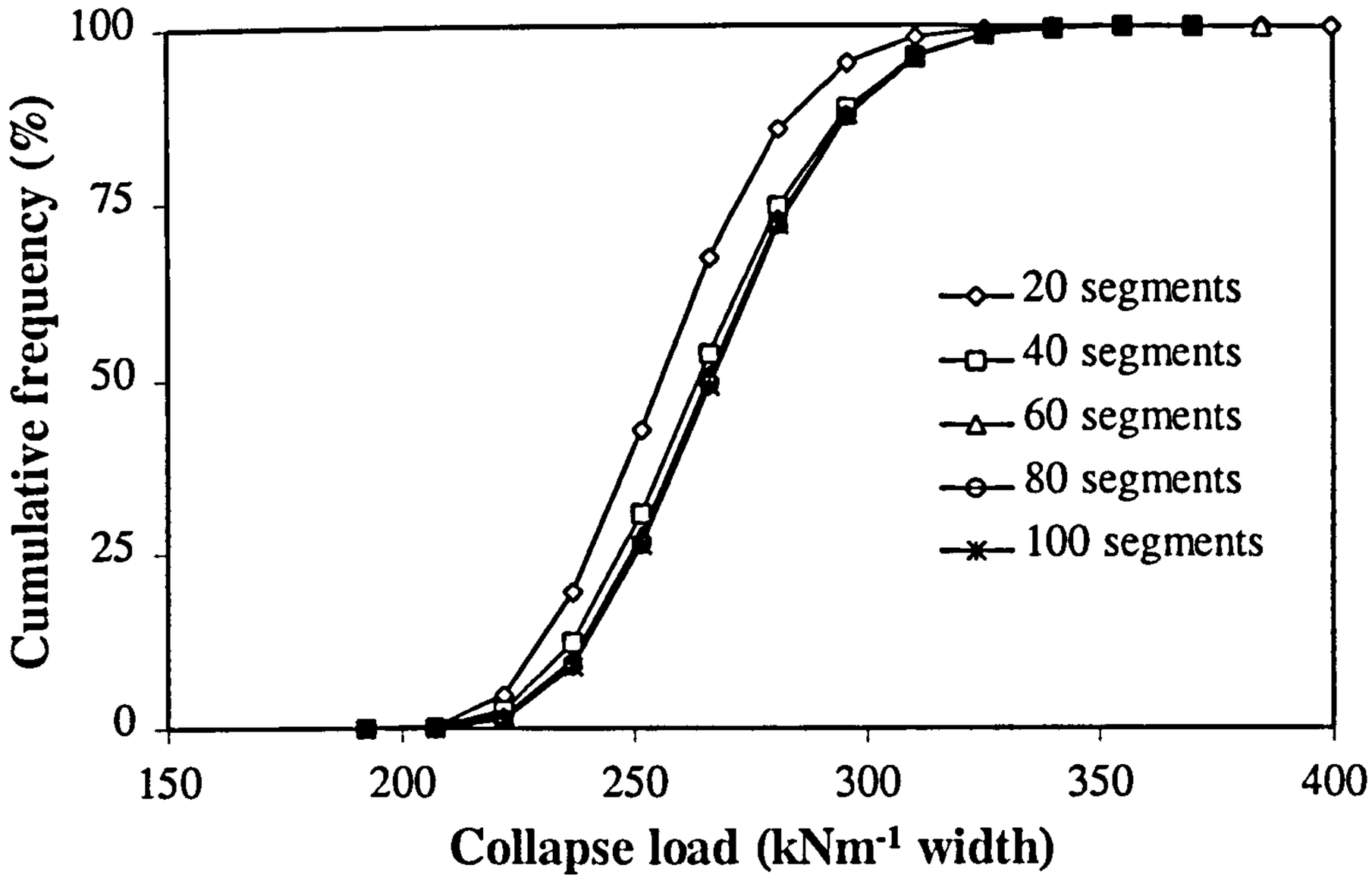

Figure 7.19 The effect of the number of segments in the arch ring

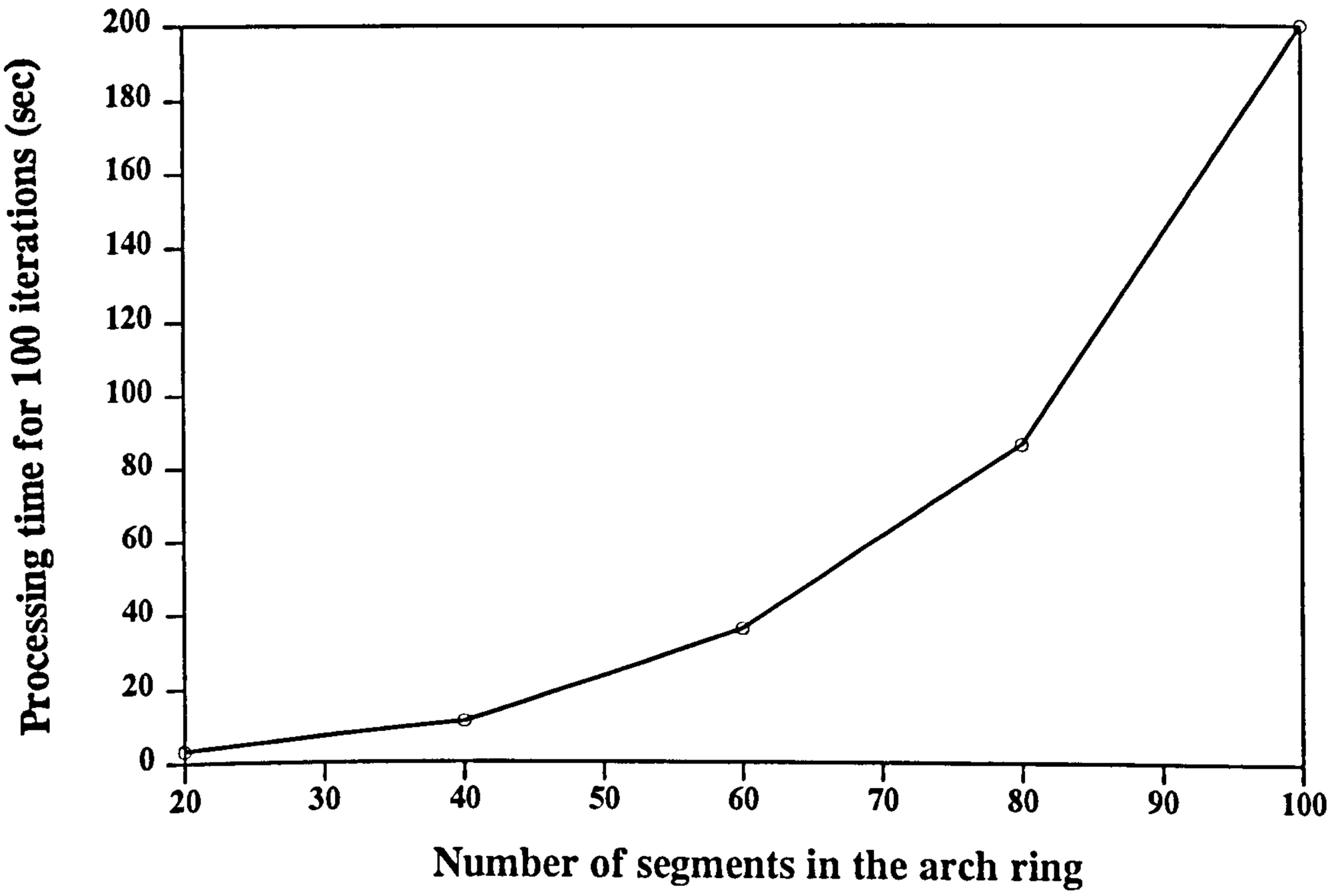

Figure 7.20 Processing time required for analysis completion

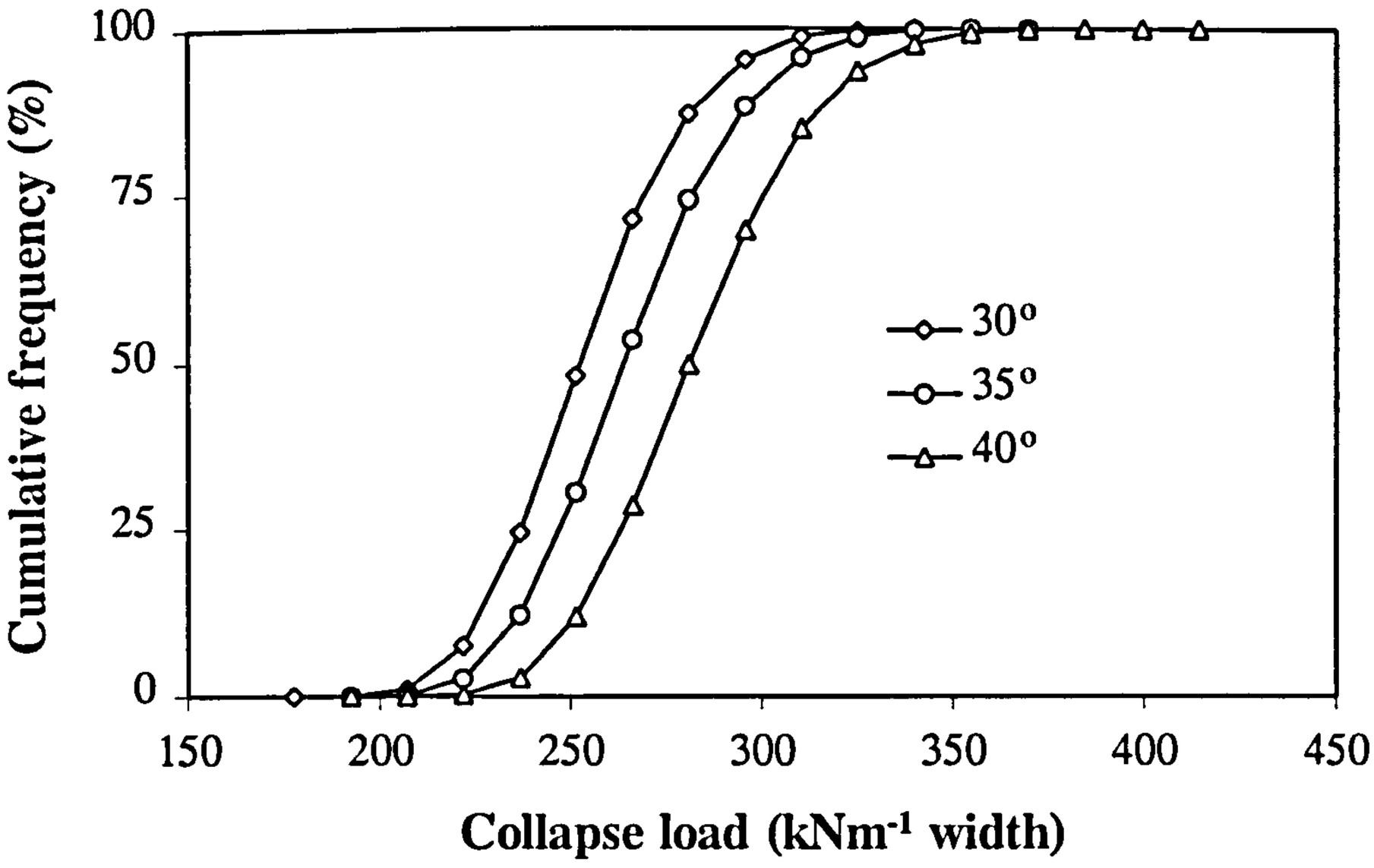

Figure 7.21 The effect of live load dispersal angle upon the collapse load

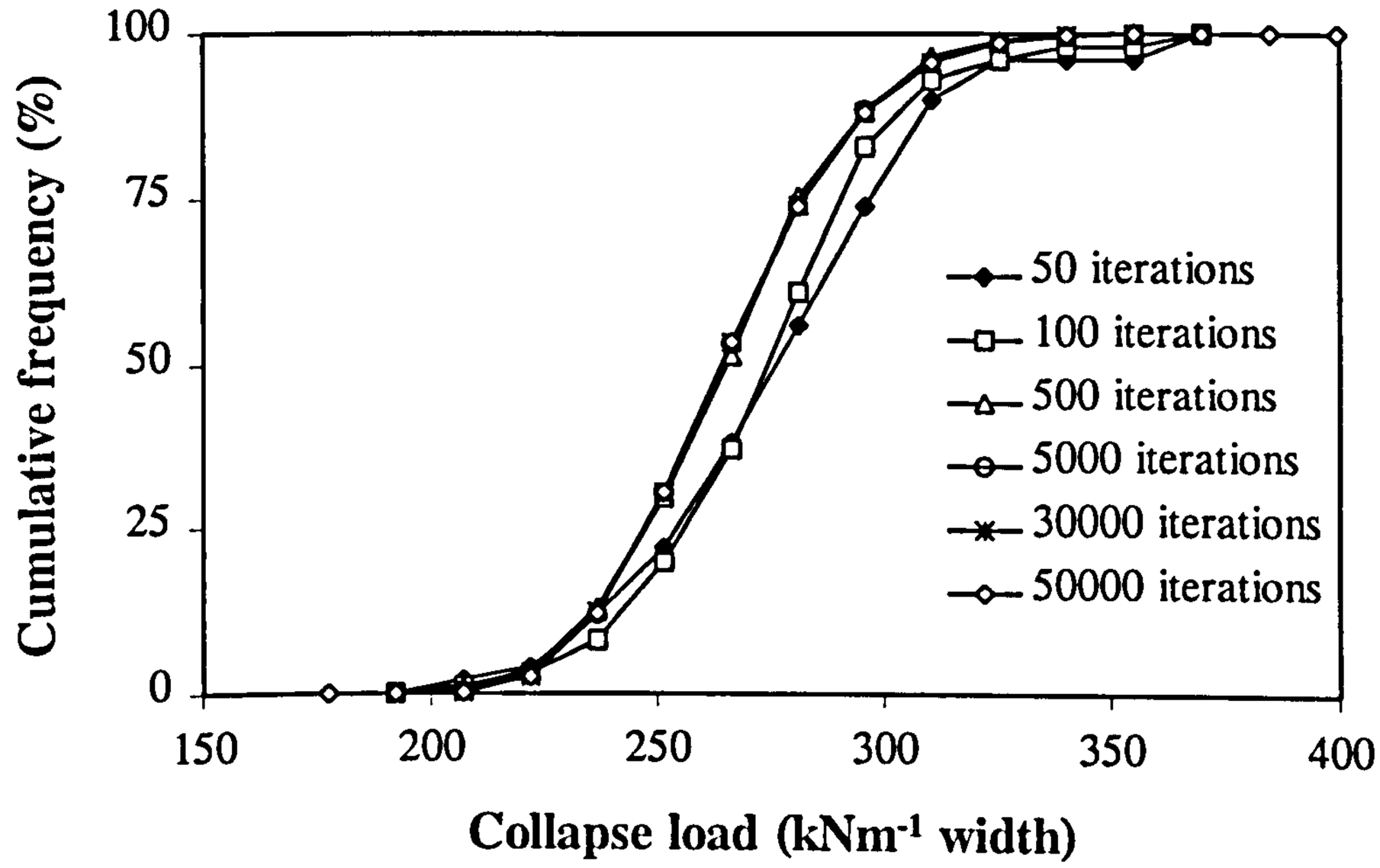

Figure 7.22 The effect of number of iterations *per* analysis

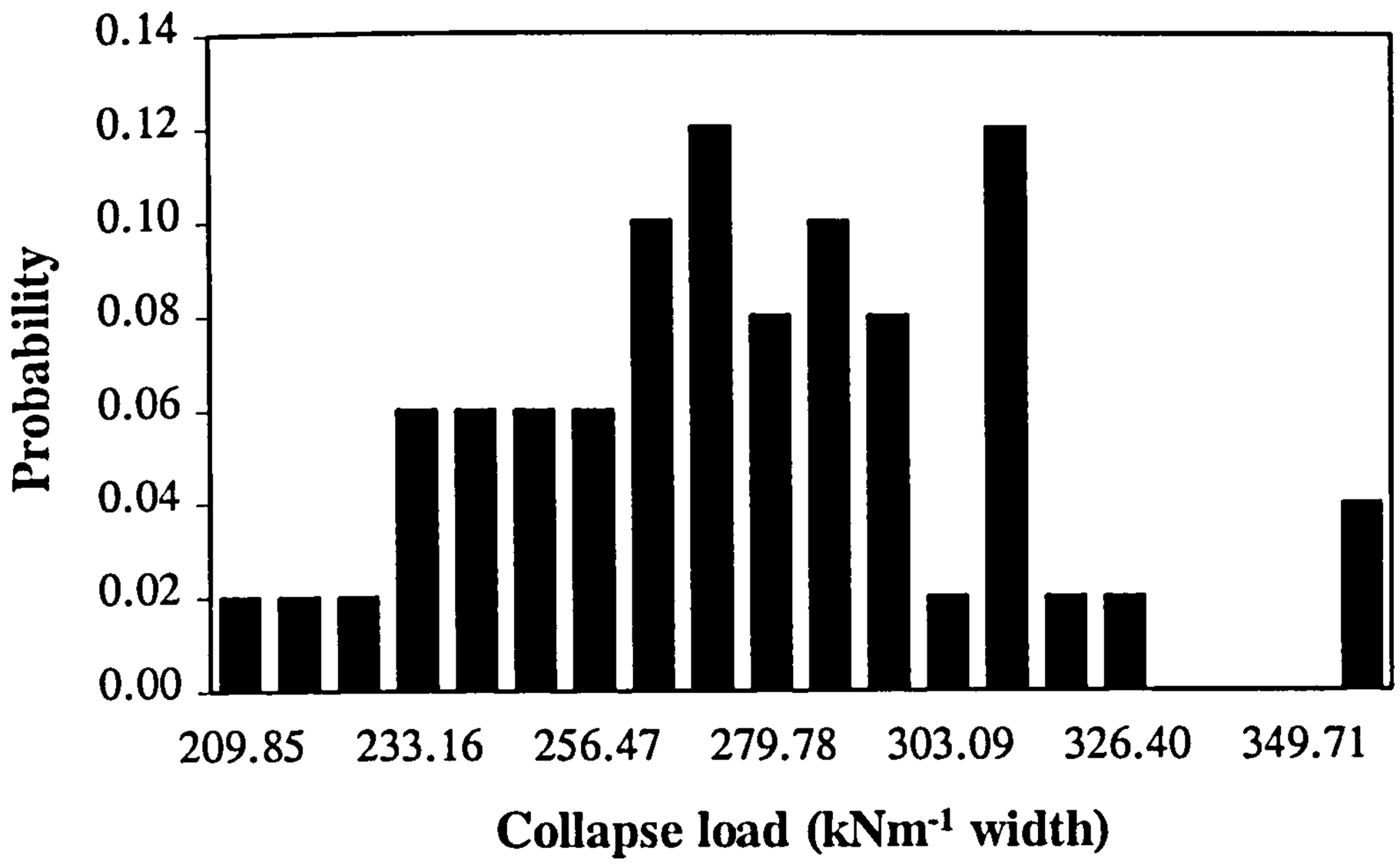

Figure 7.23 The effect of the number of iterations (50 iterations)

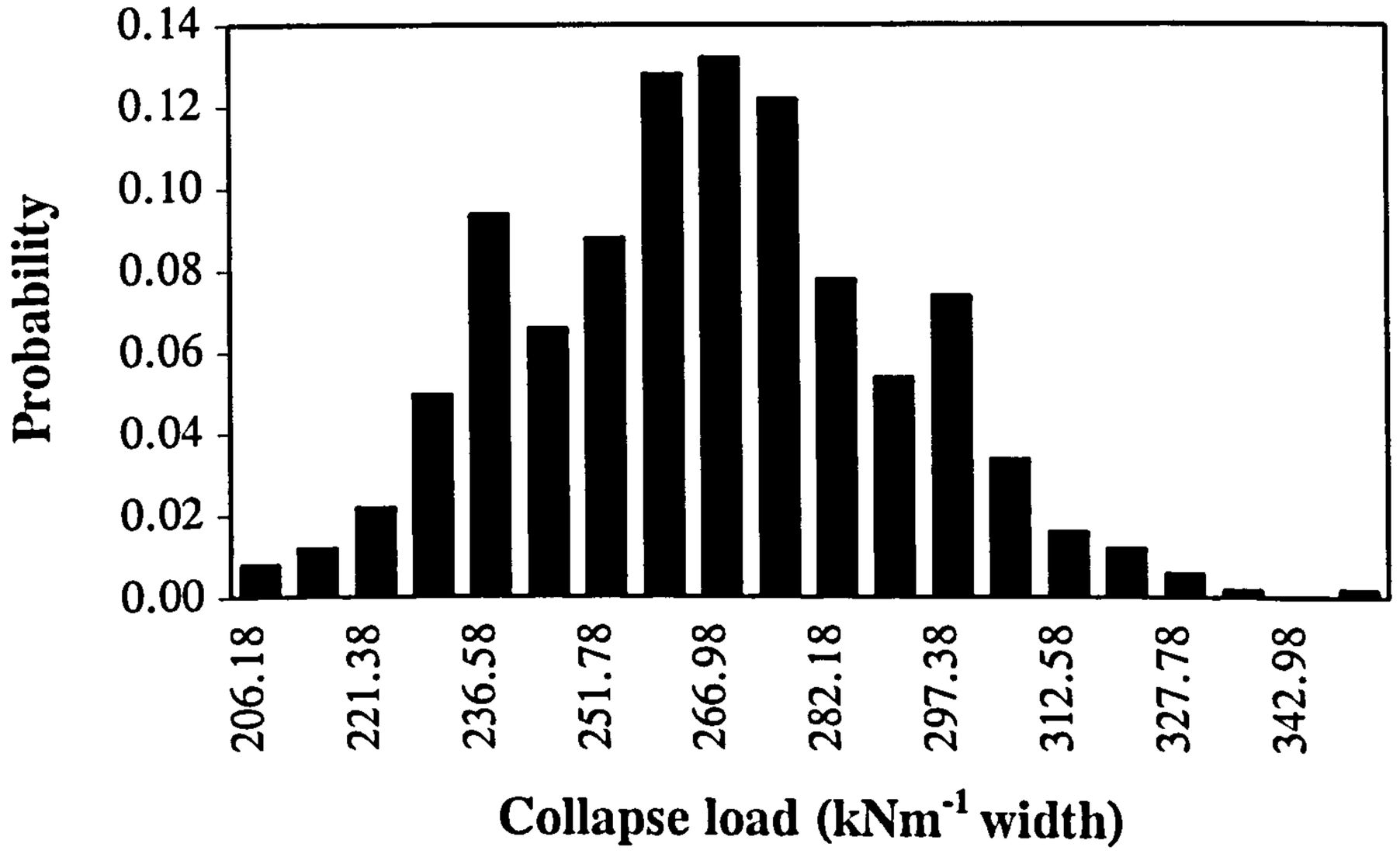

Figure 7.24 The effect of the number of iterations (500 iterations)

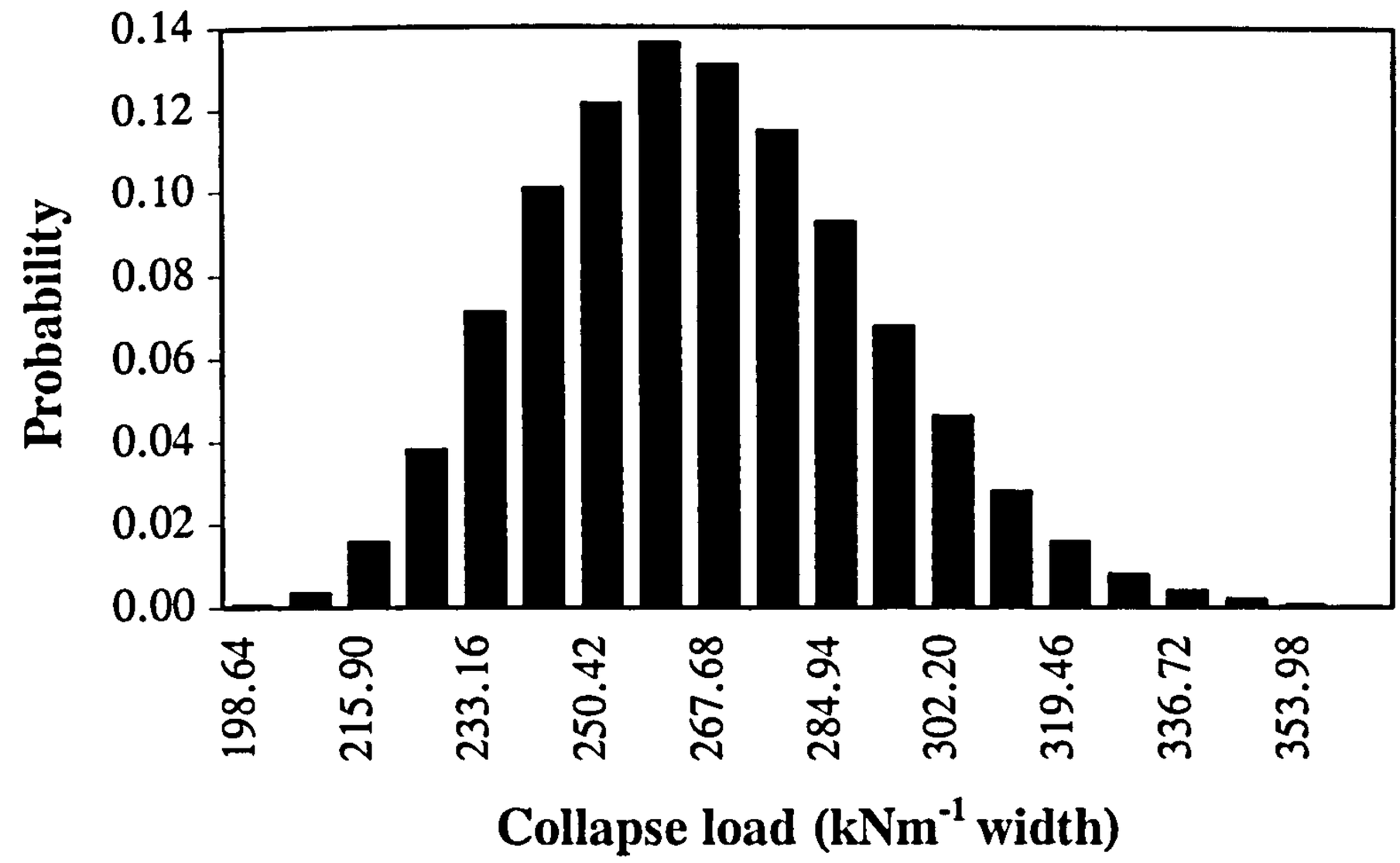

Figure 7.25 The effect of the number of iterations (30000 iterations)

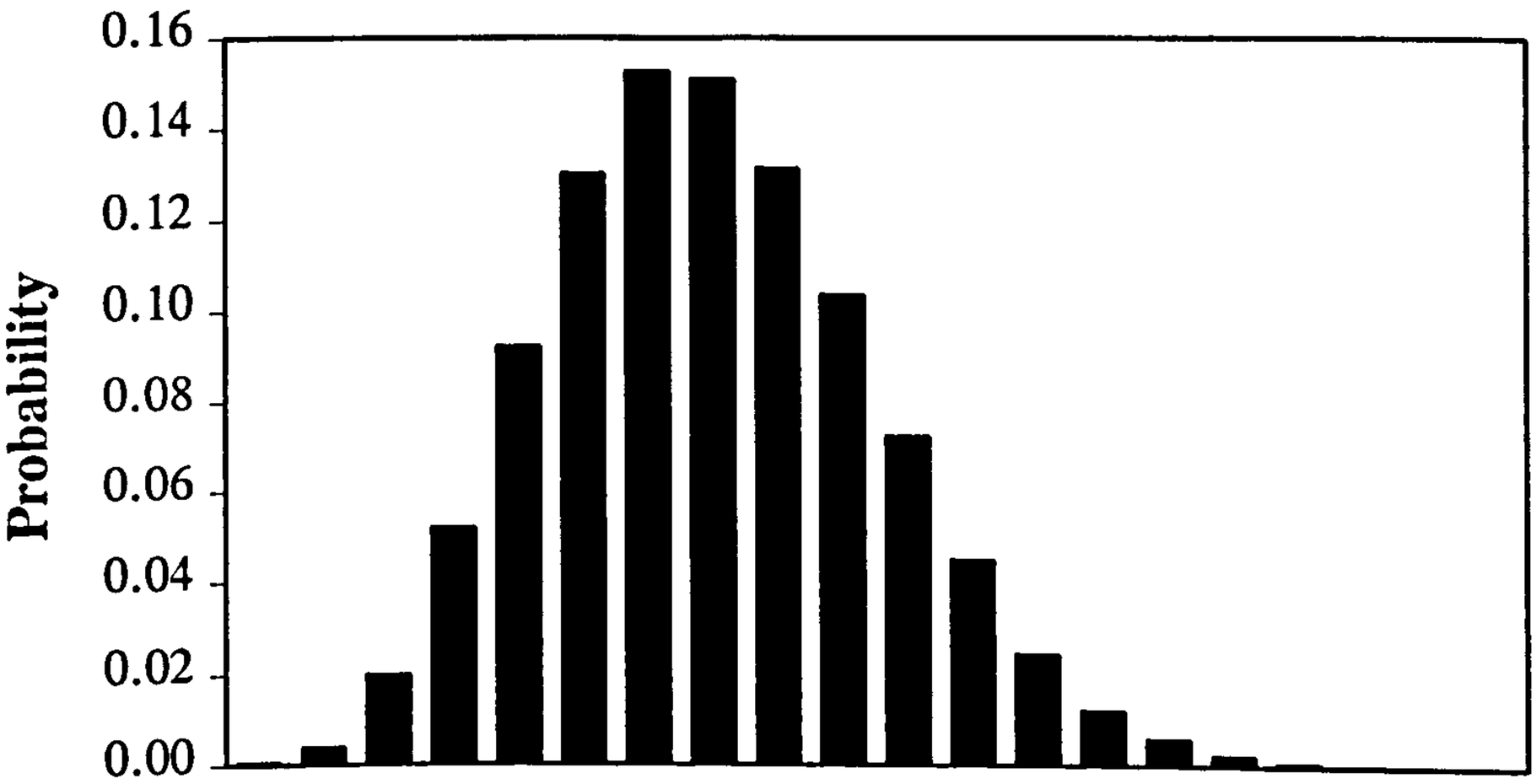

Figure 7.26 The effect of the number of iterations (50000 iterations)

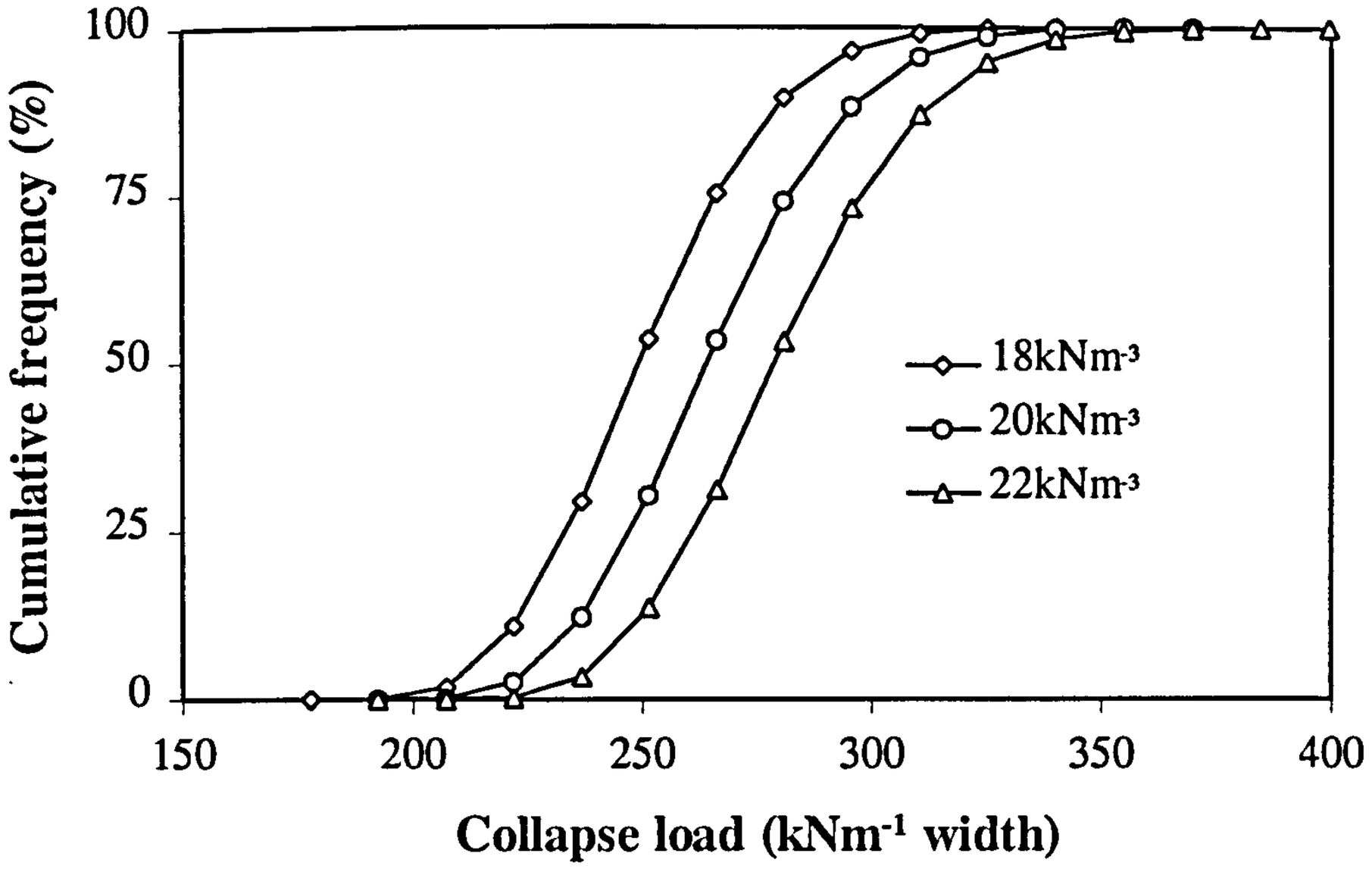

Figure 7.27 The effect of backfill bulk unit weight upon the collapse load

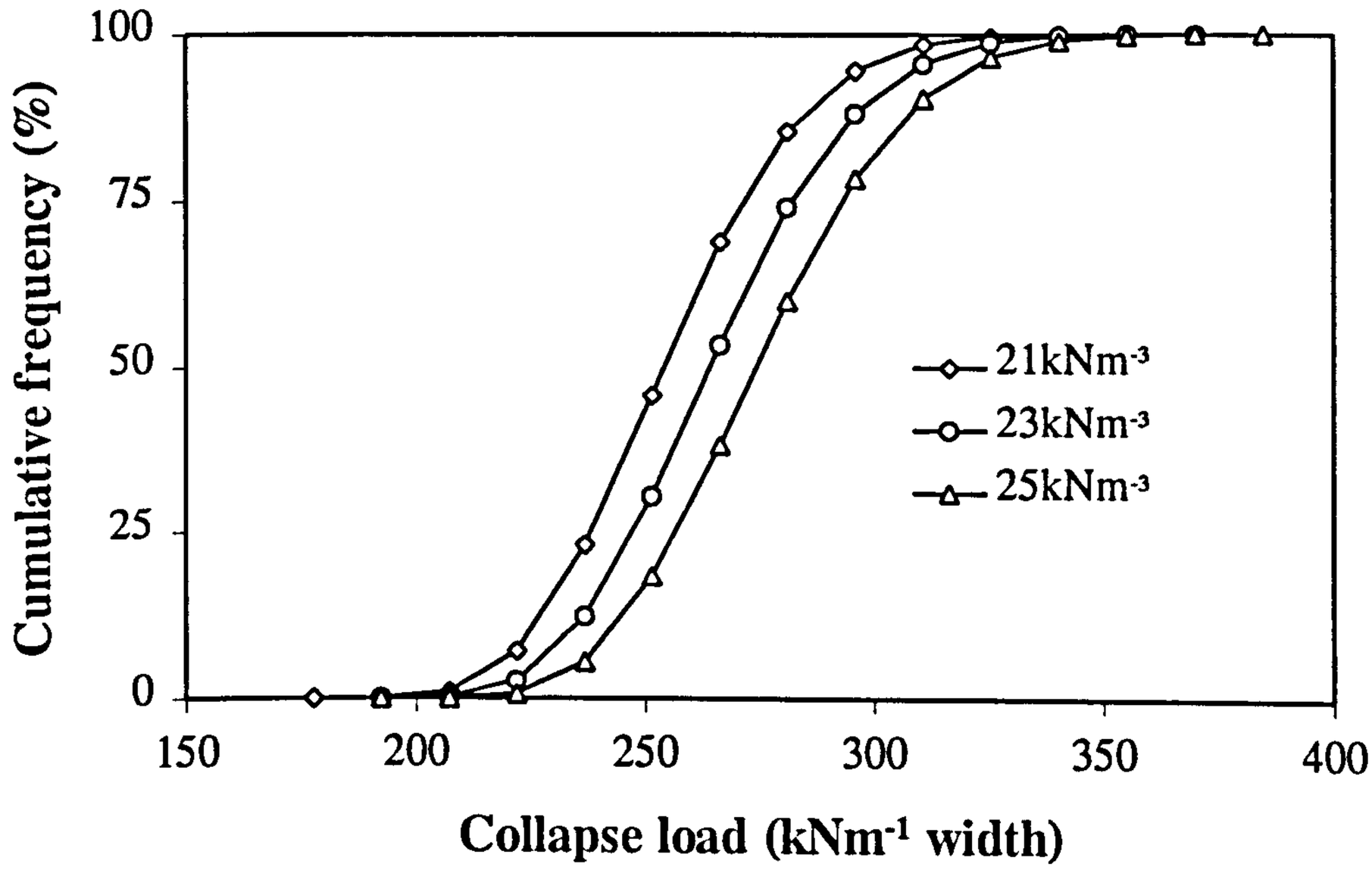

Figure 7.28 The effect of arch bulk unit weight upon the collapse load

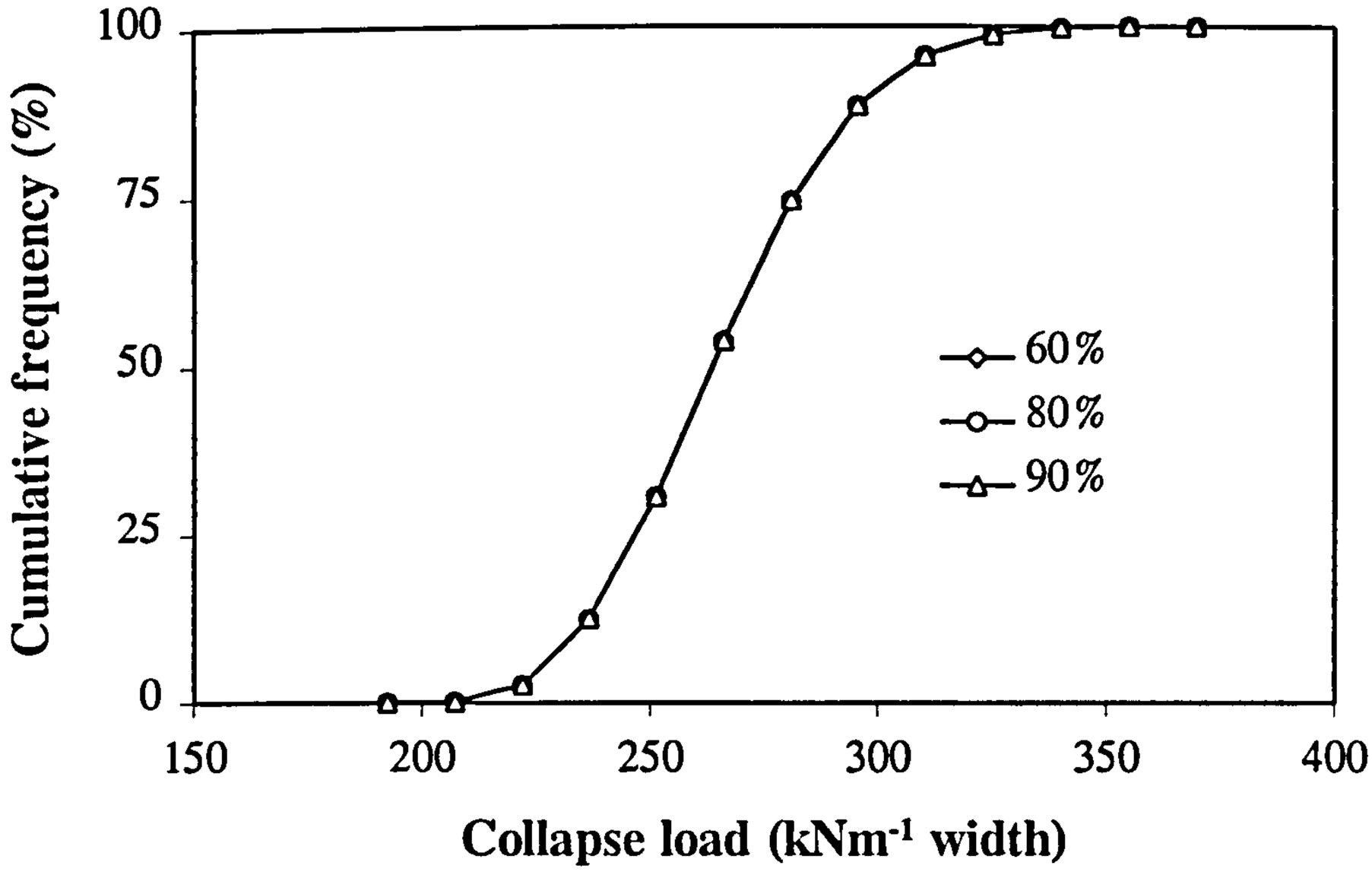

Figure 7.29 The effect of backfill active pressure mobilisation upon the collapse load

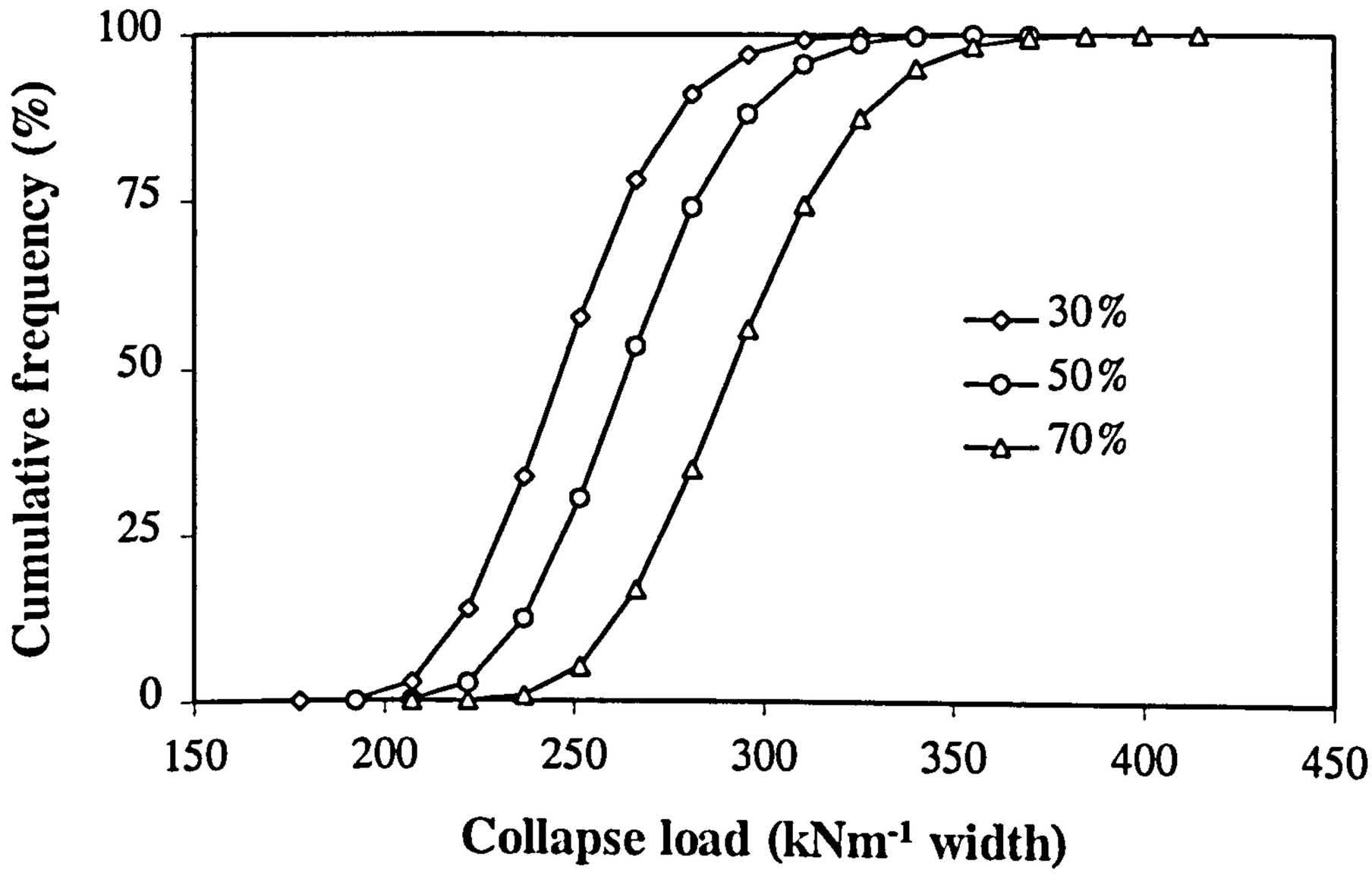

Figure 7.30 The effect of backfill passive pressure mobilisation upon the collapse load

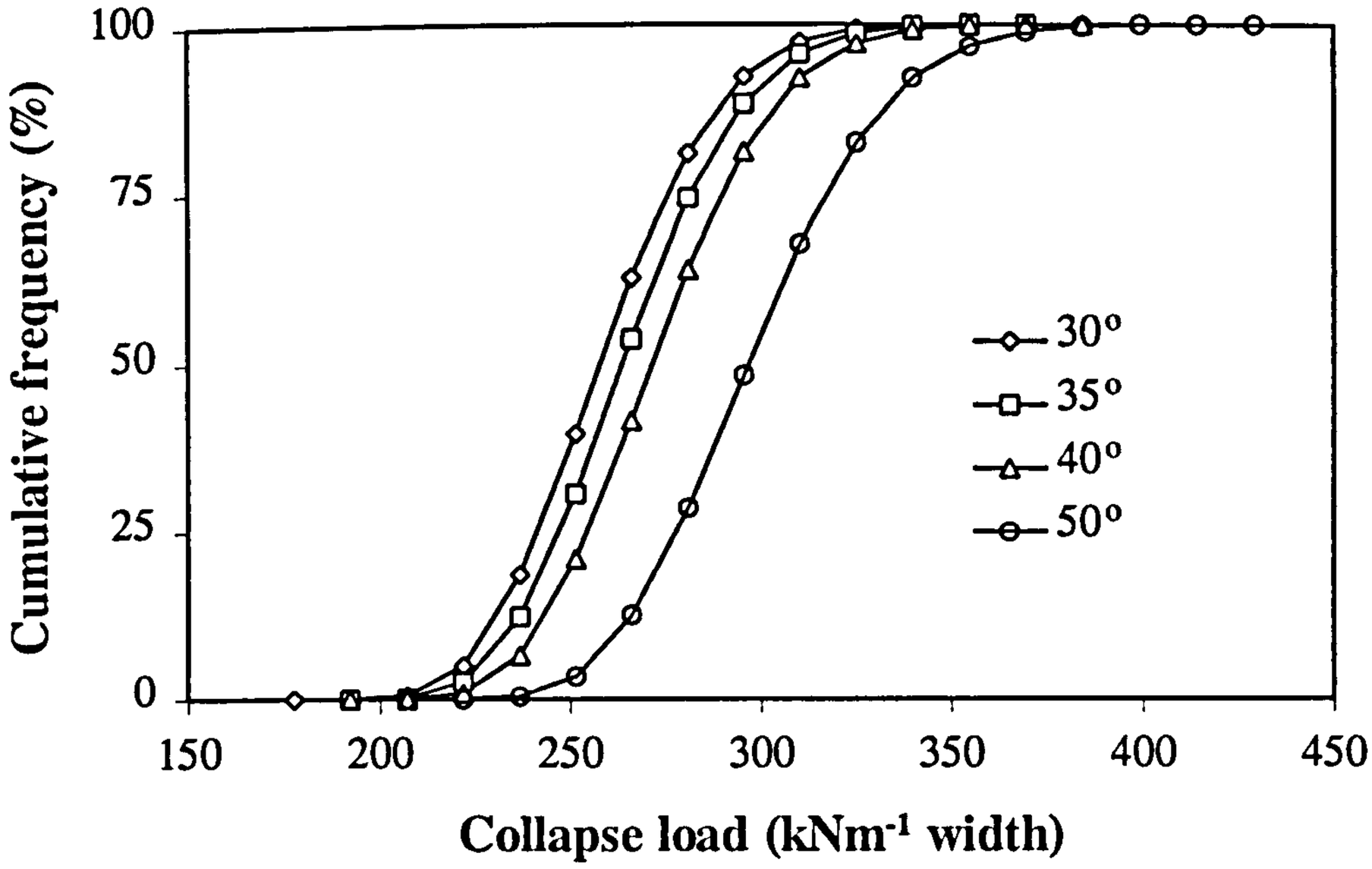

Figure 7.31 The effect of backfill angle of shearing resistance upon the collapse load

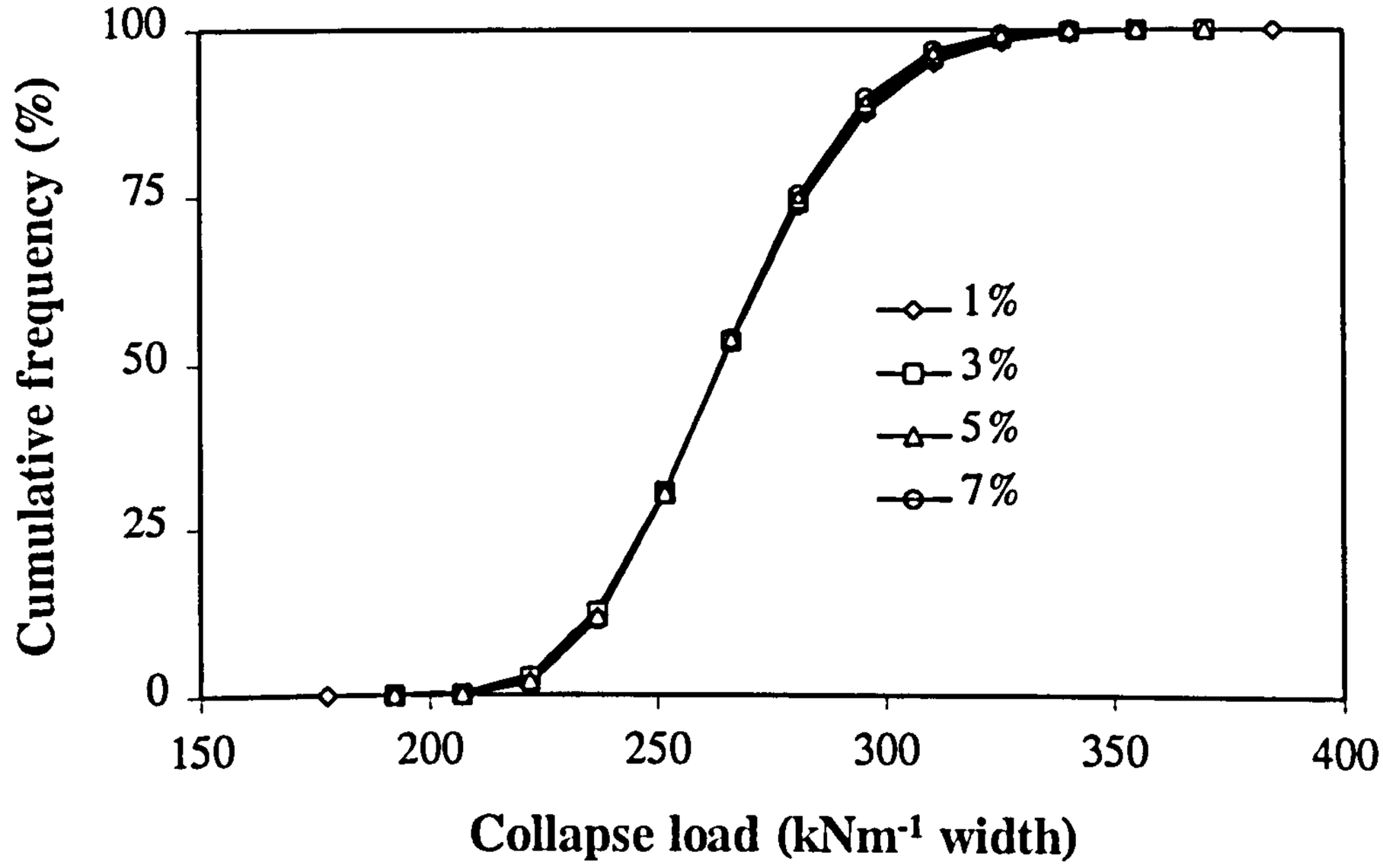

Figure 7.32 The effect of variable end limit upon the collapse load

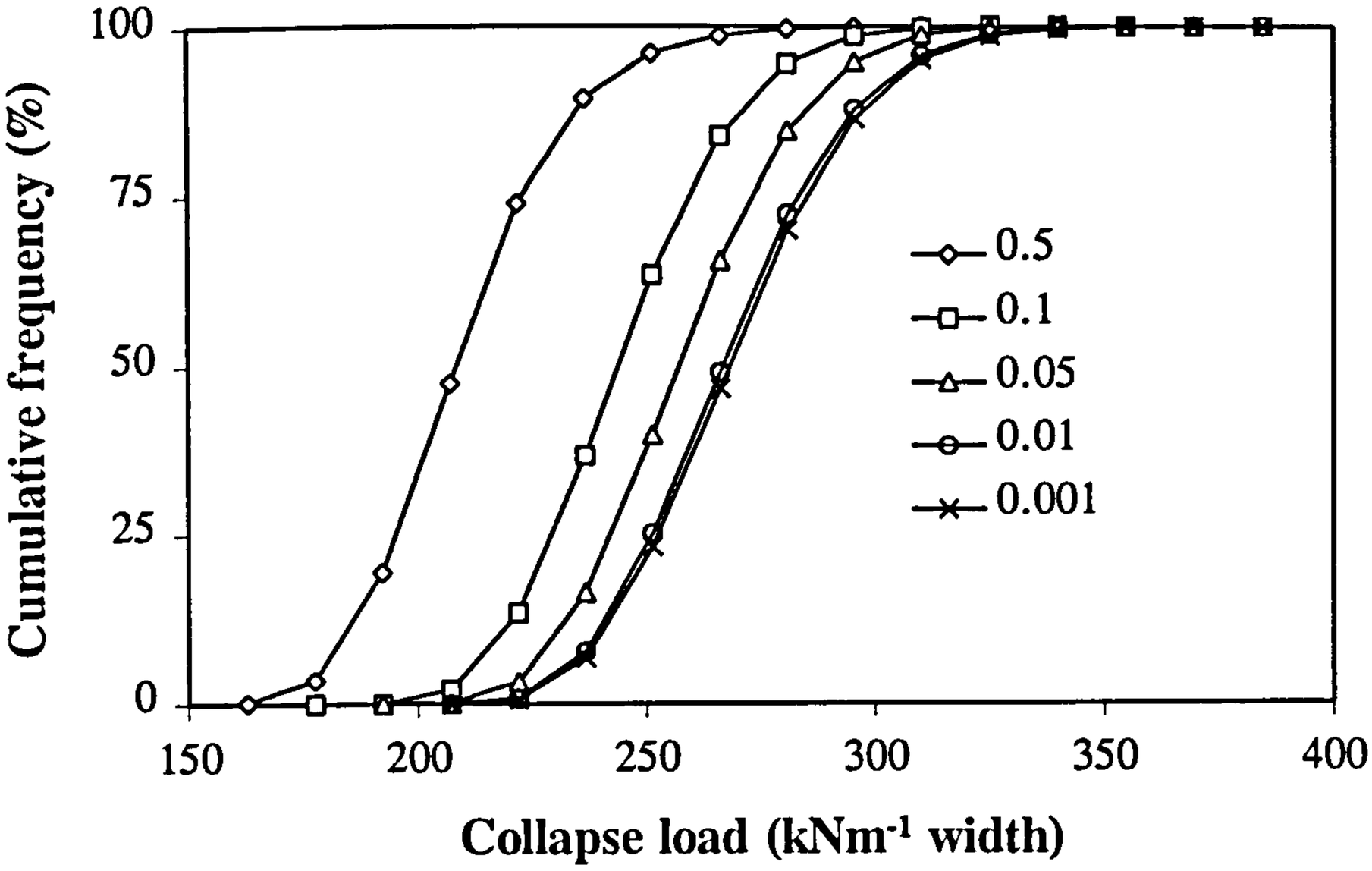

Figure 7.33 The effect of Boussinesq's limiting live load influence factor upon the collapse load

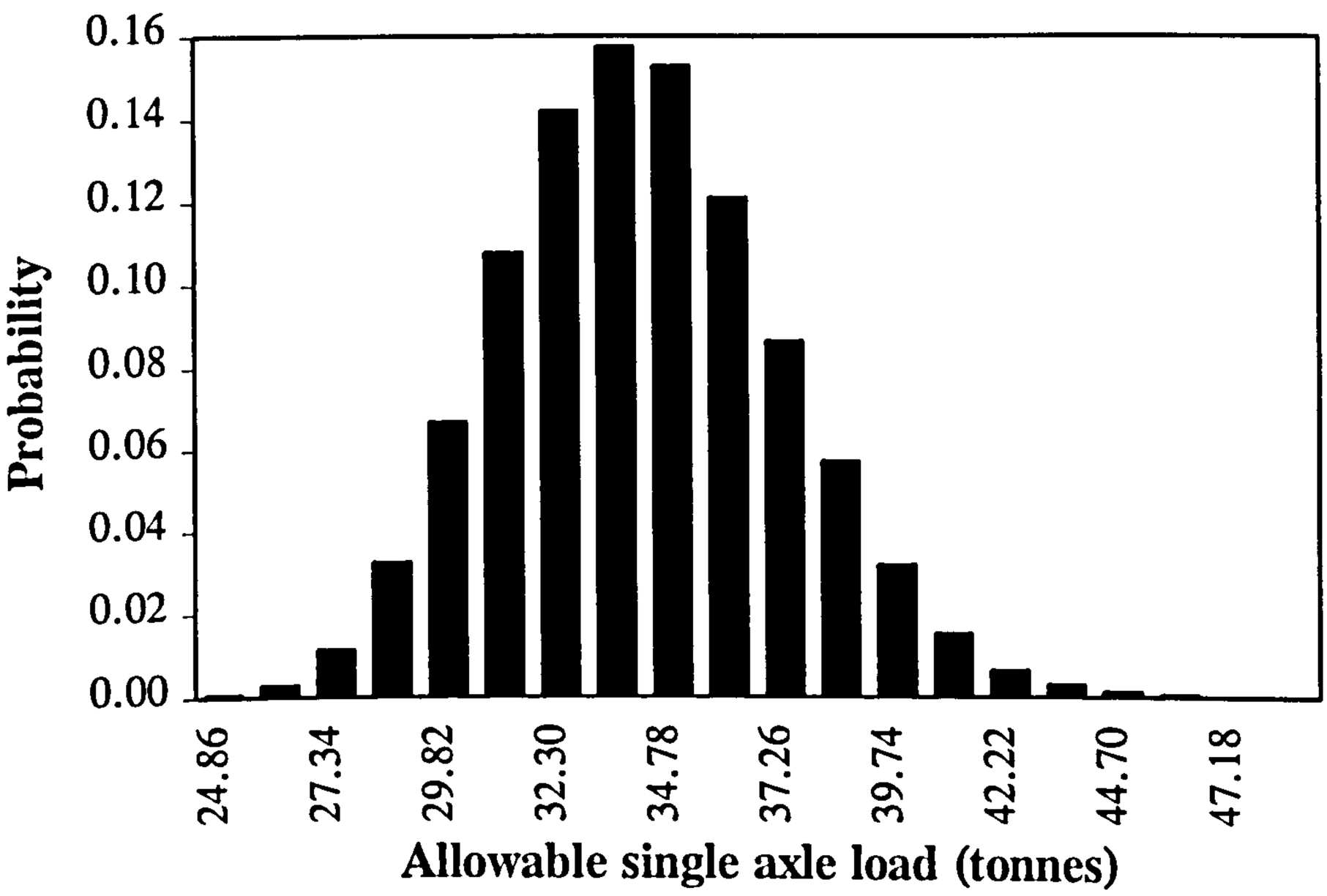

Figure 7.34 Probability distribution of allowable single axle load for Barlae bridge

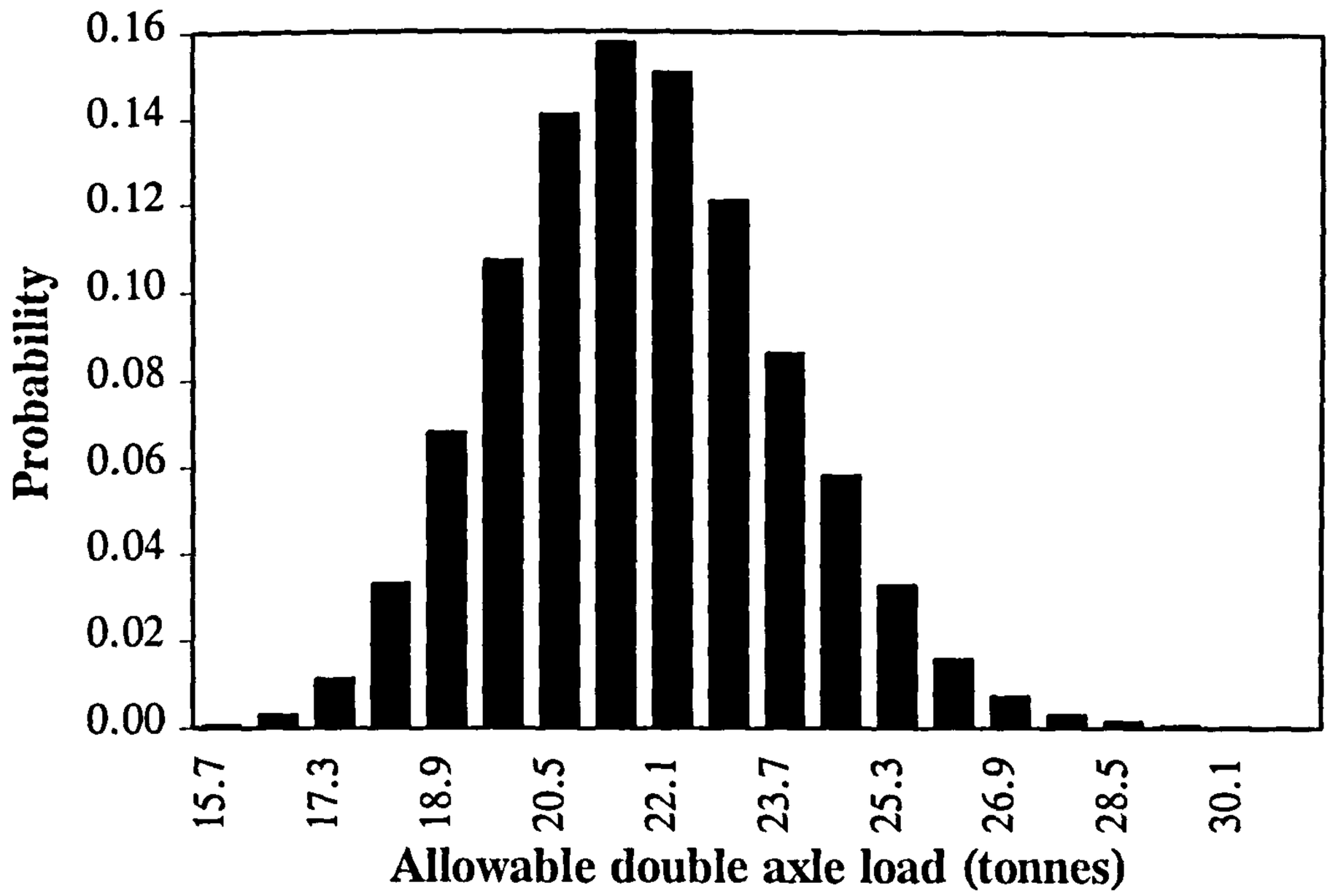

Figure 7.35 Probability distribution of double axle load for Barlae bridge

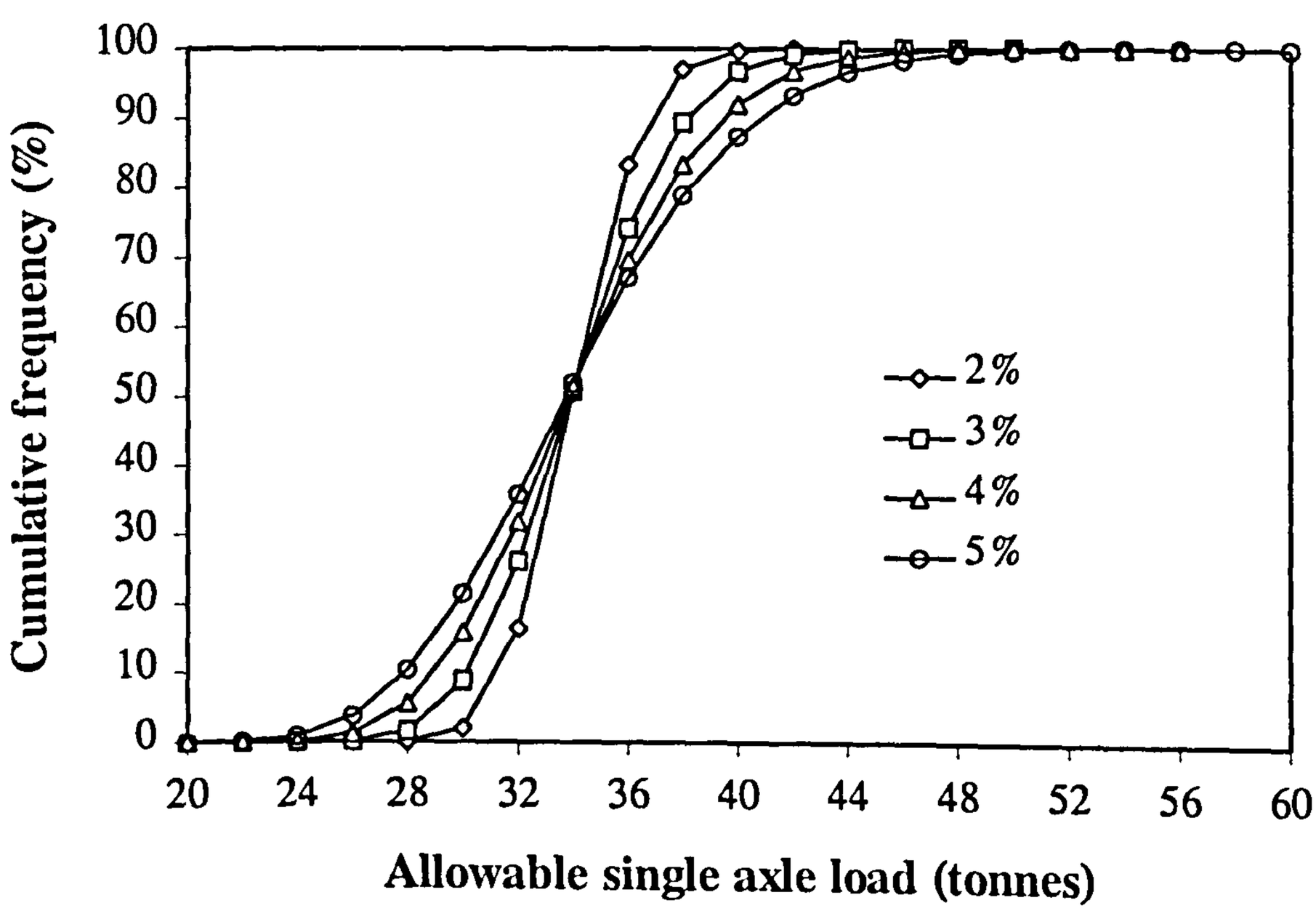

Figure 7.36 The effect of changing the coefficient of variation of the variables upon the allowable single axle load

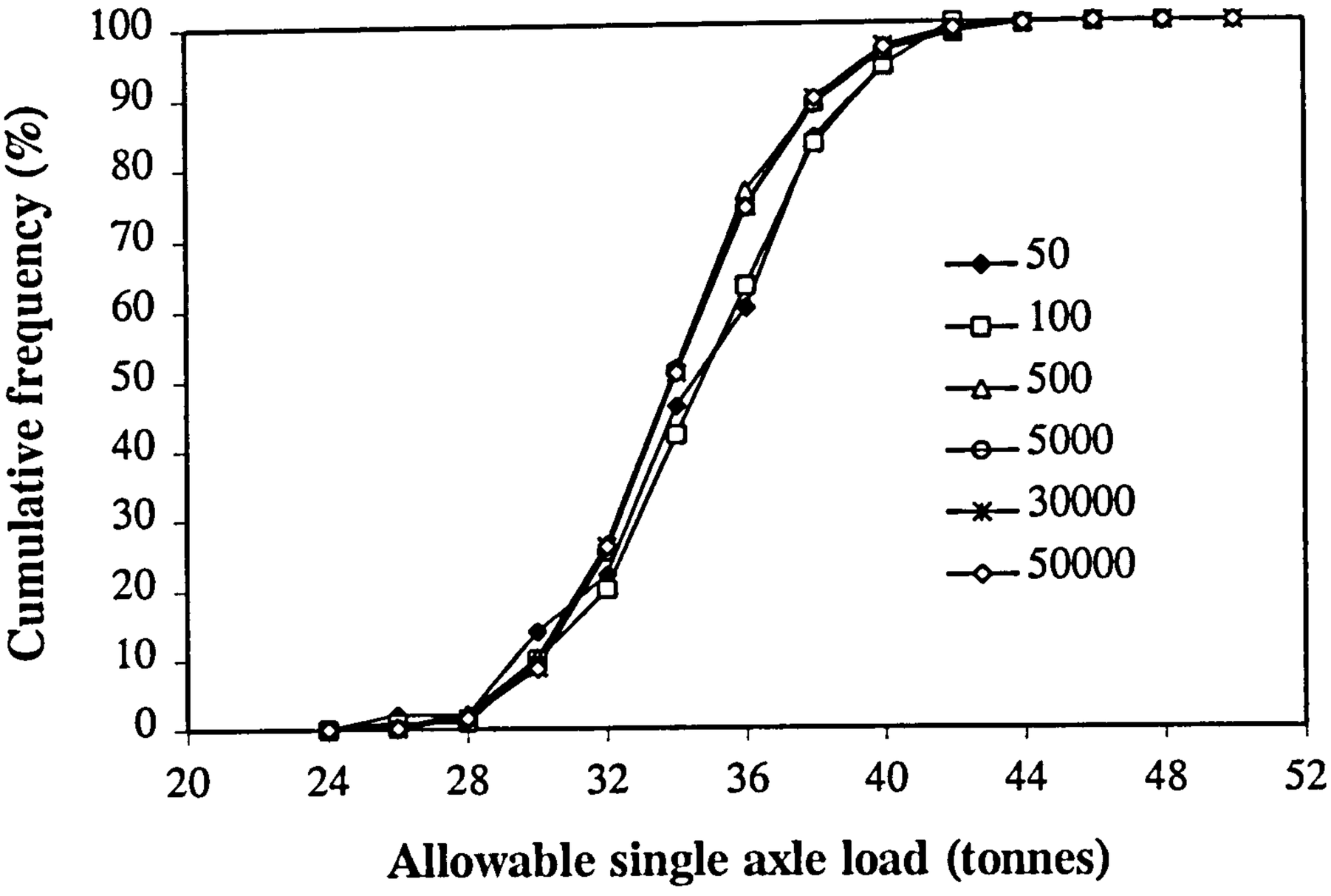

Figure 7.37 The effect of the number of iterations *per* analysis

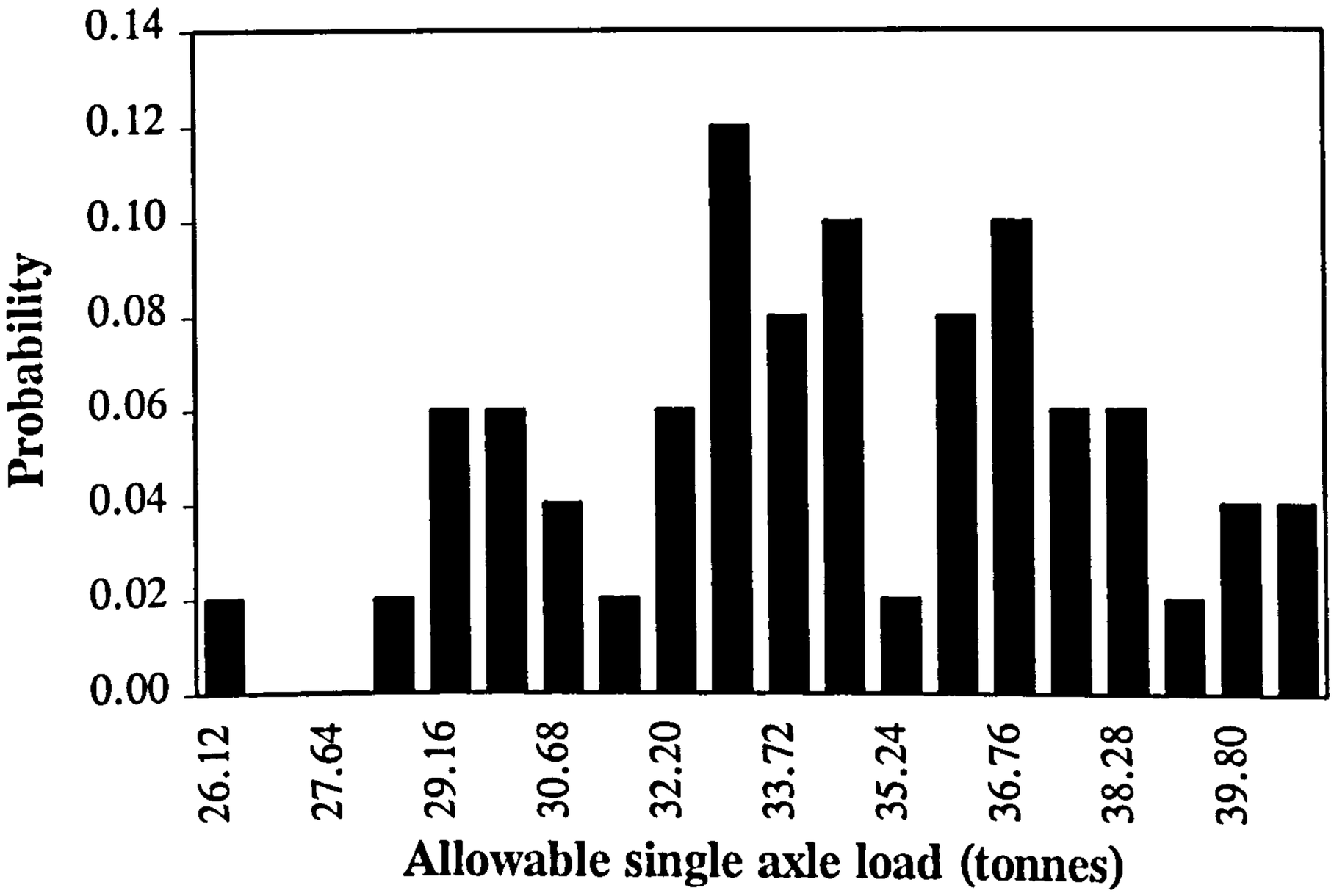

Figure 7.38 Probability distribution of allowable single axle load for 50 iterations

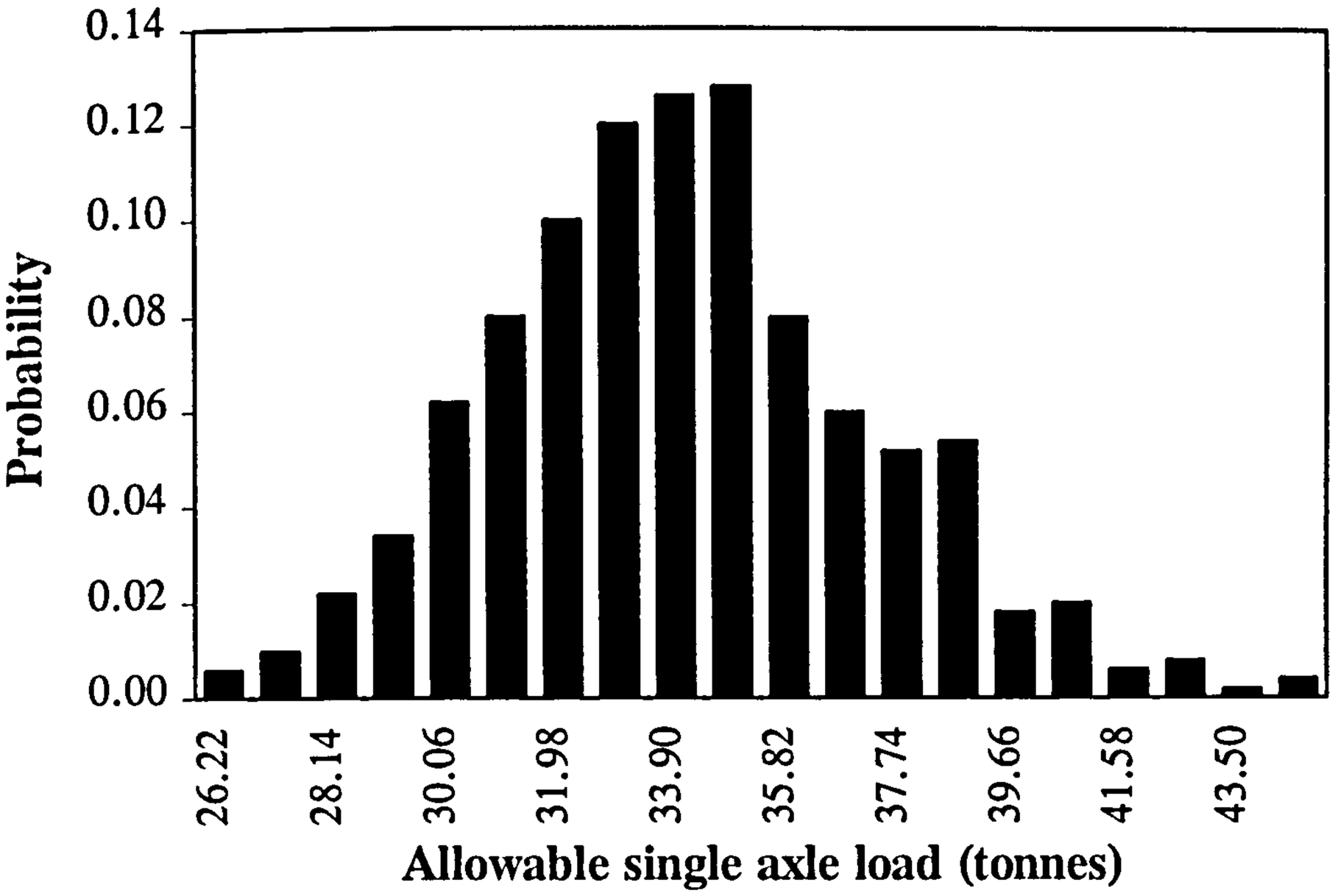

Figure 7.39 Probability distribution of allowable single axle load for 500 iterations

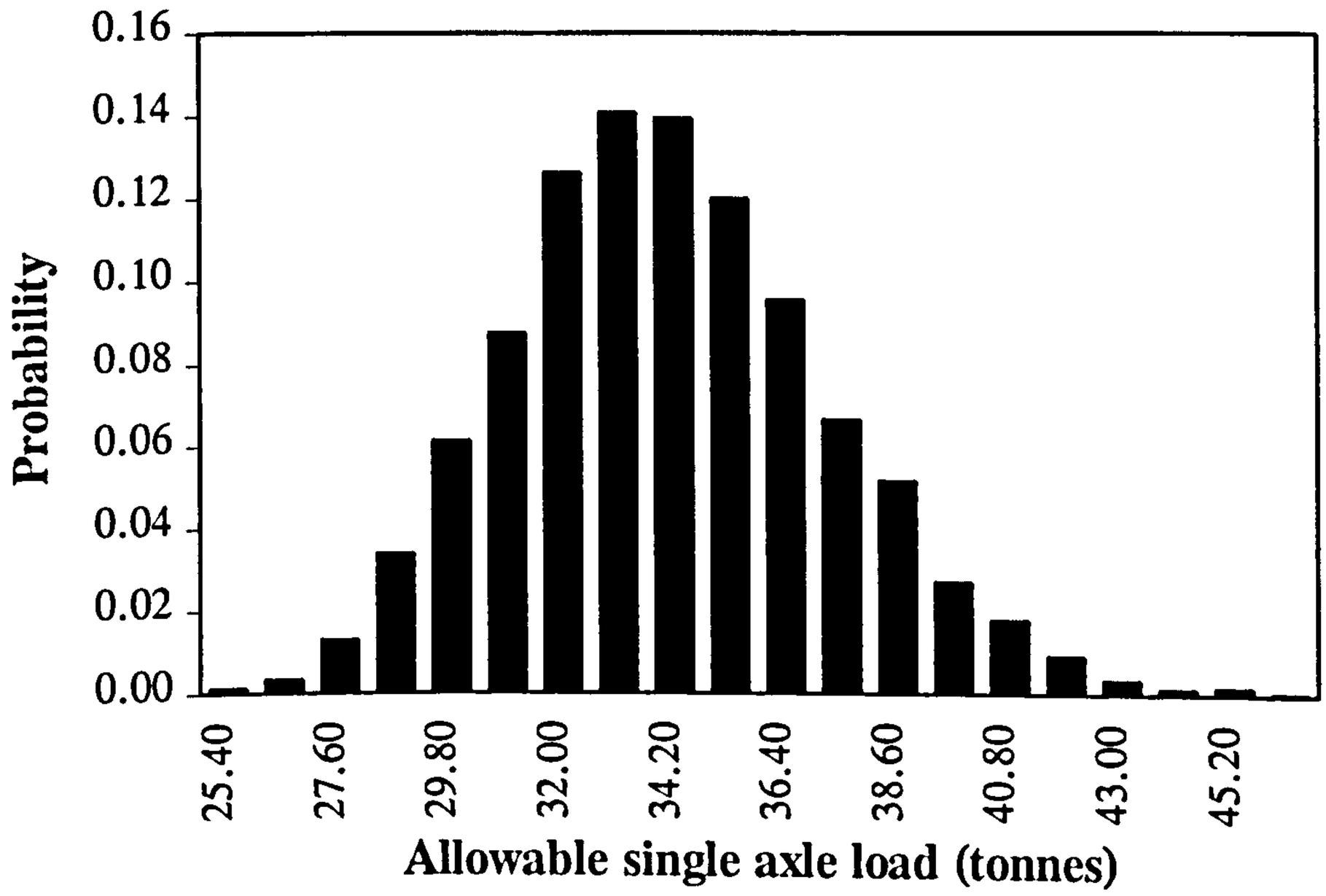

Figure 7.40 Probability distribution of allowable single axle load for 5000 iterations

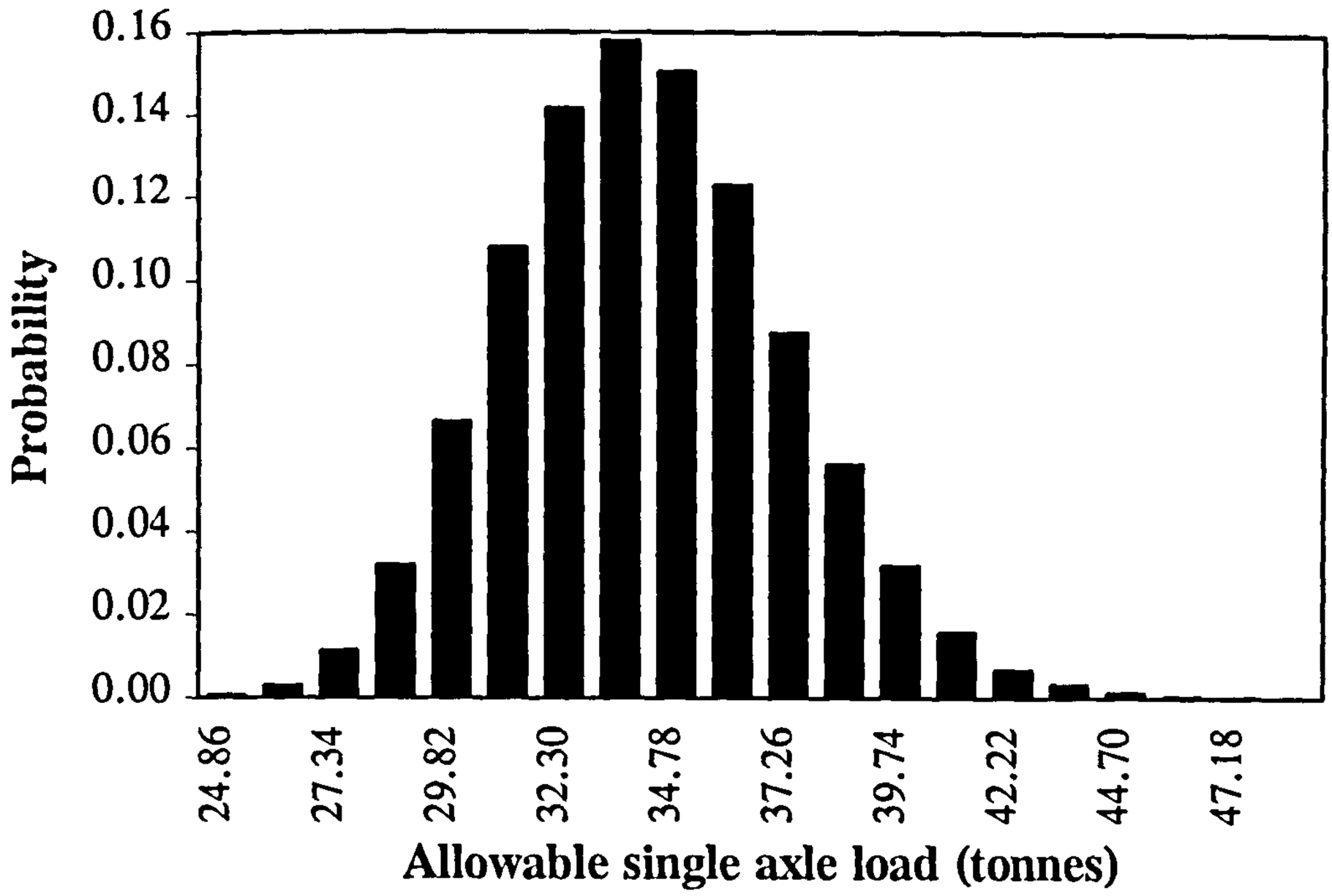

Figure 7.41 Probability distribution of allowable single axle load for 50000 iterations

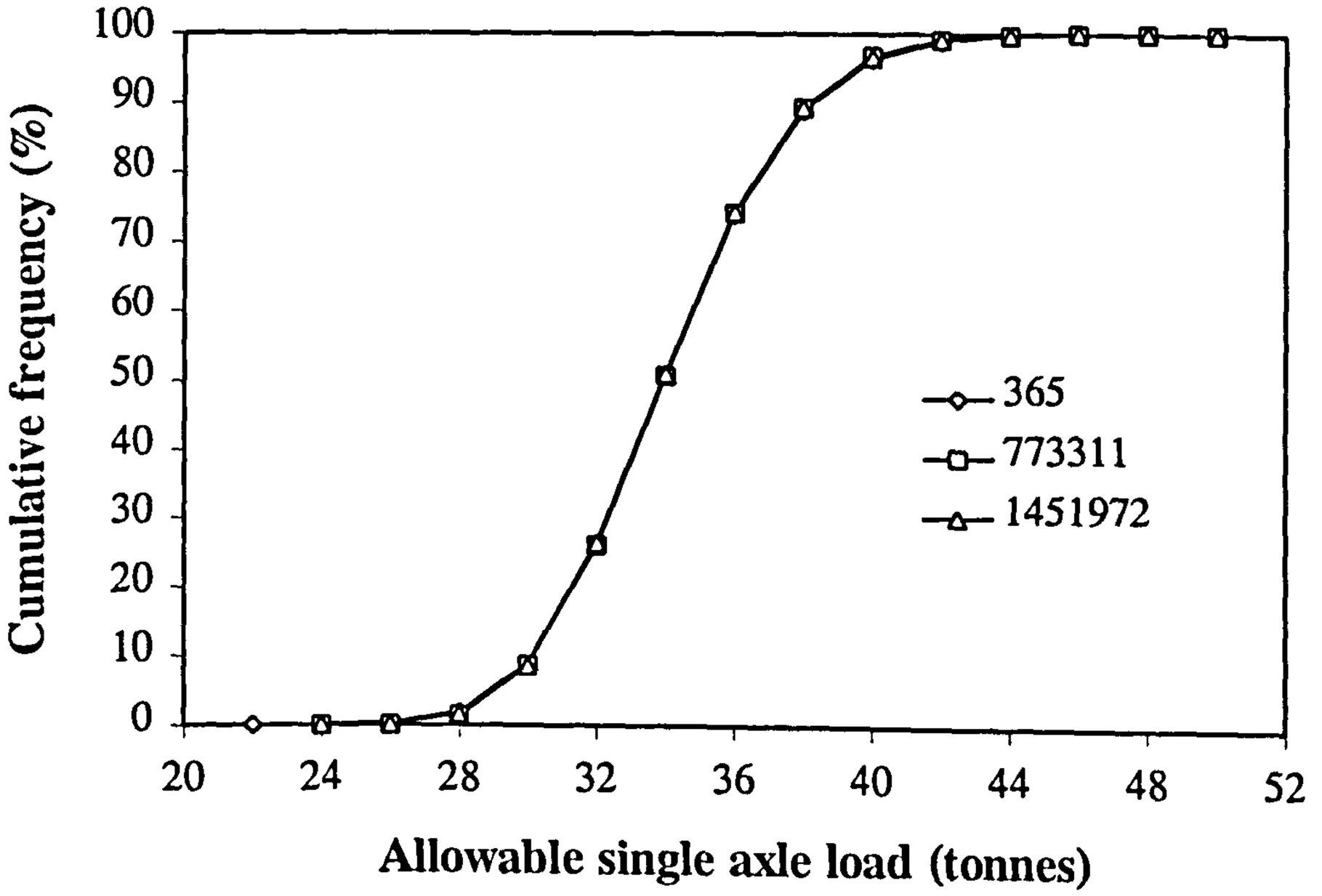

Figure 7.42 The effect of the seed for the random number generator upon the allowable single axle load

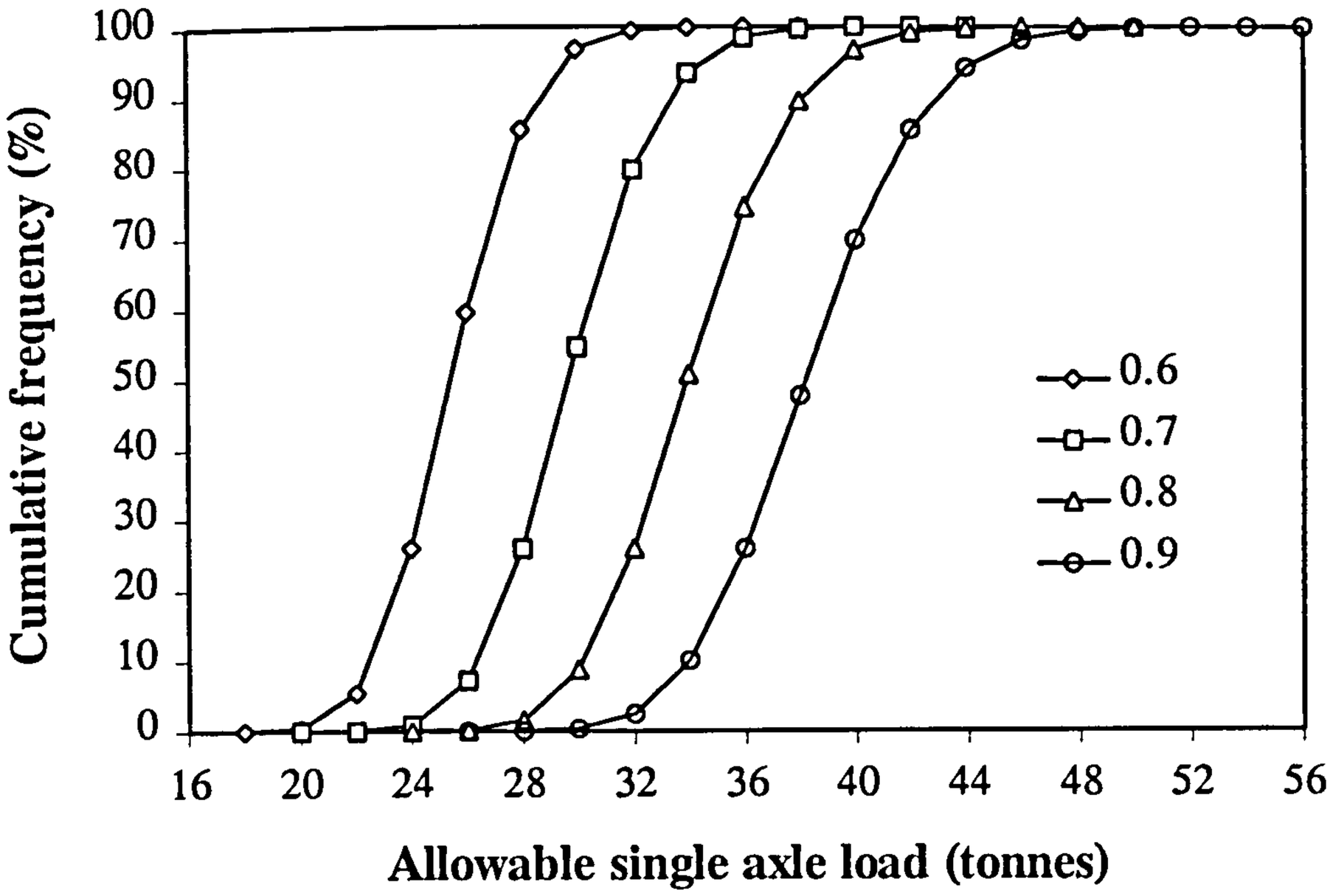

Figure 7.43 The effect of condition factor upon the allowable single axle load

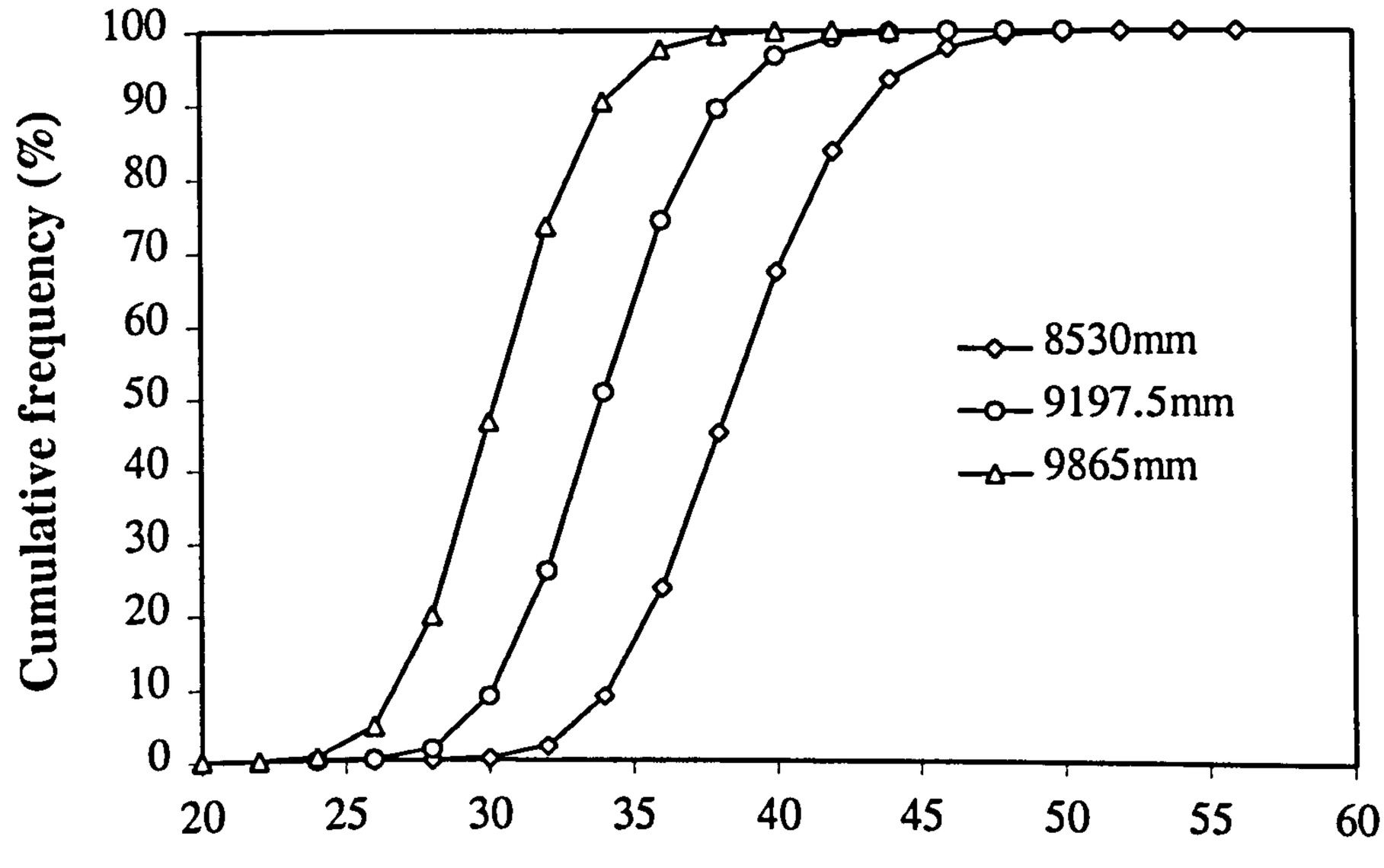

Figure 7.44 The effect of arch span upon the allowable single axle load

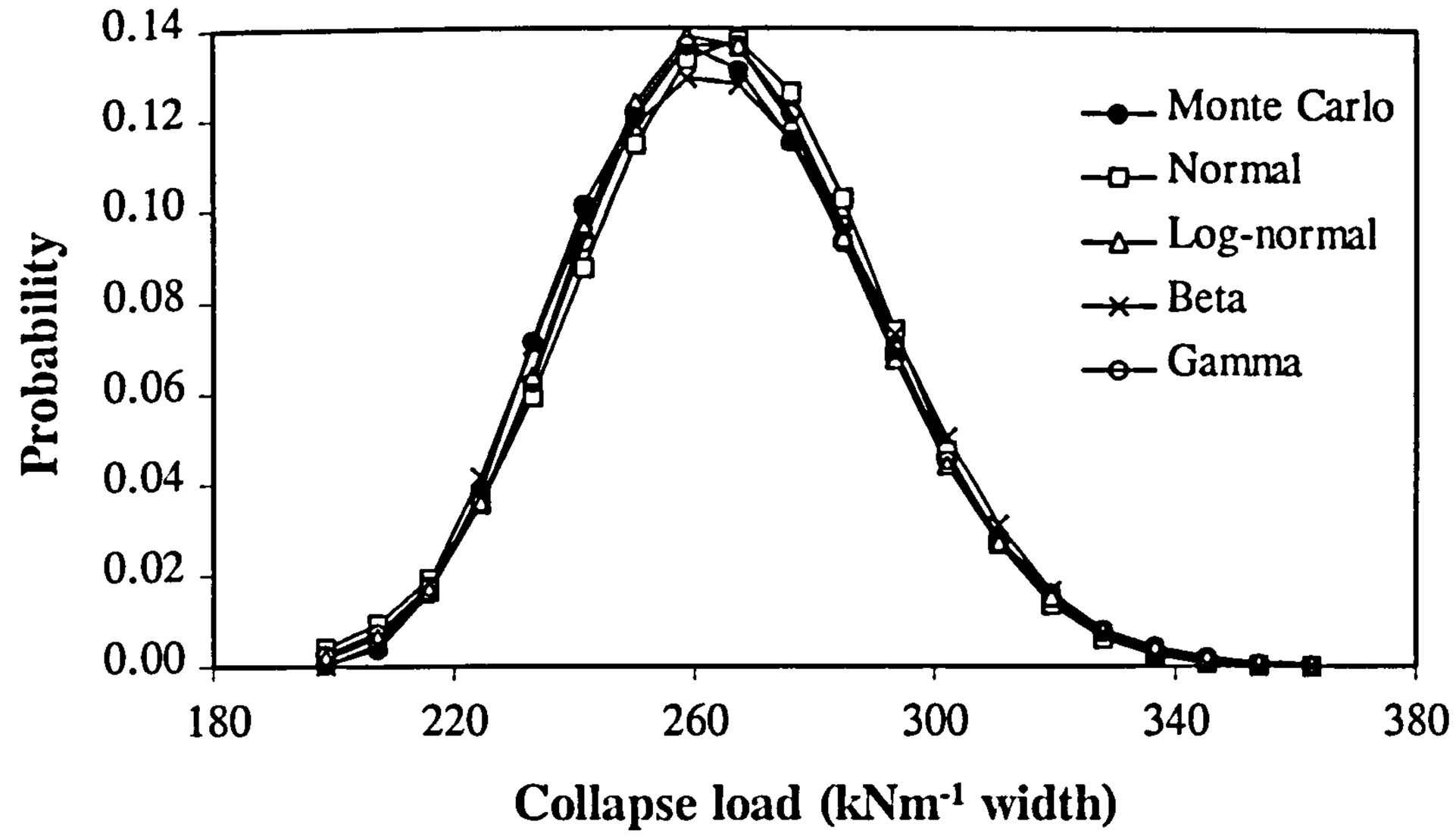

Figure 7.45 Monte Carlo and analytical distributions of the arch collapse load for Barlae bridge

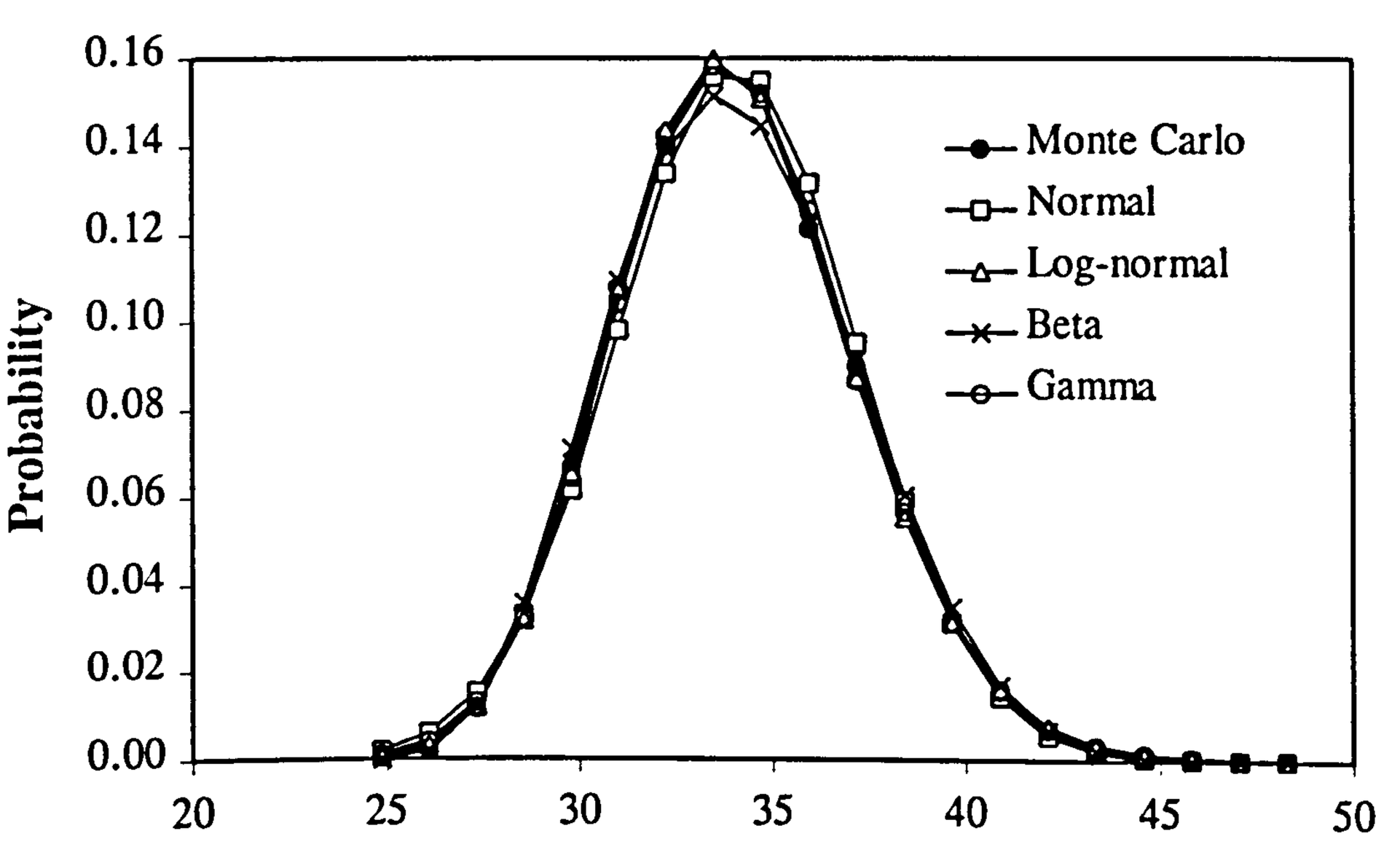

Figure 7.46 Monte Carlo and analytical distributions of the allowable single axle load for Barlae bridge

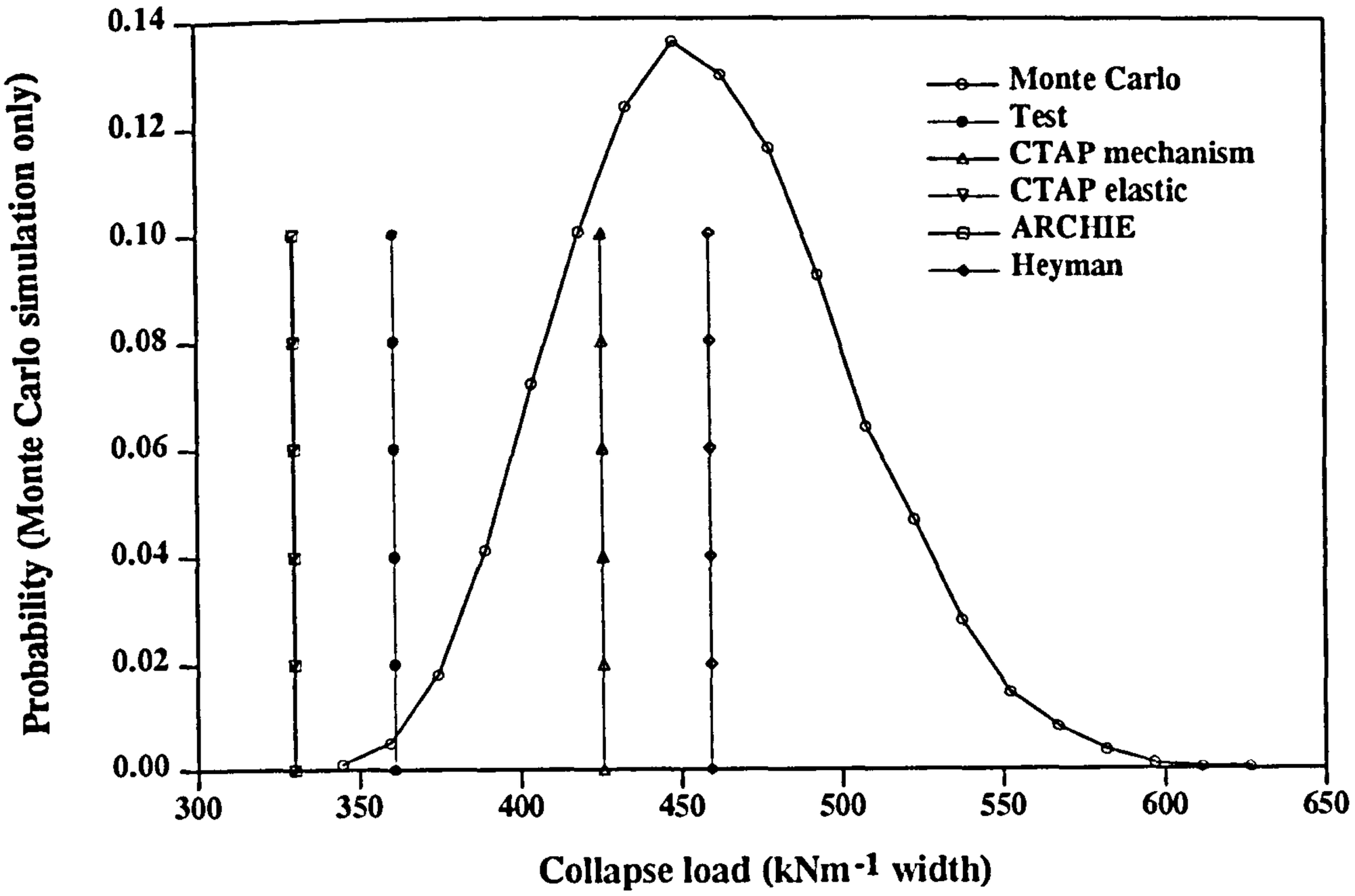

Figure 7.47 Prediction of arch collapse loads for Bridgemill

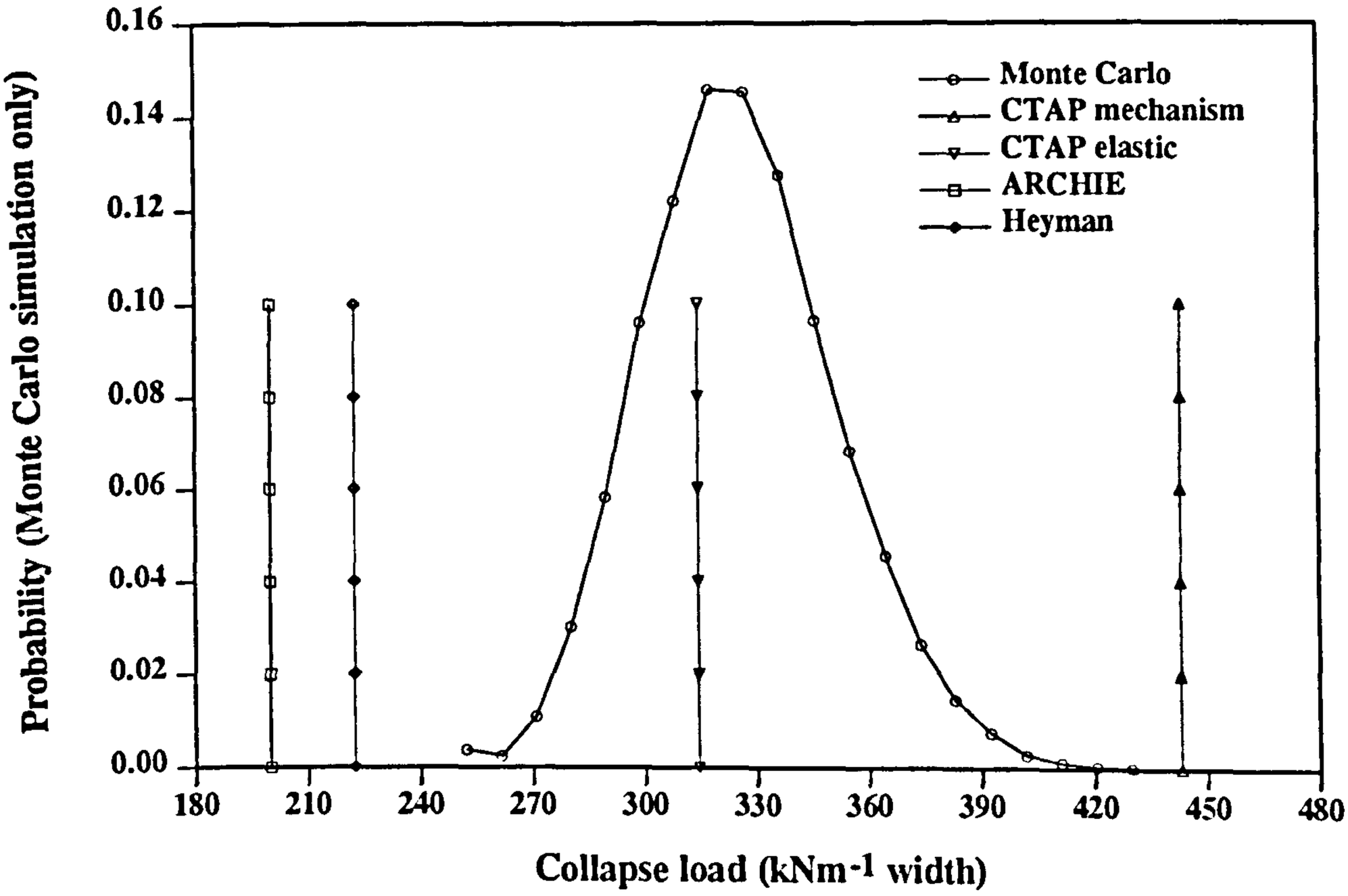

Figure 7.48 Prediction of arch collapse loads for Kimbolton Butts

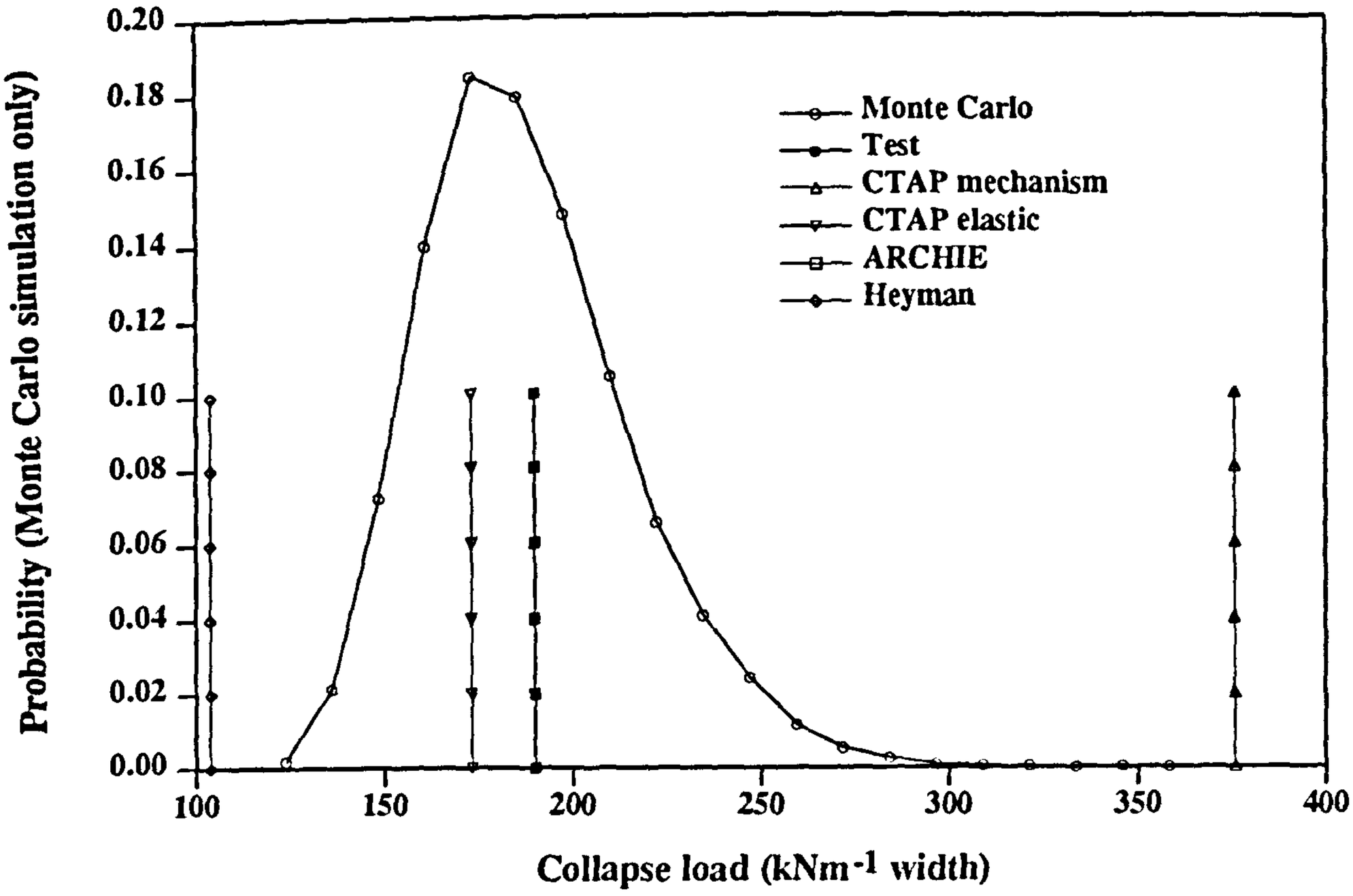

Figure 7.49 Prediction of arch collapse loads for Bolton

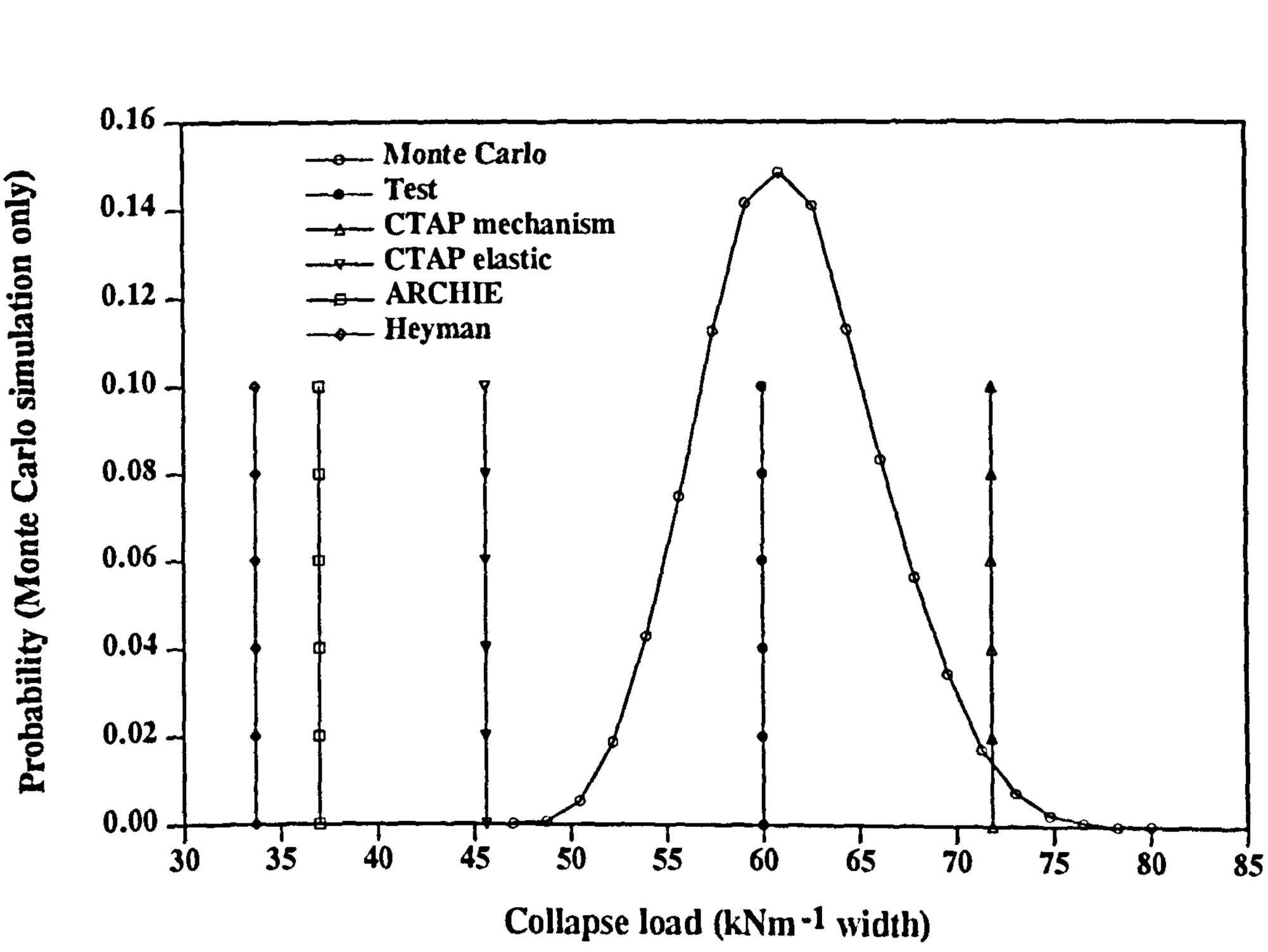

Figure 7.50 Prediction of arch collapse loads for Prestwood

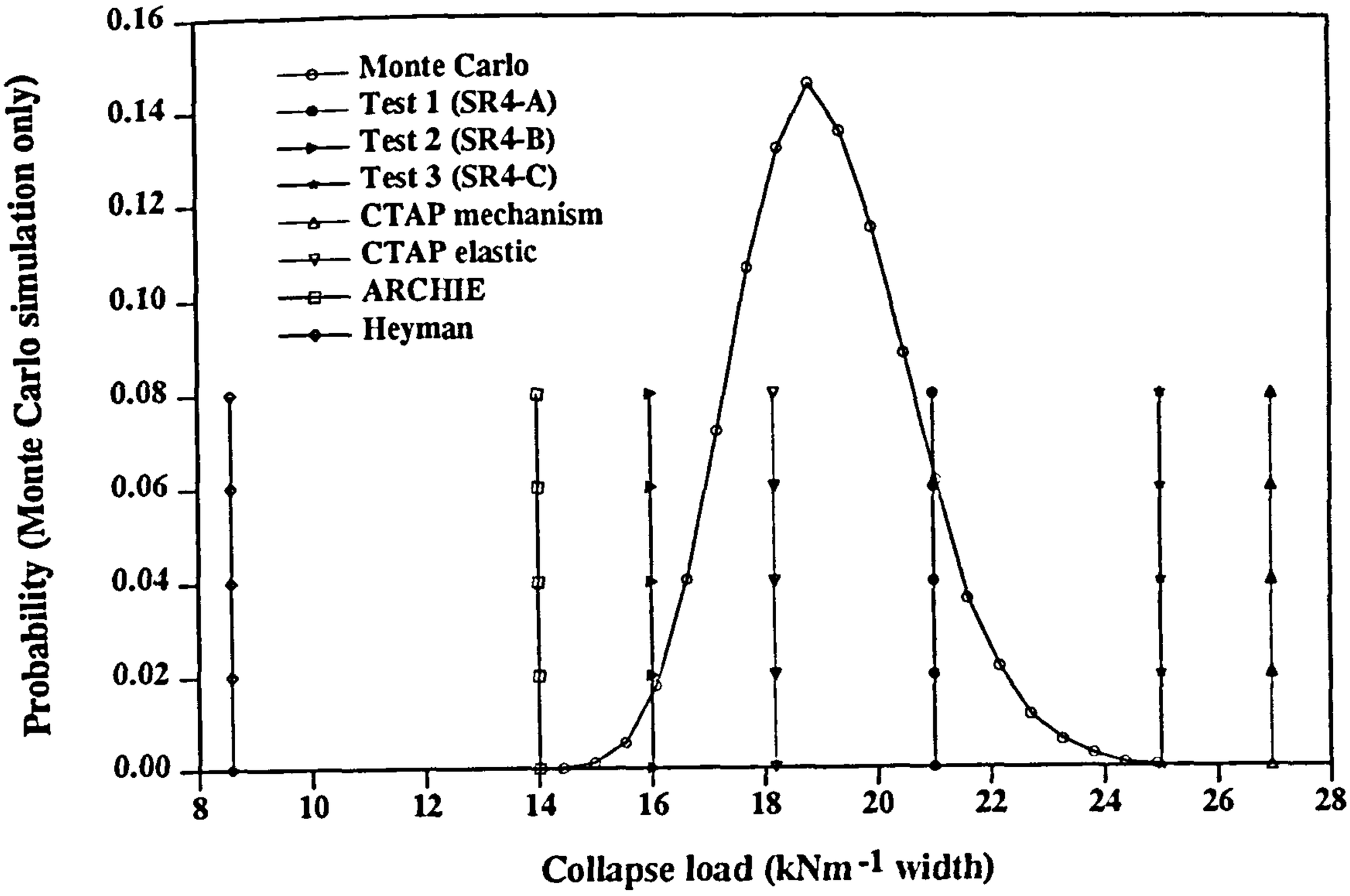

Figure 7.51 Prediction of arch collapse loads for SR4-A, SR4-B, and SR4-C

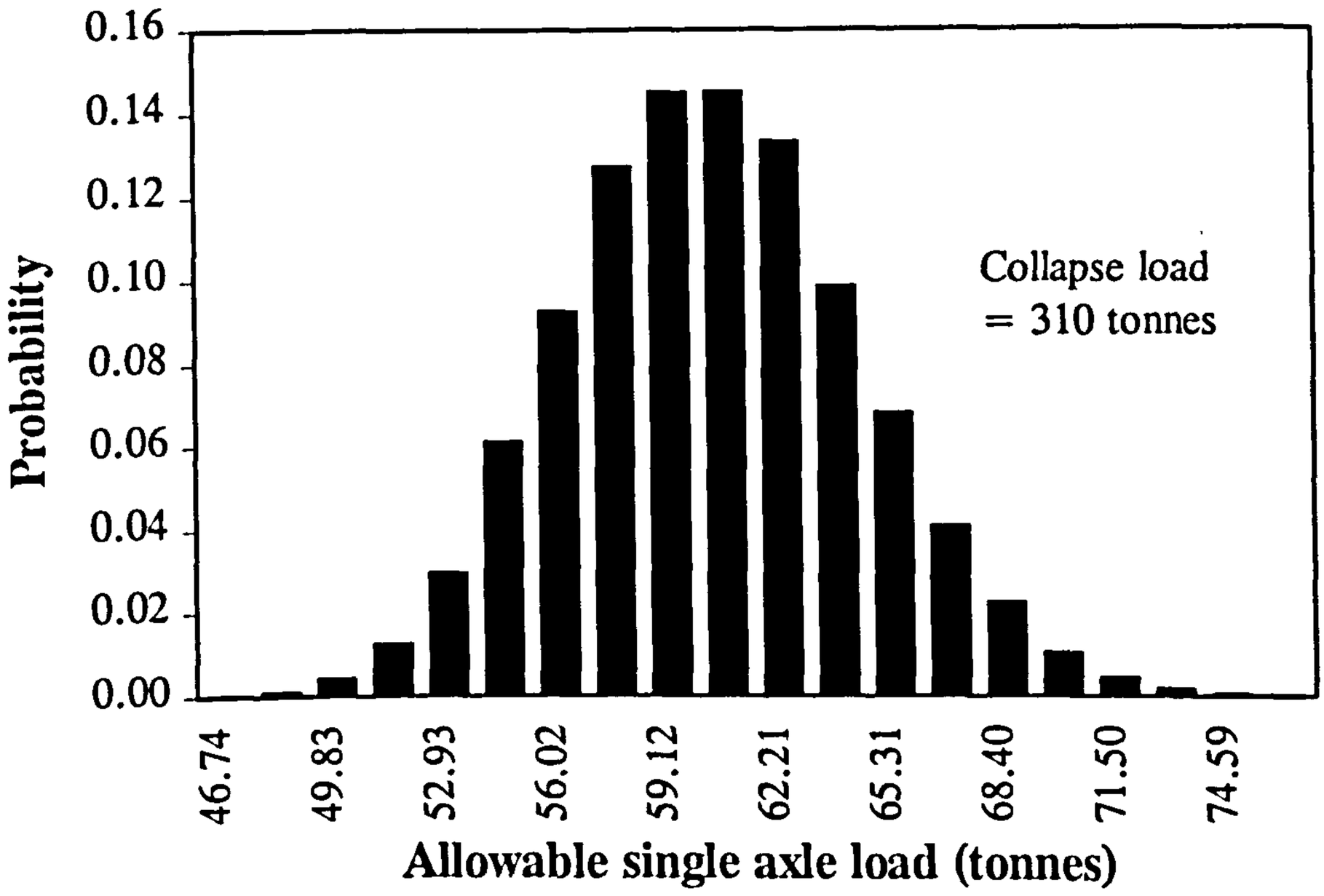

Figure 7.52 Probability distribution of the allowable single axle load for Bargower

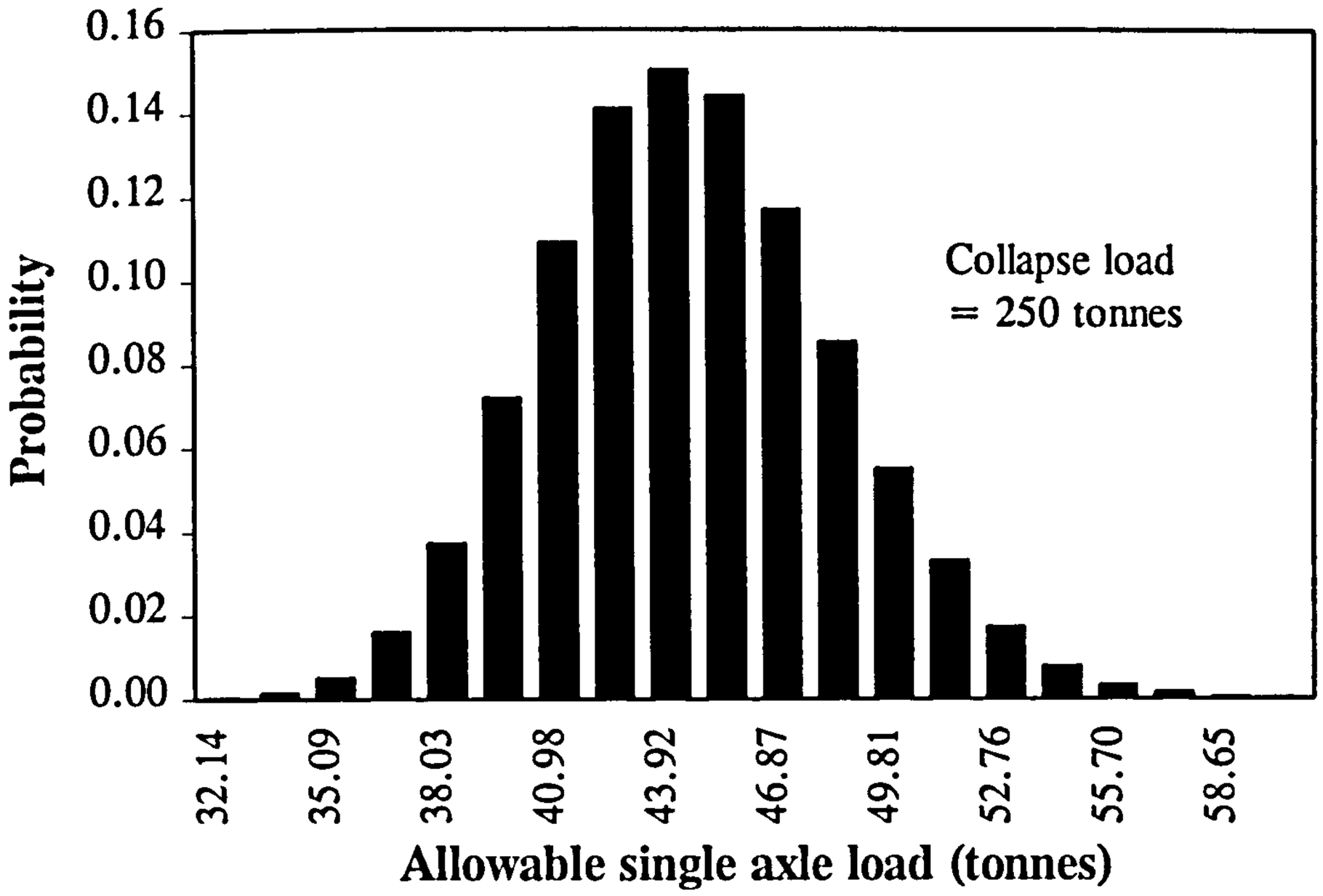

Figure 7.53 Probability distribution of the allowable single axle load for Shinafoot

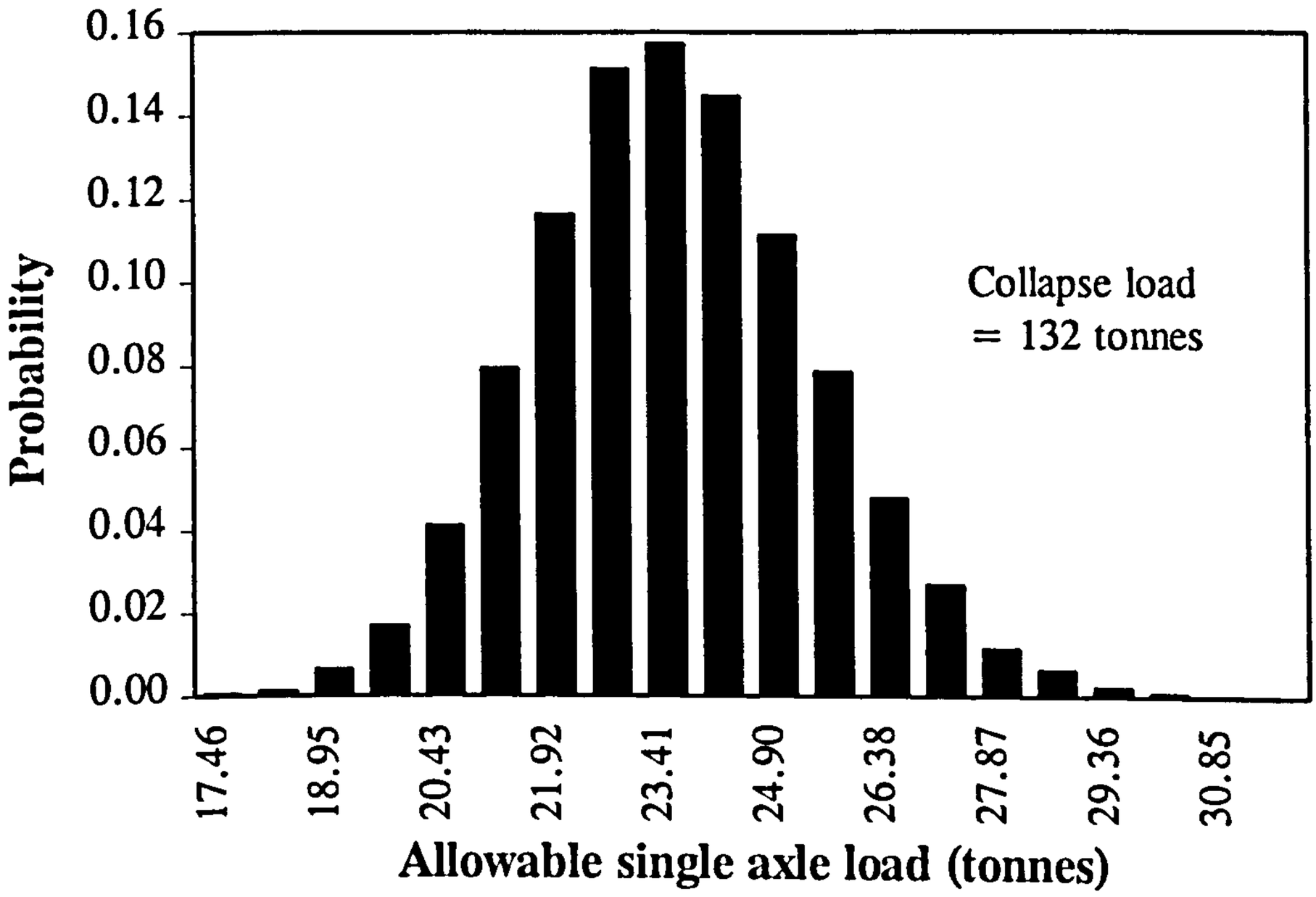

Figure 7.54 Probability distribution of the allowable single axle load for Strathmashie

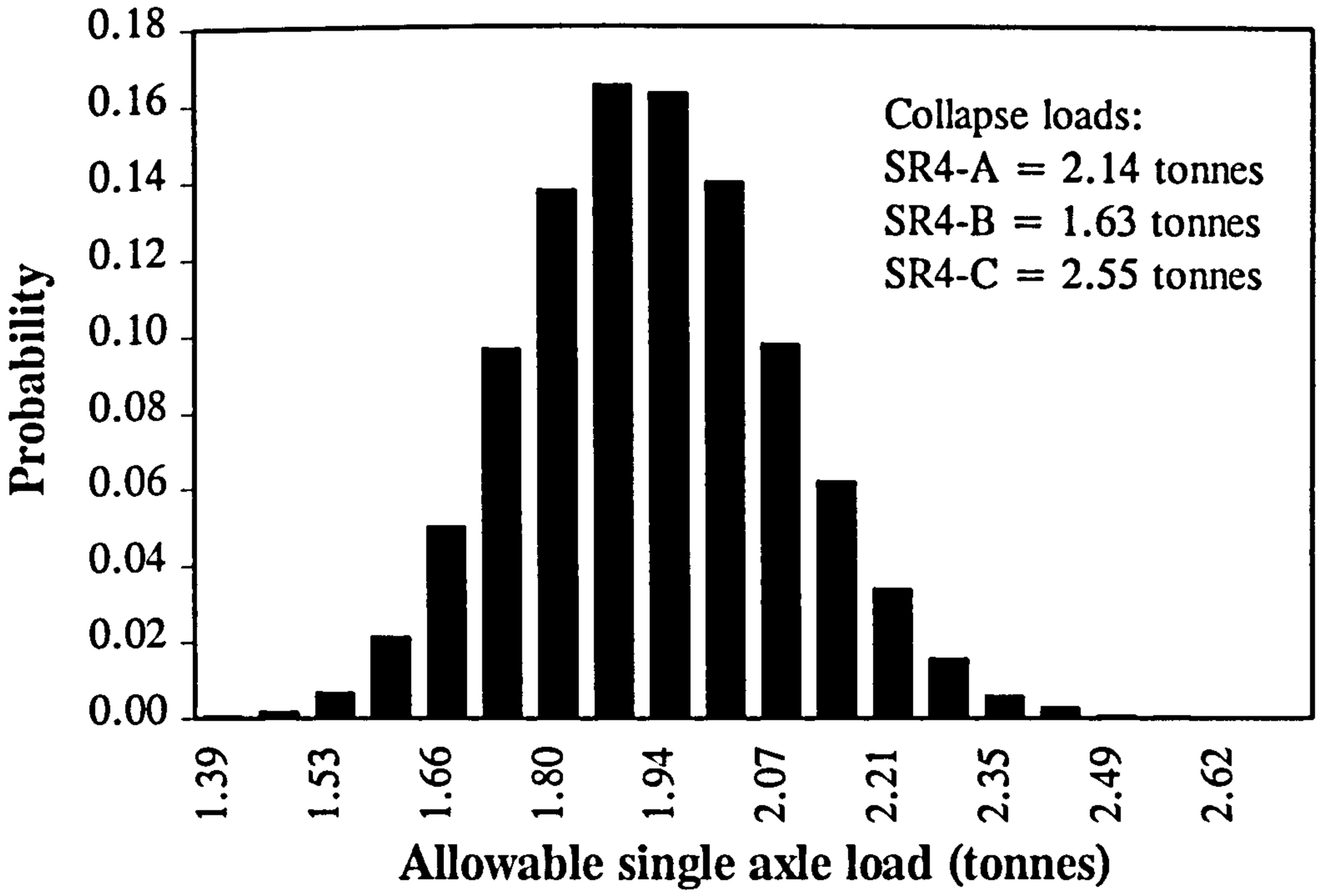

Figure 7.55 Probability distribution of the allowable single axle load for SR4-A, SR4-B, and SR4-C

CHAPTER 8

A Modified Mechanism Method Incorporating Arch Deflections

8.1 Introduction

The mechanism method is currently one of the most widely used arch bridge assessment methods in the United Kingdom. The method can be easily coded whilst soil-arch interactions can be considered, albeit in an arbitrary manner, such as the live load stress distribution and mobilisation of backfill lateral forces, without difficulty. No complex properties of the arch and backfill are needed in the mechanism method except in the case where the arch compressive strength is considered. In the past few decades, this method has been extensively explored leading to the development of many mechanism based computer codes for arch bridge assessments such as ARCHIE (SMITH, 1991a), CTAP-mechanism method (BRIDLE *et al.*, 1989), and ARCHMECH (PENG, 1997a). Besides being idealised as a 2-D plane strain structure without considering the spandrel, parapet and wings walls, the fundamental assumptions made in the mechanism method are; the arch has no tensile strength and the arch has an infinite elastic modulus. Ignoring the arch tensile strength is justifiable in the case of old arches. However, the author is concerned about the assumption of the arch having an infinite elastic modulus because the arch geometry is far from its original shape at the onset of a mechanism collapse. The mechanism method is only correct when all the forces and their locations are accurately considered. It is deemed necessary to explore the mechanism method further, although it has been used to analyse arch bridges for nearly 300 hundred years, by considering the effects of arch deflections.

A modified version of the mechanism method has been coded by the author as a FORTRAN77 routine (ARCH99.FOR). The modified mechanism method includes arch deflections and a bi-linear deflection dependent backfill pressure distribution model. The fundamental assumptions made in this modified mechanism method are; the arch has no tensile strength and is infinitely strong against compressive failure, the collapse mechanism of the arch occurs at some user-defined arch deflection, and the predicted arch collapse load is large enough to cause the predefined arch deflection. The author is aware of the limited application of this modified method since the arch deflection could only be assumed in a purely arbitrary manner. The predicted arch collapse load might not be large enough to cause the predefined arch deflection which sheds doubt on the reliability of the current modified mechanism method. It is, nonetheless, presented here as a possible improvement, a possible basis for further research and development, and as an idea for a future assessment method.

The current modified mechanism method is neither claimed to be an improvement over current conventional mechanism methods nor is it yet recommended for incorporation in routine arch bridge assessments due to the difficulty in deciding a reliable arch deflection at the moment of collapse. The main objective of the current modified mechanism method is to demonstrate that the arch deflection could significantly affect the mechanism prediction of the arch collapse load and to increase the awareness of those engineers who are using the conventional mechanism method about the reliability of their assessments.

Three full scale bridges namely Bargower (HENDRY *et al.*, 1986), Bridgemill (HENDRY *et al.*, 1985), and Strathmashie (PAGE, 1989) were studied using the author's modified mechanism method. The arch deflection was found to have dramatically affected the prediction of arch collapse loads for these arches. Apart from the arch deflection, a series of parametric studies was also performed by varying the backfill ultimate active and passive deflections, arch and backfill bulk unit weights, backfill angle of shearing resistance, and live load dispersal angle.

8.2 Method

The derivation of the current modified mechanism method is similar to that of the conventional mechanism method as presented in Chapter 7 of this thesis with the exception that a deflected arch geometry was considered as shown in Figure 8.1. The arch was divided into small segments in such a way that each arch segment followed the shape of a voussoir unit in the arch; the self-weight of each arch segment acts through its centre of gravity. The arch was deflected by specifying a vertical arch deflection on the arch extrados at point B (Figure 8.1). A bi-linear deflection dependent backfill pressure distribution model, as shown in Figure 8.2, was introduced to form the author's modified mechanism method. The model was fully described with backfill ultimate active and passive deflections, denoted by D_{ACT} and D_{PAS} respectively, and backfill angle of shearing resistance. The backfill lateral pressure coefficient was evaluated using Rankine's theory of backfill lateral resistance. All forces including the distributed equivalent live load were evaluated based on an assumed deflected arch geometry.

The extent to which the horizontal deflection required to fully mobilise the backfill passive resistance was found to be about 100mm (POTTS *et al.*, 1986) by rotating a retaining wall about its base. Similarly, full active resistance could be mobilised with a horizontal deflection between 10mm and 100mm depending on the mode of wall movements. However, the decision about the magnitude of the backfill ultimate active deflection could be made without difficulty since it has been shown in this study that it has only imperceptibly affected predictions of arch collapse load (see Section 7.5.1.10).

Just like the conventional mechanism method, three equilibrium equations can be derived by taking moments about points A, B, and C (Figure 8.1) giving Eqns 7.11, 7.12, and 7.13 respectively. The three unknowns; collapse load, and vertical and horizontal support reactions at an abutment, can then be found explicitly by solving Eqns 7.11 to 7.13. The support reactions at the other abutment can also be found by

considering the equilibrium of the whole system. The position of the thrustline can then be found easily since it represents a line of no bending moment.

8.3 Arch geometry and material properties

The salient dimensions and material properties of three arches; Bargower, Bridgemill, and Strathmashie, are given in Table 8.1. Their full scale collapse loads are also given in Table 8.1 for reference. The arch deflections, arch and backfill bulk unit weights, backfill ultimate active and passive deflections, backfill angle of shearing resistance, and live load dispersal angle were varied in a series of parametric studies. In the case of the parametric studies, only one input parameter given in Table 8.1 was varied while the other parameters were kept constant.

Table 8.1 Salient dimensions and material properties of Bargower, Bridgemill, and Strathmashie

Variable	Bargower	Bridgemill	Strathmashie
Span (mm)	10360	18290	9425
Rise (mm)	5180	2840	2990
Ring thickness (mm)	558	711	500
Fill depth (mm)	1200	203	410
Platen width (mm)	750	750	750
Load position	1/3-span point	1/4-span point	1/4-span point
Backfill bulk unit weight (kNm^{-3})	20	20	20
Arch bulk unit weight (kNm^{-3})	21	21	21
Backfill angle of shearing resistance ($^\circ$)	35	35	35
Load dispersal angle ($^\circ$)	45	45	45
D_{ACT} (mm) (see Figure 8.2)	10	10	10
D_{PAS} (mm) (see Figure 8.2)	100	100	100
Collapse load (kNm^{-1})	645	361	228

8.4 Results

This section presents the results generated using ARCH99.FOR on Bargower, Bridgemill, and Strathmashie. For the sake of clarity, the results from each arch bridge are presented in separate sections. Unless otherwise stated in the text, the arch deflection refers to the arch vertical deflection on the extrados under the load line.

8.4.1 Bargower

This section presents the results by the author's modified mechanism method on Bargower. The results obtained with benchmark input parameters as given in Table 8.1 are presented followed by the presentation of results from the parametric studies.

8.4.1.1 Standard results

Figure 8.3 shows the predicted arch collapse loads with the variation of arch vertical deflections. The full scale test collapse load and its corresponding arch deflection are also presented for a comparison. The predicted arch collapse load was 645.32kNm^{-1} width at an arch vertical deflection of 32.31mm. These results compared well with the actual arch collapse load of 645kNm^{-1} at an arch deflection of about 32mm. The corresponding collapse mode at this level is shown in Figure 8.4 with the deformed geometry of the arch and backfill being exaggerated by a factor of 4.44.

Figure 8.5 shows the effect of arch deflection on the distribution of backfill lateral pressure coefficient. With zero arch deflection, an at-rest pressure coefficient of 0.4264 was recorded around the whole arch extrados with the exception of the crown where the coefficient was zero since the slope of an intact arch at the crown is zero. By applying arch deflections, both backfill active and passive resistance were mobilised with the degree of mobilisation being dependent on the magnitude of arch deflections.

One of the consequences of introducing arch deflections was to shift a point, initially subjected to zero backfill lateral pressure, from the crown towards the side remote from the load. This was because the point on the arch extrados where its slope was zero had no longer remained at the crown of the deflected arch. With an arch vertical deflection of 13.91mm, the maximum passive pressure coefficient of 1.647 was recorded at a horizontal distance of 7193mm measured from the left abutment. This equated to 37.4% mobilisation of the full passive resistance. With a similar arch vertical deflection, full mobilisation of active resistance was recorded at most points on the loaded side. This was because full mobilisation of active resistance required only 10mm lateral deflection in this analysis. By applying arch vertical deflections of 32.31mm, 41.76mm, 52.22mm, and 62.68mm, the maximum evaluated passive pressure coefficients were 3.039, 3.690, 3.690, and 3.690 respectively. Although full mobilisation of passive resistance was recorded with an arch vertical deflection of 41.76mm and above, it covered only a limited area and its magnitude was found to be gradually reduced to the at-rest coefficient at the right abutment.

Figure 8.6 presents a comparison between the distribution of backfill lateral pressure coefficient evaluated with the bi-linear backfill lateral pressure model, as shown in Figure 8.2, and those being assumed in the conventional mechanism method. It was clear that both methods predicted significantly different distributions of backfill lateral pressure coefficient. Undoubtedly, the distribution of lateral pressure coefficient adopted in the conventional mechanism method is somewhat unrealistic since a constant mobilisation of backfill lateral resistance on each side of the arch is impossible, except for an intact arch, since horizontal deflections around the arch ring vary.

8.4.1.2 The effect of varying the backfill ultimate active deflection

Figure 8.7 shows the effect of varying the backfill ultimate active deflection (5mm, 10mm, 15mm, and 20mm) on the prediction of arch collapse load. It is evident from

Figure 8.7 that the backfill ultimate active deflection did not have any significant influence on the prediction of arch collapse load. All capacity predictions were found to converge for arch vertical deflections of 30mm and above. This was because, beyond this deflection, the backfill's full active resistance had been mobilised and the distribution of active resistance around the arch extrados remained unchanged at its full active value even with further arch deflections.

8.4.1.3 The effect of varying the backfill ultimate passive deflection

Figure 8.8 shows the effect of varying the backfill ultimate passive deflection (25mm, 50mm, 75mm, 100mm, and 140mm) on the prediction of arch collapse load. Referring to Figure 8.8, it could be seen that the lower the backfill ultimate passive deflection the greater its influence on the prediction of arch collapse load. With a backfill ultimate passive deflection of 140mm, its influence on the prediction of arch collapse load was found to be insignificant since a much larger lateral deflection was required to mobilise the passive resistance. The peak evaluated arch collapse loads with backfill ultimate passive deflections of 25mm, 50mm, 75mm, 100mm, and 140mm were 995kNm^{-1}, 847kNm^{-1}, 743kNm^{-1}, 651kNm^{-1}, and 566kNm^{-1} respectively.

Figure 8.9 shows the influence of backfill ultimate passive deflection on the distribution of backfill lateral pressure coefficient at an arch vertical deflection of 32.31mm. The lower the backfill ultimate passive deflection, the higher the backfill lateral pressure coefficient, until full passive pressure was mobilised, for a given arch vertical deflection. It could be seen from Figure 8.9 that full mobilisation of the passive resistance was reached with a backfill ultimate passive deflection of 75mm and above at an arch deflection of 32.31mm.

8.4.1.4 The effect of varying the backfill bulk unit weight

Figure 8.10 shows the effect of varying the backfill bulk unit weight on the prediction of arch collapse load. The collapse load was found to increase with an increase in the backfill bulk unit weight at any given arch deflection. By increasing the backfill bulk unit weight from $18kNm^{-3}$ to $21kNm^{-3}$, the predicted peak arch collapse load was found to increase from $602kNm^{-1}$ to $691kNm^{-1}$ at an arch vertical deflection of 41.76mm.

8.4.1.5 The effect of varying the arch bulk unit weight

Figure 8.11 shows the effect of varying the arch bulk unit weight on the prediction of arch collapse load. Increasing the arch bulk unit weight increased the arch collapse load at a given arch vertical deflection. By increasing the arch bulk unit weight from $19kNm^{-3}$ to $22kNm^{-3}$, the peak predicted arch collapse load increased from $655kNm^{-1}$ to $665kNm^{-1}$.

8.4.1.6 The effect of varying the backfill angle of shearing resistance

Figure 8.12 shows the effect of varying the backfill angle of shearing resistance on the prediction of arch collapse load. Apart from very small arch deflections, the prediction of arch collapse load was found to be higher with a higher backfill angle of shearing resistance. Referring to Figure 8.12, with a backfill angle of shearing resistance of 25°, the predicted arch collapse load was found to reduce with the increase in arch deflections. With backfill angles of shearing resistance of 35° and 45°, the predicted arch collapse loads were found to increased with arch deflections until reaching their maximae at $661kNm^{-1}$ and $901kNm^{-1}$ respectively.

8.4.1.7 The effect of varying the live load dispersal angle

Figure 8.13 shows the effect of varying the live load dispersal angle on the prediction of arch collapse load. It is clear from Figure 8.13 that increasing the live load dispersal angle resulted in an increase in collapse load over the range of arch deflections considered in this case. As a numerical example, at an arch deflection of 42mm, the collapse load predictions with load dispersal angles of 27°, 45°, and 55° were 524kNm^{-1}, 661kNm^{-1}, and 778kNm^{-1} respectively.

8.4.2 Bridgemill

This section presents the generated results for Bridgemill. The standard results, obtained with benchmark input parameters given in Table 8.1, are firstly presented followed by the presentation of results of the parametric studies.

8.4.2.1 Standard results

Figure 8.14 shows the predicted arch collapse loads at different arch deflections. For comparison, the full scale test collapse load and its corresponding arch deflection are also presented. At an arch deflection of 27mm, the author's modified mechanism method predicted a collapse load of 360kNm^{-1}. However, the full scale arch collapse load recorded was 361kNm^{-1} at an arch deflection of about 90mm. The predicted collapse mode, at an arch deflection of 27mm is shown in Figure 8.15 with a exaggeration factor of 18.52.

Figure 8.16 shows the effect of varying the arch deflection on the distribution of backfill lateral pressure coefficient. A constant at-rest coefficient of 0.4264 was recorded at zero arch deflection with the exception of the point at the crown where

the coefficient was zero since the slope at the crown was zero. With increasing arch deflection both active and passive resistance were mobilised. At an arch deflection of 27mm and above, full active resistance was recorded at almost every point on the loaded side of the arch. However, full mobilisation of the backfill passive resistance was not recorded even at an arch deflection of 100mm. At arch deflections of 15mm, 27mm, 40mm, 60mm, and 100mm, the maximum recorded backfill passive pressure coefficients were 0.89, 1.24, 1.60, 2.13, and 3.10 respectively. The full backfill passive pressure coefficient would be 3.69.

8.4.2.2 The effect of varying the backfill ultimate active deflection

The effect of varying the backfill ultimate active deflection on the capacity prediction for Bridgemill is presented in Figure 8.17. The prediction of the arch collapse load was found to be imperceptibly varied over the range of backfill active ultimate deflections from 5mm to 20mm regardless of the arch deflection. In this parametric study, all predicted arch collapse loads were found to be identical for any arch deflection of over 40mm. As shown in Figure 8.16, an arch deflection of 40mm was large enough to achieve full mobilisation of backfill active resistance on the loaded side of the arch.

8.4.2.3 The effect of varying the backfill ultimate passive deflection

Figure 8.18 shows the effect of varying the backfill ultimate passive deflection, from 25mm to 140mm, on the prediction of arch collapse load. By reducing the backfill ultimate passive deflection from 140mm to 25mm, the predicted arch collapse load increased from 350kNm^{-1} to 398kNm^{-1} at an arch deflection of 30mm. Figure 8.19 shows the effect of varying the backfill ultimate passive deflection on the prediction of the distribution of backfill lateral coefficient at an arch deflection of 60mm. No variation of the backfill lateral coefficient on the active side was observed since a 60mm arch deflection was large enough to mobilise full backfill active resistance. A

significant variation in the backfill lateral pressure coefficient was recorded on the side remote from the load over the range of backfill ultimate passive deflection (25mm to 140mm) used in this parametric study. Full passive pressures were recorded for a backfill passive ultimate deflection of 25mm over a horizontal distance from 11222mm to 16069mm measured from the left abutment (intrados). The maximum recorded backfill lateral pressure coefficients with backfill ultimate passive deflections of 140mm, 100mm, 75mm, 50mm, and 25mm were 1.64, 2.13, 2.70, 3.69, and 3.69 respectively.

8.4.2.4 The effect of varying the backfill bulk unit weight

Figure 8.20 shows the effect of varying the backfill bulk unit weight on the prediction of arch collapse load. As expected, the predicted arch collapse load was found to increase with the backfill bulk unit weight at any given arch deflection. By increasing the backfill bulk unit weight from $18kNm^{-1}$ to $21kNm^{-1}$, at an arch deflection of 30mm, the author's modified mechanism method predicted an increase in the arch collapse load from $339kNm^{-1}$ to $362kNm^{-1}$.

8.4.2.5 The effect of varying the arch bulk unit weight

Figure 8.21 shows the effect of varying the arch bulk unit weight on the prediction of arch collapse load. The arch's capacity was found to increase with a higher arch bulk unit weight at any given arch deflection. At an arch deflection of 30mm, the predicted arch collapse load increased from $335kNm^{-1}$ to $364kNm^{-1}$ with an increase in the arch bulk unit weight from $19kNm^{-3}$ to $22kNm^{-3}$.

8.4.2.6 The effect of varying the backfill angle of shearing resistance

Figure 8.22 shows the effect of varying the backfill angle of shearing resistance on the prediction of arch collapse load. There was no significant variation in the collapse load prediction at small arch deflections. However, the influence of the backfill angle of shearing resistance became apparent for arch deflections of 30mm and above; its influence was found to increase gradually with arch deflections. By increasing the backfill angle of shearing resistance from 25° to 45°, at an arch deflection of 30mm, the collapse load prediction was found to increase from 349kNm^{-1} to 363kNm^{-1}.

8.4.2.7 The effect of varying the live load dispersal angle

Figure 8.23 shows the effect of varying the live load dispersal angle on the prediction of arch collapse load. The collapse load prediction was found to be dramatically increased by increasing the live load dispersal angle from 27° to 55°. However, its influence gradually decreased with arch deflection. At an arch deflection of 30mm, increasing the live load dispersal angle from 27° to 55° increased the predicted arch collapse load from 343kNm^{-1} to 453kNm^{-1}.

8.4.3 Strathmashie

This section presents the results obtained by the modified mechanism method for Strathmashie. The standard results, obtained with benchmark input parameters given in Table 8.1, are presented. This is then followed by the presentation of results of the parametric studies.

8.4.3.1 Standard results

Figure 8.24 shows the prediction of arch collapse loads by the modified mechanism method for different levels of arch deflections. The full scale test collapse load and its corresponding arch deflection are also presented for comparison. At an arch deflection of 70mm, the modified mechanism method predicted an arch collapse load of $227kNm^{-1}$. Good agreement was achieved with the full scale test collapse load of $228kNm^{-1}$ at a deflection of 80mm. Figure 8.25 shows the predicted arch collapse mode, exaggerated by a factor of 8.25, with a limiting live load of $227kNm^{-1}$ at an arch deflection of 70mm.

Figure 8.26 shows the effect of varying the arch deflection on the distribution of backfill lateral pressure coefficient. As with the previous two arches, a constant at-rest coefficient was recorded around the arch extrados, with the exception of the point at the crown, at zero arch deflection. Full mobilisation of the backfill active resistance was recorded over almost the entire arch extrados on the loaded side with an arch deflection of 17.43mm and above. However, full mobilisation of backfill passive resistance was not recorded on the arch extrados, remote from the load, until an arch deflection of 104.7mm. However, even at an arch deflection of 104.7mm, full mobilisation of backfill passive resistance was only recorded over a limited chord length on the arch extrados on the side remote from the load; its magnitude rapidly fell to the at-rest coefficient at the right abutment.

8.4.3.2 The effect of varying the backfill ultimate active deflection

Figure 8.27 shows the effect of varying the backfill ultimate active deflection on the capacity prediction. At no point did the difference in the collapse load prediction seem significant over the range of backfill ultimate active deflections from 5mm to 20mm. At an arch deflection of about 26mm and above, the predicted arch collapse load was

found to be unchanged regardless of the variation of backfill ultimate active deflection in this parametric study.

8.4.3.3 The effect of varying the backfill ultimate passive deflection

Figure 8.28 shows the effect of varying the backfill ultimate passive deflection on the prediction of arch collapse load. In could be seen clearly from Figure 8.28 that the collapse load prediction was significantly affected by the variation of backfill ultimate passive deflection. With a backfill ultimate passive deflection of 50mm or below, the collapse load prediction increased with arch deflection until the magnitude of the arch deflection reached about 26mm. However, such a phenomenon was not observed with a backfill ultimate passive deflection of above 50mm, with which the collapse load prediction decreased with increasing arch deflection. It could also be seen from Figure 8.28 that, at higher deflections, the predicted collapse loads were lower with a lower backfill ultimate passive deflection. This was because, beyond a certain arch deflection, an increase in the backfill lateral pressure on the side remote from the load might indeed lower the prediction of arch collapse load (in this particular case) since the equilibrium of the whole arch bridge depended not only on the magnitude of all acting forces but also the points at which they acted.

Figure 8.29 shows the effect of varying the backfill ultimate passive deflection on the distribution of backfill lateral pressure coefficient at an arch deflection of 70mm. A full mobilisation of backfill passive resistance was recorded on the arch extrados, on the side remote from the load, with a backfill ultimate passive deflection of 75mm and below for an arch deflection of 70mm.

8.4.3.4 The effect of varying the backfill bulk unit weight

Figure 8.30 shows the effect of varying the backfill bulk unit weight on the prediction of arch collapse load. Its influence was found to be significant over the range of backfill bulk unit weights ($18kNm^{-3}$ to $21kNm^{-3}$) used in this parametric study. As a numerical example, the collapse load prediction increased from $210kNm^{-1}$ to $235kNm^{-1}$ for an increase in the backfill bulk unit weight from $18kNm^{-1}$ to $21kNm^{-1}$ at an arch deflection of 70mm.

8.4.3.5 The effect of varying the arch bulk unit weight

Figure 8.31 shows the effect of varying the arch bulk unit weight on the collapse load prediction. Its influence was noticeable only at small arch deflections. At an arch deflection of 70mm, an increase in the arch bulk unit weight from $19kNm^{-3}$ to $22kNm^{-3}$ resulted in an increase in the collapse load prediction from $221kNm^{-1}$ to $230kNm^{-1}$.

8.4.3.6 The effect of varying the backfill angle of shearing resistance

Figure 8.32 shows the effect of varying the backfill angle of shearing resistance on the collapse load prediction. The backfill angle of shearing resistance was found to have dramatically affected the prediction of arch collapse load. As a numerical example, at an arch deflection of 70mm, the collapse load prediction was found to increase from $193kNm^{-1}$ to $283kNm^{-1}$ with an increase in the backfill angle of shearing resistance from 25° to 45°.

8.4.3.7 The effect of varying the live load dispersal angle

Figure 8.33 shows the effect of varying the live load dispersal angle on the prediction of arch collapse load. A range of dispersal angles from 27° to 55° was used in this parametric study. The influence of the live load dispersal angle was found to be significant. At an arch deflection of 70mm, increasing the live load dispersal angle from 27° to 55° increased the collapse load prediction from 180kNm^{-1} to 243kNm^{-1}.

8.5 Discussion

This section discusses the results generated by the author's modified mechanism method as applied to Bargower, Bridgemill, and Strathmashie. A discussion about the assumptions made in this method is also presented.

8.5.1 Generated results applied to full scale arch tests

For the sake of clarity, the results generated by the current modified mechanism method on each full scale arch; Bargower, Bridgemill, and Strathmashie, are discussed in separate sections.

8.5.1.1 Bargower

The modified mechanism method has been used to analyse Bargower bridge. Parametric studies were performed to investigate the influence of the arch deflection, backfill ultimate active and passive deflections, backfill and arch bulk unit weights, backfill angle of shearing resistance, and the live load dispersal angle.

The modified mechanism method predicted an arch collapse load of 645.32kNm^{-1} width at an arch vertical deflection of 32.31mm (45mm at hinge B). These results compared well with the test maximum applied load of 645kNm^{-1} width at an arch deflection of 32mm. Referring to Figure 8.3, it could be seen that the prediction of arch collapse load increased with arch deflections until the collapse load prediction reached its maximum. The arch deflection had two major influences on the prediction of arch collapse load in this modified mechanism method. With a deflected arch, the thrustline was more easily maintained in contact with the intrados and extrados, as shown in Figure 8.1, to form the hinges necessary for mechanism failure. This therefore lowered the predicted collapse load. However, deflecting an arch also, at the same time, mobilises backfill resistance which helps to stabilise the arch. The capacity of a deflected arch therefore depends on the loss of strength due to the deflected arch geometry and the gain of strength due to mobilisation of passive resistance. In the case of Bargower bridge, the gain of strength due to mobilisation of passive resistance was found to be more significant than that lost due to the deflected arch geometry until a maximum arch vertical deflection of 41.76mm. Beyond this deflection the arch capacity was found to reduce with further arch deflections.

Figure 8.5 shows the influence of arch deflection on the distribution of backfill lateral pressure coefficient. Full mobilisation of passive resistance was found at an arch deflection of 41.76mm and above. The peak backfill passive coefficient did not occur at the crown since hinge C (Figure 8.1) was located away from the crown. A comparatively small arch vertical deflection was enough to fully mobilised the backfill active resistance.

The backfill ultimate active deflection, as expected, did not have a significant influence on the prediction of arch collapse load and the distribution of backfill pressure coefficient. This was because its magnitude was comparatively negligible when compared with the self-weight of the arch bridge and also the backfill passive resistance. It could be seen from Figure 8.7 that all predictions of the arch collapse load were identical, even for different backfill ultimate active deflections, at an arch

deflection of 30mm and above since full active resistance was mobilised beyond this level of arch deflection anyway.

The backfill ultimate passive deflection was found to have a dramatic influence on the prediction of arch collapse load and the distribution of backfill lateral pressure coefficient. It could be seen from Figure 8.8 that, with lower backfill ultimate passive deflections, the predictions of arch collapse load were found to increase with arch deflections until they reached their maximae. Its influence was particularly significant in this case since Bargower was a deep arch with a significant amount of backfill on both sides of the arch thus enhancing the effect of soil-structure interactions. However, its influence also depended on the magnitude of the backfill angle of shearing resistance. The effect would be more dramatic with a higher backfill angle of shearing resistance.

The backfill and arch bulk unit weights were found to have an influence on the prediction of arch collapse load. In the case of Bargower a substantial depth of fill of 1.2m was used to cover the arch rendering the backfill bulk unit weight so influential. However, the arch bulk unit weight was found to have a comparatively low influence on the prediction of arch collapse load since its volume was not as large as that of the backfill. It is expected that the self-weight of an arch bridge is the most important factor in determining the arch capacity since the failure load of an arch bridge is the load required to rotate three large arch segments (Figure 8.1) against gravitational attraction to form a failure mechanism.

The backfill angle of shearing resistance was found to have a significant influence on the prediction of arch collapse load. This was partly contributed to by the large fill depth over the crown and also the geometry of the arch allowing significant soil-arch interaction to take place. Large boulders were found on both sides of the arch acting as backing. This might have affected the arch behaviour during the test. However, nothing has been done in the author's analyses to modify the backfill properties in order to take into account the existence of larger boulders on both sides of the arch.

The live load dispersal angle, as expected, was found to have a significant influence on the prediction of arch collapse load. It is still a subject of dispute as to what actual live load dispersal angle is to be used in this type of analyses. A 27° dispersal angle is recommended by the Department of Transport (BD21/97, 1997a). However, a live load dispersal angle of 65° was recorded by FAIRFIELD (1994a) in a full scale test at Kimbolton Butts, Cambridgeshire. An arbitrary 45° dispersal angle was used , except in the parametric study on the load dispersal angle, in all analyses.

8.5.1.2 Bridgemill

The modified mechanism method predicted a collapse load of 360.3kNm^{-1} at an arch deflection of 27mm. The full scale arch collapse load of 361kNm^{-1} was recorded at an arch deflection of about 90mm. The arch deflection at which the arch was subjected to a maximum applied load of 361kNm^{-1} in the full scale test was much higher than that required by the modified mechanism method for an accurate prediction of the arch collapse load. At an arch collapse load of 90mm, the collapse load prediction by the modified mechanism method was much more lower at 256.7kNm^{-1}. This might be the result of ignoring the spandrel walls. In reality, the spandrel walls provide extra stiffness against the rotation of an arch. In the full scale test on Bridgemill, separation between the arch and spandrels occurred. However, this was followed immediately by a new mode of arch-spandrel interaction on the side remote from the load where a portion of the arch ring was moved towards the spandrels. This indicated that the arch was supporting part of the spandrel's self-weight, on the side remote from the load, requiring a greater live load to rotate the arch.

Figure 8.16 shows the influence of arch deflection on the distribution of backfill lateral pressure coefficient. It was no surprise that full mobilisation of backfill passive resistance was not recorded even at an arch deflection of 100mm since Bridgemill was a flat arch. At a given arch vertical deflection under the load line at the ¼-span point of

a flat arch, its corresponding arch horizontal deflections on the side remote from the load are comparatively much smaller than those in the case of a deep arch.

Unlike the backfill ultimate active deflection, the backfill ultimate passive deflection was found to affect the prediction of arch collapse load, as shown in Figure 8.18, although Bridgemill was a flat arch. However, the collapse load prediction was found to decrease with arch deflection even for a very low backfill ultimate passive deflection of 25mm. This indicated that the loss of arch strength due to deflection was more significant than the gain of stiffness due to mobilisation of passive resistance.

Both the arch and backfill bulk unit weights were found to affect the collapse load prediction. With a higher arch or backfill bulk unit weight, a higher collapse load was predicted since a larger load was required to rotate the arch against gravitational attraction. However, their influence on the collapse load prediction was not very significant as only a small amount of backfill was used to cover the arch and the arch itself was not stocky.

The backfill angle of shearing resistance did not significantly affect the collapse load predicted at small arch deflections since its influence was deflection dependent. In the case of Bridgemill, the magnitude of arch horizontal deflection on the side remote from the load was comparatively much smaller than the arch vertical deflection under the load line rendering the collapse load prediction insensitive to the variation of backfill angle of shearing resistance except in cases where arch deflections were substantial.

As shown in Figure 8.23, the influence of live load dispersal angle is significant. However, the increase in the collapse load prediction with live load dispersal angle was not linear in this case. It could be seen from Figure 8.23 that only a small increase in the collapse load prediction was recorded with an increase in the live load dispersal angle from 27° to 45°. However, a substantial increase in the collapse load prediction was observed by increasing the live load dispersal angle from 45° to 55°.

8.5.1.3 Strathmashie

The modified mechanism method predicted an arch collapse load of 227kNm^{-1} at an arch deflection of 70mm. This compared well with the full scale test collapse load of 228kNm^{-1} at an arch deflection of 80mm. At an arch deflection of 80mm, the modified mechanism method prediction was 220kNm^{-1} which was also reasonably close to the full scale test collapse load.

Full mobilisation of backfill passive resistance was recorded at an arch deflection of 104.7mm. However, that covered only about a quarter of the arch span and the backfill lateral pressure coefficient rapidly fell to its at-rest value at the right abutment.

As in the case of Bargower and Bridgemill, the influence of backfill ultimate active deflection on the collapse load prediction for Strathmashie was imperceptible. In contrast, the backfill ultimate passive deflection was found to affect the prediction of arch collapse load quite significantly as shown in Figure 8.28. Most notable was the collapse load predictions with backfill ultimate passive deflections of 50mm and lower with which the collapse load predictions were found to increase with arch deflections until an arch deflection of about 30mm. Surprisingly, the collapse load predictions were found to be lower with lower backfill ultimate passive deflections at higher arch deflections. A greater backfill lateral force acting on the side remote from the load is always claimed to be enhancing the arch's capacity. However, this might not be true if arch deflections were considered. In the case where the arch deflection is substantial to a degree where, referring to Figure 8.1, hinge C is at a point higher than hinge B, lateral forces acting on the side remote from the load at points higher than hinge B are actually inducing moments that are unfavourable to the stability of the arch.

Both the arch and backfill bulk unit weights were found to affect the collapse load prediction for Strathmashie. The backfill bulk unit weight was more influential than that of the arch since a comparatively large volume of the whole structure consisted of backfill.

As shown in Figure 8.32, the collapse load prediction was dramatically affected by backfill angle of shearing resistance. With the exception of the case where the arch deflection was zero, the collapse load prediction increased significantly with backfill angle of shearing resistance especially at arch deflections in the region of 50mm to 100mm. With a 45° of backfill angle of shearing resistance, the collapse load increased with arch deflection until an arch deflection of about 20mm.

The influence of live load dispersal angle on the collapse load prediction was significant as shown in Figure 8.33. With a load dispersal angle of 27°, the predicted arch collapse loads were found to be much more lower than those with load dispersal angles of 45° and 55° at a given arch deflection.

8.5.2 Discussion concerning the assumptions inherent in the author's method

The author's modified mechanism method assumed the arch had no tensile strength and was infinitely strong against compressive failure. The former was justifiable since most existing arches have been subjected to cyclic loadings for years and therefore their tensile strength, if any, is negligible. Furthermore, the size of a real arch bridge is comparatively large thus making the tensile strength unimportant since the magnitude of the collapse load is dominated by the force required to rotate the mass of the arch bridge against gravitational attraction. The tensile strength of an arch would be significant in the case of a newly built arch at a moderate size.

Compressive failure of the arch has been incorporated in conventional mechanism assessment (SMITH, 1991a). The arch compressive strength was claimed to be the combined compressive strength of the voussoir unit and the mortar joint. The combined compressive strength of a masonry prism is much lower than that of the voussoir unit itself since the failure of a masonry prism is due to a stretching effect induced in the mortar which has a higher Poisson's ratio. It is very clear that

compressive failure of an arch, if at all, happens at hinges, usually near the load, with a high concentrated stress due to a limited contact area between the voussoir unit and the mortar joint. This is completely different from that defined in the compressive failure of a masonry prism which has been widely used by various researchers in the mechanism method. In reality, an apparent compressive failure occurs simultaneously at the collapse of the arch. This implies that shortly before the occurrence of compressive failure the applied live load would have almost reached the maximum. Is reducing the arch ring thickness by considering a zone of thrust due to compressive failure a solution to consider the arch compressive failure in the mechanism method? The author thinks not. It would be more appropriate to say that such an arbitrary compressive failure is introduced as an indirect compromise to the assumption of infinite arch elastic modulus made in the no-deflection mechanism model.

The main difficulty in using the author's modified mechanism method is determining the arch vertical deflection of which the applied load reaches its maximum. It depends on the arch geometry as well as its material properties. Full scale tests revealed that the arch vertical deflections of which the arch capacities reached their peak values were between 20mm an 50mm. Research was carried out with a view to search for an empirical relationship relating the arch geometry and the deflection at which an arch's capacity peaked using results from previous full scale tests. An apparent disagreement was found when relating the arch deflection, at which an arch was subjected to a maximum applied load, to its geometry. Furthermore, limited availability of full scale results call into question the reliability of such an empirical relationship.

Apart from the above mentioned difficulties, the arch bridge was assumed to be idealised as a 2-D plane strain structure in the mechanism method. The method ignores the contribution from spandrel, wing, and parapet walls. In reality, the arch behaviour and the hinge positions could be different if these arches were not surrounded by these structural elements.

8.6 Conclusions

1 The author's modified mechanism method has been successfully used to analyse Bargower, Bridgemill, and Strathmashie.

2 The arch deflection was shown to have a dramatic influence on the prediction of arch collapse load and the distribution of backfill lateral pressure coefficient.

3 A bi-linear backfill lateral pressure model has been incorporated in the author's modified mechanism method rendering the distribution of backfill lateral pressure more realistic.

4 The backfill ultimate active deflection had no significant influence on the prediction of arch collapse load.

5 The backfill ultimate passive deflection had a significant influence on the prediction of arch collapse load.

6 The backfill and arch bulk unit weights were shown to have an influence on the prediction of arch collapse load.

7 The backfill angle of shearing resistance was found to have a significant influence on the prediction of arch collapse load.

8 The live load dispersal angle was found to have a significant influence on the prediction of arch collapse load.

9 Anomalies still to be researched include; definition of limiting deflection and 3-D effects.

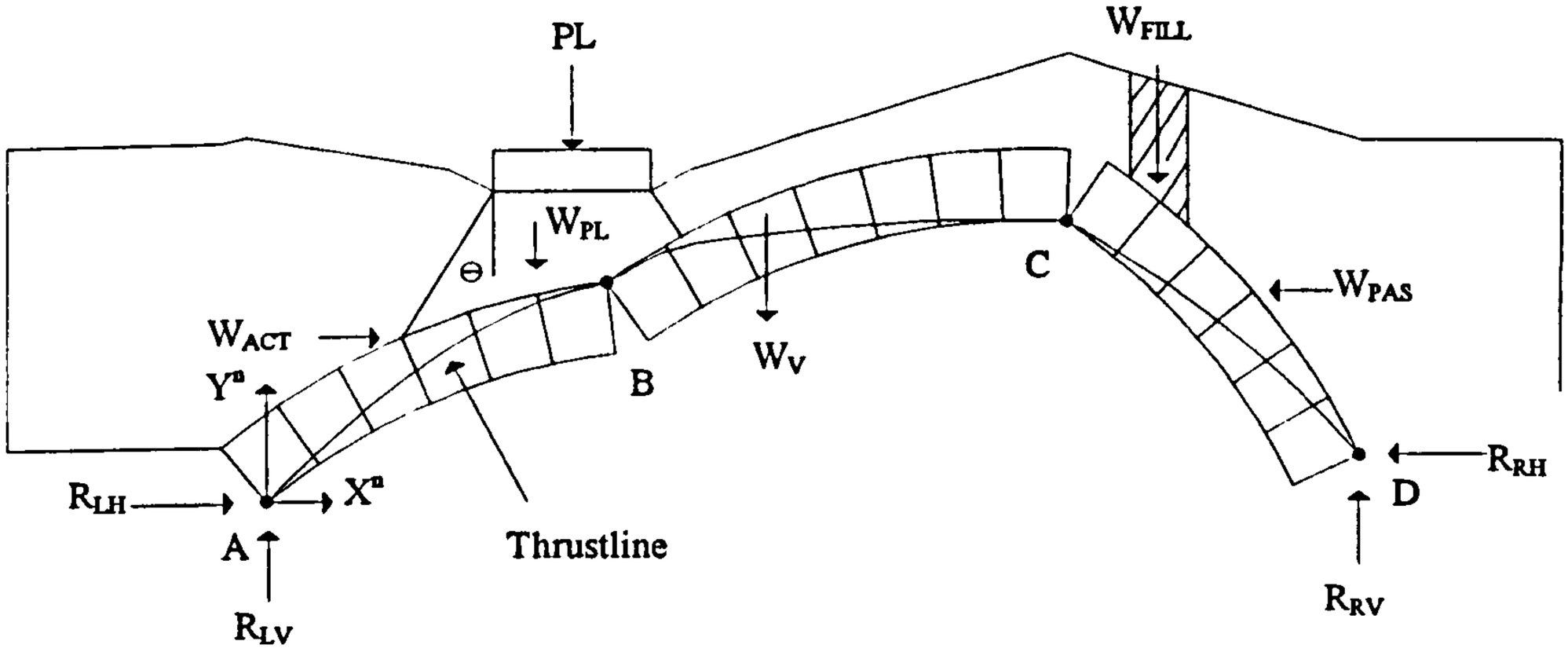

Figure 8.1 Idealisation of a deflected arch with a typical collapse mechanism

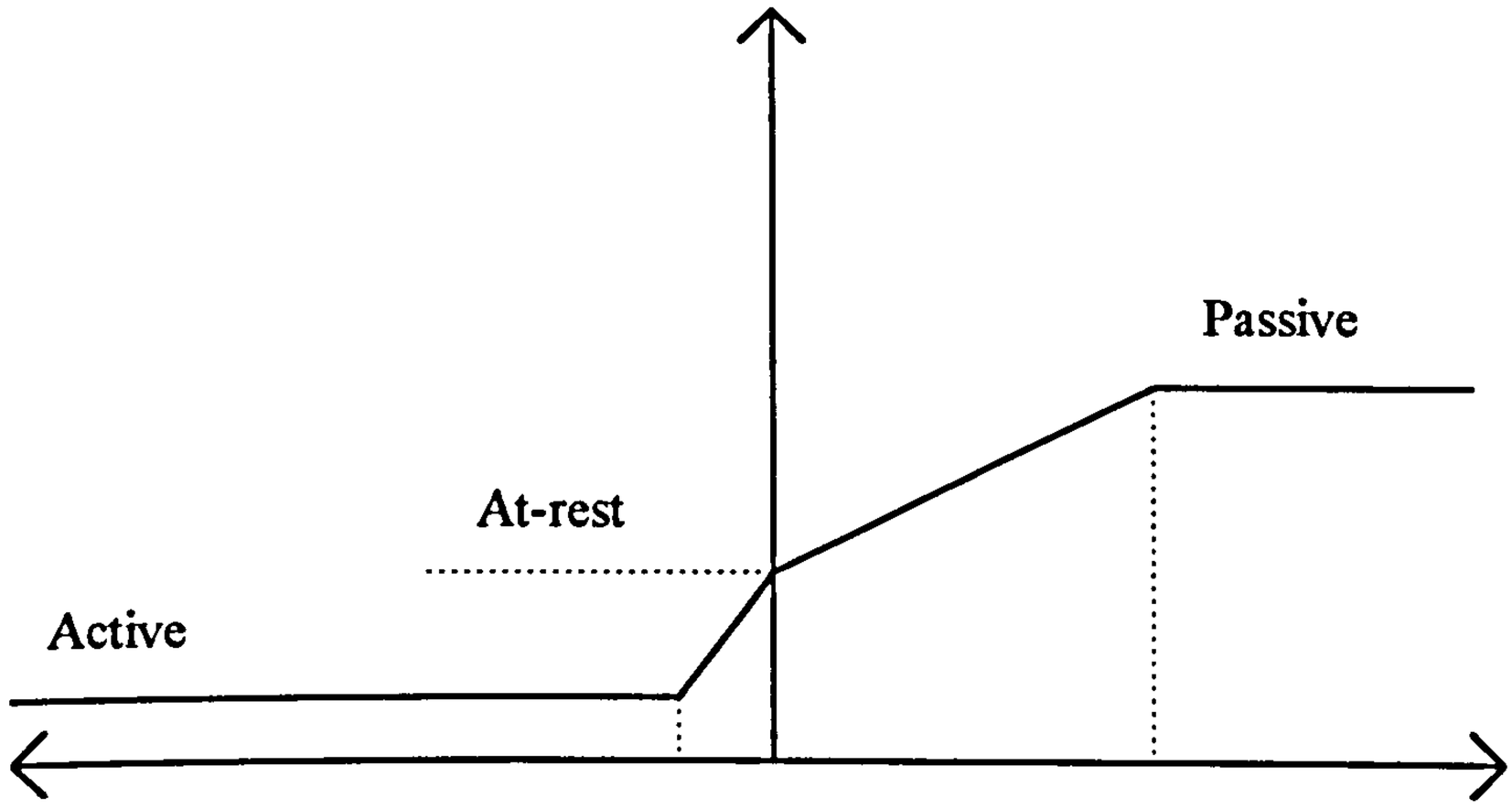

Figure 8.2 A bi-linear deflection dependent backfill pressure distribution model

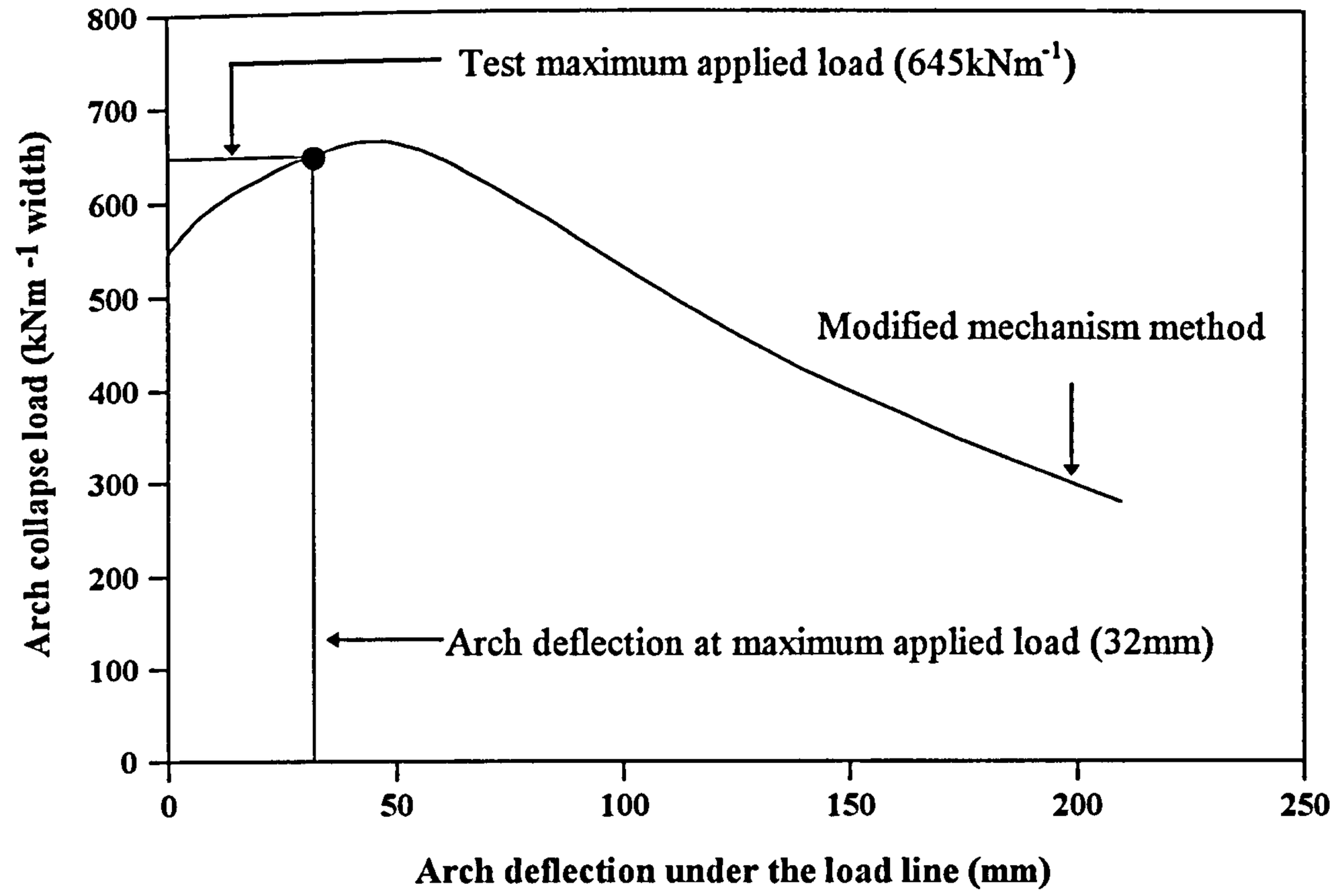

Figure 8.3 Collapse load predictions with arch deflections for Bargower

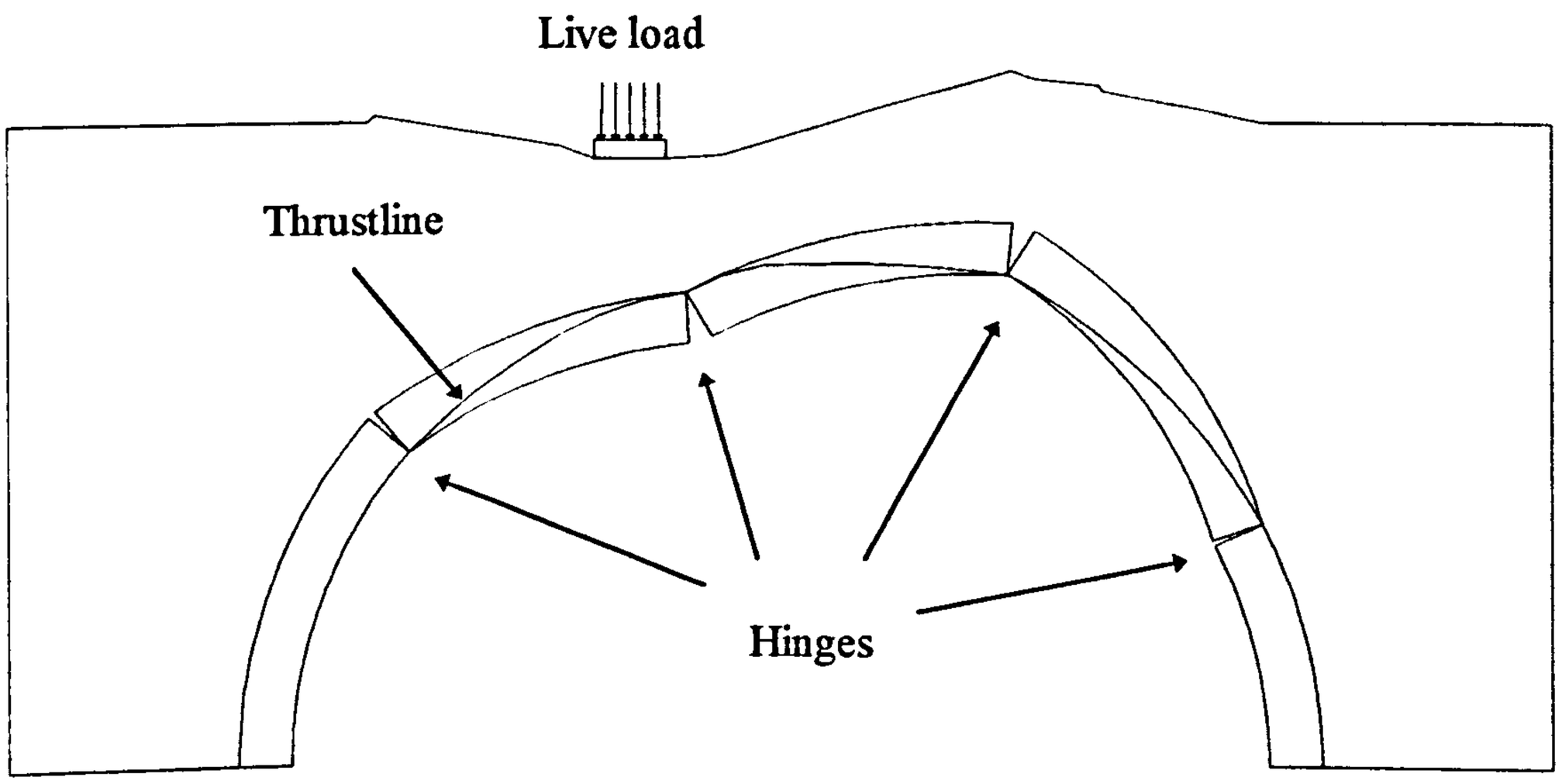

Figure 8.4 Predicted collapse mechanism at 645kNm^{-1} width for Bargower (Deformations exaggerated by × 4.44)

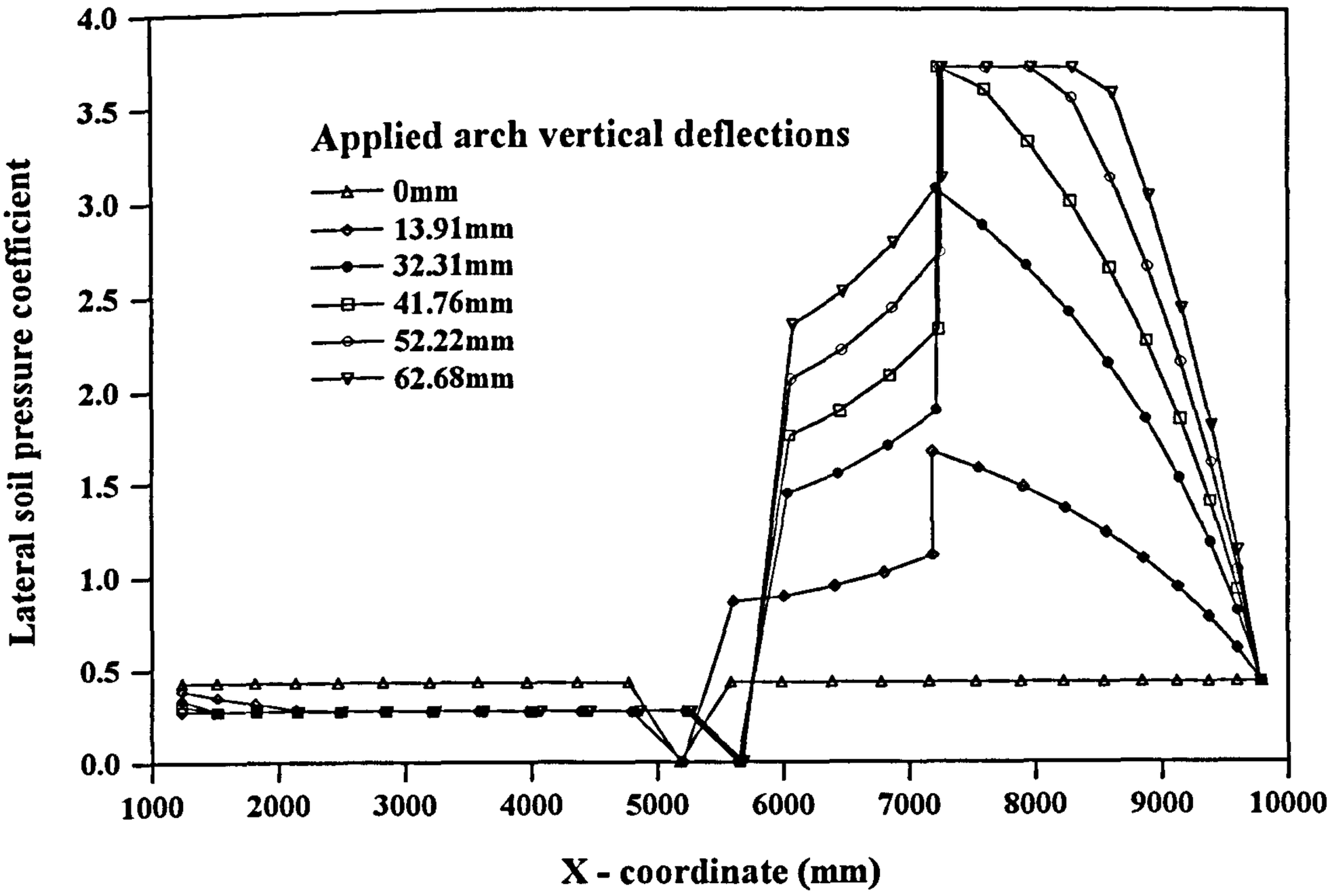

Figure 8.5 Distribution of backfill lateral pressure coefficient for Bargower

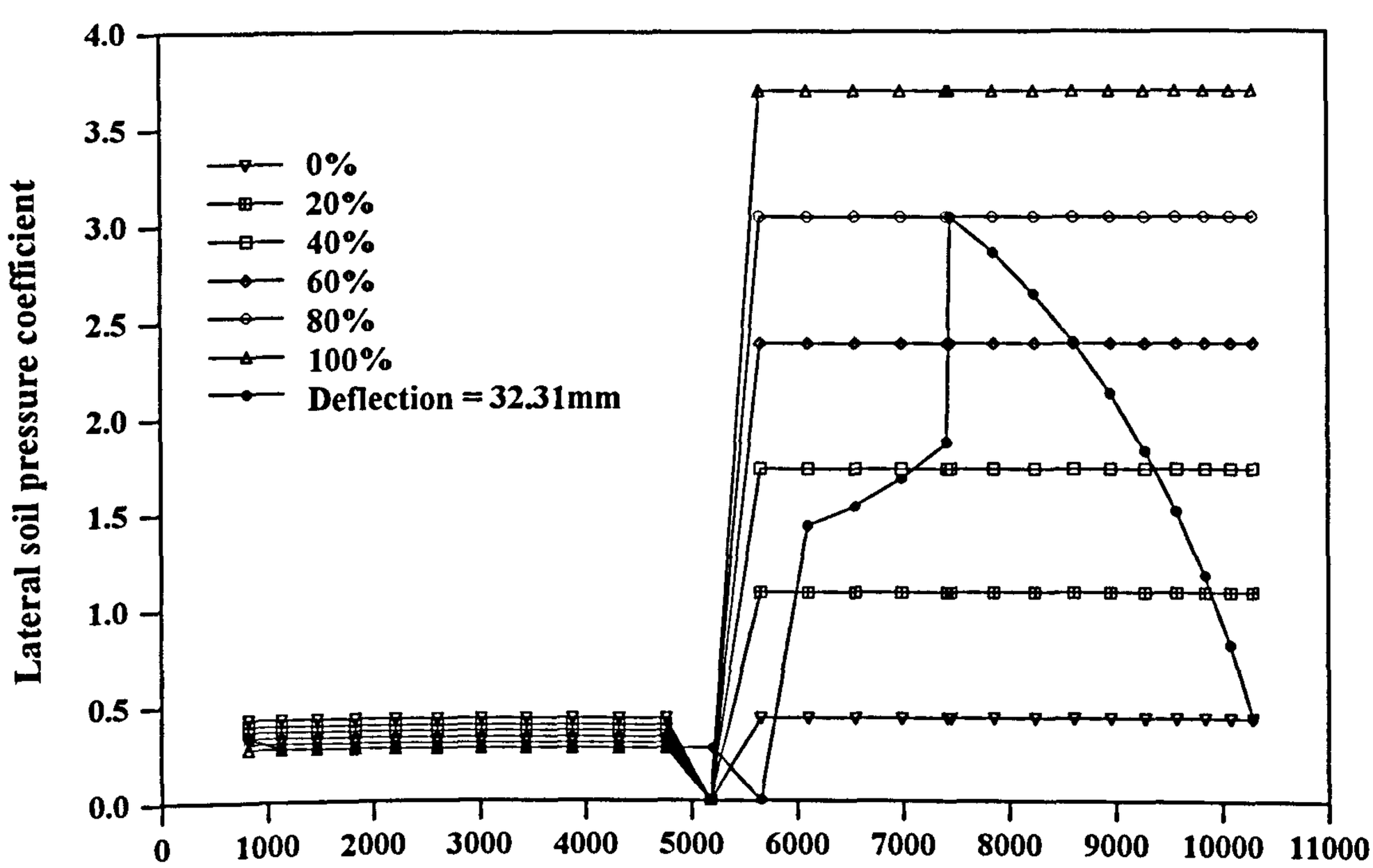

Figure 8.6 Distribution of backfill lateral pressure coefficient with and without arch deflections for Bargower

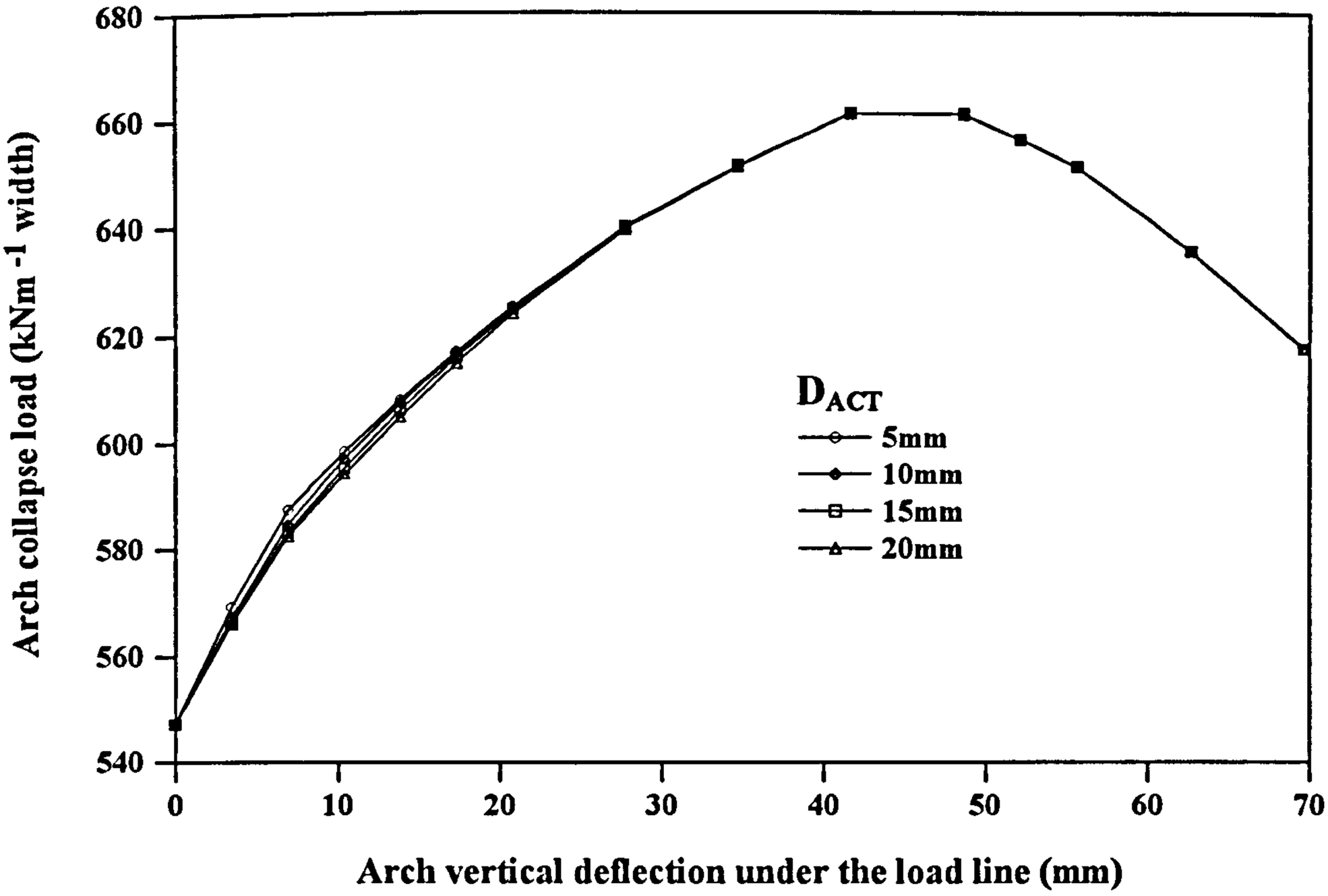

Figure 8.7 The effect of backfill ultimate active deflection on the prediction of arch collapse load for Bargower

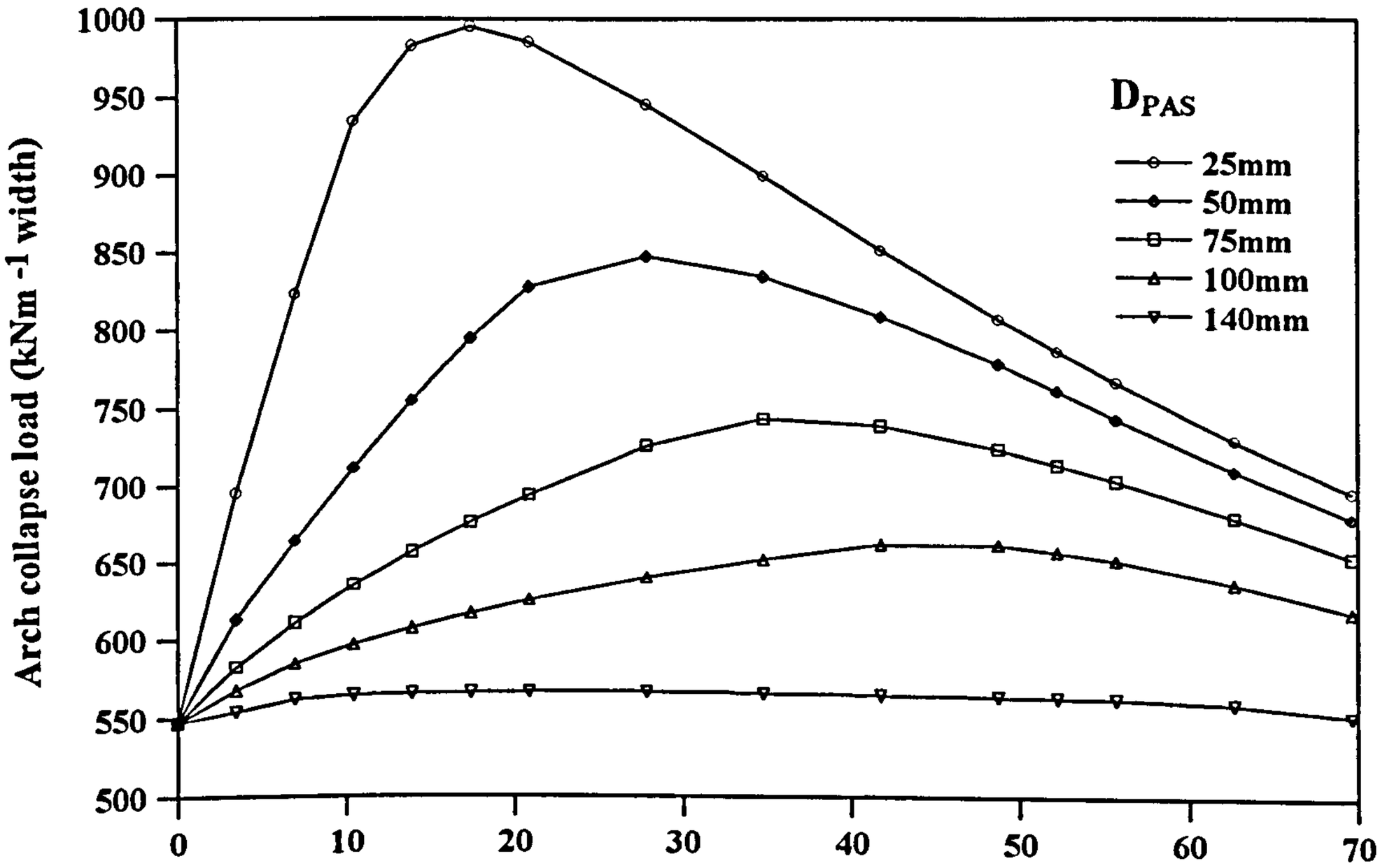

Figure 8.8 The effect of backfill ultimate passive deflection on the prediction of arch collapse load for Bargower

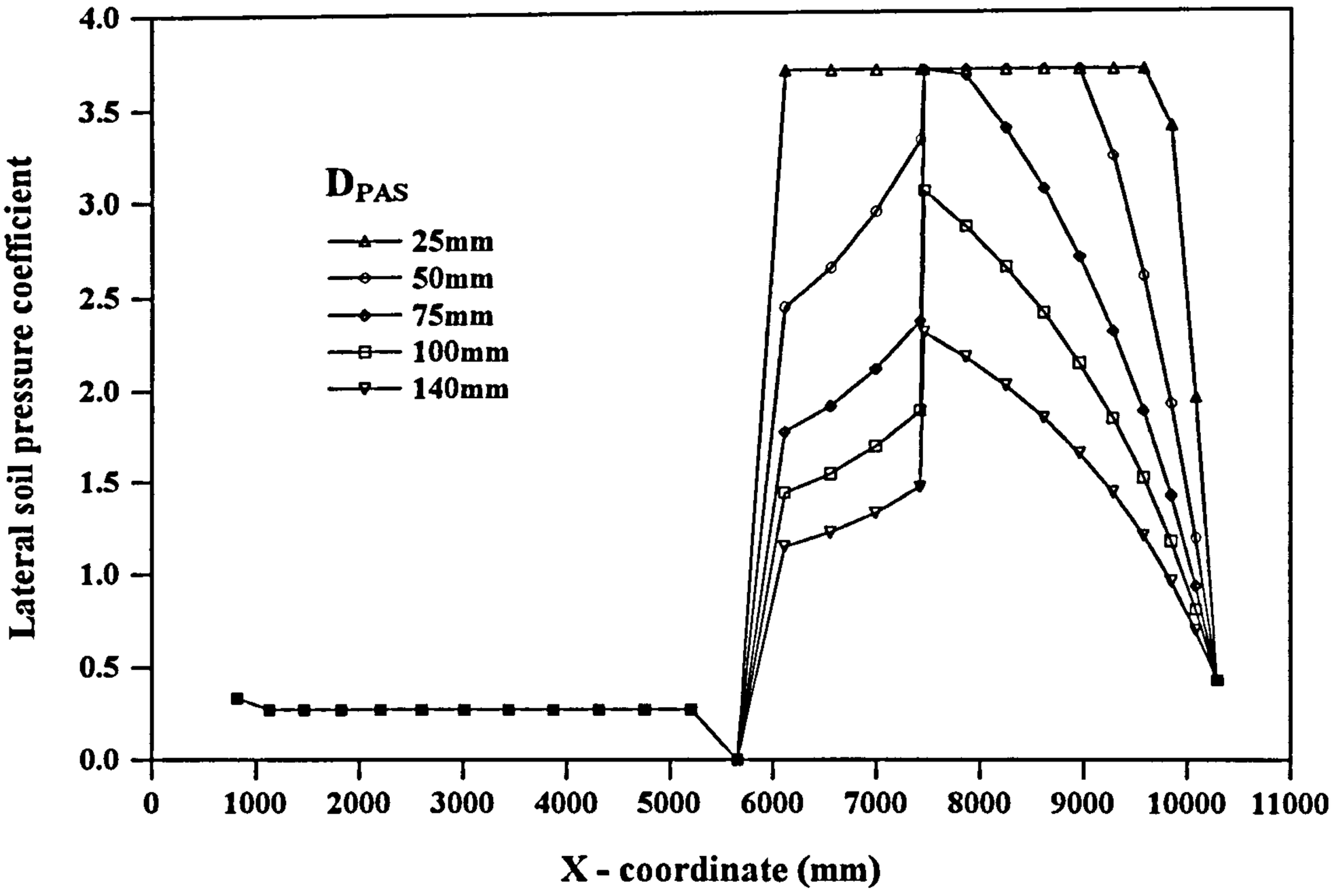

Figure 8.9 The effect of backfill ultimate passive deflection on the distribution of backfill lateral pressure coefficient for Bargower

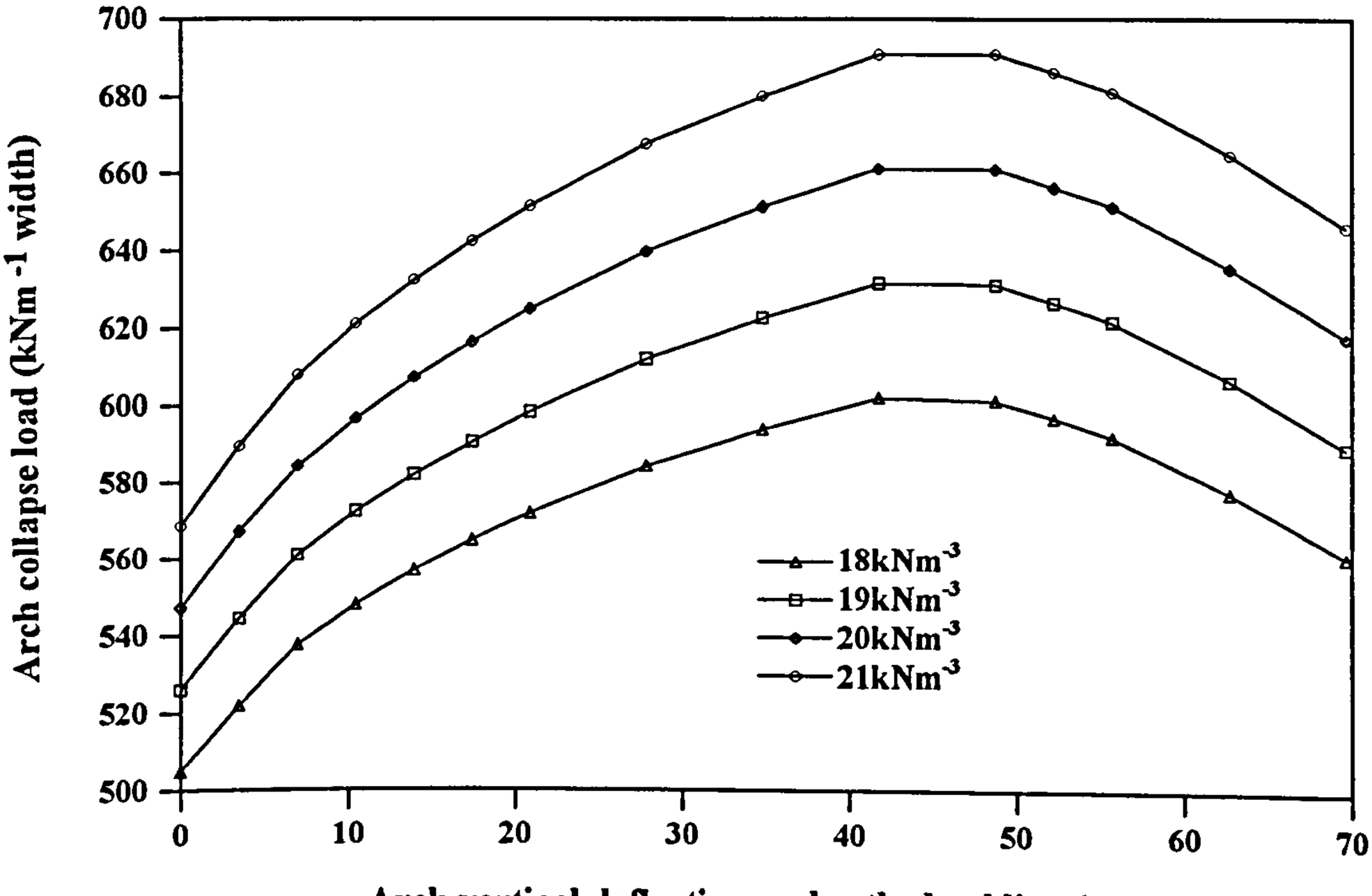

Figure 8.10 The effect of backfill bulk unit weight on the prediction of arch collapse load for Bargower

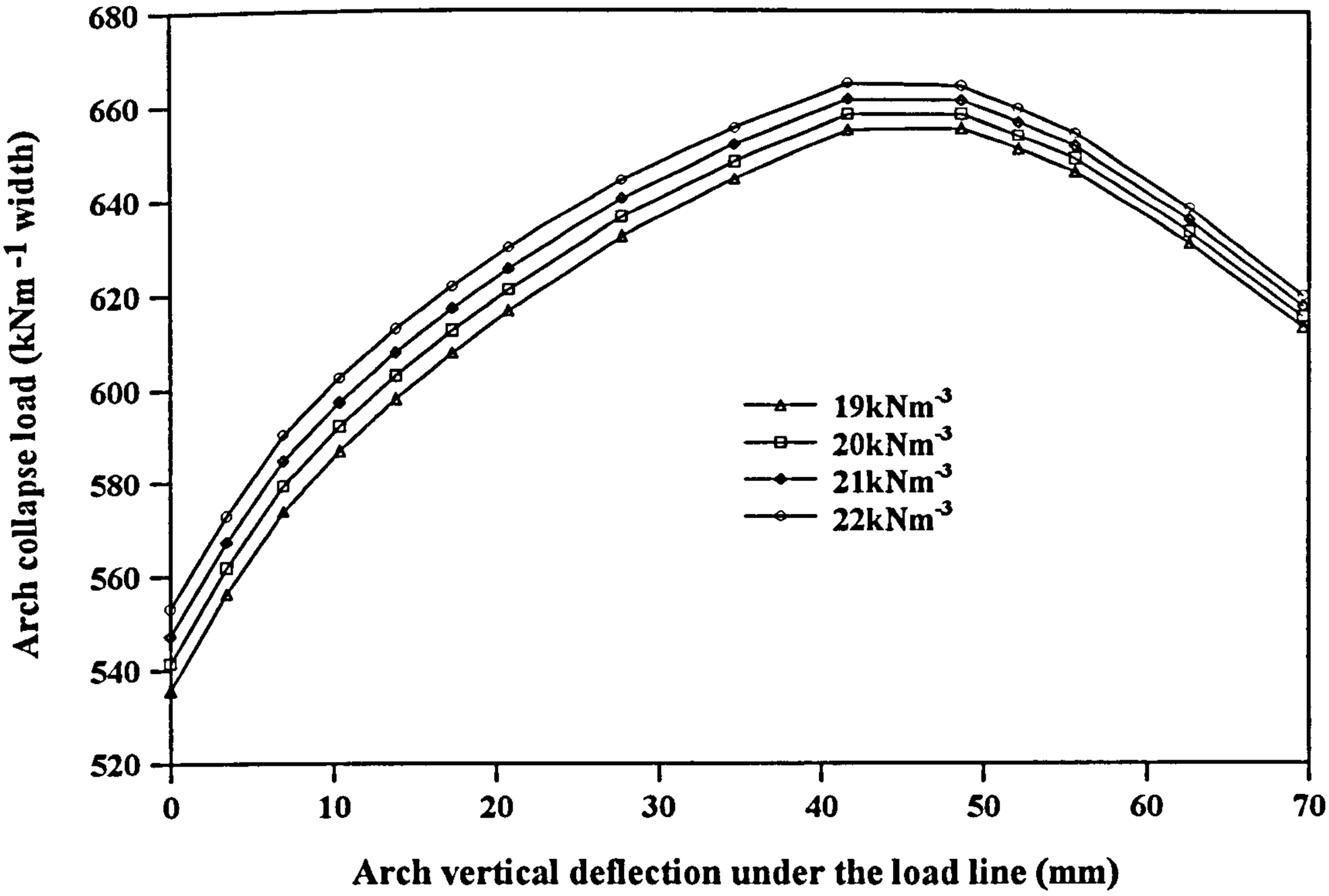

Figure 8.11 The effect of arch bulk unit weight on the prediction of arch collapse load for Bargower

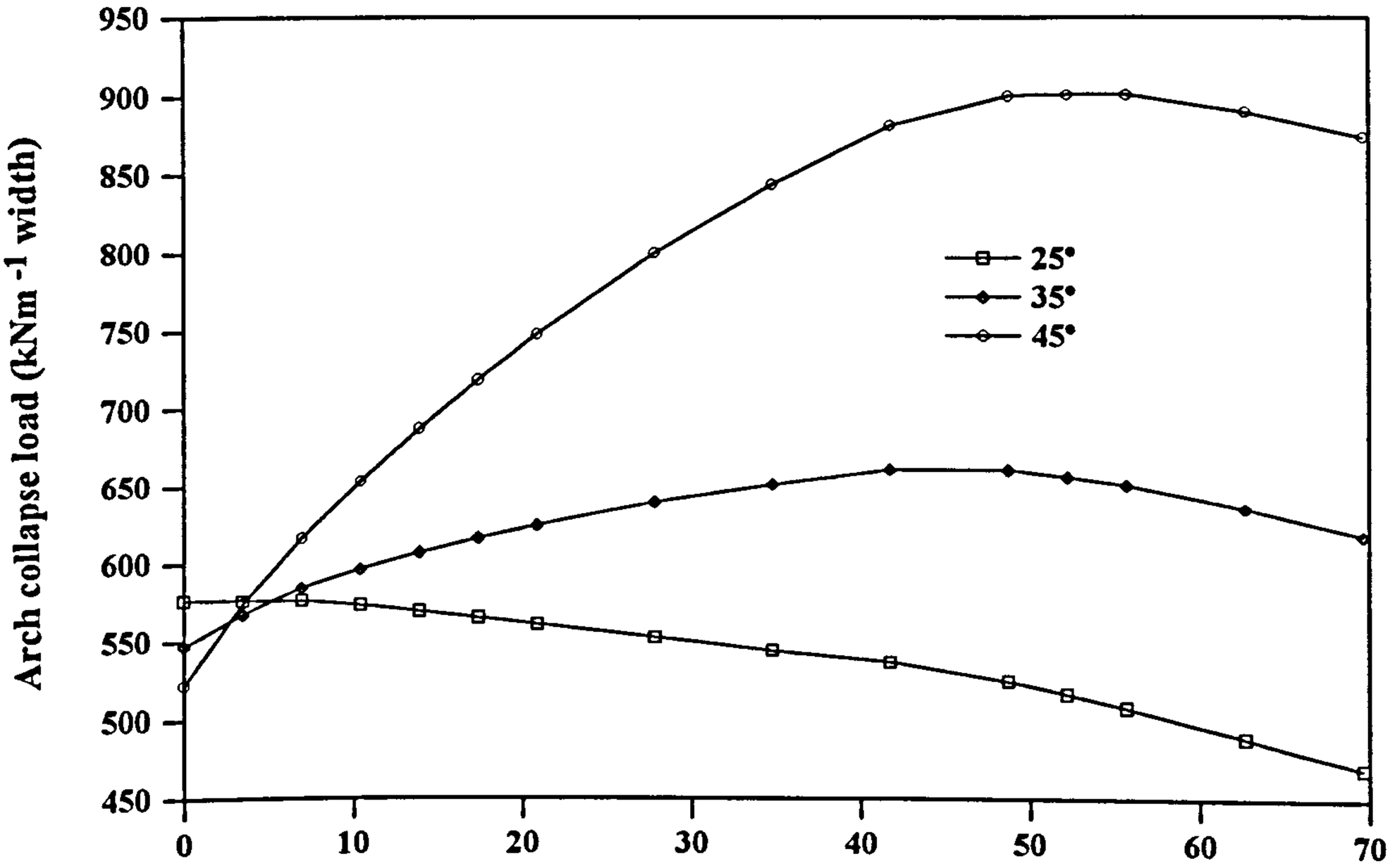

Figure 8.12 The effect of backfill angle of shearing resistance on the prediction of arch collapse load for Bargower

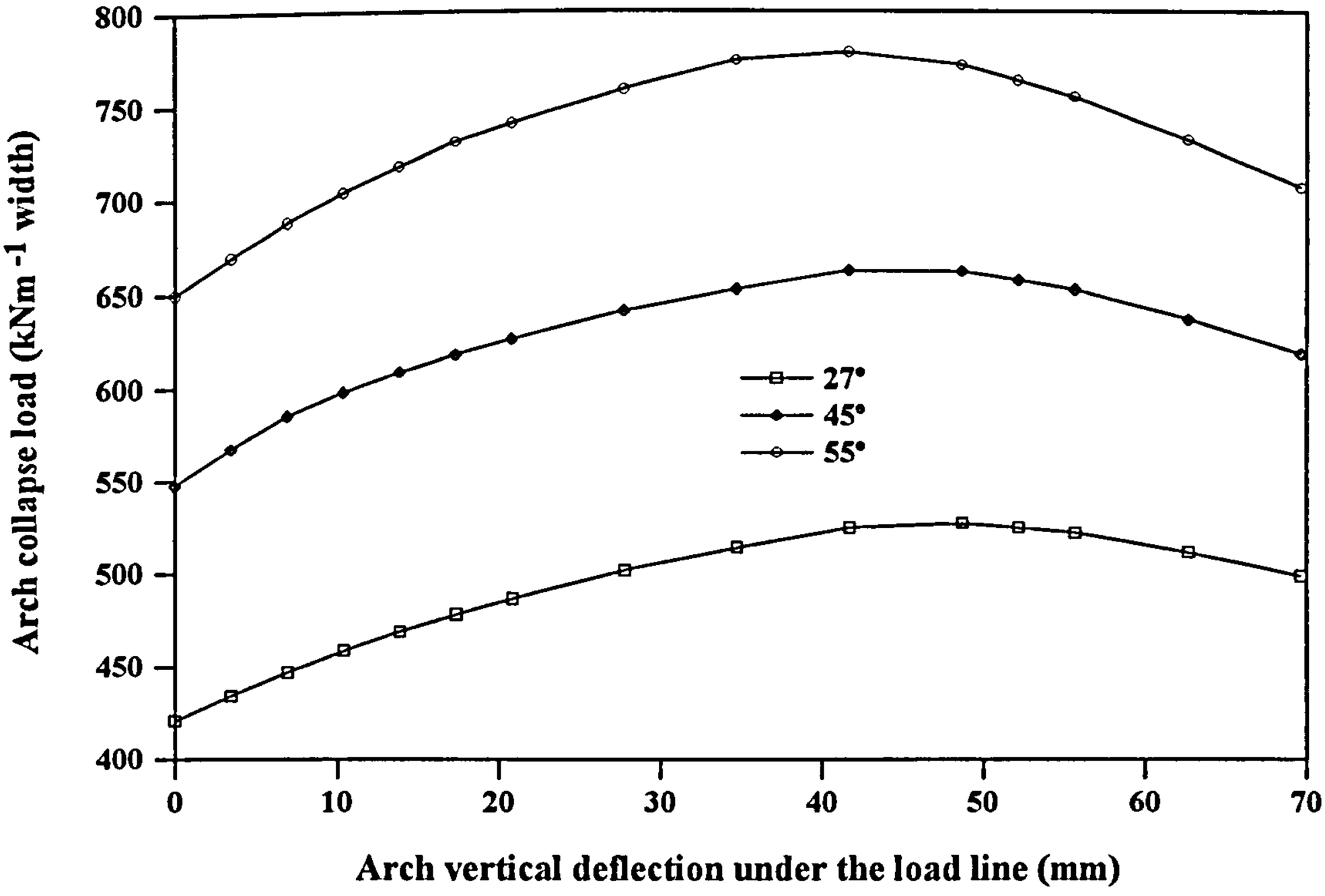

Figure 8.13 The effect of live load dispersal angle on the prediction of arch collapse load for Bargower

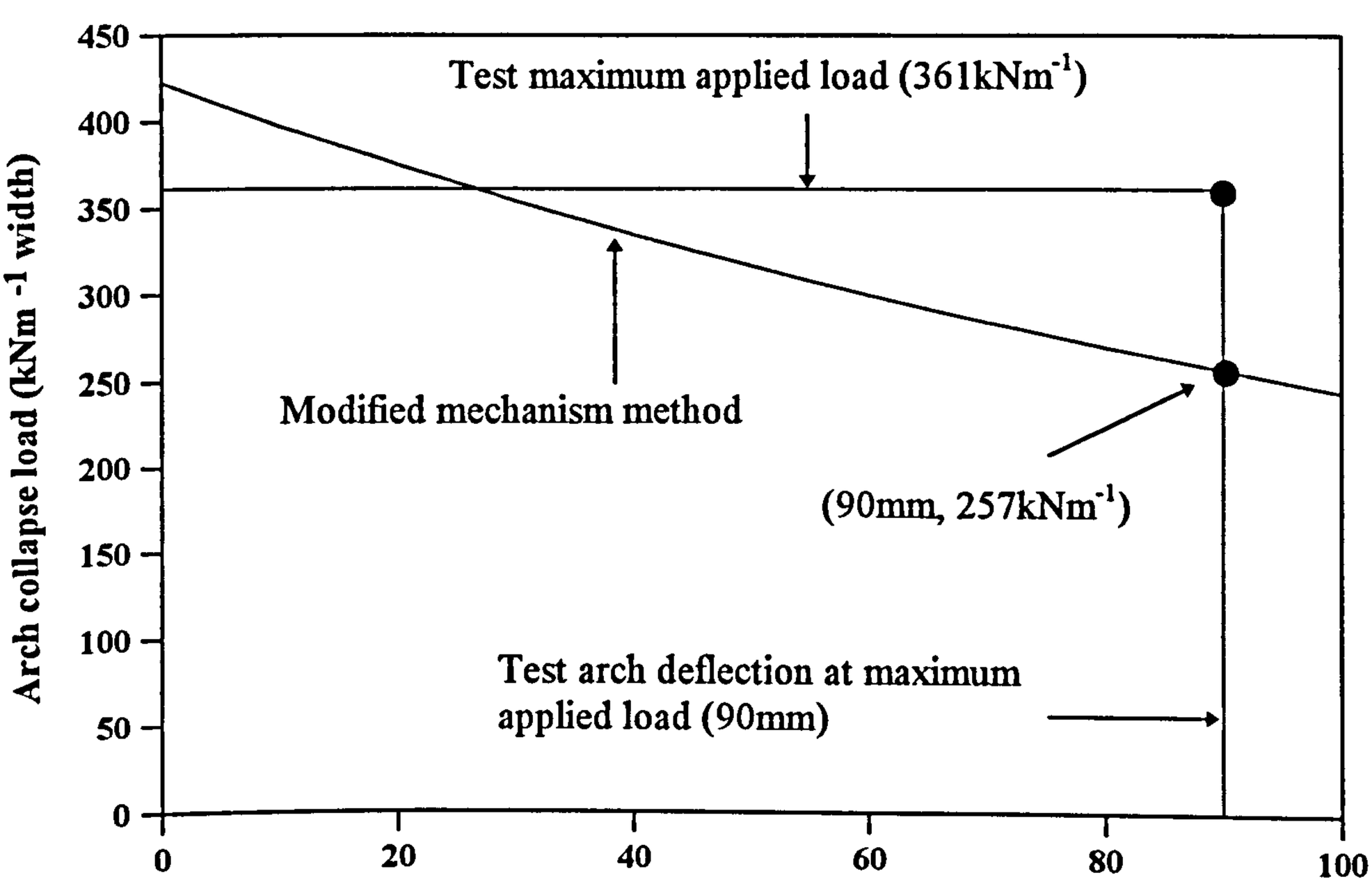

Figure 8.14 Collapse load predictions with arch deflections for Bridgemill

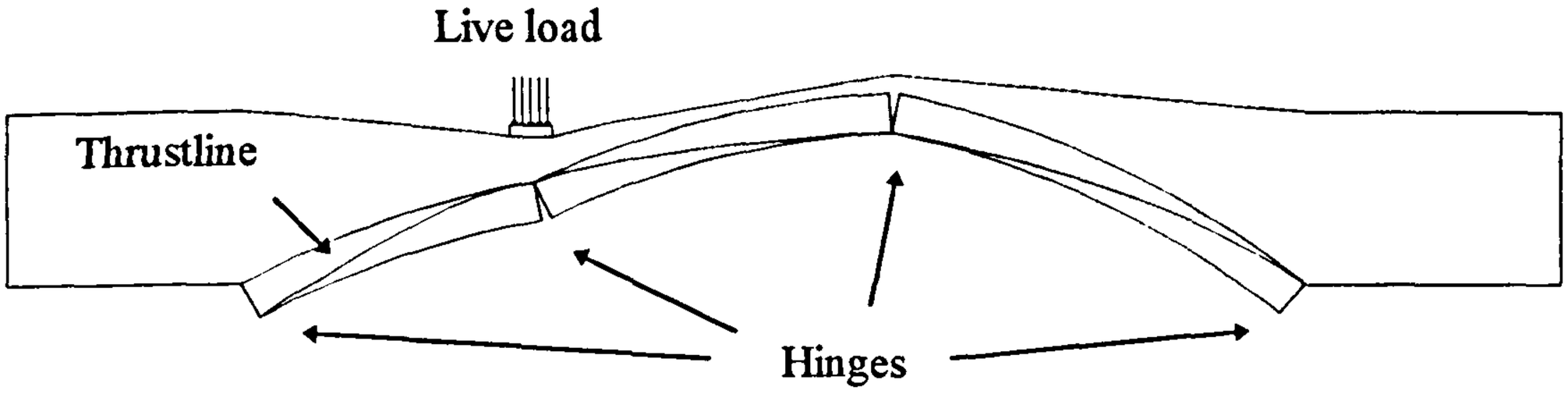

Figure 8.15 Predicted collapse mechanism at 360.3kNm^{-1} width for Bridgemill (Deformations exaggerated by × 18.52)

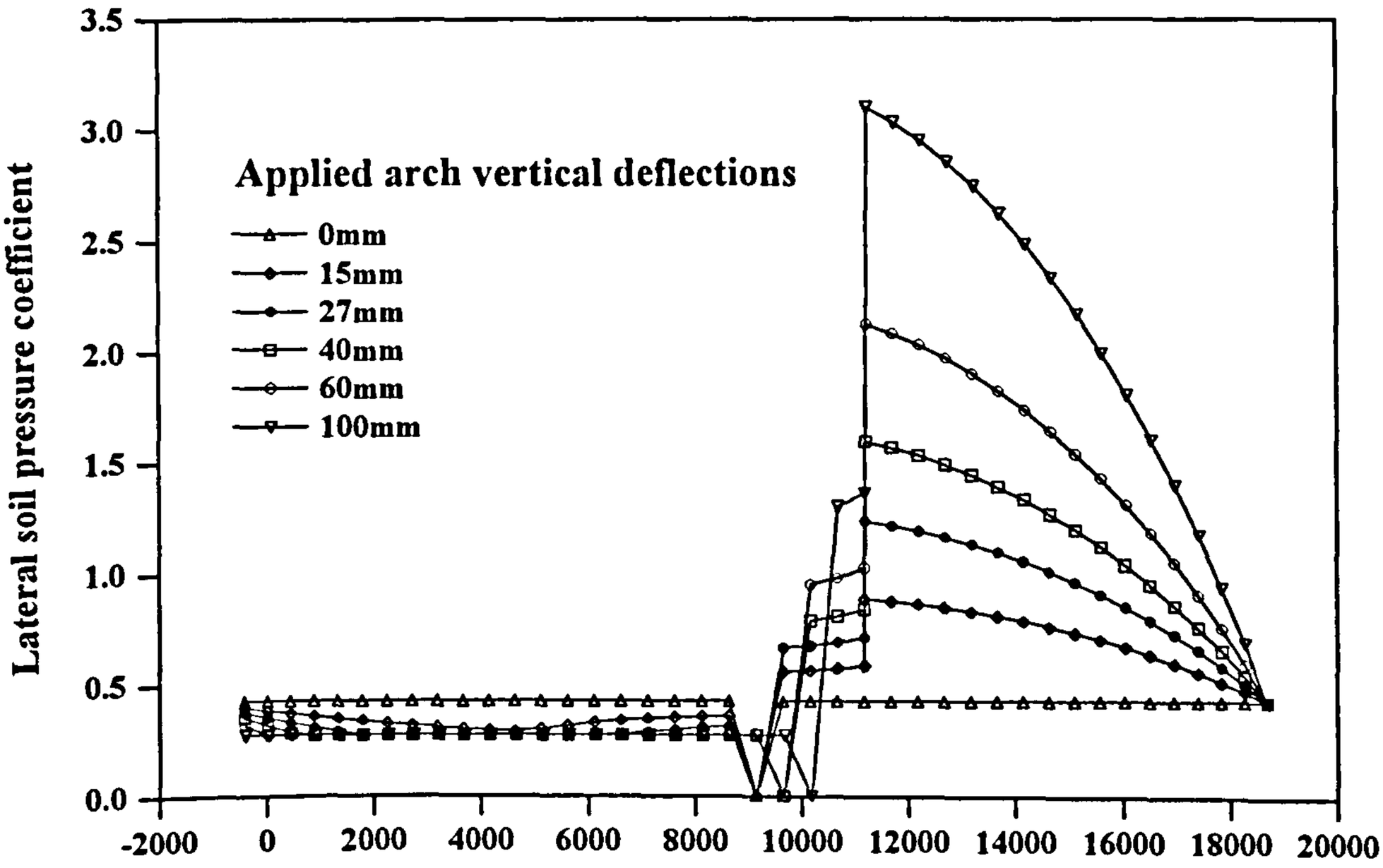

Figure 8.16 Distribution of backfill lateral pressure coefficient for Bridgemill

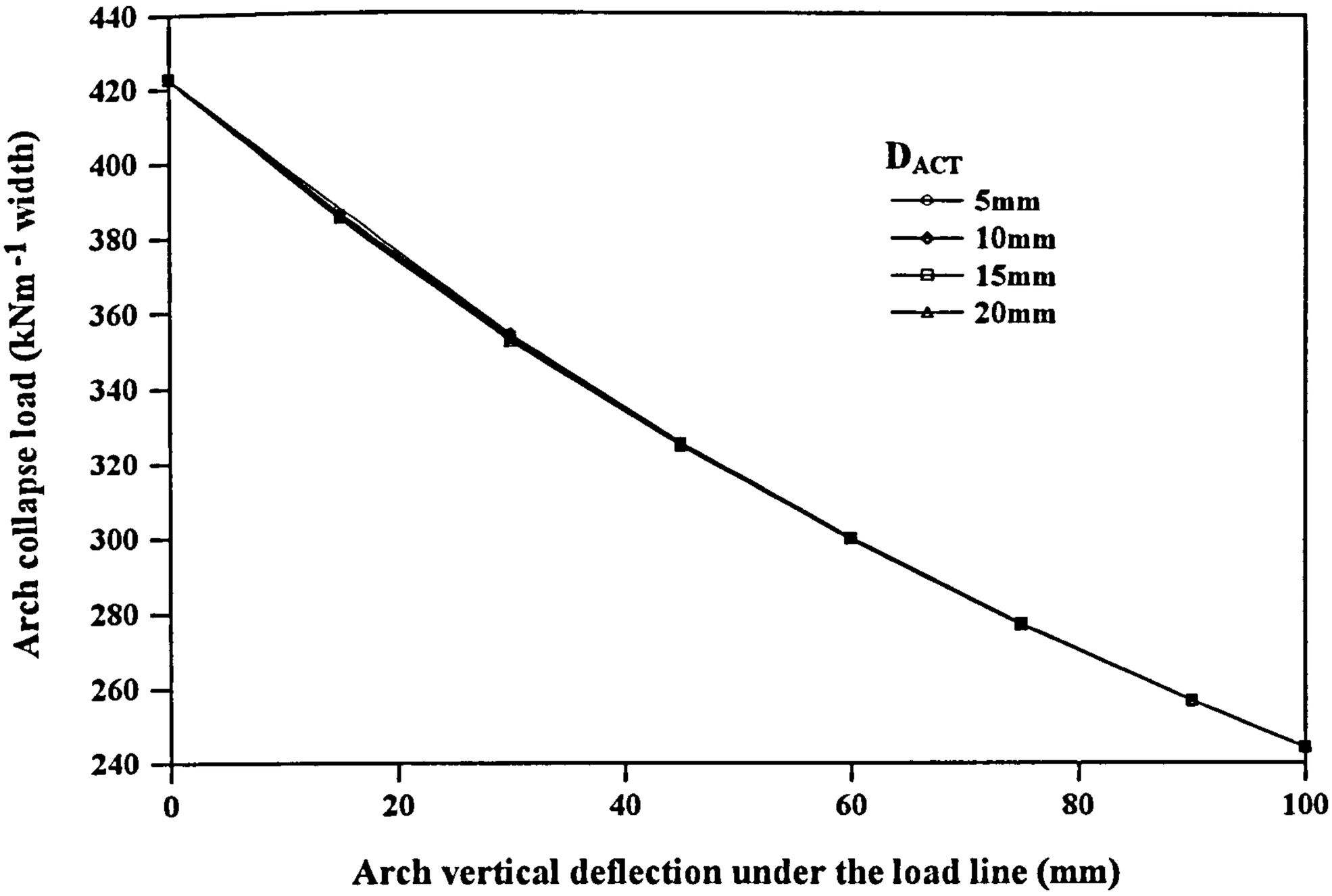

Figure 8.17 The effect of backfill ultimate active deflection on the prediction of arch collapse load for Bridgemill

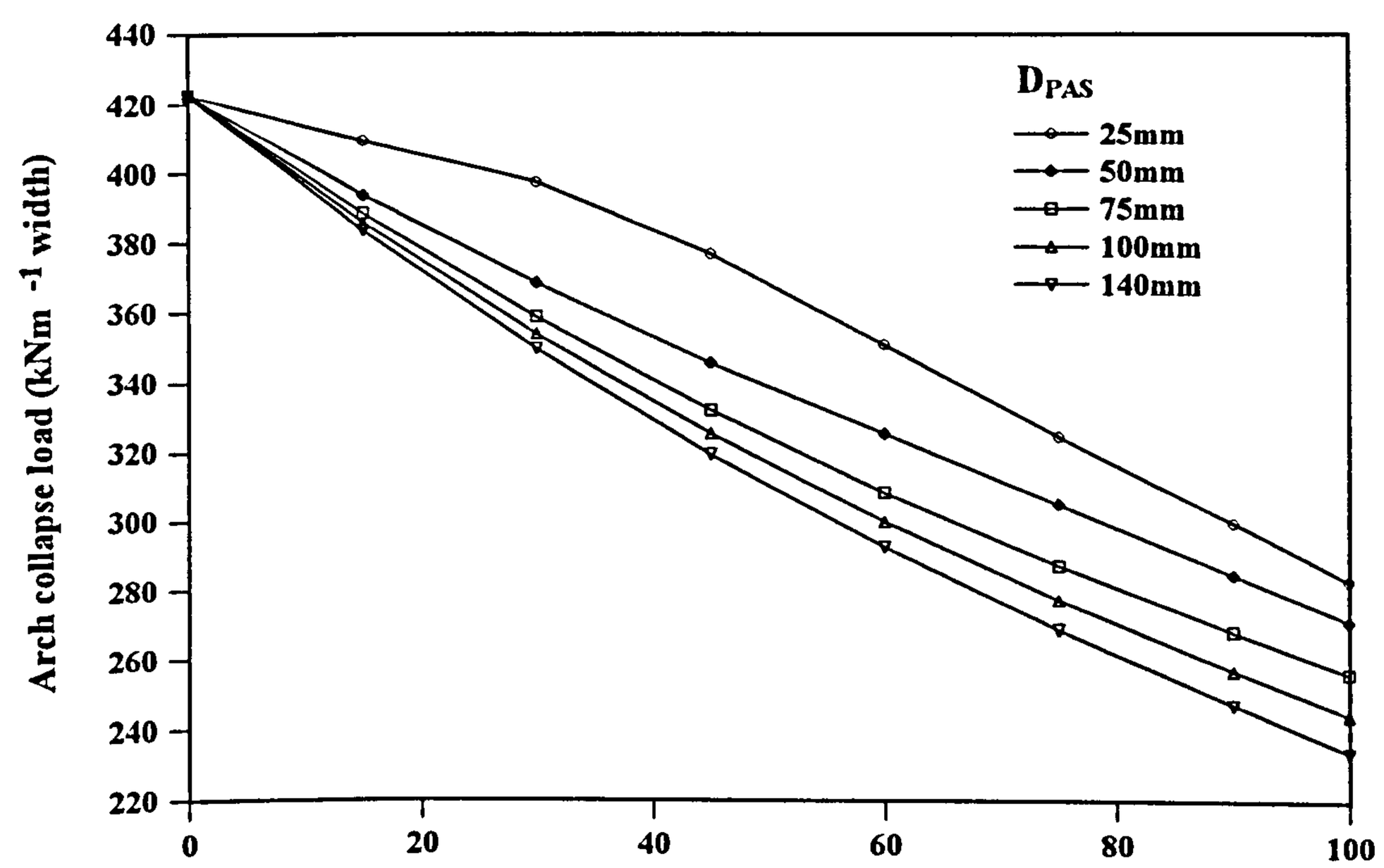

Figure 8.18 The effect of backfill ultimate passive deflection on the prediction of arch collapse load for Bridgemill

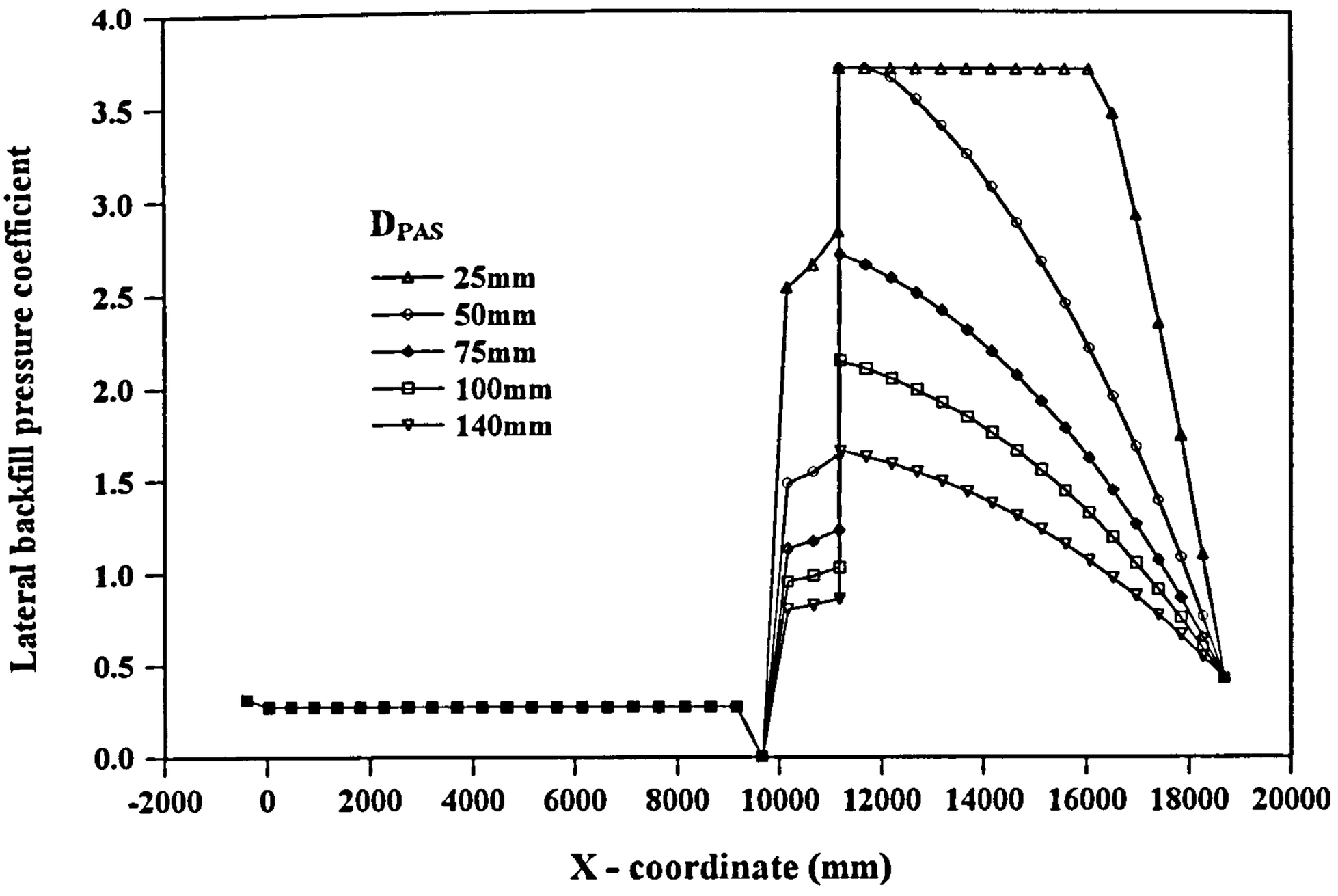

Figure 8.19 The effect of backfill ultimate passive deflection on the distribution of backfill lateral pressure coefficient for Bridgemill

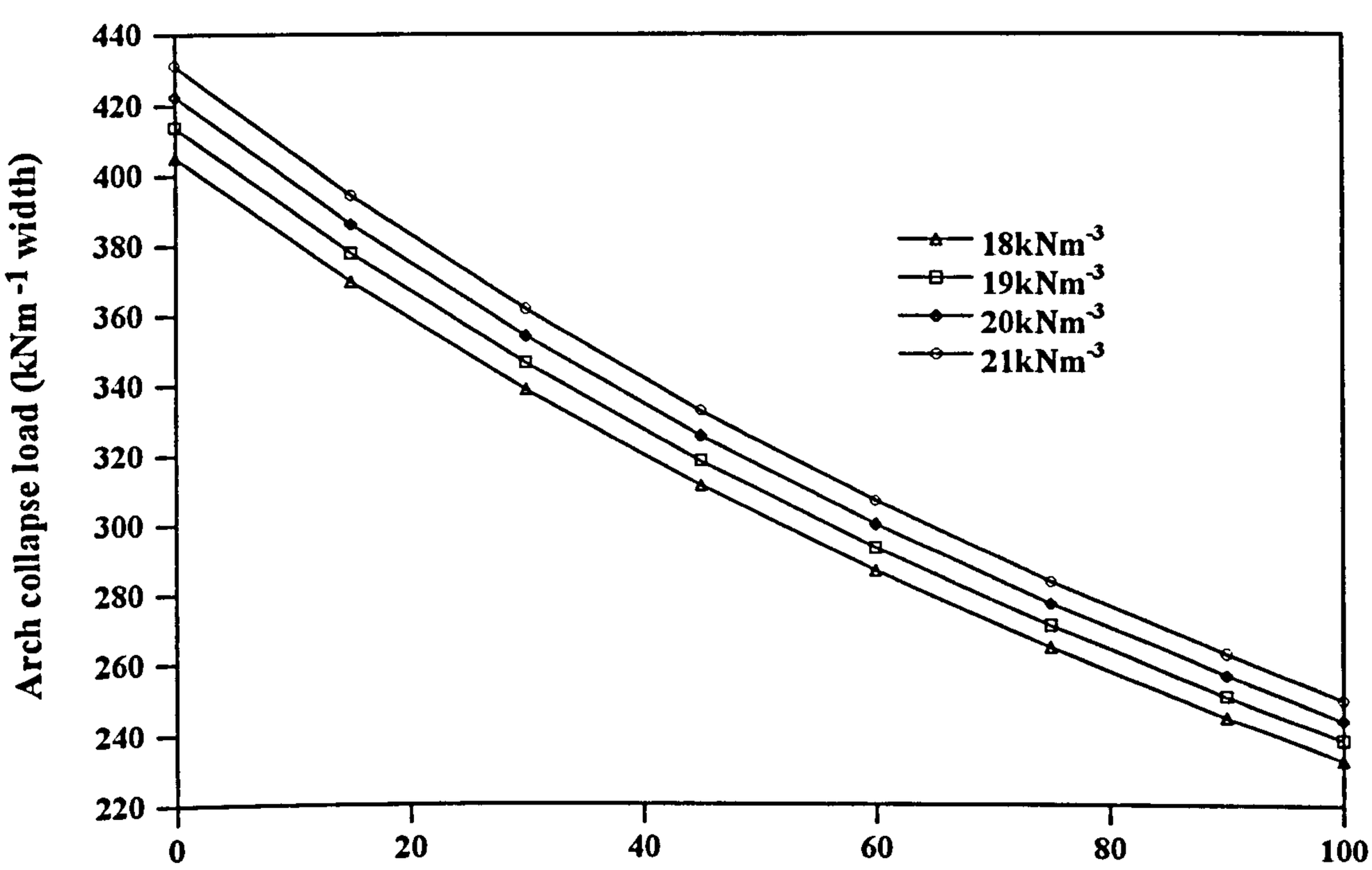

Figure 8.20 The effect of backfill bulk unit weight on the prediction of arch collapse load for Bridgemill

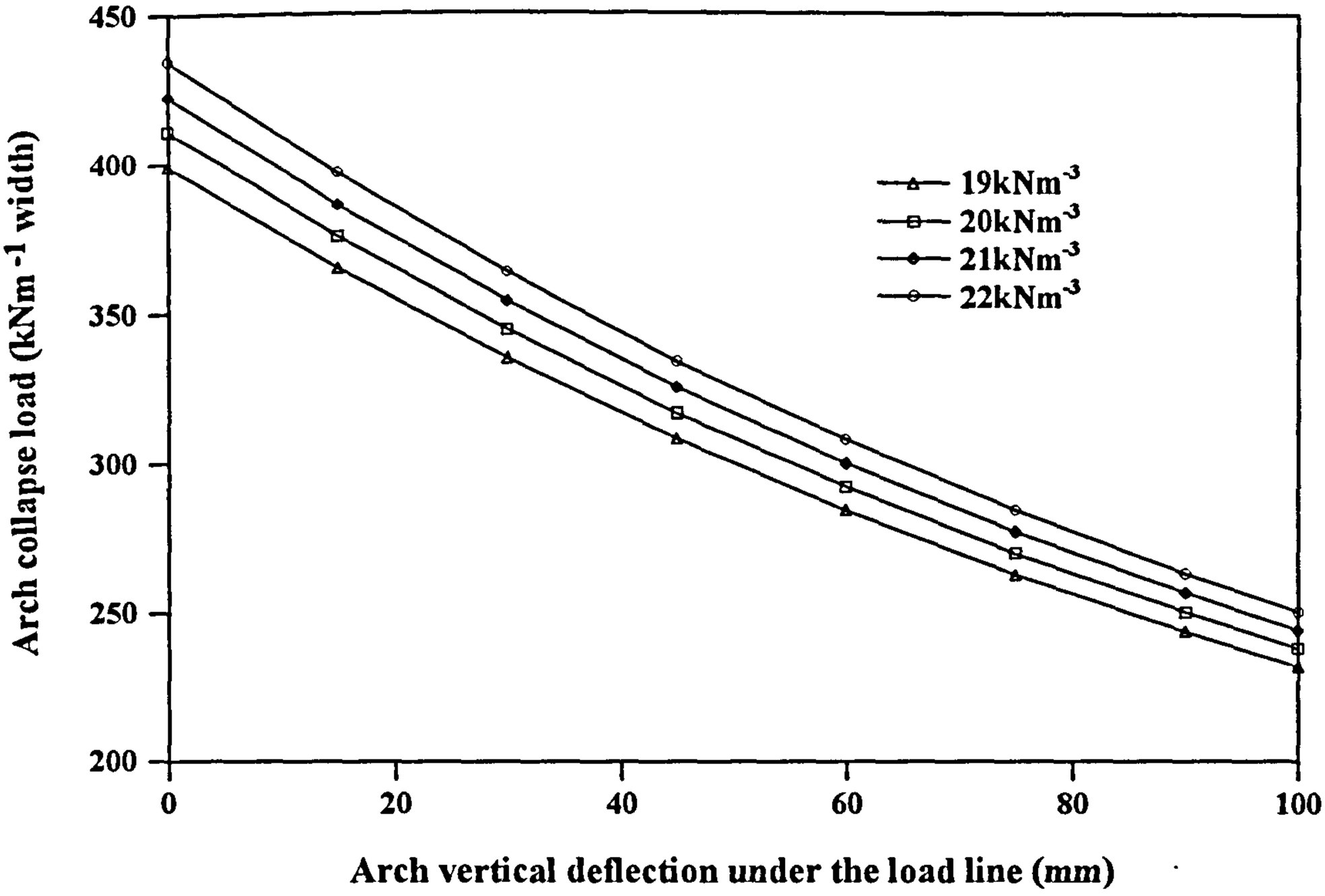

Figure 8.21 The effect of arch bulk unit weight on the prediction of arch collapse load for Bridgemill

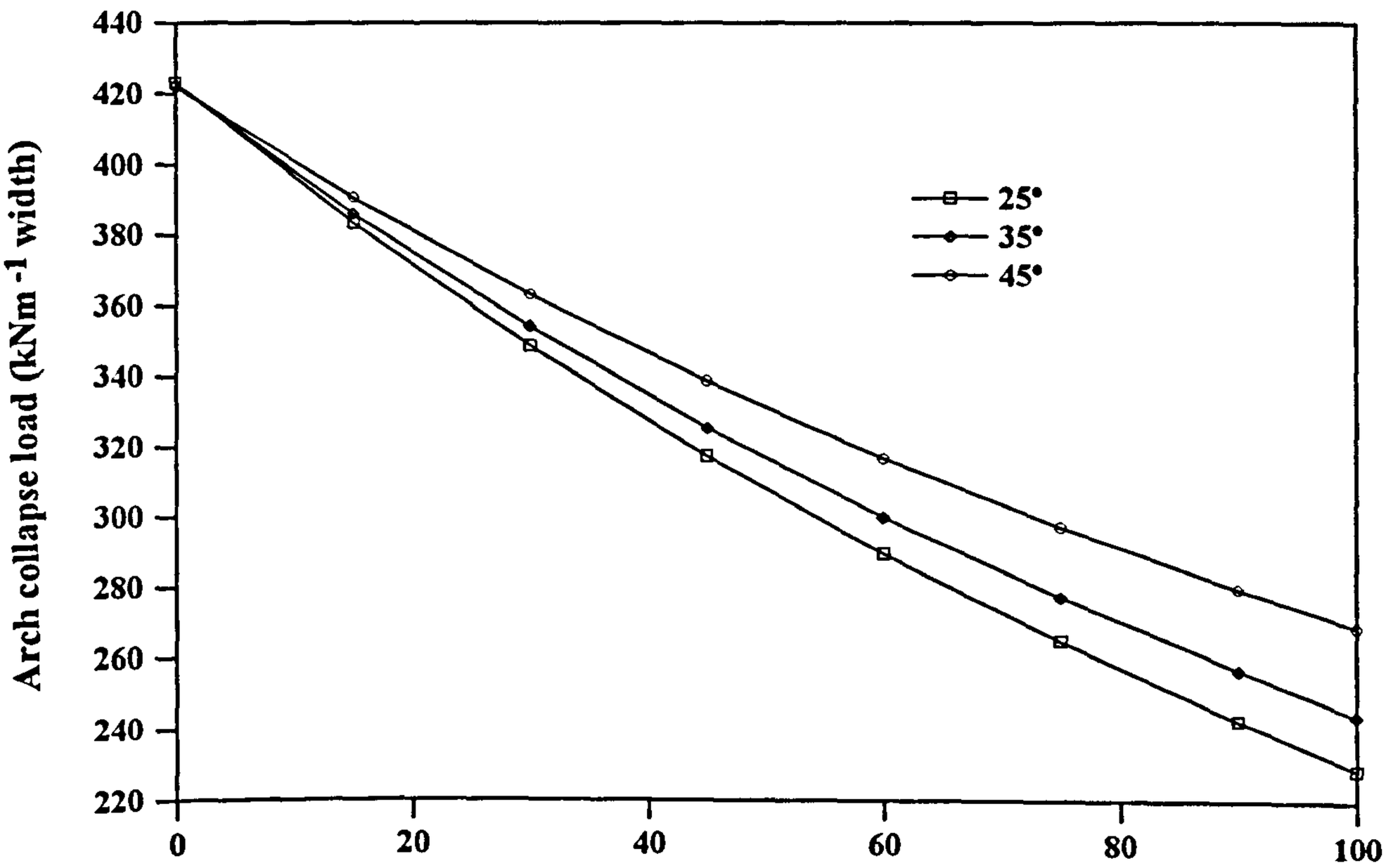

Figure 8.22 The effect of backfill angle of shearing resistance on the prediction of arch collapse load for Bridgemill

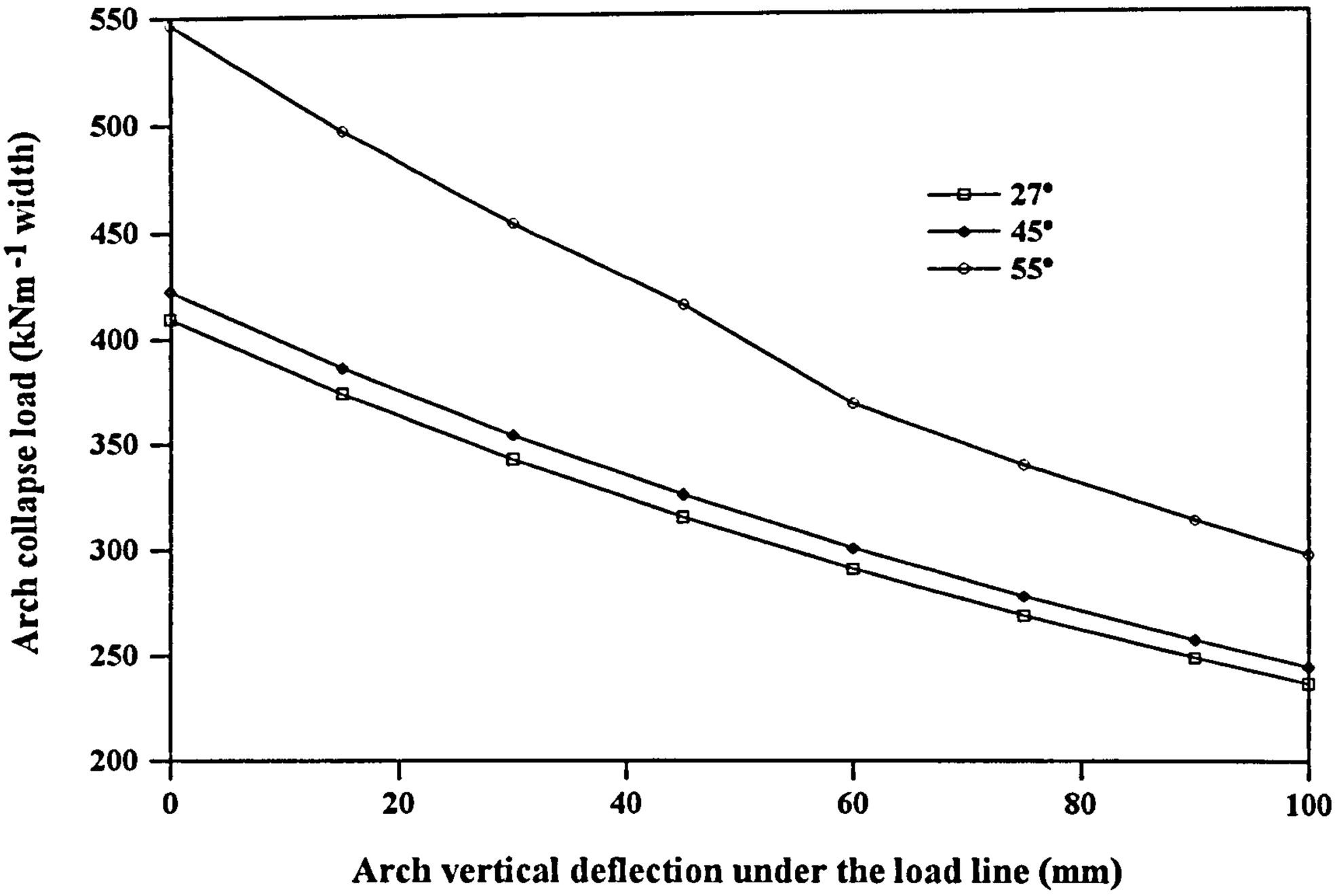

Figure 8.23 The effect of live load dispersal angle on the prediction of arch collapse load for Bridgemill

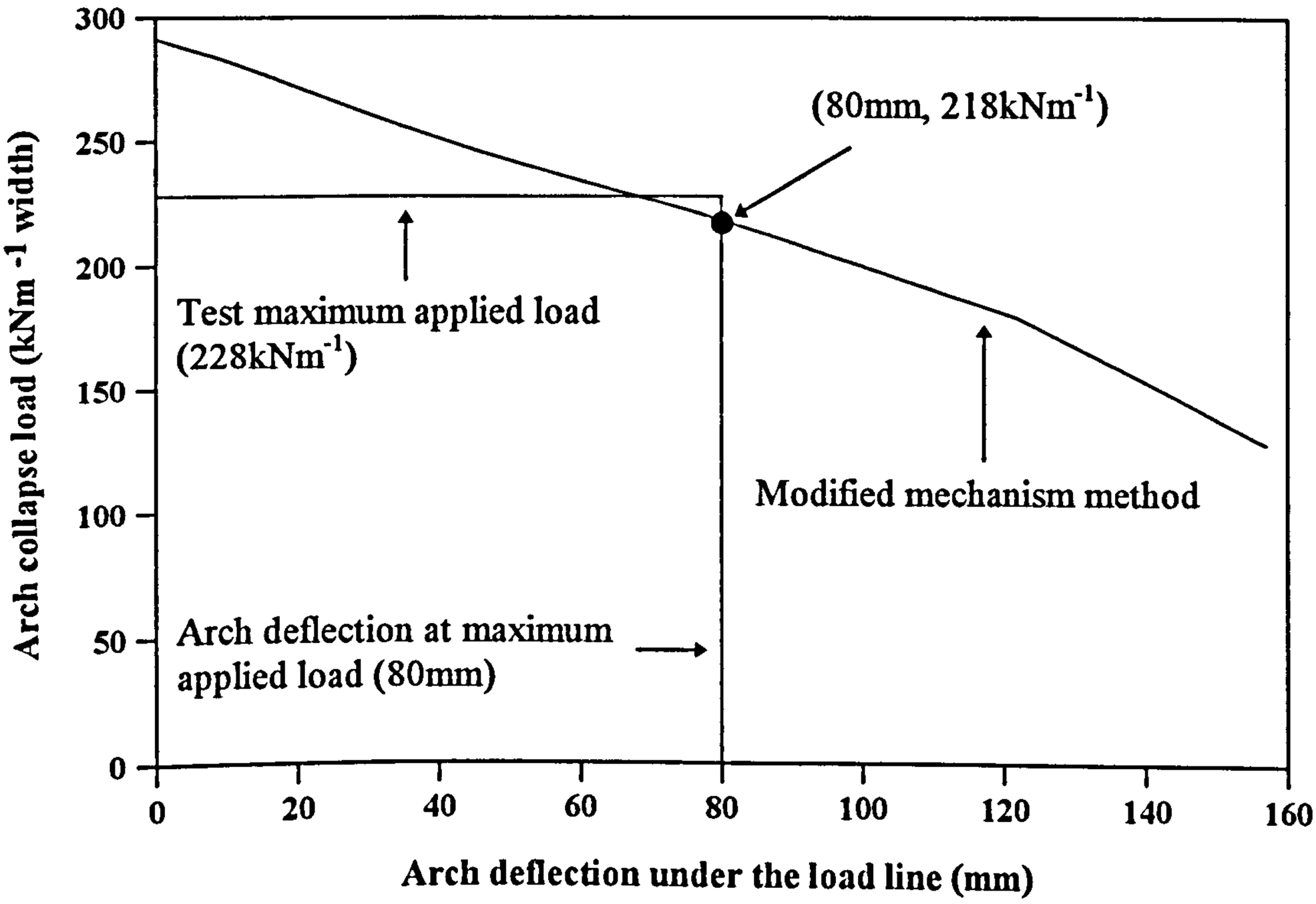

Figure 8.24 Collapse load predictions with arch deflections for Strathmashie

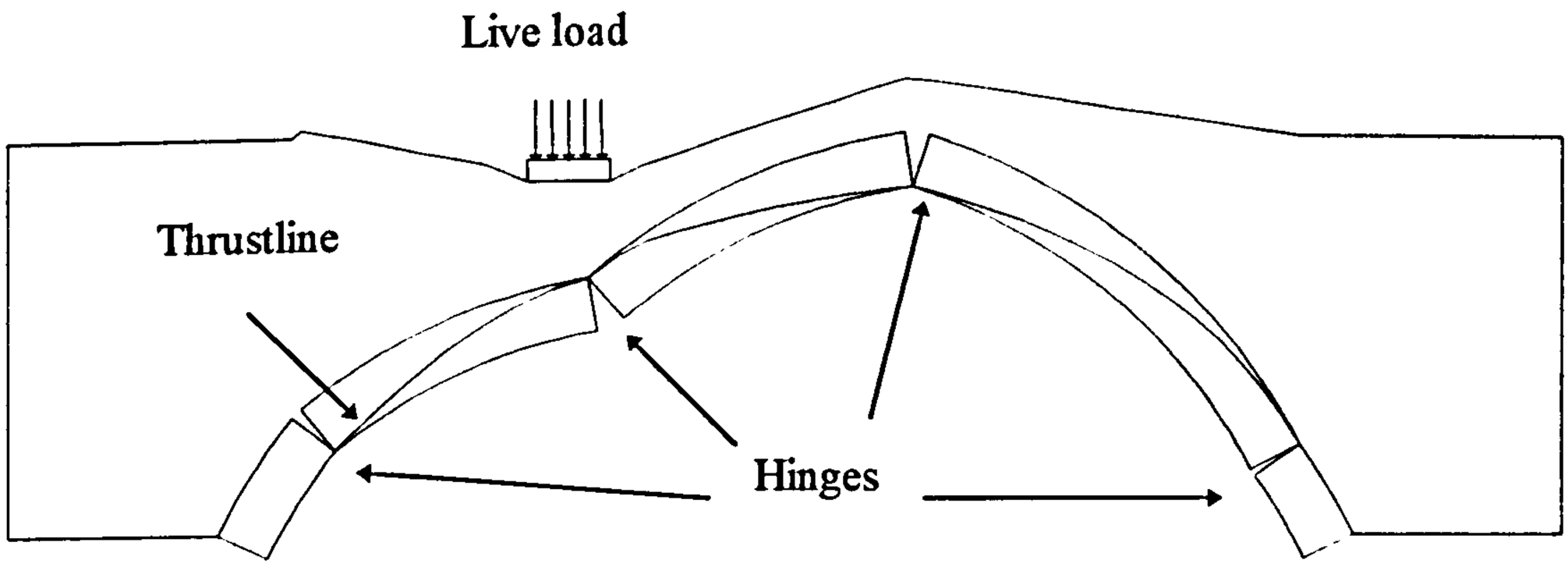

Figure 8.25 Predicted collapse mechanism at 227kNm^{-1} width for Strathmashie (Deformations exaggerated by × 8.25)

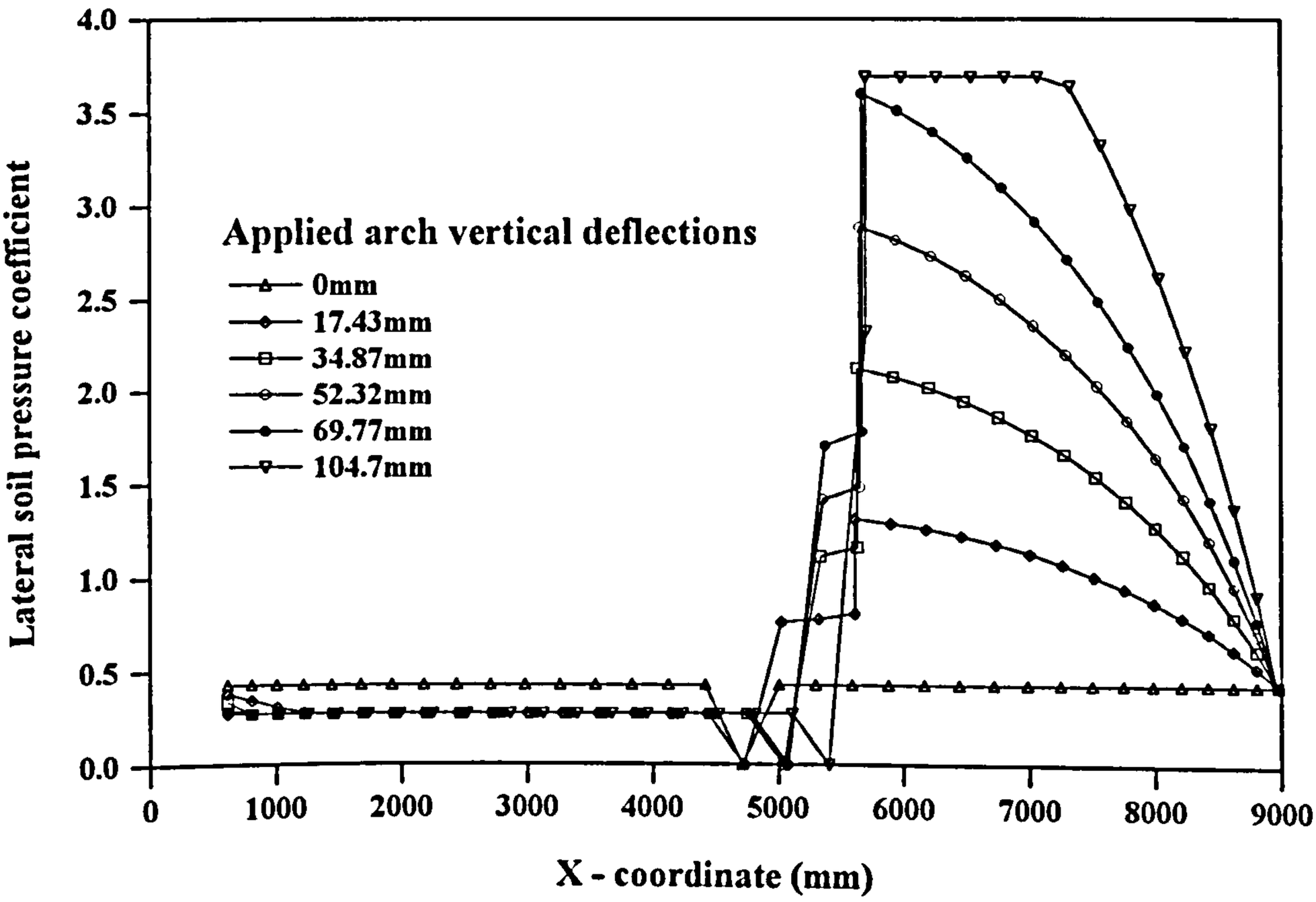

Figure 8.26 Distribution of backfill lateral pressure coefficient for Strathmashie

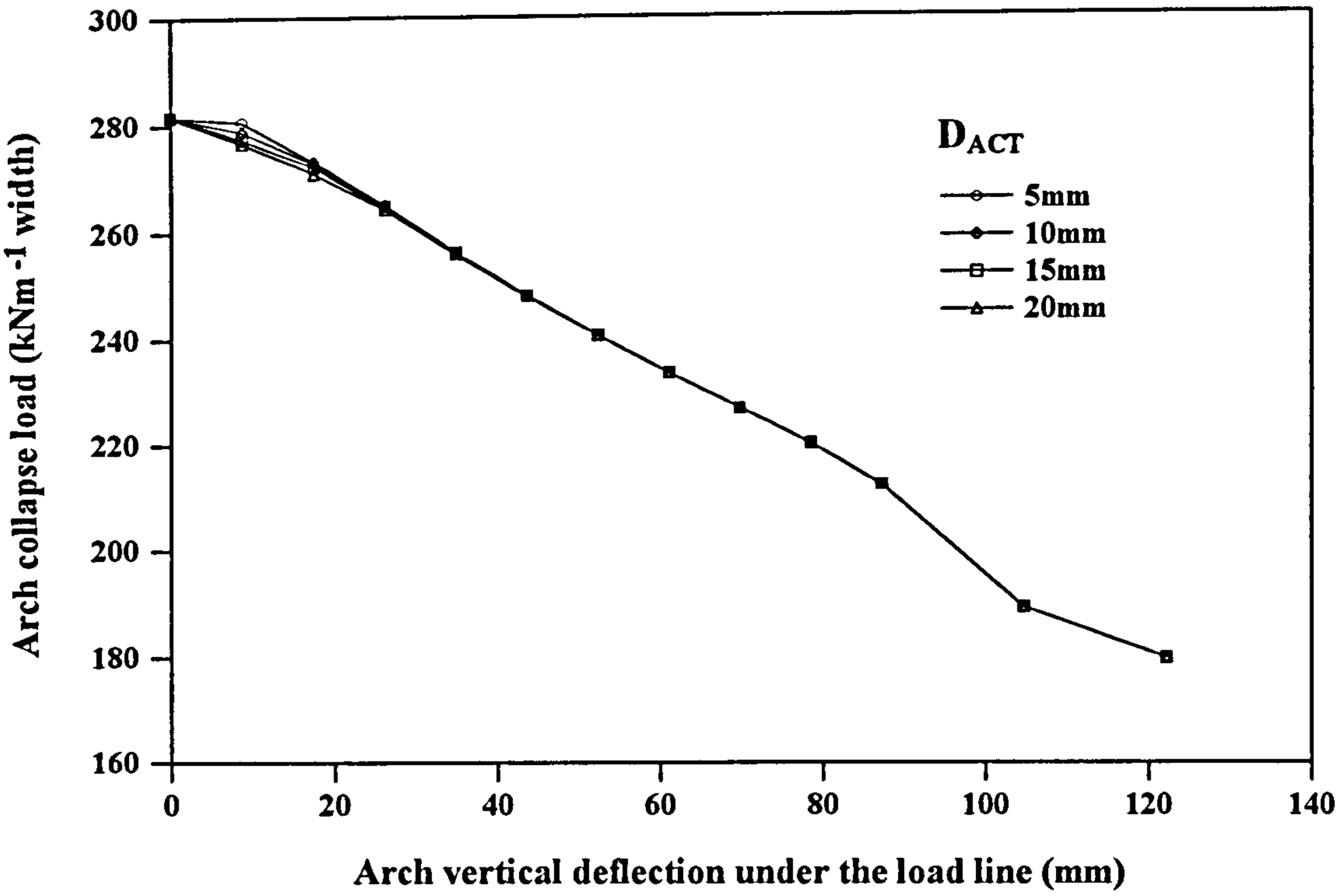

Figure 8.27 The effect of backfill ultimate active deflection on the prediction of arch collapse load for Strathmashie

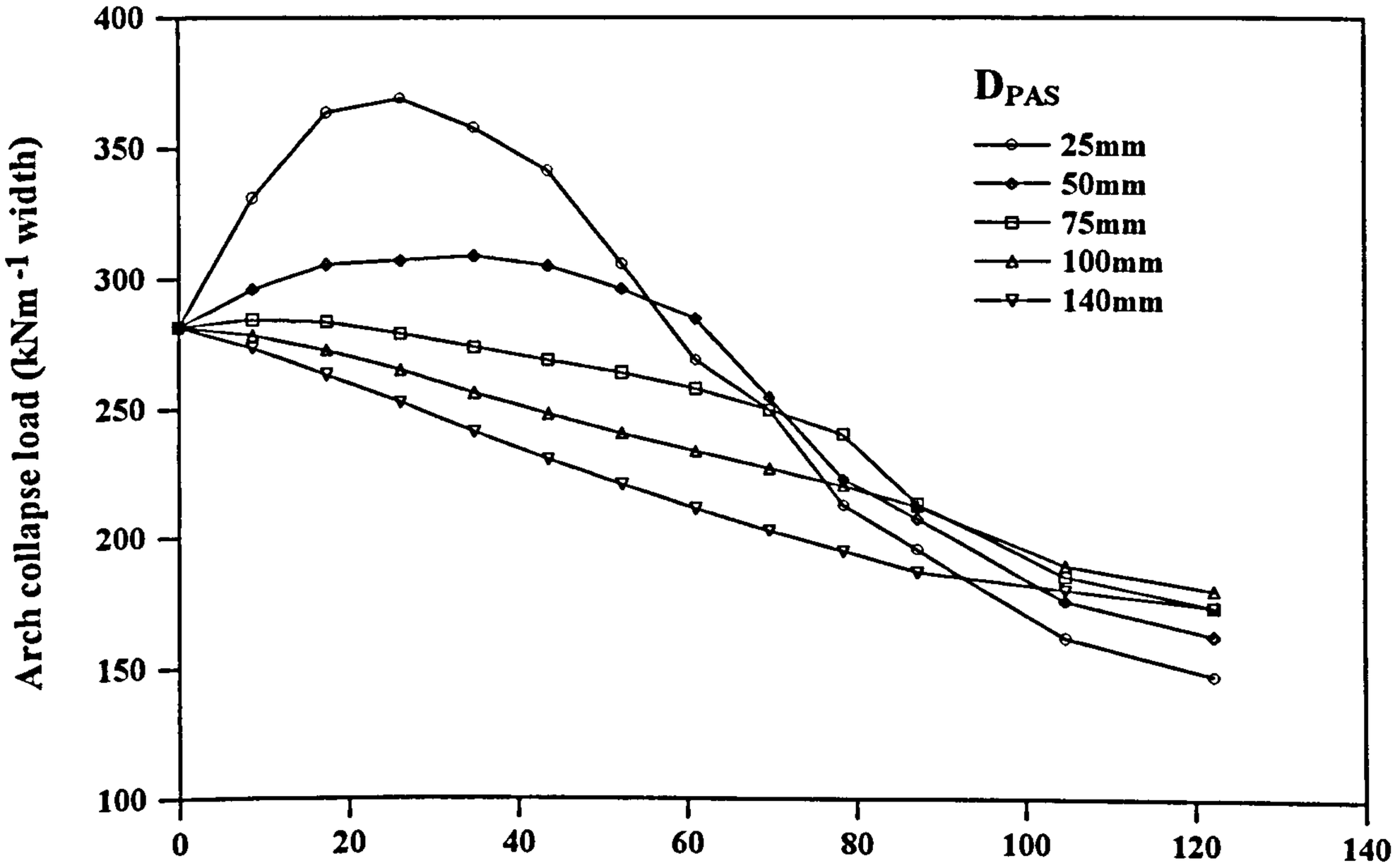

Figure 8.28 The effect of backfill ultimate passive deflection on the prediction of arch collapse load for Strathmashie

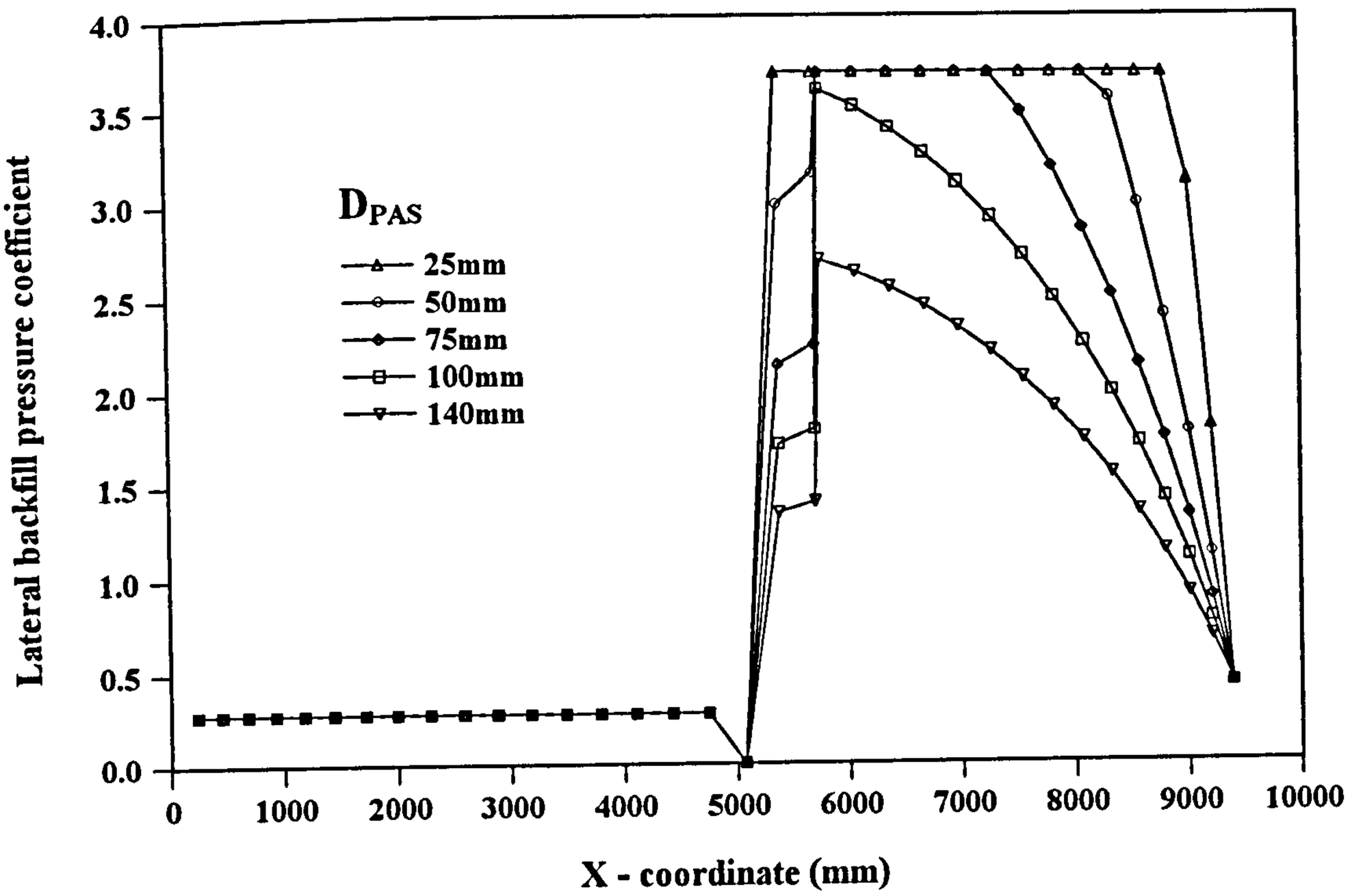

Figure 8.29 The effect of backfill ultimate passive deflection on the distribution of backfill lateral pressure coefficient for Strathmashie

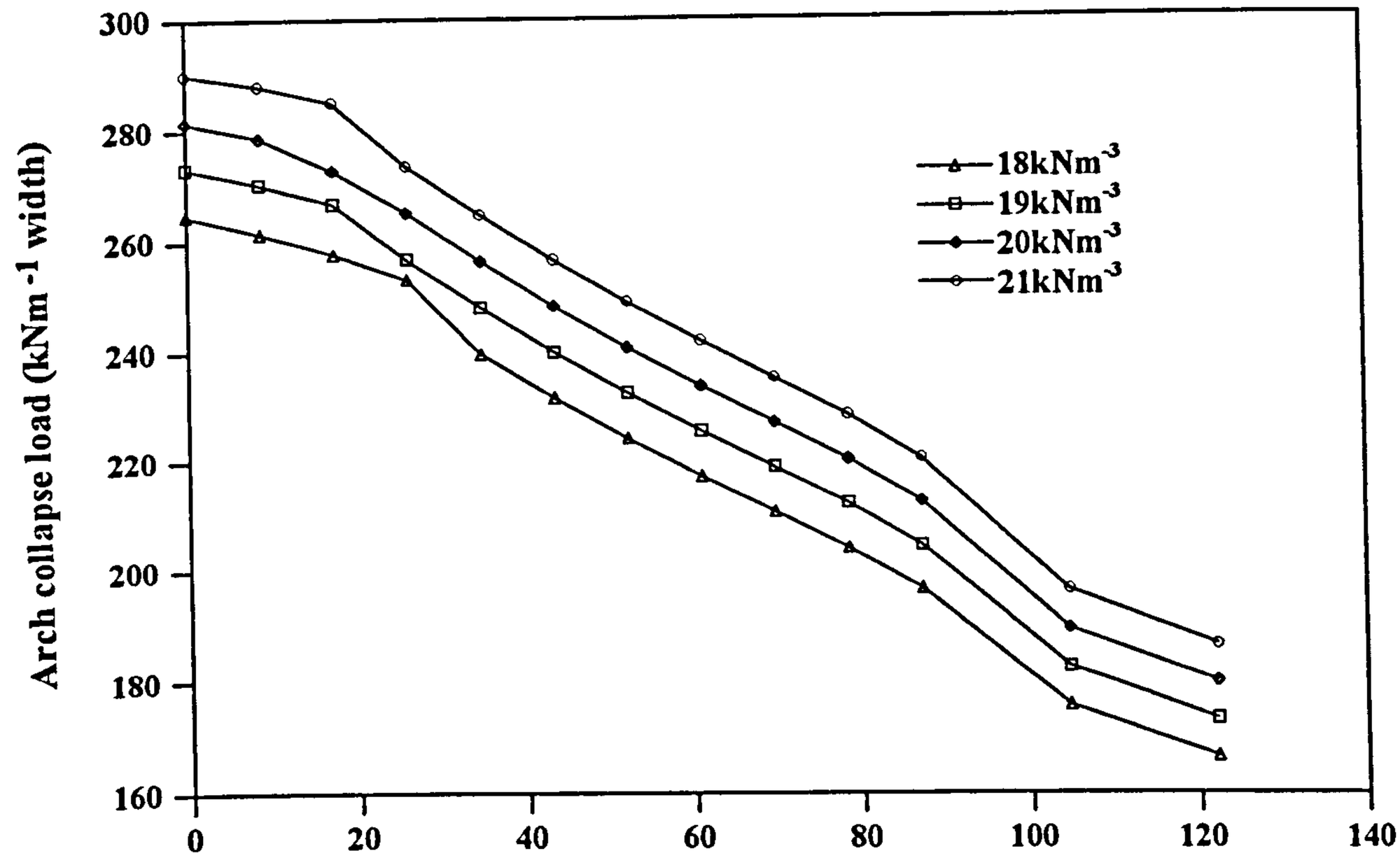

Figure 8.30 The effect of backfill bulk unit weight on the prediction of arch collapse load for Strathmashie

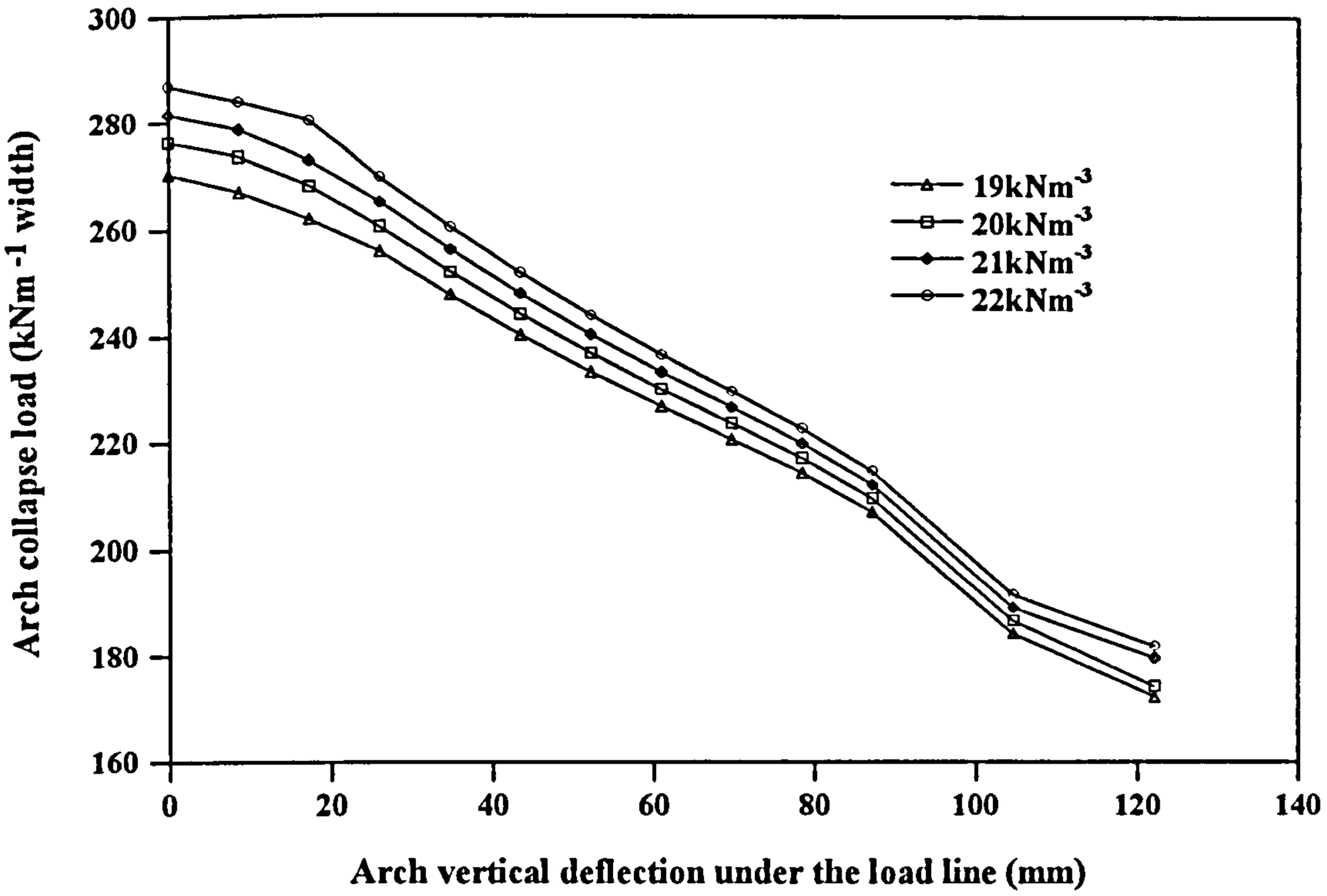

Figure 8.31 The effect of arch bulk unit weight on the prediction of arch collapse load for Strathmashie

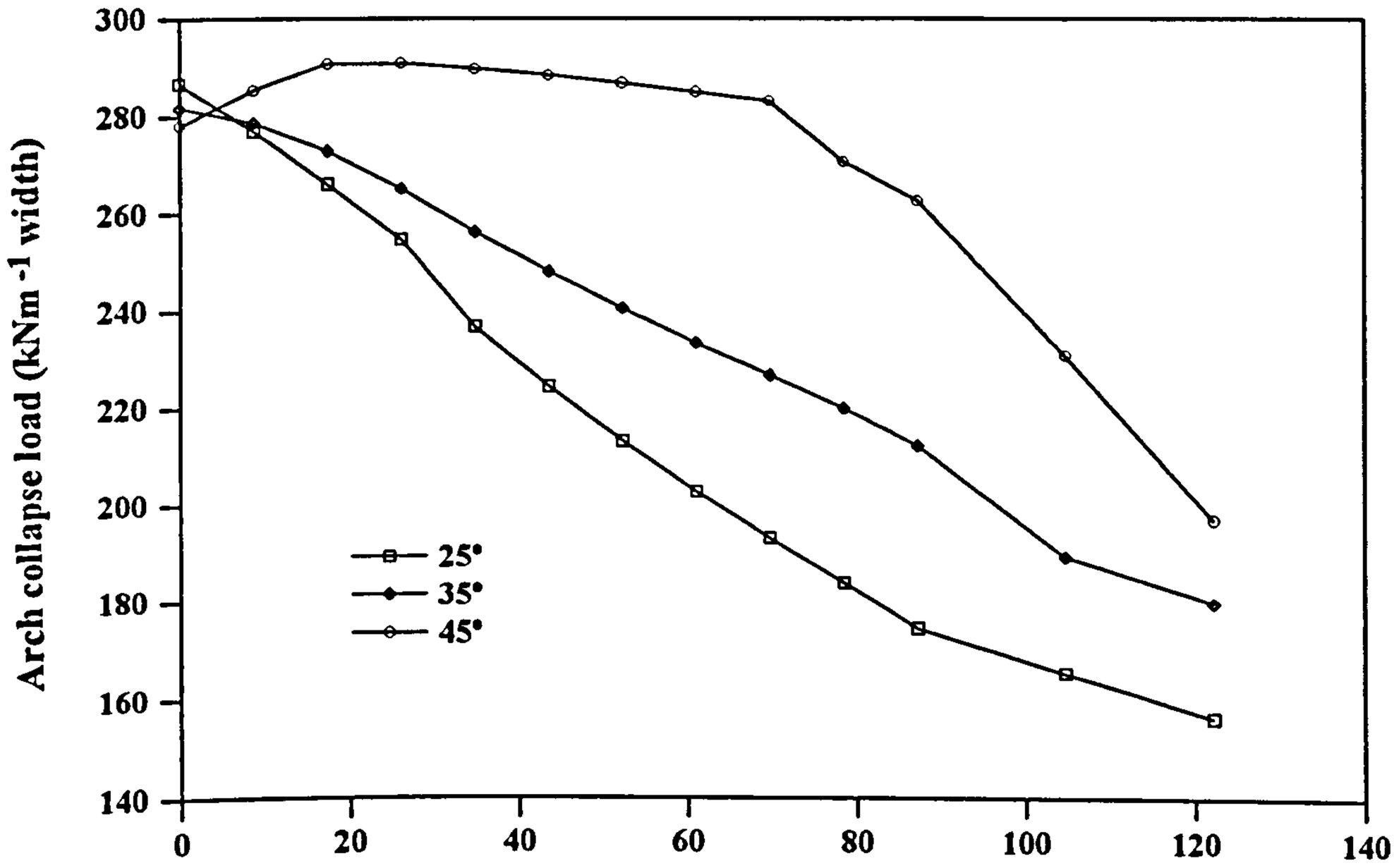

Figure 8.32 The effect of backfill angle of shearing resistance on the prediction of arch collapse load for Strathmashie

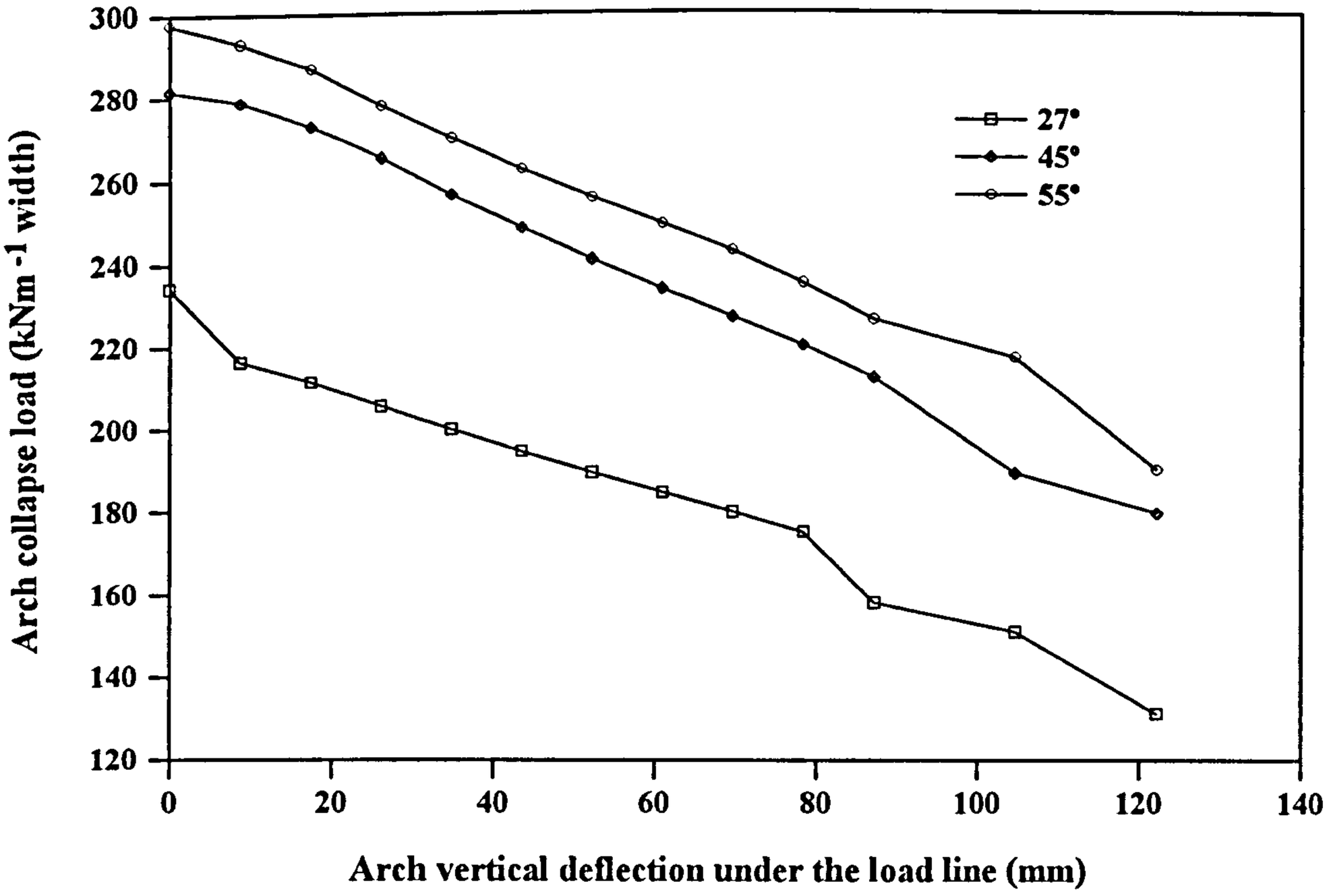

Figure 8.33 The effect of live load dispersal angle on the prediction of arch collapse load for Strathmashie

CHAPTER 9

Conclusions

9.1 Executive summary

This thesis has developed original work in the field of arch bridge assessment. The components claimed as novel are, in particular; the finite element analysis (in the sense of its application), the repeatability analysis on the large scale model tests, the risk analysis as applied to the collapse load predictions, and the updated mechanism method incorporating the author's own suggested displacement fields.

This chapter presents general conclusions followed by specific conclusions arising from each strand of the research. By drawing them together in this manner it is hoped to eliminate unnecessary duplication and present clarity of thinking in the summing up of this thesis. This thesis, in common with all of its ilk, can not claim to be exhaustive. In cognisance of this fact Chapter 10 goes on to provide the author's suggestions for further avenues of investigation.

9.2 General conclusions

1 Both linear and non-linear finite element analyses have been performed to model the live load distribution on a semicircular large scale arch and the results showed good agreement with observed experimental behaviour in terms of load spread, deflections, hinge locations, and collapse loads.

2 Repeatability tests on three nominally identical large scale arches have been carried out. These three arches collapsed at different loads ($16kNm^{-1}$, $21kNm^{-1}$ & $25kNm^{-1}$). This gave an indication of the possible spread of results.

3 Two novel arch bridge risk assessment programs have been successfully developed by integrating Monte Carlo simulation with the MEXE and mechanism methods. These gave intimations as to the reliability of any given assessment as well as accurate probabilities of failure for arches.

4 A modified mechanism has been successfully developed by incorporating arch deflections and a deflection dependent backfill lateral pressure distribution model.

9.3 Specific conclusions: finite element analysis

Both linear and non-linear finite element models have been used to analyse arch bridges. Details can be found in Chapters 3, 4, and 6 of this thesis. All finite element models used in this research were two dimensional. The following conclusions were drawn from the finite element analyses performed in this research.

1 The linear elastic finite element model detected the mobilisation of backfill passive resistance on the arch extrados on the side remote from the load.

2 The arch's elastic modulus was found to have no significant influence on the prediction of stress state on the arch extrados by the linear elastic finite element model.

3 The backfill and the pavement elastic moduli significantly affected the prediction of stress state on the extrados in the linear elastic finite element model.

4 Varying the condition of the arch and backfill (plane strain or plane stress) had no effect on the arch deflections in the linear elastic finite element analysis.

5 Both the normal and shear stresses predicted by the linear elastic finite element model were higher than those found using Boussinesq's method.

6 The arch tensile strength has been identified as the most influential arch material property in the prediction of arch collapse load by non-linear finite element analysis.

7 The arch elastic modulus had no influence on the collapse load prediction but it affected arch deformations at lower loads.

8 The arch compressive strength has been identified to have some, but not as much as often thought, influence on the collapse load prediction for full scale arches.

9 The load dispersal angle significantly affected the collapse load prediction.

10 The adopted non-linear finite element model successfully predicted a four hinge collapse mode on single span arches whilst a seven hinge collapse mode was predicted for a typical multi-span arch.

9.4 Specific conclusions: repeatability tests on large scale arch bridges

Details of the repeatability tests and the arch material sample tests can be found in Chapters 6 and 5 respectively of this thesis. Three nominally identical large scale arch bridges were built and tested to collapse to determine the repeatability of such tests. This provided valuable information since most of the arch bridge assessment methods

depend mainly on the geometry of the arch bridge. The main conclusions drawn from the collapse load repeatability and arch material sample tests are given below.

1 Three nominally identical large scale arch bridges collapsed at 21kNm^{-1}, 16kNm^{-1}, and 25kNm^{-1} width perpendicular to the arch span.

2 The load *versus* deflection relationships from all three large scale arch bridge tests were brittle and these arches lost their stiffness immediately after the formation of the first hinge.

3 No compression failures of the arch material were found in three large scale arch bridge tests.

4 On the point of collapse, four hinges were found in the arch ring in each test.

5 Hinge positions in each tests were different.

6 A total of thirty six specimens were built to determine the brick-mortar flexural bond strength: the mean, standard deviation, minimum, and maximum were 0.521MPa, 0.224MPa, 0.127MPa, and 1.179MPa respectively. The coefficient of variation of these tests was 43%.

9.5 Specific conclusions: risk analysis on arch bridges using Monte Carlo simulation

Monte Carlo simulation has been integrated with the MEXE and mechanism methods to perform risk assessments on arch bridges. Details of this study can be found in Chapter 7 of the thesis. These two risk assessment methods have been coded in FORTRAN77: MCMEXE.FOR for the MEXE method and MCMECH.FOR for the mechanism method. The main conclusions derived from this study are given below.

1 The two risk assessment programs could be used to give information about the reliability of the MEXE and mechanism assessments. Statistical information about the predicted results was made available: the mean, standard deviation, skewness, kurtosis, and range were, for the first time, all provided.

2 The standard deviation of input parameters has been identified as significantly affecting the capacity predictions. The larger the standard deviation of any of the input parameters the wider the resulting distribution of assessed collapse loads.

3 The random number generator used by the author has been identified to be appropriate.

4 Some of the input parameters have been identified as significantly affecting the collapse load prediction by MCMECH.FOR: the live load dispersal angle, the backfill and arch unit weights, the backfill passive pressure coefficient and its angle of shearing resistance.

5 The condition factor significantly affected the prediction of the allowable axle load by MCMEXE.FOR.

9.6 Specific conclusions: modified mechanism method

A modified mechanism method has been developed to determine the significance of the no-deflection assumption made in previous mechanism assessments. Details of this study can be found in Chapter 8 of the thesis. This study was important as the mechanism method has been used widely for a few decades to date for assessing arch bridges. The author's modified method has been coded in FORTRAN77 (ARCH99.FOR). The modified mechanism method is not claimed to be a useful arch bridge assessment method as it stands since the actual arch deflection on the verge on collapse has yet to be investigated. However, this study has demonstrated the

significance of the errors inherent in the no-deflection mechanism model thus giving engineers some idea about its unreliability. The following main conclusions were drawn from this study.

1 The mechanism prediction for the arch collapse load has been identified to be significantly affected by arch deflections.

2 The deflection dependent backfill lateral pressure distribution model has been successfully incorporated in the author's modified mechanism method.

3 Apart from the arch deflection, some input parameters have been identified as affecting the collapse load prediction: the backfill and arch unit weights, the backfill angle of shearing resistance, the ultimate passive deflection, and the live load dispersal angle.

9.7 Final remarks

The findings from this research, as summarised above, have led to a better understanding, both theoretically and experimentally, of backfilled arch bridges. It seems as if there has been some narrowness of thought in the way we used to build only one large scale arch and then test it to confirm the validity of newly proposed or existing arch bridge assessment models. The discrepancy of the collapse loads recorded in the repeatability tests on three nominally identical large scale arches spoke for itself. Such validation procedures are clearly unreliable. The mechanism method has been shown to be unlikely to give a reliable result as one of the most important parameters, the arch deflection, is not considered. Whilst not completely solved, the author has at least advanced incrementally towards a solution of this problem.

It could be seen in this thesis that as many arches as possible were analysed in the theoretical studies such as the non-linear finite element analysis, the Monte Carlo risk

assessment analysis, and the modified mechanism assessments. This was to ensure the subsequent conclusions covered a wider range of arches than would be the case if the author had stuck to one, and only one, arch profile.

CHAPTER 10

Recommendations For Future Research

10.1 Introduction

Recommendations for future research are outlined in this chapter to help to continue the research presented in this thesis. Some of this research could be explored further: the finite element analysis, the repeatability tests on large scale arches, the Monte Carlo risk analysis, and the modified mechanism method are all potentially worthy of more examination. The recommendations are not claimed to be any less important than that work already carried out by the author. The recommendations do however, represent distinct steps forward from the author's current findings and as such form potentially years' worth of future effort.

10.2 Finite element analysis

The LUSAS finite element analysis could be extended to three dimensions thereby including the spandrel, wing and parapet walls. Skew arches may also be analysed using such a 3-D finite element model. However, the interactions between each component of the bridge may be too complicated to be modelled and the processing time may also be too excessive.

The failure of the arch material is used as a failure criterion in most of the finite element programs for the analysis of arch bridges. This may be, in some cases, inappropriate since most arches fail by instability unless the arch tensile strength is

dominant or the arch fails under severe compression. Future research should also involve the development of a finite element model which considers the safety of arches based on geometrical stability rather than material failure.

10.3 Repeatability tests on large scale arches

It is suggested that more nominally identical arches, similar to those built by the author, could be built and tested so that more results are available to confirm the repeatability of large scale arch bridge tests. Repeatability tests could also be carried out on arches with span to rise ratios other than four as the arch tensile strength might have different effects on arches with different profiles. The variations in arch tensile strength may affect the repeatability of the test; nominally identical arches could also be built with a very weak mortar to reduce the influence of the brick-mortar bond strength.

10.4 Monte Carlo risk assessment for arch bridges

The two arch bridge risk assessment programs developed by the author based on the MEXE and mechanism methods are ready to bear the burden of the UK's arch bridge assessment programme on more than 50,000 arches. However, further work should be carried out to make these programs more user friendly by allowing the input of parameters and the output of results to be performed in a graphical environment.

On a more technical note, it is suggested that work should be carried out in collaboration with national and local road authorities so that the derived distribution of the allowable axle load by MCMEXE.FOR or the collapse load by MCMECH.FOR could be used in the assessment: the risk involved in any assessment method depends on the standard deviation of the derived distribution, the greater the standard deviation the greater the risk involved.

10.5 Modified mechanism method

One of the problems associated with the modified mechanism method is deciding an arch deflection at the onset of a mechanism collapse. A series of experimental parametric studies on large scale arches with different span to rise ratios and sizes could be carried out to derive an empirical relationship relating the arch geometry and the maximum arch deflection allowed. However, these arches should be built with a very weak mortar to reduce the influence of brick-mortar bond strength on the arch behaviour. Repeatability of these tests should also be ensured by building more nominally identical arches.

10.6 Miscellaneous recommendations for further research

Future research should also involve the design of strengthening for arch bridges since some of the bridges might not able to carry the maximum allowable weight currently imposed by the Department of Transport. Impact-echo non-destructive test can also be used for defect detection on some parts of the bridge which are inaccessible to visual inspection but much more work is needed in this field. Optimisation of the arch profile could also be carried out with a view to gain greater capacity for newly designed arches or to make best use of resources when repairing defective or damaged bridges.

10.7 Summary

The author has presented various recommendations for future research on arch bridges. Some of the recommendations are continuations of the author's work where it was either incomplete or could be further explored. However, some of the author's work such as the risk analysis and FE modelling are ready to be incorporated into national and local arch bridge assessment routines. Future projects should look at ways of transferring the author's findings to those who are assessing arch bridges. This

concludes the author's recommendations for future research and the thesis proper; what follows are the cited reference list and the Appendix containing copies of the author's publications.

References

ALI-AHMED, H. (1999). Non-destructive testing of arch bridges. Ph.D. thesis, Napier University, Edinburgh, U.K.

ARMSTRONG, D. M., SIBBALD, A., FAIRFIELD, C. A & FORDE, M. C. (1995). Modal analysis for masonry arch bridge spandrel wall separation identification. NDT & Evaluation International, 28, 6, pp. 377-386.

BARLOW, W. H. (1846). On the existence (practically) of the line of equal horizontal thrust in arches, and the mode of determining it by geometrical construction. Proc. Instn Civ. Engnrs, 5, p. 162.

BENSALEM, A., FAIRFIELD, C. A. & SIBBALD, A. (1997a). Non-destructive evaluation of the dynamic response of a brickwork arch. Proc. Instn Civ. Engnrs, Structs & Bldgs, 122, pp. 69-82.

BENSALEM, A., FAIRFIELD, C. A. & SIBBALD, A. (1997b). The effect of material stiffness upon the modal characteristics of arch bridges. Innovation in Civil and Structural Engineering, Ed. Topping, B. H. V. & Leeming, M. B., Civil - Comp Press, Edinburgh, U.K., pp. 301-309.

BENSALEM, A., ALI-AHMED, H., FAIRFIELD, C. A. & SIBBALD, A. (1998). FE modelling of the dynamic response of Kimbolton Butts bridge. Proc. 2nd Int. Conf. Arch Bridges, Venice, Italy, pp. 187-194.

BOUSSINESQ, J. (1885). Application des potentials à l'étude de l'équilibre et de mouvement des solids elastiques. Gauthier-Villars, Paris.

BRIDLE, R. J. & HUGHES, T. G. (1989). The arch revival. The Cardiff arch analysis procedure. J. Instn Highways & Transportation, 36, 10, pp. 21-22.

BRIDLE, R. J. & HUGHES, T. G. (1990). An energy method for arch bridge analysis. Proc. Instn Civ. Engnrs, 89, pp. 375-385.

BRITISH STANDARDS INSTITUTION (1985). BS3921 Specification for clay bricks. BSI, London.

BRITISH STANDARDS INSTITUTION (1990). BS1377 Methods of test for soils for civil engineering purposes. BSI, London.

BRITISH STANDARDS INSTITUTION (1992). BS5628 Code of practice for use of masonry: Part 1 Unreinforced masonry. BSI, London.

BRITISH STANDARDS INSTITUTION (1993). BS 1881 Method for determination of static modulus of elasticity in compression, Part 121. BSI, London.

CASTIGLIANO, C. A. P. (1876). Nuova teoria intorno all'equilibrio dei sistemi elastici. Trans. Acad. Sci., Turin, Italy.

CASTIGLIANO, C. A. P. (1879). Théorie de l'équilibre des systémes élastiques et ses applications. F. A. Nero, Turin, Italy.

CHETTOE, C. S. & HENDERSON, W. (1957). Masonry arch bridges: a study. Proc. Instn Civ. Engnrs, 7, pp. 723-774.

CHOO, B. S. & COUTIE, M. G. (1990a). Analysis of masonry arch bridges by a finite-element method. Proc. Forth Rail bridge Cent. Conf., London, reprinted as internal report, University of Nottingham.

CHOO, B. S. & COUTIE, M. G. (1990b). The application of the finite-element method to the study of cracking in masonry arch bridges. Proc. Conf. App. Stress Anal., Nottingham, reprinted as internal report, University of Nottingham.

CHOO, B. S. & COUTIE, M. G. (1991). Finite-element analysis of masonry arch bridges using tapered elements. Proc. Instn Civ. Engnrs, 91, pp. 755-770.

CHOO, B. S. & HOGG, V. (1994). The use of finite element analysis in the study of scale effects. Proc. Int. Conf. Bridge Assessment Management and Design, Cardiff, pp. 211-216.

CORNELL, C. A. (1969). A probability-based structural code. J. Am. Concrete Inst., 66, 12, pp. 974-985.

COULOMB, C. A. (1773). Essai sur une application des règles de maximis & minimis à quelques problèmes de statique, relatifs à l'architecture. Mémoires de mathématiques & de physique, présentés à l'Académie Royale des Sciences par divers Savants, Paris, France, 7, p. 343.

COUPLET, P. (1729). De la poussée des voûtes. Histoire de l'Académie Royale des Sciences, Paris, France, pp. 79 & 117.

CRAIG, R. F. (1997). Soil mechanics. 6th edition. Chapman & Hall, U.K.

CRISFIELD, M. A. (1984). A finite element computer program for the analysis of masonry arches. TRRL Lab. Report 1115, TRRL, Crowthorne.

CRISFIELD, M. A. (1985a). Computer methods for the analysis of masonry arches. Proc. 2nd Int. Conf. Civ. & Struct. Engng Computing, London, pp. 213-219.

CRISFIELD, M. A. & WILLS, J. (1985b). Non linear analysis of concrete and masonry structures. Proc. Conf. Finite Element Meth. Nonlinear Problems, London, pp. 640-652.

CRISFIELD, M. A. & PACKHAM, A. J. (1987). A mechanism program for computing the strength of masonry arch bridges. TRRL Lab. Report 124, TRRL, Crowthorne.

CRISFIELD, M. A. (1988). Numerical methods for the non-linear analysis of bridges. Comp. & Struct., 30, 3, pp. 637-644.

DANYZY, A. -A., -H. (1778). Méthode générale pour déterminer la résistance qu'il faut opposer à la pousée des voûtes. Histoire de l'Académie Royale des Sciences établie à Montpellier, Lyon, France, 2, p. 40.

DAS, P. (1990). Monitoring assessment procedure. Proc. 2nd Arch Bridge Res. Workshop, Bolton.

DAVEY, N. (1953). Tests on road bridges. Natnl Bldng Studies Res. Paper 16, HMSO, London.

DAVIES, S. R. (1989a). MARCH - a computer program for the assessment of masonry arches. Proc. 4th Int. Conf. Struct. Faults & Repair, 1, London, pp. 277-287.

DAVIES, S. R. (1989b). Some difficulties in the assessment of masonry arches. Proc. 4th Int. Conf. Struct. Faults & Repair, 1, London, pp. 289-295.

de GROOT, C. J. W. P. (1987). Bond in masonry. Proc. 1st Int. Conf. Struct. Engng Anal. & Modelling. Univ. of Sci. & Tech., Kumasi, Ghana.

DEPARTMENT OF TRANSPORT (1997a). The assessment of highway bridges and structures. Dept Standard BD21/97, HMSO, London.

DEPARTMENT OF TRANSPORT (1997b). The assessment of highway bridges and structures. Advice Note BA16/97, HMSO, London.

DEVORE, J & PECK, R. (1993). Statistics: The exploration and analysis of data. Duxbury Press, California.

FAIRFIELD, C. A. (1992a). Soil-structure interaction in a masonry arch bridge test. Graduates & Students Papers Competition winner, Instn Civ. Engnrs, Edinburgh.

FAIRFIELD, C. A. (1992b). Soil-structure interaction in a masonry arch bridge test. Russel Allin Prize, Instn Civ. Engnrs, London.

FAIRFIELD, C. A. & PONNIAH, D. A. (1992c). Soil-structure interaction in a masonry arch bridge test. Proc. 4th Int. Conf. Struct. Mas. for Developing Countries, Madras, India, pp. 81-89.

FAIRFIELD, C. A. & PONNIAH, D. A. (1993a). Geotechnical consideration in arch bridge assessment. J. Instn Highways & Transportation, 40, 7, pp. 11-16.

FAIRFIELD, C. A. & PONNIAH, D. A. (1993b). Earth pressure measurements at Kimbolton Butts bridge, Cambridgeshire. TRRL Sub-contractor's Report, TRL, Crowthorne.

FAIRFIELD, C. A. & PONNIAH, D. A. (1993c). Arch bridge backfill properties. Proc. 5th Int. Conf. Struct. Faults & Repair, Edinburgh, 3, pp. 269-273.

FAIRFIELD, C. A. & PONNIAH, D. A. (1993d). Soil pressure measurement for arch bridge assessment. Proc. 5th Int. Conf. Struct. Faults & Repair, Edinburgh, 3, pp. 283-288.

FAIRFIELD, C. A. (1994a). Soil-structure interaction in masonry arch bridges. Ph.D. thesis, University of Edinburgh, U.K.

FAIRFIELD, C. A. & PONNIAH, D. A. (1994b). Model tests to determine the effect of fill on buried arches. Proc. Instn Civ. Engnrs, Structs & Bldgs, 104, pp. 471-482.

FAIRFIELD, C. A. & PONNIAH, D. A. (1996). A method of increasing arch bridge capacity economically. Proc. Instn Civ. Engnrs, Structs & Bldgs, 116, pp. 109-115.

FRANCIS, A. J., HORMAN, C. B. & JEREMS, L. E. (1971). The effect of joint thickness and other factors on the compressive strength of brickwork. Proc. 2nd Int. Brickwork Masonry Conf. Stoke-on-Trent, pp. 31-37.

GAUTHIER, H. (1717). Dissertation sur l'epassieur des culées des ponts. Paris, France.

GILBERT, M. & MELBOURNE, C. (1994). Rigid-block analysis of masonry structures. J. Instn Struct. Engnrs, 72, 21/1, pp. 356-361.

GILBERT, M., HOBBS, B., MOLYNEAUX, T. (1995). The response of masonry parapets to accidental vehicle impact. Proc. 1st Int. Conf. Arch Bridges, Bolton, pp. 143-153.

GILBERT, M. (1998). On the analysis of multi-ring brickwork arch bridges. Proc. 2nd Int. Conf. Arch Bridges, Venice, Italy, pp. 109-118.

GONG, N. G. (1992). Finite element analysis of masonry arch bridges. Ph.D. thesis, Nottingham University, U.K.

GRANDET, B. (1975). Physico-chemical mechanisms of the bond between clay and cement. Proc. 3rd Int. Brick Masonry Conf. Essen, Germany, pp. 217-221.

GREGORY, D. (1697). Catenaria. Phil. Trans. Roy. Soc., 231, London, p. 637.

HARVEY, W. J. & SMITH, F. W. (1987). Semicircular arches. Proc. Instn Civ. Engnrs, 83, pp. 845-849.

HARVEY, W. J. (1988a). Application of the mechanism analysis to masonry arches. J. Instn Struct. Engnrs, 66, 5, pp. 77-84.

HARVEY, W. J. & MAXWELL, J. W. S. (1988b). Arch bridges are economic. Proc. 8th Int. Brick/Block Masonry Conf., Dublin, Eire, pp. 1302-1310.

HARVEY, W. J., VARDY, A. E., CRAIG, R. F. & SMITH, F. W. (1989). Load tests on a full scale model four metre span masonry arch bridge. TRRL Contractor Report 155, TRL, Crowthorne.

HARVEY, W. J. (1991a). Stability, strength, elasticity and thrust lines in masonry structures. J. Instn Struct. Engnrs, 69, 9/7, pp. 181-184.

HARVEY, W. J. & SMITH, F. W. (1991b). The behaviour and assessment of multi-span arches. J. Instn Struct. Engnrs, 69, 24, pp. 411-417.

HENDRY, A. W., DAVIES, S. R. & ROYLES, R. (1985). Test on stone masonry arch at Bridgemill - Girvan. TRRL Contractor Report 7, TRL, Crowthorne.

HENDRY, A. W., DAVIES, S. R. & ROYLES, R. (1986). Load tests to collapse on a masonry arch bridge at Bargower, Strathclyde. TRRL Contractor Report 26, TRL, Crowthorne.

HENDRY, A. W. (1987). The strength of two stone masonry arch bridges. *in* Structural assessment: the use of full and large scale testing. Butterworths, London, pp. 272-283.

HENLEY, E. J. & KUMAMOTO, H. (1981). Reliability engineering and risk assessment. Prentice-Hall, Englewood Cliffs, New Jersey, U.S.A.

HEYMAN, J. (1966). The stone skeleton. Int. J. Solids & Struct., 2, pp. 249-279.

HEYMAN, J. (1969). The safety of masonry arches. Int. J. Mech. Sci., 11, pp. 363-385.

HEYMAN, J. & PADFIELD, C. (1972a). Two masonry arch bridges: (1) Clare college bridge. Proc. Instn Civ. Engnrs, 52, pp. 305-318.

HEYMAN, J. & THRELFALL, B. (1972b). Two masonry arch bridges: (2) Telford's bridge at Over. Proc. Instn Civ. Engnrs, 52, pp. 319-330.

HEYMAN, J. (1980). The estimation of the strength of masonry arches. Proc. Instn Civ. Engnrs, 69, pp. 921-937.

HEYMAN, J. (1982). The masonry arch. Ellis Horwood, Chichester.

HEYMAN, J. (1996). Arches vaults and buttresses. Variorum, U.K.

HOOKE, R. (1675). A description of helioscopes, and some other instruments. London, (*sic*, actually 1675).

HOPKINS, H. J. (1970). A span of bridges. David & Charles Ltd, Newton Abbot, U.K.

HUGHES, T. G. (1995a). Analysis and assessment of twin-span masonry arch bridges. Proc. Instn Civ. Engnrs, Structs & Bldgs, 110, pp. 373-382.

HUGHES, T. G. (1995b). The assessment of a multi-span masonry arch bridge. Proc. 1st Int. Conf. Arch Bridges, Bolton, pp. 489-497.

HUGHES, T. G. & BLACKLER, M. J. (1997a). A review of the UK masonry arch assessment methods. Proc. Instn Civ. Engnrs, Structs & Bldgs, 122, pp. 305-315.

HUGHES, T. G. (1997b). Discussion on; 'FAIRFIELD, C. A. & PONNIAH, D. A. Model tests to determine the effect of fill on buried arches. Proc. Instn Civ. Engnrs, Structs & Bldgs, 1994, 104, pp. 471-482.' *Ibid.*, 123, pp. 247-250.

HUGHES, T. G., DAVIES, M. C. R. & TAUNTON, P. R. (1998). Small scale modelling of brickwork arch bridges using a centrifuge. Proc. Instn Civ. Engnrs, Structs & Bldgs, 128, pp. 49-58.

KAMF, L. (1963). Factors affecting bond between bricks and mortar. Symp. Masonry Testing, Am. Soc. Testing Matls, Sci. Tech. Press, 320, pp. 127-141.

LENCZNER, D. (1966). Strength and elastic properties of the 9" brickwork cube. Trans. Brit. Cer. Soc., 65.

LESAGE, P. C. (1810). Recueil de divers mémoires extraits de la Bibliothèque Impériale des Ponts et Chaussées. Paris, France.

LOO, Y. C. & YANG, Y. (1991a). Cracking and failure analysis of masonry arch bridges. Proc. Am. Soc. Civ. Engnrs, J. Struct. Engng, 117, 6, pp. 1641-1659.

LOO, Y. C. & YANG, Y. (1991b). Tensile strength, strain softening and the failure analysis of masonry arch bridges. Proc. Asian-Pacific Conf. Computational Mech., 1, Hong Kong, pp. 191-196.

LOO, Y. C. (1995). Collapse load analysis of masonry arch bridges. Proc. 1st Int. Conf. Arch Bridges, Bolton, pp. 239-244.

LU, D. Q. (1992). Chinese stone bridges. People's Transportation Press. *In translation from the original Chinese.*

LUSAS (1997). Finite element stress analysis system. FEA Ltd, Forge House, Kingston-upon-Thames, Surrey.

MALLINSON, R. (1989). Soil-structure interaction in masonry arch bridges. B.Eng thesis, University of Edinburgh, U.K.

MELBOURNE, C. (1987). A new arch construction technique. Proc. Int. Conf. Design & Constr. Non-conventional Structs, London, pp. 317-321.

MELBOURNE, C., QUAZZAZ, A. & WALKER, P. J. (1988). Load tests to collapse of model brickwork masonry arches. Proc. 8th Int. Conf. Brick & Block Masonry, Dublin, Eire, pp. 991-1002.

MELBOURNE, C., QUAZZAZ, A. & WALKER, P. J. (1989a). Load testing to collapse of model and full scale brickwork masonry arches. Proc. SERC Conf. Repair, London, Maintenance & Operation in Civ. Engng. Engineering Technics Press, pp. 9-4.

MELBOURNE, C., QUAZZAZ, A. & WALKER, P. J. (1989b). Influence of ring separation on the load carrying capacity of brickwork masonry arch bridges. Proc. SERC Conf. Repair, London, Maintenance & Operation in Civ. Engng. Engineering Technics Press, pp. 5-7.

MELBOURNE, C. (1989c). Mass concrete arch bridge construction. Proc. 4th Int. Conf. Struct. Faults & Repair, London, 1, pp. 331-334.

MELBOURNE, C. (1990a). Load test to collapse on a full scale six metre span brick arch bridge. Department of Transport & TRRL Contractor Report 189. TRL, Crowthorne.

MELBOURNE, C. (1990b). The behaviour of masonry arch bridges - the effect of defects. Proc. Forth Rail Bridge Centenary Conf., Edinburgh, pp. 393-401.

MELBOURNE, C. & WAGSTAFF, M. (1992a). A study of the load carrying capacity of multi-span masonry arch bridges. Internal Report, Bolton Inst. Higher Educ., Bolton.

MELBOURNE, C. & GILBERT, M. (1992b). A study of the effect of defects on the load carrying capacity of masonry arch bridges. Internal Report, Bolton Inst. Higher Educ., Bolton.

MELBOURNE, C. & WAGSTAFF, M. (1992c). The behaviour of multispan masonry arch bridges. Proc. 3rd Int. Mas. Conf., London.

MELBOURNE, C. & GILBERT, M. (1992d). The behaviour of multi-ring brickwork arch bridges containing ring separation. Proc. 3rd Int. Mas. Conf., London.

MELBOURNE, C. & WAGSTAFF, M. (1993). Load tests to collapse of three large-scale multispan brickwork arch bridges. Bridge Management 2nd Ed. Thomas Telford Ltd, pp. 227-235, London.

MELBOURNE, C. & HODGSON, J. A. (1994a). The behaviour of skew brickwork arches. Proc. Int. Conf. Bridge Assessment Management & Design, Cardiff, pp. 187-198.

MELBOURNE, C., BEGIMGIL, M. & WEEKES, L. (1994b). Construction and testing of flat arch bridge models. Contractor's Report B225, Department of Transport, London.

MELBOURNE, C., GILBERT, M. & WAGSTAFF, M. (1995a). The behaviour of multi-span masonry arch bridges. Proc. 1st Int. Conf. Arch Bridges, Bolton, pp. 489-497.

MELBOURNE, C. & TAO, H. (1995b). The behaviour of open spandrel masonry arch bridges. Proc. 1st Int. Conf. Arch Bridges, Bolton, pp. 239-244.

MELBOURNE, C. & HODGSON, J. A. (1995c). The behaviour of skewed brickwork arch bridges. Proc. 1st Int. Conf. Arch Bridges, Bolton, pp. 309-320.

MELBOURNE, C., BEGIMGIL, M. & GILBERT, M. (1995d). The load test to collapse of a 5m span brickwork arch bridge with tied spandrel walls. Proc. 1st Int. Conf. Arch Bridges, Bolton, pp. 509-518.

MELBOURNE, C. & GILBERT, M. (1995e). The behaviour of multi-ring brickwork arch bridges. J. Instn Struct. Engnrs, 73, pp. 39-47.

MELBOURNE, C., GILBERT, M. & WAGSTAFF, M. (1997). The collapse behaviour of multispan brickwork arch bridges. J. Instn Struct. Engnrs, 75, 17, pp. 297-305.

MISES, R. von. (1913). Mechanik der festen Körper im plastisch-deformablen Zustand. Nach. von der Königlichen Gesellschaft der Wissenschaften zu Göttingen, Math. -Phil. Klasse, pp. 582-592.

MOHR, O. (1871). Beiträge zur Theorie des Erddruckes, Z. Arch. u. Ing. Ver. Hannover, 17, p. 344.

MYSTRO (1997). Finite element stress analysis system. FEA Ltd, Forge House, Kingston-upon-Thames, Surrey.

NG, K. H., FAIRFIELD, C. A. & SIBBALD, A. (1998). Track bed geotechnology: its effect on the collapse load of railway arch bridges. Proc. 1st Int. Conf. Railway Engng, Uxbridge, pp. 163-168.

PAGE, J. (1987). Load tests to collapse on two arch bridges at Preston, Shropshire and Prestwood, Staffordshire. TRRL Research Report 110, TRRL, Crowthorne.

PAGE, J. (1988). Load tests on two arch bridges at Torksey and Shinafoot. TRRL Research Report 159, TRL, Crowthorne.

PAGE, J. (1989). Load tests to collapse on two arch bridges at Strathmashie and Barlae. TRRL Research Report 201. TRL, Crowthorne.

PENG, D. M. (1997a). Finite element modelling and optimum design of arch bridges. Ph.D. thesis, Napier University, Edinburgh, U.K.

PENG, D. M., FAIRFIELD, C. A. & SIBBALD, A. (1997b). Experimental validation of flat arch analysis techniques. Proc. 7th Int. Conf. Struct. Faults & Repair, 1, Edinburgh, pp. 121-128.

PENG, D. M. & FAIRFIELD, C. A. (1999). Optimal design of arch bridges by integrating genetic algorithms and the mechanism method. J. Engng Struct., 21, pp. 75-82.

PIPPARD, A. J. S., TRANTER, E. & CHITTY, L. (1936). The mechanics of the voussoir arch. J. Instn Civ. Engnrs, 4, pp. 281-306.

PIPPARD, A. J. S. & ASHBY, R. J. (1938). An experimental study of the voussoir arch. J. Instn Civ. Engnrs, 10, pp. 383-404.

PIPPARD, A. J. S. & CHITTY, L. (1941). Repeated load tests on a voussoir arch. Proc. Instn Civ. Engnrs, 17, pp. 79-86.

PIPPARD, A. J. S. (1948). The approximate estimation of safe loads on masonry bridges. Civ. Engnr in War, Instn Civ. Engnrs, 1, pp. 365-372.

PIPPARD, A. J. S. (1951). A study of the voussoir arch. Natnl Bldg Studies Res. Paper 11, HMSO, London.

PIPPARD, A. J. S. (1952). Studies in elastic structures. E. Arnold, London, pp. 276-320.

PIPPARD, A. J. S. & BAKER, J. (1968). The analysis of engineering structures. E. Arnold, London, pp. 385-403.

POLENI, G. (1748). Memorie istoriche della gran Cupola del Tempio Vaticano. Padua, Italy.

PONNIAH, D. A. & BLACKIE, K. (1989). Further considerations in the soil-structure interaction of arch bridges. Proc. 4th Int. Conf. Struct. Faults & Repair, London, 2, pp. 301-306.

PONNIAH, D. A., FAIRFIELD, C. A. & PRENTICE, D. J. (1997). Fill stresses in a new brick arch bridge subject to heavy axle-load tests. Proc. Instn Civ. Engnrs, Structs & Bldgs, 123, pp. 173-185.

POTTS, D. M. & FOURIE, A. B. (1986). A numerical study of the effect of wall deformation on earth pressure. Int. J. Num. Anal. Meth. Geomech., 10, pp. 383-405.

PRENTICE, D. J. (1996). An appraisal of the geotechnical aspects of multi-span masonry arch bridges. Ph.D. thesis, University of Edinburgh, U.K.

QIAN, L. X. (1987). The carrying capacity of Zhao Zhou stone arch bridge. J. Chinese Civ. Engng., 4, pp. 831-843.

ROBINSON, J. I., PONNIAH, D. & PRENTICE, D. (1997a). Soil pressure measurements on a multi-span brick arch. Proc. 7th Int. Conf. Struct. Faults & Repair, 1, Edinburgh, pp. 111-119.

ROBINSON, J. I., PRENTICE, D. & PONNIAH, D. (1997b). Temperature effects in a new brickwork arch bridge. Proc. 7th Int. Conf. Struct. Faults & Repair, 1, Edinburgh, pp. 159-170.

ROBINSON, J. I., PRENTICE, D. J. & PONNIAH, D. (1998). Thermal effects on a masonry arch bridge investigated using ABAQUS. Proc. 2nd Int. Conf. Arch Bridges, Venice, Italy, pp. 431-438.

ROUF, M. (1984). The fundamental properties of brickwork with particular emphasis to brickwork arches. Ph.D. thesis, University of Liverpool, U.K.

ROYLES, R. & HENDRY, A. W. (1991). Model tests on masonry arches. Proc. Instn Civ. Engnrs, 2, 91, pp. 299-321.

SAWKO, F. & TOWLER, K. (1982). Structural behaviour of brickwork arches. Proc. Brit. Ceram. Soc., 30, pp. 160-168.

SAWKO, F. & ROUF, M. (1985). A proposed numerical model for structural masonry. J. Brit. Mas. Soc., 5, pp. 22-27.

SIBBALD, A., BENSALEM, A. & FAIRFIELD, C.A. (1995). NDT of arch bridges. J. Brit. Inst. NDT, 37, 11, pp. 864-870.

SMITH, F. W., HARVEY, W. J. (1989). Full-scale test of a masonry arch. Proc. SERC Conf. Repair, Maintenance & Operation in Civ. Engng., Engineering Technics Press, London, pp. 21-27.

SMITH, F. W., HARVEY, W. J. & VARDY, A. E. (1990). Three-hinge analysis of masonry arches. J. Instn Struct. Engnrs, 68, 11, pp. 203-213.

SMITH, F. W. (1991a). Load path analysis of masonry arches. Ph.D. thesis, University of Dundee, U.K.

SMITH, F. W., HARVEY, W. J. & VARDY, A. E. (1991b). *Correspondence on*; Three-hinge analysis of masonry arches, J. Instn Struct. Engnrs, 68, 11, pp. 203-213. *Ibid.*, 69, 1, pp. 9-10.

TAYLOR, A. K. (1997). An investigation into the behaviour of blockwork masonry elements. Ph.D. thesis, Napier University, Edinburgh, U.K.

TERZAGHI, K. (1943). Theoretical soil mechanics. Wiley & Sons, New York, U.S.A.

TOWLER, K. (1981). The structural behaviour of brickwork arches. Ph.D. thesis, University of Liverpool, U.K.

TOWLER, K. (1985). Applications of non-linear finite element codes to masonry arches. Proc. 2nd Int. Conf. Civ. & Struct. Engng Computing, London, pp. 197-202.

ZIENKIEWICZ, O. C. & TAYLOR, R. L. (1989). The finite element method. 1, 4th Ed., McGraw-Hill, London.

Appendix

Published papers

The following papers derived from this thesis were published in journal or conference proceedings. A set of these papers is bound in this thesis. Full permission from the relevant publisher or copyright holder has been obtained. The pagination makes no attempts to follow that of the thesis proper; the numbering sequence follows that of the parent journal or proceedings as appropriate.

1 NG, K. H., FAIRFIELD, C. A. & SIBBALD, A. (1998). Track bed geotechnology: its effect on the collapse load of railway arch bridges. Proc. 1st Int. Conf. Railway Engng., Uxbridge, pp. 163-168.

2 NG, K. H., FAIRFIELD, C. A. & SIBBALD, A. (1999). Finite-element analysis of masonry arch bridges. Proc. Instn Civ. Engnrs J. Structs & Bldgs, 134, pp. 119-127.

3 NG, K. H., FAIRFIELD, C. A. & SIBBALD, A. (1999). Arch bridge mechanism method assessment incorporating deflection dependent soil pressure updating algorithms. Proc. 2nd Int. Conf. Railway Engng., London, ISBN 0-947644-39-3. (Highly recommended for conference award)

4 NG, K. H. & FAIRFIELD, C. A. (1999). Reliability of arch bridges by Monte Carlo simulation. Proc. 8th Int. Conf. Struct. Faults & Repair, London, ISBN 0-947644-41-5. (Highly recommended for conference award)

5 NG, K. H. & FAIRFIELD, C. A. (1999). Collapse load repeatability tests on brickwork arches. Proc. 8th Int. Conf. Struct. Faults & Repair, London, ISBN 0-947644-41-5.

TRACK BED GEOTECHNOLOGY: ITS EFFECT ON THE COLLAPSE LOAD OF RAILWAY ARCH BRIDGES

Mr Kwooi-Hock Ng, Dr Charles A. Fairfield & Professor Alan Sibbald

Department of Civil & Transportation Engineering, Napier University

10 Colinton Road, Edinburgh EH10 5DT, United Kingdom

KEYWORDS: Masonry arch bridges, Finite element analysis, stress distribution

ABSTRACT

One of the difficulties in assessing arch bridges is a lack of knowledge available to quantify soil-arch interactions. An axle load located on a rail will be distributed downwards through the ballast and subgrade onto the arch extrados. It is the stresses on the extrados that govern the subsequent load-deflection behaviour of the arch. A 2D linear elastic finite element (FE) analysis was performed to demonstrate the effects of varying both ballast and subgrade elastic moduli on the predicted extrados stress distribution. A comparison with Boussinesq's stress distribution method was also carried out. A 2D non-linear FE analysis was then performed, using the stress dispersal information gleaned from the previous linear elastic FE analysis, to predict the collapse load of a typical railway arch bridge, its associated failure mode and the load-deflection characteristic. The effect of varying the load dispersal angle on the predicted collapse load was also demonstrated using two traditional collapse load assessment methods namely Castigliano's strain energy method (in computer program form as CTAP) (Bridle & Hughes, 1990) and a mechanism method coded by the authors. It was found that the live load dispersal angle, as the result of variation of ballast and subgrade moduli, significantly affected the arch behaviour at both serviceability and ultimate limit states.

INTRODUCTION

There are approximately 33,000 masonry arch bridges in the railway network in Great Britain with most of these built during the 19th century. Engineers responsible arch bridges face difficulties assessing these old structures due to the complexity of soil-structure interaction effects. Whilst modern computerised arch bridge assessment programs are available, results are always sensitive to the load dispersal angle. Inappropriate assessments, due to inadequate knowledge of soil-arch interaction, will either jeopardise the safety of the bridge or cause an unnecessary and costly repair. The current standard (BD21/97) for the assessment of highway bridges and structures (Department of Transport, 1997) used by the Department of Transport allows a load distribution of 1 horizontal to 2 vertical. A load dispersal angle of 65° was recorded in a full scale test at Kimbolton Butts bridge, Cambridgeshire (Ponniah *et al.*, 1997). However, an ideal fixed dispersal angle is difficult to state explicitly as it is influenced by the stiffnesses of both the ballast and the subgrade.

The purpose of this study is to examine the influence of ballast and subgrade elastic moduli on the live load distribution and the predicted collapse load of a typical arch bridge. Results from the current FE method showed that the normal and shear stresses on the arch extrados were reduced with the increases in either ballast or subgrade moduli. The increase in ballast modulus also increased the capacity of the arch bridge in the non-linear FE models as a result of greater live load distribution and soil stiffness. The principal conclusion of this paper is that ballast and subgrade elastic moduli should be taken into consideration when assessing arch bridges. Arbitrary load spread angles are best avoided. The research has wider applicability to assessment of buried culverts, pipe crossings and cut and cover tunnels where the soil mechanics involved is not surprisingly very similar.

METHOD

This section describes all analytical methods used in this study. The 2D linear elastic FE model and Boussinesq's method were used for the analysis of live load stress distribution. The 2D non-linear FE, strain energy and mechanism methods were used for the ultimate limit state analysis. All analyses were carried out on a typical soil-arch system shown in Fig. 1. The imposed loading was applied on the surface of ballast at one ¼-span point through a 260mm wide load platen. A stress of 100 kPa was applied. For the 2D non-linear analysis, the loading was applied directly onto the arch extrados using the stresses obtained from previous linear elastic FE analysis.

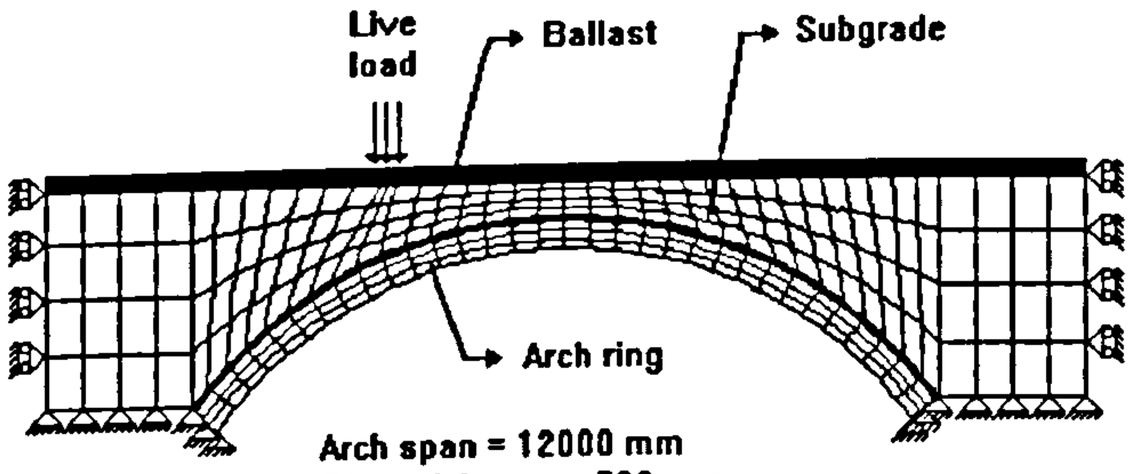

Figure 1 A 2D mesh for FE analysis

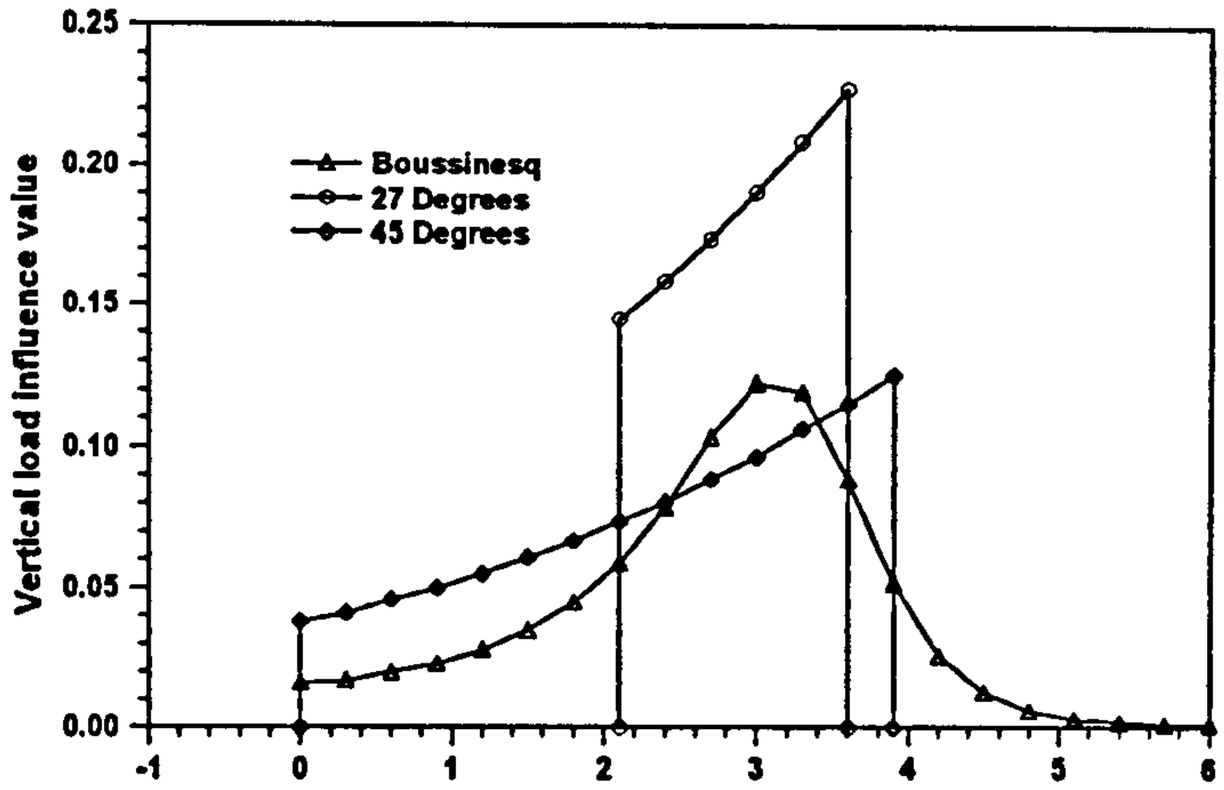

Figure 2 Boussinesq's and codified load influence factors

The FE Method

The 2D FE analysis was performed using LUSAS (FEA Limited, 1997), a commercially available finite element package. Eight-noded quadrilateral elements in conjunction with four Gaussian quadrature points were used to model the arch, backfill, and interface elements. The behaviour of backfill and interface elements was elasto-plastic with failure defined by Mohr-Coulomb yield criterion. The arch was simulated by a stress dependent Von-Mises constitutive law enabling different tensile and compressive material to be specified. The arch was assumed to be rigidly fixed to its abutments. All soil elements were restrained horizontally on both sides of the wing walls and rigidly fixed at the base. For all the FE analyses, the arch elastic modulus, Poisson's ratio and density were assumed to be 5000MPa, 0.2 and 20kN/m^3 respectively. The backfill elastic modulus, Poisson's ratio and density were 50MPa, 0.4 and 18kN/m^3 respectively. In the non-linear FE analysis, the arch tensile and compressive strength adopted were 0.35 MPa and 8MPa respective.

Boussinesq's Method

Boussinesq's solution of stresses is based on the assumption that the medium is semi-infinite, elastic, homogeneous and isotropic. The stress distribution is thus a geometrical function. The presence of three different materials, the arch ring, subgrade and ballast, clearly violates the assumptions of homogeneity and a semi-infinite soil mass. Despite the assumptions being violated, Boussinesq's method gave a reasonable pattern of stress distribution. Fig. 2 presents the live load distributions by both the codified (BD21/97) and Boussinesq's methods. It is obvious that the codified distributions are somewhat senseless with a sudden curtailment of peak stresses. The Peak influence factor by the codified method reduced from 0.228 to 0.126 with the increase in load dispersal angle from 27° to 45° respectively. This represents a decrease in peak influence factor of 45 %.

Castigliano's Strain Energy Method (Program CTAP)

This method is based on Castigliano's basic strain energy principles and has been computer coded (Bridle & Hughes, 1990). The principle of the program is to ignore tensile zones in the rib which appear due to cracking. A hinge is defined at a particular section where the tensile zone covers almost the whole section. Compared with the mechanism method, this method has extra options to allow the user to vary the arch elastic modulus, thereby monitoring or controlling the stresses and modulus of subgrade reaction. However, the arch elastic modulus and the compressive strength were kept constant at 5000MPa and 8MPa respectively as used in the FE analysis. The modulus of subgrade reaction, angle of shearing resistance and the passive pressure factor were assumed to be 9900kN/m^3, 35° and 0.5 respectively. The live load distribution was varied from 0° to 60°.

The Mechanism Method.

The mechanism method assumes the arch to be rigidly fixed at both abutments. The arch elastic modulus and the compressive strength are assumed to be infinite and the arch is assumed to have zero tensile strength. This study uses a

computerised version of method coded by the authors. The live load distribution was varied in this study from 0° to 60° and the corresponding ultimate loads predicted. The angle of shearing resistance, active and passive pressure factors were assumed to be 35° and 0.8 and 0.5 respectively.

RESULTS

The live load stress distributions obtained from the 2D linear elastic FE method for different ballast and subgrade moduli are presented. Only the imposed load was considered in this analysis. Comparisons are made with Boussinesq's results. The ultimate capacities assessed by the 2D non-linear FE method are then presented and compared with those obtained from the strain energy and mechanism methods.

Stress Distribution by 2D FE Method

The normal and shear stresses on the arch extrados due to the application of an imposed load of 100kPa located at ¼-span, with different ballast moduli, are shown in Fig. 3. The subgrade elastic modulus was kept constant at 50MPa. The peak normal stress was reduced from 14.7kPa to 12.7kPa with the ballast modulus increased from 50MPa to 300MPa. Similarly, the peak shear stress was reduced from 4.97kPa to 4.52kPa with the same increase in ballast modulus. This represented a decrease of 13.4% in peak normal stress and 9.1% in peak shear stress.

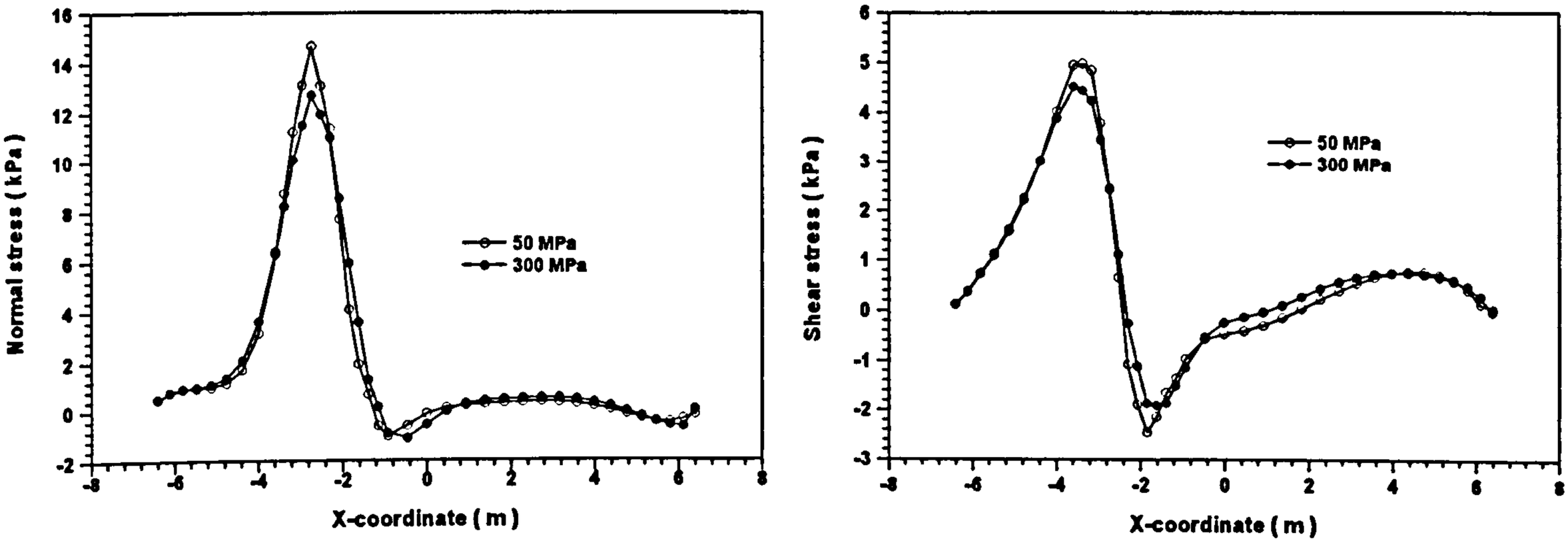

Figure 3 Normal and shear stresses with different ballast elastic moduli

Fig. 4 shows the normal and shear stresses obtained with different subgrade moduli. The ballast elastic modulus was kept constant at 300MPa. The peak normal stress was reduced from 12.7kPa to 11.3kPa and the peak shear stress was reduced from 4.5kPa to 4.0kPa with the subgrade modulus being increased from 5 MPa to 50MPa. This represented a stress decrease of 11.0% and 11.1% for the peak normal and shear stresses respectively.

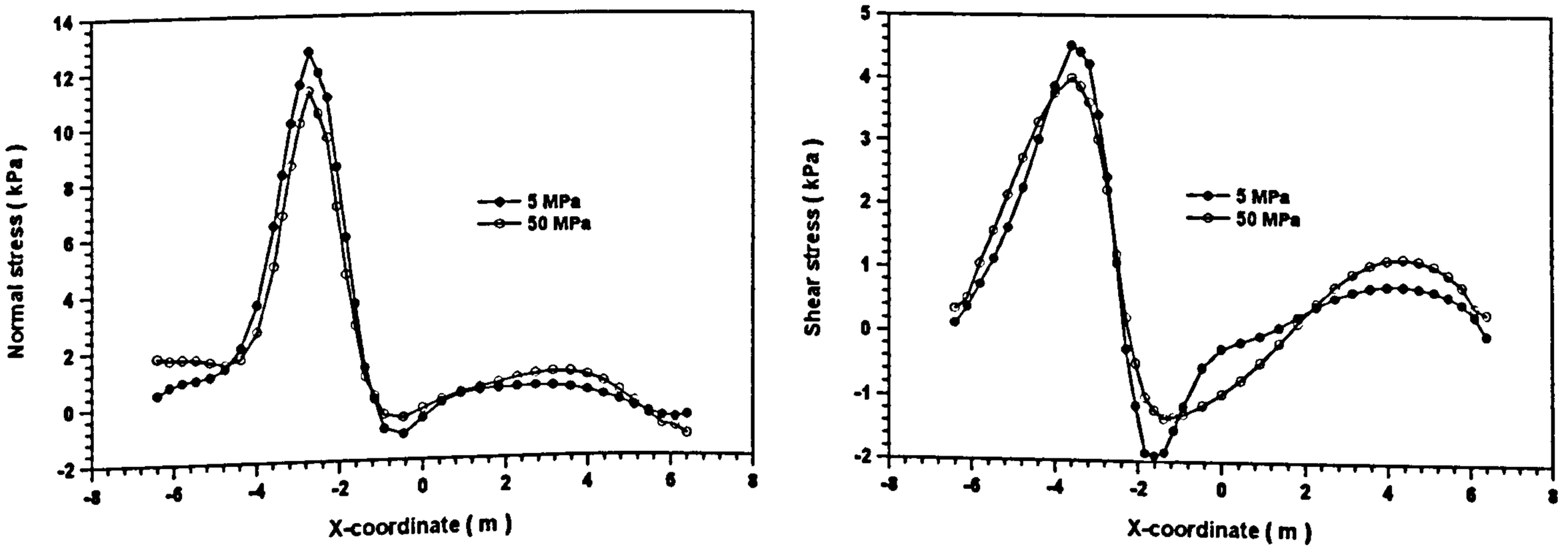

Figure 4 Normal and shear stresses with different subgrade moduli

The peak normal and shear stresses were found to be directly under the load platen at the ¼-span. A slight increase in normal stress on the side remote from the load was recorded due to the deformation of the arch ring towards the fill thus mobilising some passive resistance from the fill. This increase in normal stress was more sensitive to the increase in subgrade modulus. This would be expected as the subgrade with a higher modulus would be able to attract more stresses by virtue of its stiffness. However, at no point is this stress increase deemed significant when balanced against the applied stress of only 100kPa.

Stress Distribution by Boussinesq's Method

The normal and shear stresses on the arch extrados are presented in Fig. 5. For comparison, the FE results are also presented in Fig. 5. The ballast and subgrade elastic moduli used in the FE model were 300MPa and 50MPa respectively. The FE and Boussinesq's peak normal stresses were 12.7kPa and 10.5kPa respectively. This represents a difference in the peak normal stress in between 18.2% to 16.5%. No increase in normal stress on the side remote from the load was recorded by Boussinesq's method. This was expected as Boussinesq's method does not consider the variation of stress due to deformations. The FE and Boussinesq's peak shear stresses were 4.5kPa and 4.3kPa respectively. This represented only 6.7% to 2.2% difference in peak shear stress.

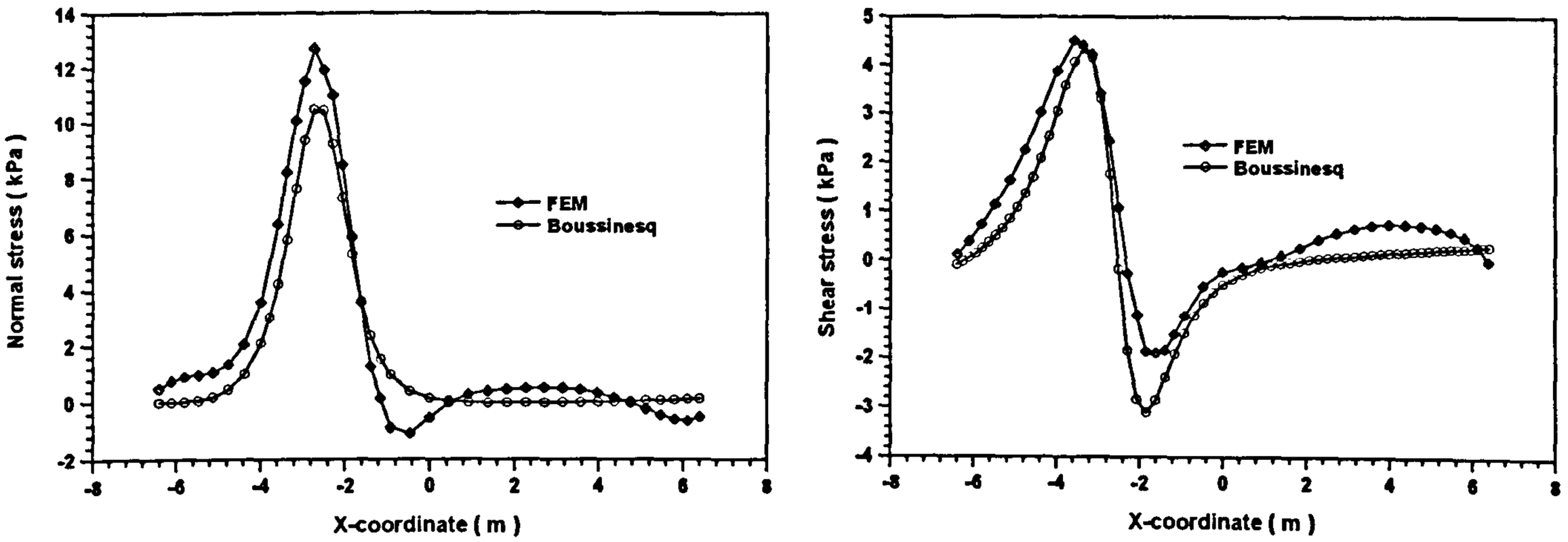

Figure 5 Normal and shear stresses by the FE and Boussinesq's methods

Ultimate Capacity by FE Method

The ultimate capacity of the arch bridge predicted by the 2D non-linear FE method is presented in Fig. 6. The ballast moduli used were 50MPa and 300MPa which resulted in collapse loads of 226kN/m and 249kN/m respectively. This represented a 10.2% increase in load carrying capacity. The ballast with a higher elastic modulus provided a higher stiffness and wider spread of the imposed load thus enhancing the capacity of the arch. The vertical deflection under the load point was also reduced with a higher ballast elastic modulus. Fig. 6 shows the failure modes predicted by the 2D non-linear FE analysis (a yielded Gauss point is symbolised by an asterisk). From Fig. 7, it is clear that a typical 4-hinge mechanism was predicted.

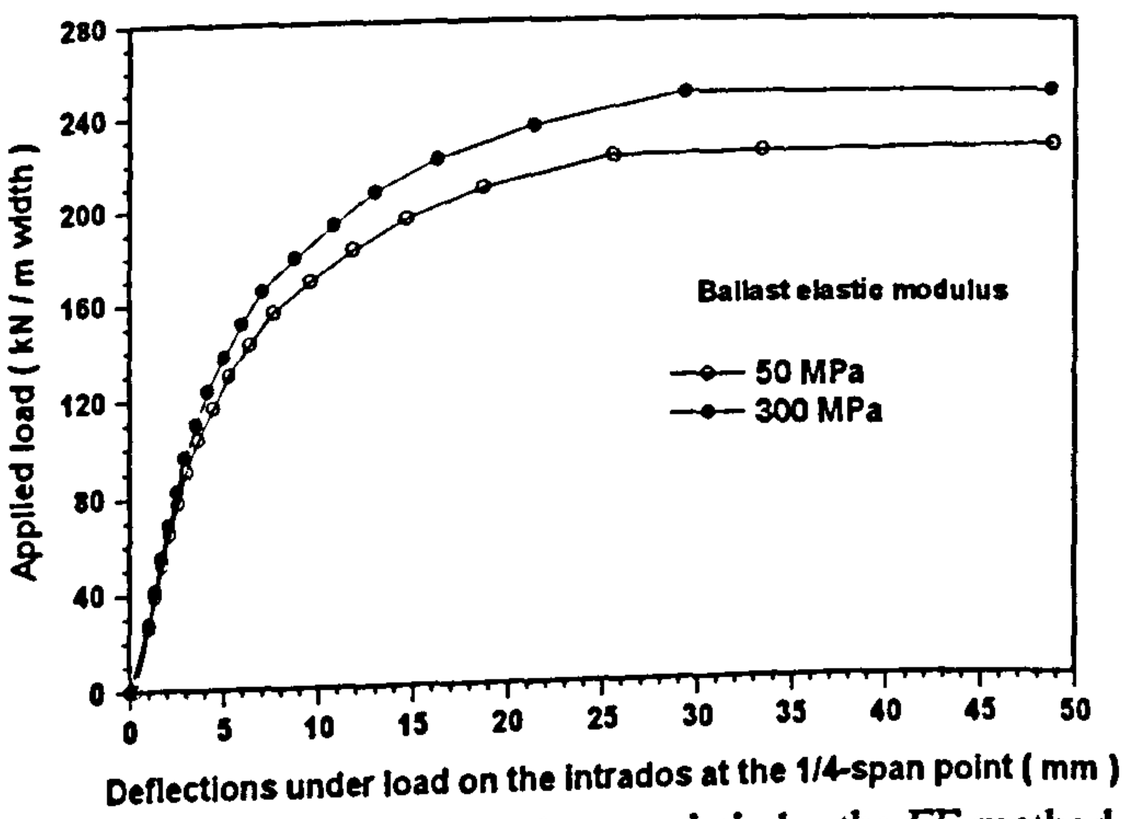

Figure 6 Load-deflection characteristic by the FE method

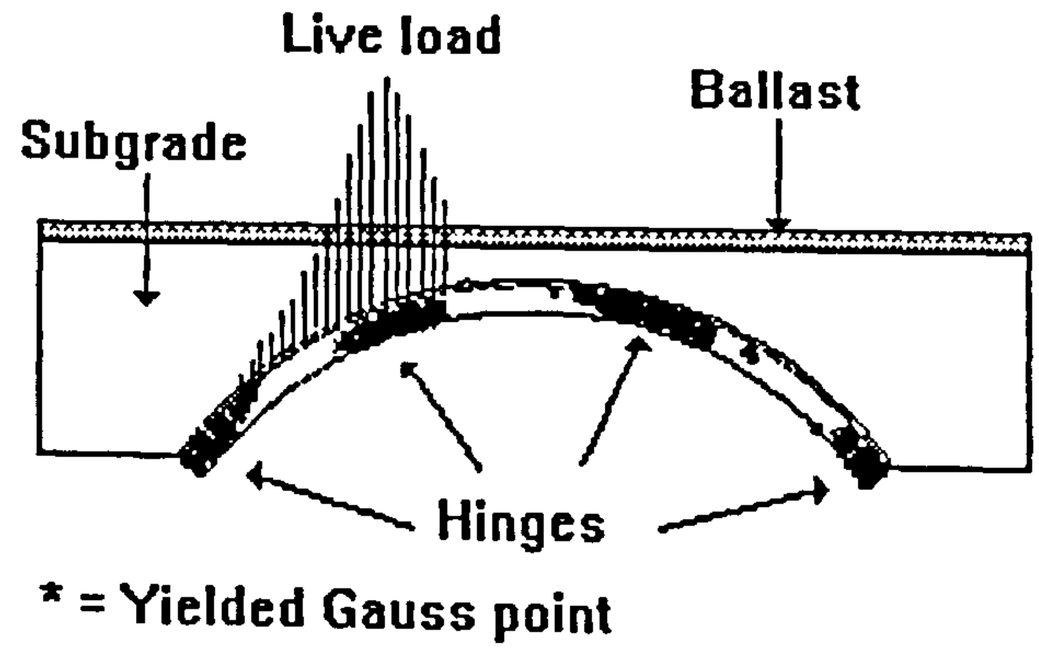

Figure 7 Predicted collapse mode by the FE method

Ultimate Capacity by CTAP and Mechanism Methods

The collapse loads assessed by CTAP and the mechanism method are presented in Fig. 8. The dispersal angle was varied from 0° to 60° on each side of the load's edge. With an increase of dispersal angle from 0° to 60°, CTAP predicted collapse loads of 171kN/m to 465kN/m, whereas the mechanism method predicted collapse at 288kN/m to 556kN/m. Unlike the FE method, CTAP and the mechanism methods do not consider the ballast and subgrade moduli in determining the load spread and the pattern of stress distribution. The dispersal angles assumed in both methods were thus imaginary. However, the increase in ultimate capacity of the arch with a higher load dispersal angle was evident in both CTAP and the mechanism methods.

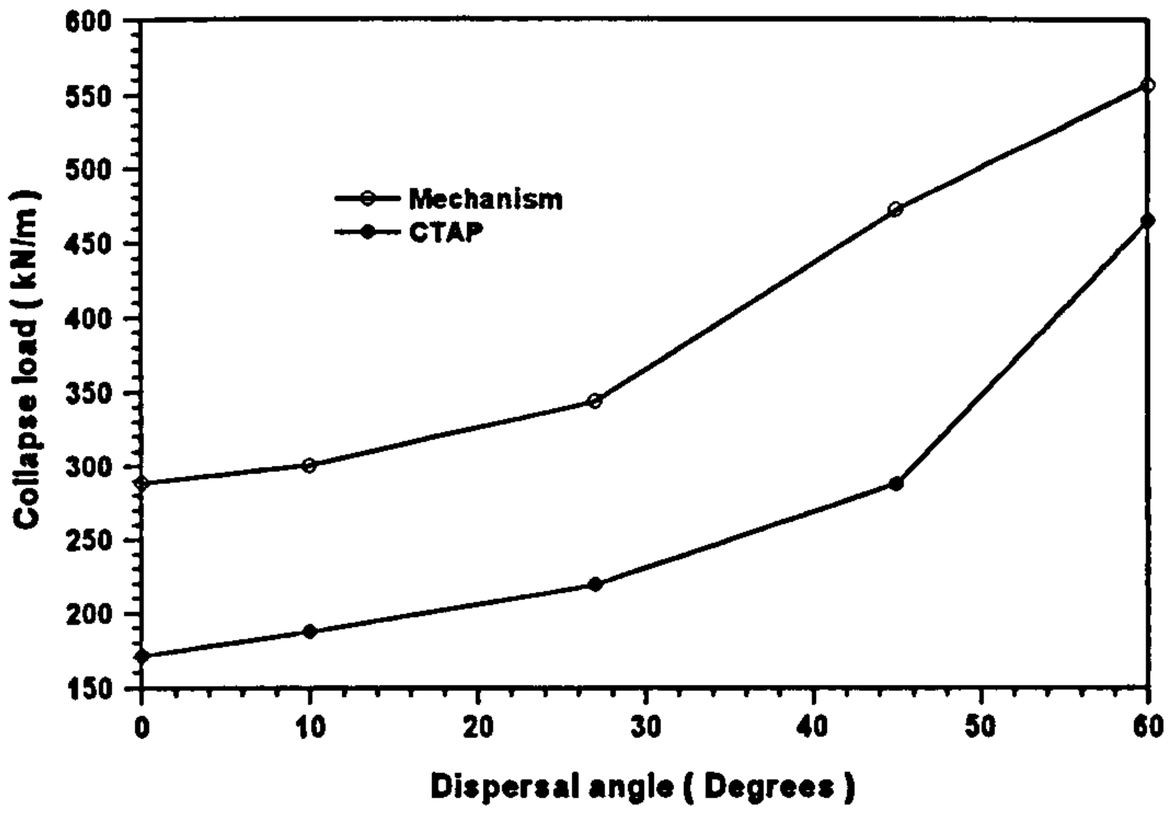

Figure 8 Ultimate loads by CTAP and the mechanism methods

DISCUSSION

The stress dispersal analyses by the 2D linear elastic FE and Boussinesq's methods are discussed. Following this, the influence of stress distribution and dispersal angle on the predicted ultimate capacity of the arch is discussed. Finally, some limitations to the stress distribution analysed by linear elastic methods are given.

2D FE and Boussinesq's Stress Distributions

The decrease in normal and shear stresses with the increase in ballast and subgrade elastic modulus was confirmed by the 2D linear elastic FE method. The ballast and subgrade with a higher elastic moduli are able to spread the imposed stress over a wider extent of the extrados which subsequently reduces the normal and shear stresses on the arch and enhances its load carrying capacity. The increase in subgrade elastic modulus also increases its stiffness which in turn enables it to provide a greater restraint against arch deformations.

Boussinesq's stress distribution, albeit with its fundamental assumptions violated in this soil-arch system, has demonstrated its potential to model a realistic trend of stress distribution. However, the magnitude of stresses predicted by Boussinesq's method was found to be lower than those from the FE predictions. This is because Boussinesq's method does not take into consideration the existence of various components in this system with widely different elastic moduli. Apparently, the arch ring with a higher elastic modulus was able to attract more stress. The stress increase was not recorded on the side remote from the load by Boussinesq's method. This was because Boussinesq's method does not consider the stress variation due to arch deformations thereby making stress calculations purely geometrical. Suffice to say, a FE analysis should be performed to obtain a more realistic stress distribution prior to the collapse analysis.

Ultimate Limit Analyses by the 2D FE, CTAP and Mechanism Methods

The increase in arch capacity with the increase in ballast elastic modulus is demonstrated by the 2D linear elastic FE method. The increase in ballast elastic modulus provides a greater load spread onto the arch extrados and also increases the overall stiffness. The arch carrying capacity was increased by 10.2% by increasing the ballast elastic modulus from 50MPa to 300MPa.

CTAP and the mechanism methods have demonstrated that the load dispersal angle had a significant effect on the predicted ultimate carrying capacity. The current codified assessment (BD21/97), recommends a load dispersal angle of about 27° regardless of the stiffnesses of ballast and subgrade or their highway engineering equivalents. With the increase in load dispersal angle from 27° to 45°, CTAP and the mechanism methods predicted capacity increases of 31% and 37% respectively.

This study has presented the influence of ballast and subgrade elastic moduli on the behaviour of stress distribution and predicted ultimate carrying capacity of a typical soil-arch system. Following this, some limitations of the current study on the linear elastic stress distribution are discussed.

LIMITATIONS

The 2D linear elastic FE method, being more sophisticated, can model the material non-homogeneities and anisotropies of this soil-arch system. However, the time required for both pre- and post-processing is larger than that required for Boussinesq's method. It is also understood that the soil remains non-elastic once loaded. In practice the distance between the load point and the arch extrados decreases as the load increases due to settlement or even failure of the foundation. This would concentrate the imposed stress onto the extrados and give greater deflections. However, foundation failure is difficult to envisage in reality with the load applied on a steel rail ably supported by stiffer ballast.

CONCLUSIONS

1. The increase in ballast elastic modulus from 5MPa to 300MPa has reduced the normal and shear stresses on the arch extrados from 14.7kPa to 12.7kPa and 4.97kPa to 4.52kPa respectively.

2. The increase in subgrade elastic modulus from 5MPa to 50MPa has reduced the normal and shear stresses on the arch extrados from 12.7kPa to 11.3kPa and 4.5kPa to 4.0kPa respectively.

3. Boussinesq's method predicted a realistic trend of live load stress distribution but with normal and shear stresses on the arch extrados lower than those produced by the FE method.

4. The 2D non-linear FE method predicted an increase in the ultimate load carrying capacity of the arch from 226kN/m to 249kN/m with an increase in the ballast elastic modulus from 50MPa to 300MPa.

5. The 2D non-linear FE model used in this study has predicted a typical 4-hinge collapse mode.

6. With an increase in the load dispersal angle from 27° to 45°, the CTAP and mechanism methods predicted a load carrying capacity increase of 31% and 37% respectively.

7. The FEA adopted here proved quick and effective to use for arch bridge assessments incorporating earth pressure effects.

REFERENCES

1 Bridle, R.J. & Hughes, T.P. (1990) 'An energy method for arch bridge analysis' Proc. Instn Civ. Engnrs, Vol. 89, pp. 375-385.

2 Department of Transport. (1997) 'Departmental Standard BD21/97: The assessment of highway bridges' HMSO, London.

3 FEA Limited. (1997) 'Finite element stress analysis system' FEA Ltd, Forge House, Kingston-upon-Thames, Surrey.

4 Ponniah, D.A., Fairfield, C.A. & Prentice, D.J. (1997) 'Fill stresses in a new brick arch bridge subject to heavy axle-load tests' Proc. Instn Civ. Engnrs J. Struct & Bldgs, Vol. 123, pp. 173-185.

Proc. Instn Civ. Engrs Structs & Bldgs, 1999, **134**, May, 119–127

Paper 11789

Written discussion closes 27 August 1999

Finite-element analysis of masonry arch bridges

K. H. Ng, BEng, C. A. Fairfield, BEng, PhD, MIHT, MInstNDT, and A. Sibbald, BSc, MSc, PhD, CEng, MICE, FInstNDT

This paper describes a method of assessing the load-carrying capacity of masonry arch bridges using the general-purpose finite-element (FE) package LUSAS. Good agreement was found, in terms of collapse loads and load–deflection characteristics, between the FE analysis adopted here and the experimental data. Three bridges were assessed: Bridgemill (actual collapse load 361 kN/m, FE collapse load 362 kN/m), Strathmashie (actual collapse load 228 kN/m, FE collapse load 226 kN/m) and Barlae (actual collapse load 296 kN/m, FE collapse load 302 kN/m). These values were based on cases where the material properties were well documented, which will not always be the case for other less well-researched arches, and therefore a parametric study involving the arch's elastic modulus, its compressive strength, its tensile strength and the backfill's load dispersal angle was carried out. The progressive development of cracking in the arch ring due to the application of live loading was also analysed. The method adopted was found to be a viable assessment tool for those bridges where the cost of potential repair/maintenance justifies what can be time-consuming FE work.

Keywords: brickwork & masonry; bridges; maintenance & inspection

Introduction

There are approximately 60 000 masonry arch bridges built between the 17th and 19th centuries in the United Kingdom now carrying traffic loads far beyond those estimated by their designers. The present initial method of assessing the load-carrying capacity of masonry arch bridges is referred to as the MEXE (Military Engineering Experimental Establishment) method defined in the Department of Transport's Departmental Standard BD21/97[1] and associated Advice Note BA16/97[2]. As mentioned later, other methods have been developed to give a more refined assessment. This method considers a limited load dispersal angle, and the strengthening effect of the lateral earth pressures is ignored. Although this method is easily applied, the use of the MEXE modification factors is subjective.

2. National roads authorities are assessing the arch bridge stock to allow increases in the maximum allowable gross vehicle weight (GVW) from 38 t to 40 t (certain bridges may have to be assessed for 44 t GVW) and in the maximum axle weight from 10 t to 11·5 t. Full-scale tests suggest that the MEXE method gives conservative results, with the consequence of heavy goods vehicles taking longer trips than would otherwise be required. This shifts traffic to bridges rated for the higher axle limits, thus speeding their deterioration. The actual safety factor on an arch bridge is very hard to find accurately by any of the current assessment methods; hence the current interest in arch analyses.

3. In this study a two-dimensional analysis was performed using LUSAS, a commercially available finite-element (FE) package.[3] Three full-scale bridge collapse tests were modelled: Bridgemill,[4] Strathmashie[5] and Barlae,[6] and the results compared with available field test data. Comparisons were also made with results obtained from other current arch bridge assessment methods: CTAP,[7] ARCHIE,[8] MEXE,[1,2] and ARCH.[9] The program CTAP, developed by Bridle and Hughes, uses Castigliano's elastic strain energy method. The MEXE results were obtained using a computerized version (MINIPONT) developed by the Department of Transport. The program ARCHIE, developed by Harvey and Smith, uses the mechanism method to assess the load-carrying capacity of arches. The program ARCH, another mechanism-method-based application, was developed by Cascade Software Ltd. Parametric studies were carried out using the adopted FE package to study the effects of variations in the arch's elastic modulus, compressive strength and tensile strength and the backfill's load dispersal angle. The influence of each parameter on the modelled behaviour of the field tests at Bridgemill, Strathmashie and Barlae was also considered.

The FE model

4. Eight-noded quadrilateral elements (one node *per* corner plus four midside nodes) were used to model the arch, backfill and extrados interface. The element type QPM8 (LUSAS designation, included here for reference purposes only), under plane stress conditions, was used to model the arch. The element type QPN8 (LUSAS designation) was used to model the

K. H. Ng, Postgraduate student, Department of Civil & Transportation Engineering, Napier University, Edinburgh

C. A. Fairfield, Senior Lecturer in Soil Mechanics, Department of Civil & Transportation Engineering, Napier University, Edinburgh

A. Sibbald, Dean of the Faculty of Engineering, Napier University, Edinburgh

backfill–extrados interface. These are standard, readily available element types proven over many years to give accurate results for a wide range of engineering problems. The behaviour of backfill and interface elements was elasto-plastic with failure defined by Mohr–Coulomb yield criterion. The arch was simulated by a stress-dependent von Mises constitutive law enabling different tensile and compressive material properties to be specified.

5. The fill above the arch ring was confined by spandrel walls and was therefore assumed to be under plane strain conditions (no strain allowed out of the plane of the span). The arch ring itself was not thus confined and was therefore assumed to be in a state of plane stress (no stress allowed out of the plane of the span). A total of 272 elements were used, of which 90 modelled the arch ring and the remaining 182 modelled the backfill and interface. Using a Pentium processor (100 MHz chip speed) with 8 Mb of RAM, a typical analysis took 1·5 h.

Loading

6. The total load on an arch bridge consists of its self-weight, including the backfill above the extrados, plus any imposed live loading. In the authors' FE analyses the imposed load was applied incrementally after the application of self-weight. The imposed load was applied to the backfill's upper, horizontal surface and distributed over the extrados in accordance with Boussinesq's elastic method. Little is known about actual load spreads through arch bridge backfills. Ponniah *et al.*[10] recorded a load dispersal angle of 65° during a field test at Kimbolton Butts bridge, Cambridgeshire; previous instrumented load tests[11] to failure have found Boussinesq's method to provide results surprisingly close to the stress states measured on the extrados. BD21/97[1] allows a dispersal angle of 26·6°, based on its 1 in 2 side slope for live-load stress distribution. For steeply haunched arch bridges with low span-to-rise ratios, the live load may be distributed beyond the springers: it would be safer to consider the entire live load as being carried by the arch. To this end, it was assumed that sliding could occur along the backfill–extrados interface in regions where the slop of the extrados exceeded the backfill's angle of shearing resistance. A similar approach was adopted by Gong.[12]

Boundary conditions

7. The arch was assumed to be rigidly fixed to its abutments, and therefore both horizontal and vertical springer displacements were zero. No significant abutment movement was recorded *in situ* for the arch bridges used in this study. However, any of the three bridges may have settled over the years, thus easing any problems by creep and/or stress relaxation. If desired, spring supports can be used to simulate abutment movement; this was not done in this study.

Backfill material properties

8. It is generally difficult to determine the backfill properties as they are inherently variable and subject to the vagaries of compaction, years of dynamic loading and possible over-consolidation. In some bridges (*e.g.* Bargower bridge, Strathclyde, tested by the University of Edinburgh in 1986), stronger, stiffer backing was found behind the arch. For the authors' current FE study, the backfill's elastic modulus and angle of shearing resistance were assumed to be 50 MPa and 35°, respectively.

Arch geometry and material properties

9. Salient dimensions of the three arch bridges analysed in this study and their material properties are presented in Table 1. These material properties, derived from the reports on the *in situ* tests, were used for the subsequent FE analyses.

FE results

10. The FE analysis was performed on three redundant arch bridges which were loaded to collapse by various researchers[4–6] as part of the Transport Research Laboratory's research programme examining the behaviour of arch bridges, their assessment methods and their analysis. A parametric study involving the arch's elastic modulus, its compressive and tensile strength, and the backfill's load dispersal angle was also carried out. For each arch analysed, results from *in situ* load tests,[4–6] the program CTAP,[7] the program ARCHIE,[8] the MEXE method[1,2] and the program ARCH[9] were compared with the authors' FE output.

Bridgemill

11. The Bridgemill bridge[4] was a red-sandstone masonry arch. The whole structure was in good condition, without any significant cracks in the vault and spandrel walls. The bridge was loaded to collapse using a transverse line load over a width of 750 mm located at one quarter-span point. The collapse load recorded was

Table 1. Arch geometries and their salient properties

Bridge	Bridgemill	Strathmashie	Barlae
Span: m	18·29	9·425	9·865
Rise at the crown: m	2·84	2·99	1·695
Width: m	8·30	5·81	9·80
Ring thickness: m	0·711	0·60	0·45
Fill depth at the crown: m	0·203	0·41	0·295
Arch ring profile	Parabolic	Segmental	Segmental
Arch elastic modulus: MPa	5000	5000	5000
Arch compressive strength: MPa	5	6	7
Arch tensile strength: MPa	0·22	0·25	0·33

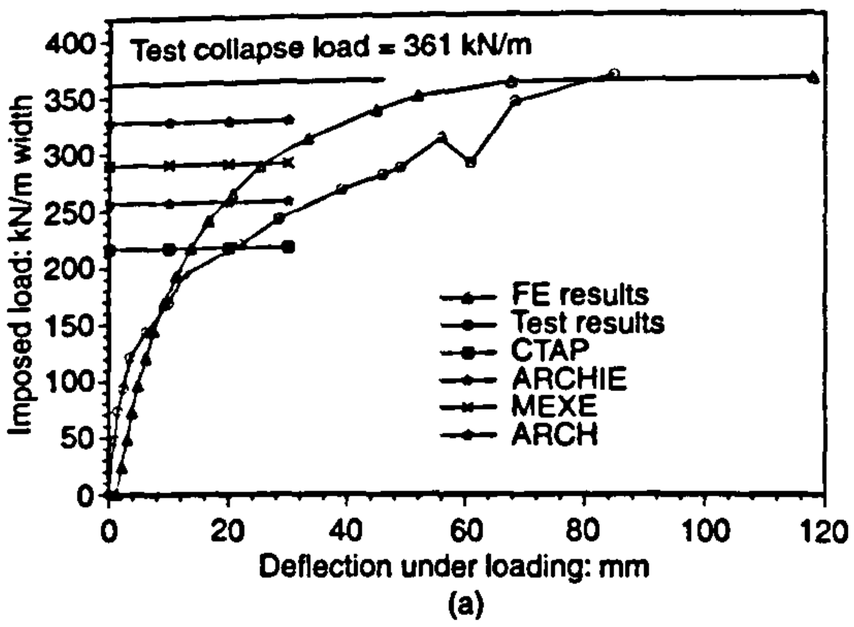

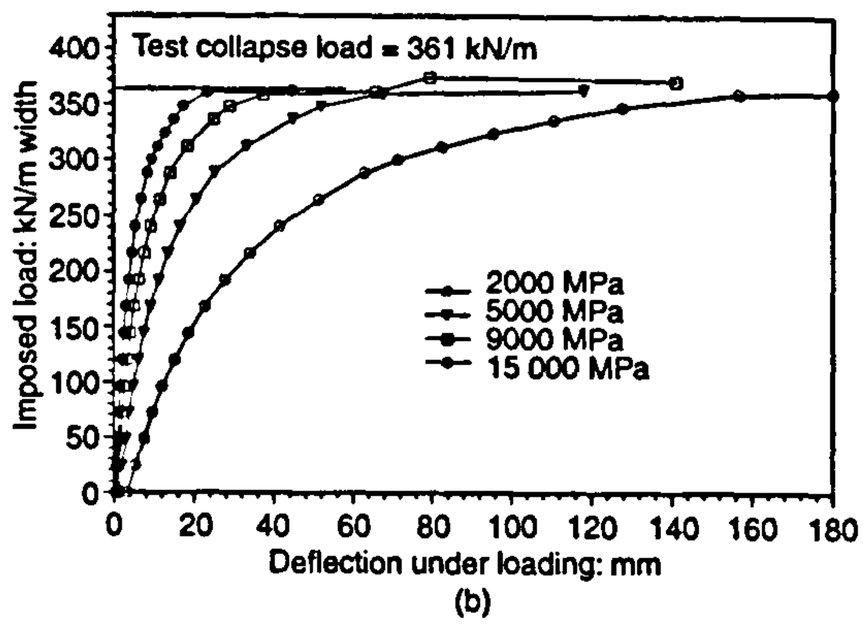

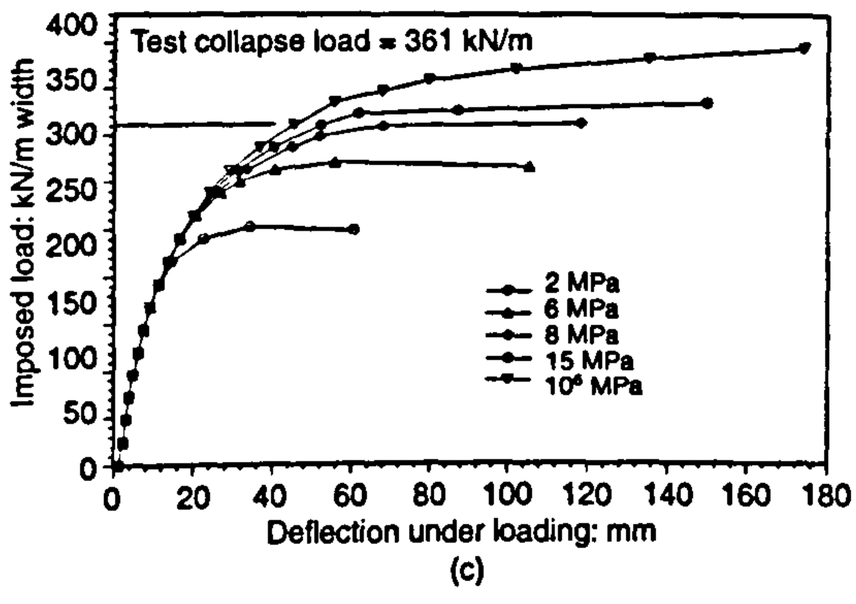

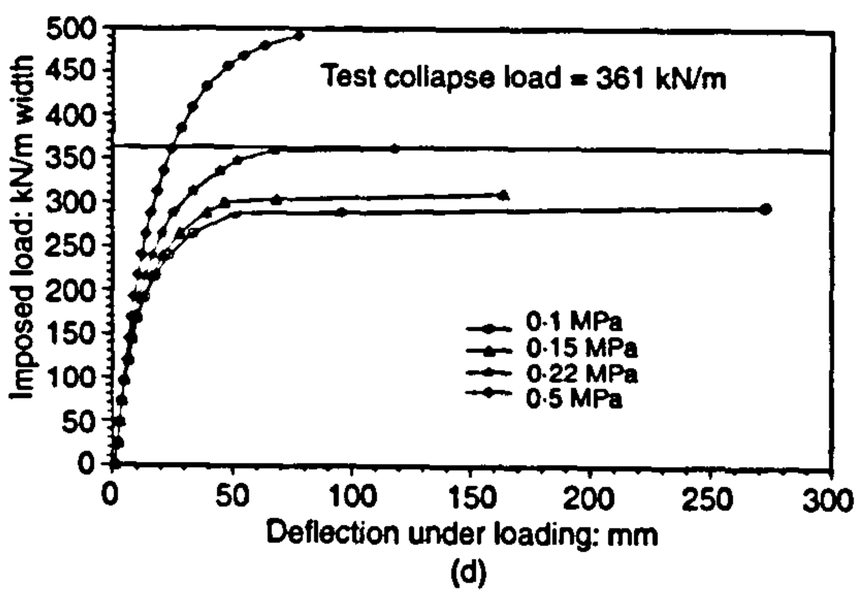

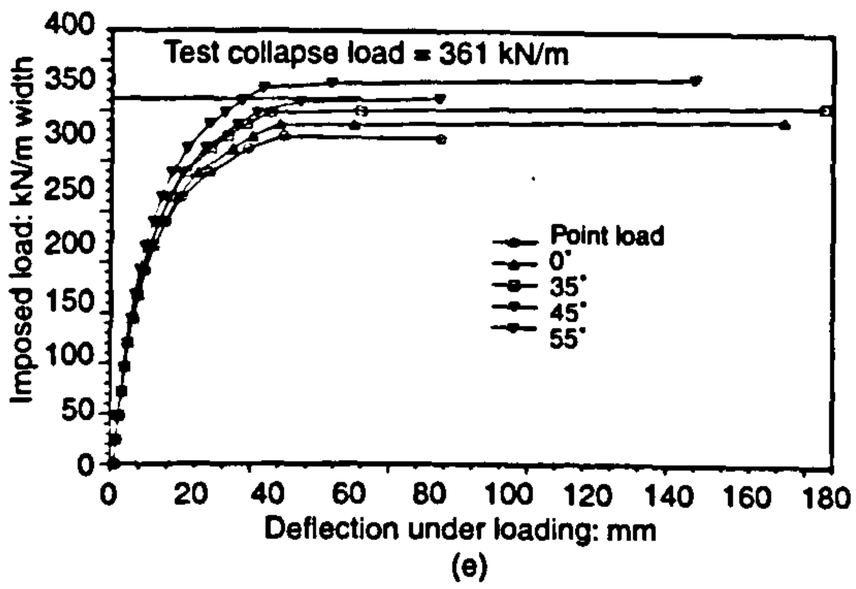

Fig. 1. (a) Load–deflection relationships for Bridgemill bridge; (b)–(e) parametric studies: (b) effect of arch elastic modulus, (c) effect of arch compressive strength, (d) effect of arch tensile strength, (e) effect of load dispersal angle

361 kN/m width perpendicular to the span. The FE result using the arch properties given in Table 1 was 362 kN/m width. Comparison was made with the experimental collapse load and the results obtained from other assessment methods: these are presented in Fig. 1(a) and discussed later. Results from the parametric study on the effects of arch elastic modulus, compressive strength, tensile strength and backfill load dispersal angle are presented in Figs 1(b)–1(e).

Strathmashie

12. The Strathmashie bridge[5] was a rubble masonry arch. Dimensionally it was in good condition but there was only a little mortar in parts of the arch and a serious longitudinal crack in the arch ring, as mentioned in the report on its testing.[5] The bridge was loaded to collapse using a transverse line load of 750 mm width located at one quarter-span point. The ultimate load recorded was 228 kN/m width perpendicular to the span. A reduced thickness of 500 mm was used in this study instead of the original thickness of 600 mm due to the aforementioned loss of mortar in the arch ring. The FE result using the arch properties given in Table 1 was 226 kN/m width. Comparison was made with the experimental collapse load and the results obtained from other assessment methods: these are presented in Fig. 2(a) and discussed later. Results from the parametric study on the effects of arch elastic modulus, compressive strength, tensile strength and backfill load dispersal angle are presented in Figs 2(b)–2(e).

Barlae

13. The Barlae bridge[6] was an ashlar masonry arch with a 29° skew. No major defects

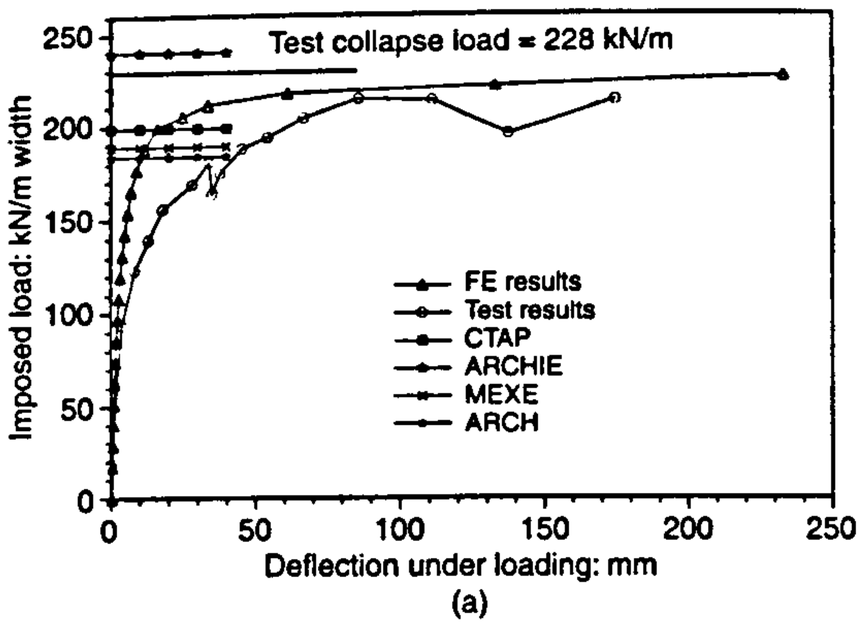

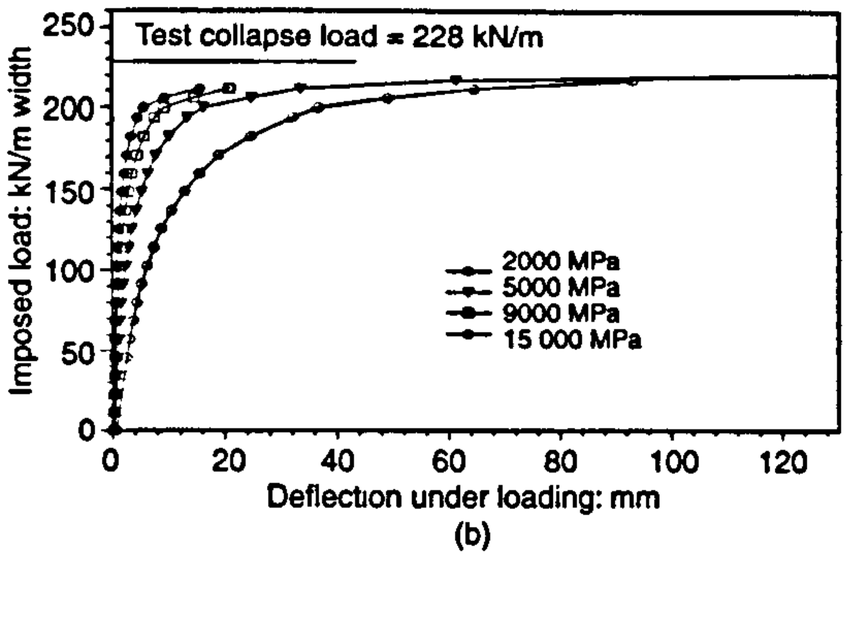

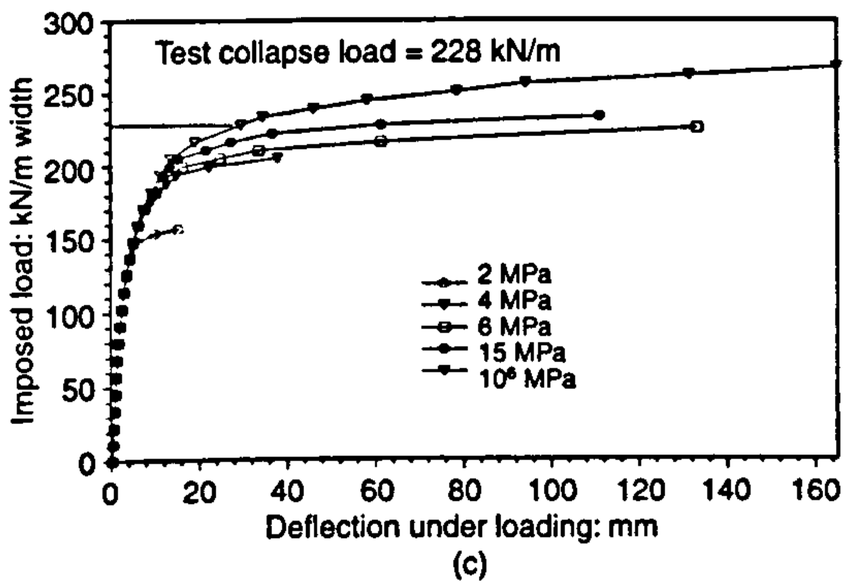

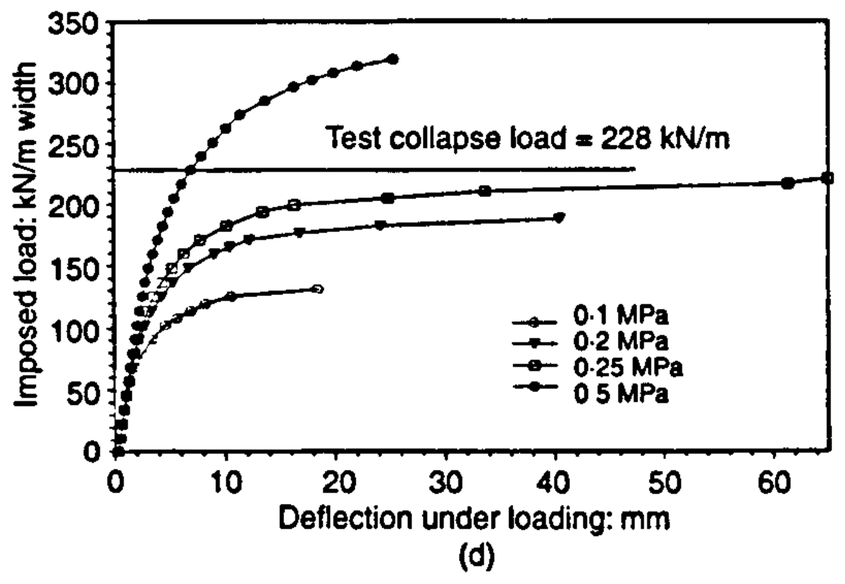

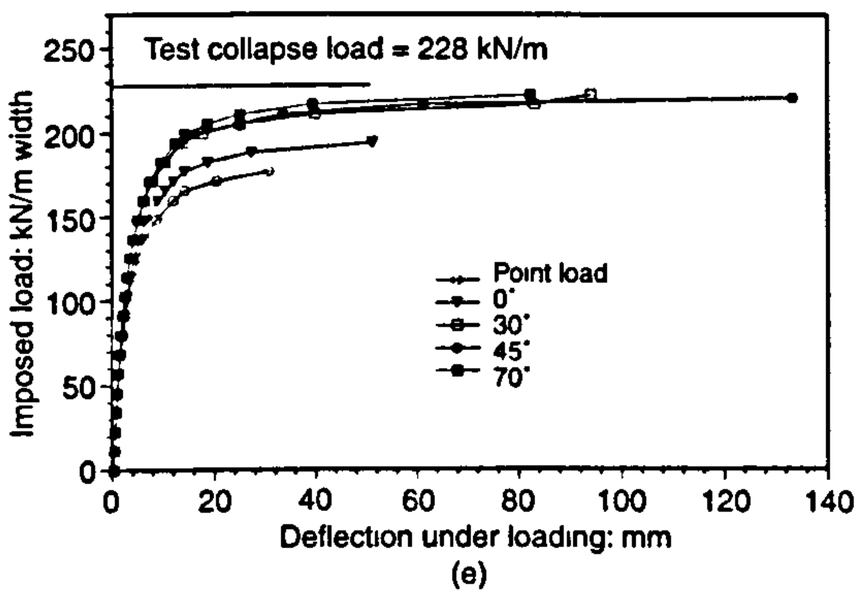

Fig. 2. (a) Load–deflection relationships for Strathmashie bridge; (b)–(e) parametric studies: (b) effect of arch elastic modulus, (c) effect of arch compressive strength, (d) effect of arch tensile strength, (e) effect of load dispersal angle

were found on the bridge, which was loaded to collapse using a transverse line load of 750 mm width located at one quarter-span point. The ultimate load recorded was 296 kN/m width perpendicular to the span. The FE result using the material properties given in Table 1 was 302 kN/m width. Comparison was made with the experimental collapse load and the results obtained from other assessment methods: these are presented in Fig. 3(a) and discussed later. Results from the parametric study on the effects of arch elastic modulus, compressive strength, tensile strength and backfill load dispersal angle are presented in Figs 3(b)–3(e).

Discussion

14. The results obtained from the authors' FE analyses are discussed below. Following this, comparisons are made between the capacity as estimated by CTAP,[7] ARCHIE,[8] MEXE[1,2] and ARCH.[9] Finally, the influence of arch elastic modulus (Fig. 4), compressive strength (Fig. 5), tensile strength (Fig. 6) and backfill load dispersal angle (Fig. 7) on the behaviour of arch bridges is discussed.

FE analysis

15. The results from the authors' FE analyses show close agreement in terms of collapse load and load–deflection characteristics for the three arches analysed here. The percentage differences between the test and FE results for the Bridgemill, Strathmashie and Barlae bridges were 0·2%, 0·7% and 2%, respectively. The FE analysis accounted for all major arch and fill material properties and was able to model material cracking and crushing as well as soil yielding. Figures 8 and 9 show the hinge locations, and the imposed loading versus depth of crack relationships for the Barlae bridge.[6] No hinges were formed across the full depth of

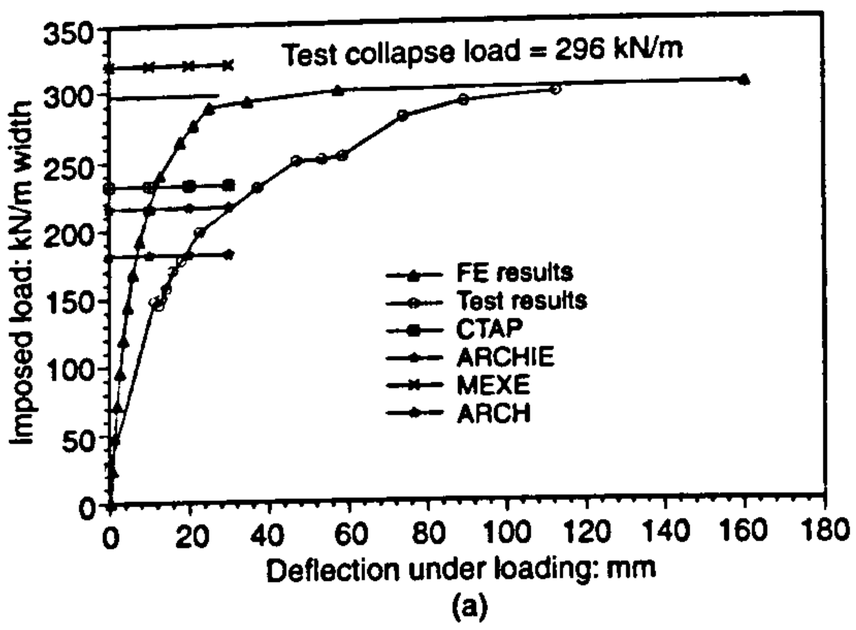

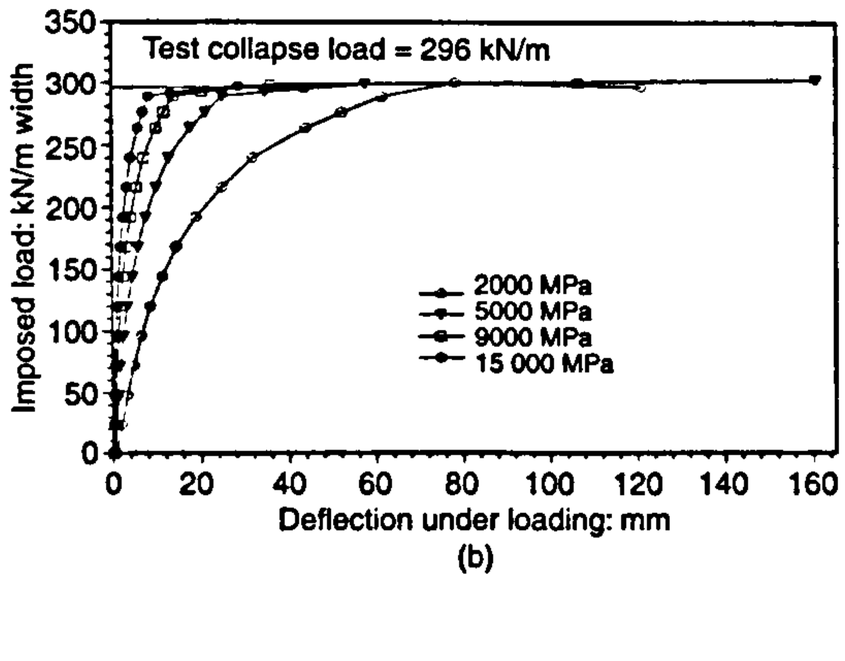

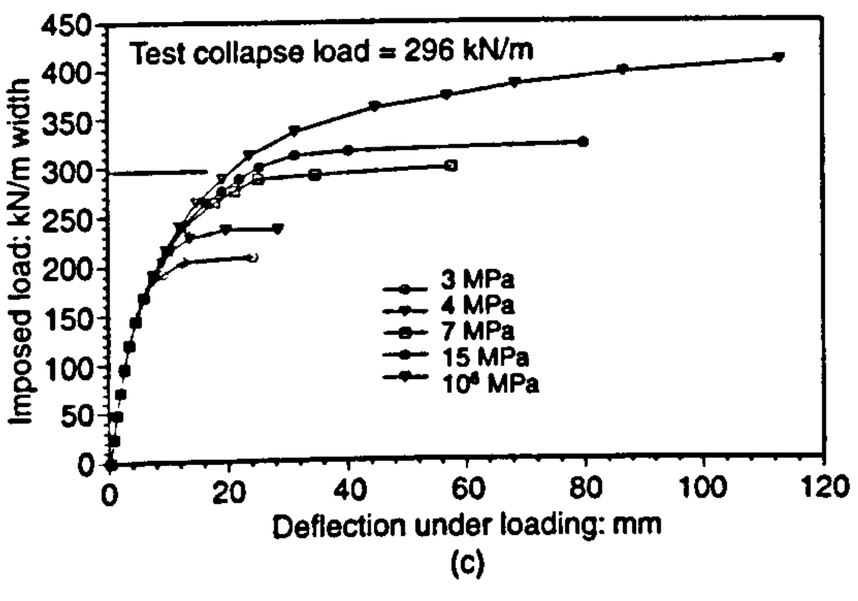

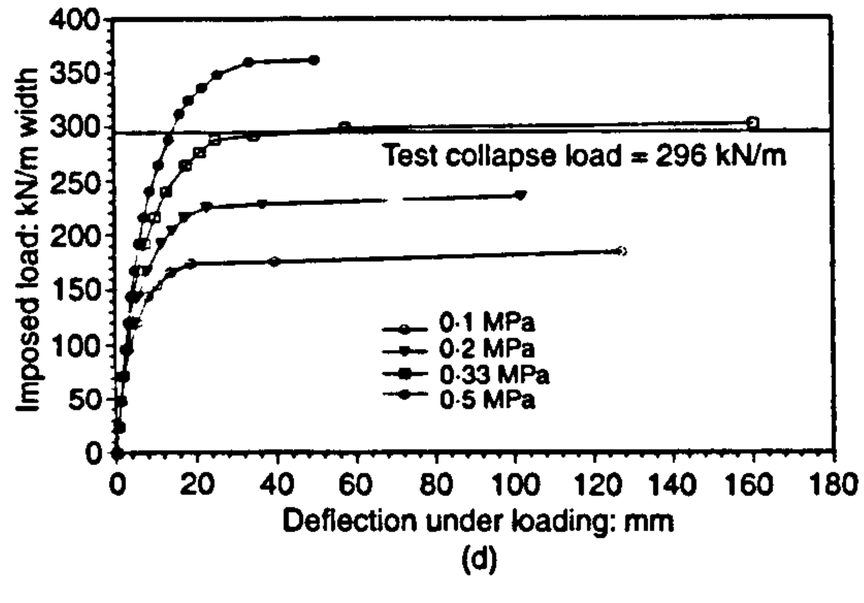

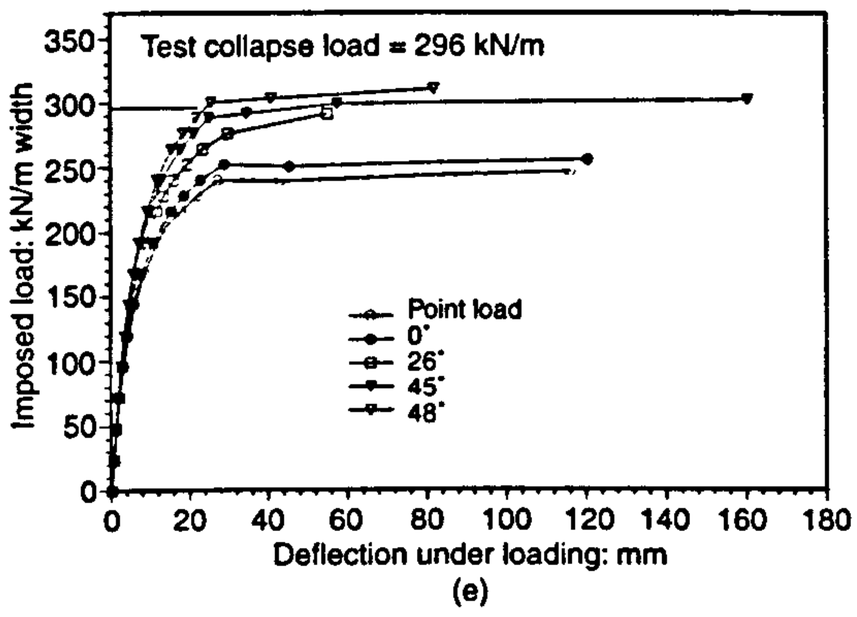

Fig. 3. (a) Load–deflection relationships for Barlae bridge; (b)–(e) parametric studies: (b) effect of arch elastic modulus, (c) effect of arch compressive strength, (d) effect of arch tensile strength, (e) effect of load dispersal angle

arch ring, since the compressive stresses induced at the hinge locations were high enough to cause material crushing. Information such as the extent of cracking, the stress level in the arch ring and its deflection at any load level is crucial for a serviceability limit state analysis.

16. Different material properties may be assigned to a single arch ring if it consists of different materials because of remedial repairs or if weak spots associated with defects are to be included. The use of two-dimensional backfill elements enables the strengthening effects of soil–structure interaction to be modelled realistically. It is common to find stronger, stiffer backings existing behind the haunches of such bridges: different backfill materials with different strengths and stiffnesses can be assigned to account for the existence of backing.

Results from other assessment methods

17. It is clear that the collapse loads estimated by the four other assessment methods used in this paper are quite diverse. This is due to different assumptions made and different theoretical models adopted. The authors are unaware of the exact material properties used in these assessment methods for these bridges; obviously, different arch and backfill material properties and load dispersal angles will result in different behaviour predictions. CTAP is the only method among those used here that gives load-versus-deflection information and details of the extent of cracking at any load level. Clearly, different methods will be more suited to different arch geometries, whereas assessment by the FE method will be applicable to any soil–arch system. The drawback of FE assessment is the amount of computing power and

user time required for data input, mesh generation and postprocessing.

18. *The MEXE method.* The MEXE method is substantially influenced by modification factors. It is not always conservative; in the case of the Barlae bridge the method overestimated the collapse load by 8·1%. For the Bridgemill and Strathmashie bridges the MEXE method gave percentage differences of −19·7% and −17·1%, respectively. It is unique among assessment methods in that different engineers can quite legitimately provide different capacity estimates for a given arch.

19. *Program CTAP, a strain energy method.* The program CTAP analyses the arch by eliminating the tensile areas of the cross-section. Lateral pressure is modelled with horizontal springs which yield at active and passive limits. The percentage differences between the actual and the CTAP-assessed results for the Bridgemill, Strathmashie and Barlae bridges are −40·2%, −12·7% and −21·6%, respectively. The authors have previously carried out model tests on wooden arches with dry sand backfill;[13] CTAP was also used to assess their collapse loads, with some success.[14] Variations of between −16% and +6·4% of the actual collapse loads were found, indicating the efficacy of CTAP as an assessment method. The one case where CTAP overestimated a collapse load occurred where the weak sand backfill underwent bearing-capacity failure, resulting in the load point becoming progressively closer to the arch extrados. This was a facet of the structure's behaviour that CTAP does not attempt to model, as full-scale masonry arch bridges have road pavements above the backfill, making bearing-capacity failure unlikely.

20. *Programs ARCHIE and ARCH: mechanism methods.* The programs ARCHIE[8] and ARCH[9] are based on the mechanism method. The mechanism method is based on assumed hinge positions for a given load configuration. Iteration to find a safe line of thrust, the arch ring depth required to contain it and hence the ultimate load is then carried out. Various methods of load dispersal through the backfill are used and program ARCHIE is able to assess an arch with some account being taken of the development of passive resistance to deformation of the unloaded side of the span. Drawbacks to this method are that information about the extent of lateral earth pressure mobilization is limited to calibration scale models,[15] FE analyses[10] and the occasional full-scale test.[16] For the three bridges assessed here, no more than 40% of the full passive pressure was allowed to develop. The percentage differences between the actual and the ARCHIE-assessed results for the Bridgemill, Strathmashie and Barlae bridges are +9·1%, +5·3% and −27·0%, respectively. These data are

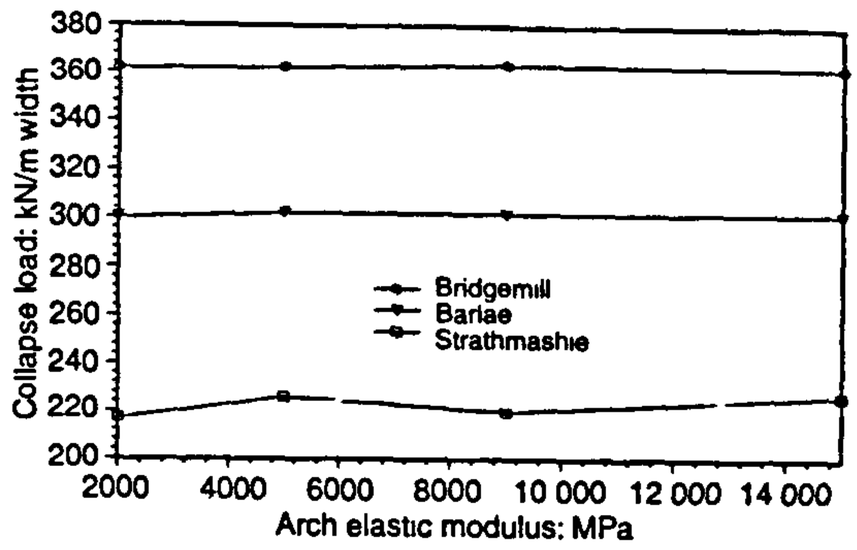

Fig. 4. Parametric study: effect of arch elastic modulus on each bridge

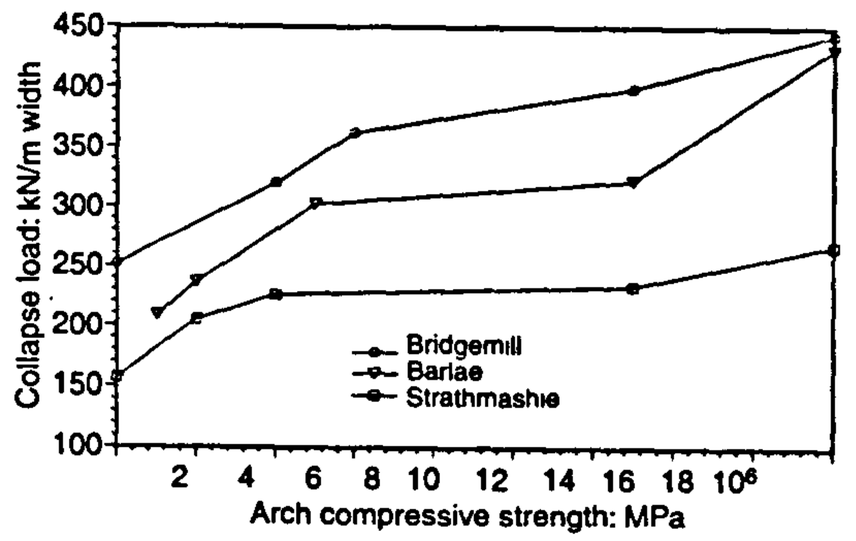

Fig. 5. Parametric study: effect of arch compressive strength on each bridge

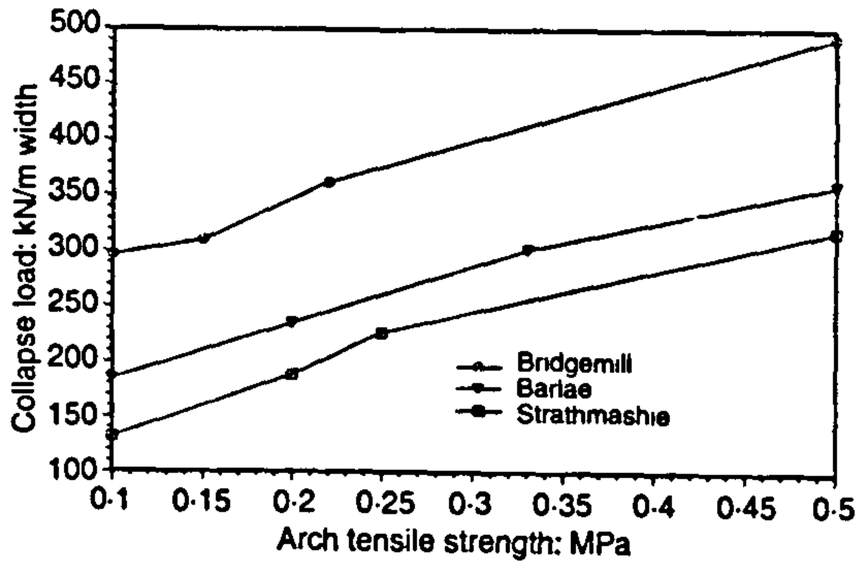

Fig. 6. Parametric study: effect of arch tensile strength on each bridge

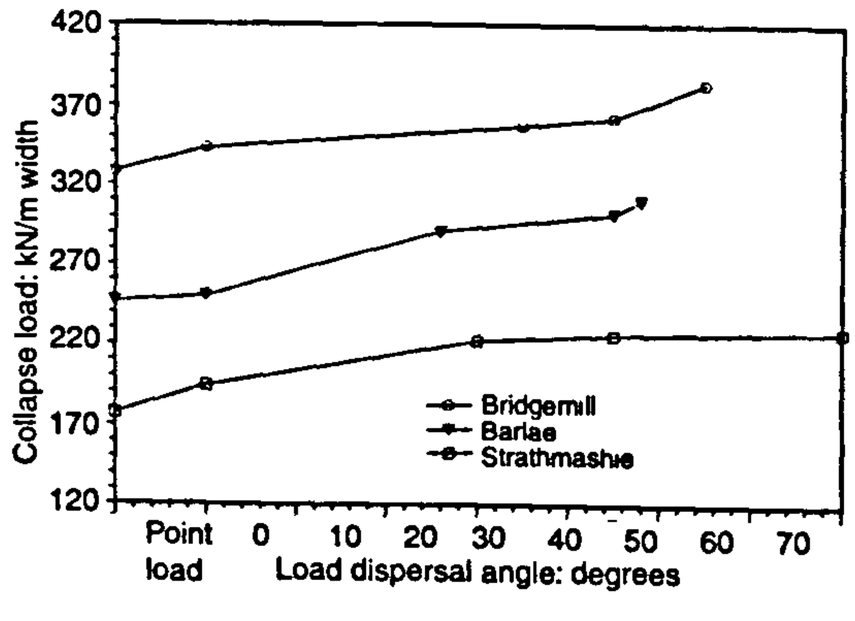

Fig. 7. Parametric study: effect of load dispersal angle on each bridge

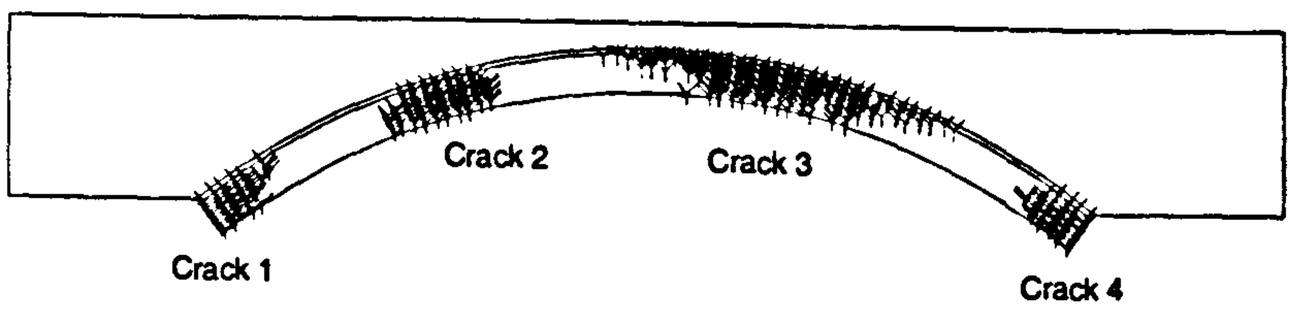

Fig. 8. Yielded zones in Barlae bridge as predicted by finite-element analysis

consistent with earlier comparisons involving the collapse load of a 2 m span brickwork arch,[11] where ARCHIE provided a difference of −19%. The percentage differences between the actual and the ARCH-assessed results for the Bridgemill, Strathmashie and Barlae bridges are −29·1%, +19·3% and −38·5%, respectively. The principal reason for the discrepancies between the assessed and actual collapse loads lies in the way the mechanism method has had to use simplified soil stress distributions on the extrados. The authors' FE results presented earlier were based on more accurate earth pressure distributions not limited by the dictates of any other assessment method.

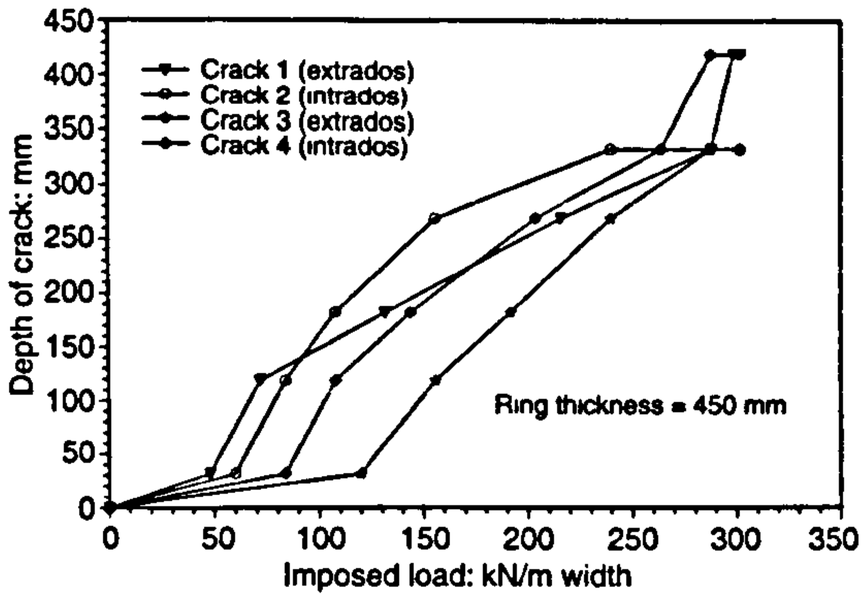

Fig. 9. Imposed loading and crack development for Barlae bridge

Analysis of the results of the FE parametric study

21. The influence of each quantity considered in the FE-based parametric study is discussed separately in the following sections. Four parameters were varied: the arch's elastic modulus, its compressive and tensile strengths, and the backfill load dispersal angle.

22. *The effect of varying the arch's elastic modulus.* It is apparent from Figs 1(b), 2(b), 3(b) and 4 that the arch's elastic modulus has no significant effect on the system's collapse load. However, this may not be true when there is an upper limit to the maximum arch deflection allowed before the onset of buckling. The major influence of the arch's elastic modulus comes in the form of its influence on the load-versus-deflection characteristic of an arch. The lower the elastic modulus of the arch ring, the more flexible the system. It is difficult to determine the value of the arch's elastic modulus as it is a composite of mortar and voussoir units. Direct compression tests on this composite material may not give reliable results because replication of the confining stresses pertinent to its *in situ* condition is difficult. The elastic modulus also has its importance diminished because the arches tended to fail with large deformations caused by rotation of segments of the arch ring; compression of the material is of lesser importance, provided a sufficiently wide gap can open under elastic compressive stresses to allow the first hinge to form. A value of around 5000 MPa is suggested by the authors to simulate accurately the load-versus-deflection characteristics.

23. *The effect of varying the arch's compressive strength.* Results of the parametric study on the effect of the arch's compressive strength are presented in Figs 1(c), 2(c), 3(c) and 5. The estimated collapse loads were sensitive to variations in arch compressive strength; values ranging from 2 MPa to 1×10^6 MPa were used. A sensible range of 2 MPa to 15 MPa was contained within this extreme variation; it is not suggested that values as high as 1×10^6 MPa are used for assessment purposes. Different values of compressive strength did not affect the initial flexibility or the deformations. For the Bridgemill bridge the FE-estimated collapse load increased from 252 kN/m to 384 kN/m (actual collapse load, 361 kN/m) as the arch's compressive strength increased from 2 MPa to 15 MPa. For the Strathmashie bridge the FE-estimated collapse load increased from 157 kN/m to 230 kN/m (actual collapse load, 228 kN/m) as the arch's compressive strength increased from 2 MPa to 15 MPa. For the Barlae bridge the FE-estimated collapse load increased from 180 kN/m to 321 kN/m (actual collapse load, 296 kN/m) as the arch's compressive strength increased from 2 MPa to 15 MPa. A realistic arch compressive strength will obviously be essential for accurate arch assessment by any method adopted.

24. *The effect of varying the arch's tensile strength.* Results of the parametric study on the effect of the arch's tensile strength are presented in Figs 1(d), 2(d), 3(d) and 6. The estimated collapse loads were sensitive to variations in arch tensile strength; values ranging from 0·1 MPa to 0·5 MPa were used. Care must be taken when selecting a value for the arch's tensile strength. On an intact arch, nominally defect-free, it is justifiable to use a higher value of arch tensile strength since at no time in the loading history has the tensile stress been large enough to cause full-depth discontinuities between the mortar beds and the voussoir units. Full-scale tests on arch bridges carried out by Davey[17] recorded a maximum tensile stress of 0·69 MPa. Ignoring the tensile strength may lead to conservative results. Non-destructive testing by the impact-echo method[18–20] can assist an engineer in making an assessment of the state of cracking in the arch.

25. Different values of tensile strength did not affect the initial flexibility or deformations. For the Bridgemill bridge the FE-estimated collapse load increased from 296 kN/m to 489 kN/m (actual collapse load, 361 kN/m) as the arch's tensile strength increased from 0·1 MPa to 0·5 MPa. For the Strathmashie bridge the FE-estimated collapse load increased from 131 kN/m to 314 kN/m (actual collapse

load, 228 kN/m) as the arch's tensile strength increased from 0·1 MPa to 0·5 MPa. For the Barlae bridge the FE-estimated collapse load increased from 184 kN/m to 360 kN/m (actual collapse load, 296 kN/m) as the arch's tensile strength increased from 0·1 MPa to 0·5 MPa. Should a test be required to determine the compressive strength, as mentioned previously, tensile tests should also be carried out on as many samples as possible at the same time.

26. *The effect of varying the backfill's load dispersal angle.* Results of the parametric study on the effect of the backfill's load dispersal angle are presented in Figs 1(e), 2(e), 3(e) and 7. Varying the backfill's load dispersal angle had a significant effect on the estimated collapse loads but little effect on the slope of the initial elastic portion of the load-versus-deformation plot. For the Bridgemill bridge the FE-estimated collapse load increased from 320 kN/m to 381 kN/m (actual collapse load, 361 kN/m) as the backfill's load dispersal angle increased from the point load case through 0° to 55°. For the Strathmashie bridge the FE-estimated collapse load increased from 175 kN/m to 220 kN/m (actual collapse load, 228 kN/m) as the backfill's load dispersal angle increased from the point load case through 0° to 70°. For the Barlae bridge the FE-estimated collapse load increased from 247 kN/m to 310 kN/m (actual collapse load, 296 kN/m) as the backfill's load dispersal angle increased from the point load case through 0° to 48°. Different ranges of load distribution angle were used because of the geometries of the different arches; at no time was load dispersal beyond the springers permitted.

27. Given the importance of soil–structure interaction effects on the assessed capacity of an arch bridge, the authors recommend selection of a load dispersal angle consistent with the Boussinesq stress distribution's least significant stress-increase contour. The relevant point on the extrados forming the limit beyond which no stress should be distributed would then be the point where the 0·1 (or 10%) stress-influence-value contour intersected the extrados. The use of Boussinesq's method and its variants for stress dispersal above arch bridges is well documented elsewhere;[13,15,21] a detailed analysis is beyond the scope of this paper.

Conclusion

28. A commercially available finite-element suite[3] has been used successfully to study the behaviour of masonry arch bridges, with the following salient findings.

(*a*) The chosen FE analysis could model the load–definition behaviour extremely well in cases where the material properties were well known. Unfortunately this is often only the case for bridges where, for research purposes, tests to collapse have been undertaken, with associated material testing. Three bridges were assessed: bridges at Bridgemill (actual collapse load 361 kN/m, FE collapse load 362 kN/m), Strathmashie (actual collapse load 228 kN/m, FE collapse load 226 kN/m) and Barlae (actual collapse load 296 kN/m, FE collapse load 302 kN/m).

(*b*) The elastic modulus of the arch ring had no significant effect on the collapse load but it did affect deformation at lower loads.

(*c*) The compressive strength of the arch ring significantly affected the collapse load but had no significant effect on the initial load–deflection behaviour. For the Bridgemill bridge the estimated collapse load increased from 252 kN/m to 384 kN/m (actual collapse load, 361 kN/m) as the arch's compressive strength increased from 2 MPa to 15 MPa. For the Strathmashie bridge the estimated collapse load increased from 157 kN/m to 230 kN/m (actual collapse load, 228 kN/m). For the Barlae bridge the estimated collapse load increased from 180 kN/m to 321 kN/m (actual collapse load, 296 kN/m) over the same range.

(*d*) The tensile strength of the arch ring significantly affected the collapse load. For the Bridgemill bridge the estimated collapse load increased from 296 kN/m to 489 kN/m (actual collapse load, 361 kN/m) as the arch's tensile strength increased from 0·1 MPa to 0·5 MPa. For the Strathmashie bridge the estimated collapse load increased from 131 kN/m to 314 kN/m (actual collapse load, 228 kN/m). For the Barlae bridge the estimated collapse load increased from 184 kN/m to 360 kN/m (actual collapse load, 296 kN/m) over the same range.

(*e*) The load dispersal angle through the backfill had some influence on the collapse load, with wider dispersal giving reduced extrados stresses and hence lower deformations and higher collapse loads. Wide differences in arch–soil system geometries mean that for a full treatment of soil–structure interaction effects such as this, each case may have to be assessed on its own merits.

(*f*) The chosen FE suite performed at least as well as any of the chosen current assessment methods in the three cases presented here. A limitation on the use of FE-based assessment would be the time and computer power required for preprocessing and analysis of the data. It is recommended that FE methods are chosen only where the implicit cost merits their use.

Acknowledgement

29. The authors thank Dr T. G. Hughes

(University of Wales, Cardiff) for the use of the program CTAP, Professor W. J. Harvey (University of Exeter) and Dr F. W. Smith (University of Dundee) for the use of the program ARCHIE, and Dr Abdelmadjid Bensalem (Transport Research Laboratory, formerly at Napier University) for his assistance on this project.

References

1. Department of Transport. *The Assessment of Highway Bridges and Structures*. HMSO, London, 1997, Departmental Standard BD21/97.
2. Department of Transport. *The Assessment of Highway Bridges and Structures*. HMSO, London, 1997, Advice Note BA16/97.
3. FEA Ltd. *LUSAS*. Finite Element Analysis Ltd, Kingston upon Thames, 1993, Version 12, user manuals.
4. Hendry A. W., Davies S. R. and Royles R. *Test on Stone Masonry Arch at Bridgemill-Girvan*. Transport Research Laboratory, Crowthorne, 1985, TRL Contractor Report 7.
5. Page J. *Load Test to Collapse on Two Arch Bridges at Strathmashie and Barlae*. Transport Research Laboratory, Crowthorne, 1989, TRL Research Report 201.
6. Page J. *Masonry Arch Bridges: State of the Art Review*. HMSO, London, 1993.
7. Bridle R. J. & Hughes T. G. An energy method for arch bridge analysis. *Proceedings of the Institution of Civil Engineers, Part 2*, 1988, **89**, 375–385.
8. Harvey W. J. Application of the mechanism analysis to masonry arches. *Journal of the Institution of Structural Engineers*, 1988, **66**, No. 20, 77–84.
9. Department of Transport. *The Assessment of Highway Bridges and Structures*. HMSO, London, 1997, Advice Note BA16/97, Annex E, 4–6.
10. Ponniah D. A., Fairfield C. A. and Prentice D. J. Fill stresses in a new brick arch subject to heavy axle load tests. *Proceedings of the Institution of Civil Engineers: Structures and Buildings*, 1997, **123**, 173–185.
11. Fairfield C. A. and Ponniah D. A. Geotechnical considerations in arch bridge assessment. *Journal of the Institution of Highways and Transportation*, 1993, **40**, No. 7, 11–16.
12. Gong N. G. *Finite Element Analysis of Masonry Arch Bridges*. PhD thesis, University of Nottingham, 1992.
13. Fairfield C. A. and Ponniah D. A. Model tests to determine the effect of fill on buried arches. *Proceedings of the Institution of Civil Engineers: Structures and Buildings*, 1994, **104**, 471–482.
14. Fairfield C. A. and Ponniah D. A. Model tests to determine the effect of fill on buried arches [Discussion]. *Proceedings of the Institution of Civil Engineers: Structures and Buildings*, 1997, **123**, 247–250.
15. Fairfield C. A. *Soil–Structure Interaction in Masonry Arch Bridges*. PhD thesis, University of Edinburgh, 1994.
16. Fairfield C. A. and Ponniah D. A. *Earth Pressure Measurements at Kimbolton Butts Bridge, Cambridgeshire*. Transport Research Laboratory, Crowthorne, 1993, TRL Sub-Contractor Report.
17. Davey N. Tests on road bridges. *National Building Studies Research*, HMSO, London, 1953, **16**.
18. Bensalem A., Fairfield C. A. and Sibbald A. Non-destructive evaluation of the dynamic response of a brickwork arch. *Proceedings of the Institution of Civil Engineers: Structures and Buildings*, 1997, **122**, 69–82.
19. Sibbald A., Bensalem A. and Fairfield C. A. NDT of arch bridges. *Journal of the British Institute of Non-Destructive Testing*, 1995, **37**, No. 11, 864–870.
20. Armstrong D. M., Sibbald A., Fairfield C. A. and Forde M. C. Modal analysis for masonry arch bridge spandrel wall separation identification. *Non-destructive Testing & Evaluation International*, 1995, **28**, No. 6, 377–386.
21. Fairfield C. A. and Ponniah D. A. A method of increasing arch bridge capacity economically. *Proceedings of the Institution of Civil Engineers: Structures and Buildings*, 1996, **116**, 109–115.

Please email, fax or post your discussion contributions to the publisher: email: ttjournals@ice.org.uk; Fax: 0171 538 9620; or post to Terri Harding, Journals Department, Thomas Telford Limited, Thomas Telford House, 1 Heron Quay, London E14 4JD.

ARCH BRIDGE MECHANISM METHOD ASSESSMENT INCORPORATING DEFLECTION DEPENDENT SOIL PRESSURE UPDATING ALGORITHMS

Mr Kwooi-Hock Ng, Dr Charles A. Fairfield & Professor Alan Sibbald
Napier University, School of the Built Environment
10 Colinton Road, Edinburgh EH10 5DT, U.K.

KEYWORDS: Masonry, arch bridges, mechanism method

ABSTRACT
There are approximately 75000 brickwork or stone arch bridges in the United Kingdom the majority of which were built in the 19th Century. The assessment of these old structures is not a simple matter due to complex arch-soil interactions. One way of assessing an arch bridge's capacity is the mechanism method. Collapse load predictions from this method depend on an assumed distribution of lateral soil pressures around the extrados regardless of the arch's deformed shape. Undoubtedly, the arch profile at the onset of failure is far from its original shape. A mechanism analysis is accurate only when all the forces and their positions are accurately located. The authors developed a modified version of the mechanism method which includes arch deflections. A bi-linear backfill pressure distribution model, for both active and passive states, has also been incorporated so that mobilisation of backfill lateral resistance depends on the arch deflections. Analyses were carried out using this modified mechanism method on a full scale arch (Bargower bridge) which was tested to collapse in 1986. Results revealed that arch deflections had a significant influence on the prediction of the collapse load.

INTRODUCTION

The assessment of old arches is not a simple matter due to complex soil-arch interactions (Ng *et al.*, 1998). One way of assessing an arch bridge's capacity is the conventional mechanism method (Heyman, 1982). Collapse load predictions from this method depend on an assumed distribution of lateral soil pressures around the extrados regardless of the arch's deformed shape. Undoubtedly, the arch profile at the onset of failure is far from its original shape. A mechanism analysis is accurate only when all the forces and their positions are accurately located. A modified version of the mechanism method which includes arch deflections and a deflection dependent backfill pressure distribution model has been developed by the authors. This study aimed to introduce this modified mechanism method. Also investigated were the influence of: arch deflection, backfill ultimate active and passive deflections, live load dispersal angle, material densities, and the backfill's angle of shearing resistance on the predicted collapse load for Bargower bridge (Hendry *et al.*, 1986).

METHOD

An intact masonry arch is statically indeterminate. However, the arch becomes determinate when three hinges form in the arch ring due to the action of live load. In the mechanism method, the arch is assumed to be on the verge of collapse under a single axle load located on the pavement surface somewhere around one ¼-span point. Four hinge positions are selected to search for the minimum collapse load taking into account all forces acting whilst still fully containing the thrustline within the arch ring. Figure 1 shows a deflected arch at its ultimate limit state with four hinges at A, B, C, and D. As in the conventional mechanism method, there are three unknowns, the live load, and the vertical and horizontal abutment reactions to be sought in order to fully describe the thrustline around the arch ring. By taking moments about A, B, and C, three equilibrium

equations (Eqns 1 to 3) can be derived. In the authors' modified mechanism method, the arch bridge was assumed to be incapable of transmitting tensile stress and was infinitely strong in compression. The arch was idealised as a 2-D plane strain structure thereby ignoring the spandrel, wing, and parapet walls.

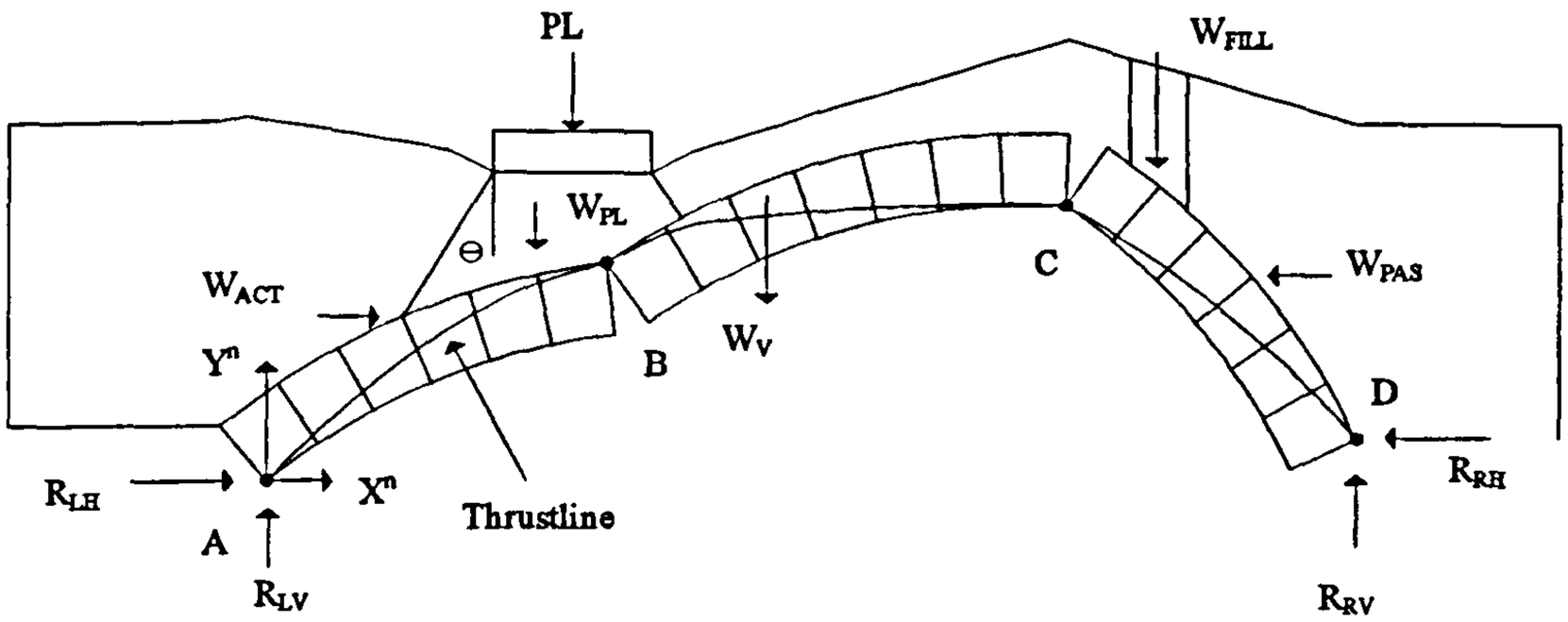

Figure 1 Idealisation of a typical arch bridge showing its failure mechanism

$$R_{RV}\left[X^D - X^C\right] = R_{RH}\left[Y^C_{IN} - Y^D_{EX}\right] + \sum_{n=C}^{D}\left[W^n_{FILL} + W^n_V\right]\left[X^n - X^C\right] + \sum_{n=C}^{D} W^n_{PAS}\left[Y^C_{IN} - Y^n_{EX}\right] \qquad \text{Eq. 1}$$

$$R_{RV}\left[X^D - X^B\right] = R_{RH}\left[Y^B_{EX} - Y^D_{EX}\right] + \sum_{n=B}^{D}\left[W^n_{FILL} + W^n_V + W^n_{PL}\right]\left[X^n - X^B\right] + \sum_{n=B}^{D}\left[W^n_{PAS} - W^n_{ACT}\right]\left[Y^B_{EX} - Y^n_{EX}\right] \qquad \text{Eq. 2}$$

$$R_{RV}\left[X^D - X^A\right] = -R_{RH}\left[Y^D_{EX} - Y^A_{IN}\right] + \sum_{n=A}^{D}\left[W^n_{FILL} + W^n_V + W^n_{PL}\right]\left[X^n - X^A\right] + \sum_{n=A}^{D}\left[W^n_{ACT} - W^n_{PAS}\right]\left[Y^n_{EX} - Y^A_{IN}\right] \qquad \text{Eq. 3}$$

By introducing Eqns 4 and 5, Eqns 1 to 3 can be expressed in matrix form as shown in Eq. 6.

$$\sum_{n=A}^{D}\left|I_n\right|_{\theta^n \le \theta} = I_p \qquad \text{Eq. 4}$$

$$W^n_{PL} = PL \times \sum_{n=B}^{D}\frac{\left|I_n\right|_{\theta^n \le \theta}}{I_P} \times \left[X^n - X^B\right] \qquad \text{Eq. 5}$$

$$\begin{bmatrix} R_{RV} \\ R_{RH} \\ PL \end{bmatrix}\begin{bmatrix} \left[X^D - X^A\right] & \left[Y^D_{EX} - Y^A_{IN}\right] & -\sum_{n=A}^{D}\frac{\left|I_n\right|_{\theta^n \le \theta}}{I_P}\left[X^n - X^A\right] \\ \left[X^D - X^C\right] & -\left[Y^C_{IN} - Y^D_{EX}\right] & 0 \\ \left[X^D - X^B\right] & -\left[Y^B_{EX} - Y^D_{EX}\right] & -\sum_{n=B}^{D}\frac{\left|I_n\right|_{\theta^n \le \theta}}{I_P}\left[X^n - X^B\right] \end{bmatrix} = \begin{bmatrix} \sum_{n=A}^{D}\left[W^n_{FILL} + W^n_V\right]\left[X^n - X^A\right] + \sum_{n=A}^{D}\left[W^n_{ACT} - W^n_{PAS}\right]\left[Y^n_{EX} - Y^A_{IN}\right] \\ \sum_{n=C}^{D}\left[W^n_{FILL} + W^n_V\right]\left[X^n - X^C\right] + \sum_{n=C}^{D} W^n_{PAS}\left[Y^C_{IN} - Y^n_{EX}\right] \\ \sum_{n=B}^{D}\left[W^n_{FILL} + W^n_V\right]\left[X^n - X^B\right] + \sum_{n=B}^{D}\left[W^n_{PAS} - W^n_{ACT}\right]\left[Y^B_{EX} - Y^n_{EX}\right] \end{bmatrix} \qquad \text{Eq. 6}$$

The three unknowns can be evaluated explicitly by solving the matrix in Eq. 6. Since the thrustline represents a line of zero bending moment, its position can be easily determined by taking moments about any point within the span of the arch.

Figure 2 shows the bi-linear backfill pressure distribution model incorporated in the modified mechanism method. This model is fully described by specifying the backfill's angle of shearing resistance, and its ultimate active and passive deflections. The backfill lateral pressure coefficient is evaluated using Rankine's theory of lateral earth pressure.

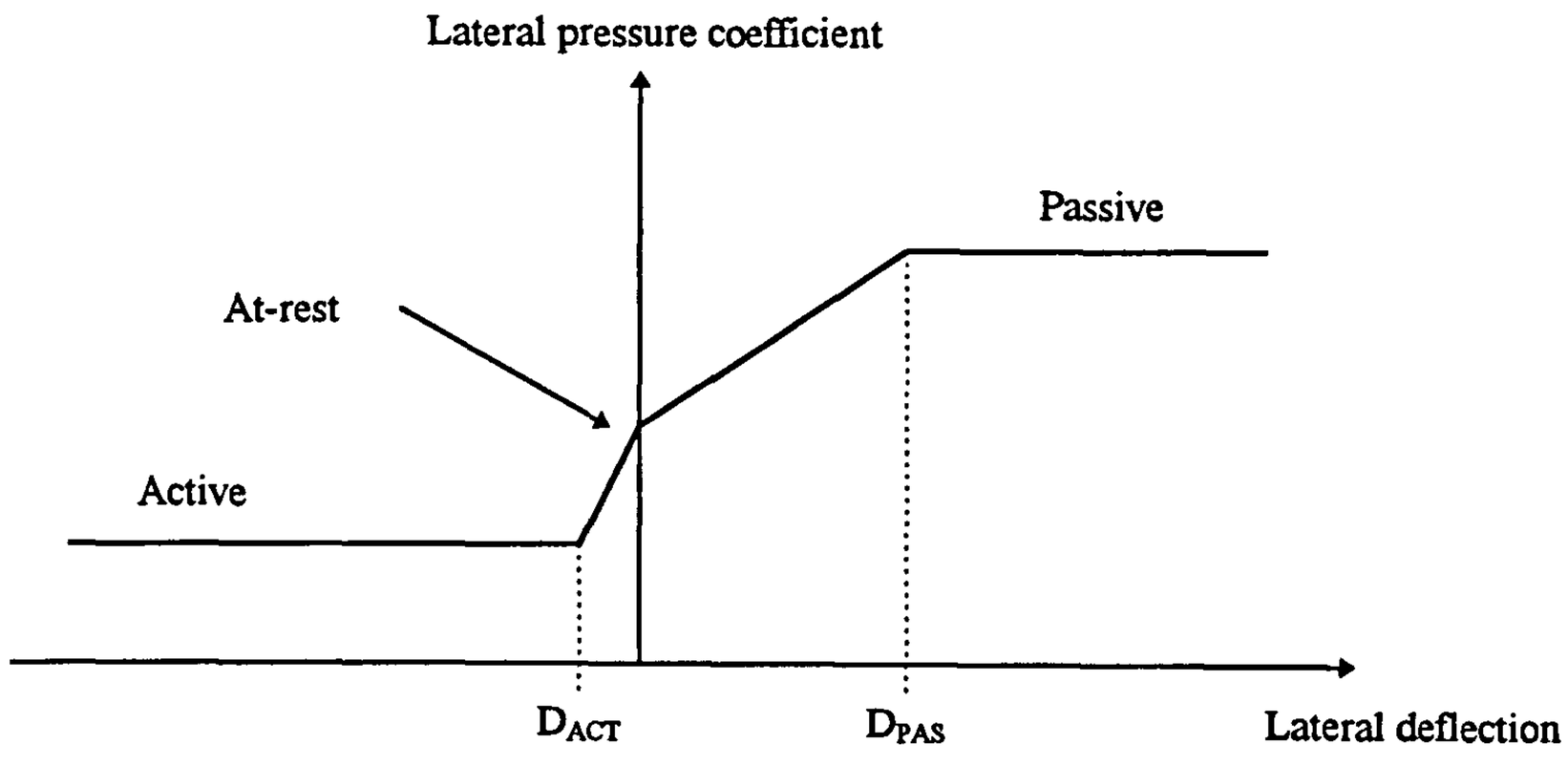

Figure 2 Bi-linear backfill lateral pressure model

This modified mechanism method has been coded in FORTRAN-77 for use in bridge assessment research. The particular subject of this paper, Bargower bridge, has the geometrical and material properties given in Table 1. In the ensuing parametric study, each parameter was varied individually whilst keeping the rest unchanged with their baseline values as in Table 1. The program allowed the user to specify an arch vertical deflection at hinge B (see Figure 1).

Table 1 Arch properties used in the modified mechanism method

Variable	Magnitude
Span	10360mm
Rise	5180mm
Ring thickness	558mm
Fill depth over the crown	1200mm
Width of load platen	750mm
Location of load platen's centreline	Directly above one $^1/_3$-span point
Backfill's bulk unit weight	$20kNm^{-3}$
Arch ring's bulk unit weight	$21kNm^{-3}$
Backfill's angle of shearing resistance	35°
Load dispersal angle	45°
Ultimate active lateral deflection	10mm
Ultimate passive lateral deflection	100mm

BARGOWER BRIDGE

Bargower bridge was built in 1859 with a span of 10360mm, a 16° skew angle, and a semicircular profile. Its geometrical and material properties were given in Table 1. No major defects were observed before testing and its condition was described as "moderate". However, the most significant defects found related to the tilt of the parapet walls and the longitudinal crack visible in the vault. At a depth of about 1m below the road surface, the fill was composed of large boulders interspersed with fine sand and silt. Above this level, the fill was a silty sand. The arch was tested to collapse using a line load of 750mm width located at one $^1/_3$-span point. The maximum recorded applied load was 645kN/m width. Failure was due to a combination of compressive and mechanism failures.

RESULTS

Results generated with the standard input variables given in Table 1 are presented. These are followed by the presentation of results from a parametric study which involved the ultimate active and passive lateral deflections, backfill and arch unit weights, backfill angle of shearing resistance, and live load dispersal angle. Unless otherwise stated the arch vertical deflection refers to that under the load platen's centreline.

Baseline Case Analytical Results For Bargower Bridge

Figure 3 shows the predicted variation in arch collapse load for different permitted arch vertical deflections. The predicted arch collapse load was 645kN/m width (*i.e.* matching that observed experimentally) only for an arch vertical deflection of 32.31mm. The corresponding collapse mode at this level is shown in Figure 4 with the deformed geometry exaggerated by a factor of 4.44.

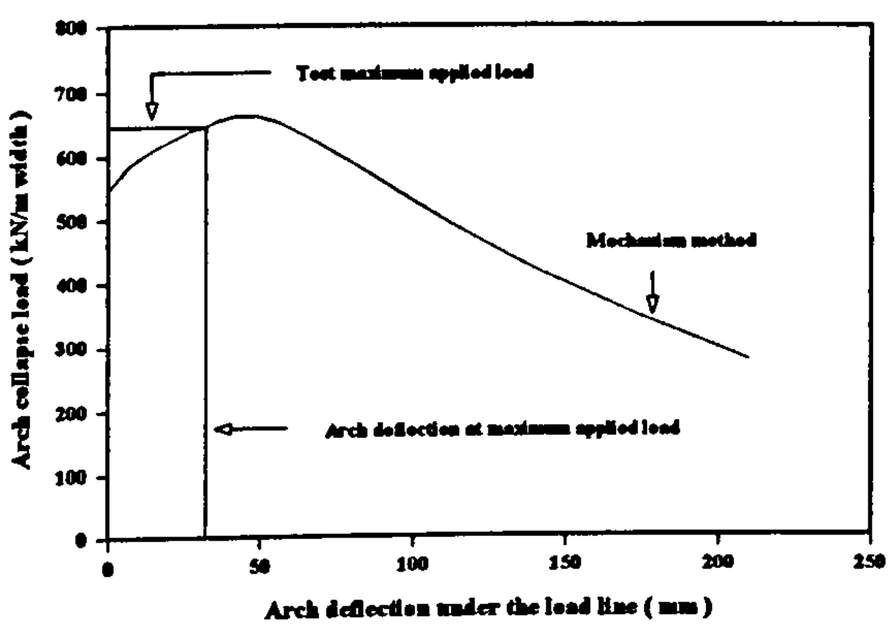

Figure 3 Collapse load *versus* arch deflection allowed

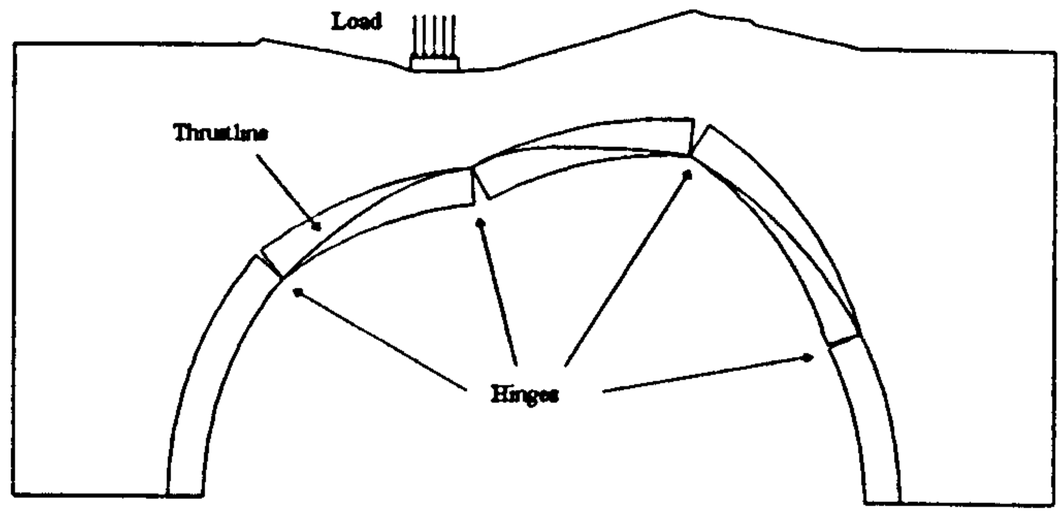

Figure 4 Predicted mechanism at 645kN/m

Figure 5 shows the effect of arch deflection on the distribution of backfill lateral pressure coefficient. With no arch deflection, an at-rest pressure coefficient of 0.4264 was recorded everywhere around the extrados except at the crown where the coefficient was zero since the slope of an intact arch at the crown is zero. By applying arch deflections, both backfill active and passive resistances were mobilised with the degree of mobilisation dependent on the arch deflection. One of the consequences of introducing arch deflections was to shift the point initially subjected to no backfill lateral pressure, from the crown towards the side remote from the load. This was because the point where the extrados had zero slope had no longer remained at the crown under the applied deflection. With an arch vertical deflection of 13.9mm, the maximum passive pressure coefficient was found to be 1.647 at a horizontal distance of 7193mm measured from the left abutment. This was equal to 37.4% mobilisation of full passive resistance. For a similar arch vertical deflection, full mobilisation of active resistance was recorded at most points on the loaded side. This was because full mobilisation of active resistance required only 10mm lateral deflection in this analysis. By applying arch vertical deflections of

32.31mm, 41.76mm, 52.22mm, and 62.68mm, the maximum evaluated passive coefficient were 3.039, 3.690, 3.690, and 3.690 respectively. Although a zone of full mobilisation of passive resistance was recorded with an arch vertical deflection of 41.76mm and beyond, it covered only a limited area and its magnitude was found to be gradually reduced to the at-rest coefficient at the right abutment.

Figure 6 presents a comparison between the distribution of backfill lateral pressure coefficient evaluated using the authors' bi-linear model (see Figure 2) and those being assumed in the conventional mechanism method. It is clear that both methods predicted significantly different distributions of backfill lateral pressure coefficient. Undoubtedly, the distribution of lateral pressure coefficient adopted in the conventional mechanism method is somewhat unrealistic since a constant mobilisation of backfill lateral resistance on each side of the arch is impossible as horizontal deflections vary around the arch ring.

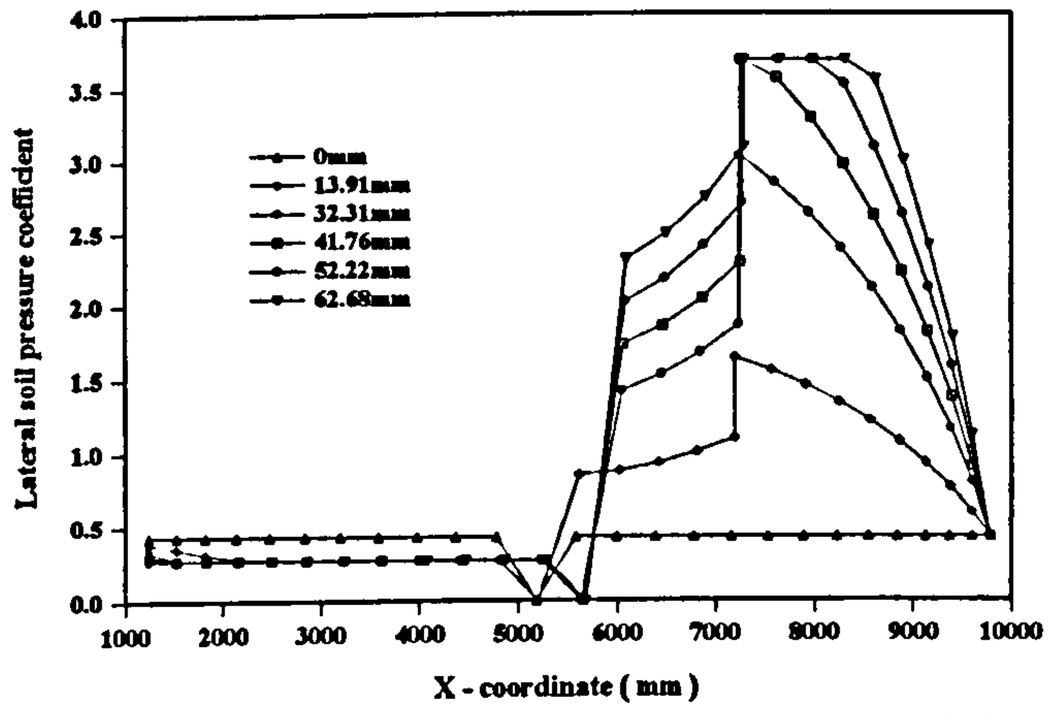

Figure 5 Distribution of lateral pressure coefficient

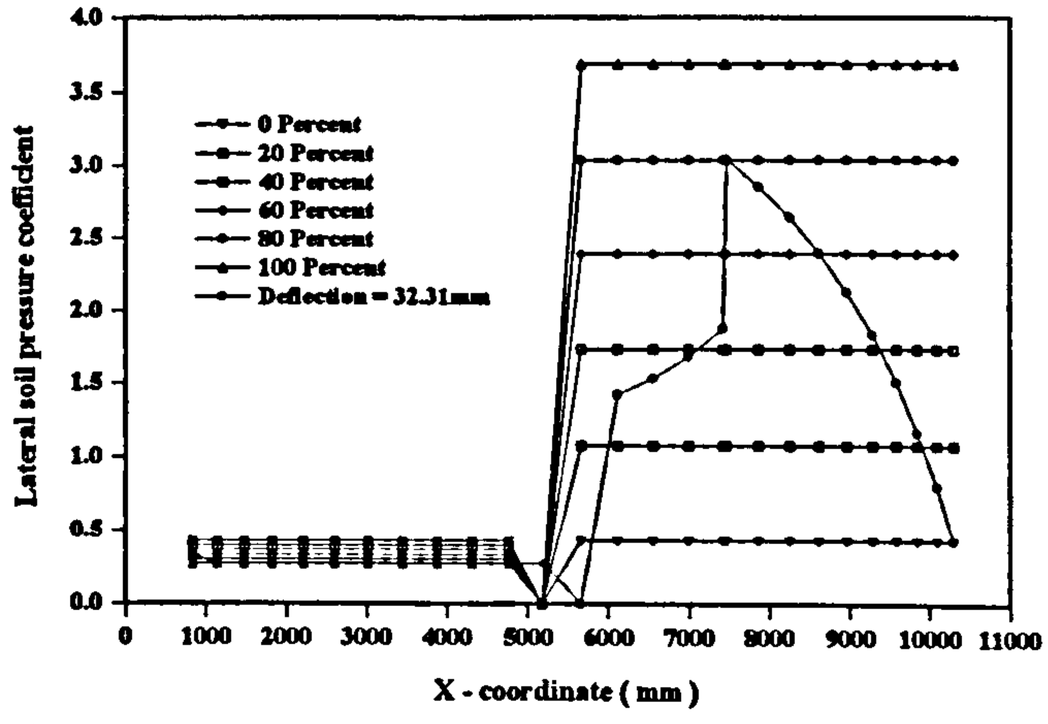

Figure 6 Distribution of lateral pressure coefficient with and without arch deflections

The Effect Of Varying The Backfill Ultimate Active Deflection

Figure 7 shows the effect of varying the backfill's ultimate active deflection on the collapse predictions. The ultimate active deflection did not have a significant influence on the assessment. All collapse load predictions converged for arch deflections over 30mm. Beyond 30mm deflection, the backfill's full active resistance had been mobilised and the distribution of active resistance around the extrados remained unchanged at its full active value even for further increases in arch deflection.

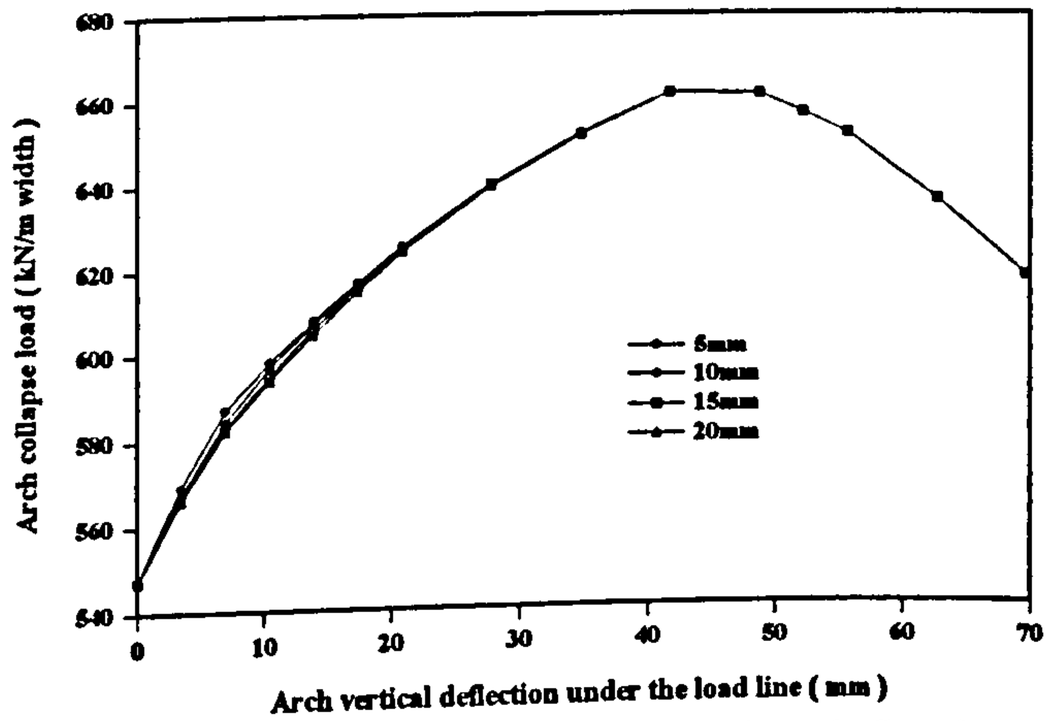

Figure 7 The effect of ultimate active deflection on the prediction of collapse load

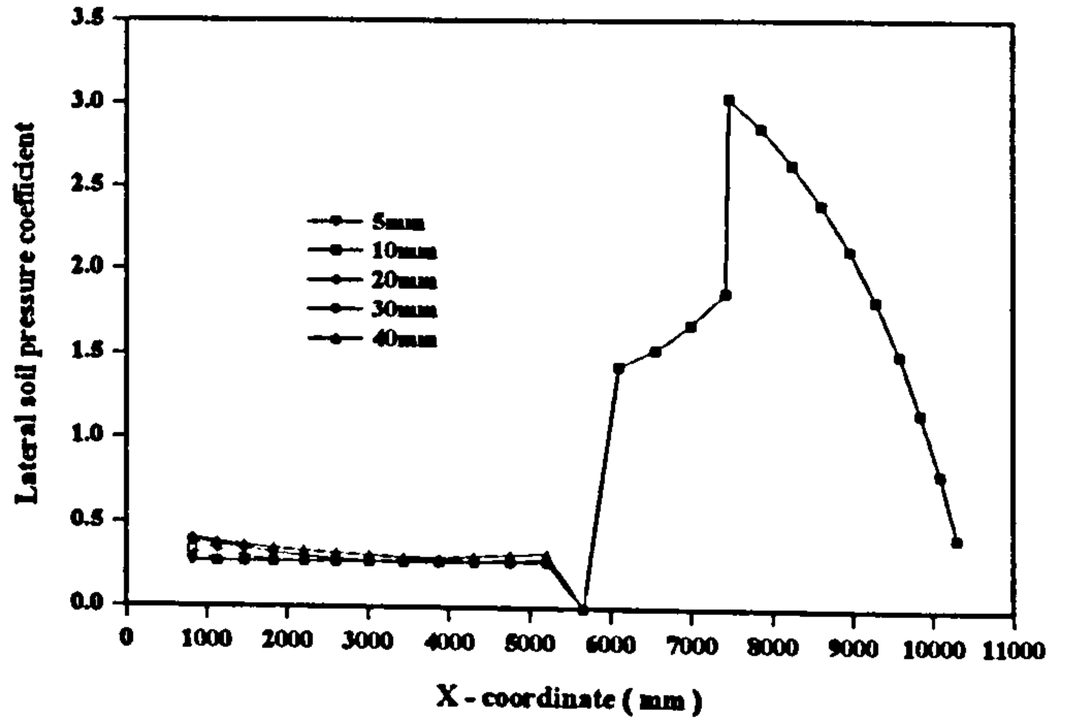

Figure 8 The effect of ultimate active deflection on the distribution of lateral pressure coefficient

Figure 8 shows the effect of varying the backfill's ultimate active deflection on the distribution of backfill lateral pressure coefficient with an arch deflection of 32.31mm. Its influence on the distribution of active pressure coefficient was not significant since the difference between at-rest and active coefficient was small compared with the range over which the passive coefficient could vary from the at-rest state.

The Effect Of Varying The Ultimate Passive Deflection

Figure 9 shows the effect of varying the ultimate passive deflection on the collapse load prediction. The lower the backfill ultimate passive deflection the greater its influence on the assessment. With a backfill ultimate passive deflection of 140mm, its influence on the assessment was insignificant since a much larger lateral deflection was required to mobilise the passive resistance. The peak evaluated arch collapse loads with backfill ultimate passive deflections of 25mm, 50mm, 75mm, 100mm, and 140mm were 995kN/m, 847kN/m, 743kN/m, 651kN/m, and 566kN/m respectively. Figure 10 shows the ultimate passive deflection's influence on the distribution of backfill lateral pressure coefficient for an arch vertical deflection of 32.31mm. The lower the backfill ultimate passive deflection, the higher the backfill lateral pressure coefficient. Full mobilisation of passive resistance was reached at a backfill ultimate passive deflection of 75mm with an arch vertical deflection of 32.31mm.

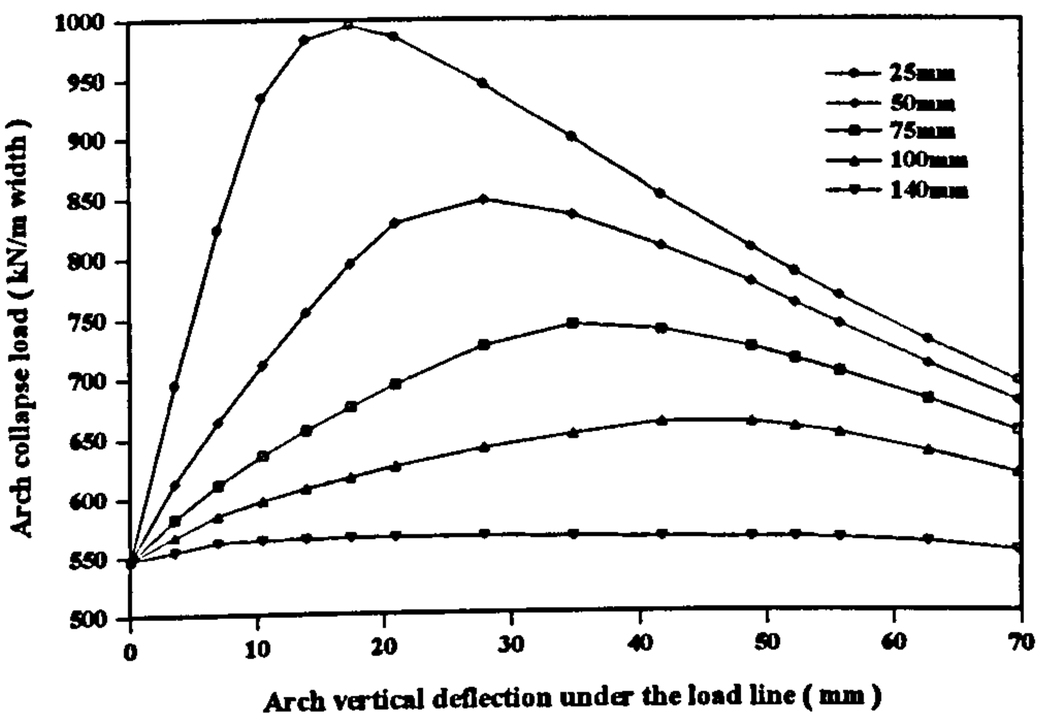

Figure 9 The effect of backfill ultimate passive deflection on the collapse load prediction

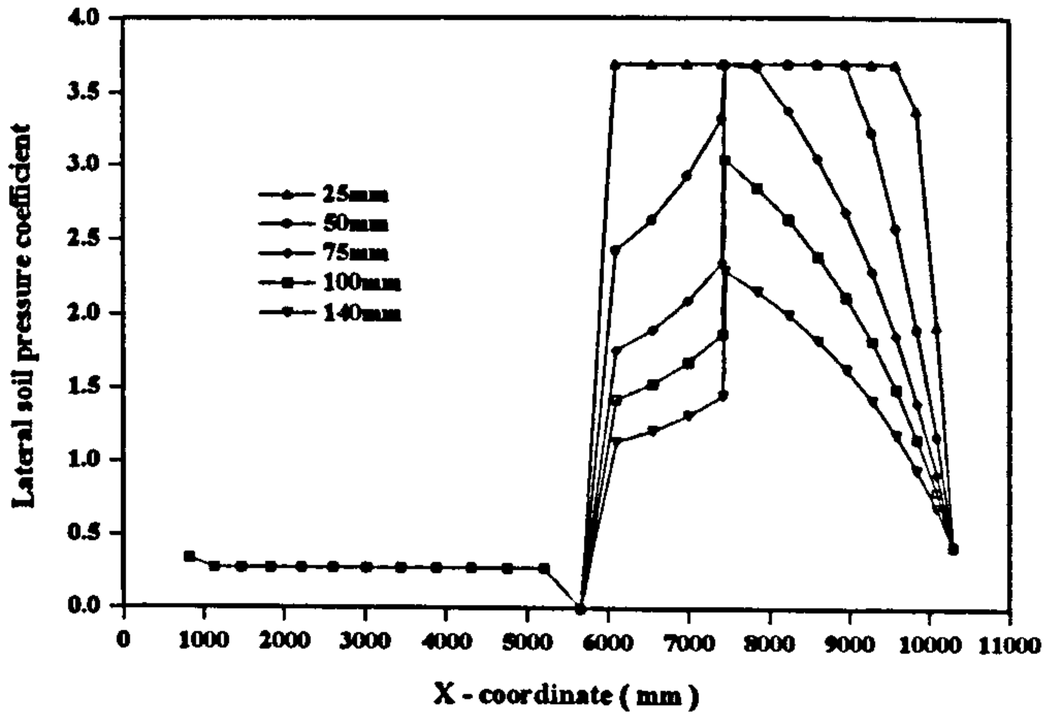

Figure 10 The effect of ultimate passive deflection on the backfill lateral coefficient distribution

The Effect Of Varying The Backfill Unit Weight

Figure 11 shows the effect of varying the backfill's unit weight on the collapse load prediction. The predicted capacity increased with the backfill unit weight for a given arch vertical deflection. By increasing the backfill unit weight from 18kN/m^3 to 21kN/m^3, the predicted peak arch collapse load increased from 602kN/m to 691kN/m for an arch vertical deflection of 41.76mm.

The Effect Of Varying The Arch Unit Weight

Figure 12 shows the effect of varying the arch unit weight on the prediction of arch collapse load. Increasing the arch unit weight was shown to increase the prediction of arch collapse load for a given arch vertical deflection. By increasing the arch unit weight from 19kN/m^3 to 22kN/m^3, the peak predicted arch collapse load was found to increase from 655.04kN/m to 664.50kN/m.

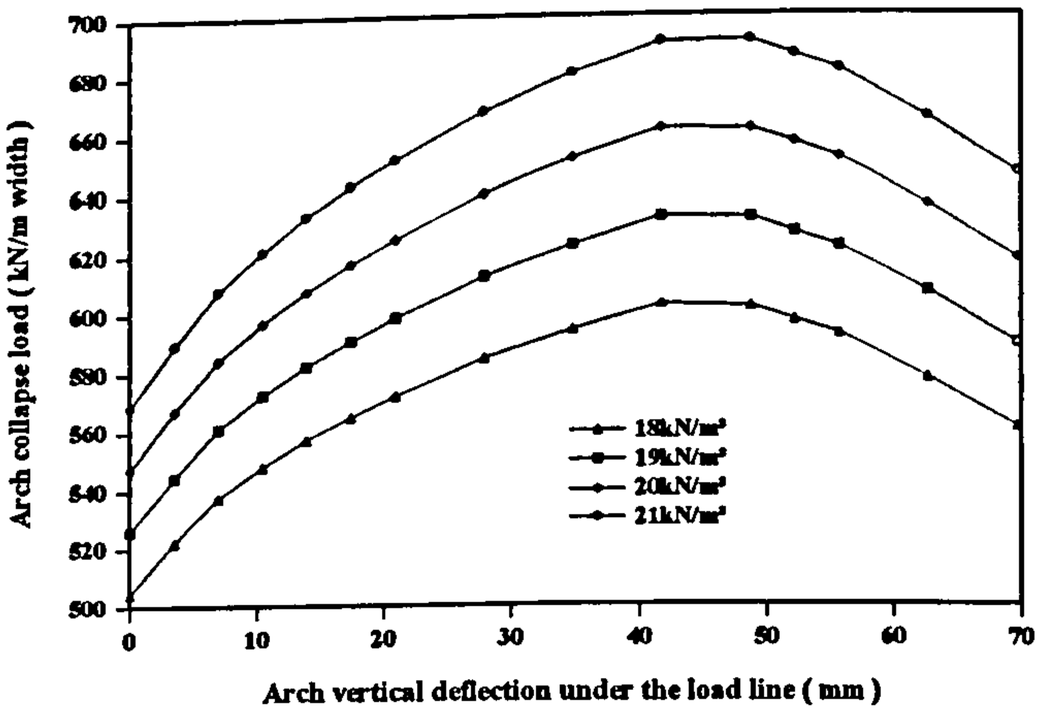

Figure 11 The effect of backfill unit weight on the collapse load

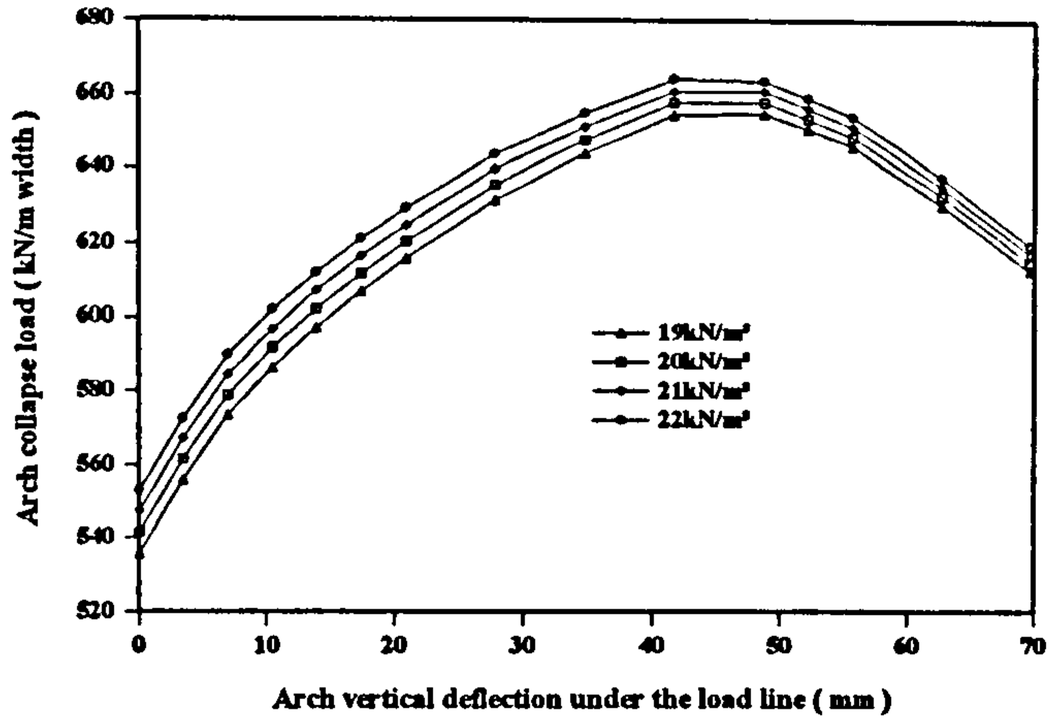

Figure 12 The effect of arch unit weight on the collapse load

The Effect Of Varying The Backfill Angle Of Shearing Resistance

Figure 13 shows the effect of varying the backfill's angle of shearing resistance on the predicted capacity. With the exception of very small arch vertical deflections, the capacity was higher with a higher backfill angle of shearing resistance. The trend in the relationship between arch deflection and predicted arch collapse load was influenced by the backfill's angle of shearing resistance. Referring to Figure 13, a backfill angle of shearing resistance of 25° gave a predicted collapse load that was reduced with increasing arch vertical deflections. With backfill angles of shearing resistance of 35° and 45° the predicted arch collapse loads increased with arch vertical deflections until reaching their maxima at 661kN/m and 901kN/m respectively.

The Effect Of Varying The Live Load Dispersal Angle

Figure 14 shows the effect of varying the live load dispersal angle on the collapse load prediction. Increasing the live load dispersal angle increased the assessed capacity over the range of arch deflections considered.

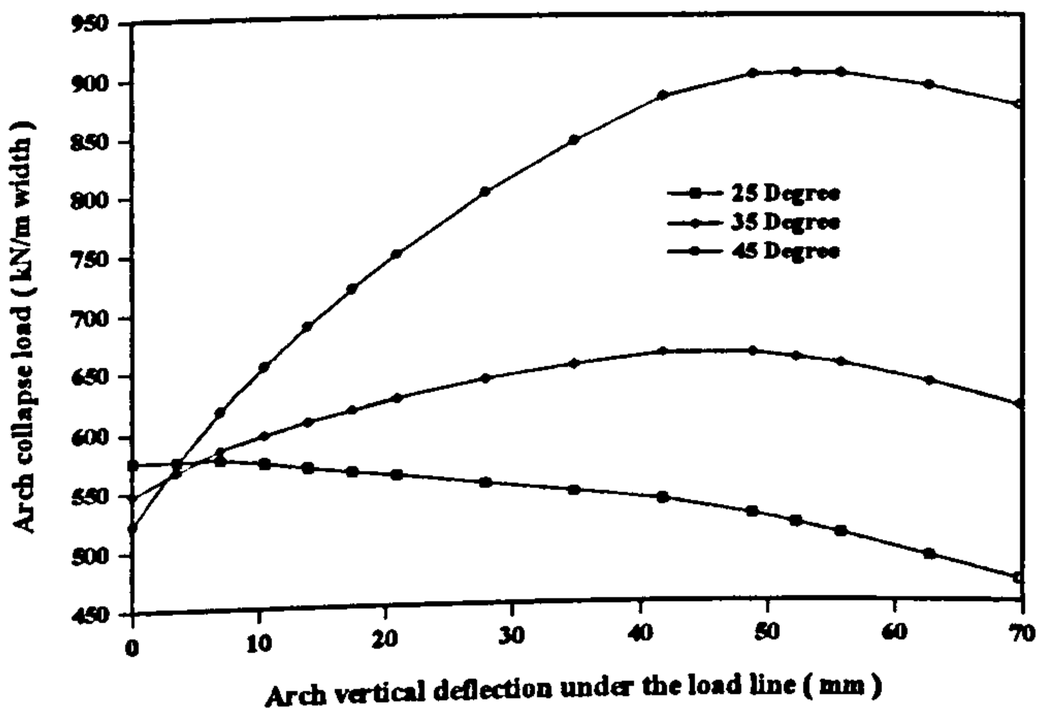

Figure 13 The effect of backfill angle of shearing on the collapse load prediction

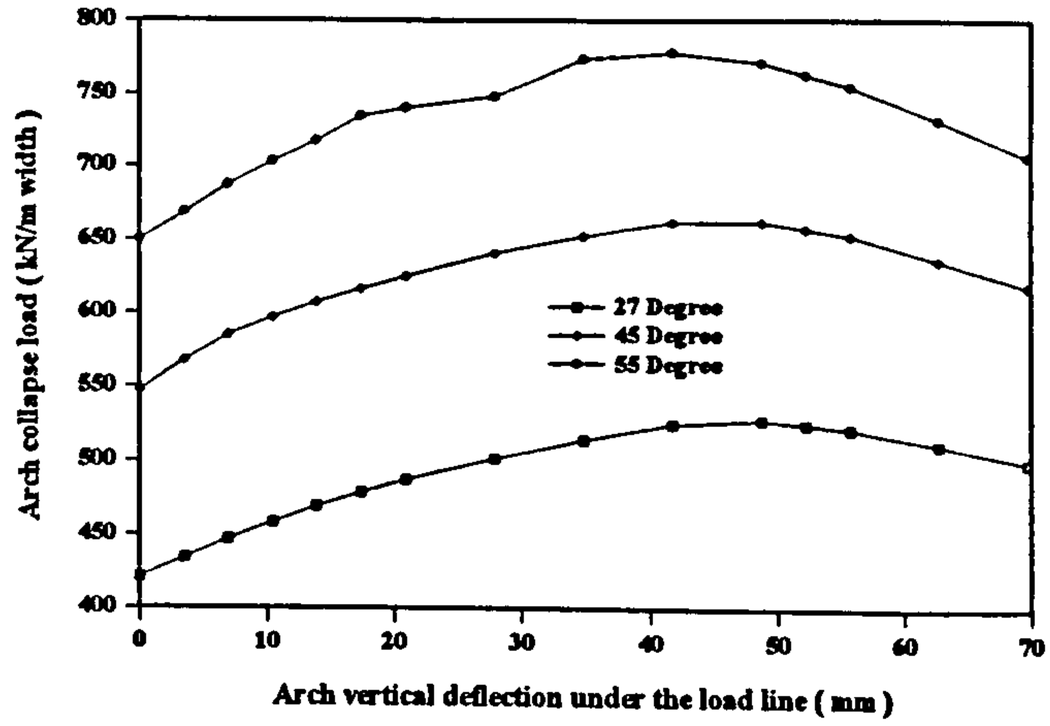

Figure 14 The effect of live load dispersal angle on the collapse load prediction

DISCUSSION OF KEY RESULTS

The modified mechanism method has been used to analyse Bargower bridge. Parametric studies were performed to investigate the influence of the arch deflection, ultimate active and passive deflections, backfill and arch unit weights, backfill angle of shearing resistance, and the live load dispersal angle.

The modified mechanism method predicted an arch collapse load of 645kN/m width with an arch vertical deflection of 32.31mm (equivalent to 45mm vertical movement at hinge C). These results compared well with the test maximum applied load of 645kN/m width with an arch vertical deflection of 32mm ± 0.5mm. Referring to Figure 3, it could be seen that the prediction of arch collapse load was found to increase with arch deflection until it reached its maximum. The arch deflection had two major influences on the capacity prediction in this modified mechanism method. With a deflected arch, the thrustline migrates more readily to the intrados and extrados, as shown in Figure 1, to form the failure mechanism thereby lowering the predicted collapse load. However, deflecting an arch also, at the same time, mobilises backfill resistance which helped to stabilise the arch. The capacity of a deflected arch depended on the loss of strength due to the deflected arch geometry and the gain of strength due to mobilisation of passive resistance. In the case of Bargower bridge, the gain of strength due to mobilisation of passive resistance was found to be more significant that lost due to the deflected geometry until a maximum vertical deflection of 41.76mm. Beyond this deflection the arch capacity was reduced with further arch deflections.

Figure 5 showed the influence of arch deflection on the backfill's lateral pressure coefficient distribution. A full mobilisation of the passive resistance was found at an arch deflection of 41.76mm. The peak backfill passive coefficient did not occur at the crown since hinge C (Figure 1) was located away from the crown. A comparatively small arch vertical deflection was enough to fully mobilised the backfill's active resistance.

The backfill ultimate active deflection, as expected, did not have a significant influence on the predicted collapse load and distribution of backfill pressure coefficient. This was because active forces were negligible compared to the system's self-weight and the backfill's passive resistance. It could be seen from Figure 7 that at, and above, 30mm vertical arch deflection, all capacity predictions were identical (regardless of the backfill's chosen ultimate active deflection) because the active resistance was fully mobilised.

The backfill's ultimate passive deflection had a dramatic influence on the prediction of arch collapse load and the distribution of backfill lateral pressure coefficient. It could be seen from Figure 9 that, with lower backfill ultimate passive deflections, the predictions of arch collapse load were found to increase with arch deflections until they reached their maxima. Its influence was particularly significant in this case since Bargower bridge was a deep arch with a significant amount of backfill on both sides of the span enhancing the soil-structure interaction effects. However, its influence also depended on the backfill's angle of shearing resistance. The effect would be more dramatic with a higher backfill angle of shearing resistance.

The backfill and arch unit weights influenced the capacity predictions. In the case of Bargower bridge a substantial depth of fill of 1.2m was used to cover the arch rendering the backfill unit weight so influential. However, the arch's unit weight was found to have a comparatively low influence on the capacity assessment as its volume was not as large as the backfill's. It is expected that the self-weight of an arch bridge is the most important factor in determining an arch's capacity since the failure load of an arch bridge is the load required to rotate three large arch segments (Figure 1) against gravitational attraction to form a mechanism.

The backfill angle of shearing resistance had a significant influence on the prediction of arch collapse loads. This arose partly from the large fill depth over the crown as well as the geometry of the arch allowing

substantial soil-structure interaction to take place. As mentioned previously, boulders were found on both sides of the arch acting as backing. This might have affected the system's behaviour during testing. However, nothing has been done in the authors' analyses to modify the backfill properties to account for the existence of this stiffer backing around the haunches.

The live load dispersal angle, as expected, had a significant influence on the collapse load predictions. It is still a subject of dispute as to what actual live load dispersal angle should be used in this type of analysis. A 27° dispersal angle is recommended by the Department of Transport (DETR, 1997). However, a live load dispersal angle of 65° was recorded in the full scale testing of Kimbolton Butts bridge, Cambridgeshire (Ponniah *et al.*, 1996). A 45° dispersal angle was used in this research, except during the parametric study on the load dispersal angle itself.

DISCUSSION OF THE UNDERLYING ASSUMPTIONS IN THE AUTHORS' METHOD

The authors' modified mechanism method assumes that the arch has no tensile strength and is infinitely strong in compression. The former is justifiable since most existing arches have been subjected to cyclic loading for over 100 years and therefore their residual tensile strength, if any, is negligible. The tensile strength of an arch would be more important only in the case of a newly built arch.

The compressive failure of the arch has been incorporated in conventional mechanism assessments (Smith, 1991). The arch's compressive strength was claimed to be the combined compressive strength of the voussoir unit and the mortar joint. The combined compressive strength of a masonry prism is much lower than that of the voussoir unit itself since the failure of a masonry prism is due to a stretching effect induced in the mortar which has a higher Poisson's ratio. It is very clear that the compressive failure of an arch, if any, happens at hinges, usually near the load line, with a high concentrated stress due to a limited contact area between the voussoir unit and the mortar joint. This is completely different from that defined in the compressive failure of a masonry prism which has been widely used by various researchers in the mechanism method. In reality, an apparent compressive failure occurs simultaneously with the collapse of the arch. This implies that shortly before the occurrence of compressive failure the applied live load would have almost reached the maximum. Is reducing the arch ring thickness by considering a zone of thrust due to compressive failure a solution adequately considering potential compressive failure in the mechanism method?

LIMITATIONS OF THE AUTHORS' METHOD

One of the difficulties in using the authors' modified mechanism method is determining the arch vertical deflection at which the applied load reaches its maximum. This depends on the arch geometry as well as its material properties. Full-scale tests revealed that the arch vertical deflections by which the arch capacity reached its maximum were between 20mm and 50mm. More work is underway to search for an empirical relationship, using full-scale test results, to relate an arch's vertical deflection with which it achieved its maximum capacity to its geometry.

Apart from the aforementioned difficulties, the arch bridge is assumed to be idealised to a 2-D plane strain structure in the mechanism method. This ignores contributions from the spandrel, wing, and parapet walls. In reality, the arch behaviour and hinge positions change if the arch is not surrounded by these various walls.

CONCLUSIONS

1. A modified mechanism method has been successfully used to analyse Bargower bridge. A bi-linear backfill lateral pressure model was incorporated into the simple mechanism method making the backfill lateral pressure distribution more realistic.

2. Arch deflections dramatically affected the capacity assessment and backfill lateral pressure coefficients.

3. The backfill's ultimate passive deflection significantly influenced the predicted collapse load but the corresponding active state deflections had little effect on the assessed capacity.

4. The backfill and arch unit weights influenced the predicted collapse load: the former was more influential due to the backfill's greater mass as a proportion of the total systems self-weight.

5. The backfill's angle of shearing resistance and its ability to disperse live load had a significant influence on the predicted collapse load.

REFERENCES

Department of Transport. (1997) *Departmental Standard BD21/97: The assessment of highway bridges and structures.* HMSO, London, U.K.

Hendry, A.W., Davies, S.R., Royles, R., Ponniah, D.A., & Forde, M.C. (1986) *Load test to collapse on a masonry arch bridge at Bargower, Strathclyde.* TRL Contractor Report 26, TRL, Crowthorne, U.K.

Heyman, J. (1982) *The masonry arch.* Ellis Horwood, Chichester, U.K.

Ng, K.-H., Fairfield, C.A. & Sibbald, A. (1998) Track bed geotechnology: its effect on the collapse load of railway arch bridges. *Proc 1st Int. Conf. Railway Engng*, Uxbridge, U.K.

Ponniah, D.A., Prentice, D.J. & Fairfield, C.A. (1996) The effect of the overlying fill on stresses in a new arch bridge, *Recent Advances in Bridge Engng*, CIMNE, Barcelona, Spain.

Smith, F. W. (1991) *Load path analysis of masonry arches.* Ph.D. Thesis, Univ. of Dundee, Dundee, U.K.

RELIABILITY OF ARCH BRIDGES BY MONTE CARLO SIMULATION

Mr K.-H. Ng & Dr C.A. Fairfield
Napier University
School of the Built Environment
10 Colinton Road
Edinburgh EH10 5DT,U.K.

KEYWORDS: Masonry arch bridges, Monte Carlo simulation, Mechanism method

ABSTRACT
A novel risk assessment program for masonry arch bridges integrating the Monte Carlo simulation with the mechanism method has been developed by the authors. A parametric study was carried out on Barlae bridge involving: arch span, live load dispersal angle, backfill lateral pressure mobilisation, material bulk unit weight, and backfill angle of shearing resistance. These parameters, along with their standard deviations were amongst those most significantly affecting collapse load predictions. Apart from these, the convergence of the results was also checked by varying the number of iterations, the random number generator's seed, the number of arch segments, and each variable's end limit. This integrated Monte Carlo simulation is offered for incorporation within routine assessment methods. Its principal benefit lies in providing engineers with a feel for the reliability of their analyses.

INTRODUCTION

There are around 75,000 brickwork or stone arch bridges in the U.K. most of which were built between the 18th and 20th Centuries. Despite their age, these arches still carry enormous traffic loads which are ever increasing both in magnitude and frequency. Such increases compelled highway authorities to undertake assessment and strengthening works on many masonry arch bridges. The masonry arch bridge is a complex three dimensional structure with contributions to its capacity coming from soil-arch interactions, spandrel, parapet, and wing walls. In most assessment methods, the arch is idealised as a simple 2-D plane strain system. Soil-arch interaction is often considered in a speculative manner and material properties are assumed constant, isotropic and/or homogeneous. These idealisations and assumptions can render a capacity prediction no better than an educated guess.

METHOD

The current risk assessment program integrating the Monte Carlo simulation and the mechanism method has been coded by the authors as a FORTRAN77 algorithm. The program starts by generating the random variables and then evaluating the arch's collapse load distribution. Finally the program carries out statistical analyses on the derived results. A brief description of the two methods (traditional mechanism analysis and Monte Carlo simulation) follows.

Mechanism Method

An intact masonry arch is statically indeterminate but becomes determinate when three hinges form in the ring. In this method, the arch bridge is assumed to be at the onset of collapse under a single line load located on the pavement surface above one ¼-span point. Four hinges are to be searched for iteratively to find the minimum collapse load whilst still fully containing the thrustline within the arch ring. Figure 1 shows an arch at its ultimate limit state with four hinges formed at A, B, C, and D. There are three unknowns; the collapse load, and the vertical and horizontal abutment reactions. Three equilibrium equations can be derived by taking moments about A, B, and C giving Eqns (1), (2) and (3) respectively.

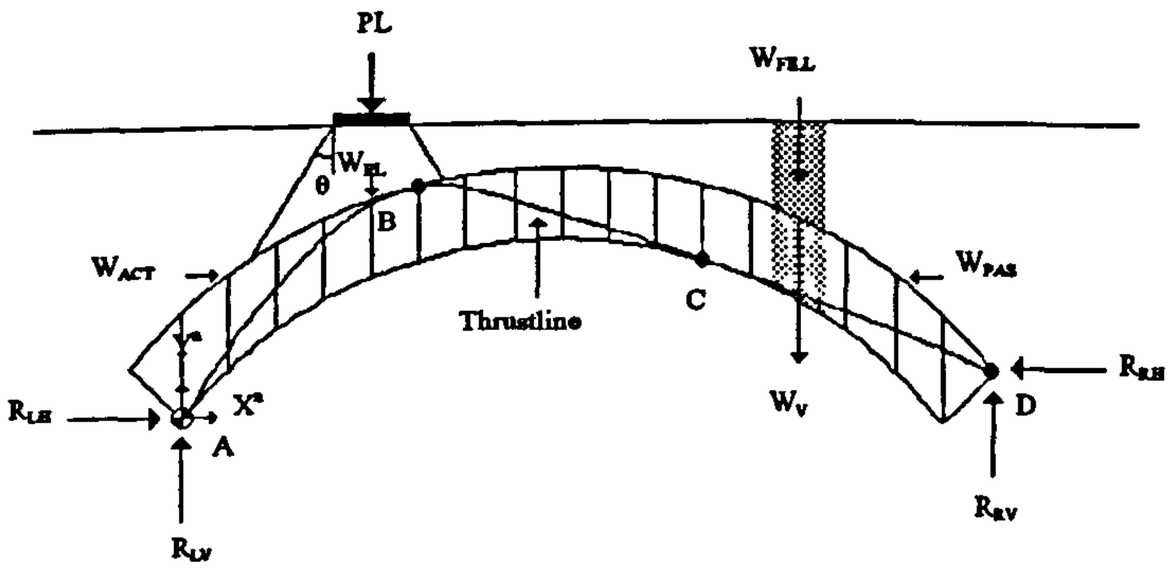

Figure 1. Idealisation of an arch bridge with a typical collapse mechanism under load, PL shown

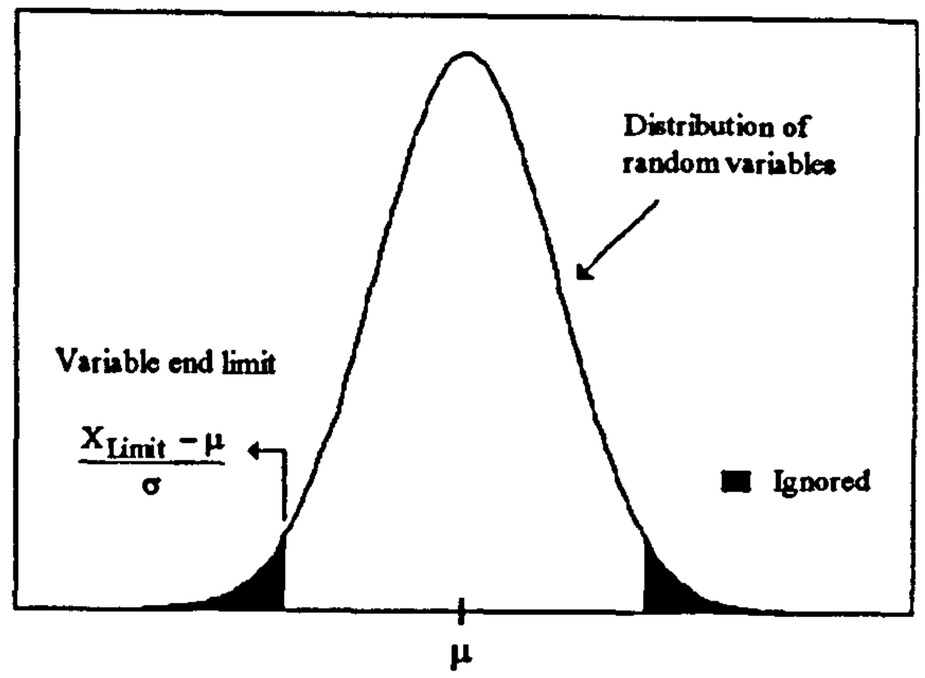

Figure 2. Distribution of random variables and the variable end limits

$$R_{RV}\left[X^D - X^C\right] = R_{RH}\left[Y_{IN}^C - Y_{EX}^D\right] + \sum_{n=C}^{D}\left[W_{FILL}^n + W_V^n\right]\left[X^n - X^C\right] + \sum_{n=C}^{D} W_{PAS}^n\left[Y_{IN}^C - Y_{EX}^n\right] \quad (1)$$

$$R_{RV}\left[X^D - X^B\right] = R_{RH}\left[Y_{EX}^B - Y_{EX}^D\right] + \sum_{n=B}^{D}\left[W_{FILL}^n + W_V^n + W_{PL}^n\right]\left[X^n - X^B\right] + \sum_{n=B}^{D}\left[W_{PAS}^n - W_{ACT}^n\right]\left[Y_{EX}^B - Y_{EX}^n\right] \quad (2)$$

$$R_{RV}\left[X^D - X^A\right] = -R_{RH}\left[Y_{EX}^D - Y_{IN}^A\right] + \sum_{n=A}^{D}\left[W_{FILL}^n + W_V^n + W_{PL}^n\right]\left[X^n - X^A\right] + \sum_{n=A}^{D}\left[W_{ACT}^n - W_{PAS}^n\right]\left[Y_{EX}^n - Y_{IN}^A\right] \quad (3)$$

Introducing Eqns (4) and (5) allows Eqns (1) to (3) to be expressed in matrix form (Eqn (6)).

$$\sum_{n=A}^{D}\left|I_n\right|_{\theta^n \le \theta} = I_p \quad (4)$$

$$W_{PL}^n = PL \times \sum_{n=B}^{D}\frac{\left|I_n\right|_{\theta^n \le \theta}}{I_P} \times \left[X^n - X^B\right] \quad (5)$$

$$\begin{bmatrix} R_{RV} \\ R_{RH} \\ PL \end{bmatrix}\begin{bmatrix} \left[X^D - X^A\right] & \left[Y_{EX}^D - Y_{IN}^A\right] & -\sum_{n=A}^{D}\frac{\left|I_n\right|_{\theta^n \le \theta}}{I_P}\left[X^n - X^A\right] \\ \left[X^D - X^C\right] & -\left[Y_{IN}^C - Y_{EX}^D\right] & 0 \\ \left[X^D - X^B\right] & -\left[Y_{EX}^B - Y_{EX}^D\right] & -\sum_{n=B}^{D}\frac{\left|I_n\right|_{\theta^n \le \theta}}{I_P}\left[X^n - X^B\right] \end{bmatrix} = \begin{bmatrix} \sum_{n=A}^{D}\left[W_{FILL}^n + W_V^n\right]\left[X^n - X^A\right] + \sum_{n=A}^{D}\left[W_{ACT}^n - W_{PAS}^n\right]\left[Y_{EX}^n - Y_{IN}^A\right] \\ \sum_{n=C}^{D}\left[W_{FILL}^n + W_V^n\right]\left[X^n - X^C\right] + \sum_{n=C}^{D} W_{PAS}^n\left[Y_{IN}^C - Y_{EX}^n\right] \\ \sum_{n=B}^{D}\left[W_{FILL}^n + W_V^n\right]\left[X^n - X^B\right] + \sum_{n=B}^{D}\left[W_{PAS}^n - W_{ACT}^n\right]\left[Y_{EX}^B - Y_{EX}^n\right] \end{bmatrix} \quad (6)$$

The arch collapse load, and all abutment reactions can be found explicitly by solving Eqn (6). The thrustline, representing a line of zero bending moment, is then located by taking moments about any point.

Monte Carlo simulation

The mechanism method analyses were performed in conjunction with a Monte Carlo simulation whereby the mechanism method was re-run many times. All variables in this simulation were produced by a computer based random number generator and were different for each iteration. Each variable was generated from a Gaussian distribution with specified mean and standard deviation. Statistical checks were carried out for all generated random variables so that they were close to their predefined means and standard deviations. Results revealed that accuracy of the generated random variable depended on the number of iterations: a minimum of 5000 iterations was sufficient for achieving acceptable accuracy.

Measures were also taken to prevent random variables being generated outwith a reasonable range. Referring to Figure 2, two limits were set in such a way that the probability represented by the shaded area on each side was equal to a predefined limit. This limit is subsequently referred to as the variable end limit.

Finally the analysis consisted of a series of statistical evaluations of the generated results in terms of mean, standard deviation, skewness, kurtosis, and range. The probability of overestimating the collapse load can also be evaluated with this program if the actual collapse load is known. Table 1 shows the standard set of parameters used in this Monte Carlo simulation. The probability of failure in this paper refers to the probability of overestimating the arch collapse load. In the case of the parametric study, only one parameter was varied at one time; other parameters were kept constant as given in Table 1.

Table 1 Standard values for the variables used in the analysis of Barlae bridge

Variable	Value	Variable	Value
Span	9197.5mm	Permitted backfill active pressure mobilisation	80%
Rise	1695mm	Permitted backfill passive pressure mobilisation	50%
Ring thickness	450mm	Backfill angle of shearing resistance	35°
Backfill depth at the crown	295mm	Location of the centreline of load platen	2299mm
Width of load platen	750mm	Variable's standard deviation	3%
Backfill bulk unit weight	20kNm^{-3}	Seed for random number generator	773311
Arch bulk unit weight	23kNm^{-3}	Number of iterations	30000
Live load dispersal angle	35°	Variable end limit	3%
Number of arch segments	40		

BARLAE BRIDGE

Barlae bridge was an ashlar masonry arch with a 29° skew angle. It was tested to collapse by the Transport Research Laboratory (Page, 1989). No major defects were found on the bridge before applying a transverse 750mm wide line load at the ¼-span point. The ultimate load recorded was 296kN/m width perpendicular to the span. The arch span, rise at the crown, ring thickness and fill depth at the crown were 9197.5mm, 1695mm, 450mm and 295mm respectively. Since the arch was skewed, there was no clear indication as to how to consider the arch span in the current 2-D analysis. The span was taken as 9197.5mm, the average of the shortest and longest distances measured square along the bridge. A range of possible spans will be considered in the ensuing parametric study anyway to allay fears of conservatism.

RESULTS

The following sections present data from the Monte Carlo simulation and mechanism method on a parameter by parameter basis. A summary of the statistics applicable to the predicted collapse load (mean, standard deviation, skewness, kurtosis, range, and probability of failure) is given in Table 2 for those parameters significantly affecting the collapse load. Comparisons were also made with capacity predictions by CTAP (Bridle & Hughes, 1990), ARCHIE (Smith, 1991), and a plastic analysis (Heyman, 1982).

Standard results

Figure 3 shows results from the Monte Carlo simulation using the variables listed in Table 1. A classical bell shaped distribution was obtained. The full scale test at Barlae revealed that the arch collapsed at 296kN/m width. The shaded region in Figure 3 represents the probability of overestimating the collapse load; here this amounted to 11.8%. The statistical properties (mean, standard deviation, skewness, kurtosis, maximum and minimum) of the predicted arch collapse load distribution were 265kN/m, 18.2kN/m, 0.21, 2.75, 332.4kN/m, and 213.1kN/m respectively.

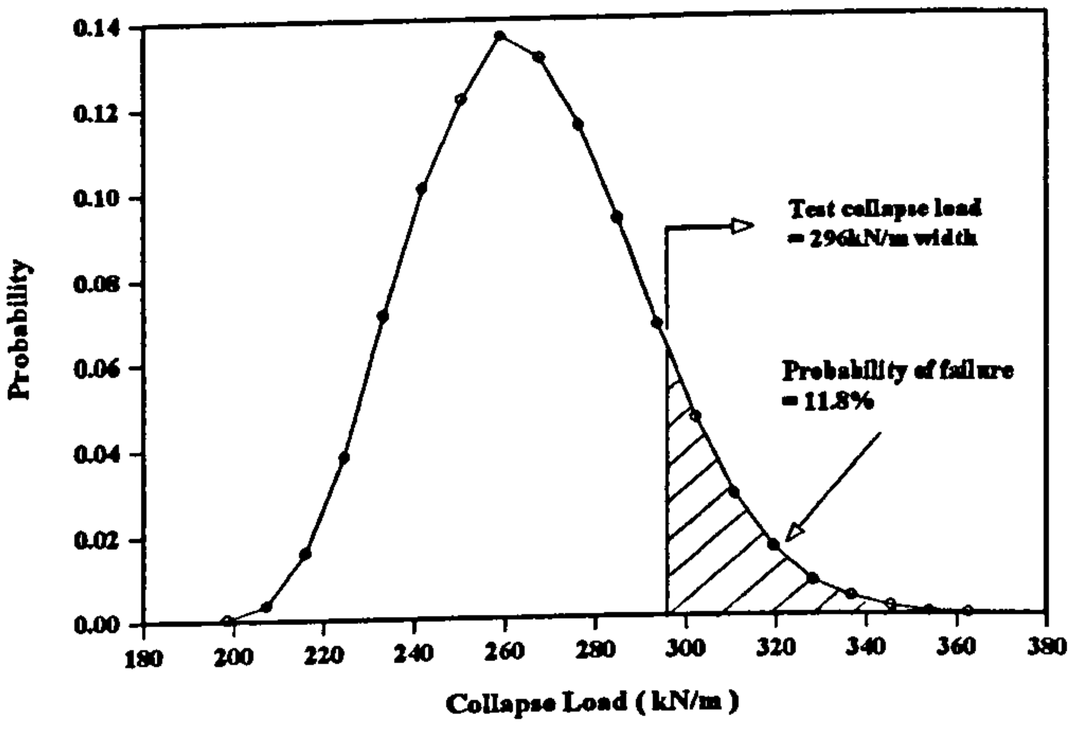

Figure 3. Distribution of predicted collapse loads

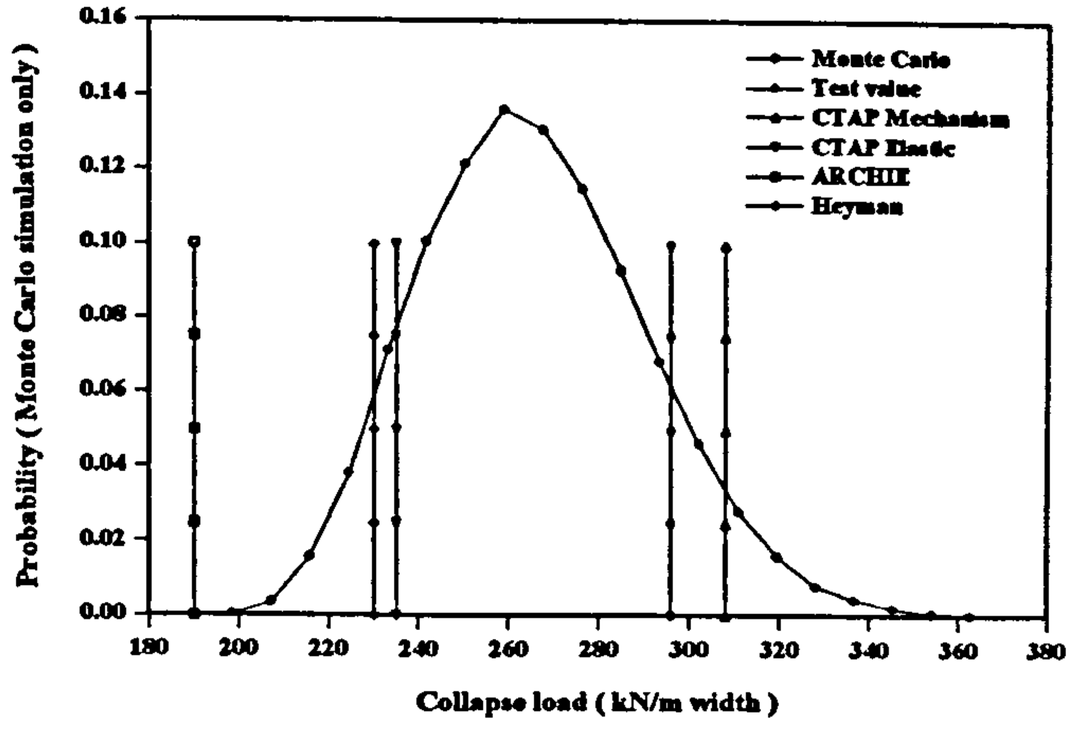

Figure 4. Comparison with other assessment methods

Figure 4 presents a comparison of results from the current Monte Carlo simulation, CTAP's mechanism method, CTAP's elastic cracking analysis, ARCHIE (mechanism method), and Heyman's plastic method. A compressive strength of 8MPa was assigned to the arch ring in CTAP's mechanism assessment and ARCHIE. The actual arch collapse load was also included for comparison. The mean arch collapse load from the current Monte Carlo simulation was 265.6kN/m (10.3% lower than the actual arch collapse load of 296kN/m). CTAP's mechanism assessment, CTAP's elastic cracking analysis, ARCHIE, and Heyman's plastic method predicted collapse loads of 308kN/m, 235kN/m, 190kN/m, and 230kN/m respectively.

The effect of varying the standard deviation of the input variables

Figure 5 shows the effect of varying the standard deviation of every input parameter on the predicted capacity. The analysis was carried out with standard deviations equal to 2%, 3%, 4%, and 5% of the mean. It was clear from Figure 5 that the larger the standard deviation, the wider the spread in the predicted capacity distribution. By increasing the standard deviation from 2% to 5% the predicted mean collapse load rose from 265kN/m to 270kN/m. Similarly, the standard deviation of the predicted arch collapse load rose from 18kN/m to 42kN/m. The failure probability, p_f also rose from 5.1% to 24.7% due to a wider spread of predicted collapse loads.

The effect of varying the seed for the random number generator

The seed values adopted for this parametric study were 819, 773311, and 4552466. Regardless of the value of the seed for the subsequent computer generation of random numbers it was clear, from Figure 6, that at no point were the results different from each other. From Table 2, it was also apparent that the statistical properties of the predicted arch collapse load distribution remained unaltered.

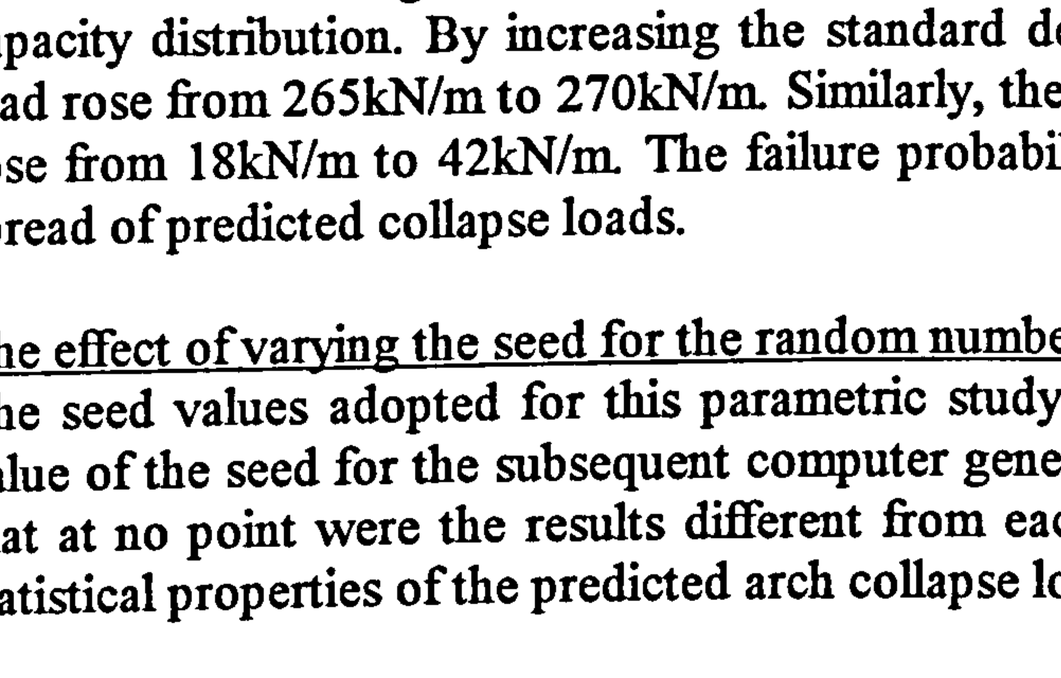

Figure 5. The effect of input variable standard deviation

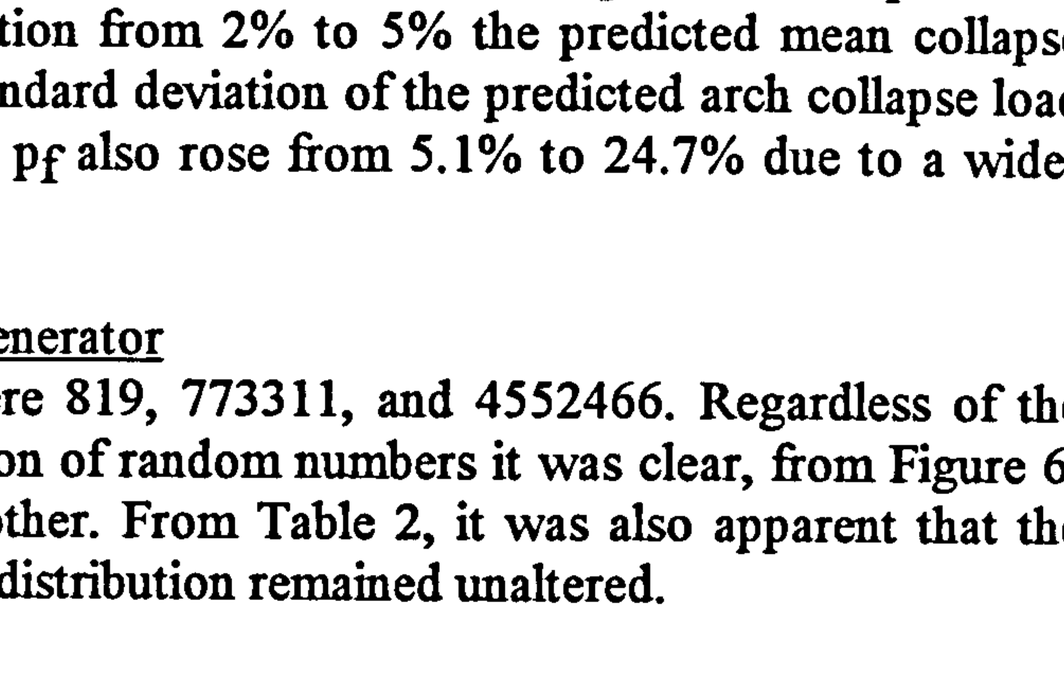

Figure 6. The effect of random number generator seed

Table 2 Statistical properties of the generated collapse load results

Variable	Value	Mean capacity (kN/m)	S.D (kN/m)	Skewness	Kurtosis	Max. load (kN/m)	Min. load (kN/m)	p_f (%)
Standard deviation	2%	265	18.2	0.21	2.75	332	213	5.13
	5%	270	41.5	0.59	3.45	482	167	24.7
Arch span (mm)	8530	276	27.6	0.42	3.08	400	197	22.6
	9197.5	266	24.9	0.33	2.92	367	194	11.8
	9865	260	23.1	0.29	2.87	364	191	6.90
Number of segments	20	257	22.9	0.42	3.32	388	194	5.30
	40	266	24.9	0.33	2.92	367	194	11.8
	100	268	23.9	0.32	2.89	370	202	12.8
Load dispersal angle	30°	254	23.4	0.36	2.99	356	187	4.69
	35°	266	24.9	0.33	2.92	367	194	11.8
	40°	283	26.7	0.33	2.96	410	206	30.2
Number of iterations	50	276	32.2	0.30	3.26	361	206	26.0
	5000	265	24.9	0.34	2.99	356	199	11.5
	50000	266	24.8	0.34	2.94	389	192	11.9
Backfill unit weight	18kNm^{-3}	251	23.5	0.33	2.92	345	183	3.55
	20kNm^{-3}	266	24.9	0.33	2.92	367	194	11.8
	22kNm^{-3}	281	26.2	0.33	2.92	388	205	27.0
Arch unit weight	21kNm^{-3}	255	23.9	0.33	2.91	354	187	5.44
	23kNm^{-3}	266	24.9	0.33	2.92	367	194	11.8
	25kNm^{-3}	276	25.9	0.33	2.92	380	202	21.6
Passive pressure mobilised	0.3	248	23.7	0.34	2.92	344	181	2.97
	0.5	266	24.9	0.33	2.92	367	194	11.8
	0.7	293	27.2	0.32	2.92	407	215	44.0
Angle of shearing resistance	30°	260	24.5	0.33	2.92	359	190	7.75
	40°	273	25.5	0.32	2.92	378	200	18.9
	50°	299	28.3	0.32	2.95	416	218	52.0

The effect of varying the arch span

As previously mentioned Barlae bridge had a 29° skew. The authors assumed the arch was under 2-D plane strain conditions. The span was undefined for such an idealisation. The longest and shortest distances along the arch span were 9865mm and 8530mm respectively. A parametric study was carried out with spans of 8530mm, 9197.5mm, and 9865mm; the results are presented in Figure 7. By increasing the arch span from 8530mm to 9865mm, the predicted mean collapse load fell from 276kN/m to 260kN/m. Similarly, the predicted standard deviation of the collapse load fell from 28kN/m to 23kN/m. Such an increase in span also reduced the probability of failure from 23% to 6.9%.

The effect of varying the number of arch segments

Figure 8 shows the effect of varying the number of arch segments on the collapse load prediction. The numbers of segments used in this parametric study were; 20, 40, 60, 80, and 100. The results converged when the number of arch segments was 40 or greater. By increasing the number of arch segments from 20 to 100, the predicted mean collapse load increased from 257kN/m to 268kN/m. The predicted standard deviation of the collapse load increased from 23kN/m to 24kN/m. The failure probability increased from 5.3% to 13% for the same increase in the number of segments. Increasing the number of segments had a significant influence on the processing time. By increasing the number of segments from 20 to 100, the processing time *per* 100 iterations rose from 3.2s to 200s on a 100MHz Pentium based computer.

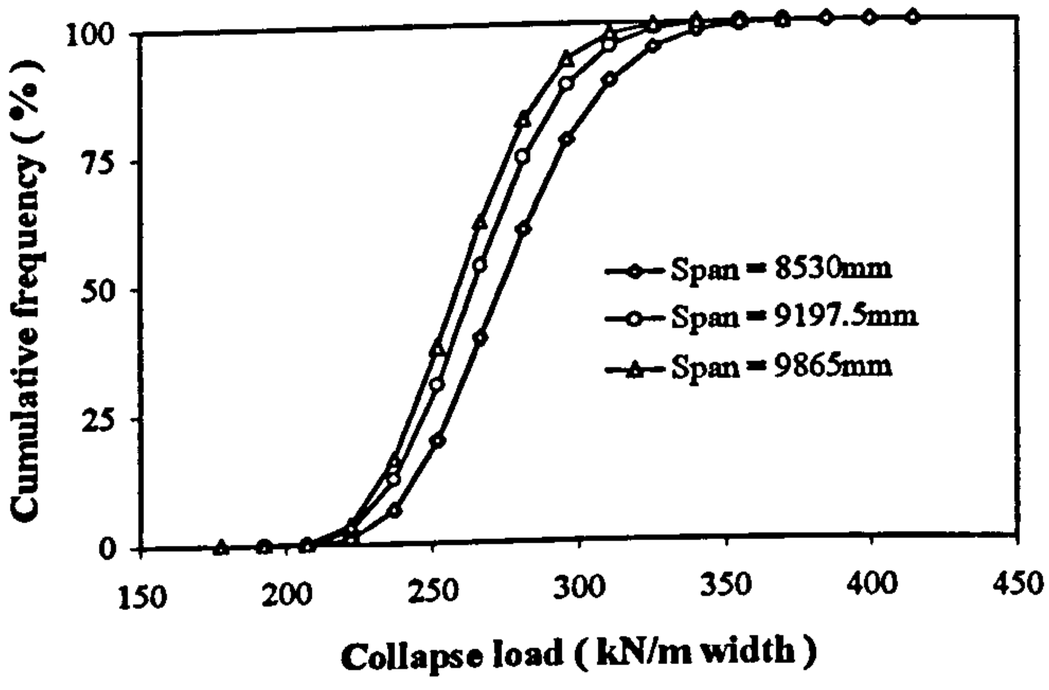

Figure 7. The effect of the arch span

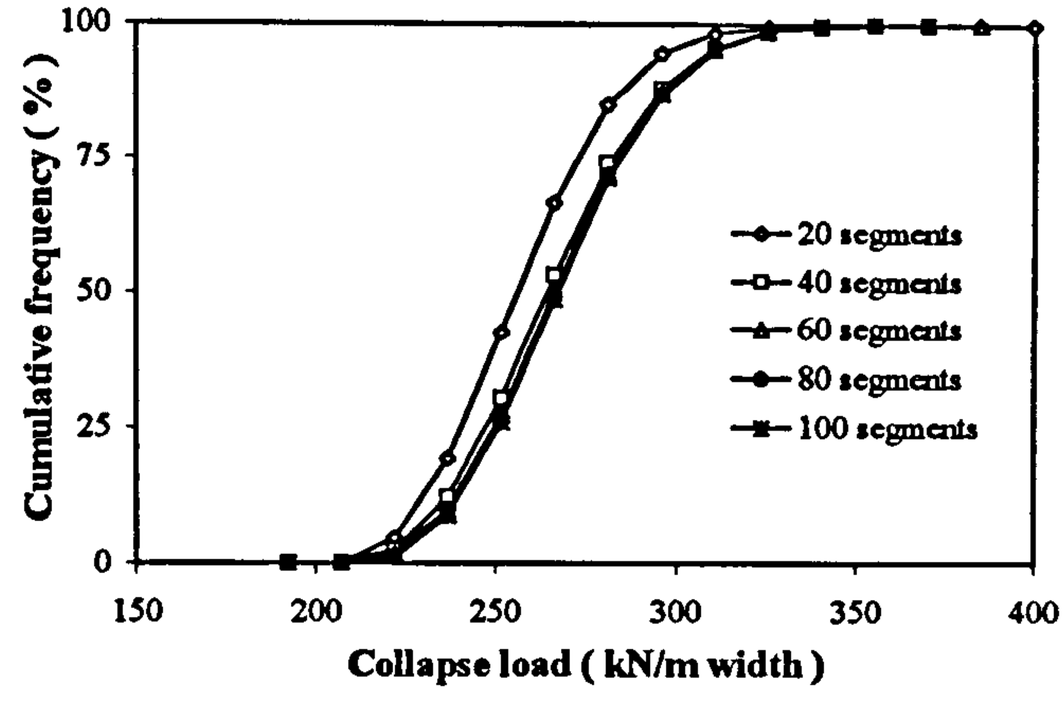

Figure 8. The effect of the number of arch segments

The effect of varying the live load dispersal angle

Figure 9 shows the effect of varying the live load dispersal angle on the collapse load prediction. The live load dispersal angles used in this parametric study were 30°, 35°, and 40° from each side of the loaded area's edge. By increasing the load dispersal angle from 30° to 40° the predicted mean collapse load increased from 254kN/m to 283kN/m. The standard deviation of the predicted collapse load increased from 23kN/m to 27kN/m. The same increase in load dispersal angle increased the probability of failure from 4.7% to 30%.

The effect of varying the number of iterations

Figure 10 shows the effect of varying the number of iterations on the collapse load prediction. The number of iterations used in this parametric study were 50, 100, 500, 5000, 30000, and 50000. The influence of this parameter was much less significant for 500 or more iterations. It was clear that the more iterations used *per* analysis the smoother the resulting distribution. By increasing the number of iterations from 50 to 50000, the predicted mean collapse load fell from 276kN/m to 266kN/m whilst its standard deviation fell from 32kN/m to 25kN/m. The failureprobability also fell from 26% to 12%. These decreases were non-linear: the majority of the decrease happened for runs using below 500 iterations.

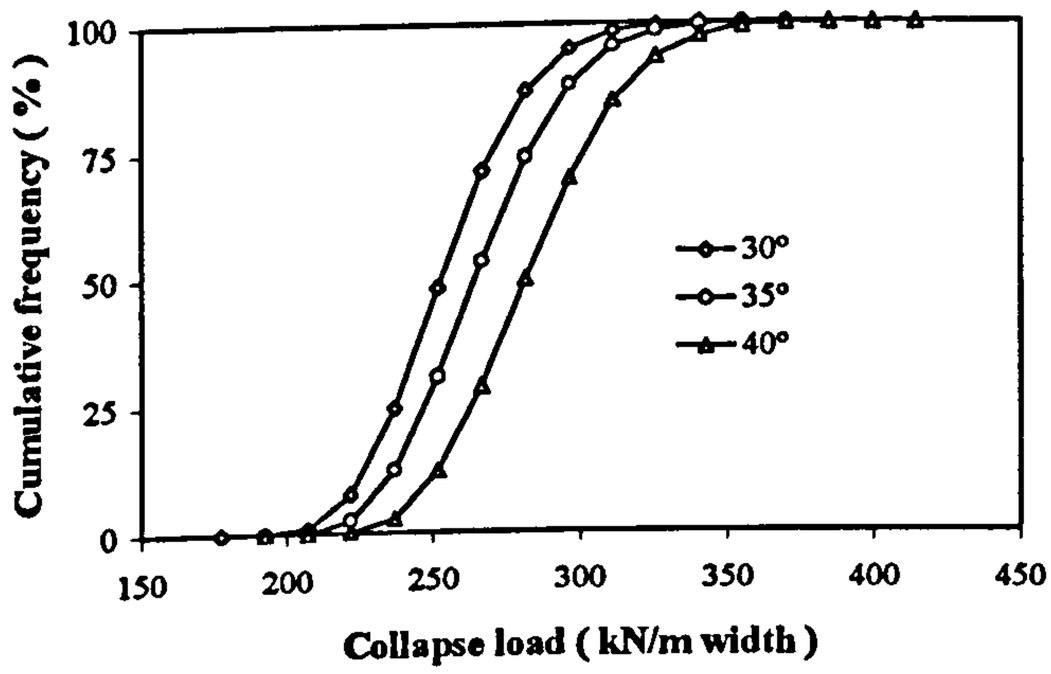

Figure 9. The effect of live load dispersal angle

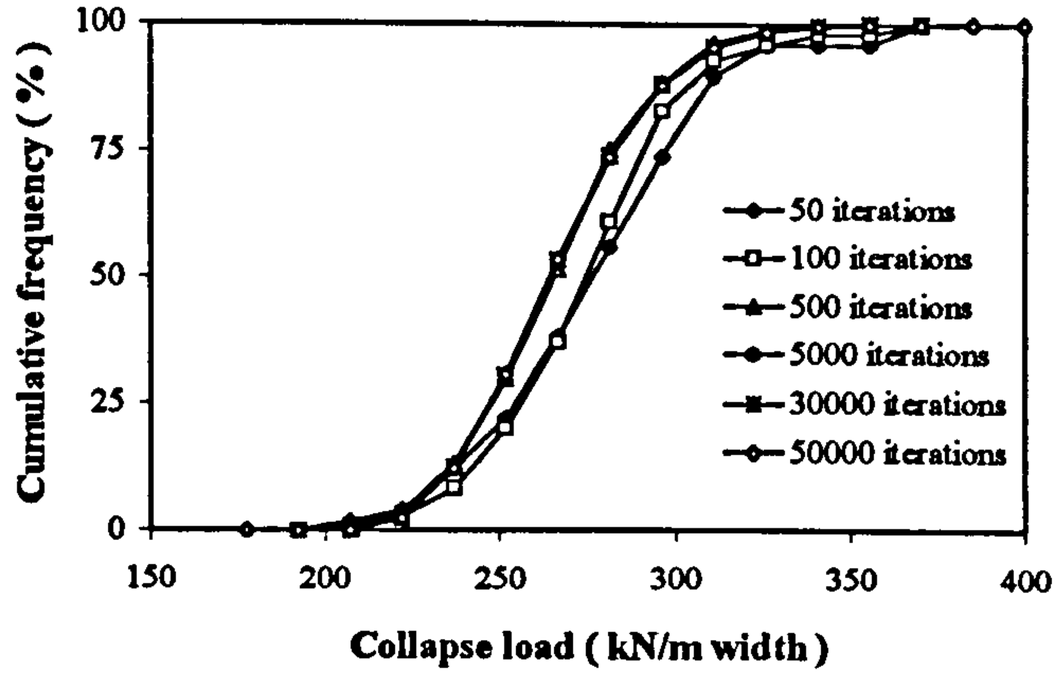

Figure 10. The effect of number of iterations

The effect of varying the backfill's bulk unit weight

Figure 11 shows the effect of varying the backfill's bulk unit weight on the collapse load prediction. The parametric study was carried out with unit weights of 18kNm^{-3}, 20kNm^{-3}, and 22kNm^{-3}. The unit weight had a significant influence on the predicted capacity. With an increase in backfill unit weight of 4kNm^{-3} the predicted mean collapse load rose from 251kN/m to 281kN/m. Similarly, the predicted standard deviation rose from 24kN/m to 26kN/m whilst the failure probability increased from 3.5% to 27%.

The effect of varying the arch's bulk unit weight

Figure 12 shows the effect of varying the arch's bulk unit weight on the collapse load prediction. Three different unit weights were used in this parametric study: 21kNm^{-3}, 23kNm^{-3}, and 25kNm^{-3}. The unit weight significantly influenced capacity predictions; increasing it from 21kNm^{-3} to 25kNm^{-3} increased the predicted mean collapse load from 255kN/m to 276kN/m whilst increasing the standard deviation from 24kN/m to 26kN/m. The same increase caused the failure probability to rise from 5.4% to 22%.

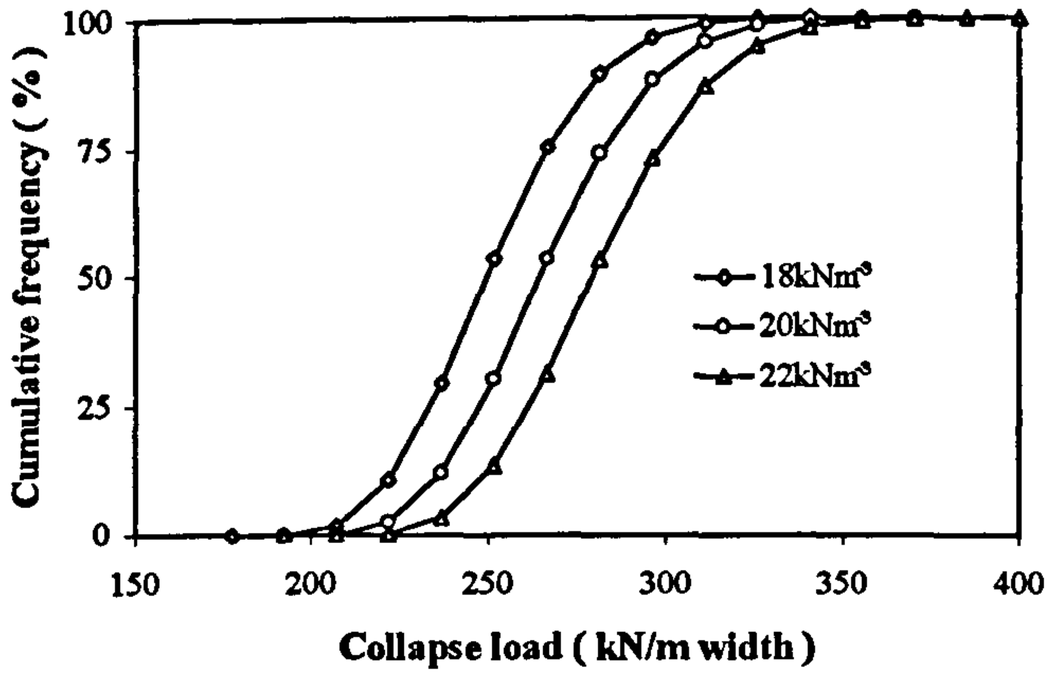

Figure 11. The effect of backfill bulk unit weight

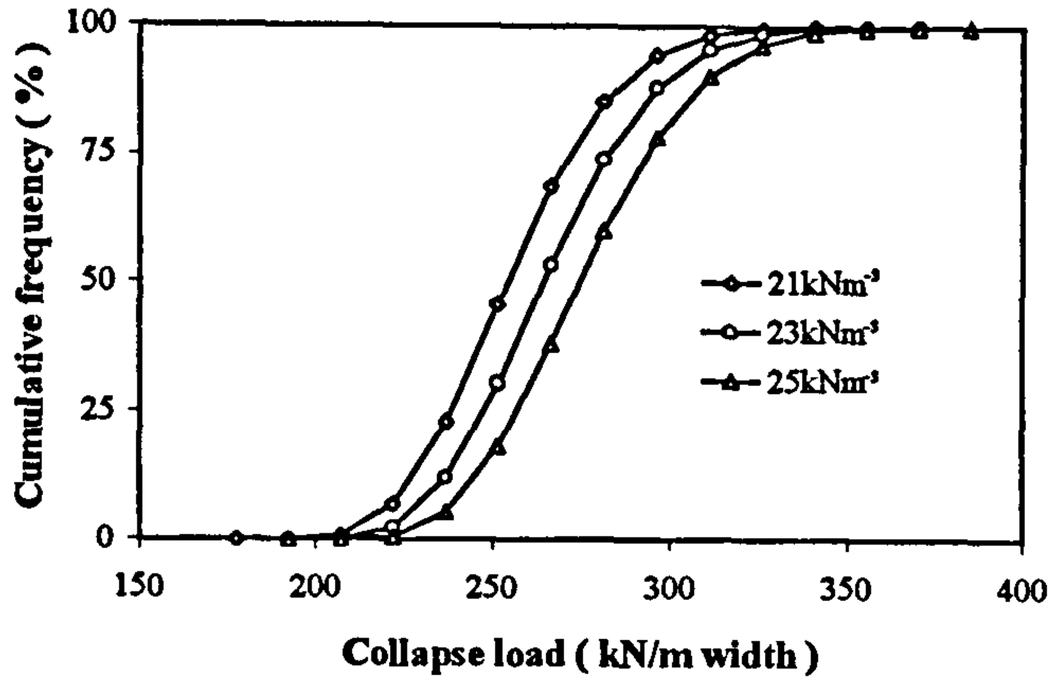

Figure 12. The effect of arch bulk unit weight

The effect of varying the backfill active pressure

Figure 13 shows the effect of varying the mobilised percentage of full backfill active pressure on the collapse load prediction. The active pressure coefficients used were the traditional Rankine coefficients. The percentages of this active pressure which were permitted to be mobilised were 60%, 80%, and 90% (corresponding to coefficients of 0.6, 0.8, and 0.9 respectively). There was no noticeable influence on the predicted results. The mean, standard deviation and failure probability were unchanged.

The effect of varying the backfill passive pressure

Figure 14 shows the effect of varying the mobilised percentage of full backfill passive pressure on the collapse load prediction. The percentage of full passive pressure permitted to be mobilised were: 30%, 50%, and 70% (corresponding to coefficients of 0.3, 0.5, and 0.7 respectively). The backfill passive pressure significantly influenced the capacity predictions. Increasing the percentage of full backfill passive pressure mobilised from 30% to 70% caused the predicted mean collapse load to increase from 248kN/m to 293kN/m. Its standard deviation increased from 24kN/m to 27kN/m. This increase in the backfill passive pressure significantly increased the probability of failure from 2.97% to 44%.

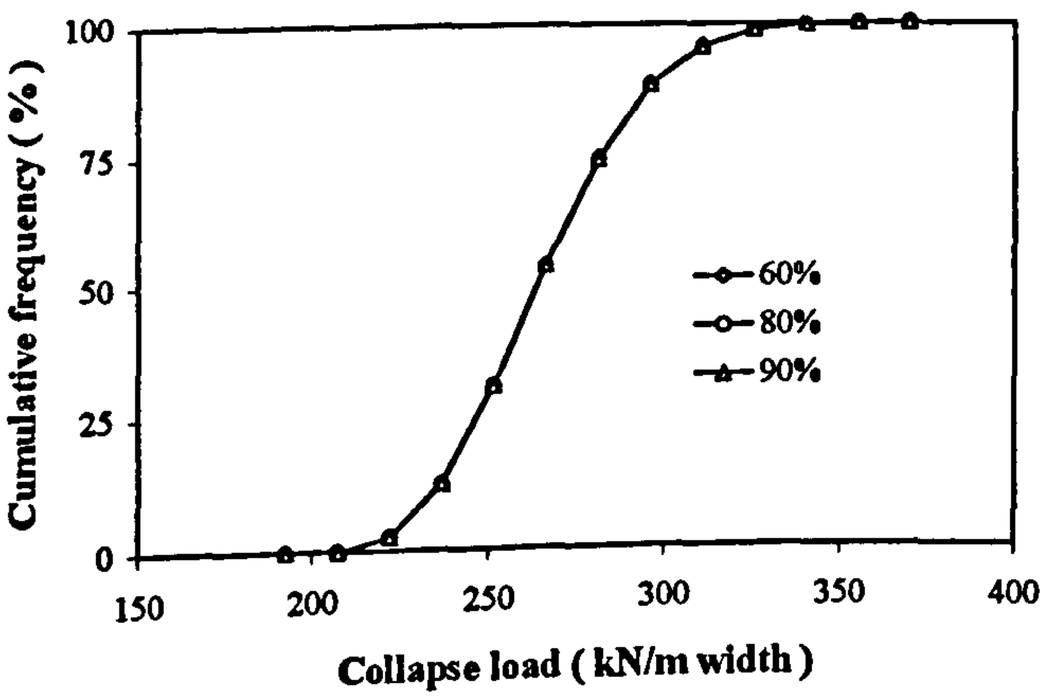

Figure 13. The effect of mobilised percentage of full backfill active pressure

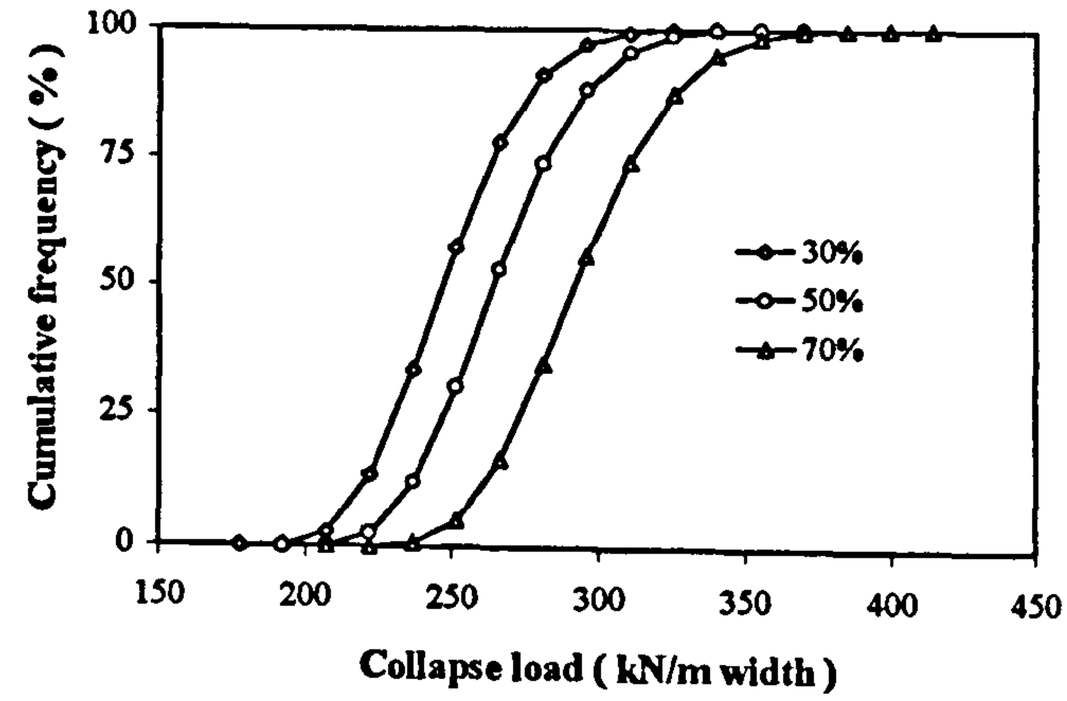

Figure 14. The effect of mobilised percentage of full backfill passive pressure

The effect of varying the backfill's angle shearing resistance

Figure 15 shows the effect of varying the backfill's angle of shearing resistance, ϕ on the collapse load prediction. The backfill angles of shearing resistance used in this parametric study were 30°, 35°, 40°, and 50°. The backfill angle of shearing resistance influenced the capacity predictions especially at higher values. Increasing the backfill angle of shearing resistance from 30° to 50° increased the collapse load prediction from 260kN/m to 299kN/m whilst increasing its standard deviation from 24kN/m to 28kN/m. The failure probability also rose significantly from 7.7% to 52% for the same increase in angle of shearing resistance.

The effect of changing the variable end limit

Figure 16 shows the effect of changing the variable end limit on the collapse load prediction. Four different variable end limits were used (1%, 3%, 5%, and 7%). Regardless of the value used no significant difference in the capacity prediction occurred. The predicted mean, standard deviation and failure probability were also found to be practically unchanged.

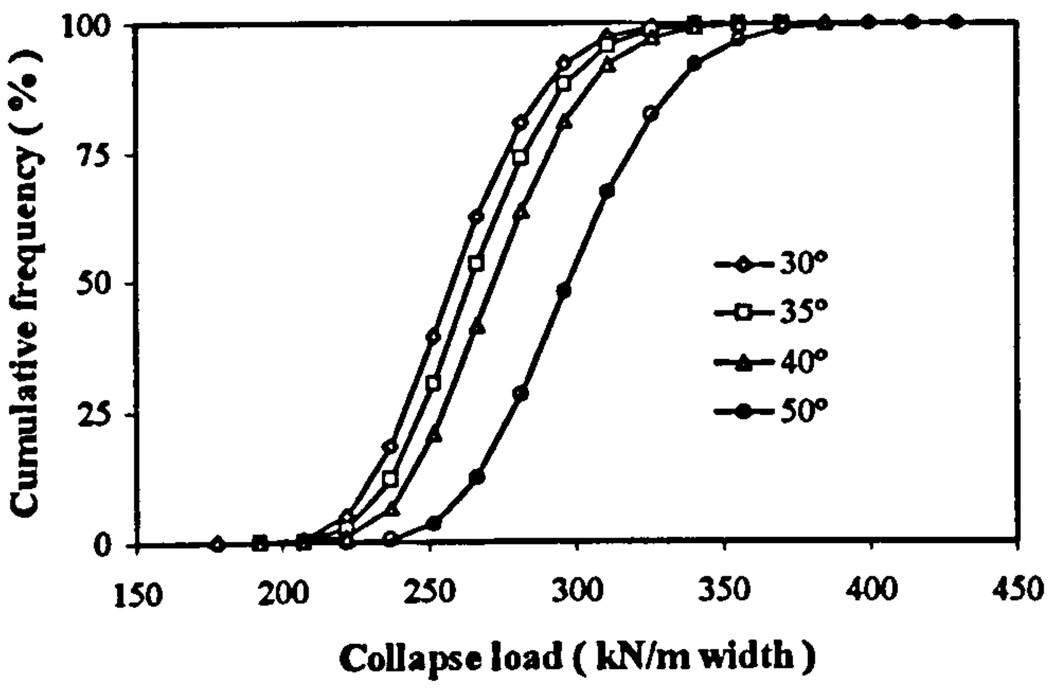

Figure 15. The effect of backfill ϕ value

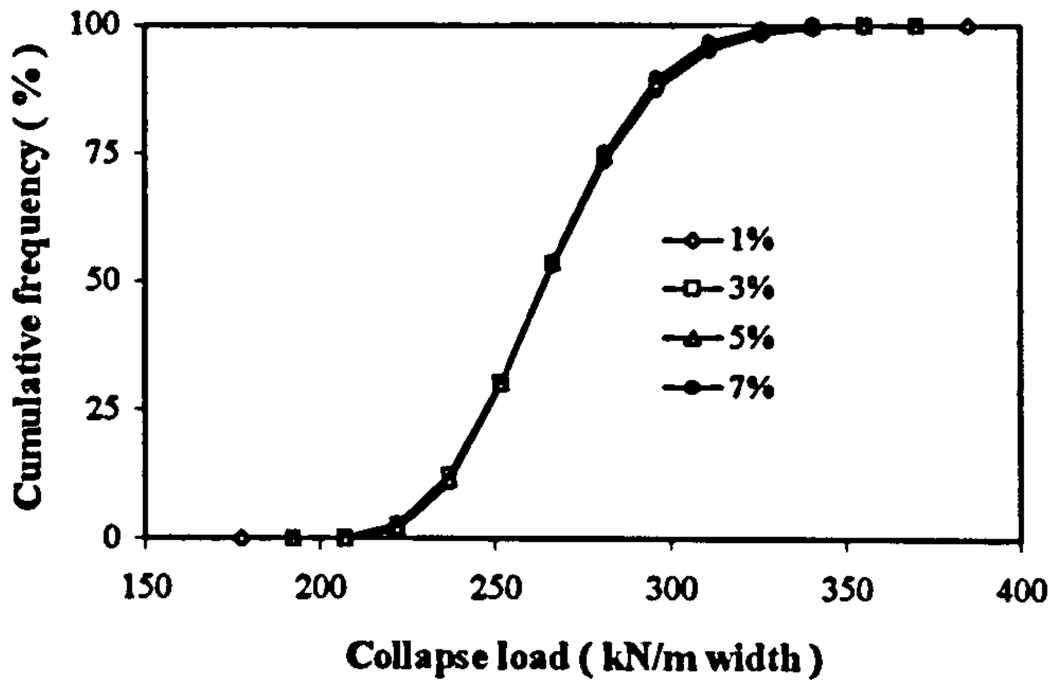

Figure 16. The effect of variable end limit

DISCUSSION

The results obtained from the authors' Monte Carlo simulation and mechanism method analysis are discussed. The influence of each parameter used in this simulation is also discussed. Following this, some limitations of the method are discussed.

Monte Carlo simulation and mechanism method

A Monte Carlo simulation has been successfully incorporated into the mechanism method for the analysis of Barlae bridge. Unlike other arch bridge assessment methods, the current Monte Carlo simulation gives statistical information about the predicted arch collapse load. The risk involved in assessing an arch bridge can be measured by analysing the standard deviation of the collapse load distribution. The larger this is, the greater the risk involved: such information can help an engineer to have some idea of the reliability of their assessment. The parametric studies carried out showed that some variables had a significant influence on the collapse load prediction most notably: the variable's standard deviation, the arch's span, the live load dispersal angle, the arch and backfill unit weights, the permitted mobilisation of backfill passive pressure, and the backfill's angle of shearing resistance.

The influence of the number of arch segments and number of iterations depended on their magnitudes. Parametric studies have to be performed to search for a minimum number of arch segments and the number of iterations in such a way that any increase in their magnitudes does not significantly affect the collapse load prediction. In this study, 40 arch segments and 30000 iterations were appropriate.

The standard deviations of input variables have been shown to affect the predicted results. In this study, the standard deviations for all input variables were set to be similar at any one time. However, the program also allows the user to specify different standard deviations for each input variable. The range of standard deviations used in this study was between 2% to 5%. This was deemed appropriate since most of the geometrical properties of the arch bridge are unlikely to be unduly dispersed about their respective means. However, individual analyses should be performed for parameters such as load dispersal angle, arch and backfill unit weights, backfill lateral pressures, and angle of shearing resistance which are difficult to find from what may only be a cursory survey and inspection of a bridge.

The influence of the seed for the random number generator was insignificant because different values of this seed only varied the sequence in which random numbers were generated. Provided a sufficient number of iterations is used, the statistical properties of the generated random numbers will not differ significantly.

Parametric studies carried out on both the arch and backfill bulk unit weights revealed that both parameters significantly influenced the capacity predictions. This was expected as the failure of an arch bridge is usually a mechanism involving rotation of several sections of the ring, usually three, against gravitational attraction and restraining pressure from the backfill. The higher the arch and backfill unit weights, the larger the live load required to form the failure mechanism.

A parametric study on the mobilisation of backfill passive pressure showed it significantly influenced the capacity predictions. In contrast, the backfill active pressure mobilisation was found to have no influence on the predicted results. Both Rankine's active and passive earth pressure coefficients involve the backfill's angle of shearing resistance. A maximum of 70% passive pressure mobilisation was used here because it was thought unlikely that full passive resistance could be mobilised in such a soil-arch system. Alternatively full mobilisation of the active state would be possible but as active pressures are so much lower than their passive counterparts they were still unable to influence the collapse load predictions.

LIMITATIONS OF THE METHOD

The mechanism method has been widely used for arch bridge analysis because no complicated computations are required and it is quick. However, the method is based on many unrealistic assumptions such as the arch having no spandrels, wing walls, and parapet. Many subjective judgements have to be made when using this method such as the live load dispersal angle, active/passive pressure coefficients and the backfill's angle of shearing resistance. Ongoing research is involved with the development of a modified mechanism method including arch deflections and a deflection dependent bi-linear backfill lateral pressure model (Ng *et al.*, 1999). This revealed that the arch deflections significantly affected the collapse loads predicted by the mechanism method. It was justifiable since the mechanism prediction is only accurate if all forces and their positions are considered accurately. A problem lies in the concerns over what deflection an assessing engineer should adopt as the ultimate limit state case. Subjectively this is however, no more difficult or arbitrary than the choice of lateral earth pressure coefficients.

A major drawback arising from this Monte Carlo simulation is the processing time required for a sufficient number of iterations. However, most of the processing time was occupied with the evaluation of collapse load distributions and not spent generating random variables. The standard deviations for all input variables can only be assumed subjectively because there is no such information available and it is highly unlikely that cursory site investigation will provide such data from field measurements. Over the wide range of bridges built in any one Local Authority area a database of experience will gradually have been built up concerning the likely variability in some of the more common material properties. One of the benefits of this type of risk based assessment is that it allows an engineer faced with a complex problem to examine the possibilities previously unavailable through use of any other traditional or modern arch assessment methods in isolation.

CONCLUSIONS

1. Monte Carlo simulation has been successfully incorporated into the mechanism method to perform risk analysis based arch bridge assessment.

2. The following parameters significantly affected the output collapse load distribution: the standard deviations of the input variables (a standard deviation between 2% to 5% of the variable's mean is recommended), the arch span, the passive pressure acting on the extrados and the backfill's angle of shearing resistance.

3. The following parameters did not affect the output collapse load distribution: the seed for random number generation, the active pressure acting on the extrados, and each variable's end limit.

4. A total of 40 arch segments or more is recommended for such analyses. Increasing the number of segments increased the processing time significantly. More than 5000 iterations are recommended for convergence of the solution and smoothness of the resultant collapse load distribution.

5. The method has provided more realistic capacity assessments which could enable an assessing engineer to improve upon current axle load limits for critical arch bridges.

ACKNOWLEDGEMENT

The authors thank: Prof. W. J. Harvey (University of Exeter) and Dr F. W. Smith (University of Dundee) for the use of program ARCHIE and Dr T. G. Hughes (Cardiff University) for the use of program CTAP.

REFERENCES

Bridle, R. J. & Hughes, T. G. (1990) An energy method for arch bridge analysis. *Proc. Inst. Civ. Engnrs*, 89, 2, pp. 375-385.

Heyman, J. (1982) *The masonry arch.* Ellis Horwood, Chichester.

Ng, K.-H., Fairfield, C. A. & Sibbald, A. (1999) Arch bridge mechanism method assessment incorporating deflection dependent soil pressure updating algorithms. *Proc. 2nd Int. Conf. Railway Engineering*, London Engineering Technics Press, *under review.*

Page, J. (1989) Load tests to collapse on two arch bridges at Strathmashie and Barlae. *TRL Research Report 201*, TRL, Crowthorne.

Smith, F. W. (1991) Load path analysis of masonry arches. *Ph.D. Thesis*, University of Dundee.

COLLAPSE LOAD REPEATABILITY TESTS ON BRICKWORK ARCHES

Mr K.-H. Ng & Dr C. A. Fairfield
Napier University
School of the Built Environment
10 Colinton Road
Edinburgh EH10 5DT, U.K.

KEYWORDS: Masonry arch bridges, Repeatability, Finite element analysis

ABSTRACT
A pilot experimental study was carried out at Napier University by building three nominally identical large scale (2m span, 0.5m rise, ½-brick ring) soil backfilled brickwork arch bridges. These structures were tested to collapse to investigate the repeatability of the ultimate load measured by such large scale tests. Although similar tests have been carried out previously, repeatability tests have not been carried out mainly because of cost. It was therefore deemed necessary to conduct a series of repeatability tests on large scale model arches to give engineers an idea of the reliability of their assessed results whilst recognising the inherent uncertainties in existing experimental data. Before breaking the first arch, five analytical studies were performed to predict the system's behaviour up to ultimate limit state. The analytical methods used as predictors were: SOILARCH (a mechanism based method coded by the authors), a mechanism method (program ARCHIE), a Castigliano elastic strain energy method (program CTAP), the MEXE method, and a 2-D non-linear finite element analysis. It was found that the results predicted by these methods were significantly different. This was mainly because of the differing assumptions and idealisations they incorporate. The experimental data from three nominally identical arches was superimposed and collapse load ranges, rather than mock-precise collapse load values, were recommended.

INTRODUCTION

In recent years, arch bridges have been actively researched. Engineers have come to the view that underestimate the capacity of many arches because vehicles with weights far beyond assessed allowable limits have been crossing without significant distress for years. It is now economically important to search for a more reliable capacity assessment to eliminate the possibility of abandoning or repairing arch bridges which were perfectly adequate.

Recently, many numerical methods have been proposed (Gong, 1992, Smith, 1991, and Bridle & Hughes, 1990) for analysing arch bridges. With assumed material properties and idealised geometries for arch and backfill, results predicted by these methods bear considerable resemblance to those observed in recent full-scale tests. However, arch bridges are complex 3-D structures and are subjected to a wide range of material variability and geometrical imperfections. A question has to be asked on whether nominally identical arches will yield identical collapse loads. This is particularly important as the geometry of an arch bridge is the dominant factor in determining its capacity in all assessment methods.

A pilot experimental study was carried out on three nominally identical model arches with a span to rise ratio, s = 4; these were tested to collapse to investigate their repeatability. Before testing the first arch, analyses were performed to predict the behaviour up to ultimate limit state using various assessment methods: SOILARCH (Ng, 1998), program ARCHIE (Smith, 1991), program CTAP (Bridle & Hughes, 1990), the MEXE method, and a 2-D non-linear finite element (FE) analysis.

DESIGN AND CONSTRUCTION OF THE ARCHES

Three nominally identical arch bridges (all s = 4) were built in the laboratory. The brick, backfill, mortar mix and construction method were kept unchanged throughout. The first, second and third arches are referred to as SR4-A, SR4-B and SR4-C respectively. All the arches were circular segmental spanning of 2m, with a width of 1m in a 102.5mm thick ring of Engineering Class B bricks. Each arch was supported by a rigid concrete abutment. Each arch ring consisted of 32 courses of brick set in a 1:1:6 (cement:lime:sand) mortar. Cube tests revealed an elastic modulus, Poisson's ratio, and compressive strength of: 6867MPa, 0.263 and 4.90MPa respectively. The average brick-mortar bond strengths for SR4-A, SR4-B, and SR4-C were found to be 0.542MPa, 0.471MPa, and 0.550MPa respectively with a standard deviation and the coefficient of variation, considering all test specimens, of 0.22MPa and 43% respectively. The spandrel and wing walls were not structural and only served to retain the backfill. To avoid interference with the arch ring, a gap of 10mm was provided between the arch ring and the spandrel walls. Heavy duty polythene strips were lapped 100mm over the arch extrados and fixed to the inner surface of the timber spandrel wall up to a height of 100mm above the arch. Figure 1 shows a photograph of one model (SR4-B) with spandrel, wing and end walls before being backfilled with sand.

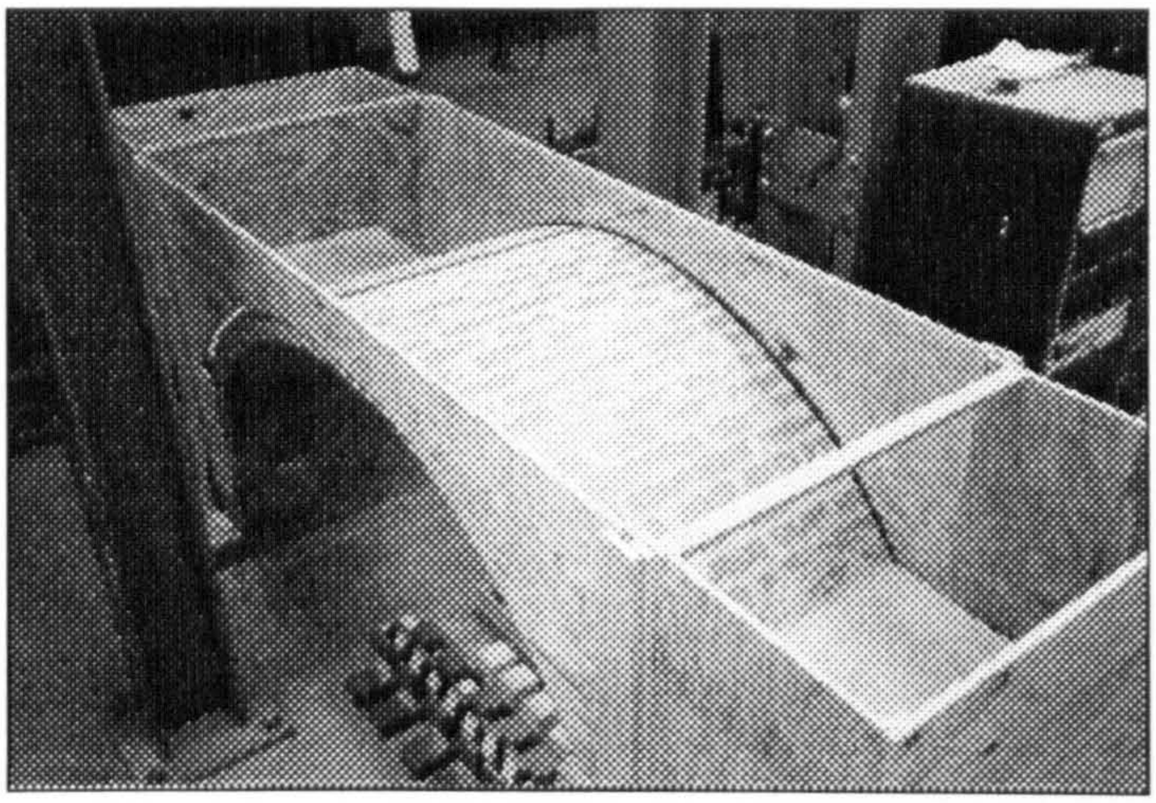

Figure 1 The bare extrados before backfilling (Model SR4-B)

BACKFILL

The bulk unit weight of the backfill was 14.86kNm^{-3} and its depth at the crown was 150mm. A series of tests were carried out to determine the backfill's moisture content, apparent cohesion, angle of shearing resistance and particle size distribution. The backfill moisture contents for SR4-A to SR4-C were 12.5% to 12.0%. The backfill was dry sieved to find its particle size distribution (Figure 2 shows the backfill's to be a uniform sand). The backfill was subjected to a series of QU triaxial tests on 100mm diameter samples compacted to a bulk unit weight of 14.86kNm^{-3}. Results are presented (Figure 3) showing the backfill's apparent cohesion as zero and its angle of shearing resistance 30.5°.

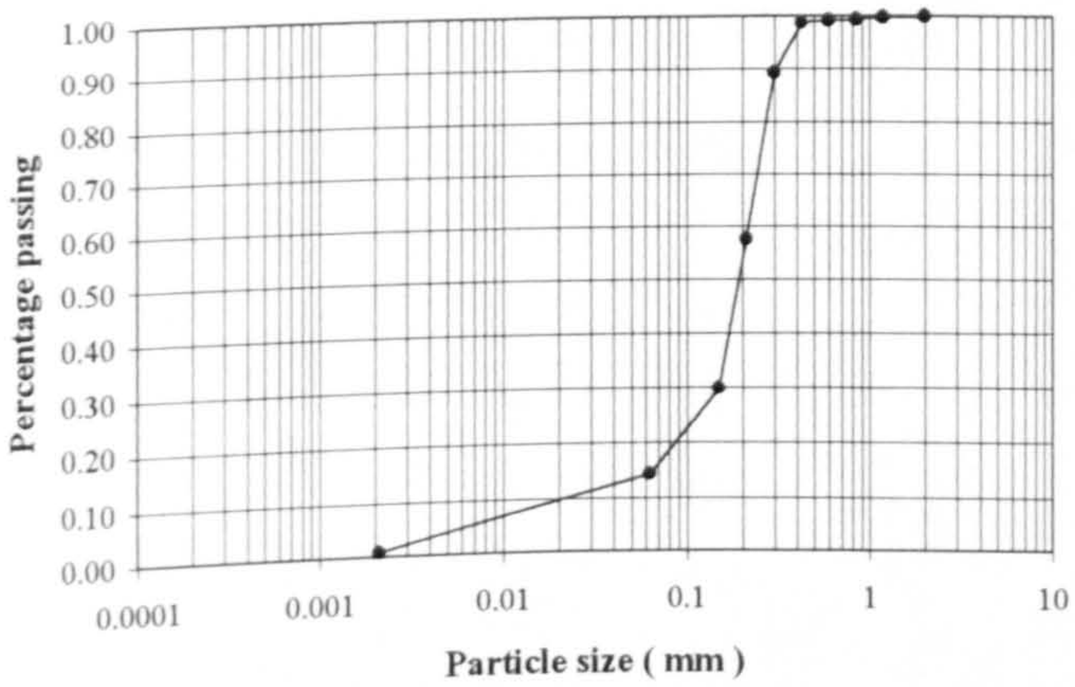

Figure 2 Particle size distribution of the backfill

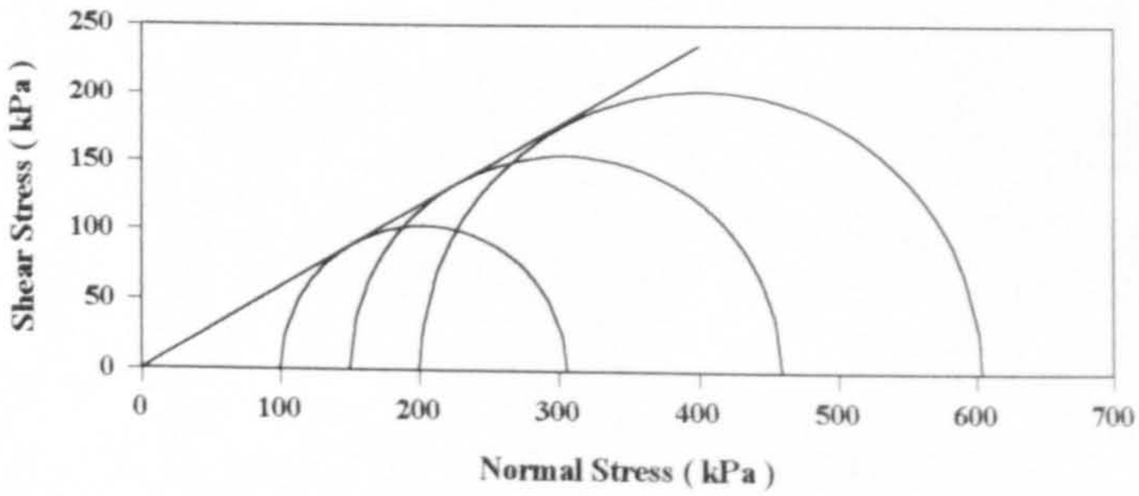

Figure 3 Backfill shear strength (triaxial tests, ϕ=35°)

LOADING SYSTEM

A 100 tonne hydraulic jack was used to impose live loads to the arches. Two steel anchors were bolted to the laboratory's strong floor to form a reaction frame against which the jacks could push the arch down by applying line load at the ¼-span. The imposed load from the jack was applied to the backfill surface at the ¼-span point through a 180mm wide spreader beam covering the whole width of the arch. A calibrated load cell was placed between the jack and the spreader beam to measure the imposed load. To prevent excessive vertical displacement and bearing capacity failure at the load line, a woven geotextile strip (380mm × 1000mm) was placed directly under the load platen.

DISPLACEMENT MEASUREMENTS

Linear variable differential transducers (LVDTs) were used to measure arch deflections. The LVDTs were connected to a datalogger for reading and storing their output. All LVDTs were calibrated using the same system over their entire working ranges. Twelve LVDTs, eight of long (100mm) and four of short (50mm) travel type, were used in each test to measure arch deflections at the positions shown in Figure 4. The LVDTs were not mounted directly under the arch; deflections were taken off rigid timber platforms glued to the intrados and projecting 50mm away from the structure. This avoided having to remove the expensive instrumentation to prevent it getting damaged by falling masonry.

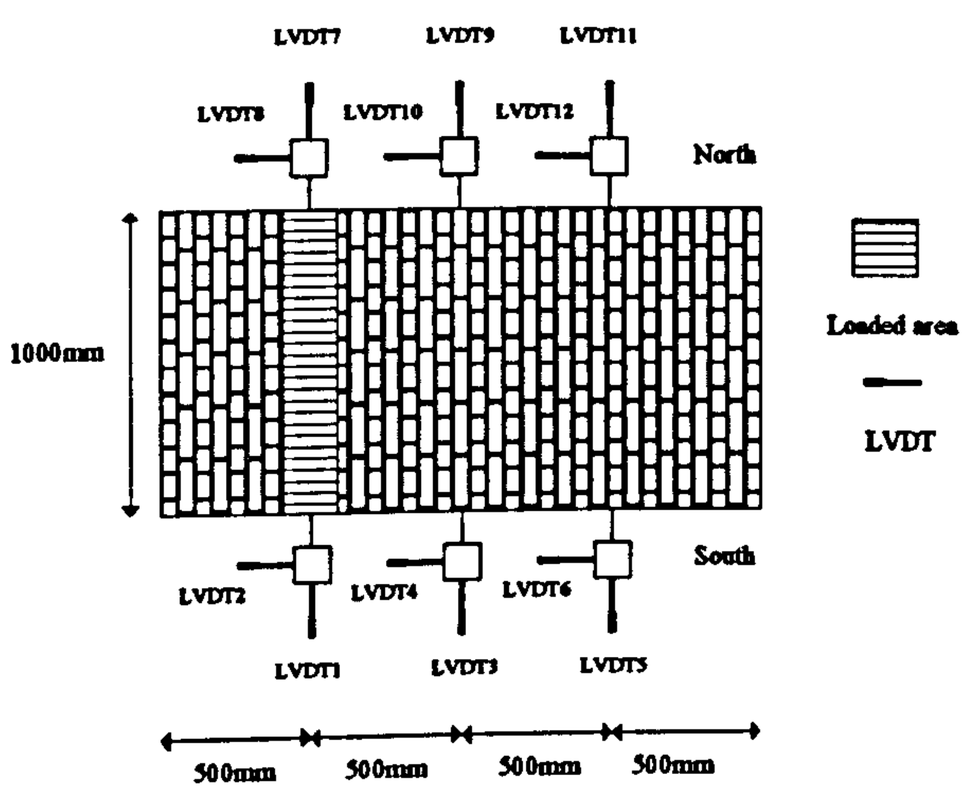

Figure 4 LVDT locations (plan view)

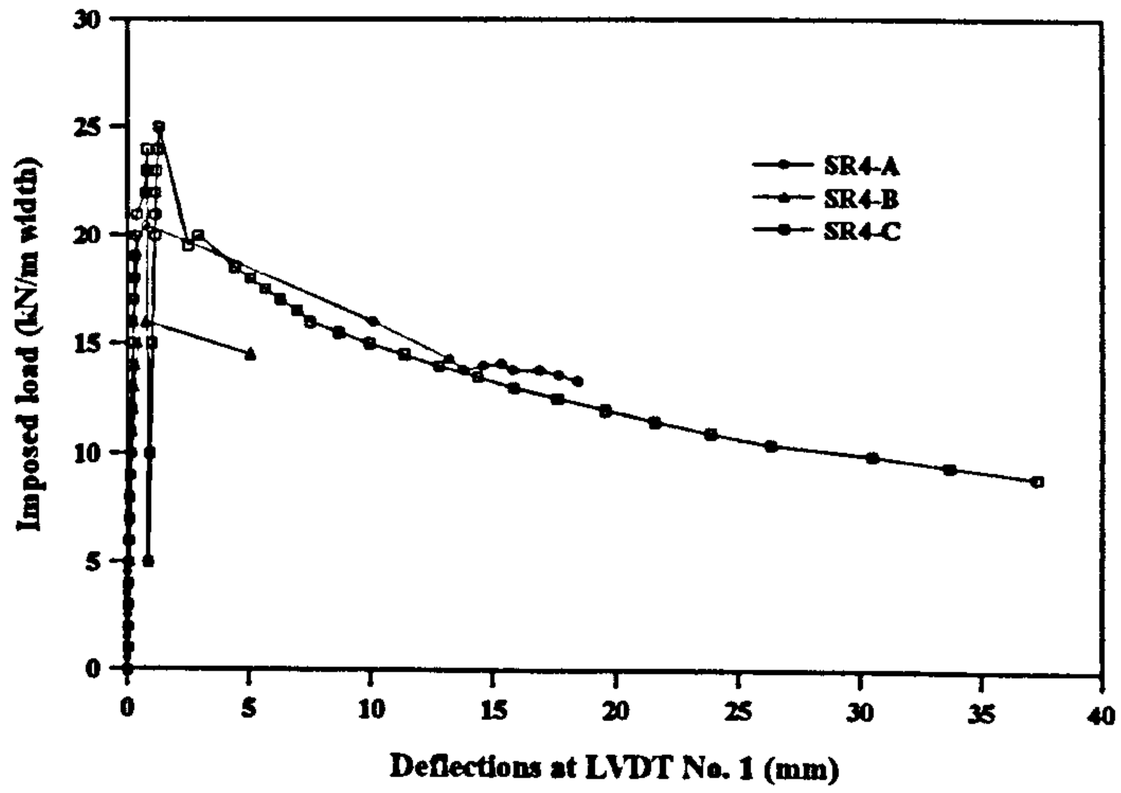

Figure 5 Load *vs* vertical deflection at the ¼-span

EXPERIMENTAL RESULTS

This section presents the experimental results from the three large-scale nominally identical arch tests. A load increment of 0.5kN *per* metre width (hence the units of kNm^{-1}), perpendicular to the span, was used followed by visual inspection of the arch for the onset of cracking. As a summary of the experimental results, Table 1 gives the collapse loads and hinge locations for each test. The hinge locations are represented by their mortar joint numbers. Each of the 33 joints was numbered from the left abutment. The order of presentation in Table 1 does not represent the order in which the hinges actually formed. The load *versus* vertical deflection plots at the ¼-span point on the intrados are presented in Figure 5.

Table 1 Collapse loads and hinge locations

Arch	Collapse load (kNm^{-1} width)	Hinge location (mortar joint no.)
SR4-A	21	1, 12, 22, 33
SR4-B	16	3, 10, 21, 33
SR4-C	25	1, 9, 19, 33

Experimental Behaviour Of Model SR4-A

The arch collapsed at a maximum applied ¼-span live load of 21kNm^{-1} width perpendicular to the span. The arch finally collapsed with four hinges at joint numbers 1, 12, 22, and 33. The load *versus* vertical deflection curve at the intrados ¼-span point was presented in Figure 5.

No signs of damage to the arch were observed before loading. At an imposed load of 10kNm^{-1}, the arch vertical deflection at the ¼-span point was only 0.102mm. No signs of hinge formation were seen at this load. When loaded to 17kNm^{-1} width, bearing capacity failure started beneath the loaded area but the settlement was small because of the geotextile strip beneath the load platen. A small soil tensile crack also formed near the load platen. The arch still showed no signs of distress at a load of 20kNm^{-1}. However, a more obvious settlement was noticed at this load. When the load increased to 21kNm^{-1}, an obvious hinge was formed in the arch ring at an interface near the ¼-span point (joint 12). This followed by an immediate loss of arch stiffness and a rapid increase in its deflection. The load fell rapidly from 21kNm^{-1} to 16kNm^{-1} resulting in increased vertical deflection at the ¼-span point from 0.752mm to 10.097mm. Such a significant arch deflection caused the formation of another three hinges in the arch ring at joints 1, 22, and 33. Further application of live load was accompanied by rapid increases in deflection and no loads higher than the previous maximum could be applied to the arch. A large tensile crack was observed on the surface of backfill at about other ¼-span point remote from the load. With the load reduced to 13.3kNm^{-1}, collapse of the arch looked imminent and all LVDTs were removed to avoid damage. On re-loading, the arch deflection increased further and the arch finally collapsed in a mechanism. No signs of compressive failure of the arch material were seen.

Experimental Behaviour Of Model SR4-B

The arch collapsed at a maximum applied ¼-span live load of 16kNm^{-1} width perpendicular to the span. The arch finally collapsed with four hinges at joint numbers 3, 10, 21, and 33. Figure 6 shows SR4-B shortly before collapse. The load versus vertical deflection plot at the intrados ¼-span point was presented in Figure 5. No signs of damage to the arch were observed before loading. When loaded to 9kNm^{-1}, small settlements at the load platen was noticed. Careful inspection of the arch revealed no cracks were formed in the arch ring at this load level.

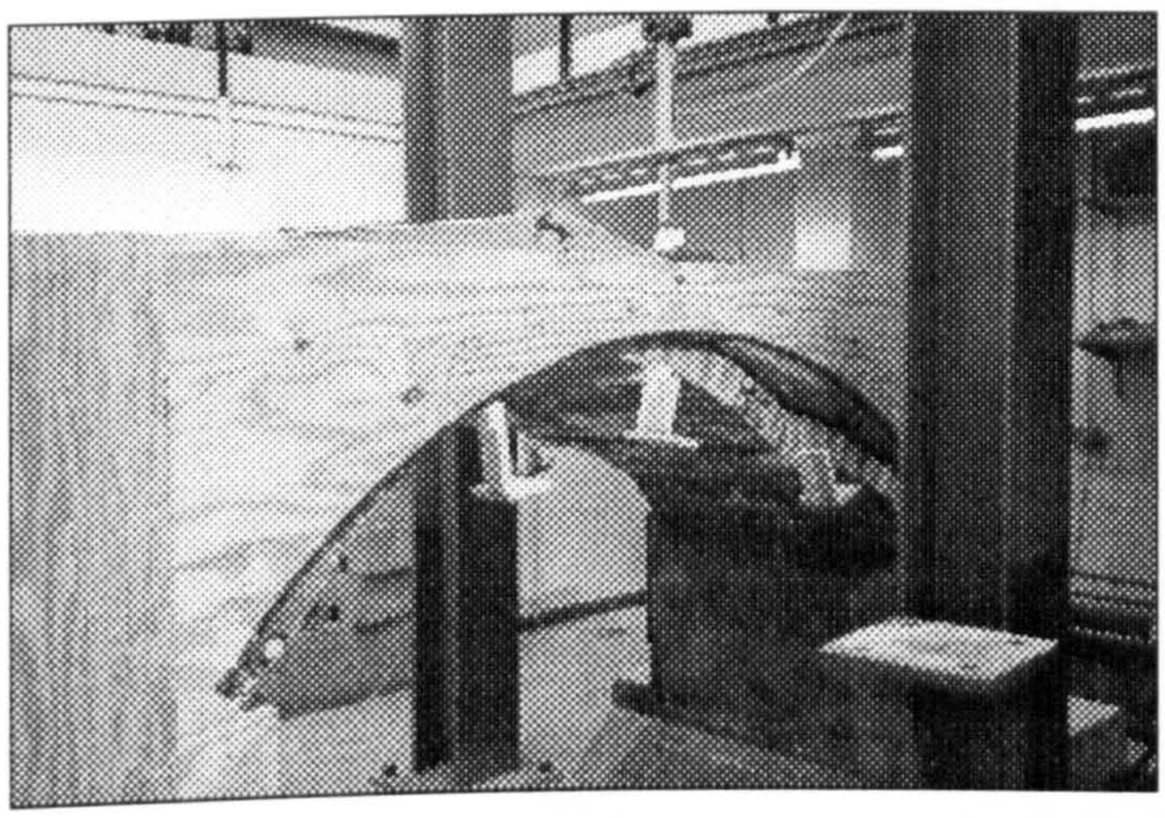

Figure 6 Arch SR4-B shortly before collapse

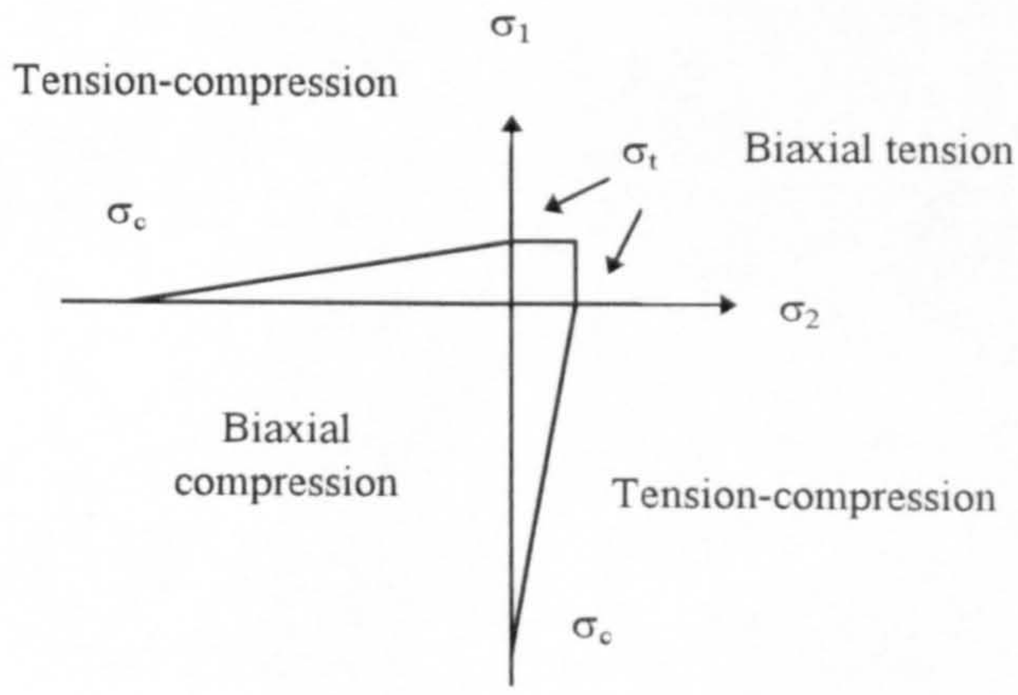

Figure 7 Failure envelope for biaxial concrete model

When the arch was loaded to 16kNm^{-1}, an apparent hinge was formed in the arch ring near the ¼-span point (joint 10). The applied load quickly dropped from 16kNm^{-1} to 14.5kNm^{-1} with an increase in arch vertical deflection, at the ¼-span point, from 0.709mm to 5.03mm. As the load fell, due to increasing deflection, three more hinges formed in the arch ring (joints 3, 21, and 33). All LVDTs were removed to

prevent damage; further loading revealed that the arch was not far from collapse after the load was decreased from its maximum to 13kNm^{-1}. On re-loading, no loads higher than 16kNm^{-1} could be applied. The deflection increased substantially resulting in a large tensile crack on the surface of backfill opposite the loaded strip. The arch finally collapsed in a mechanism with no signs of material compressive failure.

Experimental Behaviour Of Model SR4-C

The arch collapsed at a maximum applied ¼-span live load of 25kNm^{-1} width perpendicular to the span. The arch finally collapsed with four hinges at joints 1, 9, 19, and 33. The load *versus* vertical deflection plot at the intrados ¼-span point was presented in Figure 5. No signs of damage were noticed before testing. No obvious signs of distress were observed until the live load reached 12kNm^{-1} at which small settlements of the load platen occurred. However, no hinges or cracks were observed in the arch ring. At 18kNm^{-1}, the load platen was found to be slightly tilted with its base moved towards the side remote from the load. However, further loads were still being applied to the arch. When loaded to 20kNm^{-1}, the tilting of the load platen was significant and further increases in live load would have caused the platen to become unstable. The applied load was therefore decreased to zero and the whole loading system re-levelled. On re-loading, a load increment of 5kNm^{-1} was applied until the load reached its previous maximum at 20kNm^{-1}. The load *versus* deflection results show that the arch did not fully recover its original shape before re-loading. At 20kNm^{-1} after the re-loading, the vertical deflection at the ¼-span was 0.324mm which was higher than the 0.316mm recorded at the same load before the adjusting the loading system.

After the load reached 20kNm^{-1} the previous 0.5kNm^{-1} load increments were used. When loaded to 24kNm^{-1} the jack had to be readjusted due to tilting of the load platen. As before, the hydraulic jack was fully relaxed and the whole loading system adjusted. The arch was then re-loaded in 5kNm^{-1} increments to its previous maximum of 24kNm^{-1}. The load increment was then re-reduced to 0.5kNm^{-1}. When the live load reached 25kNm^{-1}, the first hinge occurred at joint 9 near the ¼-span point. As happened previously for SR4-A and SR4-B, the arch lost most of its stiffness immediately after formation of the first hinge. The formation of three more hinges at joints 1, 19, and 33 occurred soon afterwards. Further application of live loads, albeit not exceeding the previous maximum of 25kNm^{-1}, substantially increased the arch deflection. An obvious tensile crack was formed on the surface of backfill opposite the loaded strip. As the applied live load was reduced to 9kNm^{-1}, the arch vertical deflection at the ¼-span was 37.3mm. All LVDTs were then removed as a complete collapse of the arch was imminent. Further increase in the arch deflection caused the arch to collapse in a mechanism. Material compressive failure was not observed.

ANALYTICAL METHODS FOR COMPARATIVE ASSESSMENT

Five assessment methods were used: SOILARCH, ARCHIE, CTAP-elastic cracking, MEXE, and 2-D non-linear FE analysis. In addition to the arch geometry, additional input variables required by any assessment method are given below. For consistency between assessment methods a partial factor of safety on applied load of 1 was used throughout.

The mobilisation of backfill passive resistance in SOILARCH, ARCHIE, and CTAP was assumed to be at 80% of the full Rankine value. A compressive strength of 30MPa was assigned to the arch in the ARCHIE analysis. A 45° dispersal angle was adopted in both SOILARCH and CTAP methods. In the MEXE analysis, the span to rise ratio factor, profile factor, material factor, joint factor and condition factor were considered to be 1.000, 0.898, 0.822, 0.770 and 0.600 respectively. A low value of condition factor was used to account for the absence of structural spandrel walls in the authors' model arches.

For the 2-D non-linear FE analysis, eight-noded quadrilateral elements in conjunction with nine Gaussian quadrature points were used to model the arch and backfill. The analysis was performed using commercially available software (LUSAS Version 11-46). A total of 96 elements were used for the arch ring, 128 for the backfill, and 32 for the extrados interface. The biaxial stress-strain model for concrete was

used to describe the failure of the arch material (see Figure 7). It is justified that this model, although being unable to consider material failure subjected to biaxial compression, is deemed suitable for this analysis since no compressive failure of the arch material actually occurred. It has been revealed (Loo, 1995) that the arch collapse load is insensitive to variations in arch compressive strength. Loo's FE analyses considered failures in both biaxial compression and tension. The strain softening model used in the current constitutive model is depicted in Figure 8. A thin layer interface element was used to model the soil-arch interactions around the extrados. The behaviour of the backfill and interface elements was elasto-plastic with failure defined by Mohr-Coulomb yield criterion. All elements were assumed to be in a plane stress condition. Results revealed that the predictions were not significantly affected by using different conditions; plane strain or plane stress. Table 2 gives the material properties used as benchmark values in the FE analyses. A parametric study was performed by varying the arch compressive and tensile strengths, arch elastic modulus, tension softening factor, backfill elastic modulus, and live load dispersal angle. Analyses were also carried out without interface elements and with plane strain conditions in the backfill.

Table 2 Benchmark input variables for the FE analyses

Property	Arch	Backfill
Elastic modulus (MPa)	8000	15
Poisson's ratio	0.2	0.4
Bulk unit weight (kNm^{-3})	21	14.86
Compressive strength (MPa)	30	N/A
Tensile strength (MPa)	0.3	N/A
Strain softening factor	8	N/A
Angle of shearing resistance (°)	N/A	30.5

Results

Figure 9 shows the results from the parametric study on the backfill passive pressure coefficient by SOILARCH, ARCHIE, and CTAP. Results for the parametric study on the live load dispersal angle by SOILARCH and CTAP are presented in Figure 10. Individual data from each assessment method is presented section-by-section following Figure 9.

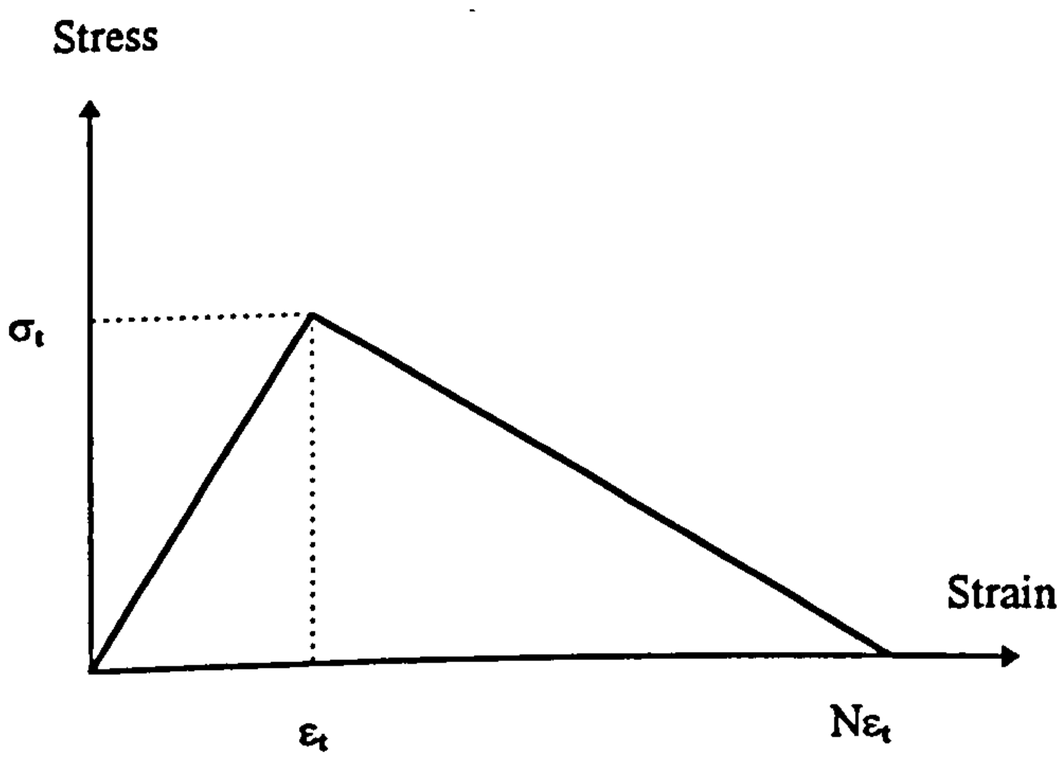

Figure 8 Stress-strain curve for the arch material

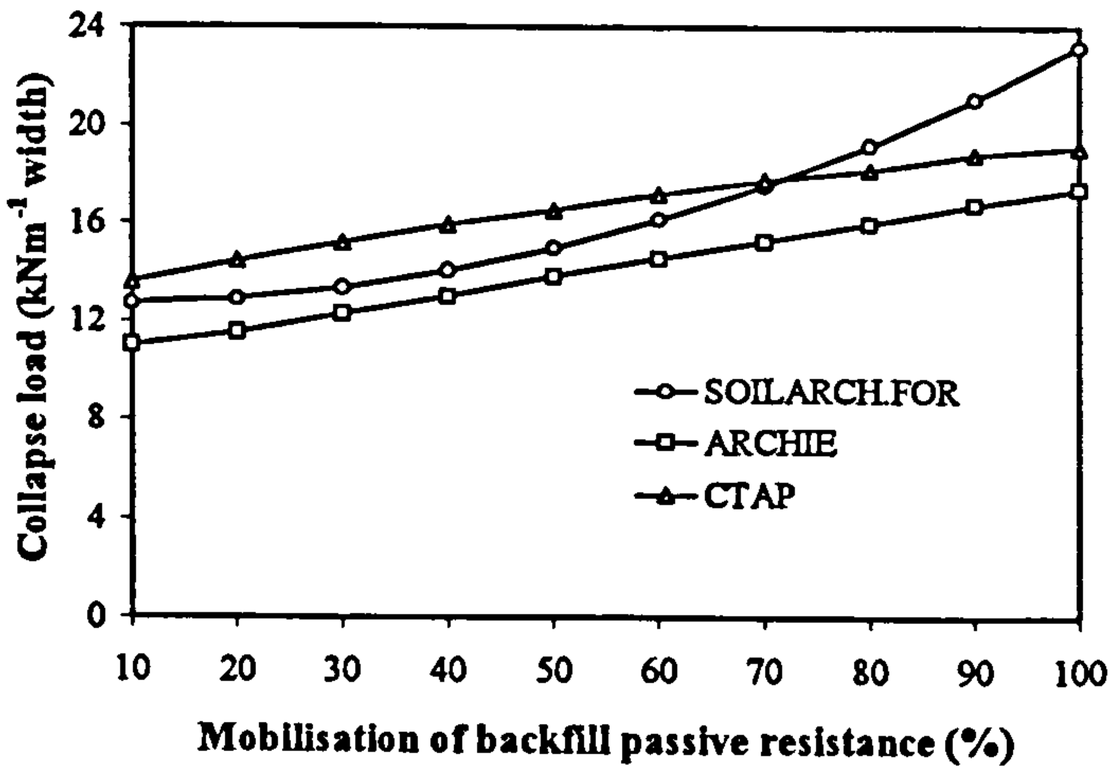

Figure 9 The effect of varying the backfill passive resistance

Arch Assessment By SOILARCH

Parametric studies were carried out by varying the backfill passive pressure coefficient and the live load dispersal angle: data are presented in Figures 9 and 10 respectively. By increasing the mobilisation of

backfill passive resistance from 10% to 100%, SOILARCH predicted an increase in collapse load from 12.76kNm^{-1} to 23.23kNm^{-1}. Similarly, increasing the load dispersal angle from 10° to 60° resulted in an increase in collapse load from 12.80kNm^{-1} to 22.31kNm^{-1}. However, the maximum arch collapse load from these parametric studies was still below the maximum experimental collapse load of 25kNm^{-1}. This might be because the mechanism method ignored the contribution from the brickwork's tensile strength.

Arch Assessment By The Mechanism Method: Program ARCHIE

The backfill passive pressure coefficient was varied in a parametric study and results presented in Figure 9. By increasing the mobilisation of backfill passive resistance from 10% to 100%, the predicted arch collapse load was found to increase from 11kNm^{-1} to 17.4kNm^{-1}. Such an increase was approximately linear. As can be seen from Figure 9, the collapse loads predicted by ARCHIE were lower than those from SOILARCH and CTAP. The live load dispersal angle could not be varied in this method and therefore it was not included in the parametric study.

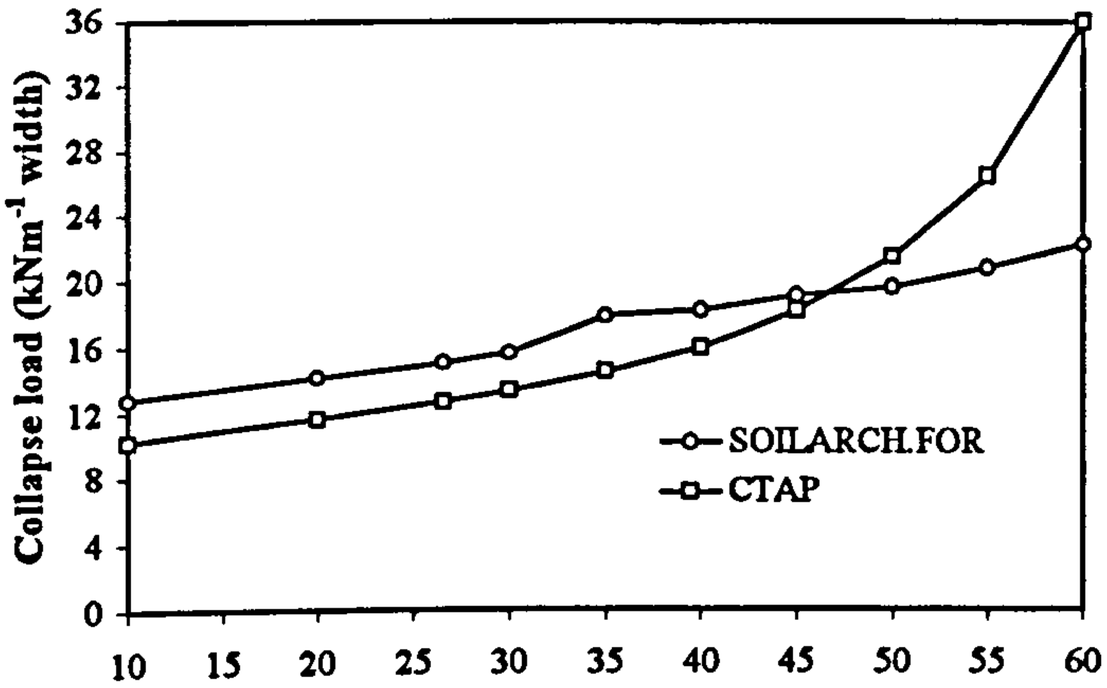

Figure 10 The influence of live load dispersal angle

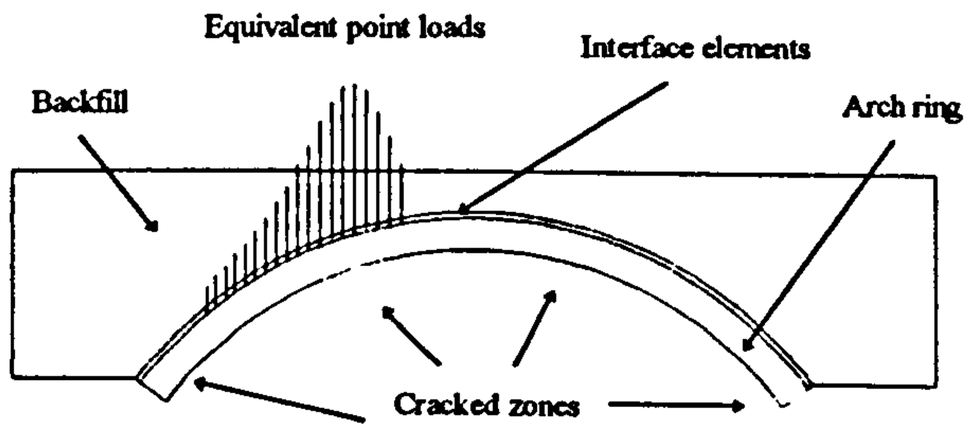

Figure 11 Collapse mode predicted by FE analysis

Arch Assessment By CTAP's Elastic Cracking Analysis

The backfill passive pressure coefficient and the live load dispersal angle were varied in the parametric studies and results are presented in Figures 10 and 11 respectively. By increasing the mobilisation of backfill passive resistance from 10% to 100%, CTAP predicted an increase in the arch collapse load from 13.62kNm^{-1} to 19.12kNm^{-1}. The predicted collapse loads are higher than those predicted by ARCHIE. However, its predictions are only higher than those by SOILARCH.FOR for the mobilisation of backfill passive resistance from 10% to 70%. The live load dispersal angle was increased from 10° to 60° resulting in an increase in the collapse load from 10.31kNm^{-1} to 36kNm^{-1}. Such an increase is approximately quadratic. CTAP's predictions are lower than those by SOILARCH.FOR for the dispersal angle from 10° to 45° and higher for the dispersal angle from 50° to 60°.

Arch Assessment By The MEXE Method

The allowable single axle load predicted by the MEXE method was 18.98kNm^{-1}. This figure lay between the maximum and minimum experimental arch collapse loads. However, it must be emphasised that the MEXE method only gives allowable axle loads not a predicted collapse load. If a factor of safety of 3.4 were applied, as recommended by current standard BD 21/97 (Department of Transport, 1997), then the predicted arch collapse load would be 64.53kNm^{-1}. Although the derivation of the MEXE method was conservative in that it ignored lateral soil forces and allowed only limited load distribution, it still predicted a capacity above the actual collapse loads.

Arch Assessment By 2-D FE Analysis Using LUSAS

Figure 11 shows the collapse mode predicted by the 2-D FE model at a load of 26kNm^{-1} using the benchmark input variables given in Table 2. The load *versus* deflection plot from this analysis was even more brittle than those recorded experimentally. The deflections given by the FE analysis were due to the bending of the arch making them much smaller than in reality. Failure of the arch in this FE analysis was defined by full propagation of a crack along a section through the arch ring. By increasing the arch tensile strength from 0.1MPa to 0.6MPa, the FE method predicted an increase in collapse load from 18kNm^{-1} to 39kNm^{-1}. Similarly, increasing the tension softening factor from 5 to 20 caused the collapse load to increase from 24kNm^{-1} to 31kNm^{-1}. No significant changes were found by varying the arch compressive strength from 10MPa to 1×10^{6}MPa; arch elastic modulus from 6000MPa to 9000MPa; backfill elastic modulus from 10MPa to 25MPa; or live load dispersal angle from 27° to 60°.

The FE prediction of the arch collapse load without interface elements was found to be 25kNm^{-1} which was only 1kNm^{-1} lower that that with interface elements. A more rigid connection between the arch and the backfill might have acted as a stress concentration resulting in a lower collapse load. A similar prediction of the arch collapse load was found by treating the backfill as if it were in plane strain conditions. Little difference was thought to arise between plane stress or plane strain conditions as the Poisson's ratio for the arch was only 0.2.

DISCUSSION OF THE EXPERIMENTAL RESULTS

The main finding of this study is that nominally identical arches may yield significantly different collapse loads. The collapse loads for SR4-A, SR4-B, and SR4-C were 21kNm^{-1}, 16kNm^{-1}, and 25kNm^{-1} respectively. Such a significant discrepancy in the collapse load was believed to be due to variations of arch tensile strength as it was the only property of the whole structure that was almost impossible to keep uniform for the three arches. The brick-mortar bond strength was between 0.13MPa and 1.18MPa with a mean, standard deviation, and coefficient of variation of 0.52MPa, 0.22MPa, and 43% respectively. Such a high coefficient of variation raised concerns as to whether the mean brick-mortar bond strength should be used to represent the arch tensile strength. What was the actual arch tensile strength at the region under the load point? If the tensile strength of the joint where the first hinge occurred was low, the whole arch could collapse at a much lower load. However, this would only be true when the arch tensile strength dominates the behaviour as was the case for those arches tested here. The load *versus* deflection plots (see Figure 5) were brittle. Each arch lost much of its stiffness immediately after formation of the first hinge. The maximum applied live load was that to cause the formation of the first hinge. The failure of these arches was due to material tensile failure although the final collapse took the form of a mechanism.

Any arch bridge assessment method which ignores the contribution of tensile strength would underestimate the capacity of these arches. The mechanism method was deemed inappropriate in this case, aside from disregarding the arch's tensile strength it failed to replicate the models' behaviour because the maximum applied load did not occur with the formation of a mechanism but was the load needed to overcome the tensile strength at the first hinge. The 2-D FE model was more realistic as it simulated crack propagation in the arch ring: failure of the arch was defined by tensile failure of the arch material for these cases.

DISCUSSION OF THE ANALYTICAL RESULTS

SOILARCH, ARCHIE and CTAP are likely to underestimate the collapse load in this study since arch tensile strength is excluded in these methods. The collapse load prediction by these methods could be arbitrarily increased by increasing the mobilisation of backfill passive resistance. By increasing the mobilisation of backfill passive resistance from 10% to 100%, SOILARCH, ARCHIE and CTAP predicted increases in collapse load from 12.76kNm^{-1} to 23.23kNm^{-1}, 11kNm^{-1} to 17.4kNm^{-1}, and 13.62kNm^{-1} to 19.12kNm^{-1} respectively. However, the use of a high percentage of backfill passive resistance is

unjustifiable, other than to indirectly compensate for ignoring the arch's tensile strength. Each arch achieved its maximum applied live load with only small deflections for which the lateral earth pressure mobilised would be only slightly higher than the at-rest state.

The MEXE method, although claimed to be conservative because it ignores backfill lateral resistance and allows only limited live load distribution, predicted a reasonable allowable single axle load of 18.98kNm^{-1}. No further comment on the MEXE method could be made as the provisional axle load and all the modification factors are purely empirical and might be subjectively manipulated by any end-user.

Among all the input variables used in the 2-D FE based parametric study, the arch tensile strength and the tension softening factor were found to be most influential. The arch compressive strength, arch and backfill elastic moduli, and live load dispersal angle were found to have insignificantly affected the prediction over the range examined. By increasing the arch tensile strength from 0.1MPa to 0.6MPa, the FE analysis predicted a collapse load increase from 18kNm^{-1} to 39kNm^{-1}. Increasing the tension softening factor from 5 to 20 resulted in an increase in the predicted collapse load from 24kNm^{-1} to 31kNm^{-1}. It was expected that the arch tensile strength and its tension softening factor were likely to have a greater influence on the capacity prediction since collapse in the FE analysis was governed by tensile failure of the arch. The predicted collapse load using the benchmark input variables given in Table 2 was 26kNm^{-1}. This prediction was still higher than all the experimental collapse loads even with a low arch tensile strength of 0.3MPa. However, if an arch tensile strength of 0.5MPa (approximately the mean brick-mortar bond strength) was used, the predicted arch collapse load would be much higher at 35kNm^{-1}. For this study, the arch tensile strength was recommended to lie between 0.2MPa and 0.3Mpa; the tension softening factor should lie between 5 and 8 for more reasonable capacity assessments.

CONCLUSIONS

1. Three nominally identical arches had significantly different capacities from 16kNm^{-1} to 25kNm^{-1}.
2. The load-deflection plots for all arches tested in this study were brittle due to a sudden release of tensile energy at brick-mortar interfaces where hinges formed.
3. The maximum applied live load required to overcome the tensile strength at the first hinge in each arch was higher than that required to form a mechanism.
4. Each arch lost its stiffness immediately after formation of the first hinge.
5. No compressive failure of the arch ring was seen in these tests.
6. Using arbitrarily high backfill passive pressures, SOILARCH, ARCHIE and CTAP predicted reasonable collapse loads for these arches.
7. The arch's tensile strength and tension softening factor were most influential for FE capacity assessment.

REFERENCES

Bridle, R.J. & Hughes, T.G., (1990), An energy method for arch bridge analysis. *Proc. Inst. Civ. Engnrs*, 89 (2): 375-385.

Department of Transport, (1997), *Departmental Standard BD21/97 The assessment of Highway Bridges and Structures*. HMSO, London.

Gong, N.G., (1992), *Finite element analysis of masonry arch bridges*. PhD Thesis, Nottingham Univ.

Loo, Y.C., (1995), Collapse load analysis of masonry arch bridges. *Proc. 1st Int. Conf. Arch Bridges*, Thomas Telford Ltd, Bolton, 239-244.

Ng, K.-H., (1999), *Analysis of masonry arch bridges*. PhD Thesis, Napier University, Edinburgh.

Smith, F.W., (1991), *Load path analysis of masonry arches*. PhD Thesis, Univ. of Dundee.